NASA Contractor Report 198525

Experimental Study of Vane Heat Transfer and Film Cooling at Elevated Levels of Turbulence

Forrest E. Ames
Allison Engine Company
Indianapolis, Indiana

September 1996

Prepared for
Lewis Research Center
Under Contract NAS3–25950

National Aeronautics and
Space Administration

NASA Contractor Report 198525

Experimental Study of Vane Heat Transfer and Film Cooling at Elevated Levels of Turbulence

Forrest E. Ames
Allison Engine Company
Indianapolis, Indiana
EDR No. 17792

Prepared for
Lewis Research Center
under CONTRACT NAS3-25950

NASA

National Aeronautics and
Space Administration

Office of Management

Scientific and Technical
Information Program
1996

Table of Contents

List of Figures

List of Tables

Appendices

Nomenclature

C	airfoil chord length
Cf/2	skin friction coefficient, $Cf/2 = \tau_0/(\rho U_\infty^2)$
Cp	specific heat at constant pressure
D	coolant hole diameter
DR	density ratio, ρ_c/ρ_∞
Ebar	mass averaged kinetic energy loss coefficient
$E_1(k_1)$	one dimensional energy spectrum of u', $E_1(k_1) = U_\infty E_1(f)/2/\pi$
$E_2(k_1)$	one dimensional energy spectrum of v', $E_2(k_1) = U_\infty E_2(f)/2/\pi$
f	frequency, 1/s
K	thermal conductivity
k_1	wavenumber, $k_1 = 2\pi f/U_\infty$
Lu	energy scale, $Lu = 1.5\ |u'|^3/\varepsilon$
Lx	longitudinal integral scale
Ma_{ex}	Mach number based on exit conditions
omega	total perssure loss coefficient, $(Pt_{in}-Pt_{ex})/(Pt_{in}-Ps_{ex})$, also ω
P	pressure
P	pitch, hole to hole spanwise spacing
PReqv	equivalent pressure ratio, (Pc-Pt)/(Pt-Ps)
Ps	static pressure
Pt	total pressure
Q	surface heat flux boundary condition
Re	Reynolds number
$Re_{\delta 2}$	momentum thickness Reynolds number, $Re_{\delta 2} = \rho_\infty U_\infty \delta_2/\mu_\infty$
Red2	momentum thickness Reynolds number, $Red2 = \rho_\infty U_\infty \delta_2/\mu_\infty$
Re_{ex}	exit Reynolds number, $Re_{ex} = \rho_{ex} U_{ex} C/\mu$
$Re\lambda$	Taylor Reynolds number, $Re\lambda = \rho\ u'\ \lambda/\mu$
S	surface arc, (cm)
St	Stanton number, $h/(\rho U Cp)$
St_0	low turbulence case Stanton number for figure 4.4 and for film cooling with low inlet turbulence
St_0	high turbulence case Stanton number for film cooling with high inlet turbulence
T	temperature
Tt	stagnation temperature
Tu	turbulence intensity, $Tu = u'/U_\infty$
Tuv	normal component turbulence intensity, $Tuv = v'/U_\infty$
Tu_0	turbulence level at reference position
U	streamwise velocity
u'	RMS streamwise fluctuation velocity
VR	velocity ratio, Uc/U_∞
v'	RMS normal fluctuation velocity (normal to streamwise velocity and generally normal to vane surface
w'	RMS spanwise fluctuation velocity

Nomenclature (continued)

X	streamwise distance along the airfoil, except for tables 2.1, 2.2, 2.3, and 2.4
Y	normal distance from the vane surface, except for tables 2.1, 2.2, 2.3, and 2.4
Z	cross span distance from the endwall

Greek Symbols

δ_1	displacement thickness, $\delta_1 = \int_0^\infty (1 - \rho U/\rho_\infty U_\infty)\, dy$
δ_2	momentum thickness, $\delta_2 = \int_0^\infty \rho U/\rho_\infty U_\infty (1 - \rho U/\rho_\infty U_\infty)\, dy$
ε	turbulent dissipation
η_{ad}	adiabatic wall effectiveness, also η, $\eta_{ad} = (Taw-Tr)/(Tco-Tr)$
λ	lateral dissipation scale or Taylor microscale, $\lambda = (15\, \nu\, u'^2/\varepsilon)^{1/2}$
ν	dynamic viscosity
μ	kinematic viscosity
μ_m	eddy diffusivity
τ_0	wall shear stress
ω	total perssure loss coefficient, $(Pt_{in}-Pt_{ex})/(Pt_{in}-Ps_{ex})$, also omega

Subscripts

∞	references to free stream conditions
aw	adiabatic wall
c	coolant (static pressure, recovery temperature)
co	coolant outlet
core	average value in region unaffected by wall or wake
ex	references to vane exit static pressure tap plane location
in	references to inlet static pressure tap plane location
r	recovery

Summary

A four vane subsonic cascade was used to investigate the influence of high intensity turbulence on vane film cooling effectiveness distributions. The influence of film cooling on surface heat transfer, boundary layer development, and exit losses was also examined. For this study a high level, large scale inlet turbulence was generated with a mock combustor (12 %) and was used to contrast results with a low level (1 %) of inlet turbulence. The three geometries chosen to study in this investigation were one row and two staggered rows of downstream cooling on both the suction and pressure surfaces in addition to a showerhead array. The downstream rows consisted of holes with a 30° incline relative to the surface and in the streamwise direction with a spanwise pitch to diameter ratio of 3. The showerhead array consisted of 5 rows of 20° spanwise slanted holes. The streamwise spacing of the showerhead rows was 3.84 diameters while the spanwise hole spacing was 6.4 diameters. Velocity ratios ranging from 0.3 to 0.56 were chosen for the suction surface film cooling while velocity ratios of 0.5, 1.0, and 1.5 were chosen for the pressure surface array. The showerhead array was run over equivalent pressure ratios (Pc-Pt)/(Pt-Ps,ex) of 0.0175, 0.07, and 0.35.

Film cooling was found to have only a moderate influence on the heat transfer coefficients downstream from arrays on the suction surface where the boundary layer was turbulent. However, film cooling was found to have a substantial influence on heat transfer downstream from arrays in laminar regions of the vane such as the pressure surface, the stagnation region, and the near suction surface. Generally, heat transfer augmentation was found to scale on velocity ratio, or equivalently pressure ratio. In relative terms, the augmentation in the laminar regions for the low turbulence case was found to be higher than the augmentation for the high turbulence case. The absolute levels of heat transfer were always found to be the highest for the high turbulence case.

The turbulence was found to have a substantial impact on effectiveness. The high turbulence had the greatest effect on the pressure side where the relative levels of turbulence are highest. For the double row, the effectiveness levels dropped to less than 50% of the low turbulence condition for all cases. For the single row, spanwise mixing was responsible for the rapid drop in centerline effectiveness levels, while turbulent diffusion in the normal direction was found to be more gradual. The turbulence also caused a large reduction in film cooling protection from the showerhead array. For the suction surface array, the effectiveness levels were higher for the high turbulence case immediately downstream from the cooling array due to the difference in the upstream boundary layer profiles. Far downstream from the suction surface array, effectiveness levels for the high turbulence case dropped below the low turbulence case.

Velocity profiles downstream from the cooling arrays have been documented to illustrate the interaction of turbulence and film cooling with vane boundary layer development. Exit loss distributions have also been taken to document the influence of film cooling on losses with and without high inlet turbulence.

Chapter 1

Introduction

According to Scrivener (1990), turbine inlet temperatures have increased by about 20° C per year driven by the resulting enhancement to engine performance. Part of this temperature rise has been accommodated by improvements in materials and the rest has been realized through progressive enhancement of component cooling capabilities. As turbine inlet temperatures increase, the heat transfer designer is charged with developing cooling configurations with higher effectiveness levels. At the same time, cooling air flow is limited by the accompanying deterioration in performance, allowing less room for conservatism.

The chief difficulty in developing a durable cooling design is the accurate assessment of gas path heat transfer. Predicting gas path heat transfer is complicated by effects of combustor generated and wake turbulence, hot streaks, and secondary flows. Furthermore, due to increasing inlet and coolant temperatures, film cooling coverage is desirable on more and more components. The effective use of film cooling protection requires accounting for the dissipating effects of turbulence on adiabatic effectiveness and augmenting effects of discrete hole film cooling jets on the local heat transfer coefficient distribution.

Over the years, a large body of film cooling data has been documented in the open literature. The large majority of these data has been taken using flat plate configurations at low free stream turbulence levels. A majority of these data has been taken using geometries in which hole length to diameter ratio and plenum configurations vary significantly from real components. Most data provide only adiabatic effectiveness values, yet designers also need to know how the discrete cooling jets alter the heat transfer coefficient distribution. Also, designers need to be able to account for the combined influence of turbulence and component geometry.

Currently, advanced cooling designs for components require a combination of warm rig and engine testing. Warm rig tests screen advanced designs for deficiencies in an attempt to improve the design prior to engine tests. Warm rig tests can also provide detailed data which allow comparisons with design system predictions. Only engine tests can verify the full interaction of the combustion, turbine, and secondary flow systems across the range of mission variables. These tests add substantial costs to the development of engines.

The risk and cost of developing advanced engines is becoming prohibitively expensive. In order to remain competitively advanced we need to streamline the way new technologies are developed. Our best change to reduce the time and overall cost of reliably integrating advanced cooling schemes into our latest engines is to spend more resources in the technology development phase to prove and improve cooling technologies prior to engine integration and testing. A more comprehensive approach to cooling technology development will take more resources initially but not more time and should substantially improve initial reliability and performance. While time to market is critical to obtain a foothold in a developing market, initial

reliability is crucial for maintaining and expanding customer base. Additionally, while detailed bench top and component testing of cooling schemes is currently indicated, our ability to accurately model complex internal and external configurations is rapidly improving. Joint experimental and computational modeling programs have the longer term potential to reduce our current dependence on comprehensive testing and eventually improve our time to market without jeopardizing initial reliability.

The objective of this contract is to study the influence of free stream turbulence on film cooling effectiveness and the interaction of discrete cooling jets on the surface heat transfer coefficient. For this study, a vane with a film cooling configuration representative of an advanced design was used. The heat transfer distribution for the base vane, the vane with showerhead array, and the vane with one and two rows of downstream film cooling has been documented. The heat transfer and film cooling tests were run at both high (13%) and low (1%) level of turbulence, at two Reynolds numbers (500,000 and 800,000), and at three coolant to free stream velocity ratios for the different configurations and conditions. Also, boundary layer profiles have been taken downstream from the film cooling arrays to determine how the turbulence boundary condition is altered by the showerhead and downstream film cooling jets. This report documents heat transfer data, film cooling data, and velocity and turbulence profiles downstream from the different film cooling arrays. These data provide useful information to designers on how turbulence dissipates film cooling protection and how discrete jets influence the surface heat transfer distributions. Additionally, these data are comprehensive enough to be useful for predictive comparisons.

Background

Comprehensive reviews on discrete hole film cooling are given by both Rohsenow, Harnett, and Ganic' (1985) in the "Handbook of Heat Transfer Applications," 2nd Edition, and by Crocker and L'Ecuyer (1988) in the Purdue University report ME-TSPC-TR-88-17. Some of the listed effects for discrete hole film cooling include density ratio, velocity ratio, pitch to diameter ratio, hole Reynolds number, boundary layer thickness to diameter ratio, curvature, acceleration, and turbulence. Additionally, both of these reviews indicate that discrete hole film cooling can substantially effect the heat transfer coefficient around and downstream from the injection site.

L'Ecuyer and Soechting (1985) characterize discrete hole film cooling with 35° holes with a P/D of 3 in three general regimes based on the coolant-to-free stream velocity ratio. They describe the mass addition regime for velocity ratios at or below 0.25. In this regime they suggest effectiveness levels increase with blowing ratio due to increased thermal capacity of the coolant. However, they indicate that the effectiveness distribution is independent of the individual values of density ratio and velocity ratio. They call the range of velocity ratios from 0.25 through 0.8 the mixing regime because the effectiveness distribution depends on the opposing influences of increased thermal capacitance with increasing blowing ratio and increased coolant penetration with increased momentum ratio. Finally, L'Ecuyer and Soechting call the range of velocity ratios above 0.8 the penetration regime. In this regime the effectiveness

distribution is dominated by excessive coolant penetration and augmented diffusivity due to the jet/free stream interaction. Further, turbulent diffusion is important in mixing the coolant's thermal effect toward the surface.

Based on the Handbook of Heat Transfer Applications, hole Reynolds number was found to have only a minor effect on effectiveness. Boundary layer displacement thickness to diameter ratio (δ_1/D) appears to have only a small effect below a value of 0.25 but appears to have a substantial effect above this value. Curvature has been demonstrated to have a substantial effect on film cooling effectiveness. Generally, convex curvature produces averaged effectiveness values above a flat plate while concave curvature reduces effectiveness values below that of a flat plate. The effect of acceleration seems to be more complicated. At low values of the acceleration parameter K, researchers generally report increases for moderate values of K but decreases for large values of K. Comparisons between a single row of holes and a double row of staggered holes generally indicate that a double row of staggered holes gives much more spanwise uniform effectiveness distributions. Additionally, a double row of staggered holes gives a higher average level of effectiveness than two single rows superposed, particularly at higher velocity ratios. Crocken and L'Ecuyer report that increasing pitch to diameter ratios of holes reduces both average effectiveness levels and spanwise uniformity.

The handbook on Heat Transfer Applications indicates that spanwise averaged values of normalized heat transfer are around 1.0 for velocity ratios up to 1 for a row of inclined tubes. Conversely, Crocker and L'Ecuyer report that for most practical film cooling applications, the normalized heat transfer is greater than unity.

The effect of turbulence on film cooling effectiveness was recently studied by Bons, MacArthur, and Rivir (1994) for a single row of 35° holes with a pitch to diameter ratio of 3 over turbulence levels ranging from 1 to 17 percent. They generally found that turbulence substantially reduced centerline effectiveness at moderate velocity/blowing ratios showing an increasing effect with increasing turbulence levels downstream distance. The effect was considerably less dramatic at higher velocity/blowing ratios. Additionally, they found that the turbulence had a dramatic influence in enhancing the spanwise uniformity of the effectiveness distribution. For the 17% turbulence case, spanwise uniformity was achieved within an X/D of 10.

The effect of plenum flow and hole length has also been found to have a significant effect on film cooling jet trajectories. Thole (1996) recently completed a study on the influence of coflow and counter flow on film cooling jets from short holes. In the study, one side of the hole was found to stay completely separated -- the downstream side for coflow in the plenum and the upstream side of the hole for counterflow. The resulting velocity field around the jet is considerably removed from the attached and largely radially uniform profile typically studied in much of the archival literature.

A number of film cooling studies have been conducted on turbine vane and blade shapes over the years. Some of these studies include Buck and Prakash (1995), Abuaf, Bunker, and Lee

(1995), Ou, Han, Mehendale, and Lee (1994), Mehendale, Han, Ou, and Lee (1994), Abhari and Epstein (1994), Ou and Han (1993), Takeishi, Aoki, Sato, and Tsukagoshi (1991), Nirmalan and Hylton (1990), and Dring, Blair, and Joslyn (1979). Generally, at similar blowing ratios pressure surface film cooling has been found to be substantially lower than suction surface effectiveness. On the suction surface, film cooling appears to cause immediate transition for the laminar or transitional boundary layer [also see Mayle (1991)]. On the pressure side, film cooling can cause substantial increases in heat transfer which increase with increasing velocity ratios. Film cooling with rotation is lower than stationary blade film cooling. Also there exists a strong radial outward component to pressure surface film cooling jet trajectory on a rotating blade.

Showerhead Film Cooling

Some recent studies on showerhead (or leading edge) film cooling include Salcudean et. al (1994), Gartshore et.al (1993), Ou, Mehendale, and Han (1992), and Mehendale and Han (1992). These studies show that depending on geometry and velocity ratio, spanwise oriented leading edge cooling jets may pair leaving portions of the downstream surface unprotected by leading edge coverage. This can lead to atypical streamwise distributions in effectiveness. Velocity ratio has a substantial effect on augmenting laminar teat transfer coefficients in the stagnation region but only a mild influence on heat transfer to the turbulent boundary layer. Additionally, free stream turbulence has a substantial influence on reducing film cooling effectiveness, particularly for lower blowing ratios. Results from previously mentioned turbine airfoil studies indicate that showerhead cooling is more effective on the suction surface compared to the pressure surface.

Combustor Generated Turbulence

Combustor generated turbulence is the inlet boundary condition for the first stage rotor and developing relevant inlet turbulence characteristics is critical to the validity of any heat transfer or film cooling study. Some studies applicable to the stator inlet condition include, Ames (1994), Goebel, Abuaf, Lovett, and Lee (1993), Moss and Oldfield (1991, 1992), Ames and Moffat (1990), Bicen and Jones (1986), and Zimmerman (1979). These studies indicate that combustor turbulence levels are high and very much dependent on the geometry of the combustor. Additionally, turbulence scales are large and scale on the combustor dimensions. Moss and Oldfield measured combustor exit spectra with and without combustion and concluded that there was little measurable change in turbulence level or normalized spectra with burning. Additionally, they indicated that the turbulence produced by Ames and Moffat in their mock combustor was consistent with the scale and level produced by their own real combustors. The turbulence levels reported by Ames and Moffat ranged from 15 to 17 percent. Bicen and Jones measured levels ranging from 13 to 20 percent based on the bulk exit velocity. Zimmerman measured turbulence levels ranging from 7 to 10 percent at the exit of a helicopter combustor and found turbulence level went up with combustion. Goebel, Abuaf, Lovett, and Lee found turbulence level decreased substantially with combustion for combustors with high levels of swirl.

Effects of Turbulence on Heat Transfer

The influence of mock combustor and grid turbulence have been previously studied by Ames (1994, 1995) and pertinent references on the effects of turbulence on heat transfer are documented there.

Implications for Film Cooling Technology Development

The references discussed previously indicate that film cooling is a complex multivariable problem. Turbulence, hole length, spacing, and angle, pressure gradient, boundary layer state, curvature, plenum feed, velocity, density ratio, and rotation all influence film cooling performance. Additionally, film cooling has been found to have a strong influence on the local heat transfer coefficient for laminar boundary layers. Because of the overall complexity and interaction of the turbulence, film cooling, and heat transfer problem, film cooling must be studied on geometries that are similar to their configuration in an engine.

The turbulence boundary condition is another important consideration in any film cooling study. Bons, MacArthur, and Rivir (1994) have shown the dramatic effect of turbulence on film cooling effectiveness. The surface of a first stage vane can see an extreme variation in local turbulence level. On the near pressure surface, the turbulence level can be as high or higher than the inlet level while typical turbulence levels on the suction surface of a vane are 1/3 to 1/4 of the inlet turbulence level due to the increase in the velocity across the nozzle. While an appropriate turbulence inlet condition is important for relevant vane film cooling and heat transfer measurements, developing a low baseline condition is useful in order to get a better appreciation for the influence of the turbulence and to help relate archival data on flat plate film cooling at low turbulence to the present investigation.

The general objective of the present study has been to investigate both the influence of turbulence on film cooling and the effect of film cooling to vane heat transfer. In this study a high level of large scale turbulence was generated with a mock combustor as well as a low level of turbulence to help ground the experiment. Both the adiabatic effectiveness and the heat transfer have been determined for a range of practical conditions for three film cooling geometries. These geometries included a vane with a showerhead array, a vane with one row of film cooling on the suction and pressure surface, and a vane with two downstream rows of film cooling on the suction and pressure surface. In addition to the film cooling and heat transfer data, velocity and turbulence measurements were also taken for the boundary layers a few diameters downstream from the film cooling rows. Also, for several pressure ratios for the three vane geometries, exit total pressure surveys were taken to examine the losses.

Chapter 2

Experimental Apparatus and Baselining

The experimental apparatus used in this investigation as well as the data acquisition and reduction procedures are documented in this section. This chapter provides detailed information on the geometry of the cascade, vanes, turbulence generator, and heat transfer apparatus. The data acquisition and data reduction procedures are overviewed. This section is intended to provide enough detail on the cascade geometry and the quality of the data to allow use of this data for predictive assessment.

Facility Description

The four vane cascade used in this study is connected to an in draft blower. The blower is rated at 1.13 m^3/s (2400 SCFM) with a pressure rise of 10.34 kPa (1.5 psia). The Plexiglas walled cascade was originally built by Zimmerman (1990) for three component laser anemometer measurements. The cascade was modified for the present experiments to allow for access with hot wire anemometry probes and pressure probes. A schematic of the cascade is shown in figure 2.1. The cascade uses four, 4.5 times scale, C3X vanes. The vanes are a two dimensional slice from a design for a helicopter engine. This vane geometry was previously used by Nealy, et. al. (1983), for measurements of heat transfer distributions in a warm cascade rig. The present cascade has a row of 9 inlet static pressure taps spanning two vane passages at 3.68 cm upstream from the inlet plane of the vanes to monitor inlet flow uniformity. In addition, the cascade has a row of exit static pressure taps to monitor exit flow periodicity. The inlet flow uniformity was controlled using the upper and lower bleed flow adjustments. The exit periodicity was set up using the upper and lower tailboards. The probe access ports, which are labeled 1 through 8, accommodated a 14.73 cm long probe used to traverse across the turbine passage and the exit. This probe was pivoted about the access ports using a slider linkage on a lead screw drive table. The location of the probe access points or pivot points is given in table 2.1 and is referenced to the lower right hand corner of figure 2.1. The position numbers referenced in table 2.1 relate to the numbers written over the pivot points in figure 2.1. The inlet access ports, which are also labeled 1 through 8, accommodated inlet total pressure, temperature, and hot wire probes used to reference and survey the inlet conditions. These ports are located 3.68 cm upstream from the vane leading edge plane and are spaced four to a passage.

The vane geometry is shown in figure 2.2 and the vane coordinates are given in table 2.2 as taken from reference 30. The vane as shown in figure 2.2 is rotated 180 degrees from its orientation in figure 2.1. In tables 2.2, 2.3, and 2.4 the columns labeled arc refer to distance along the surface of the vane from the stagnation point where positive is on the suction surface and negative is on the pressure surface. The geometric

values for the vane including true chord, axial chord, spacing, height, throat, calculated air exit and stagger angles, and leading edge and trailing edge diameters are also tabulated on figure 2.2. A second coordinate system was chosen to show the instrumentation and film cooling geometries as well as the finite element mesh in tables 2.3 and 2.4 and in later figures. This alternate coordinate system is marked X2 versus Y2 in these tables and figures and is shown for clarity on figure 2.2.

Turbulence Generator

Two inlet turbulence boundary conditions were developed for this study. The conditions consisted of a low turbulence base case and a case with simulated combustor turbulence. Figure 2.3 shows the inlet geometry for the low turbulence configuration. The inlet consisted of an inlet filter to remove dust from the air, two nylon screens to reduce the inlet velocity fluctuations, an eight to one 2-D contraction nozzle to reduce the level of streamwise turbulence intensity, and a 25.4 cm long, rectangular section. The rectangular section is connected to the cascade.

The test section configuration with the simulated combustor is shown in figure 2.4. The combustor is attached directly to the inlet plane of the cascade. The flow conditioning screens are not used in this configuration and the air filter section is connected directly to the inlet of the combustor simulator.

A schematic of the simulated combustor is shown in figure 2.5. The overall length of the turbulence generator is 45.72 cm. The inlet of the simulator is 59.06 cm wide by 42.54 cm high. Air flow is directed from the inlet plenum through the rear and side panels of the simulator liner. Flow through the rear slots combines with flow through the first row of holes in the side panel to create a recirculation zone inside the simulator liner. The second row of holes in the side panels simulate dilution jets. The simulator takes a two to one contraction from the liner into the inlet of the cascade through a 15.24 cm long nozzle.

Pressure Vane Description

A schematic of the film cooled vane used to measure the surface pressure distribution is shown in figure 2.6. The locations of the .079 cm O.D. stainless steel tubes used for the static pressure taps are indicated by the symbols. The tubes were cast into the vane and static taps were located by drilling through the surface into the tubes. The surface location of the static taps are given in table 2.3 both in terms of X and Y coordinates and also in terms of surface distance. The stagnation point is located at tap 18.

Three film cooled C3X vanes for determining the surface pressure distribution were built for this study. The geometries had (1) a showerhead array, (2) a showerhead array with one row of pressure surface and suction surface film cooling, and (3) a showerhead array with two stagger rows of pressure surface and suction surface film cooling. The showerhead array consisted of 5 staggered rows of 20 degree spanwise

incline 0.132 cm diameter holes with spanwise spacing of 0.847 cm. The surface arc of the row locations at the hole centerlines were -0.254, 0.254, 0.762, 1.270, and 1.778 cm. The pressure surface holes consisted of one and two staggered rows of 30 degree streamwise inclined 0.132 cm diameter holes with a spanwise spacing of 0.396 cm. The hole centerline plane of the single row of holes intersected the surface at an arc location of -2.72 cm from the stagnation region. The second row of holes was spaced 0.39 cm upstream from row one or at a surface arc of -2.33 cm. The suction surface holes consisted of one and two staggered rows of 30 degree streamwise inclined 0.159 cm diameter holes with a spanwise spacing of 0.478 cm. The hole centerline plane of the single row of holes intersected the surface at an arc location of 6.93 cm from the stagnation region. The second row of holes was spaced 0.48 cm upstream from row one or at a surface arc of 6.45 cm. The nominal wall thickness for the pressure and suction surface arrays was 0.292 cm producing hole length to diameter ratios of 4.5 on the pressure surface and 3.67 on the suction side. The nominal wall thickness for the showerhead array was 0.254 cm producing hole length to diameter ratios of about 5.7. The plenum runs from an arc location of -2.78 cm on the pressure side to a location of 7.24 cm on the suction surface. The inner surface of the plenum is constructed by the intersection of perpendiculars from these points.

The baseline pressure distribution for the low turbulence case is given in figure 2.7. The measured pressure distribution, shown with symbols, is compared to a prediction based on an unpublished stream function formulation for compressible flow. In general, the comparison looks quite favorable. This pressure distribution was taken with the baseline vane. The coordinates for the pressure tap locations for the baseline vane are given in Ames (1994). The surface coordinates are also documented with the baseline pressure distributions given in appendix A.2. The experimentally determined stagnation point is located between the 17th and 18th static pressure tap. The figure shows 18 taps before the stagnation point because the tap on the trailing edge is included on the pressure side rather than the suction side.

Heat Transfer Vane and Acquisition Description

A schematic of the vane used for the heat transfer measurements is shown in figure 2.8. The locations of the thermocouples used for surface temperature measurement are indicated by the symbols. Table 2.4 gives the locations of the thermocouples in terms of X and Y coordinates and in terms of surface arc. The fine gauge chromel - alumel thermocouples were cast into the vane. Not shown on the figure is the 0.025 mm thick Inconel foil used to generate the constant heat flux on the vane. The heating started at an X location of 1.0 cm on the pressure surface and ended at an X location of 1.0 cm on the suction surface. Prior to the beginning of heating, the foils were soldered to a 0.254 mm thick and 6.35 mm wide copper bus bar. A shallow indentation was milled in the airfoil surface to accommodate the bus bars. The Inconel foil was bonded to the outside of a 0.127 mm Kapton backing material. The Kapton was adhered to the airfoil surface using a high temperature acrylic adhesive. The resulting foil surface on the vane was aerodynamically smooth and visually attractive.

A finite element analysis (FEA) was made for the epoxy vane in order to reduce the uncertainty in the surface heat flux and temperature due to conduction through the vane. The surface normal heat flux determined from analysis is added to the flux dissipated in the foil. The calculated surface normal heat flux due to conduction is also used to correct for the difference between the measured temperature in the outer surface of the epoxy and the surface temperature. The mesh used for the calculation is shown in figure 2.9. The mesh over the solid portion of the vane is 21 elements by 8 elements while the mesh for the hollow section is 18 elements by 3 elements. The analysis was set up to run on a commercial spreadsheet.

Heat transfer baselining tests were conducted at the low turbulence condition using the hollow vane without any cooling holes. The procedure included running the test without heating to obtain the recovery temperatures along the vane. Next, the test was conducted with the vane heated. The heated case surface temperatures were input into the finite element analysis (FEA). The FEA analysis provided the extra surface normal heat flux due to conduction through the epoxy vane and the surface temperature which was extrapolated from the vane thermocouples to the outer surface of the foil. The heat transfer coefficient was determined from the net surface heat flux and the surface-to-recovery temperature difference. The net heat flux was determined from the foil heat flux plus the conduction heat flux less the radiation heat flux. The radiative heat flux was estimated by assuming the foil had an emissivity of 0.2 and was radiating to a black body with a temperature equal to the inlet temperature. The maximum estimate for radiative loss amounted to about 1.8 percent of the local heat flux.

A comparison between the experimentally determined Stanton number distribution for the hollow vane (Q3L8B01) and the previously determined distribution from the solid vane (HTB300) from Ames (1994) is shown in figure 2.10. Additionally, the Stanton number distribution predicted from the measured pressure distribution using a finite difference boundary layer calculation (STAN7, Kays, 1987) is also shown in figure 2.10. The comparison on the pressure surface between the hollow vane and both the solid vane and the calculation is very good. The calculated start up at the stagnation point is a little off from the experimental data and is probably due to the difference between the actual velocity and temperature distributions and the ones input into the boundary layer code. On the near suction surface, the hollow vane distribution falls about 4.5 percent below both the solid vane data and boundary layer calculation. The estimated uncertainty for the heat transfer coefficient is +/- 5 percent and excluding interpolated values in the transition region after accounting for the influence of Reynolds number in the laminar and turbulent regions, the root mean square variation between the data sets is +/- 2 percent. On the suction surface, as the boundary layer develops along the adverse pressure gradient, the code calculates boundary layer separation and cannot continue. The calculated point of separation appears to be near the point where the vane has a laminar separation and then transitions. This comparison between the hollow vane, solid vane, and predicted Stanton number distributions along the vane gives confidence in the experimental method.

Heat Transfer with Film Cooling and Adiabatic Effectiveness Measurements

Heat transfer distributions with film cooling and adiabatic effectiveness measurements were taken with the hollow vane shown schematically in figure 2.8. Prior to acquiring heat transfer and effectiveness distributions, a foil with drilled holes arrays for the downstream cooling on the pressure and suction surfaces was applied to the hollow heat transfer vane. The resistance of the foil was determined prior to drilling any holes and subsequent to the drilling of each array. The knowledge of the foil resistance outside the array and within it allowed for the accurate specification of the surface heat flux outside of and within the arrays.

A comparison between the baseline Stanton number distribution with undrilled and drilled foil is shown in figure 2.11. For this test, the drilled holes in the foil were filled to eliminate roughness effects. Essentially, the agreement is excellent in the stagnation region. Downstream from the arrays on the suction and pressure surfaces the heat transfer is slightly reduced. This reduction in Stanton number can be attributed to the higher heat flux around the array which increases the local enthalpy thickness. This comparison demonstrates that the drill holes in the foil do not significantly affect the accuracy of the Stanton number distribution.

The tests to determine heat transfer with film cooling and adiabatic effectiveness distributions were made in a coupled manner. First, the adiabatic wall temperature distribution was determined. Next, the temperature distribution for the heated test case was acquired. Finally, the foil heater was turned off and the film cooling air was heated to enable acquisition of the surface temperature distribution with film cooling. When heat is dissipated in the foil, the epoxy surrounding the plenum increases in temperature resulting in a rise in temperature of the cooling air prior to exiting the film cooling holes. Ideally for the heat transfer case, the total temperature of the film cooling air should equal the total temperature of the cascade inlet air. This condition provides the local heat transfer coefficients as affected by the vorticity and turbulence of the free stream and jet interaction. Since achieving this balanced temperature condition is not experimentally feasible, accounting for the temperature pickup of the film cooling air in the holes and the resulting influence of the adiabatic temperature distribution is important. Similarly, the heated film cooling air transfers thermal energy to the unheated vane prior to exiting from the film cooling holes and this heat loss must be accounted for in determining the adiabatic temperature distribution. Also, since the adiabatic temperature distribution is significantly affected with film cooling, the conduction within the vane must be accounted for. If the vane heat transfer distribution is known, then the impact of conduction on the surface temperature can be determined by adjusting the measured temperature by the local heat flux divided by the local heat transfer coefficient. Therefore, on this epoxy vane with nonneglible conduction, the problem of determining the heat transfer and adiabatic film cooling distributions was coupled.

Each row of downstream film cooling holes was drilled individually in order to accurately measure the flow rates in the holes,. The furthest downstream row of holes on the suction surface was drilled first since the suction surface required the lowest plenum pressure. For example, at a velocity ratio below about 0.6 for a row of suction surface holes, the required plenum pressure is low enough to produce inflow in some of the showerhead and all of the pressure surface holes. The film cooling tests proceeded from one row on the suction side to two and then to one row on the pressure side and then to two. For the pressure side film cooling, the suction surface holes were taped closed to enable the accurate determination of the film cooling flow rate to the array. In order to more accurately account for the temperature rise or loss of the film cooling air and to more accurately estimate the conduction around the holes, the finite element analysis around the holes was refined.

For the showerhead film cooling the foil with the drilled downstream film cooling holes was removed then the downstream pressure and suction surface hole arrays were filled with epoxy and the surface was smoothed. Next, a foil was drilled with the showerhead array and installed on the vane. The procedure followed for acquiring and analyzing data and for ensuring its quality was similar to the procedure followed for the downstream film cooling holes. The one difference for the showerhead array was that the flow rate was set based on the required plenum to inlet total pressure ratio rather than the total flow rate to the array.

Data Acquisition and Reduction

This experiment used a PC based data acquisition system. Pressure measurements were made using a Scanivalve and two -- 6.89 kPa pressure transducers calibrated against an Ametek dead weight tester. Steady state voltage signals were read using an HP 3456A digital multimeter with 100 nanovolt sensitivity and 2.5 microvolt accuracy. Signals were multiplexed using an HP 3497A scanner. The pressure and hot wire probes were traversed using two Unislide lead screw drive tables and an Anahiem Automation stepper motor controller. The hot wire signals were collected using an Analog Devices RTI-860 board with simultaneous sample and hold capability and a 200 kHz throughput (50 kHz per channel in simultaneous mode). The hot wires were powered with two DISA 55M system constant temperature anemometer bridges. The hot wire signal was zeroed and amplified to take advantage of the full 12 bit resolution of the data acquisition card. The probes were calibrated against a low free stream turbulence jet and the calibration was fit to a fourth order polynomial. Jorgensen's decomposition (see Frota, 1982) was used to determine the instantaneous velocity vector. For exit measurements with the X-wire, two 20 kHz active low pass filters were used to eliminate the possibility aliasing.

Pressure and thermocouple voltages were read 10 or more times for each data point using an integrating voltmeter. For mean measurements single wire voltages were read 16,384 times at each point at intervals of two or more time constants. Mean X-wire measurements were determined from 8192 independent points. Velocity time records for determining power spectra for both the single wire and X wire were determined from 40 records of 8192 points. Power spectra were calculated for each of the 40 records and then

averaged. Dissipation was estimated by fitting a -5/3 slope line through the power spectra in the region of the inertial subrange using the following relationship.

$$E_1(k_1) = 18/55\ A\ \varepsilon^{2/3} k^{-5/3}$$

Where the constant A is taken as 1.62 for consistency with Ames and Moffat (1990). The energy scale is defined as $Lu = 1.5\ |u'|^3/\varepsilon$ similar to Hancock and Bradshaw (1983) but using the dissipation estimated from the inertial subrange of the spectrum. By defining the dissipation in this manner, the energy scale has a clear relationship with the power spectra.

Data Uncertainties

The data uncertainties were estimated based on the root mean square method (see Kline and McClintok, 1953). Determination of total pressure resulted in an absolute uncertainty of about one percent at the inlet and about 0.25 percent at the exit. Determination of the velocity from the pressure at the inlet and exit had an uncertainty of about two percent due to the uncertainty in the local static pressure. The mean velocity as determined by single wire anemometry had an uncertainty of about two percent. The single largest source of uncertainty in U was due to room temperature variations which could range by as much as 9.5 degrees C during some days. The response of the hot wire due to this temperature change was compensated for. The change in anemometer voltage due to the variation in the electronics temperature was not compensated for. The uncertainty in the turbulence level determined from the single wire was estimated to be about 3 percent. The X-wire velocity had an uncertainty of about 3 percent due to both random fluctuations, room temperature variation, and errors due to binormal fluctuations (w') combined with the probe angle of attack (see Wubben, 1991). The estimated uncertainty in u' and v' was four percent for the X-wire at relatively low angles of attack (less than 7 degrees), increasing for greater values. The absolute uncertainty in the heat transfer coefficient was estimated to be +/- 5 percent. The primary sources of uncertainty included the uncertainty in the dissipated heat flux, the uncertainty in the conducted heat flux due to the uncertainty in the epoxy's conductivity, and the uncertainty in surface to adiabatic wall temperature difference due to room air temperature variations and calibration error.

Table 2.1 Exit/Passage Traverse Access Coordinates

Pos No.	X(cm)	X(in)	Y(cm)	Y(in)
1	16.307	6.420	32.169	12.665
2	17.323	6.820	35.217	13.865
3	18.339	7.220	38.265	15.065
4	19.355	7.620	41.313	16.265
5	20.498	8.070	44.742	17.615
6	21.514	8.470	47.790	18.815
7	22.530	8.870	50.838	20.015
8	23.546	9.270	53.886	21.215

Table 2.2 C3X Vane Surface Coordinates

Pos No.	X (cm)	X (in)	Y (cm)	Y (in)	Arc (cm)	Arc (in)
1	0.110	0.0432	11.655	4.5885	0.938	0.3693
2	0.389	0.1533	12.189	4.7988	1.541	0.6067
3	0.766	0.3015	12.676	4.9907	2.157	0.8491
4	1.272	0.5009	13.023	5.1273	2.771	1.0908
5	1.874	0.7379	13.138	5.1723	3.383	1.3321
6	2.471	0.9727	12.994	5.1157	3.997	1.5736
7	2.983	1.1746	12.654	4.9818	4.612	1.8159
8	3.399	1.3380	12.198	4.8022	5.229	2.0587
9	3.738	1.4715	11.682	4.5991	5.846	2.3017
10	4.027	1.5855	11.136	4.3844	6.464	2.5448
11	4.289	1.6884	10.577	4.1640	7.082	2.7880
12	4.533	1.7845	10.009	3.9407	7.699	3.0311
13	4.765	1.8759	9.437	3.7153	8.317	3.2744
14	4.987	1.9634	8.861	3.4884	8.935	3.5176
15	5.202	2.0480	8.281	3.2604	9.552	3.7607
16	5.411	2.1303	7.700	3.0316	10.170	4.0039
17	5.616	2.2109	7.118	2.8022	10.787	4.2470
18	5.817	2.2902	6.534	2.5723	11.405	4.4902
19	6.016	2.3685	5.949	2.3420	12.023	4.7335
20	6.213	2.4459	5.363	2.1115	12.641	4.9766
21	6.407	2.5226	4.777	1.8806	13.259	5.2199
22	6.600	2.5983	4.190	1.6495	13.876	5.4631
23	6.789	2.6730	3.601	1.4179	14.494	5.7065
24	6.976	2.7463	3.012	1.1859	15.112	5.9498
25	7.157	2.8179	2.422	0.9536	15.730	6.1929
26	7.333	2.8872	1.830	0.7205	16.348	6.4360
27	7.502	2.9537	1.236	0.4865	16.965	6.6793
28	7.662	3.0167	0.639	0.2516	17.583	6.9225
29	7.812	3.0754	0.041	0.0162	18.199	7.1651
30	7.816	3.0772	-0.005	-0.0021	18.246	7.1835
31	7.808	3.0741	-0.052	-0.0203	18.293	7.2020
32	7.788	3.0661	-0.093	-0.0368	18.340	7.2203
33	7.757	3.0540	-0.129	-0.0507	18.386	7.2387

Table 2.2 C3X Vane Coordinates (Continued)

Pos No.	X (cm)	X (in)	Y (cm)	Y (in)	Arc (cm)	Arc (in)
34	7.718	3.0386	-0.154	-0.0607	18.433	7.2571
35	7.674	3.0211	-0.168	-0.0662	18.480	7.2754
36	7.627	3.0027	-0.170	-0.0669	18.526	7.2939
37	7.582	2.9849	-0.159	-0.0625	18.573	7.3122
38	7.541	2.9688	-0.136	-0.0534	18.620	7.3307
39	7.508	2.9558	-0.103	-0.0404	18.667	7.3491
40	7.485	2.9468	-0.062	-0.0243	-13.288	5.2314
41	7.319	2.8814	0.356	0.1401	-12.838	-5.0545
42	7.148	2.8143	0.774	0.3046	-12.387	-4.8768
43	6.974	2.7455	1.189	0.4683	-11.936	-4.6992
44	6.795	2.6752	1.604	0.6313	-11.485	-4.5217
45	6.612	2.6030	2.015	0.7935	-11.034	-4.3442
46	6.424	2.5290	2.425	0.9549	-10.583	-4.1666
47	6.231	2.4531	2.833	1.1153	-10.132	-3.9892
48	6.033	2.3751	3.238	1.2748	-9.681	-3.8116
49	5.830	2.2951	3.641	1.4333	-9.231	-3.6341
50	5.620	2.2127	4.040	1.5906	-8.779	-3.4565
51	5.405	2.1280	4.436	1.7466	-8.329	-3.2790
52	5.183	2.0407	4.829	1.9012	-7.878	-3.1014
53	4.955	1.9507	5.218	2.0542	-7.427	-2.9239
54	4.719	1.8579	5.602	2.2055	-6.976	-2.7464
55	4.476	1.7622	5.982	2.3550	-6.525	-2.5689
56	4.225	1.6633	6.356	2.5025	-6.074	-2.3913
57	3.965	1.5612	6.725	2.6476	-5.623	-2.2139
58	3.697	1.4557	7.087	2.7903	-5.173	-2.0364
59	3.420	1.3466	7.443	2.9303	-4.722	-1.8590
60	3.134	1.2338	7.791	3.0673	-4.271	-1.6815
61	2.837	1.1171	8.131	3.2011	-3.820	-1.5040
62	2.531	0.9966	8.462	3.3313	-3.369	-1.3265
63	2.215	0.8720	8.783	3.4577	-2.919	-1.1491
64	1.888	0.7435	9.093	3.5801	-2.468	-0.9716
65	1.552	0.6110	9.393	3.6981	-2.017	-0.7942
66	1.205	0.4745	9.681	3.8116	-1.566	-0.6166
67	0.849	0.3344	9.958	3.9204	-1.116	-0.4393
68	0.500	0.1968	10.212	4.0203	-0.684	-0.2692
69	0.385	0.1515	10.304	4.0565	-0.537	-0.2112
70	0.282	0.1111	10.409	4.0982	-0.389	-0.1532
71	0.194	0.0763	10.527	4.1446	-0.242	-0.0952
72	0.121	0.0477	10.656	4.1951	-0.094	-0.0371
73	0.065	0.0256	10.792	4.2488	0.053	0.0209
74	0.026	0.0104	10.934	4.3048	0.201	0.0790
75	0.006	0.0025	11.080	4.3623	0.348	0.1370
76	0.000	0.0000	11.166	4.3961	0.434	0.1709
77	0.005	0.0018	11.228	4.4204	0.496	0.1953
78	0.022	0.0085	11.374	4.4780	0.643	0.2532
79	0.057	0.0224	11.517	4.5343	0.791	0.3112

Table 2.3 C3X Vane Pressure Tap Locations

No.	X2(cm)	X2(in)	Y2(cm)	Y2(in)	Arc(cm)	Arc(in)
1	0.907	0.357	0.161	0.063	-12.573	-4.950
2	1.653	0.651	0.317	0.125	-11.811	-4.650
3	2.402	0.946	0.460	0.181	-11.049	-4.350
4	3.153	1.241	0.587	0.231	-10.287	-4.050
5	3.907	1.538	0.700	0.275	-9.525	-3.750
6	4.663	1.836	0.795	0.313	-8.763	-3.450
7	5.421	2.134	0.870	0.342	-8.001	-3.150
8	6.181	2.433	0.922	0.363	-7.239	-2.850
9	6.942	2.733	0.952	0.375	-6.477	-2.550
10	7.704	3.033	0.953	0.375	-5.715	-2.250
11	8.466	3.333	0.924	0.364	-4.953	-1.950
12	9.225	3.632	0.862	0.339	-4.191	-1.650
13	9.981	3.929	0.763	0.301	-3.429	-1.350
14	10.456	4.117	0.676	0.266	-2.946	-1.160
15	11.544	4.545	0.445	0.175	-1.829	-0.720
16	12.200	4.803	0.225	0.089	-1.143	-0.450
17	12.800	5.040	0.011	0.004	-0.508	-0.200
18	13.305	5.238	0.033	0.013	0.000	0.000
19	13.760	5.417	0.249	0.098	0.508	0.200
20	14.087	5.546	0.635	0.250	1.016	0.400
21	14.316	5.636	1.088	0.429	1.524	0.600
22	14.474	5.699	1.571	0.619	2.032	0.800
23	14.511	5.713	2.200	0.866	2.667	1.050
24	14.230	5.602	2.895	1.140	3.429	1.350
25	13.627	5.365	3.347	1.318	4.191	1.650
26	12.899	5.078	3.550	1.398	4.953	1.950
27	12.393	4.879	3.582	1.410	5.461	2.150
28	11.882	4.678	3.585	1.411	5.969	2.350
29	10.631	4.185	3.371	1.327	7.239	2.850
30	9.885	3.892	3.216	1.266	8.001	3.150
31	9.142	3.599	3.044	1.198	8.763	3.450
32	8.403	3.308	2.859	1.126	9.525	3.750
33	7.666	3.018	2.665	1.049	10.287	4.050
34	6.931	2.729	2.464	0.970	11.049	4.350
35	6.197	2.440	2.259	0.889	11.811	4.650
36	5.465	2.151	2.050	0.807	12.573	4.950
37	4.733	1.863	1.838	0.723	13.335	5.250
38	4.002	1.576	1.622	0.638	14.097	5.550
39	3.273	1.288	1.401	0.552	14.859	5.850
40	2.545	1.002	1.175	0.463	15.621	6.150
41	1.820	0.716	0.940	0.370	16.383	6.450
42	1.099	0.433	0.694	0.273	17.145	6.750
43	0.383	0.151	0.434	0.171	17.907	7.050
44	0.001	0.000	0.162	0.064	18.415	7.250

Table 2.4 C3X Vane Thermocouple Locations

Surface thermocouple positions

	X2(cm)	X2(in)	Y2(cm)	Y2(in)	Arc(cm)	Arc(in)
1	1.748	0.688	0.361	0.142	-11.709	-4.610
2	2.497	0.983	0.502	0.198	-10.947	-4.310
3	3.249	1.279	0.629	0.248	-10.185	-4.010
4	4.004	1.576	0.738	0.291	-9.423	-3.710
5	4.761	1.874	0.831	0.327	-8.661	-3.410
6	5.520	2.173	0.904	0.356	-7.899	-3.110
7	6.281	2.473	0.953	0.375	-7.137	-2.810
8	7.044	2.773	0.978	0.385	-6.375	-2.510
9	7.807	3.073	0.977	0.385	-5.613	-2.210
10	8.569	3.374	0.943	0.371	-4.851	-1.910
11	9.329	3.673	0.875	0.345	-4.089	-1.610
12	10.085	3.970	0.772	0.304	-3.327	-1.310
13	10.461	4.119	0.707	0.278	-2.946	-1.160
14	11.648	4.586	0.422	0.166	-1.727	-0.680
15	12.305	4.844	0.219	0.086	-1.041	-0.410
16	12.806	5.042	0.036	0.014	-0.508	-0.200
17	13.300	5.236	0.058	0.023	0.000	0.000
18	13.743	5.411	0.269	0.106	0.508	0.200
19	14.064	5.537	0.645	0.254	1.016	0.400
20	14.293	5.627	1.098	0.432	1.524	0.600
21	14.449	5.689	1.576	0.621	2.032	0.800
22	14.486	5.703	2.296	0.904	2.769	1.090
23	14.135	5.565	2.946	1.160	3.531	1.390
24	13.523	5.324	3.361	1.323	4.293	1.690
25	12.795	5.037	3.538	1.393	5.055	1.990
26	12.039	4.740	3.549	1.397	5.817	2.290
27	10.710	4.217	3.360	1.323	7.163	2.820
28	10.212	4.021	3.262	1.284	7.671	3.020
29	9.716	3.825	3.155	1.242	8.179	3.220
30	8.975	3.534	2.978	1.172	8.941	3.520
31	8.237	3.243	2.790	1.098	9.703	3.820
32	7.501	2.953	2.594	1.021	10.465	4.120
33	6.767	2.664	2.392	0.942	11.227	4.420
34	6.033	2.375	2.186	0.861	11.989	4.720
35	5.301	2.087	1.976	0.778	12.751	5.020
36	4.569	1.799	1.763	0.694	13.513	5.320
37	3.839	1.511	1.546	0.609	14.275	5.620
38	3.110	1.224	1.323	0.521	15.037	5.920
39	2.383	0.938	1.097	0.432	15.799	6.220
40	1.660	0.653	0.860	0.338	16.561	6.520

Table 2.4 C3X Thermocouple Locations (continued)

Plenum wall thermocouples positions

No.	X2(cm)	X2(in)	Y2(cm)	Y2(in)	Arc(cm)	Arc(in)
41	11.694	4.604	0.580	0.229	-1.727	-0.680
42	12.358	4.865	0.375	0.148	-1.041	-0.410
43	12.840	5.055	0.200	0.079	-0.508	-0.200
44	13.262	5.221	0.218	0.086	0.000	0.000
45	13.635	5.368	0.394	0.155	0.508	0.200
46	13.912	5.477	0.714	0.281	1.016	0.400
47	14.141	5.567	1.163	0.458	1.524	0.600
48	14.289	5.625	1.609	0.634	2.032	0.800
49	14.325	5.640	2.262	0.891	2.769	1.090
50	14.013	5.517	2.839	1.118	3.531	1.390
51	13.457	5.298	3.212	1.265	4.293	1.690
52	12.776	5.030	3.375	1.329	5.055	1.990
53	12.049	4.744	3.384	1.332	5.817	2.290
54	10.740	4.229	3.198	1.259	7.163	2.820
55	10.672	4.201	1.343	0.529		
56	10.808	4.255	2.013	0.792		
57	10.676	4.203	2.695	1.061		

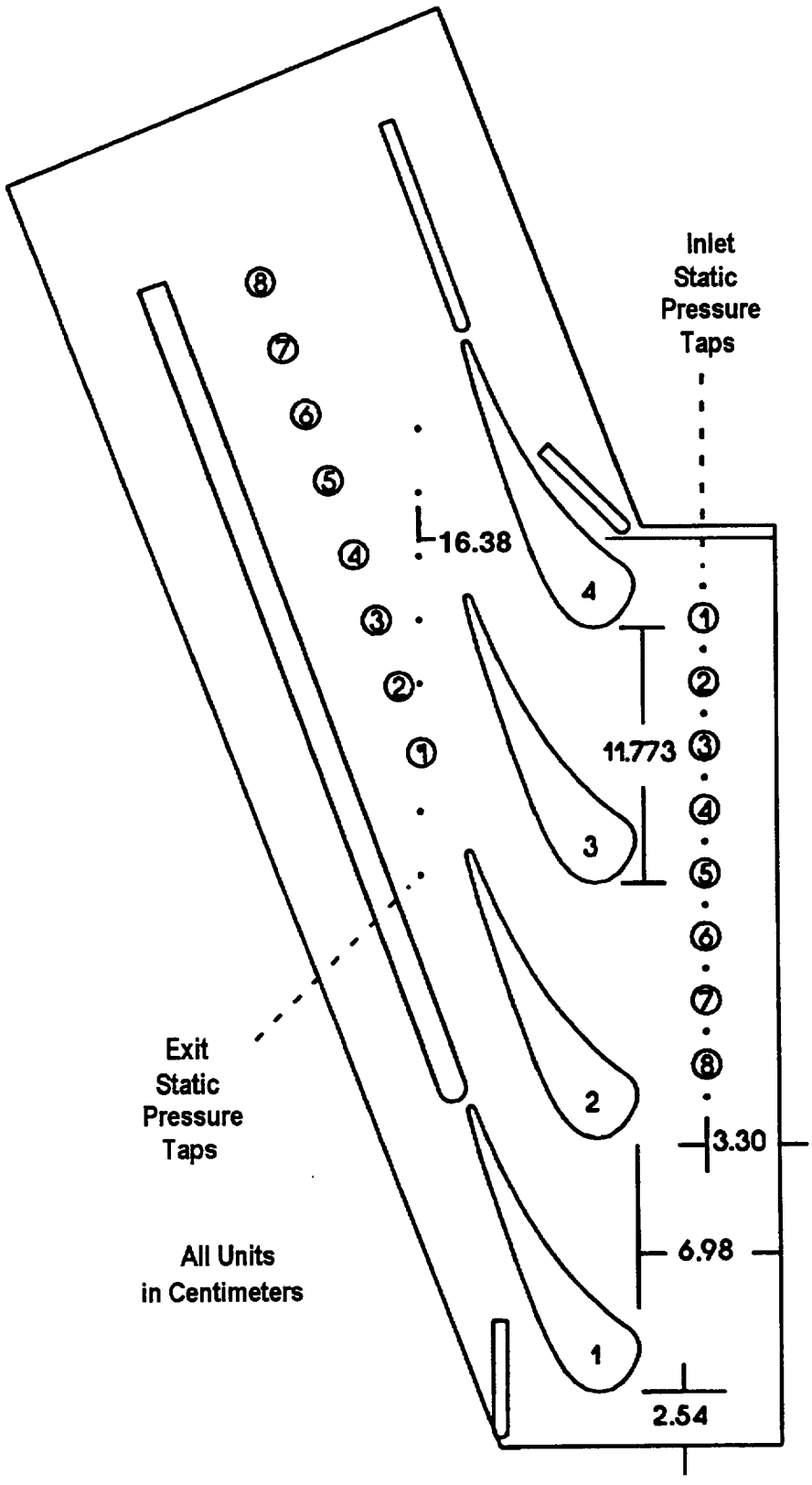

Figure 2.1 Schematic of four vane C3X cascade

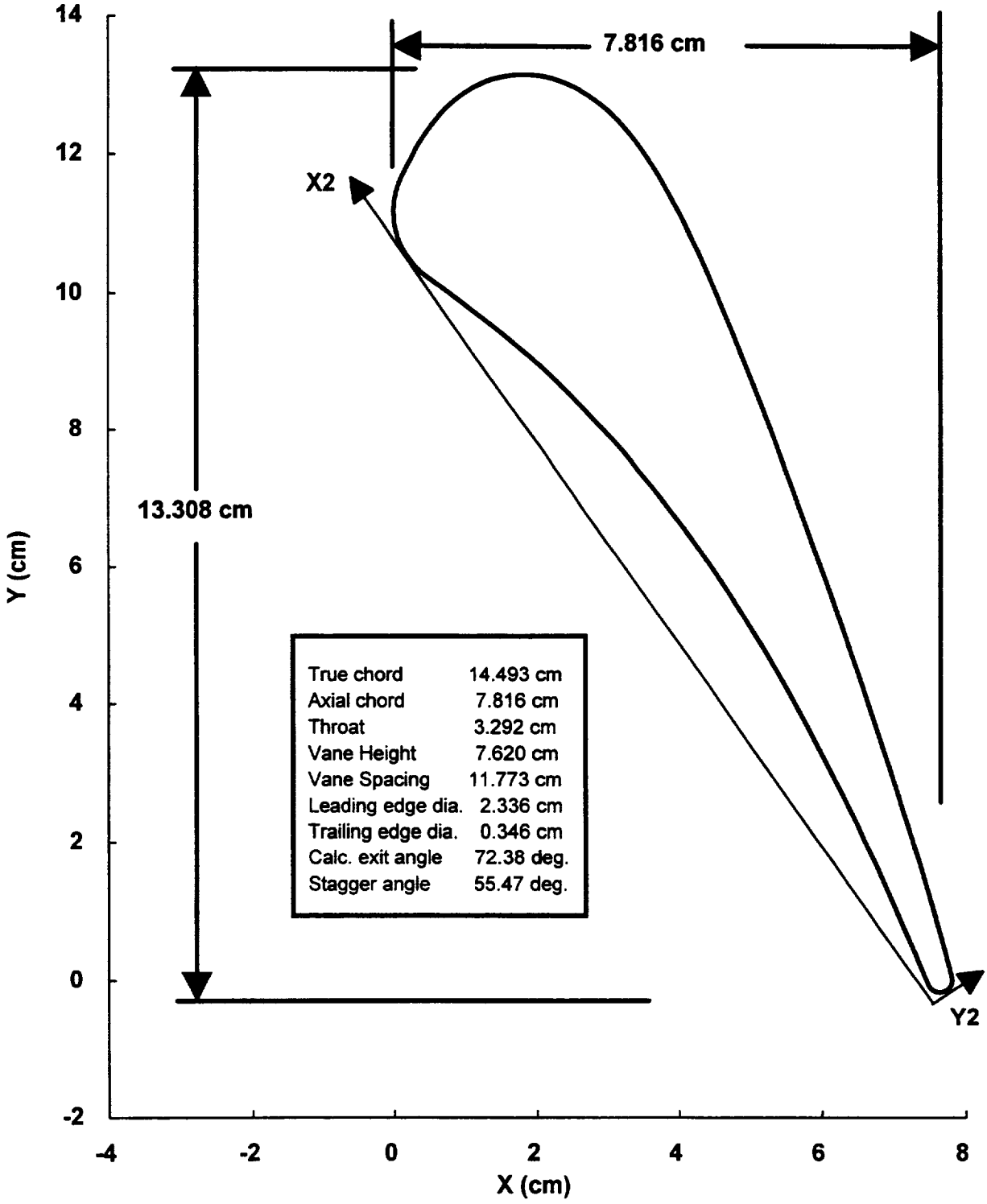

Figure 2.2 C3x vane geometry

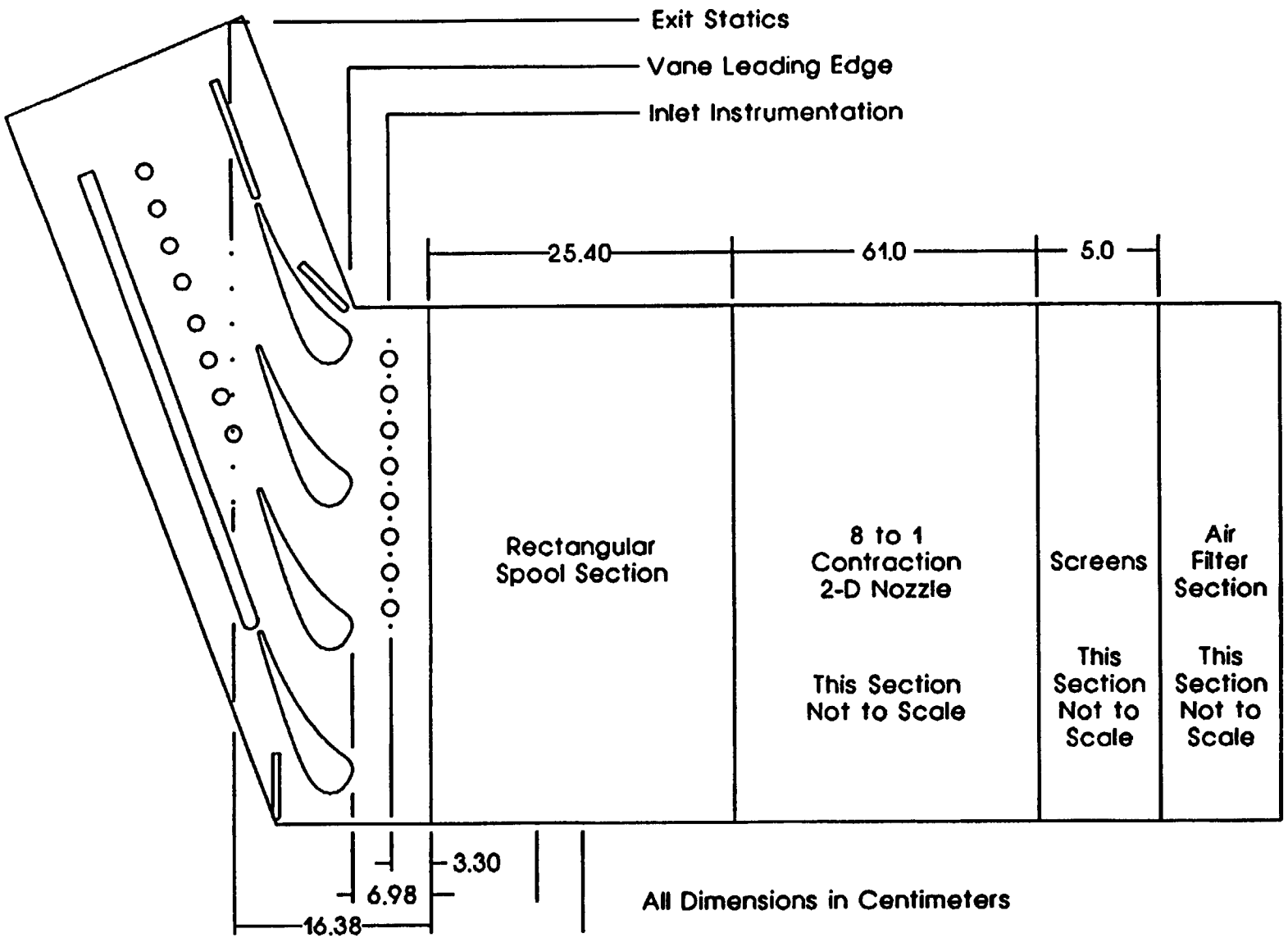

Figure 2.3 Cascade inlet setup for low turbulence condition

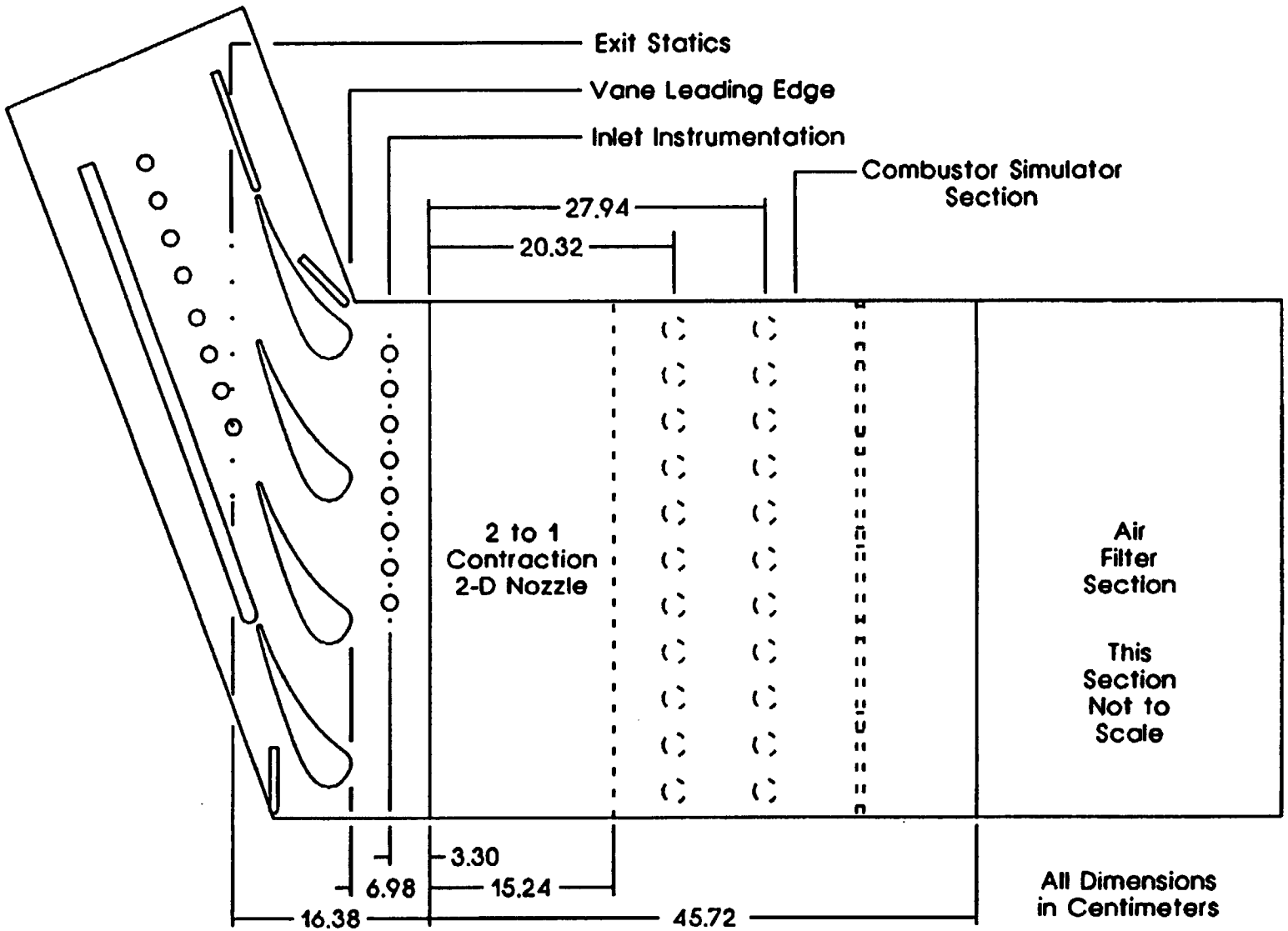

Figure 2.4 Cascade inlet setup for combustor in close position

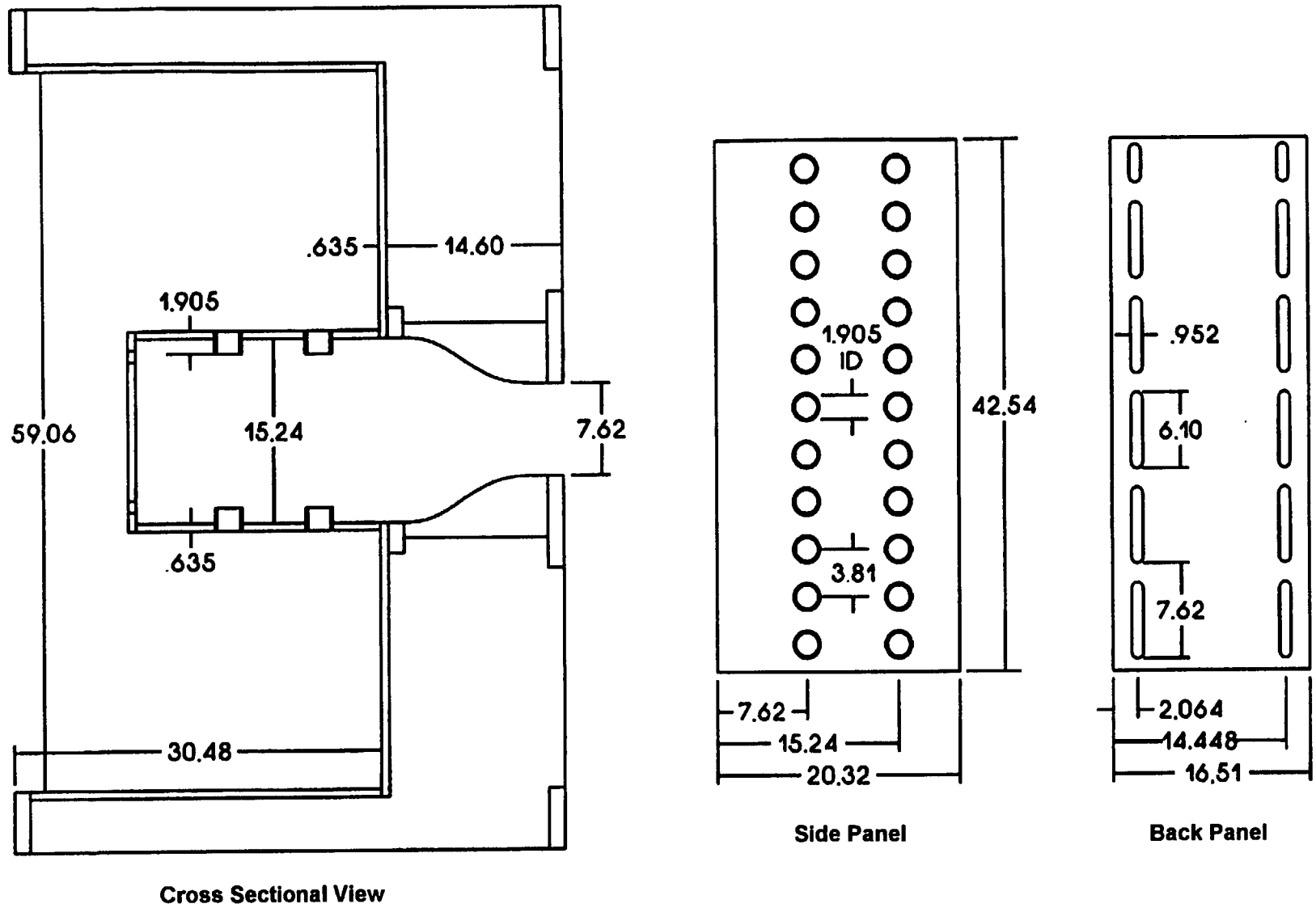

Figure 2.5 Schematic of mock combustor turbulence generator

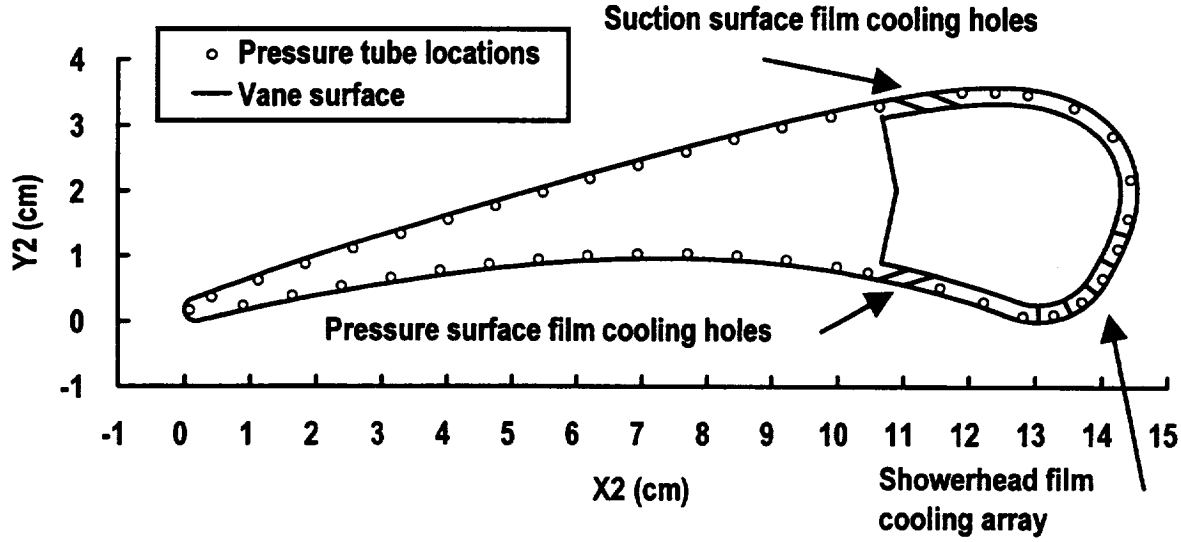

Figure 2.6 C3X vane pressure tap locations

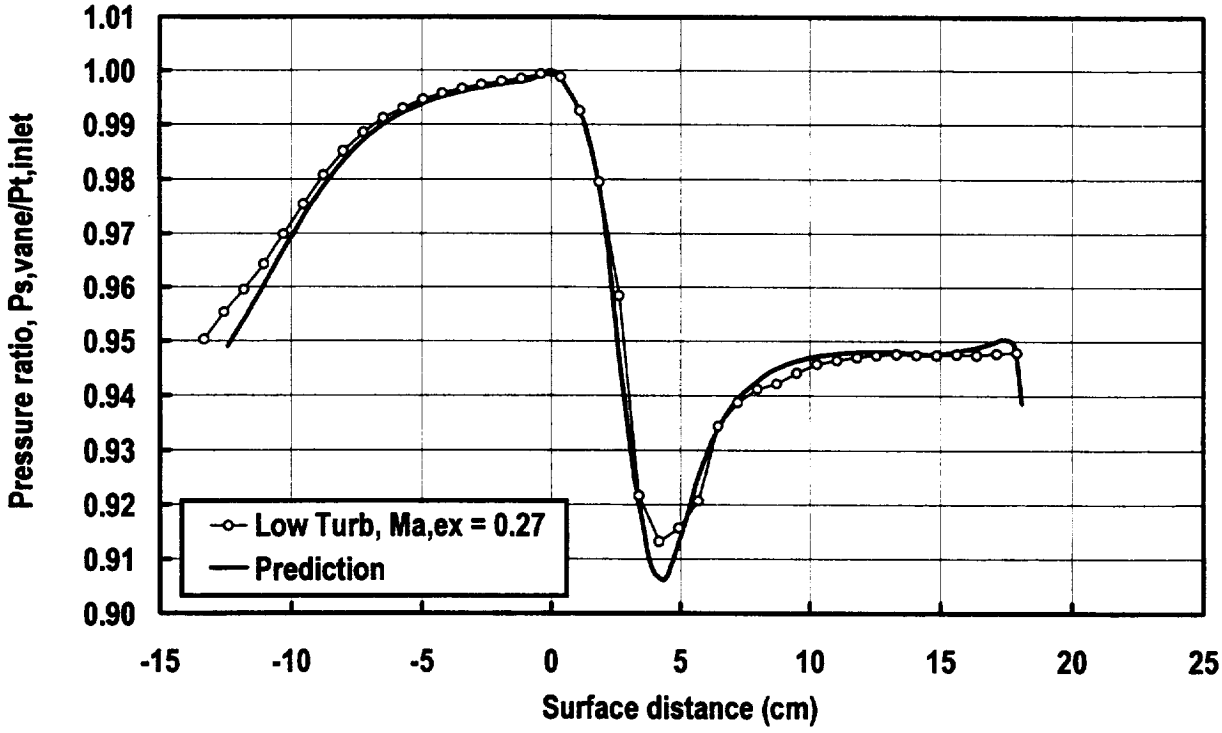

Figure 2.7 Comparison of measured and predicted pressure profiles

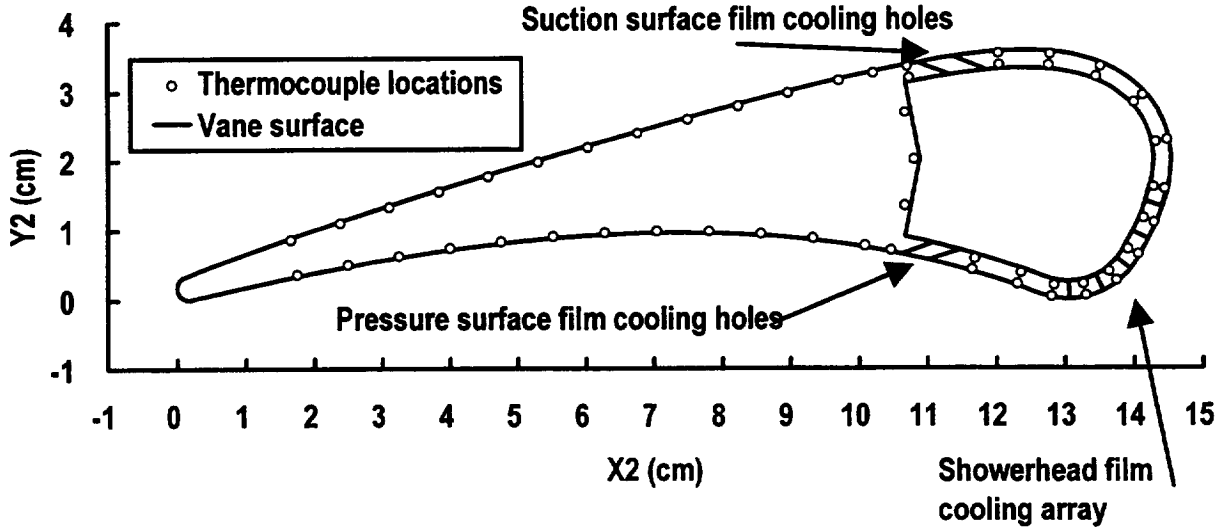

Figure 2.8 C3X vane thermocouple locations

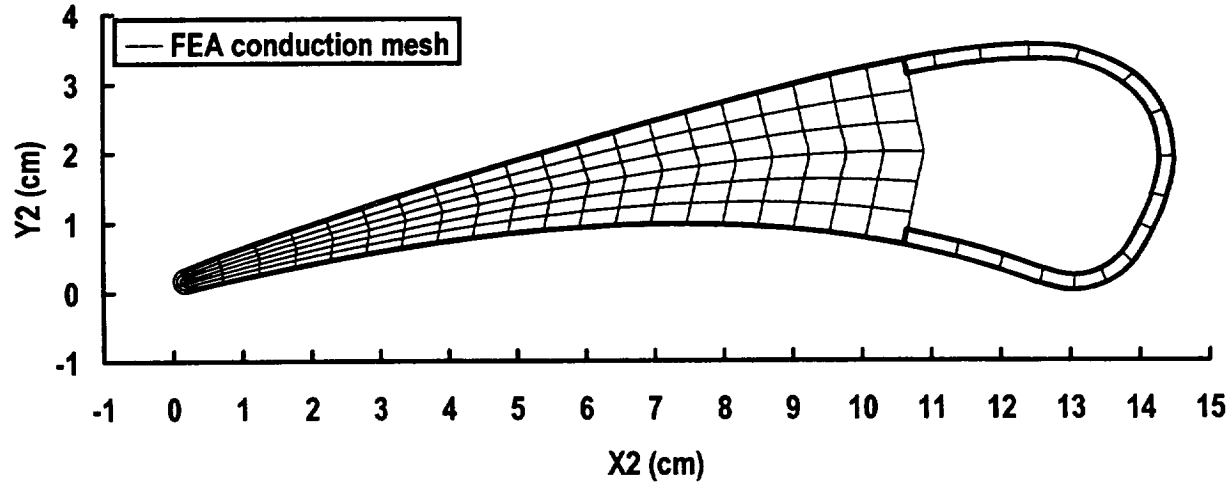

Figure 2.9 C3X finite element mesh for film cooled vane analysis

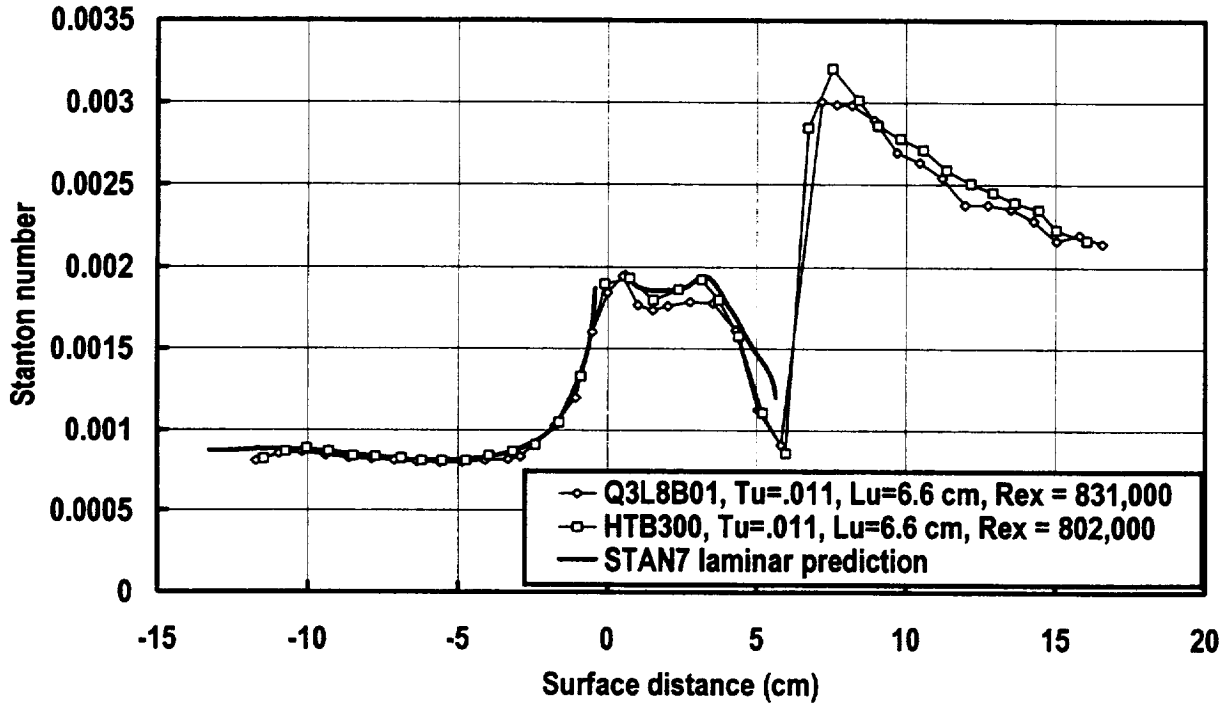

Figure 2.10 Comparison of hollow and solid vane baseline heat transfer with STAN7

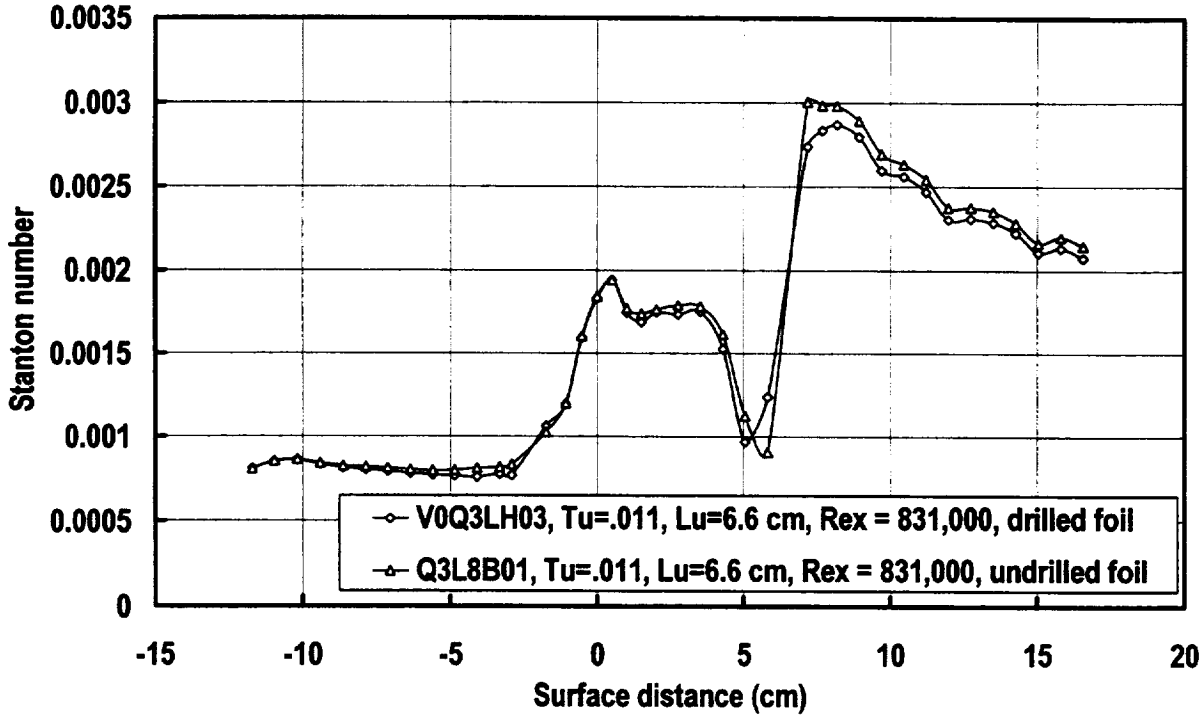

Figure 2.11 Drilled and undrilled Stanton number distributions

Chapter 3

Inlet Conditions

This chapter provides documentation for the inlet conditions into the cascade for this vane turbulence and heat transfer study. Descriptions are given for the inlet velocity, total pressure, and turbulence components distributions. In addition, the inlet turbulence scale, and one dimensional spectra are also discussed.

Inlet Velocity

The cascade inlet velocity distribution was detailed by both total pressure measurements and hot wire measurements. Figure 3.1 shows cross span inlet velocity distributions at one Z position (equivalent to circumferential spacing in an engine) for the two turbulence conditions. Both turbulence inlet conditions had good inlet uniformity. Based on the inlet total pressure measurements, the low turbulence condition total pressure distributions were consistent within about 0.3 percent in the region of the flow outside the boundary layers or the "core" region of the flow. The combustor simulator had RMS variations in pressure of about one percent. The variation in velocity is very close to one half of the total pressure variation.

Figure 3.2 shows the inlet velocity distribution in the circumferential direction based on the inlet static pressure taps. The inlet plane for the inlet static taps is located 3.68 cm upstream of the leading edge plane of the vanes. A vane shape is shown in the figure to provide the circumferential position of vane 3 relative to the static pressure tap positions. The upper and lower bleed flow adjustment blocks, as pictured in figure 2.1 of chapter 2, are used to establish inlet plane periodicity. Typical uniformity between vanes is within one percent.

Typical inlet boundary layer profiles based on total pressure measurements are shown in figure 3.3. Momentum thickness Reynolds numbers, skin friction coefficients, and turbulence levels for the velocity profiles based on inlet total pressure measurements are given in table 3.1. The low turbulence configuration had the largest momentum thickness and the lowest skin friction coefficient. Surprisingly, the inlet momentum thickness for the combustor in the close position [comb(1)] was not a great deal different than for the low turbulence case. Table 3.1 shows a significant difference between momentum thickness Reynolds numbers determined with a total pressure probe and momentum thickness Reynolds numbers determined with a single wire probe. Determining the edge of the boundary layer is uncertain for a boundary layer subjected to a high turbulence level due to the very gradual velocity gradients at the boundary layers edge. The small velocity gradients are also combined with the variations in velocity

imposed during the generation of turbulence and not thoroughly mixed out. An additional complication is probe blockage which produces a mild velocity gradient in the hot wire measurements as the probe is withdrawn from the opposite wall. Total pressure measurements do not exhibit this problem. The effect of blockage on the static reference pressures can be removed by referencing taps in the same location but in a different passage. Because of this potential error in the single wire velocity profiles caused by probe blockage in the inlet channel, the total pressure measurements are viewed as the most accurate. Comparison of the skin friction estimates show these values are consistent within ten percent. One discrepancy does exist for the momentum thicknesses determined for the first low turbulence condition. This variation is likely the result of differences in the transition origin which may be due to subtle differences in the alignment between the 8 to 1 contraction nozzle and the inlet spool.

Inlet Turbulence

Typical cross span distributions of the inlet turbulence level are given in figure 3.4. Based on single wire surveys, the streamwise core region (The core region is the region of flow where the turbulence is largely unaffected by the wall.) turbulence levels for the baseline configuration and the close combustor are 1.0 percent and 12.8 percent. It should be noted that the turbulence characteristics determined for the turbulence generator were taken 3.68 cm upstream from the vane inlet plane. The values quoted for the turbulence generator need to be adjusted for the 3.68 cm of additional decay. A simple method to estimate this change in turbulence level which is reasonably accurate over a short distance is $Tu = 1/\{1/Tu_0 + X/(2\ Lu_\infty)\}$. This equation can be developed by integrating the kinetic energy equation for turbulence, assuming that gradients in Y can be neglected and that dissipation can be estimated from the definition of Lu assuming that Lu is constant. Figure 3.5 shows the inlet turbulence profiles for the combustor simulator in the close position [comb(1)]. The turbulence level is about 13.2 percent for the u' component and about 15.5 percent for the v' component which in this case is normal to the endwall. The ratios of v'/u' for the combustor is 1.18.

One Dimensional Power Spectra

One dimensional spectra for both the streamwise and normal fluctuation velocities are shown for the combustor simulator in the close position in figure 3.6. Both the u' and v' spectra show a full decade of -5/3 slope in the inertial subrange. The presence of a substantial inertial subrange is typical of spectra with high turbulence Reynolds numbers. A Taylor Reynolds, Re_λ, number of over 100 is necessary for a well developed inertial subrange. The Taylor Reynolds number of this flow is about 270.

Isotropic relations yield that $E_2(k_1) = 4/3\ E_1(k_1)$ [Hinze (1975)] in the inertial subrange. In the spectra shown, the values of $E_2(k_1)$ and $E_1(k_1)$ match this relationship within 7 percent. This consistency indicates that although the v' component of turbulence is 18 percent higher than the u' component for this buildup, the small scale eddies show

isotropy within experimental accuracy. This small scale isotropy implies that in the inlet region of a first stage turbine, isotropic relationships ought to be reasonably valid.

Figure 3.7 shows one dimensional spectra for the v' component of turbulence at a range of distances from the wall for the close combustor condition. The spectra are plotted as a function of wavenumber. As the probe gets closer to the wall, the measured spectra show less and less energy in the lower frequency eddies. Yet, in the smaller wave number eddies, the spectra remain reasonably constant. This figure implies that the near wall distribution of the v' component of turbulence is dependent on the distribution of energy in the smaller wave number spectra. Based on relationships for the inertial subrange, the distribution of the higher frequency spectra is determined from the dissipation rate. The energy scale, Lu, which is based on the dissipation rate can therefore be expected to correlate the near wall distribution of v'^2. If we assume that the eddy diffusivity in the free stream fluid near the wall scales on v' and y, then the near wall distribution of eddy diffusivity ought to scale on Lu, Tu, and y. Since this free stream fluid is entrained into the boundary layer and has been shown to augment boundary layer heat transfer and skin friction, Lu is a logical scale to use in correlating the effects of turbulence on heat transfer.

Turbulent Scales

Nominally, the energy scale for the combustor turbulence was 3.36 cm A complete list of scales determined from the inlet turbulence is given in Appendix A.1.

Table 3.1 Inlet Velocity Profile Parameters

Velocity profiles from total pressure

Condition	Files	U_∞ (m/s)	Cf/2	U_{core} (m/s)	$Re_{\delta 2}$
Low	CI2R8P2	29.88	0.00224	29.73	1183
Low	CI6R8P2	29.84	0.00216	29.83	1392
Comb(1)	SI2R8P	28.13	0.00259	29.13	1070
Comb(1)	SI6R8P	29.08	0.00232	29.55	1286

Velocity profiles from single wire

Condition	Files	U_∞ (m/s)	Cf/2	U_{core} (m/s)	$Re_{\delta 2}$	Tu
Low	I2R8C2	29.78	0.00294	29.69	514	0.012
Low	I6R8C2	29.44	0.00239	29.51	1139	0.009
Comb(1)	I2R8CB	29.01	0.00241	29.46	1897	0.142
Comb(1)	I6R8CB	29.71	0.00212	29.54	2588	0.132

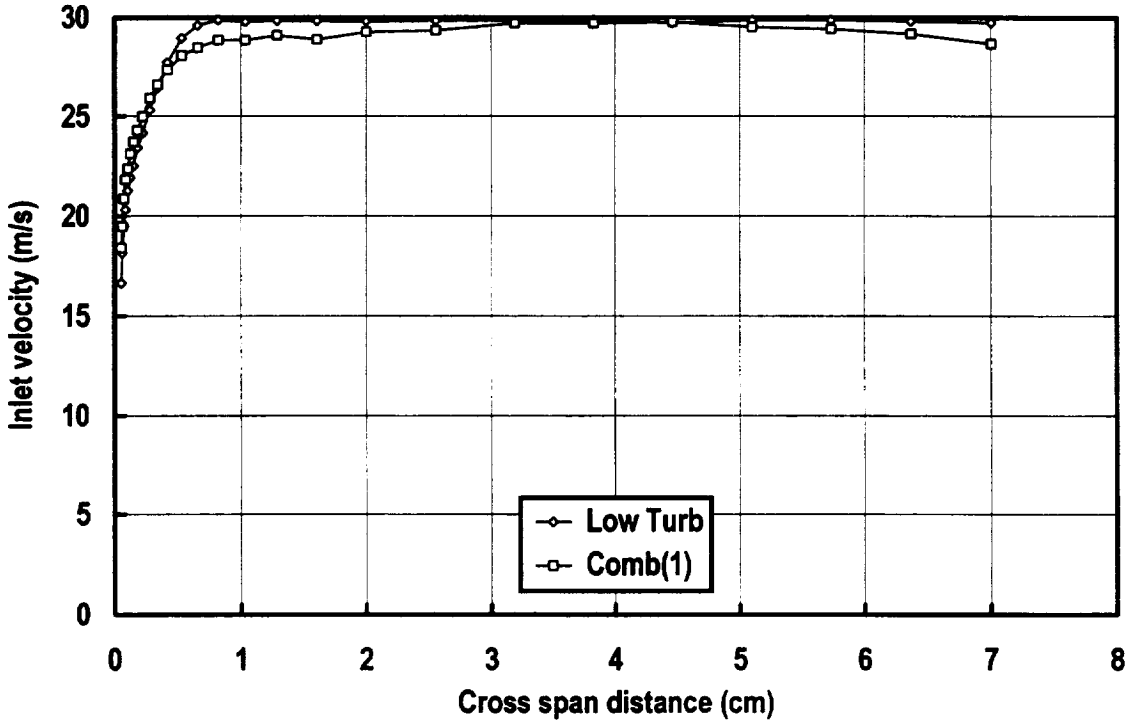

Figure 3.1 Comparison of total pressure inlet velocities

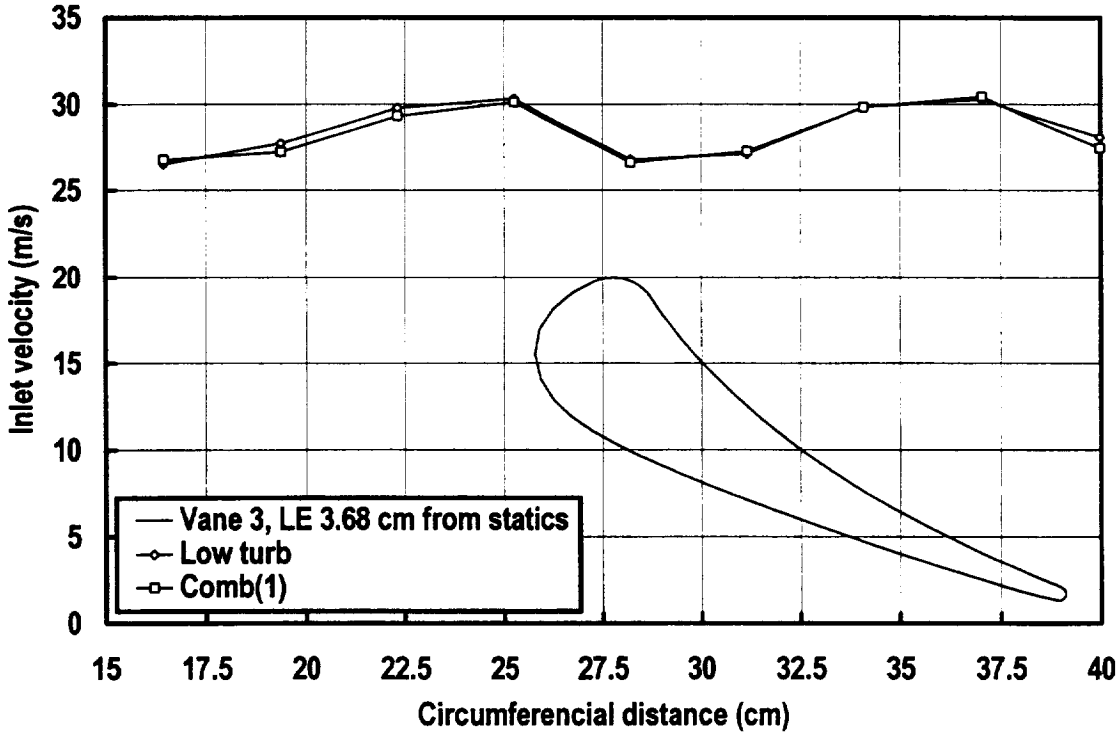

Figure 3.2 Circumferential distribution of inlet velocity based on static pressure

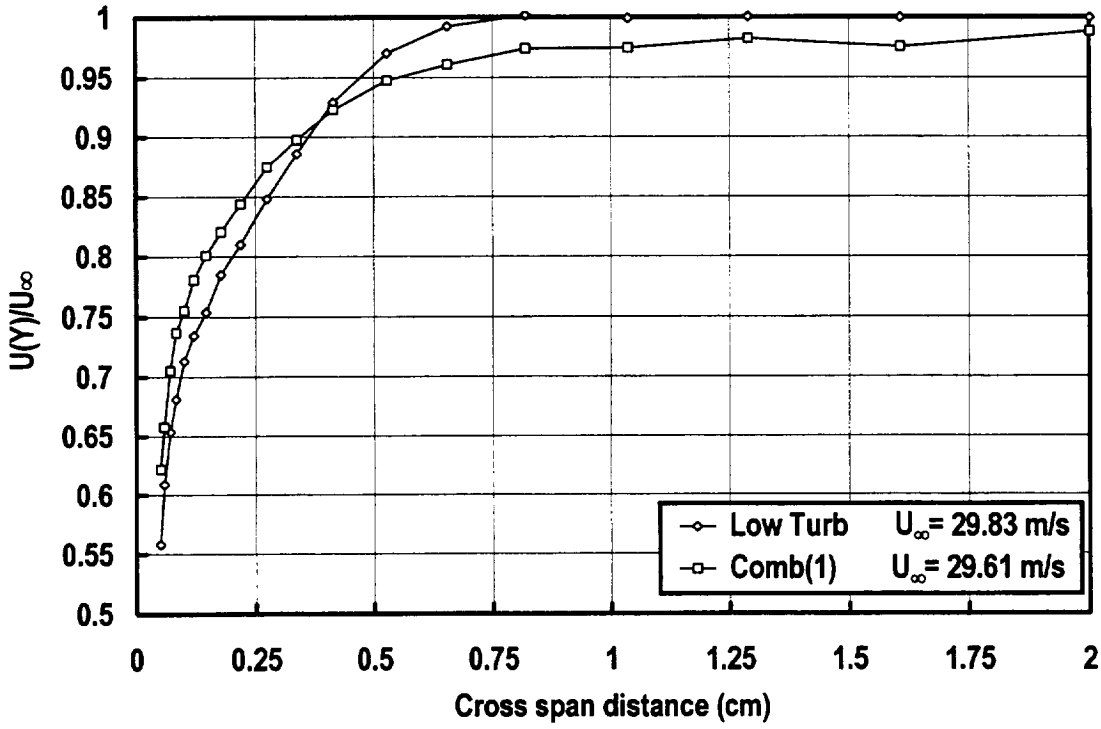

Figure 3.3 Comparison of total pressure based inlet boundary layer profiles

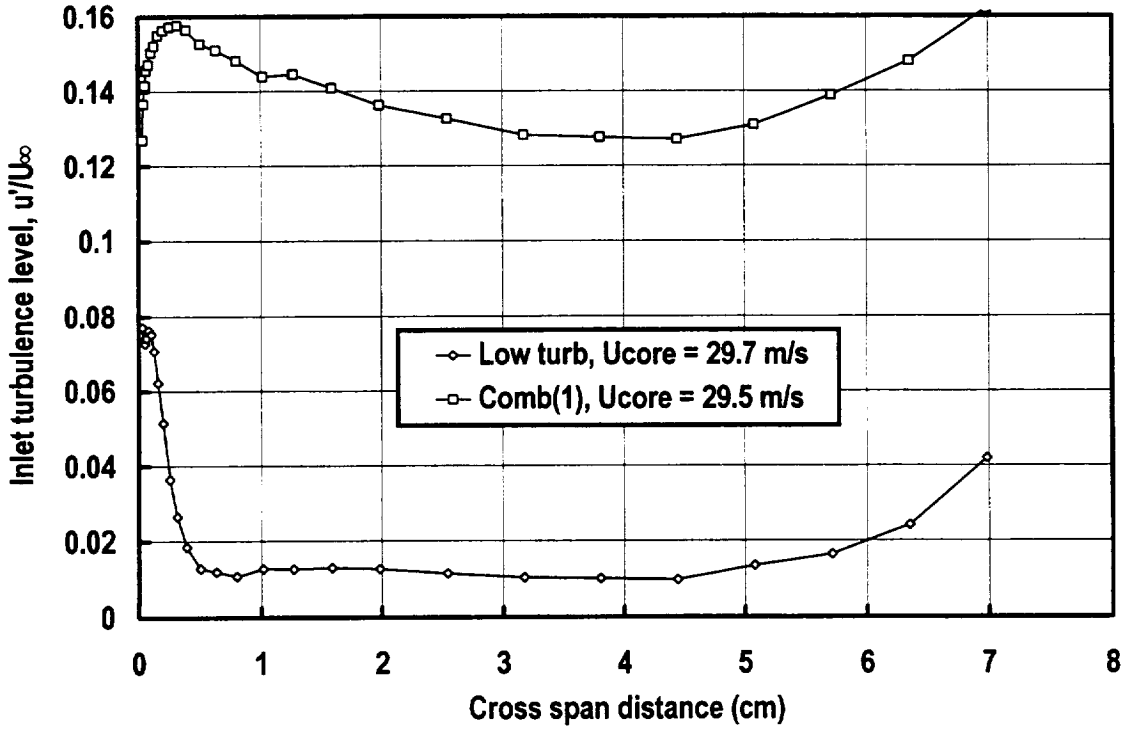

Figure 3.4 Comparison of inlet turbulence level for high and low turbulence, U_∞= 30 m/s

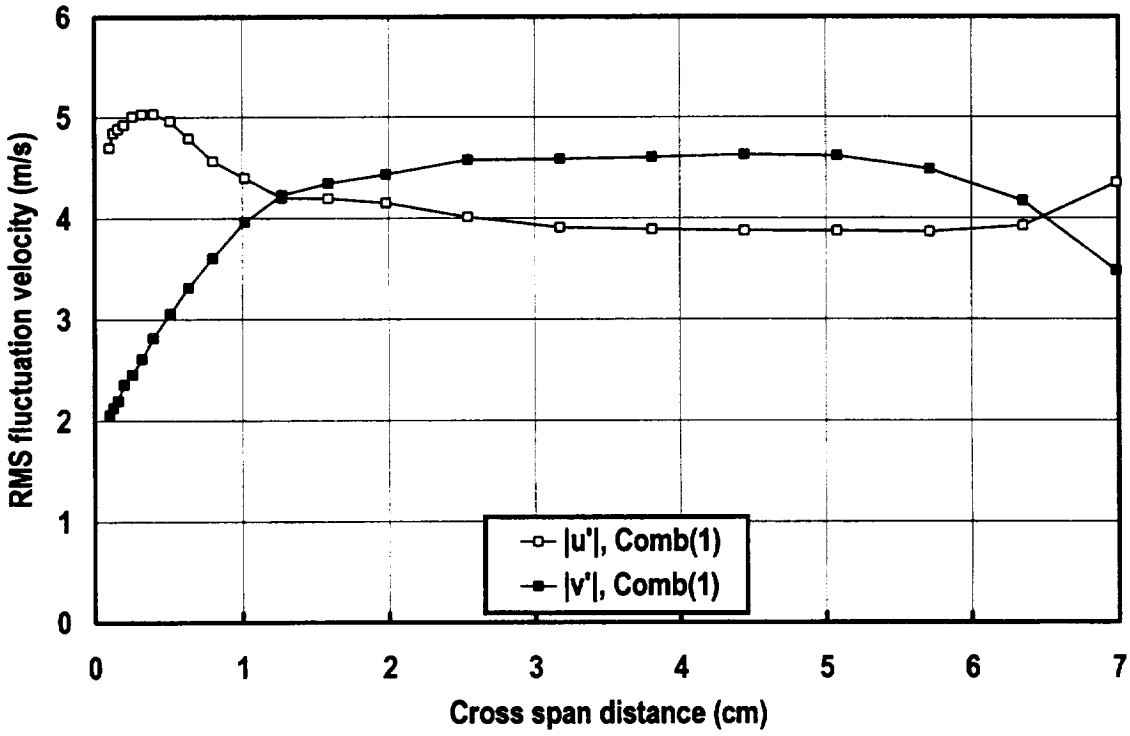

Figure 3.5 Cross span survey of turbulence components, Comb(1), $U_\infty = 30$ m/s

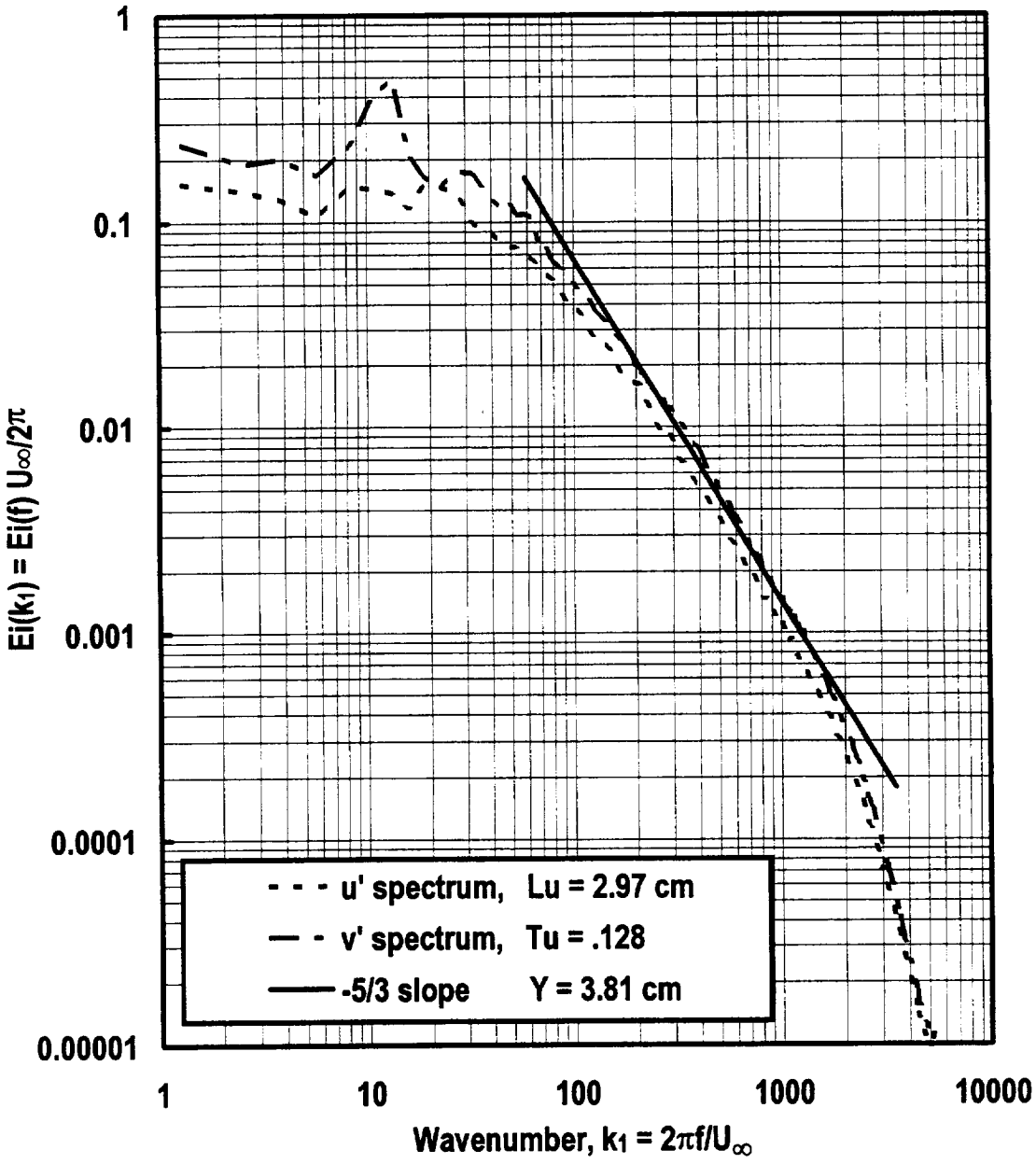

Figure 3.6 One dimensioinal spectra of u' and v' for Comb(1) showing inertial subrange isotropy, U_∞ = 30 m/s

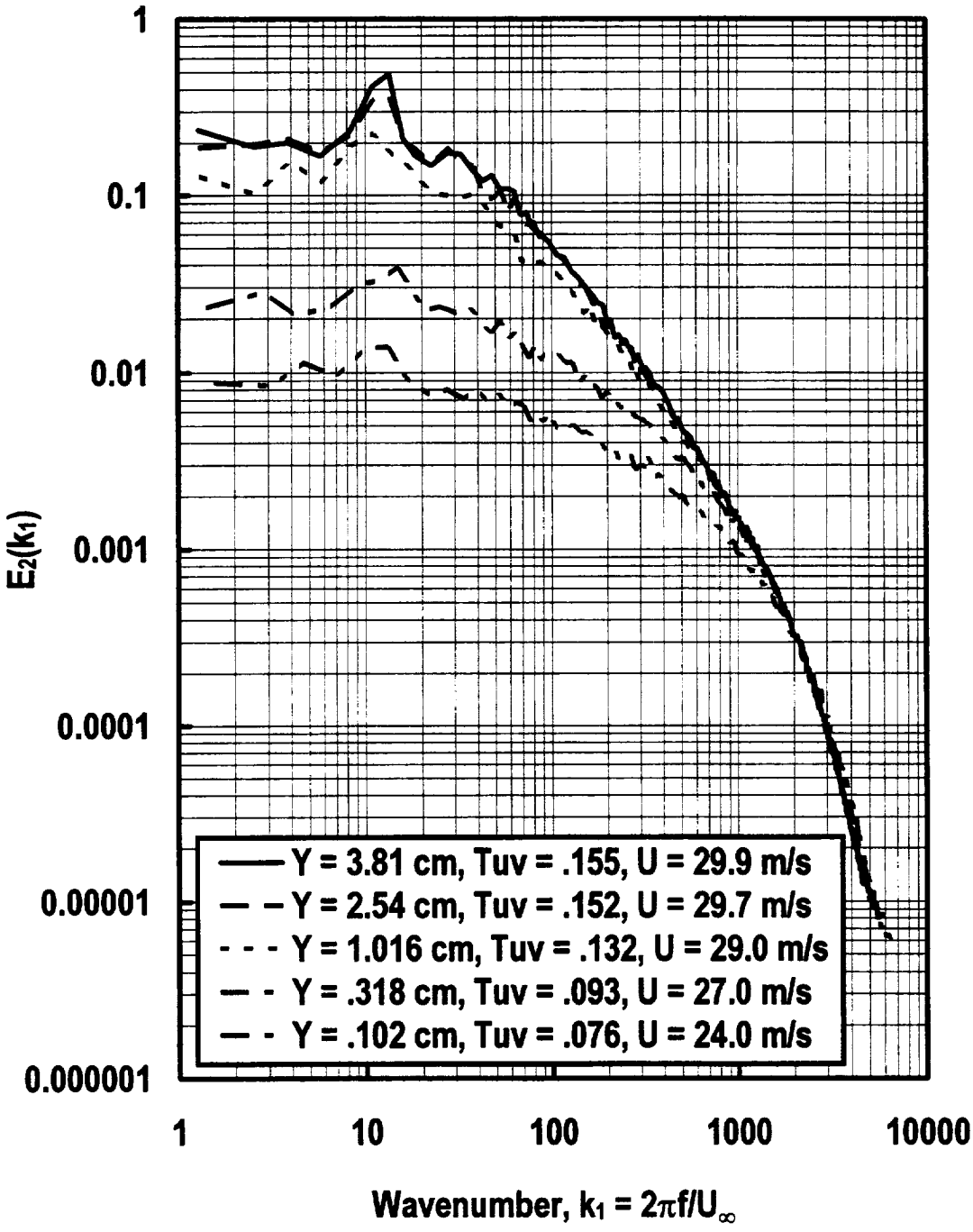

Figure 3.7 Comparison of v' spectra for various Y showing low wavenumber attenuation, Comb(1)

Chapter 4

Heat Transfer with Film Cooling

This chapter examines the influence of film cooling on vane heat transfer with and without high free stream turbulence. Initially, a comparison of the base vane heat transfer is examined with respect to the influence of high free stream turbulence. In order to demonstrate the quality of the data, the base vane data are compared to previous data from Ames (1994). The influence of film cooling on heat transfer is then examined for suction surface film cooling, pressure surface film cooling, and showerhead film cooling. The data are examined across a relevant range of film cooling velocity ratios and the data are presented in terms of both Stanton number distributions and Stanton number augmentation ratios, St/St0. These data are intended to provide the heat transfer designer with relevant examples of heat transfer augmentation on a vane subjected to a realistic turbulence inlet condition.

Base Vane Results

Heat transfer distributions for the hollow vane used in this study were taken for both the low turbulence condition and for the mock combustor in the close position, comb(1), at Reynolds numbers of about 800,000 and 500,000 and were compared to the previous data of Ames (1994). All heat transfer and film cooling data were taken near the midspan of the vane. Figure 4.1 shows a comparison between the new hollow vane data and the solid vane data from Ames (1994) at a Reynolds number of around 800,000 at the two turbulence conditions. Generally, the data compare quite favorably. For the low turbulence case, the Reynolds number varies by about 4 percent. The difference in Stanton number due to Reynolds number variations in the laminar region is expected to scale on the -0.5 power while in the turbulent region the expected scaling of Stanton number is Reynolds number raised to the -0.2 power. When this scaling is applied to the low turbulence case, the root mean square (RMS) deviation between the two data sets, excluding two points in the transitional region, is two percent. The RMS variation between the high turbulence data sets is also two percent.

A comparison between the current data and the data of Ames (1994) at an exit Reynolds number based on chord length of around 500,000 is given in figure 4.2. Again, the agreement between the current data and the data of Ames is quite good. For the low turbulence condition, the RMS variation is about 3 percent while the RMS variation for the high turbulence case is 2 percent. The four conditions which were rerun to enable comparisons between the current data, which used a heat transfer vane with a hollow leading edge, and the previous data taken at these conditions given in Ames (1994) show good agreement. In addition, a comparison between the current data and a finite difference boundary layer calculation (STAN7) shown in figure 2.10 also exhibit close agreement. The consistency of these comparisons helps establish confidence in the

experimental method. The RMS deviations between the data sets taken with different vanes are consistent within the estimated +/- 5 percent absolute uncertainty in the heat transfer coefficient. The relative uncertainty in the experimental data for run to run comparison purposes is estimated to be 2.4 percent.

Heat transfer data were also taken at low and high turbulence conditions at a Reynolds number of about 950,000. Prior to the start of this research program, the tunnel inlet filtration system was modified and the improvement resulted in a lower pressure drop across the filter section. This change has enabled the facility to reach an exit Reynolds number approaching 1,000,000 with the mock combustor in line. Figure 4.3 shows a comparison between the low turbulence and mock combustor turbulence case at an exit Reynolds number of 950,000. The distributions are qualitatively similar to the lower Reynolds number cases. The comparisons between the low and combustor turbulence cases at the three exit Reynolds numbers allow a comparison of the augmentation ratios as a function of Reynolds number. Figure 4.4 shows the Stanton number augmentation ratios of the high level combustor turbulence cases divided by the low turbulence cases for an equivalent Reynolds number. The data show the dependence of augmentation ratio on Reynolds number. The average augmentation of the pressure surface data, using a simple average of the Stanton number ratio of all the pressure surface points yields a ratios of 1.440, 1.555, and 1.618 and exit Reynolds numbers of 515,000; 805,000; and 955,000. These ratios compare with ratios of 1.464 and 1.556 at Reynolds numbers of 510,000 and 790,000 for the previous data of Ames (1994). Using averaged results at 500,000 and 800,000, the dependence of Stanton number augmentation (St/St0-1) on Reynolds number was found to scale on the 0.46 power between 500,000 and 800,000 and on the 0.50 power between 500,000 and 950,000. This compares to a dependence on Reynolds number raised to the 0.41 power for the comb(1) turbulence as determined in Ames (1994) and an average dependence scaling on the 1/3 power determined for the three cases of high turbulence investigated in the study. These present data indicate that the dependence of Stanton number augmentation on Reynolds number may be higher than the previously estimated values. However, the variations found in the Reynolds number dependence between the studies are within the estimated uncertainty of the data.

Film Cooling Effects on Suction Surface Heat Transfer

Heat transfer distributions were taken for the hollow vane for suction surface film cooling. These data sets were taken with adiabatic film cooling effectiveness measurements (reported in chapter 5) using the vane thermocouple instrumentation due to the coupled nature of the problem. The adiabatic film cooling distributions allowed the modification of the unheated wall boundary condition for heat transfer due to the heat up of air in the cooling plenum and film cooling holes. The heat transfer distribution together with the calculated surface heat flux allowed correction of the adiabatic film cooling effectiveness due to conduction effects in the epoxy vane. A more detailed description of this process is given in chapter 2.

The selection of velocity ratios to study for suction surface film cooling was based on conditions which typically exist in the design of advanced first stage vanes. For advanced engines with hot inlet temperatures, coolant to gas temperature ratios, based on hot streak temperatures, can often exceed 2. For a feed pressure which equals the inlet total pressure and with a hole Cd equal to 0.67 the coolant to gas velocity ratio would be around 0.47 assuming the local static pressure was close to the exit static pressure. For higher feed pressures and lower gas to coolant temperature ratios, the velocity ratio could be somewhat higher than this, while more internal pressure drop and higher relative gas inlet temperatures would yield a lower velocity ratio. According to L'Ecuyer and Soechting (1985) velocity ratio was found to be useful in characterizing film cooling for a range of density ratios for a single row of film cooling with 3 diameter spacing in the spanwise direction and with 35° holes. In addition, similar velocity ratios should produce similar velocity fields and mixing. Because this study was limited to density ratios of around 1.0, setting comparable velocity ratios was believed to be the best way to produce relevant levels of heat transfer augmentation.

One Row of Suction Surface Holes. Vane Stanton number distributions for 1 row of suction surface film cooling are shown in figure 4.5. These data were taken with two staggered rows of film cooling drilled in the foil on the suction and the pressure surface but only one row of 30° holes with a spanwise spacing of 3 diameters was drilled in the vane on the suction surface for these tests. The holes in the foil without corresponding holes in the vane were filled with epoxy to produce a smooth finish on the vane surface. The finite element analysis was refined in the areas of the holes to account for the extra heat flux around the drilled regions in the foil and also to account for the cooling inside of the holes in a two dimensional sense and on the plenum surface. Previous to this run, the conductances around the hollow portion of the vane were tuned to account for the uncertainty in the outside to inside thermocouple spacing. Due to the three dimensional nature of the conduction around the holes, the measuring points closest to the holes have the highest level of uncertainty. The calculated Stanton number just upstream of row of film cooling holes gave inconsistent results and is not shown in the figure.

The Stanton number distribution for the close combustor condition, comb(1), in figure 4.5 shows an increase downstream from the row of holes which diminishes in the downstream direction. This behavior is consistent for both levels of turbulence. Based on single wire measurements taken about 12 diameters downstream from the row of holes, the flow accelerates around the holes due to the blockage of the coolant jet while downstream from the holes, at these velocity ratios, the near wall thermal boundary condition is modified by the addition of the jet fluid. The effect on heat transfer by the modification of the thermal boundary condition is somewhat reduced due to the low velocity of the fluid. As the flow develops downstream from the film cooling, both the thermal and momentum deficit of the film cooling fluid gradually mix out in the spanwise direction. As this mixing progresses, the influence of the film cooling on heat transfer is seen to diminish.

The heat transfer augmentation downstream from a single row of holes is characterized in terms of Stanton number ratio for the low turbulence condition versus X/D in figure 4.6. The distance downstream from the hole, X, was referenced from the trailing edge of the hole. The augmentation ratio shows a significant rise immediately downstream from the row of film cooling but quickly decreases in the streamwise direction. The range of velocity ratios is relatively narrow for this single row of holes and the data can be reasonably characterized by a curve which averages the four data sets. Figure 4.7 shows a similar comparison for the high turbulence condition, comb(1). The trends are similar to the low turbulence data. Again the four curves appear to be quite consistent and can be reasonably characterized by a single average. The average Stanton number ratio for the eight data sets is shown in figure 4.8. The curve varies from the averaged distributions given in figures 4.6 and 4.7 by less than two percent. This line provides a good representation of the Stanton number ratio results for a single row of holes with a pitch to diameter ratio of 3. However, the two dimensional technique used to acquire these data cannot be expected to provide accurate results in the near hole region. The region around and just downstream of a single row of holes should be considered as a region for further study.

Two Staggered Rows of Suction Surface Holes. Vane Stanton number distributions for 2 rows of suction surface film cooling are shown in figure 4.9. These data were taken with two staggered rows of film cooling holes drilled in the foil on the suction and the pressure surface but only the suction surface was drilled with 30° holes through the vane at a spanwise spacing of 3 diameters. The pressure surface holes in the foil were filled with epoxy and sanded to produce a smooth finish on the vane surface. The finite element analysis was refined in the areas of the holes to account for the extra heat flux around the drilled regions in the foil and also to account for the cooling inside of the two rows of holes, in a two dimensional sense, and on the plenum surface. Due to the three dimensional nature of the conduction around the holes, the measuring points closest to the holes have the highest level of uncertainty. The plenum surface thermocouple just upstream of the first row of film cooling holes was lost when the suction surface holes were drilled and data at this position are not shown in the figure.

The Stanton number distribution for the close combustor condition, comb(1), in figure 4.9 shows a peak immediately downstream from the row of holes which diminishes in the streamwise direction. This behavior is consistent for both levels of turbulence. Based on single wire measurements taken about 12 diameters downstream from the last row of holes, the near wall thermal boundary condition is modified by the addition of the jet fluid as evidenced by the low momentum fluid near the wall. The effect on heat transfer by the modification of the thermal boundary condition is somewhat reduced due to the low velocity of the fluid. As this mixing progresses, the influence of the film cooling on heat transfer is seen to diminish.

The heat transfer augmentation downstream from the two rows of holes is characterized in terms of Stanton number ratio for the low turbulence condition in figure 4.10. The augmentation ratio shows a significant rise immediately downstream from the last row of film cooling but quickly decreases in the streamwise direction. The range of velocity ratios is relatively narrow for this double row of holes and the data can be reasonably characterized by a curve which averages the four data sets. Figure 4.11 shows a similar comparison for the high turbulence condition, comb(1). The trends are similar to the low turbulence data. Again the four curves appear to be quite consistent and can be reasonably characterized by a single average. The averaged Stanton number ratio distribution for the eight data sets is shown in figure 4.12. The curve varies from the average distributions given in figures 4.10 and 4.11 by less than two percent. This line provides a good representation of the Stanton number ratio results for two staggered rows of holes with a pitch to diameter of 3. While the two dimensional technique used to acquire these data cannot be expected to provide accurate results in the very near hole region, the two dimensionality of two staggered rows of holes is expected to be much better than that of a singe row of holes. Based on single wire measurements, the spanwise uniformity 12 diameters downstream of the two staggered rows is quite good for the high turbulence case. Also, the thermocouples embedded in the epoxy see a temperature which is averaged locally due to conduction effects. For two rows of holes at the high turbulence level, by an X/D of 5, the curve in figure 4.12 is believed to be representative of the span averaged Stanton number ratio within the uncertainty band of the data.

Film Cooling Effects on Pressure Surface Heat Transfer

The selection of velocity ratios to study for pressure surface film cooling was based on conditions which typically exist in advanced first stage vanes. On the pressure surface, pressure coefficients typically ranges from very low values near the stagnation region to values which approach unity near the trailing edge. Feed pressures for first stage vanes are limited by the pressure drop across the combustor but feed pressures for the first stage rotor and subsequent vanes can be considerably higher. In order to reproduce the physics of mixing expected across a full range of relevant velocity ratios for pressure surface film cooling, velocity ratios of 0.5, 1.0, and 1.5 were chosen. A velocity ratio of 0.5 produces a velocity deficit which must be mixed out by the free stream fluid. A velocity ratio of one provides fluid at a velocity near the free stream value. And a velocity ratio of 1.5 provides a jet of fluid. These three conditions (wake, equal velocity, and jet) should provide the full range of mixing regimes with respect to the free stream. Since this study was limited to density ratios of around 1.0, setting comparable velocity ratios was believed to be best way to produce relevant levels of heat transfer augmentation.

One Row of Pressure Surface Holes. Vane Stanton number distributions for a single row of 30° pressure surface holes for the low turbulence condition are shown in figure 4.13. The holes on the suction surface were taped shut for taking the pressure

surface film cooling and heat transfer data to insure an accurate measurement of the coolant flow. The data in this region are not shown for that reason. The level of pressure surface augmentation is very high. Fortunately, the pressure surface of a first stage vane row never sees a low level of turbulence. The heat transfer behavior is unlike the behavior on the suction surface where the effects were largely confined to the near hole region. Apparently, the film cooling jets on the pressure surface set up some type of structure for this low turbulence boundary layer which persists to the trailing edge of the vane.

Stanton number augmentation ratios are shown in figure 4.14 for the low turbulence case taken over the three velocity ratios and at a lower Reynolds numbers for one velocity ratio. For the jet to free stream velocity ratio of 1.5, the augmentation reaches over 70 percent. The level of augmentation for the 1.0 and 0.5 velocity ratios is much lower. The level of augmentation increases with velocity ratio but not in an orderly fashion. Based on single wire measurements taken about 9 diameters downstream from the hole exit plane, the velocity distribution is very much a function of the spanwise position for the low turbulence case indicating that the heat transfer distribution is likely to have some spanwise dependence as well. The low inlet turbulence condition set up for these measurements has little relevance to actual conditions which exist in turbines.

Vane Stanton number distributions for a single row pressure surface holes for the high turbulence condition are shown in figure 4.15. The absolute level of heat transfer is greater than the low turbulence case but the level of augmentation is lower. The heat transfer augmentation is similar to that on the suction surface in that the effects are largely confined to the near hole region. The Stanton number augmentation ratios are shown in figure 4.16 for the high turbulence case for the three velocity ratios and also for the lower Reynolds number. These ratios are determined from Stanton numbers with high turbulence and pressure side cooling ratioed over values from the high turbulence case for the base vane. A comparison between Stanton number distributions for the high and low turbulence cases for the two Reynolds numbers shown in figure 4.16 are given in figures 4.1 and 4.2. While the augmentation ratios are much lower than the low turbulence case they are much higher than the suction surface data. In terms of the absolute augmentation in the heat transfer coefficient, the peak increase on the pressure side for the 0.5 velocity ratio is similar to the increase on the suction side for the same velocity ratio. Also, the peak in augmentation on the pressure side scales consistently with velocity ratio. In the downstream region, both the 1.5 and 0.5 velocity ratios have higher levels of augmentation. This difference is likely due to mixing resulting from the free stream to coolant jet velocity difference. The high and low Reynolds numbers at a velocity ratio of 1.0 show comparable augmentation ratios. Based on single wire measurements taken about 9 diameters downstream from the hole exit plane, the velocity distribution has very good spanwise uniformity for the high turbulence case indicating that the heat transfer distribution is likely to have good spanwise uniformity as well.

Two Staggered Rows of Pressure Surface Holes. Vane Stanton number distributions for the two staggered rows of 30° pressure surface holes for the low turbulence condition are shown in figure 4.17. Similar to the single row of holes, the level of pressure surface augmentation is very high. The heat transfer behavior shows both effects confined to the near hole region and effects that provide a sustaining level of heat transfer augmentation. Though the level of heat transfer is high, the low level of inlet turbulence is not consistent with conditions which exist in the first stage nozzle of a combustion turbine.

Stanton number augmentation ratios for the double row of holes for the low turbulence level are shown in figure 4.18 for the three velocity ratios along with a second Reynolds numbers at a velocity ratio of 1.0. For the highest jet to free stream velocity ratio the augmentation reaches over 180 percent. The level of augmentation of the 1.0 and 0.5 velocity ratios produce much lower augmentation in the near hole region but produce a consistent level of about 60 percent in the downstream region.

Vane Stanton number distributions for a double row of staggered pressure surface holes for the high turbulence condition are shown in figure 4.19. The absolute level of heat transfer is greater than the low turbulence case but the level of augmentation is lower. The heat transfer augmentation is similar to that on the suction surface in that the effects are largely confined to the near hole region. The Stanton number augmentation ratios are shown in figure 4.20 for the high turbulence case for the three velocity ratios and also for the lower Reynolds number. While the augmentation ratios are lower than the low turbulence case they are much higher than the suction surface data. The peak in augmentation scales consistently with velocity ratio and the data look similar but about double the level of the single row data for the high turbulence condition. Unlike the single row data, all three velocity ratios show low but similar levels of augmentation in the downstream region. Like the single row, the high and low Reynolds numbers at a velocity ratio of 1.0 show consistent augmentation ratios. The measured velocity profiles reported in Chapter 6 show good uniformity in the downstream region indicating the heat transfer augmentation is uniform as well.

Showerhead Cooling Effects on Vane Heat Transfer

The showerhead cooling tests were taken subsequent to the downstream film cooling tests. The downstream film cooling foil was removed from the vane and the film cooling holes were filled with epoxy and smoothed. Showerhead holes were drilled in the new foil prior to applying the foil to the vane. A description of the 5 row array of 20° holes is given in detail in chapter 2. Since the conduction around the showerhead holes is three dimensional and the generated heat flux is two dimensional, the heat transfer and adiabatic effectiveness could not be reliably reported. The showerhead array in this study was fed by a common plenum. Since the surface static pressure distribution across the five rows varies considerably, the conditions were set by controlling the static pressure in the plenum. A typical coolant total to inlet total pressure ratio for a vane might be 1.02.

For an exit Mach number of 0.7 this pressure ratio would equate to an equivalent pressure ratio {(Pc-Pt)/(Pt-Ps,ex)} of 0.07. Similarly, equivalent pressure ratios of 0.0175 and 0.35 were chosen for investigation, corresponding to coolant to inlet pressure ratios of 1.005 and 1.10 for a vane with an exit Mach number of 0.7.

Vane Stanton number distributions for the low turbulence condition for the three equivalent pressure ratios are shown in figure 4.21. Generally, the laminar regions show high levels of augmentation while the turbulent regions actually show a decrease in heat transfer presumably due to a thickened boundary layer. The boundary layer was only measured in one spanwise location and while the momentum thickness of the suction surface boundary layer was not significantly thicker than the base vane profile the skin friction was found to be significantly lower.

The Stanton number augmentation ratios for the suction surface at the low turbulence condition are shown in figure 4.22. In the region before transition, the augmentation for the highest pressure ratio is as high as 55 percent. The augmentation appears to be both a function of pressure ratio and Reynolds number but augmentation does not vary systematically with pressure ratio. The high augmentation levels in the region starting at an X/D of 30 indicate that the showerhead cooling promotes earlier transition. In the turbulent region, the augmentation level shows heat transfer at or below the base vane level.

The Stanton number augmentation ratios for the pressure surface at the low turbulence condition are shown in figure 4.23. The augmentation ratios are high and appear to be a function of both pressure ratio and Reynolds number. The ratios increase as the Stanton number decreases in the near pressure surface and then gradually decrease but maintain a consistently high level over the entire pressure surface. While these levels of augmentation are very high, the low level of inlet turbulence is not relevant to conditions which exist at the inlet to first stage vanes.

Vane Stanton number distributions for the high turbulence condition for the three equivalent pressure ratios are shown in figure 4.24. Generally, the laminar regions show high levels of augmentation but unlike the low turbulence condition, the augmentation decreases significantly with X/D. The level of heat transfer increase is lower than the low turbulence case. However, the absolute level of heat transfer for the high turbulence case is as high or higher everywhere compared to the low turbulence case.

The Stanton number augmentation ratios for the suction surface at the high turbulence condition are shown in figure 4.25. In the region before transition, the augmentation for the highest pressure ratio is as high as 30 percent. The augmentation is a clear function of pressure ratio. In the turbulent region, the augmentation level shows heat transfer at the base vane level.

The Stanton number augmentation ratios for the pressure surface at the high turbulence condition are shown in figure 4.26. The augmentation ratios range over 35

percent for the highest pressure ratio and are a function of pressure ratio. The Stanton number ratios in the near hole region are highest and decrease with X/D.

Conclusions

Film cooling was found to have a substantial influence on heat transfer augmentation for both the high and low turbulence conditions for the laminar regions of the flow and exhibited a much smaller effect on the turbulent regions of the flow. Heat transfer augmentation due to film cooling was found to strongly depend on the velocity ratio or pressure ratio of the cooling array. The film cooling had the biggest influence near the holes for the high turbulence case. Also, the effect of film cooling was largest near the holes for the turbulence boundary layer on the suction surface for both cases. The influence of the film cooling on heat transfer was found to be more persistent in the laminar regions for the low turbulence cases. The low turbulence cases had significantly higher levels of augmentation than the high turbulence cases but the high turbulence cases all exhibited higher absolute levels of heat transfer for a given film cooling condition than the low turbulence cases. While the Stanton number augmentation ratios for the low turbulence cases were very high, they are not relevant from an engineering standpoint, since low turbulence levels do not exist at the entrance to first stage nozzles. However, the levels of Stanton number augmentation ratio found in the laminar regions for the high turbulence condition are substantial and heat transfer designers need to have both a general understanding of this problem and the design tools to deal with this situation. This heat transfer research should provide some of the needed understanding and these data can be used to help develop applicable tools. A more detailed understanding of the heat transfer problem is still needed in and around the holes and for arrays at different locations in terms of the pressure coefficient, on the pressure surface.

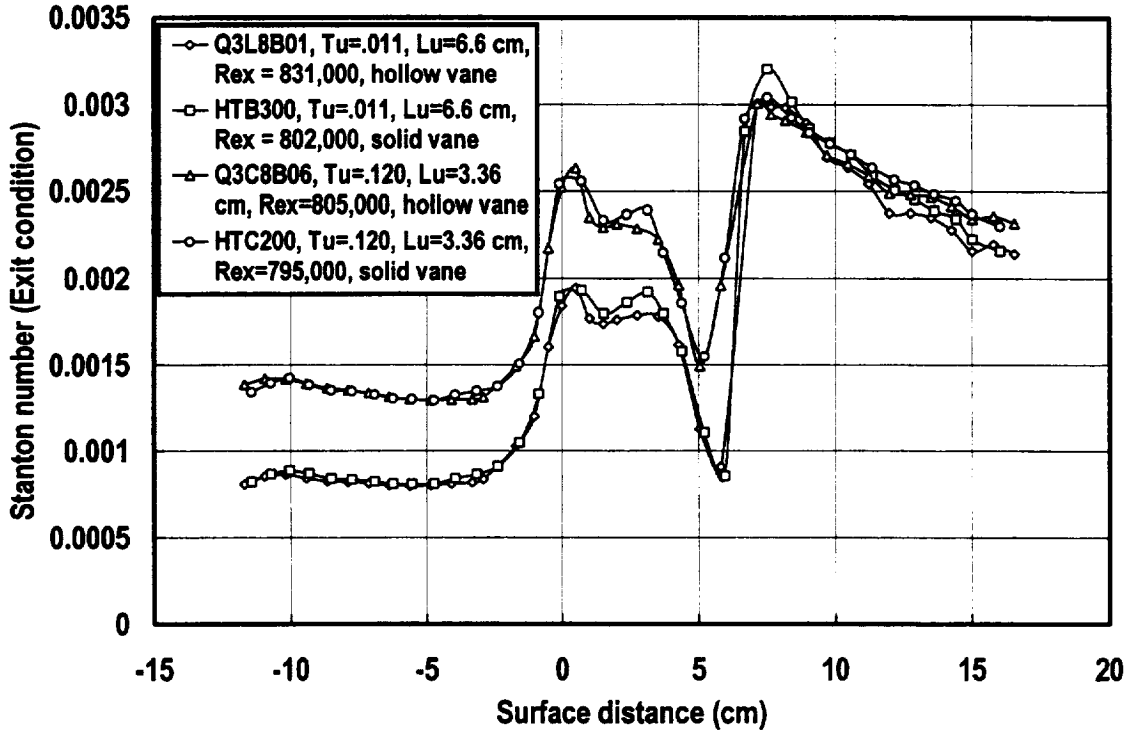

Figure 4.1 Comparison of Stanton number distribution with high and low turbulence with hollow vane and solid vane data, $Re_{,ex}$ = 800,000

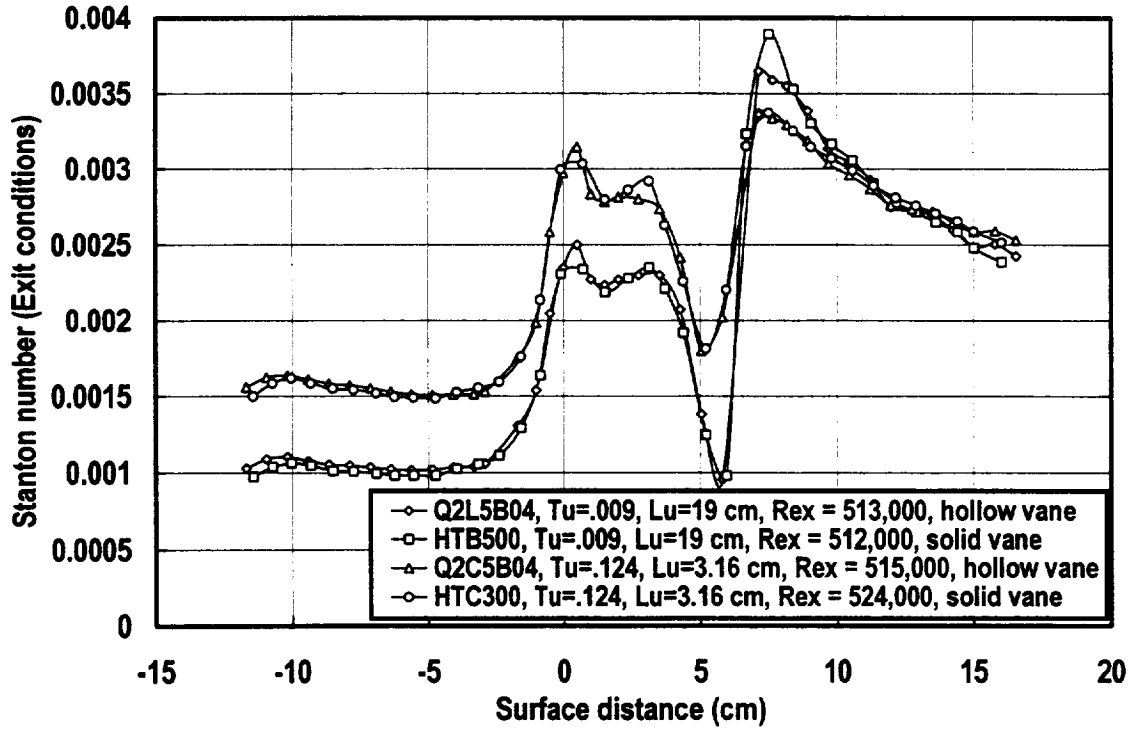

Figure 4.2 Comparison of Stanton number distribution with high and low turbulence with hollow vane and solid vane data, $Re_{,ex}$ = 510,000

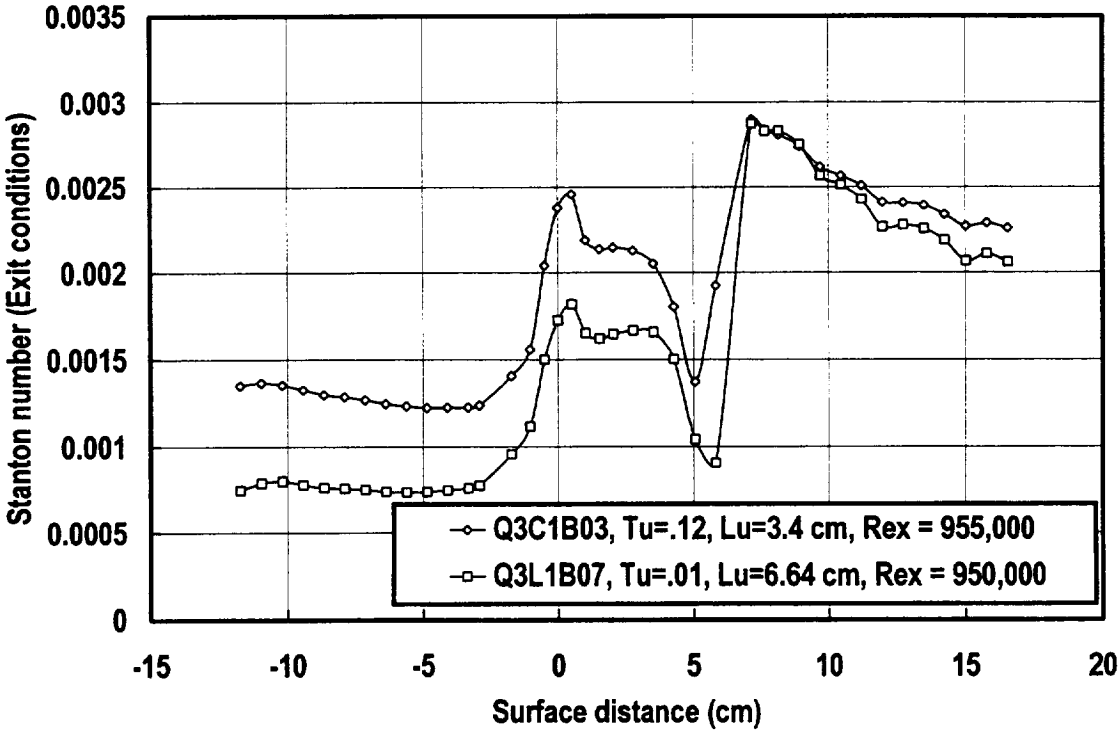

Figure 4.3 Comparison of Stanton number distribution with high and low turbulence for hollow vane, $Re_{,ex}$ = 950,000

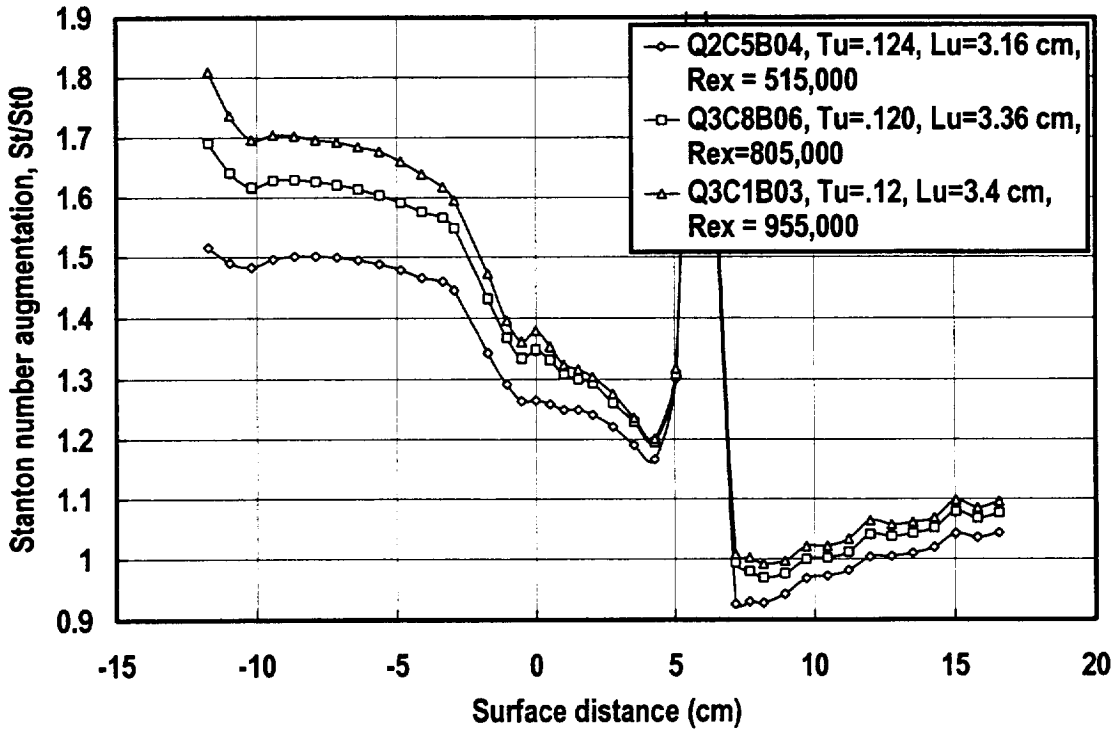

Figure 4.4 Comparison of Stanton number ratios for high/low turbulence for various Reynolds numbers

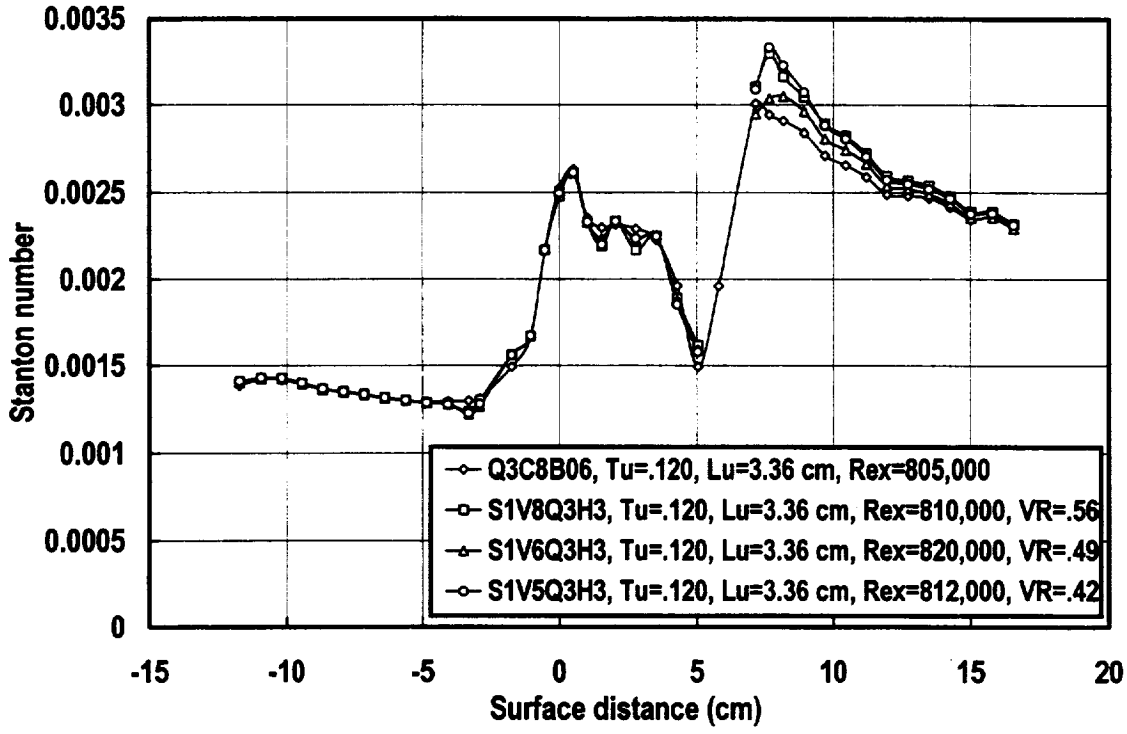

Figure 4.5 Suction surface Stanton number distribution with 1 row of holes, Comb(1)

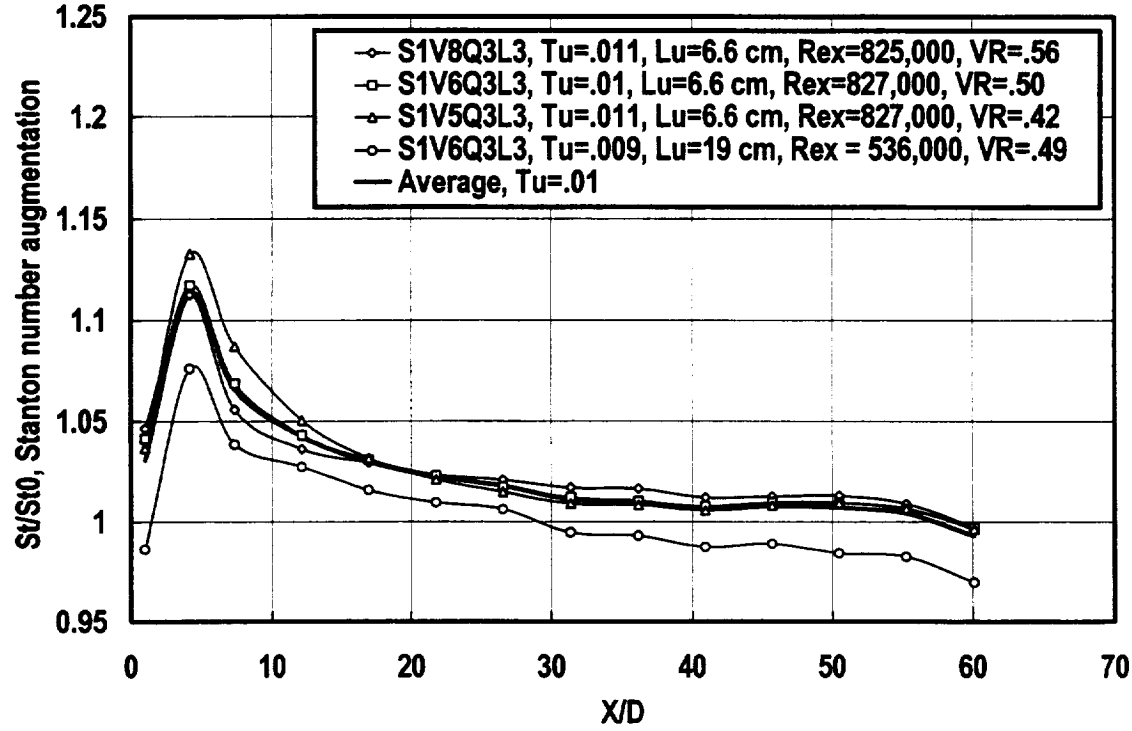

Figure 4.6 Stanton number ratio, low turbulence, 1 row, 30°, suction surface, S/D=3

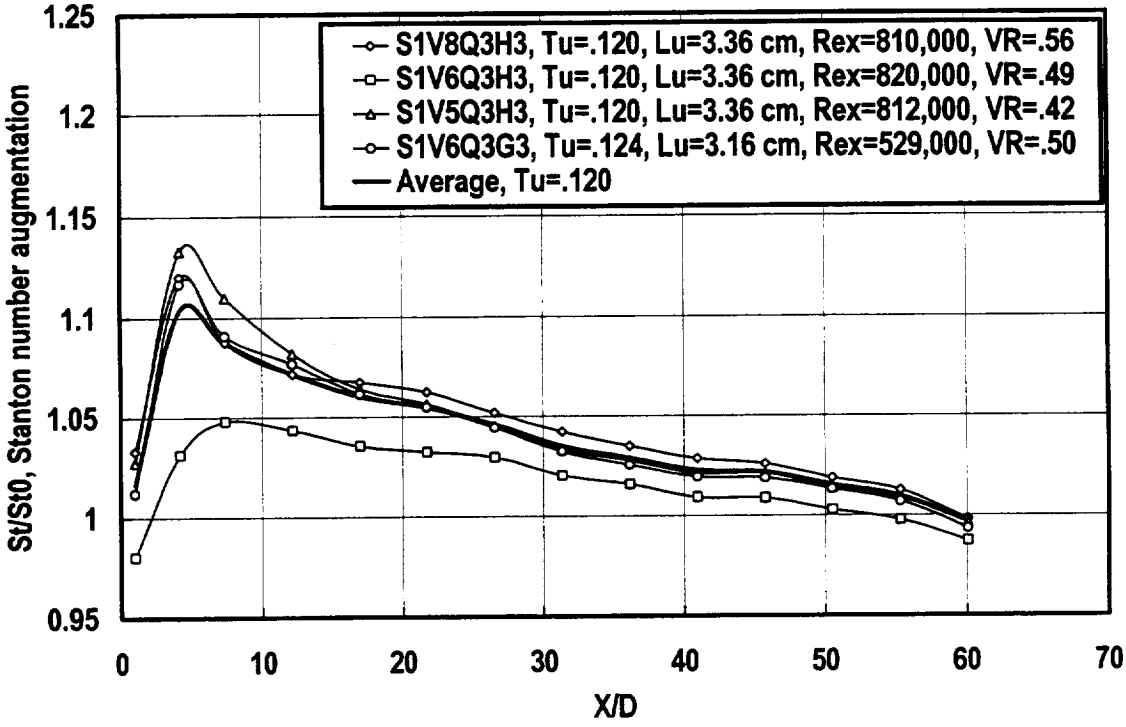

Figure 4.7 Stanton number ratio, Comb(1), 1 row, 30°, suction surface, S/D=3

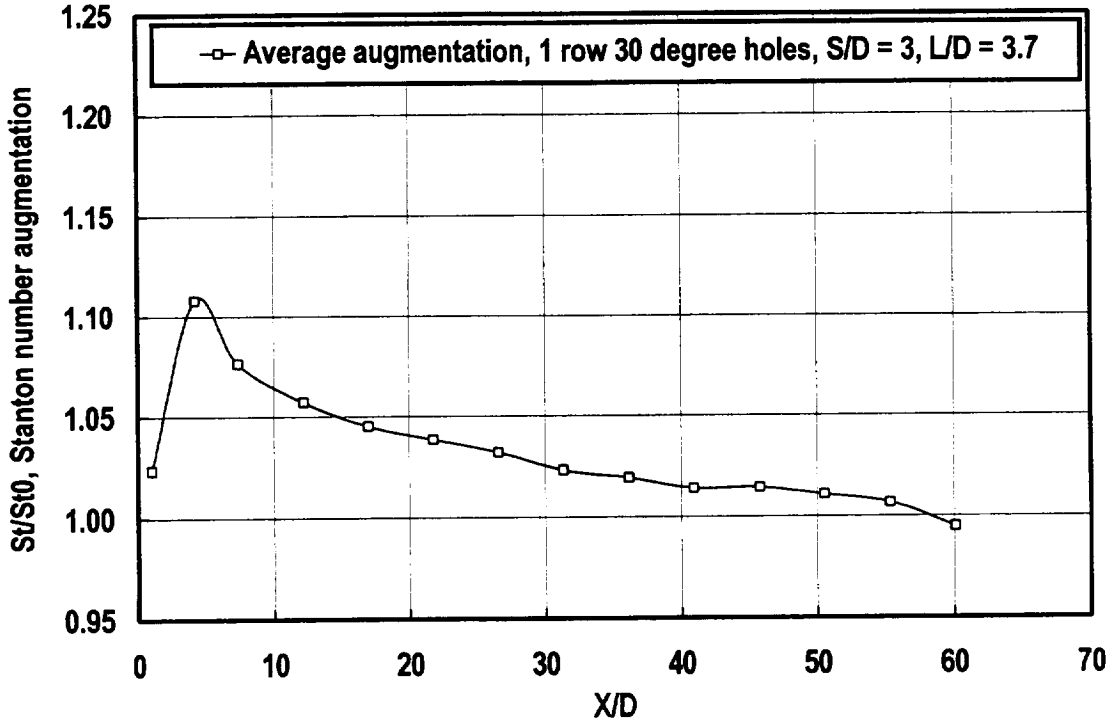

Figure 4.8 Average Stanton number ratio for 1 row of 30° holes, suction surface, S/D=3.

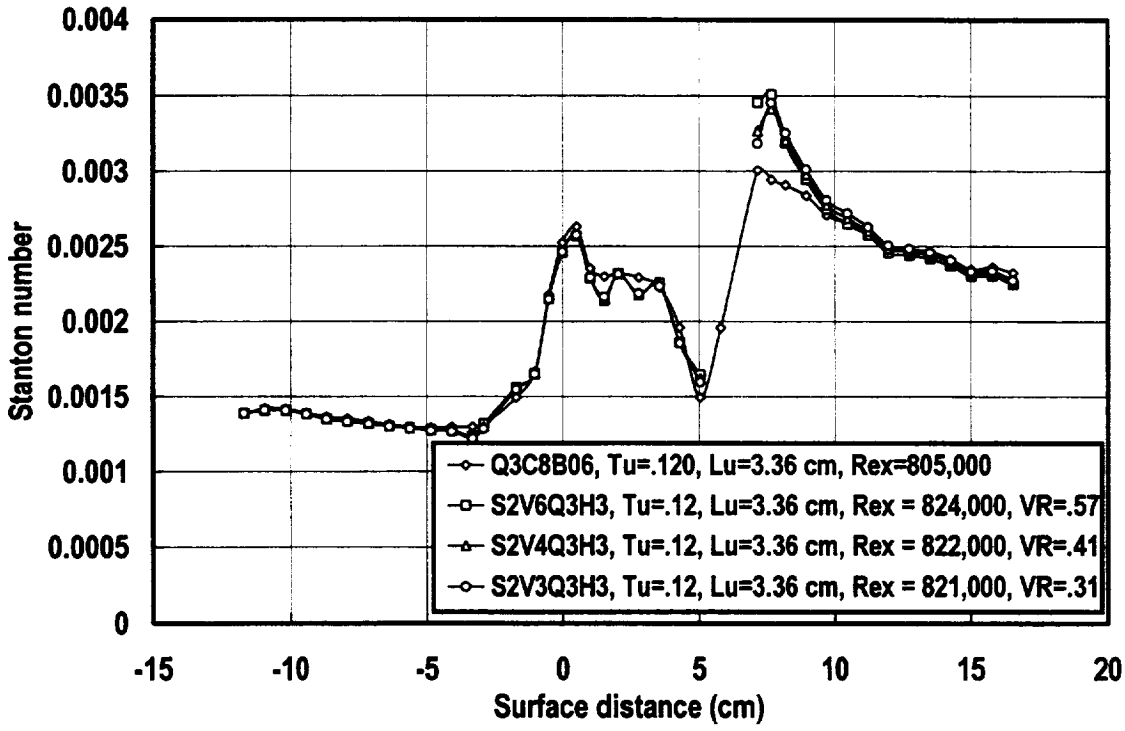

Figure 4.9 Suction surface Stanton number distribution with 2 rows of holes, Comb(1)

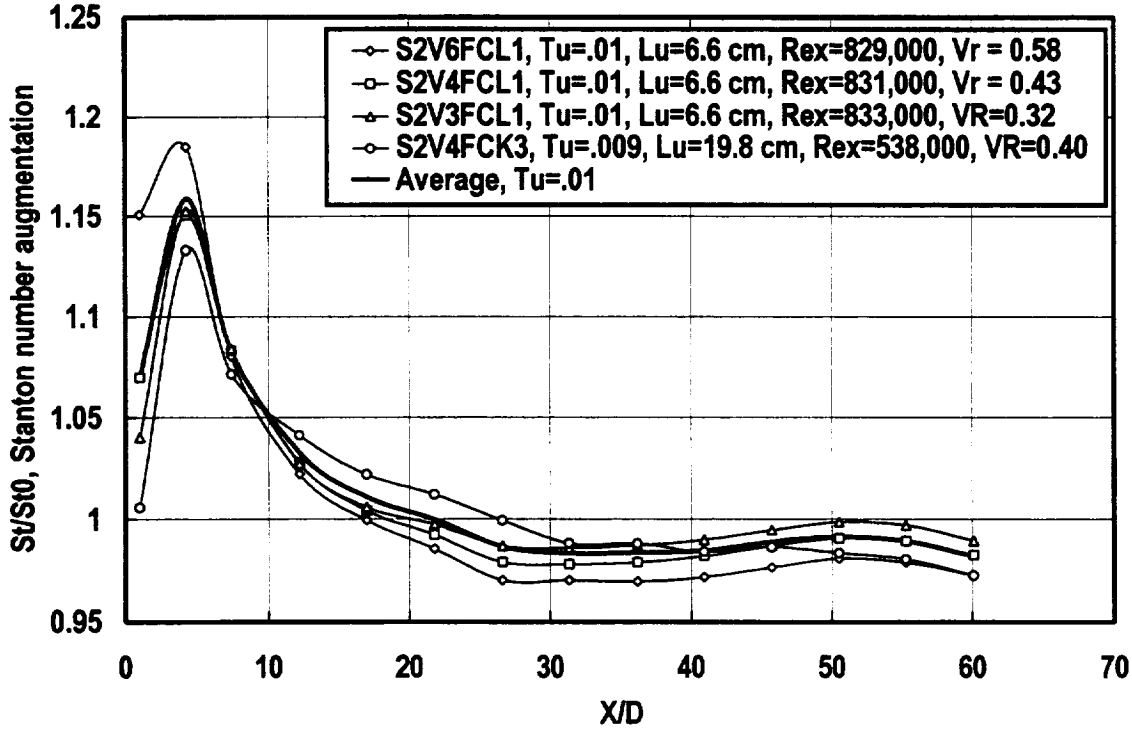

Figure 4.10 Stanton number ratio, low turbulence, 2 rows, 30°, suction surface, S/D=3

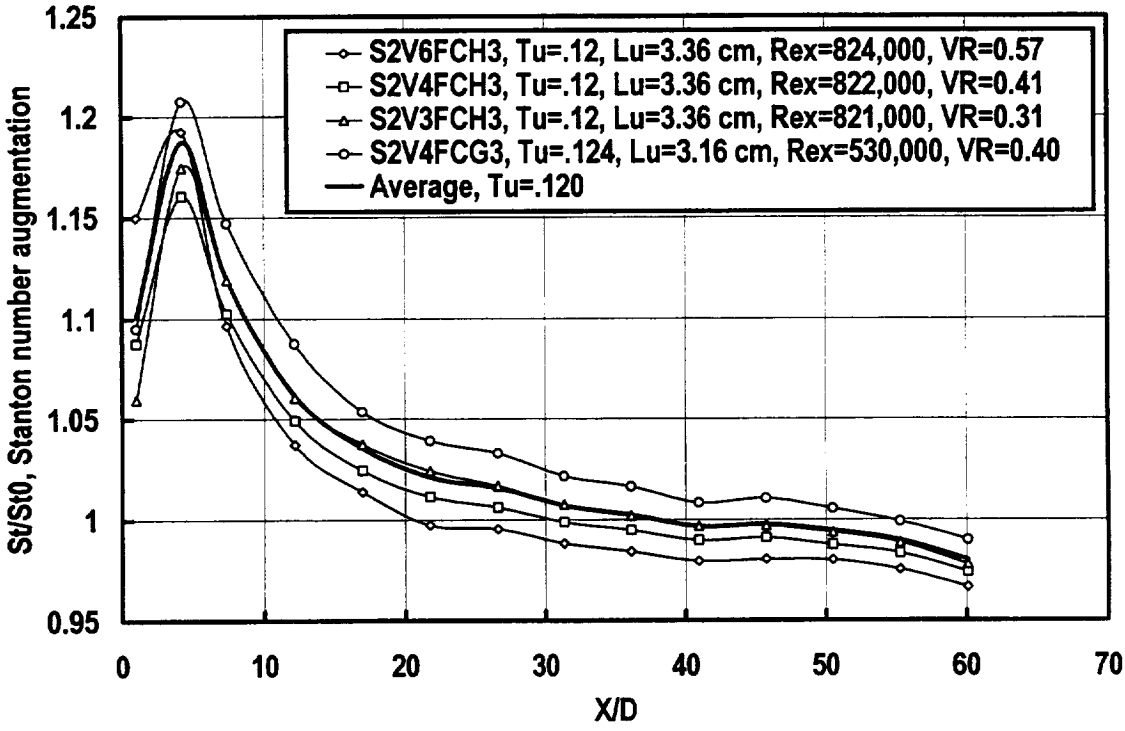

Figure 4.11 Stanton number ratio, Comb(1), 2 rows, 30°, suction surface, S/D=3

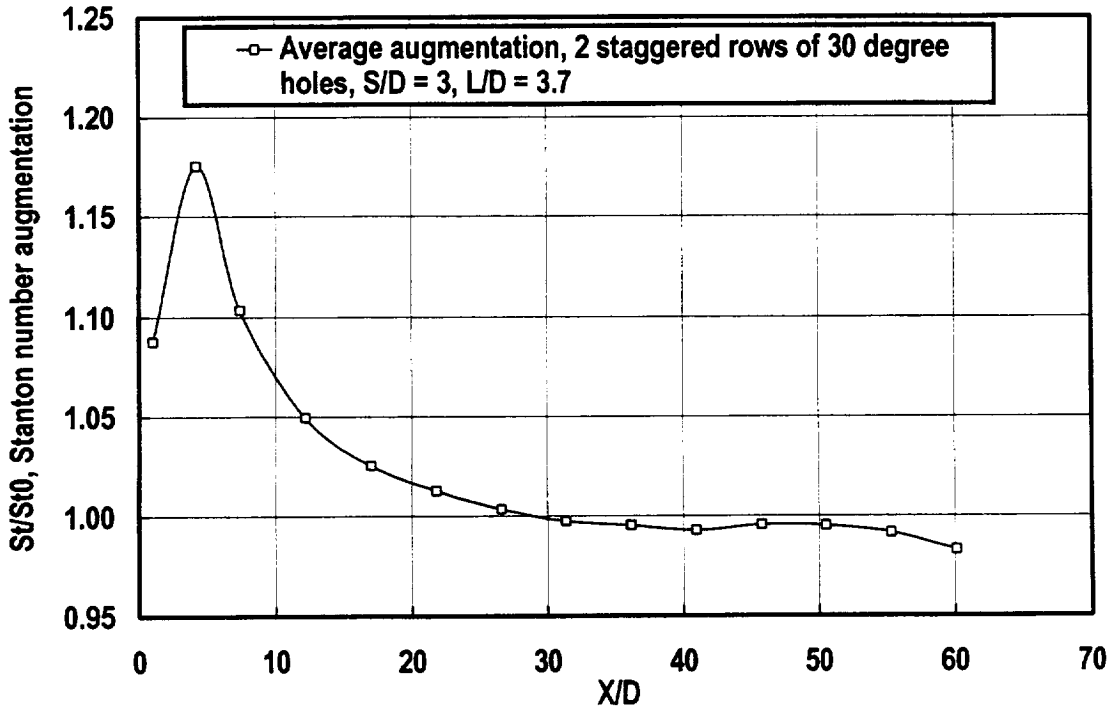

Figure 4.12 Average Stanton number ratio, 2 rows of 30° holes, suction surface, S/D=3.

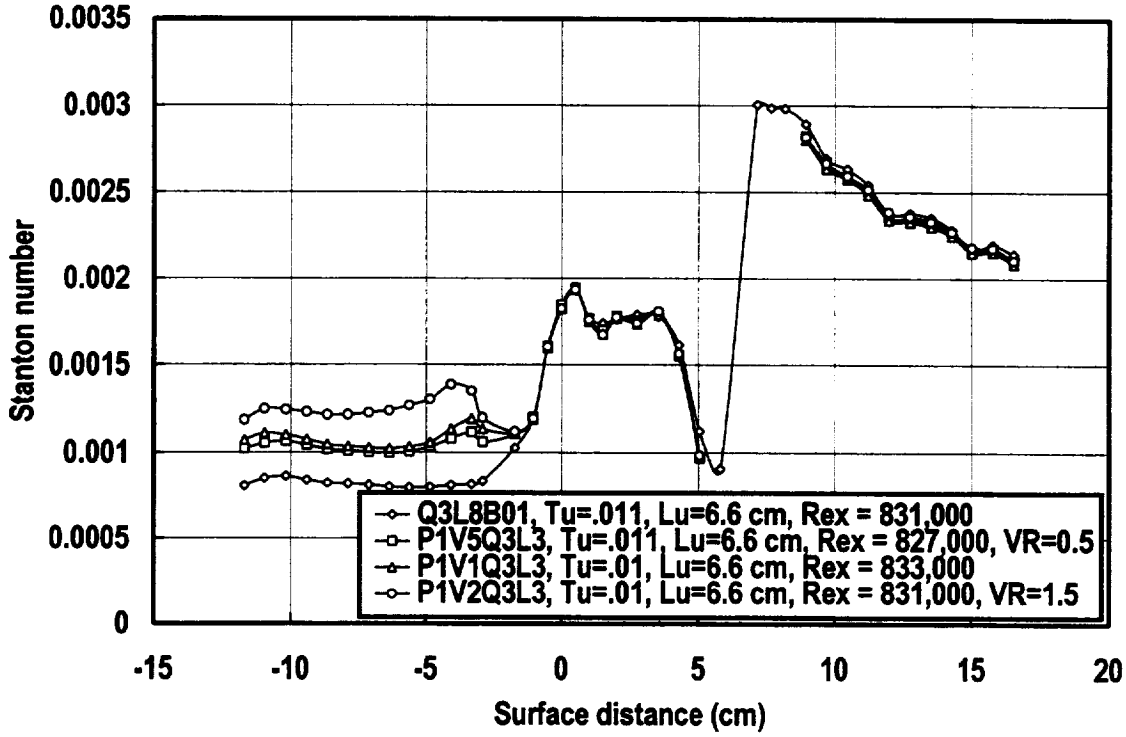

Figure 4.13 Pressure surface Stanton number distribution with 1 row of holes, low turb.

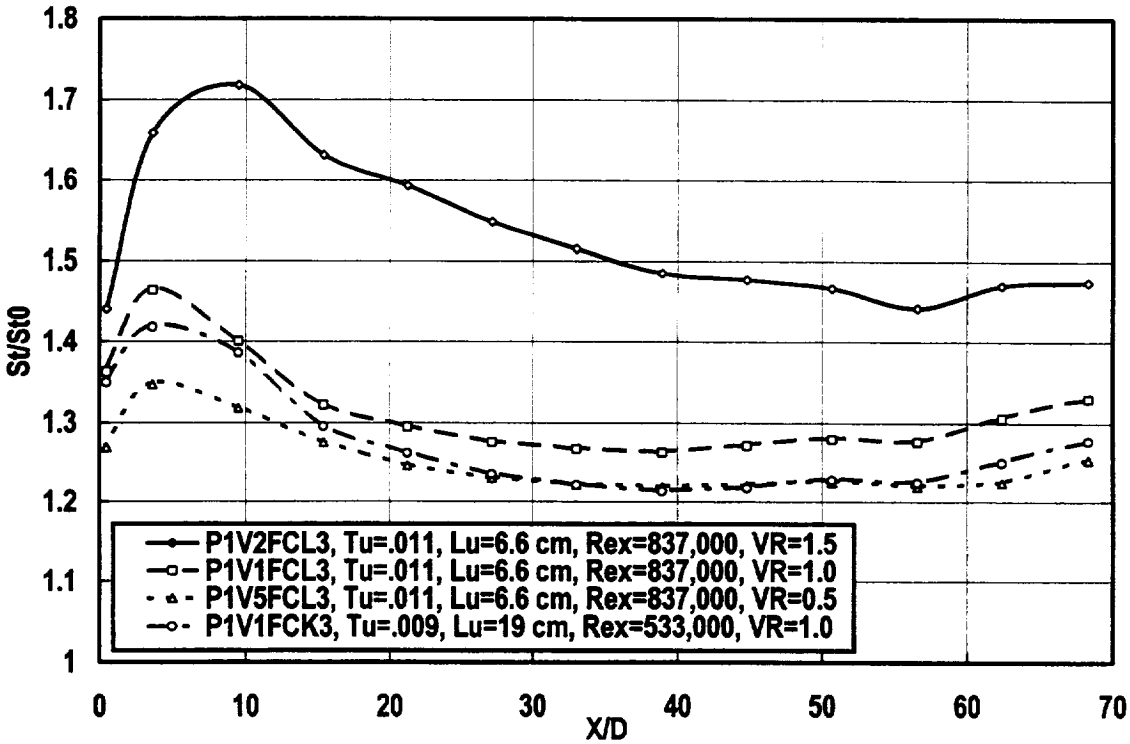

Figure 4.14 Stanton number ratio, low turbulence, 1 row, 30°, pressure surface, S/D=3

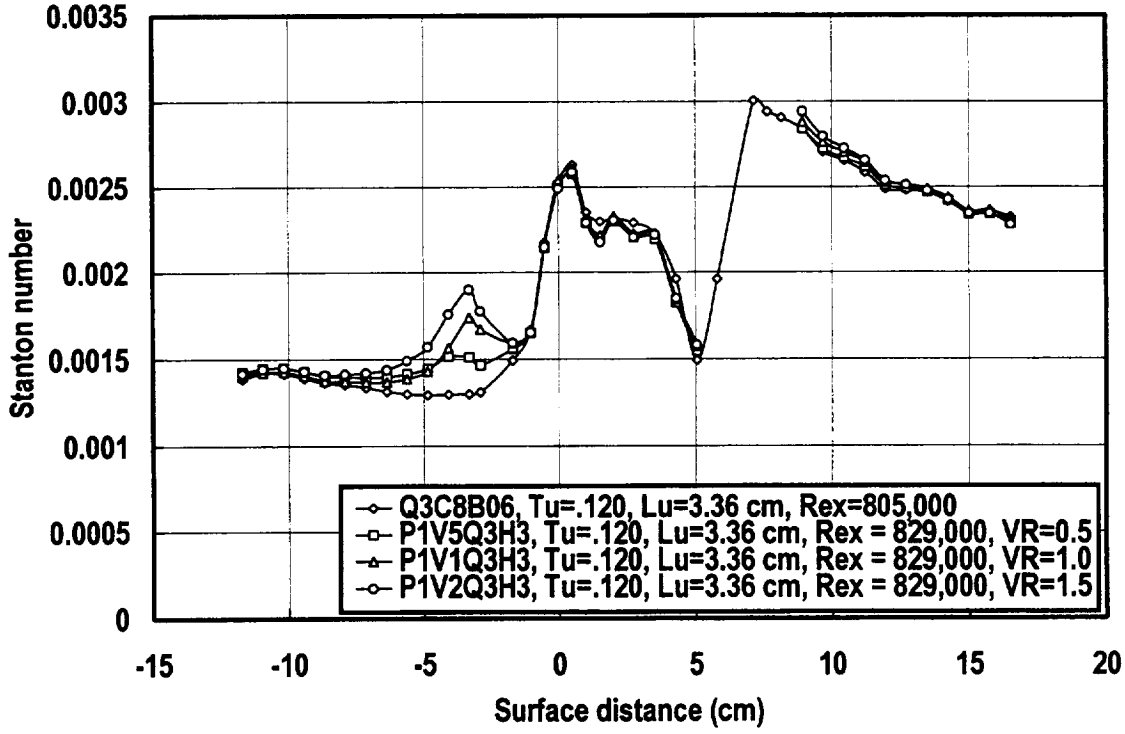

Figure 4.15 Pressure surface Stanton number distribution with 1 row of holes, Comb(1)

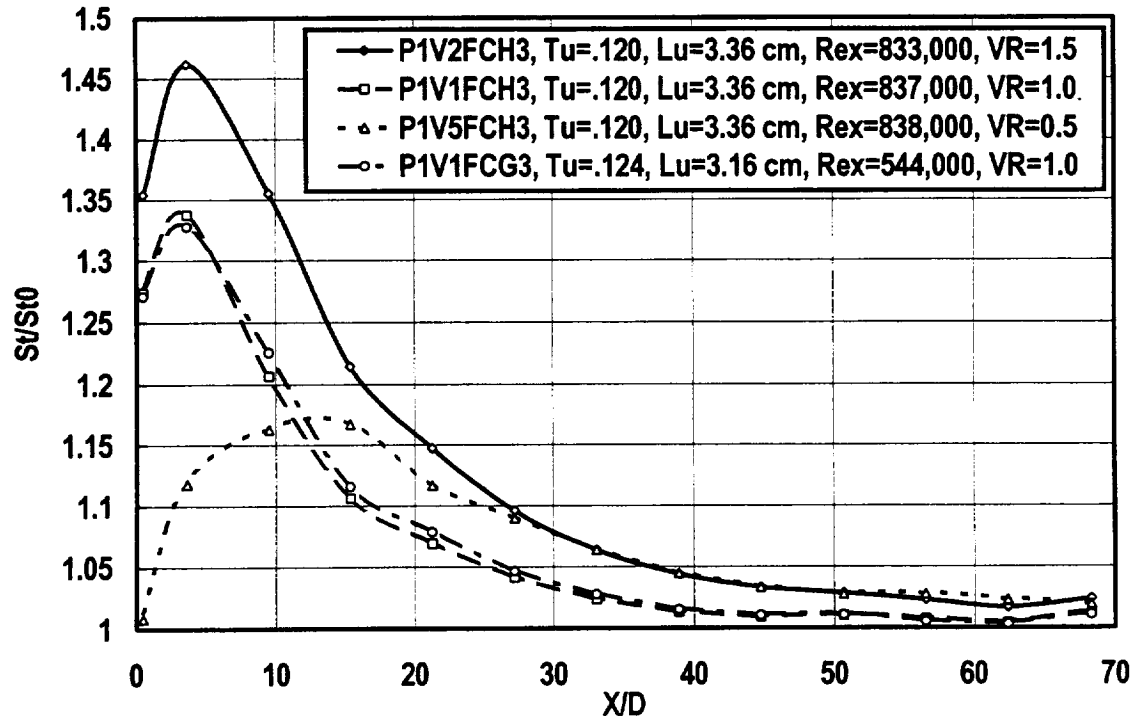

Figure 4.16 Stanton number ratio, Comb(1), 1 row, 30°, pressure surface, S/D=3

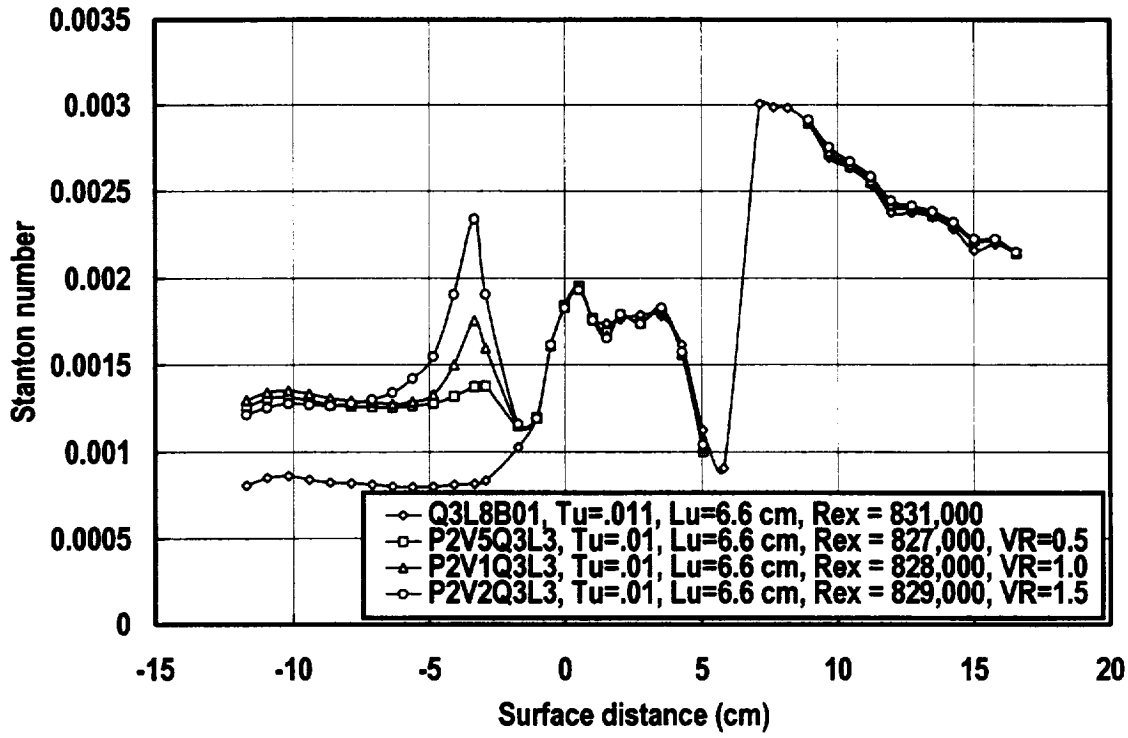

Figure 4.17 Pressure surface Stanton number distribution with 2 rows of holes, low turb.

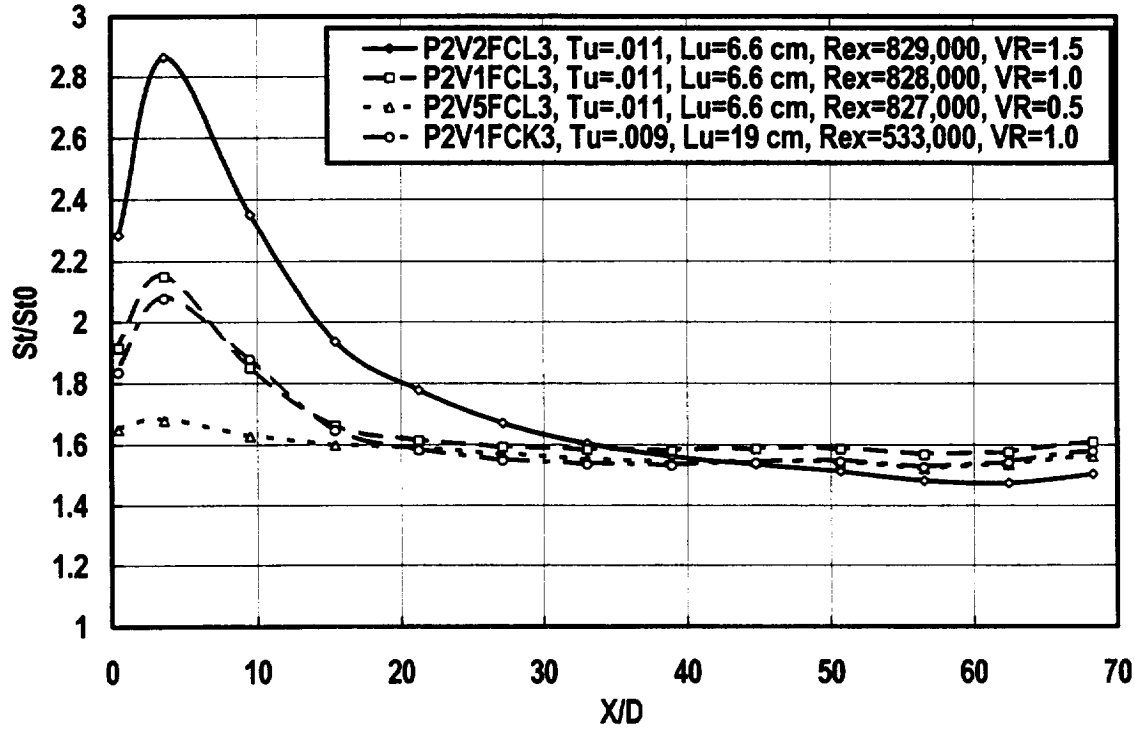

Figure 4.18 Stanton number ratio, low turbulence, 2 rows, 30°, pressure surface, S/D=3

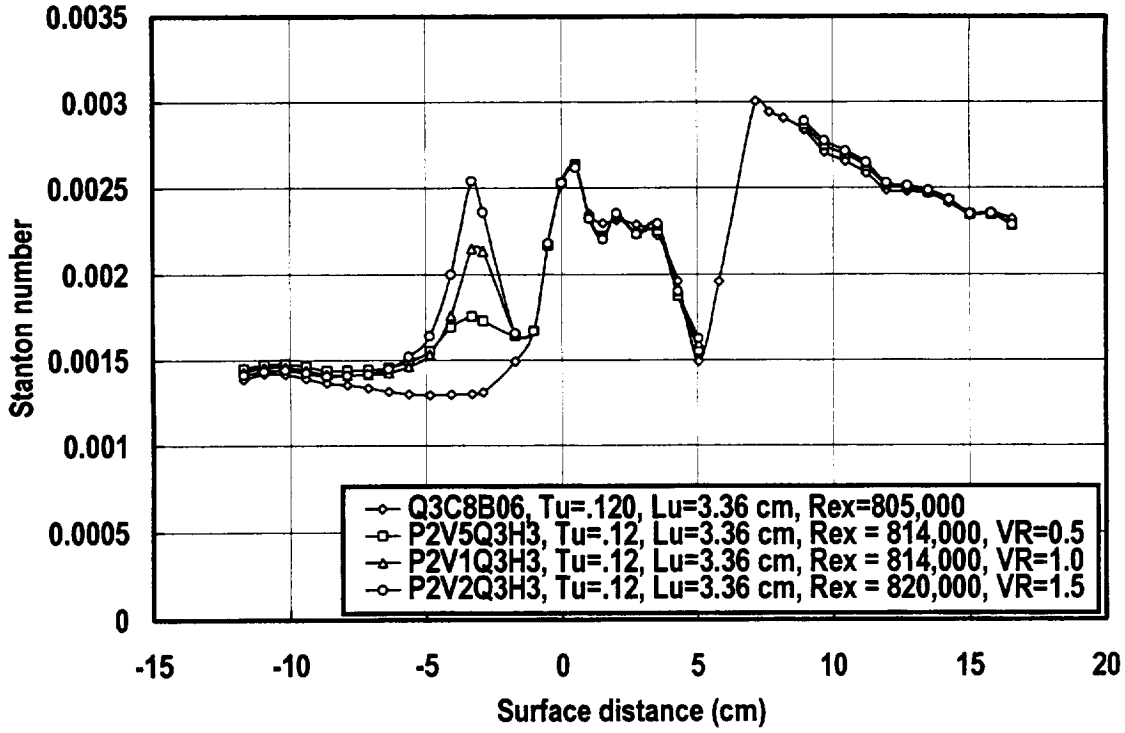

Figure 4.19 Pressure surface Stanton number distribution with 2 rows of holes, Comb(1)

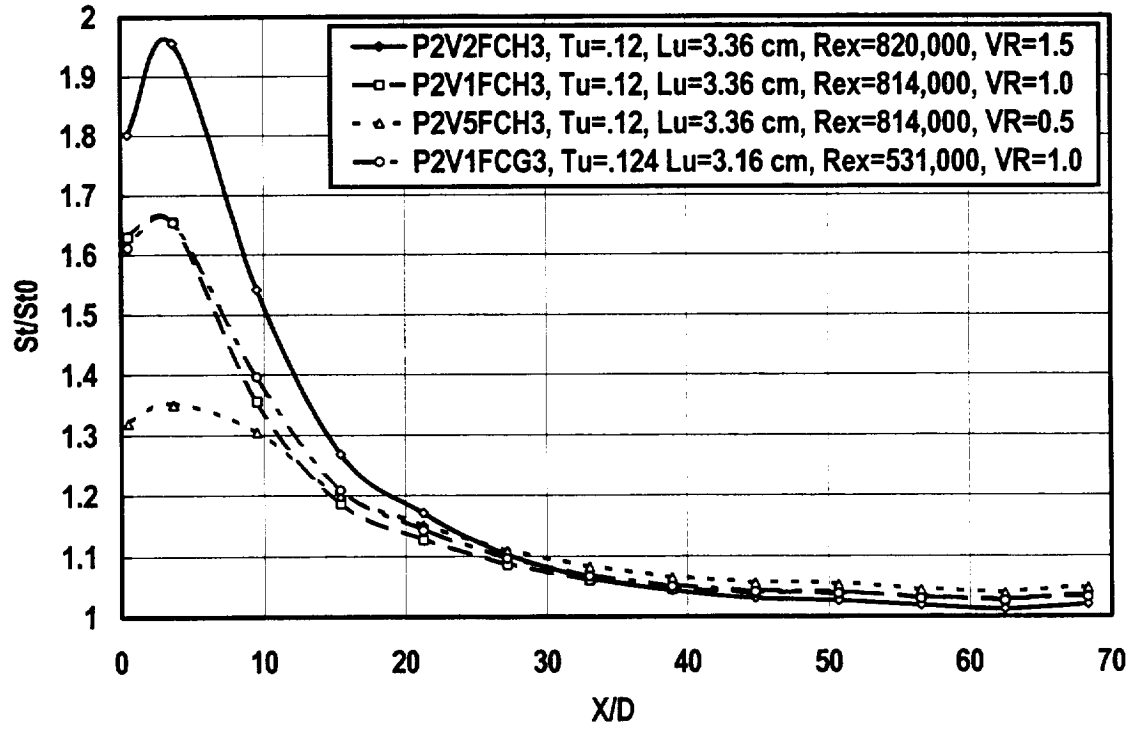

Figure 4.20 Stanton number ratio, Comb(1), 1 row, 30°, pressure surface, S/D=3

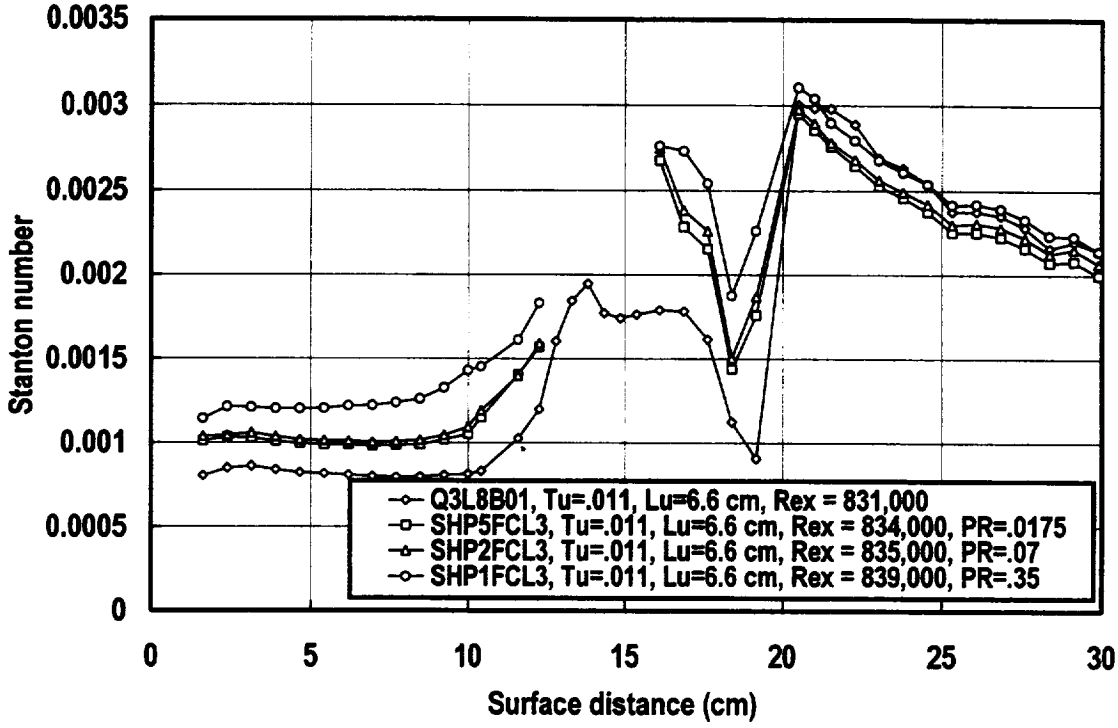

Figure 4.21 Stanton number distribution for showerhead cooling, low turbulence

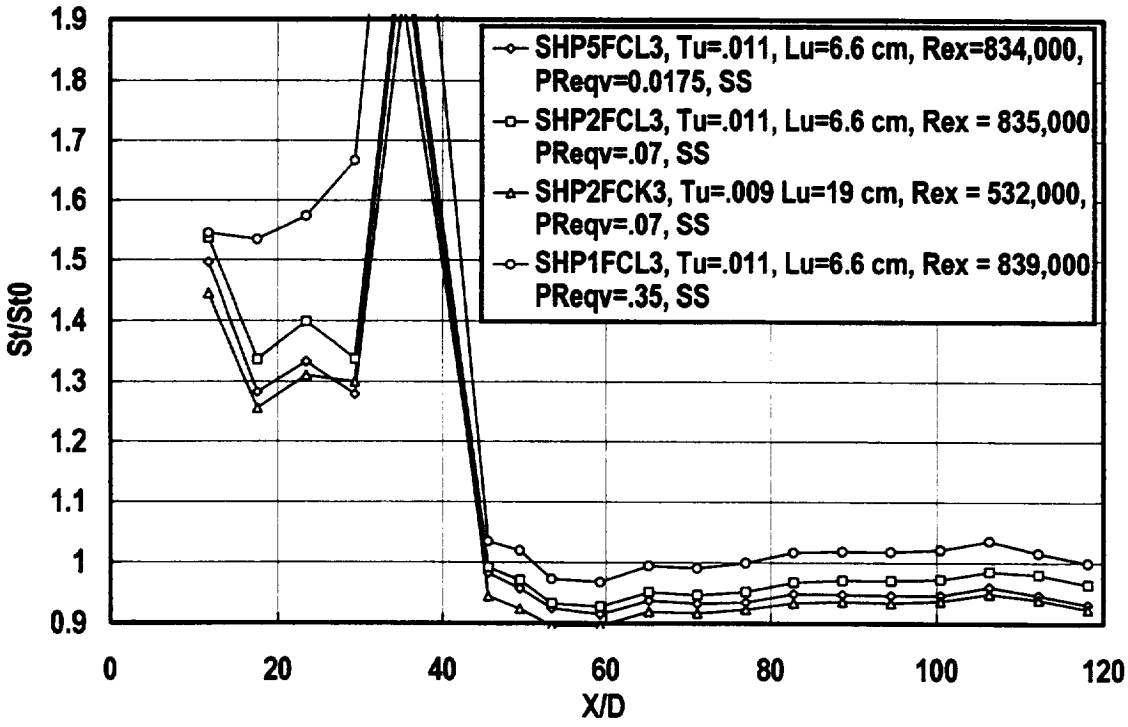

Figure 4.22 Stanton number ratio, showerhead array, low turbulence, suction surface

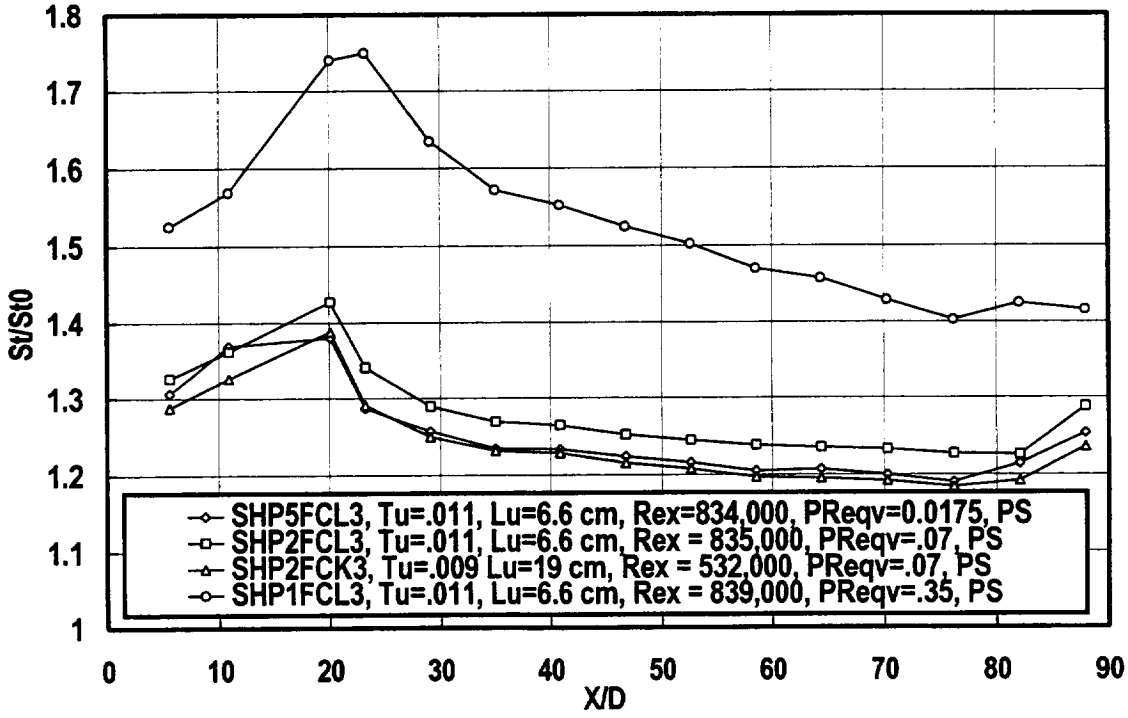

Figure 4.23 Stanton number ratio, showerhead array, low turbulence, pressure surface

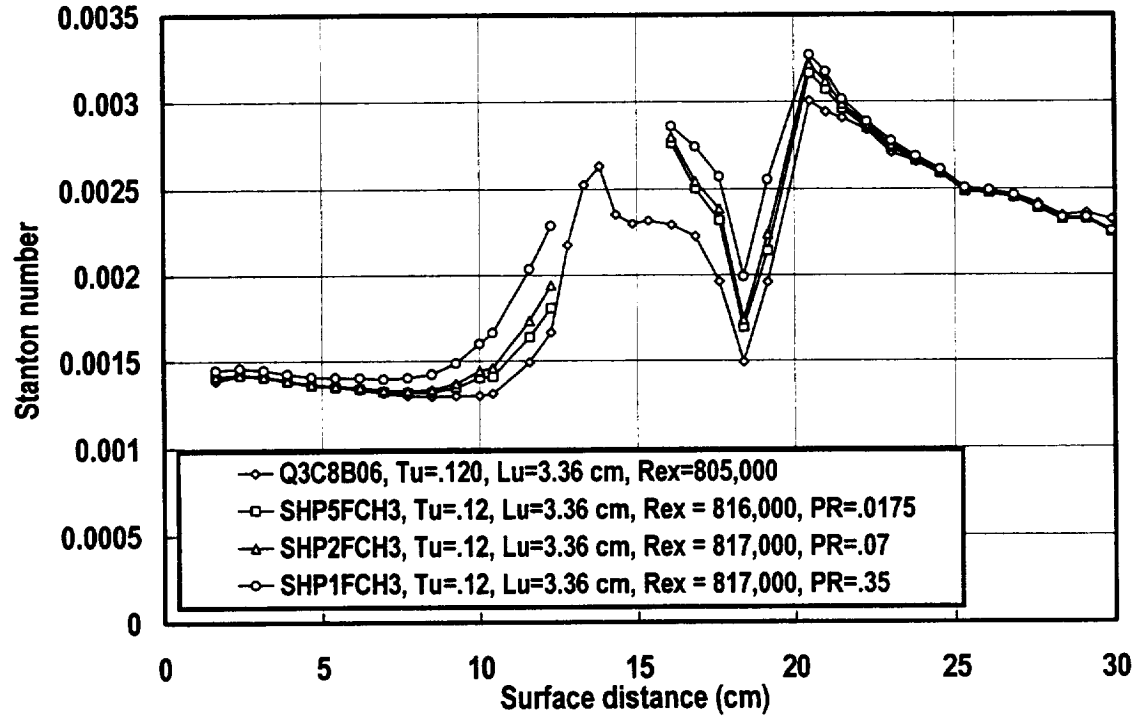

Figure 4.24 Stanton number distribution for showerhead cooling, Comb(1)

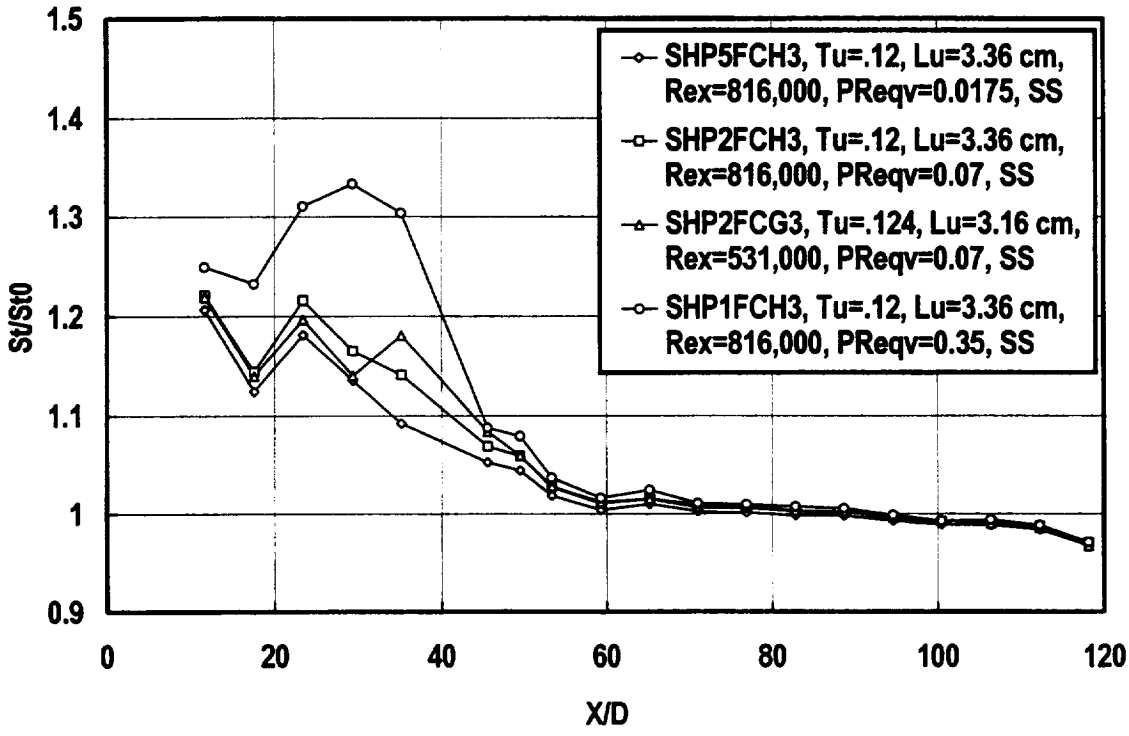

Figure 4.25 Stanton number ratio, showerhead array, Comb(1), suction surface

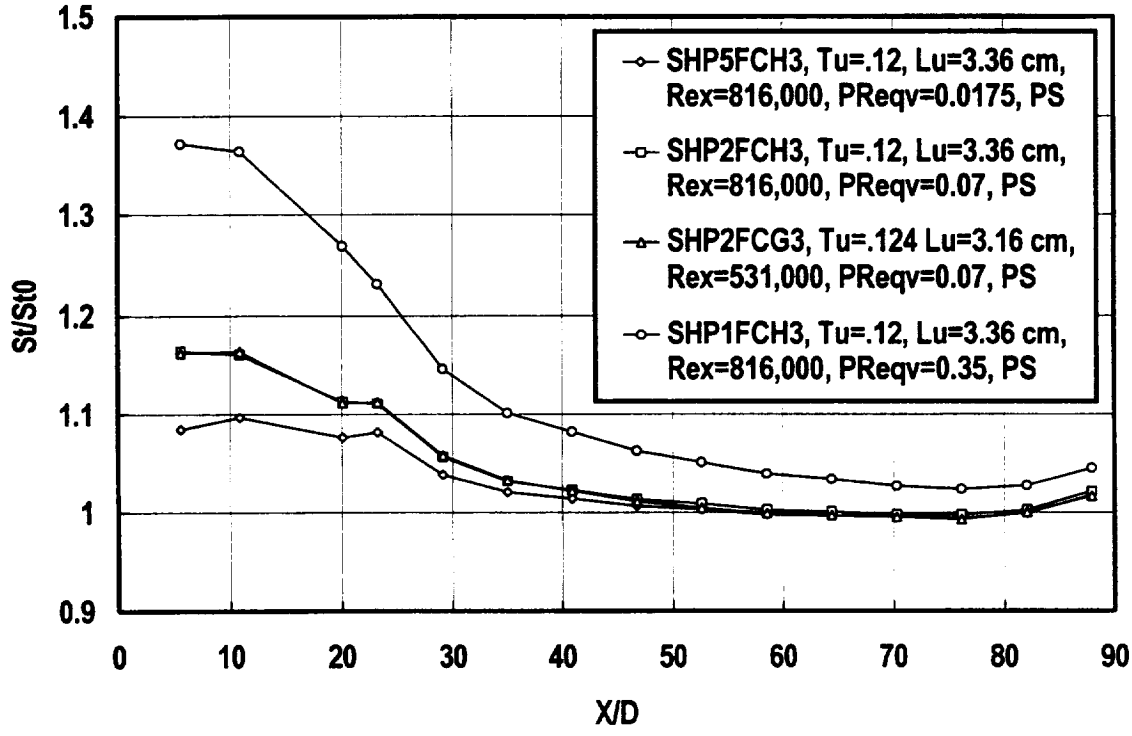

Figure 4.26 Stanton number ratio, showerhead array, Comb(1), pressure surface

Chapter 5

The Influence of Turbulence on Film Cooling

This chapter examines the influence of turbulence and vane cooling geometries on film cooling effectiveness. This chapter documents the adiabatic film cooling data taken for the various geometries, turbulence conditions, and velocity ratios investigated. The intent of these measurements has been to develop a set of data to study the dissipative nature of turbulence on various vane film cooling geometries.

All the film cooling distributions were taken at free stream to coolant temperature ratios of about 0.94. While this density ratio is significantly below the density ratios seen in an engine, which can range to values over 2.0, the back to back results at low and high turbulence levels document the dispersion of film cooling protection by relevant levels of turbulence. These data will serve as a basis to develop tools to account for the enhanced diffusion of coolant due to the free stream turbulence.

In this chapter effectiveness distributions for one row and two staggered rows of film cooling for both the pressure and suction surface over a range of relevant velocity ratios with high and low inlet turbulence are presented. The pressure surface array is located on the near pressure surface where the pressure coefficient is 0.058 for the single row and 0.055 for the double row. The suction surface array is located downstream from a strong adverse pressure gradient where the pressure coefficient is around 1.25. These film cooling arrays all have 30° slant holes with a pitch to diameter ratio of three. Effectiveness distributions downstream from a showerhead cooling array are also reported. The showerhead array consists of five rows of staggered 20° spanwise slant holes. Details of the geometries are presented in chapter two. The inlet conditions are fully documented in chapter three. Heat transfer distributions which compliment these effectiveness measurements are presented in chapter four. Chapter six presents boundary layer profiles taken with and without film cooling over the range of film cooling conditions.

The film cooling measurements were taken using the vane thermocouples due to the coupled nature of the heat transfer and film cooling problem. Simply put, the adiabatic temperature distribution downstream from the holes is needed to correct for the heat up of air in the plenum and holes during the heat transfer test. Similarly, determining the adiabatic temperature distribution requires knowledge of the surface heat transfer distribution to correct the surface temperature for conduction which takes place across the epoxy vane. The thermocouples are located along a single plane of the vane surface at midspan and with a reasonable level of variation are located directly downstream of a hole centerline for the single row hole array. The effectiveness measurements reported for the single row could best be interpreted as centerline

effectiveness data. For the double hole arrays, the data are sufficiently close to full coverage to be interpreted as averaged effectiveness data.

Turbulence Effects on Suction Surface Film Cooling

The selection of velocity ratios to study for suction surface film cooling was based on conditions which typically exist in the design of advanced first stage vanes. A discussion of this rational is given in the corresponding section of chapter four. Essentially feed pressures, temperature ratios, and the hole's discharge coefficient set the velocity ratio on the suction surface to a value in the neighborhood of 0.5. Because this study was limited to density ratios of around 1.0, setting comparable velocity ratios was believed to be the best way to produce film cooling effectiveness distributions showing a relevant response to the influence of high turbulence.

One Row of Suction Surface Holes. A comparison of the low turbulence film cooling effectiveness data for one row of film cooling holes is shown in figure 5.1 as a function of X/D, where X is taken as the distance downstream from the hole exit. The velocity ratios at the hole row range from 0.42 to 0.56 and the data also show the effect of Reynolds number. Based on measurements of the base vane suction surface boundary layer 12 diameters downstream from the hole exit plane using a hot wire, the ratio between the displacement thickness and the hole diameter, δ_1/D, is 0.22. The ratio might be a bit higher for the lower Reynolds number case. The near hole trend shows the lower velocity ratio data to have a higher peak effectiveness while the higher velocity ratio data have a higher effectiveness downstream. The lower Reynolds number data show a lower effectiveness which may be due to a higher δ_1/D ratio. Ratios of δ_1/D greater than 0.25 have been found to have reduced levels of adiabatic effectiveness. The suction surface boundary layer is developing under an adverse pressure gradient which means that more low momentum fluid is close to the wall compared to a zero pressure gradient which could magnify the effects of boundary layer thickness on film cooling.

A comparison of the high turbulence adiabatic film cooling data is shown in figure 5.2. The velocity ratios for these data range from 0.42 through 0.56. A second Reynolds number point is taken for the 0.50 velocity ratio. These trends are similar to the low turbulence data with the exception of the Reynolds number comparison. In this case the data taken at the two Reynolds numbers and at a similar velocity ratio (0.50) show very similar results. Based on downstream measurements of the suction surface boundary layer using a hot wire, the ratio between the displacement thickness and the hole diameter, δ_1/D, is 0.195 while the skin friction is about 16 percent higher than the low turbulence data.

A comparison between the data taken at both a low and a higher level of turbulence is shown in figure 5.3. Based on previous investigations, the low turbulence data would be expected to produce a higher level of effectiveness than the

higher turbulence data, throughout the downstream region. However, the inlet free stream turbulence changes the development of the suction surface boundary layer, producing a lower displacement thickness at the injection location. These higher levels of effectiveness near the holes can be attributed to the thinner, fuller boundary layer. The turbulence, as expected, can be seen to dissipate the film cooling protection more rapidly than the low turbulence condition. Relative to the peak measured effectiveness for the two cases, the far down stream effectiveness of high turbulence case is only 75 percent of the ratio for the low turbulence case, indicating the dissipative nature of the turbulence in the far field.

Two Staggered Rows of Suction Surface Holes. A comparison of the low turbulence film cooling data for the two stagger rows of film cooling holes is shown in figure 5.4. The velocity ratios at the hole row range from 0.3 to 0.56 and the data also show the effect of Reynolds number. As indicated for the single row data, the ratio between the displacement thickness and the hole diameter, δ_1/D, is 0.22. This ratio might be a bit higher for the lower Reynolds number case. The near hole trend shows that the 0.3 and 0.4 velocity ratio data have a higher peak effectiveness while the 0.56 velocity ratio data have a higher effectiveness downstream. The lower Reynolds number data show a lower effectiveness which may be due to a higher δ_1/D ratio than the higher Reynolds number data.

A comparison of the high turbulence adiabatic film cooling data is shown below in figure 5.5. Again, the velocity ratios for these data range from 0.3 through 0.56. A second Reynolds number point is taken for the 0.40 velocity ratio. As indicated for the single row data, the ratio between the displacement thickness and the hole diameter, δ_1/D, is 0.195. The trends of this comparison are similar to the low turbulence data with the exception of the Reynolds number comparison. In this case the data taken at the two Reynolds numbers and at a similar velocity ratio (0.40) show similar levels of effectiveness.

A comparison between the data taken at both a low and a higher level of turbulence is shown below in figure 5.6 for a velocity ratio of 0.42. Based on previous investigations, the low turbulence data would be expected to produce a higher level of effectiveness than the higher turbulence data, throughout the downstream region. However, the inlet free stream turbulence changes the development of the suction surface boundary layer, producing a lower displacement thickness and steeper profile at the injection location. These higher levels of effectiveness near the holes can be attributed to the thinner, fuller boundary layer. The turbulence, as expected, can be seen to dissipate the film cooling protection more rapidly than the low turbulence condition. Relative to the peak measured effectiveness for the two cases, the far down stream effectiveness of high turbulence case is only 74 percent of the ratio for the low turbulence case, indicating the dissipative nature of the turbulence in the far field.

Turbulence Effects on Pressure Surface Film Cooling

The selection of velocity ratios to study for pressure surface film cooling was based on conditions which typically exist in advanced first stage vanes. A discussion of this rational is given in the corresponding section of chapter four. Essentially, pressure coefficients on the pressure surface typically range from very low values near the stagnation region to values which approach unity near the trailing edge potentially allowing for a wide range of velocity ratios. Velocity ratios of 0.5, 1.0, and 1.5 were chosen to provide a full range of mixing regimes (wake, equal velocity, and jet) with respect to the free stream. Since this study was limited to density ratios of around 1.0, setting comparable velocity ratios was believed to be best way to produce relevant comparisons between the effectiveness distributions at low and high turbulence.

One Row of Pressure Surface Holes. The adiabatic effectiveness results for our single row of holes for the low turbulence condition is shown in figure 5.7. These results indicate that for a low turbulence inlet, a velocity ratio of around 0.5 is needed to produce good levels of film cooling protection. Since the thermocouple distribution is essentially right downstream from a hole, the effectiveness distribution should be interpreted as centerline data. The Reynolds number comparison at the velocity ratio of 1.0 shows little difference. Due to the very thin boundary layers on the pressure surface, the δ_1/D ratio is expected to be a small fraction of the value where cooling performance has been found to degrade.

The results for the single row of holes with the high turbulence condition is shown in figure 5.8. In the near hole region, the peak effectiveness is a clear function of velocity ratio with the lowest ratio, 0.5, having the highest effectiveness. In the downstream region, the higher velocity ratios have a higher level of effectiveness. When compared to the lower turbulence level case, the higher velocity ratios have similar effectiveness levels. In the near hole region, the effectiveness levels for the high turbulence cases are even slightly higher than the low turbulence condition. In the situation of high velocity ratios, where the coolant jet penetrates the boundary layer, the enhanced mixing due to the free stream turbulence improves near hole effectiveness by mixing the coolant down to the wall. Though no spanwise effectiveness measurements were made, the velocity profiles taken 9 diameters downstream from the hole exits showed good spanwise uniformity from downstream of the holes to in between them. This uniformity suggests that spanwise coverage is significantly improved with the high turbulence which is supported by the work of Bons, MacArthur, and Rivir who found that midline effectiveness was equal to centerline effectiveness by an X/D of 10.

Figure 5.9 shows a comparison of adiabatic effectiveness distributions for the two turbulence levels at a velocity ratio of 0.5. The effectiveness in the near hole region is strongly dissipated by the high turbulence while in the downstream region, the reduction is an even greater percentage. The spanwise uniformity of the velocity profiles in the near downstream region suggest that spanwise mixing is responsible for much of the near

hole degradation. However, in the far downstream region, the reduction must be due to normal mixing, since the jets are expected to merge by an X/D of around 40 for this velocity ratio. A comparison between suction surface and pressure surface effectiveness distributions for the high turbulence case and a velocity ratio of 0.5 is shown in figure 5.10. The initial level of effectiveness is lower for the pressure surface distribution and the downstream effectiveness is also much lower. Since the high turbulence level on the pressure side rapidly mixes the coolant in the spanwise and normal directions and due to the high acceleration along the pressure side, these two distributions are difficult to compare.

Two Staggered Rows of Pressure Surface Holes. The adiabatic effectiveness results for our double row of holes for the low turbulence condition is shown in figure 5.11. The results indicate that on the pressure surface, good levels of film cooling protection can be obtained with two staggered rows of holes for a wide range of velocity ratios. Unlike the suction surface data, the low turbulence pressure surface data taken at the same velocity ratio compare closely. Since the pressure surface has very thin boundary layers, the δ_1/D ratio is expected to be only a fraction of the ratio (0.25) where film cooling performance has been found to degrade. The shape of the near hole effectiveness curve at a velocity ratio of 0.5 is different for the pressure surface compared to the suction surface but the levels of film cooling are generally comparable. Past an X/D of 15 the pressure surface effectiveness is much lower than the suction surface data at the 0.5 velocity ratio and by an X/D of around 50 to 60, the pressure surface effectiveness is on the order of 50 percent of the suction surface value. The strong acceleration seen on the pressure surface is clearly responsible for degrading film cooling performance past an X/D of 15.

The adiabatic effectiveness results for the high turbulence condition are shown for two staggered rows of 30° holes in figure 5.12. In the near hole area, the peak effectiveness does not appear to be strongly affected by velocity ratio although the location of the near hole peak can be seen to move downstream somewhat with increasing velocity ratio. Downstream the effect of turbulent mixing is clearly present. The effectiveness levels of the high turbulence data are significantly lower than the effectiveness levels of the low turbulence data. Assuming the effectiveness distribution for two staggered rows of holes is roughly equivalent to the spanwise average effectiveness, turbulence has been shown to have a significant influence on the dissipation of pressure surface cooling effectiveness.

Figure 5.13 compares the effect of turbulence on pressure side film cooling with a velocity ratio of 0.5 for our double row of holes. The comparison indicates the strong effect of the turbulence in mixing away film cooling protection. Due to the low local velocity at this location on the pressure surface, the turbulence level is quite high. The reduction in film cooling protection, $\eta_{(Tu=.12)}/\eta_{(Tu=.01)}$ reaches a ratio below 0.45 by the furthest downstream station.

The relative influence of turbulence on pressure surface adiabatic effectiveness is shown in figure 5.14 in terms of the local adiabatic effectiveness for the high turbulence case ratioed by the effectiveness for the low turbulence case for the same Reynolds number and velocity ratio ($\eta_{(Tu=.12)}/\eta_{(Tu=.01)}$). While some significant variations exist in the near hole region, past an X/D of 10 the data clearly show a strong trend indicating a significant but gradual degradation in film cooling performance due to the turbulence. From an X/D of 10 to 68 the data have been averaged to show the mean effectiveness ratio. The gradual decrease in effectiveness with X/D is sound from a physical basis since the coolant jet energy difference with the free stream is an integral quantity.

Turbulence Effects on Showerhead Cooling Effectiveness

Showerhead cooling arrays are typically fed by a common plenum and the surface static pressure distribution across the five rows varies considerably. A typical coolant total to inlet total pressure ratio for a vane might be 1.02. For an exit Mach number of 0.7 this pressure ratio would equate to an equivalent pressure ratio {(Pc-Pt)/(Pt-Ps,ex)} of 0.07. Equivalent pressure ratios of 0.0175 and 0.35 were also chosen for investigation which correspond to coolant to inlet pressure ratios of 1.005 and 1.10 for a vane with an exit Mach number of 0.7.

Suction Surface. The adiabatic effectiveness distribution on the suction surface downstream from the showerhead array is shown as a function of X/D for three equivalent pressure ratios and a second Reynolds number in figure 5.15. The showerhead array can be seen to provide a good level of film cooling coverage which is not strongly affected by the pressure. Although the variation in coolant total pressure produces a big change in the showerhead jet velocities in close proximity with the stagnation point, the change in pressure has a smaller effect on jet velocities for the rows of holes further downstream on the suction surface where the surface static pressure is much lower. The showerhead effectiveness distributions show more variation than the downstream film cooling arrays. These variations are caused by the spanwise trajectories of the coolant jets which begin turning in the downstream direction as the flow leaves the holes. The jets from the showerhead array can join with jets from adjacent rows and produce regions of very good coverage and regions of poorer coverage. This same problem has been observed by Salcudean, et. al (1994).

The adiabatic effectiveness distributions for the higher turbulence case are compared in figure 5.16. In the downstream region they order on pressure ratio variation but they do not show a strong variation with pressure ratio. The data do give evidence of the influence of turbulence as indicated by the lower effectiveness values seen in figure 5.16. A comparison between the effectiveness distribution for the high and low turbulence level at an equivalent pressure ratio of 0.07 is shown in figure 5.17. The high turbulence effectiveness is 90 percent of the low turbulence effectiveness at an X/D of about 12 but the ratio decayed to only 45 percent of the protection at the furthest downstream location. Even though the external turbulence level is only about 4 percent

along the suction surface, based on the average of u' and v', the enhancement to turbulent mixing applied over a relatively long distance effectively reduces the film cooling protection in the downstream direction. In an effort to get a quantitative estimate of the influence of the turbulence on showerhead film cooling effectiveness, the local value of effectiveness taken for the high turbulence case was ratioed by the local value for the corresponding condition from the low turbulence case. These comparisons are shown in figure 5.18. The lower two pressure ratios, including the lower Reynolds number case, show a consistent level of degradation of cooling performance. An average of these three cases is displayed by the heavy solid line which shows a ratio of only 40 percent by the last measuring station. The higher pressure ratio case shows a distribution with similar trends but with less degradation in cooling performance. The larger mass of cooling which the higher pressure ratio jets provide along with the greater penetration of the jets into the free stream results in more of a thermal dilution effect.

Pressure Surface. Adiabatic film cooling measurements taken on the pressure for the low and high turbulence cases are shown in figures 5.19 and 5.20. The effectiveness distributions for the low turbulence case is given as a function of pressure ratio in figure 5.19. The data show clear structural effects due the cooling jets where gaps in effectiveness are evident and may be due to joining of adjacent jets which causes peaks and gaps in cooling protection. The peak level of effectiveness is produced by the lowest pressure ratio. The near pressure surface has a relatively low velocity and increasing pressure ratio would tend to cause increased penetration of the cooling jet. Jet lift off does not lead to good film cooling protection. Figure 5.20 shows the effectiveness distributions for the high turbulence case and the reverse trend of higher pressure ratios producing higher levels of effectiveness is present. Clearly, the high turbulence on the pressure side has a dramatic effect on the effectiveness level for the lower pressure ratios. The high pressure ratio case has effectiveness levels for the high turbulence case which are similar to the low turbulence case. The high mass flow of these jets combined with their penetration through the boundary layer must cause a thermal dilution effect which is less sensitive to the turbulent mixing. A comparison of the effectiveness distributions for the high and low turbulence cases for an equivalent pressure ratio of 0.07 is shown in figure 5.21. The difference in the level of effectiveness is dramatic and can only be attributed to the high free stream turbulence. The ratio of the local adiabatic effectiveness for the different cases for the pressure side is shown in figure 5.22. The ratios decrease with decreased pressure ratio, suggesting cooling performance is largely dependent on mass flow rate. When cooling air is well mixed with the free stream, cooling performance is largely dependent on mass flow rate.

Conclusions

The influence of mock combustor turbulence was found to have a dramatic effect on pressure surface film cooling. The process of mixing film cooling protection away in the normal direction was found to be gradual but significant based on the results from the double row of staggered holes on the pressure side, which are comparable to averaged effectiveness distributions. The high turbulence had reduced the effectiveness level to an

average of 45 percent of the low turbulence level by the last measurement location. The single row of holes on the pressure side showed a more immediate reduction in effectiveness for the lowest velocity due to spanwise mixing as evidenced by the spanwise uniformity in velocity profiles. This strong spanwise mixing is also consistent with observations by Bons, MacArthur, and Rivir (1994). The influence of turbulence on cooling protection was less substantially reduced for the higher velocity ratios of the single row where the cooling protection was already poor.

The influence of turbulence on suction surface effectiveness was seen to be more complicated due to the interaction of the free stream turbulence with the suction surface boundary layer and the boundary layers corresponding interaction with the film cooling jets. The high turbulence produced a boundary layer with significantly higher skin friction and the fuller near wall profile apparently improved effectiveness in the near hole region. Further downstream, the effect of the turbulence was seen as the cooling performance of the high turbulence case deteriorated more rapidly.

The dissipation of cooling performance by the high inlet turbulence was found to be more substantial for the showerhead array on the suction surface. This difference was probably due to the longer streamwise distance the turbulence had to act. The highest pressure ratio showed a reduced influence of the turbulence due to the thermal dilution effect of the high mass flow rate. The level of cooling protection produced by the showerhead was poor on the pressure surface and showed regions of poor coverage. With the high turbulence, the protection was driven largely by the mass flow rate.

Generally, the turbulence was found to gradually mix away cooling protection in the normal direction producing effects that could be dramatic far downstream. The turbulence dissipated protection more rapidly in the spanwise direction. The pressure surface with its higher relative level of turbulence was affected more than the suction surface. Higher blowing and velocity ratios generally were less affected than lower blowing ratios due to the thermal dilution effect of the higher mass flows. More data is needed on the pressure surface in and around the holes and for arrays located in regions of higher relative velocities.

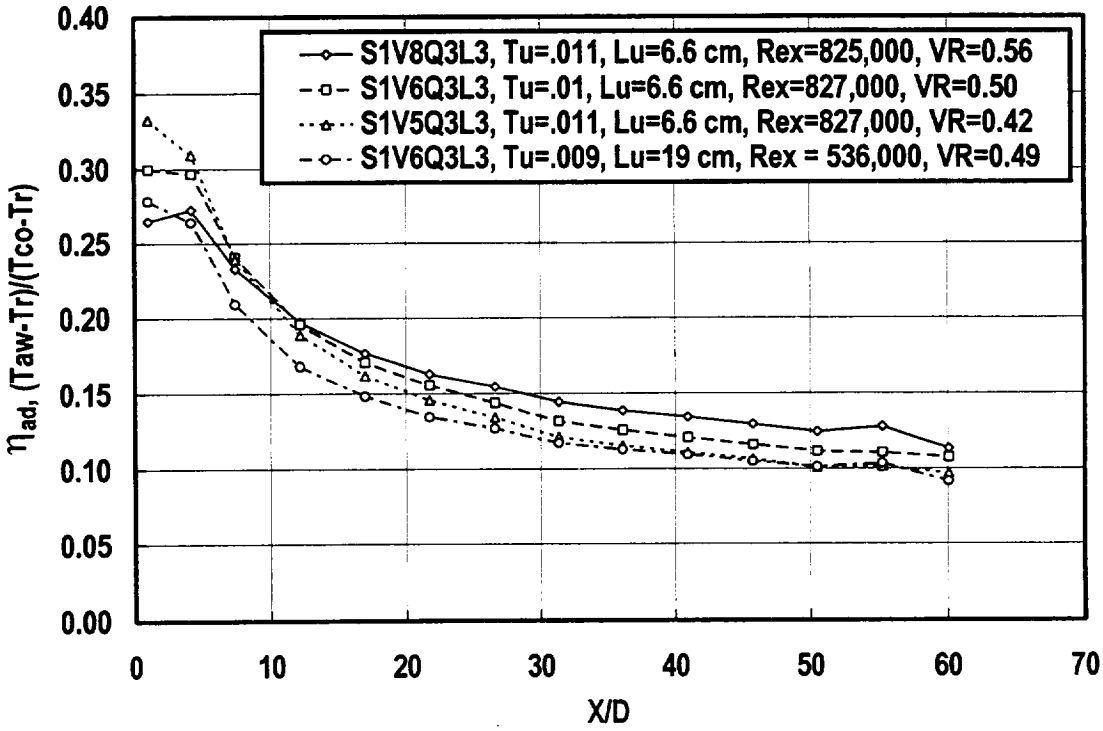

Figure 5.1 Comparison of velocity ratio and Reynolds number effects on adiabatic effectiveness, 1 row 30° suction surface, low turbulence, DR=0.94

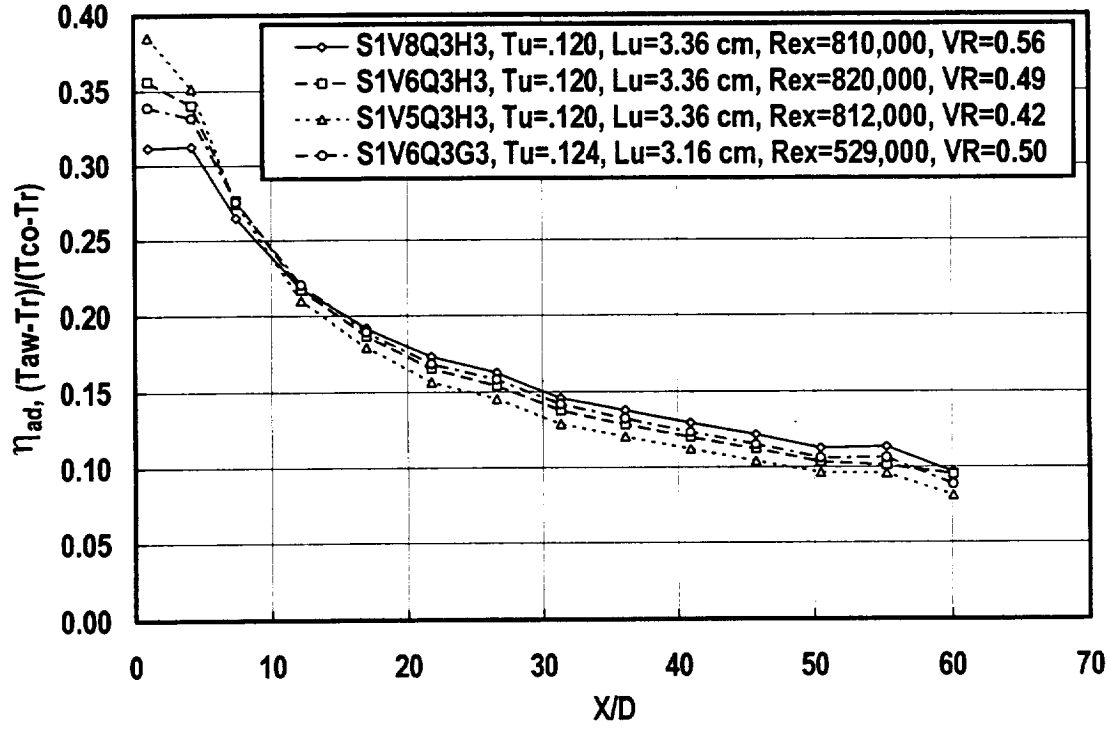

Figure 5.2 Comparison of velocity ratio and Reynolds number effects on adiabatic effectiveness, 1 row 30° suction surface, comb(1), DR=0.94

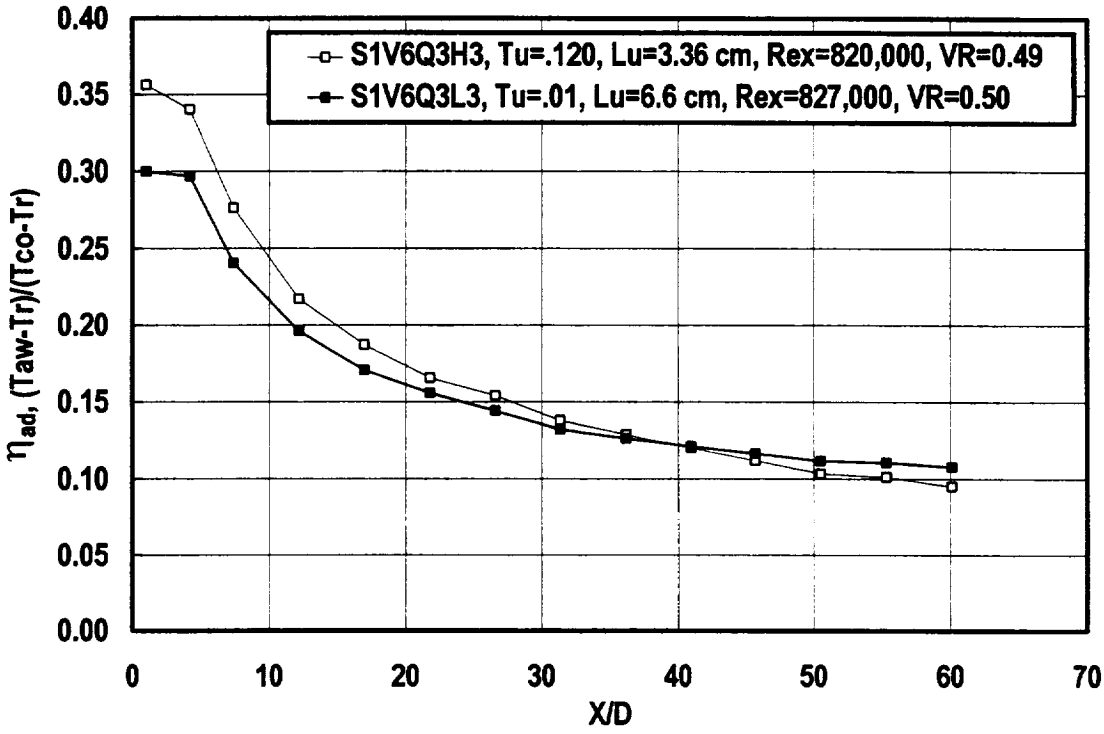

Figure 5.3 Comparison of adiabatic effectiveness with high and low turbulence, 1 row 30° suction surface, VR = 0.5, DR=0.94

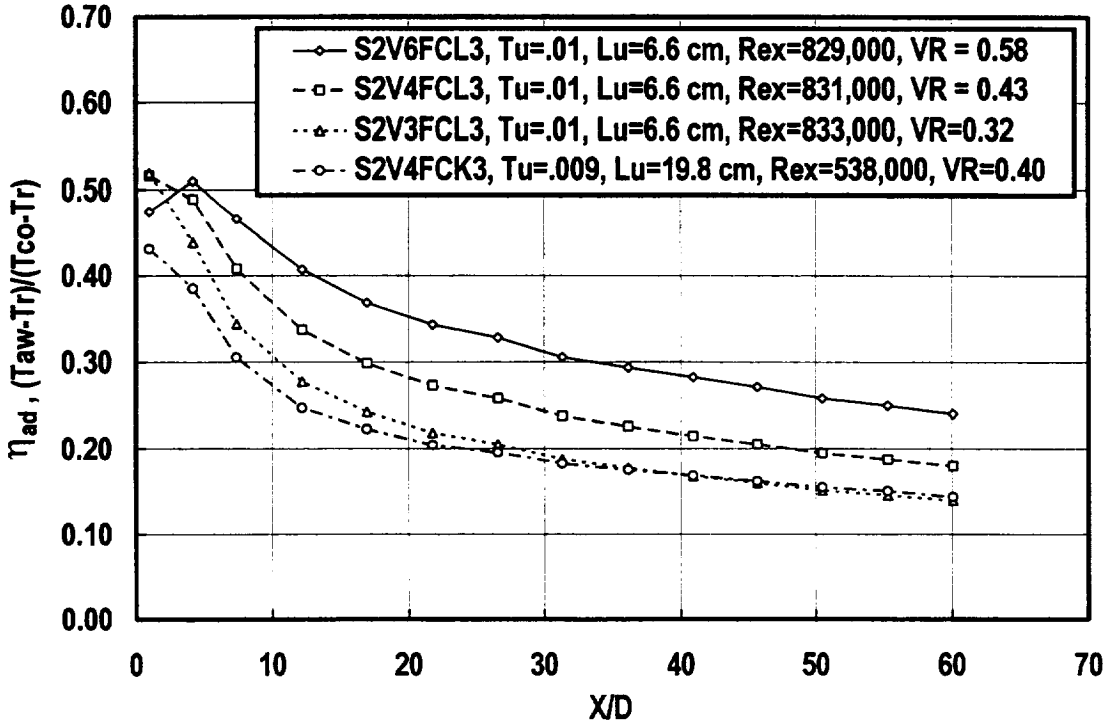

Figure 5.4 Comparison of velocity ratio and Reynolds number effects on adiabatic effectiveness, 2 rows 30° suction surface, low turbulence, DR=0.94

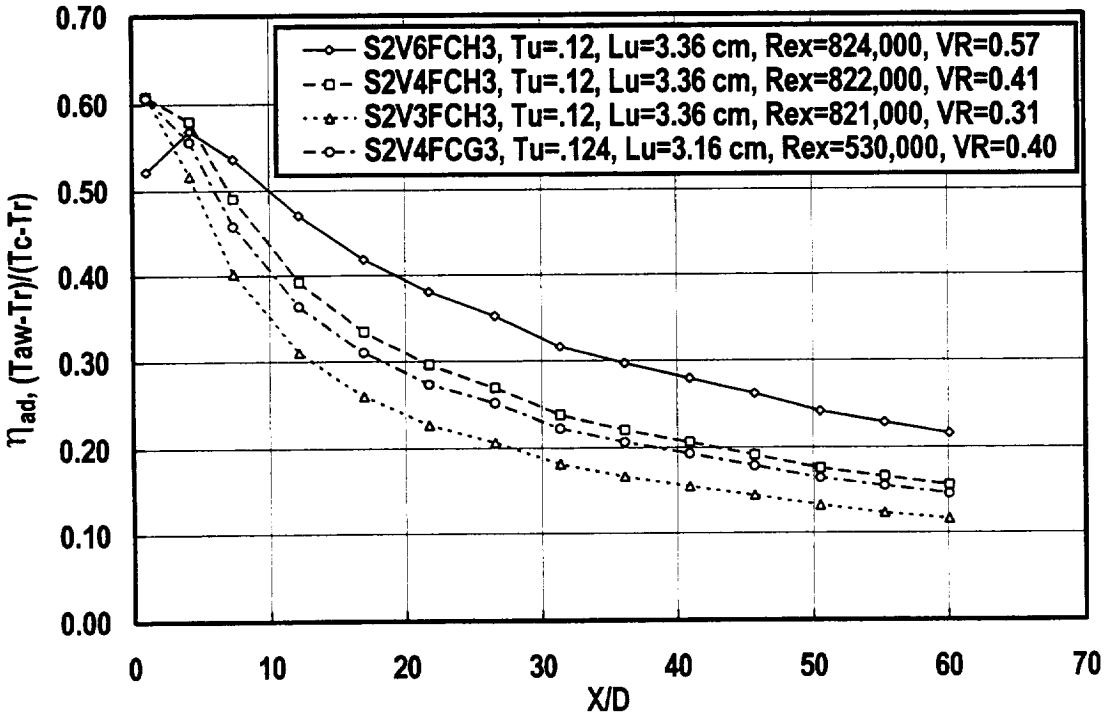

Figure 5.5 Comparison of velocity ratio and Reynolds number effects on adiabatic effectiveness, 2 rows 30° suction surface, comb(1), DR=0.94

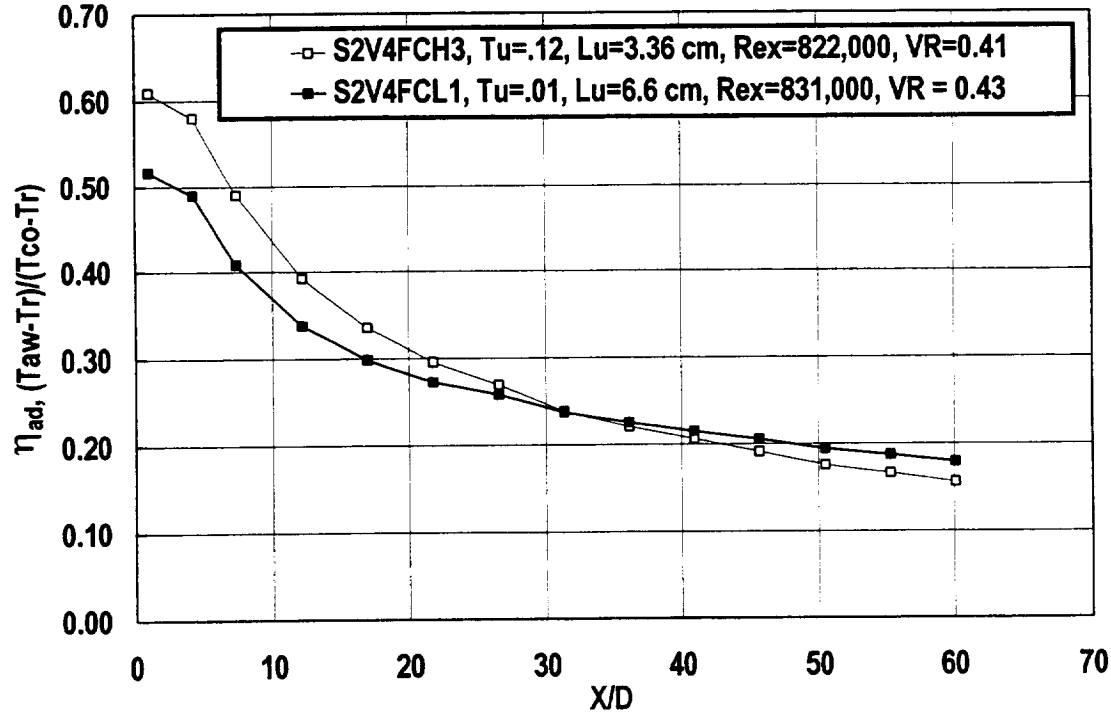

Figure 5.6 Comparison of adiabatic effectiveness with high and low turbulence, 2 rows 30° suction surface, VR = 0.42, DR=0.94

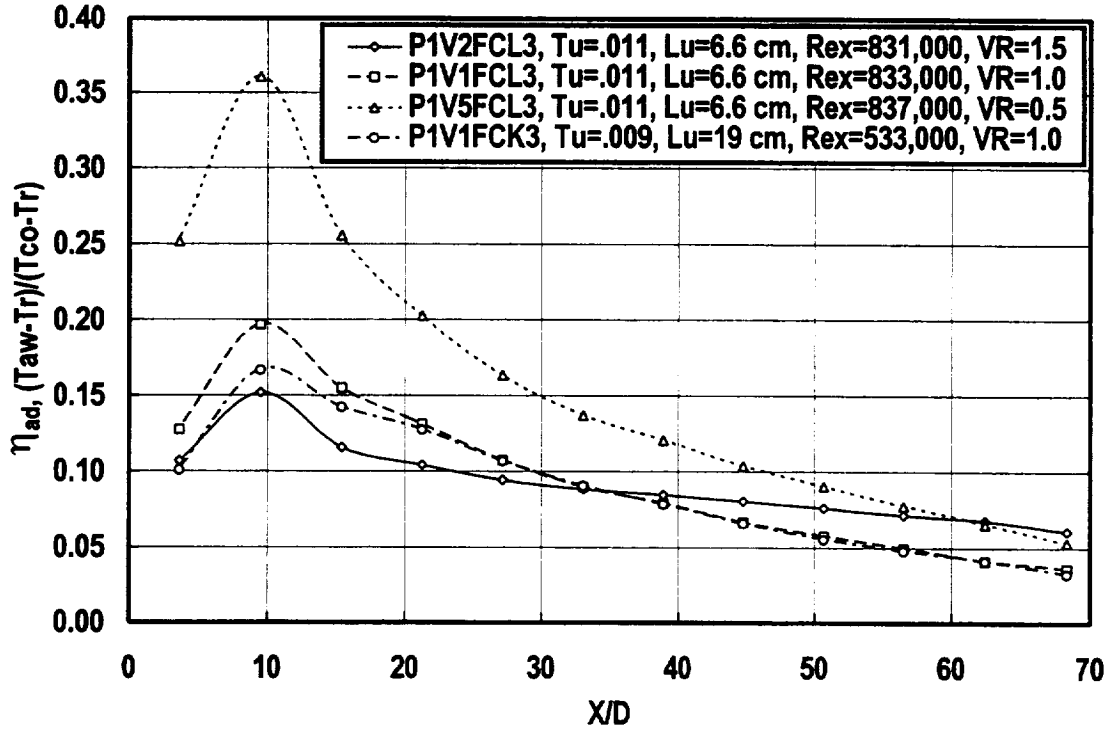

Figure 5.7 Comparison of velocity ratio and Reynolds number effects on adiabatic effectiveness, 1 row 30° pressure surface, low turbulence, DR=0.94

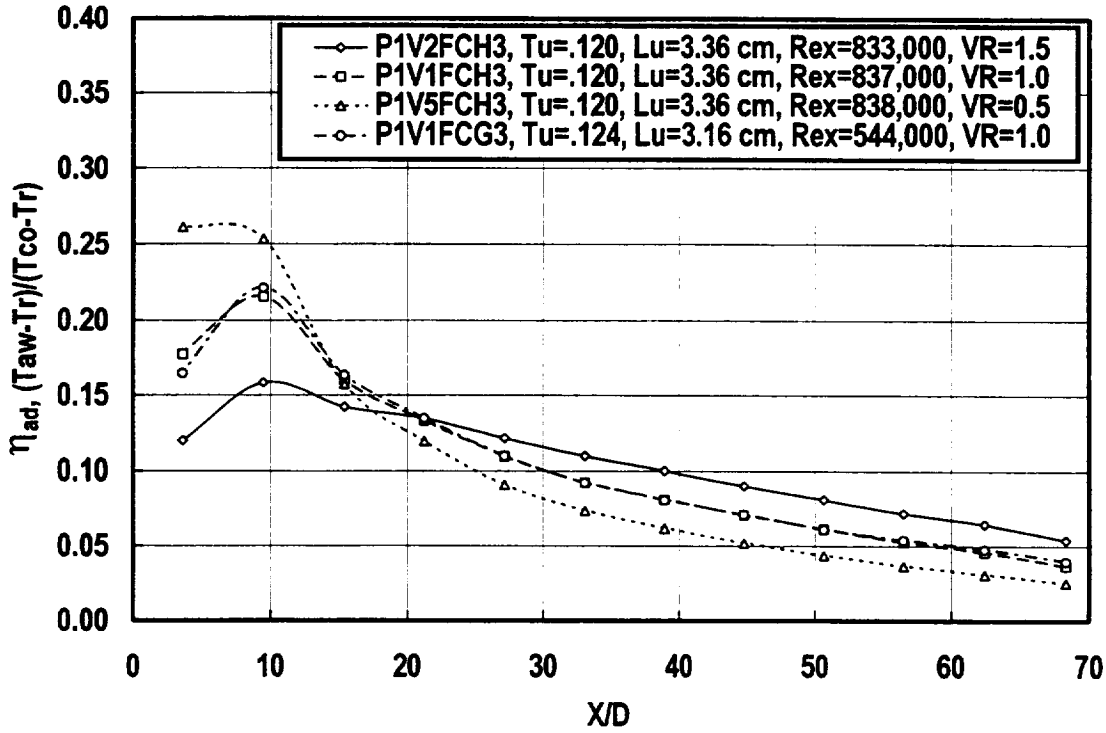

Figure 5.8 Comparison of velocity ratio and Reynolds number effects on adiabatic effectiveness, 1 row 30° pressure surface, comb(1), DR=0.94

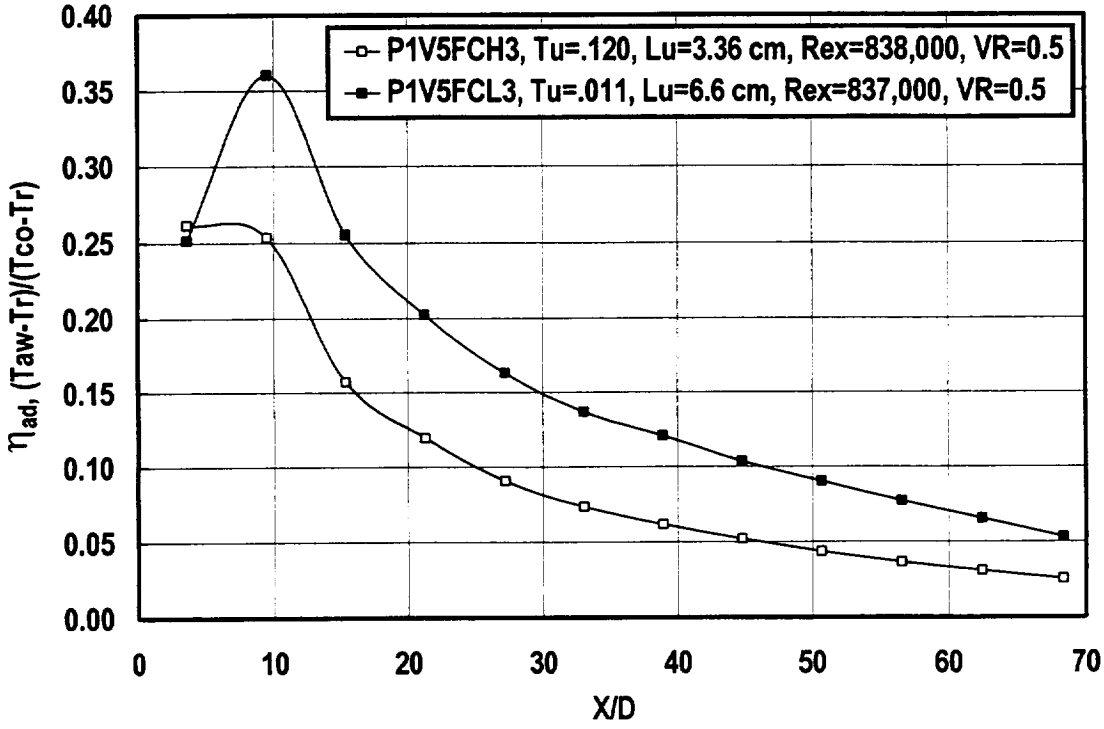

Figure 5.9 Comparison of adiabatic effectiveness with high and low turbulence, 1 row 30° pressure surface, VR = 0.5, DR=0.94

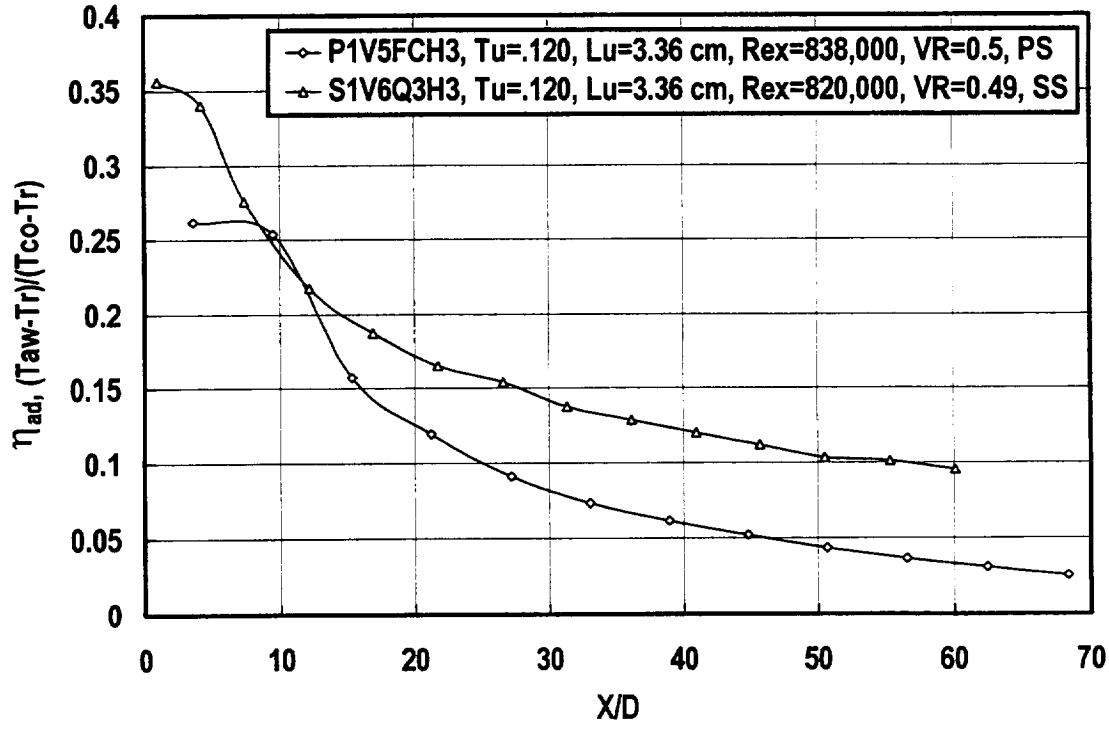

Figure 5.10 Comparison of pressure and suction surface adiabatic effectiveness, 1 row of 30° holes, P/D = 3, comb(1), DR=0.94

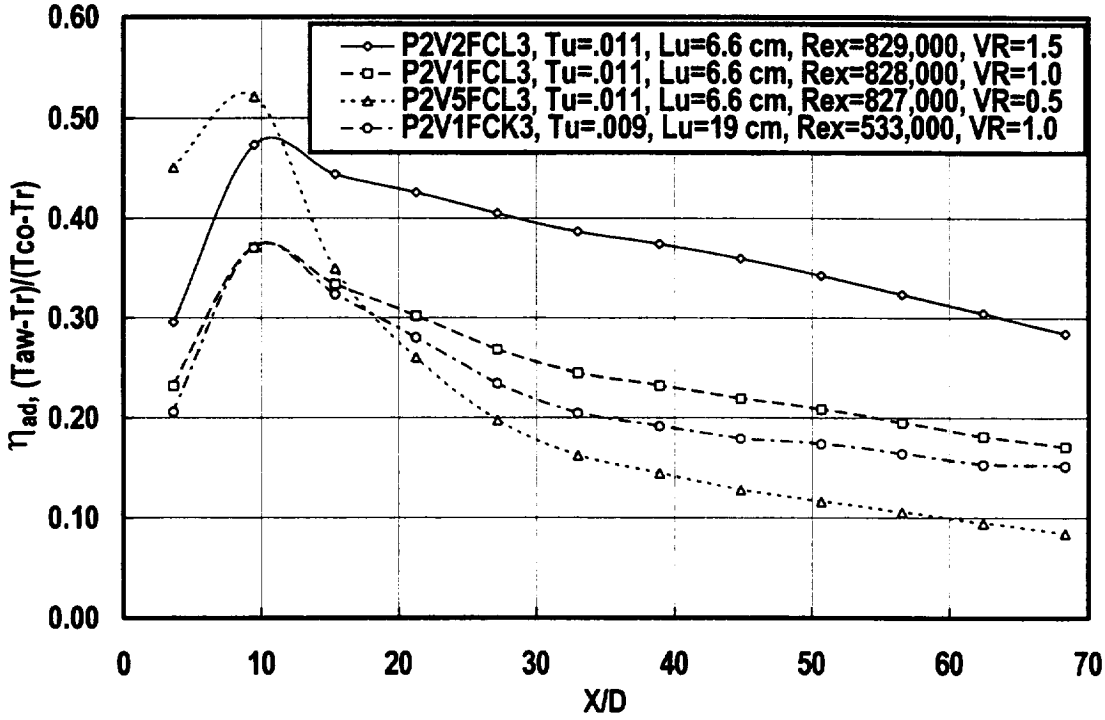

Figure 5.11 Comparison of velocity ratio and Reynolds number effects on adiabatic effectiveness, 2 rows 30° pressure surface, low turbulence, DR=0.94

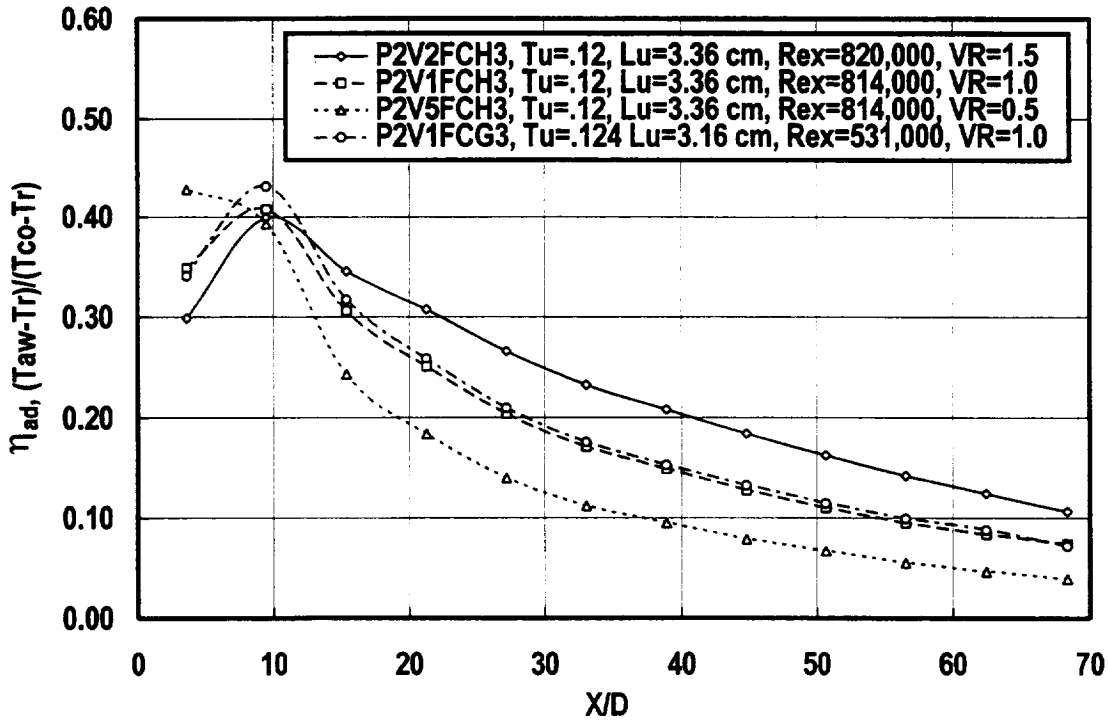

Figure 5.12 Comparison of velocity ratio and Reynolds number effects on adiabatic effectiveness, 2 rows 30° pressure surface, comb(1), DR=0.94

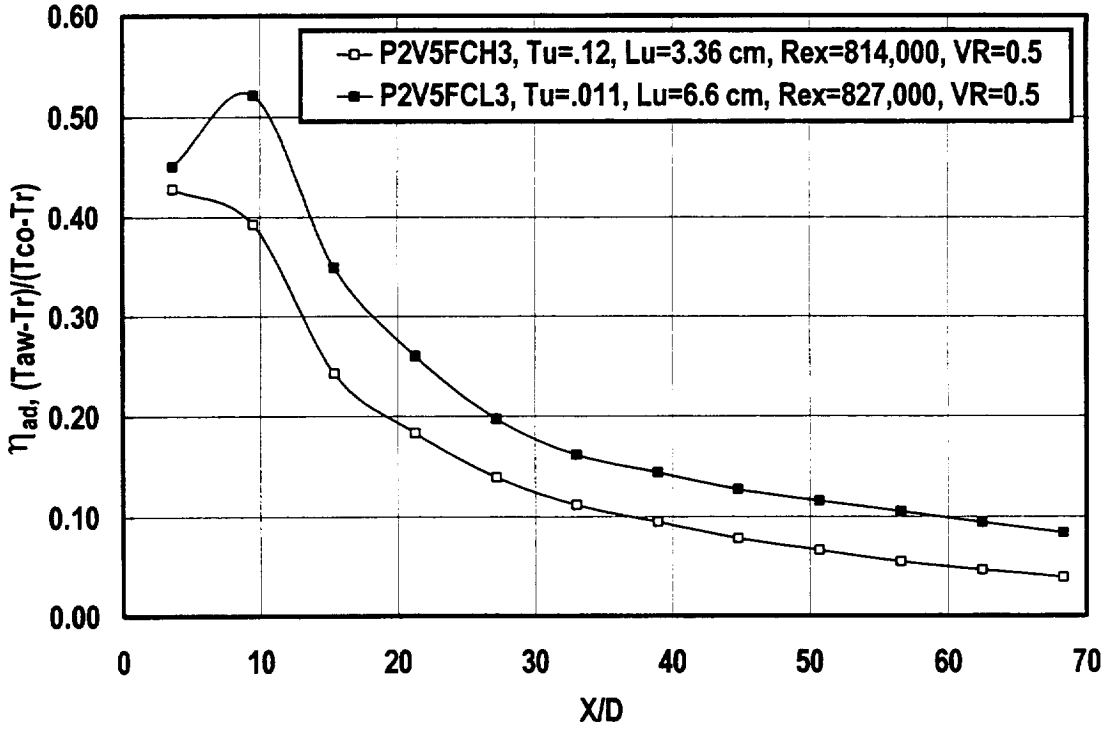

Figure 5.13 Comparison of adiabatic effectiveness with high and low turbulence, 2 rows 30° pressure surface, VR = 0.5, DR=0.94

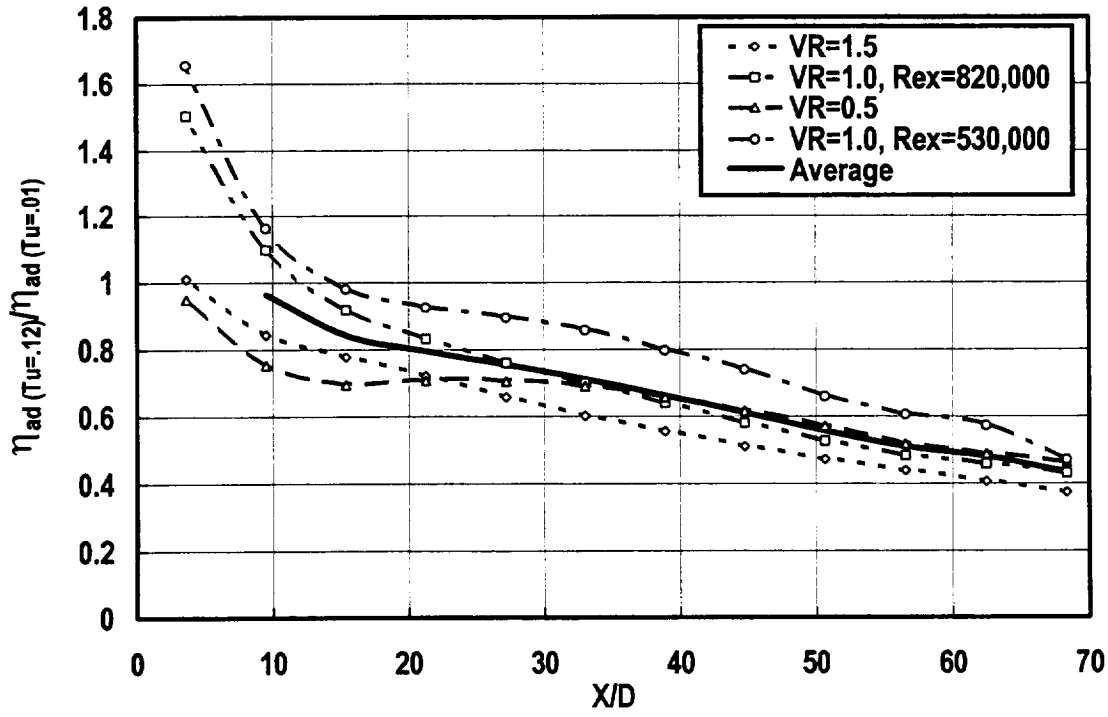

Figure 5.14 Influence of turbulence on relative level of pressure surface adiabatic effectiveness, 2 rows, 30° holes, DR = 0.94, S/D=0.3

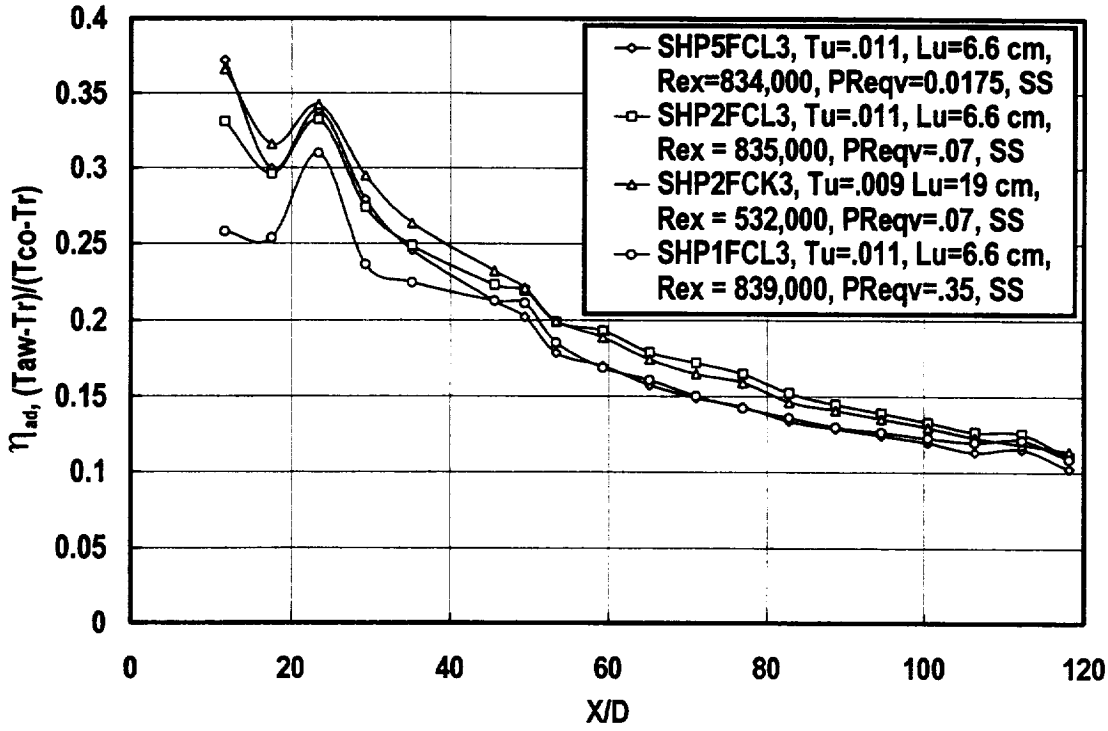

Figure 5.15 Comparison of pressure ratio and Reynolds number effects on showerhead adiabatic effectiveness, suction surface, low turbulence, DR=0.94

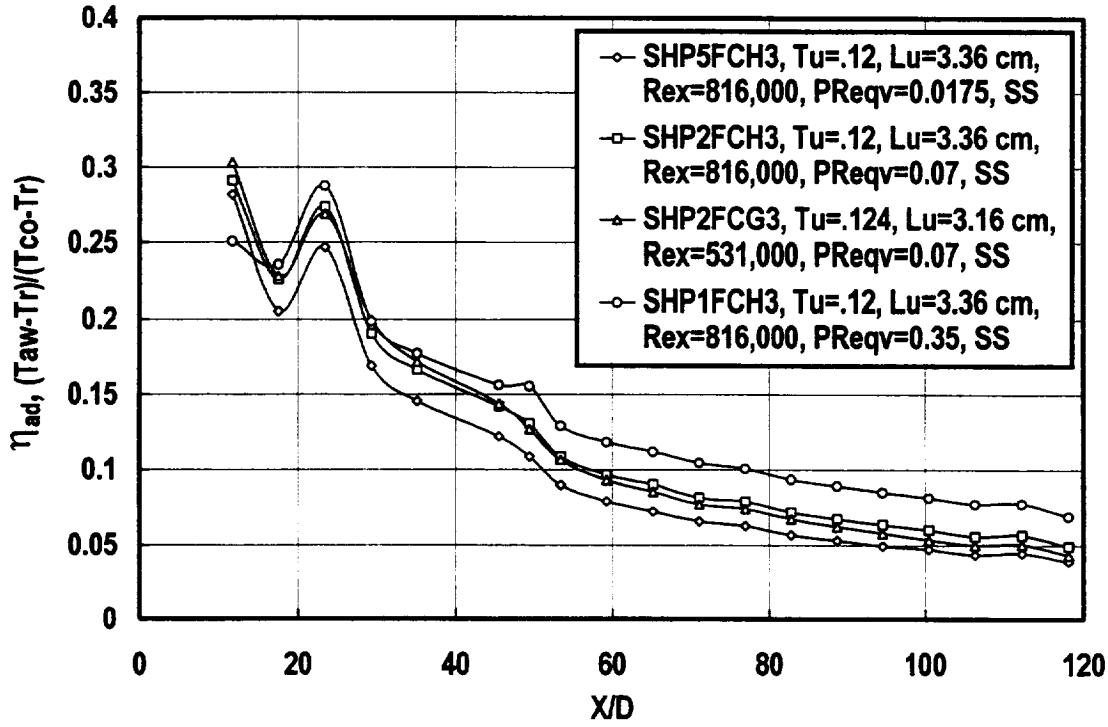

Figure 5.16 Comparison of pressure ratio and Reynolds number effects on showerhead adiabatic effectiveness, suction surface, comb(1), DR=0.94

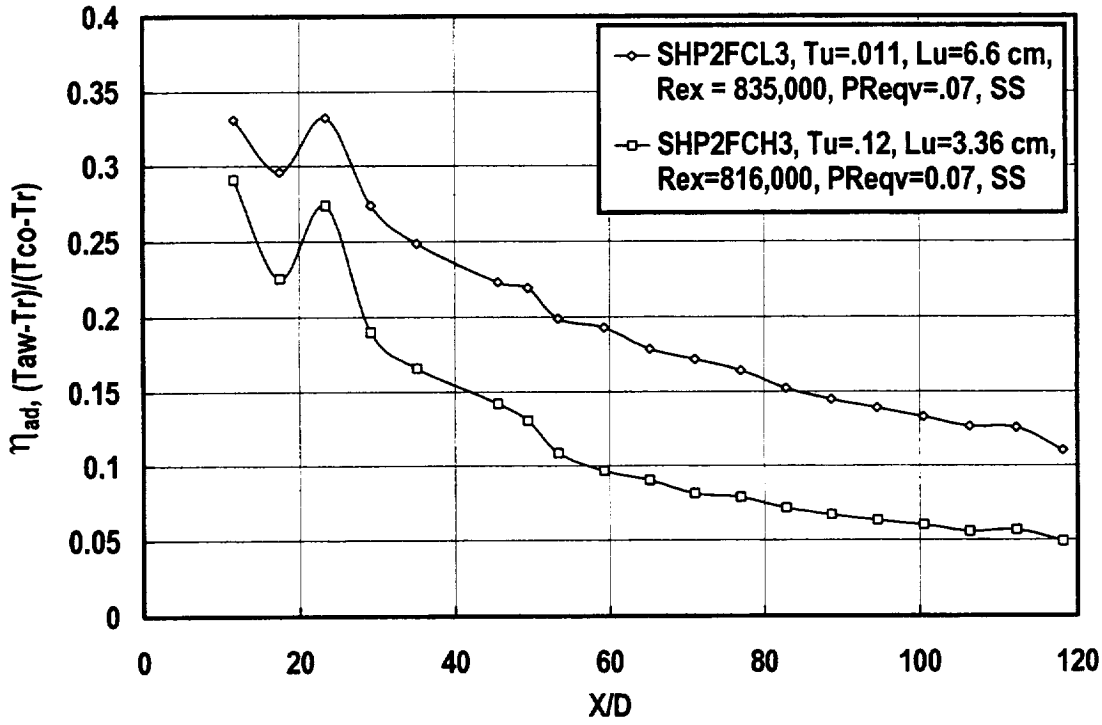

Figure 5.17 Comparison of showerhead adiabatic effectiveness with high and low turbulence, suction surface, PReqv = 0.07, DR=0.94

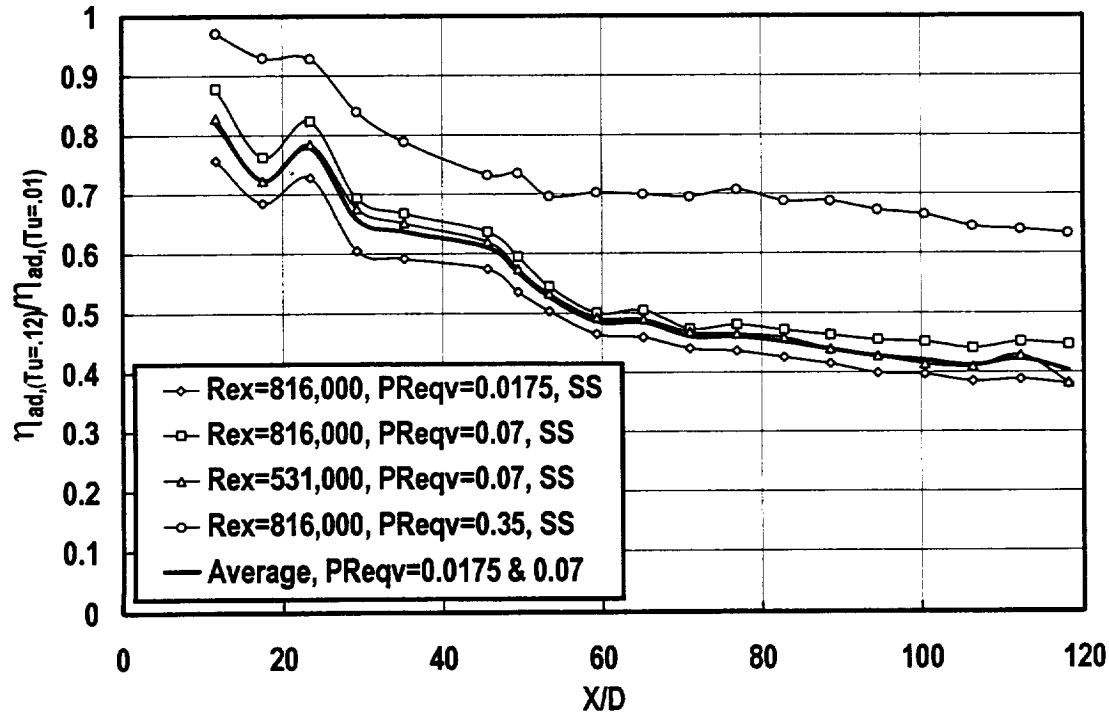

Figure 5.18 Influence of turbulence on relative level of suction surface adiabatic effectiveness for showerhead array, DR = 0.94

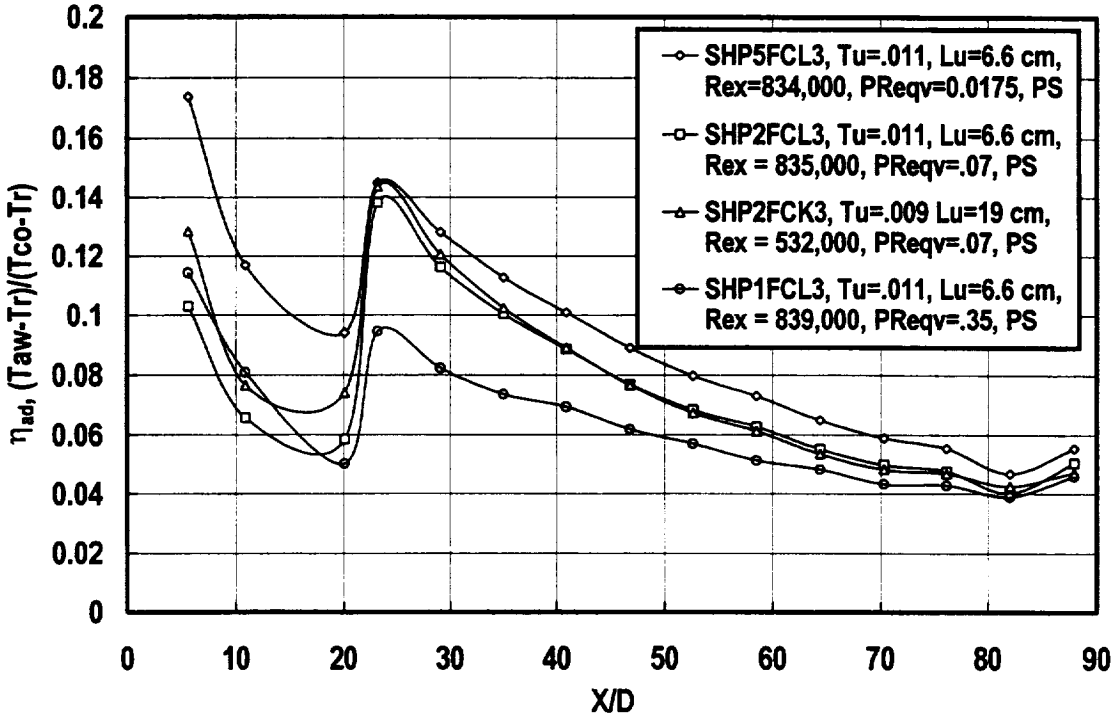

Figure 5.19 Comparison of pressure ratio and Reynolds number effects on showerhead adiabatic effectiveness, pressure surface, low turbulence, DR=0.94

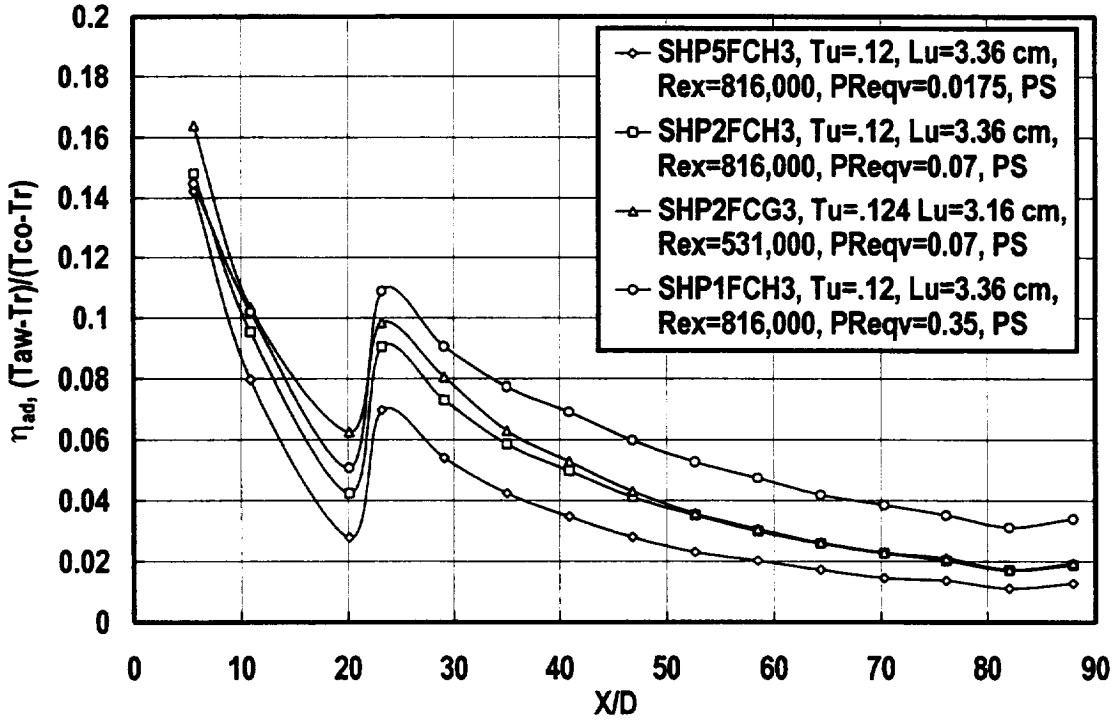

Figure 5.20 Comparison of pressure ratio and Reynolds number effects on showerhead adiabatic effectiveness, pressure surface, comb(1), DR=0.94

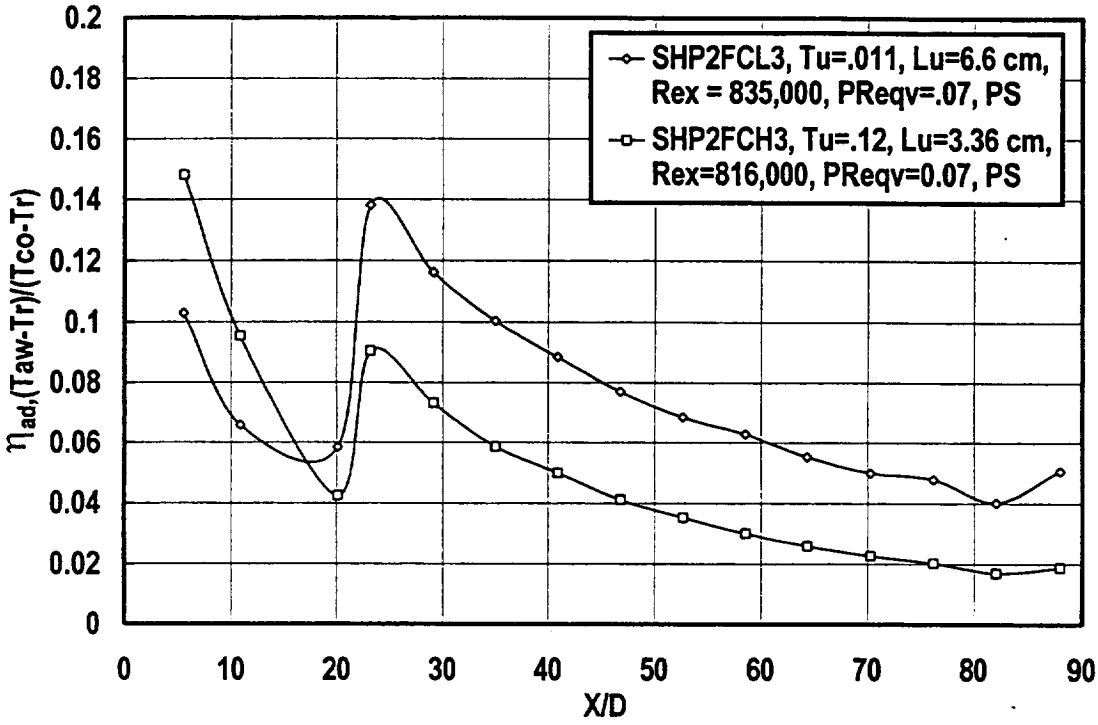

Figure 5.21 Comparison of showerhead adiabatic effectiveness with high and low turbulence, pressure surface, PReqv = 0.07, DR=0.94

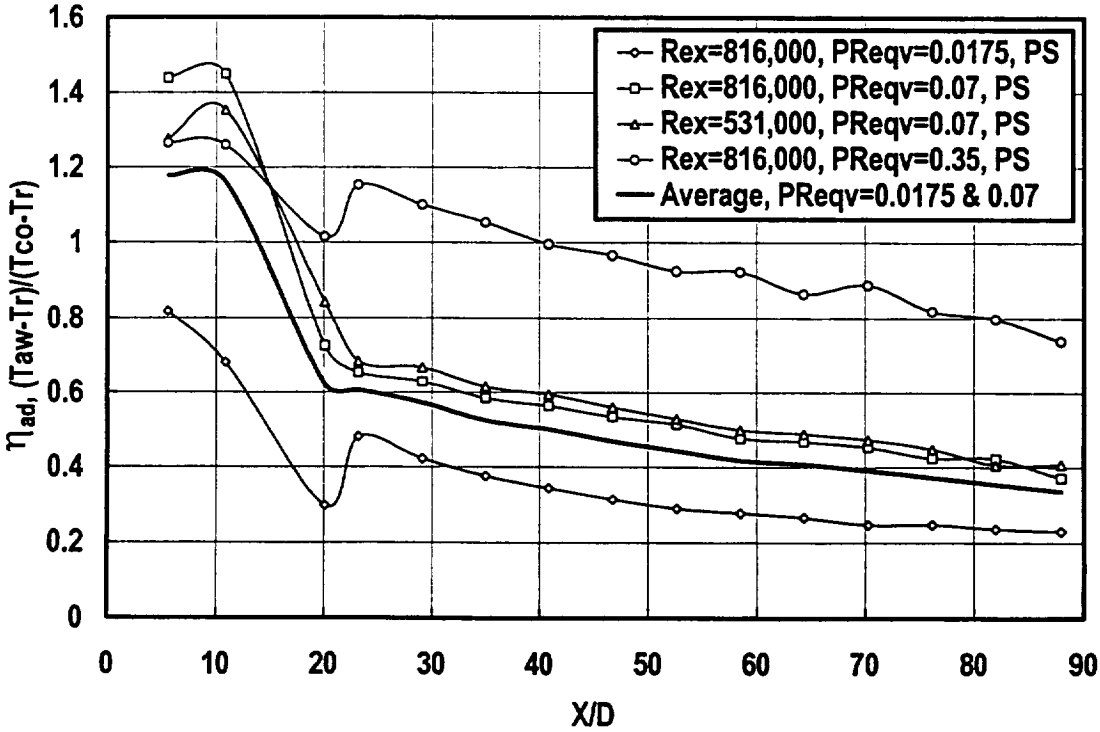

Figure 5.22 Influence of turbulence on relative level of pressure surface adiabatic effectiveness for showerhead array, DR = 0.94

Chapter Six

Velocity Profiles with Film Cooling

This chapter examines the interaction of turbulence and discrete hole film cooling on the pressure and suction surface boundary layers. Velocity profiles downstream from film cooling arrays are documented in this chapter for the various geometries, turbulence conditions, and velocity ratios investigated. These measurements were made to provide details of the interaction of turbulence and film cooling with vane surface boundary layer development. These data offer both qualitative information which aids in understanding how turbulence affects film cooling and also how film cooling alters surface heat transfer. Additionally, the velocity and turbulence distributions have value for grounding predictive comparisons of the velocity field.

All the velocity profiles were taken with a subminiature single wire probe with an active length of about 25 mm and a diameter of 2.5 microns. On the pressure surface all the measurements were taken the equivalent of nine hole diameters from the downstream edge of the last row of holes. The arc that the probe made from the pressure surface, pivoting around pivot port 1 is shown in figure 6.1. On the suction surface all the profiles were taken the equivalent of 12 diameters from the downstream edge of the last row of holes. The arc that the probe made for the suction surface pivoting around pivot port 5 is also given in figure 6.1. Turbulence profiles and some spectra were taken in addition to the velocity profiles and the data are detailed in appendices A.4 and A.5. The profiles were taken by first traversing from the wall after placing the probe as visually close as possible using the reflection of the probe on the vane surface. Next, the probe was traversed from a position of about 0.10 cm above the surface toward the surface in approximately 0.0254 mm steps until the probe touched the surface. Contact with the surface was determined by a substantial reduction in the near wall velocity gradient. The absolute Y location for the turbulence boundary layers on the suction surface was determined by using the Ludwieg - Tillman correlation [as adapted by White (1974)] for estimating skin friction and fitting the nearest couple of points in the profile to a canonical sublayer distribution. The average velocity gradient in the channel from the maximum velocity to the region just outside the pressure surface was used to estimate the variation in the wall potential velocity due to streamline curvature in the channel.

The job of estimating the absolute position on the pressure surface was much more difficult. Due to the acceleration, turbulence, and film cooling the boundary layer developing on the pressure surface does not compare well with a typical Blasius laminar boundary layer. For the low turbulence base vane case, the boundary layer could be fit to a calculated profile but with high turbulence and/or the addition of film cooling air no such tool could be used. Typically, the absolute Y position was specified by using the gradient of the two points prior to contact with the surface and extrapolating the gradient

to the surface. The absolute Y position of the pressure surface boundary layer is probably over estimated by an increment ranging from 0.025 to 0.04 mm.

In this chapter comparisons of velocity profiles taken at different spanwise locations are given for the various velocity ratios for both the single and double row of film cooling. On the suction surface profiles were only taken for a velocity ratio of 0.5, since all the velocity ratios are in the same regime of flow. For the showerhead cooling arrays, only one profile for each pressure ratio was taken. These velocity profiles are believed to be representative for the high turbulence case but a significant spanwise variation may exist for the low turbulence case. In addition to the velocity profiles, turbulence profiles were also taken. Comparisons are shown in this chapter for the suction surface boundary layers and the pressure surface fluctuating velocity distributions are documented in Appendix A.4.

Suction Surface Velocity Profiles with Film Cooling and Turbulence Effects

The velocity ratio of film cooling on the suction surface of a first stage vane is typically on the order of 0.5. This velocity ratio is due to the ratio of available coolant to inlet total pressures, the inlet to coolant temperature ratio, the Cd of the film cooling hole, and the local surface static pressure. Since these variables do not change greatly the variation of relevant velocity ratios for suction surface film cooling is not large. A coolant to gas velocity ratio of 0.5 was selected for study and is representative of the entire range.

A comparison of the base vane velocity profile for the high and low turbulence case is shown in figure 6.2. The profiles show that the near wall velocity gradient is higher for the high turbulence case due to the enhanced mixing by the turbulence. Also, the estimated momentum thickness Reynolds number is about six percent higher for the low turbulence case while the skin friction estimated from the momentum thickness Reynolds number and shape factor is 16 percent higher for the high turbulence case. This comparison indicates that the flow field turbulence which is on the order of four percent for the high inlet turbulence case, significantly augments the skin friction, indicating the turbulence has a substantial effect on the developing boundary layer.

A comparison between the base vane profile and three film cooling boundary layer profiles is shown in figure 6.3 for the low turbulence case with a single row of 30° holes with a pitch to diameter ratio of 3. The profile downstream from the hole (Z/D = 0) shows a large velocity deficit and a low level of skin friction. The blockage by the film cooling jet results in an enhancement to the skin friction for the profiles in between the holes at Z/D positions of 0.75 and 1.50. These profiles also have a slightly larger velocity deficit than the baseline profile as indicated by their momentum thickness Reynolds number. The profiles for the comparable case with high free stream turbulence are shown in figure 6.4. Unlike the low turbulence case, the profiles at Z/D's of 0.0 and 0.75 are quite similar indicating mixing has redistributed the velocity deficit in the spanwise

direction. The momentum thickness Reynolds number at Z/D of 1.5 indicates spanwise mixing has redistributed some low momentum fluid to the centerline as well.

A comparison of u' fluctuating velocity profiles for the three spanwise film cooling profiles and the base vane profile is shown in figure 6.5 for the low turbulence case. The base vane profile and the profile taken at a Z/D of 1.5 are nearly identical and give evidence that spanwise mixing has had no effect at this Z/D location. The profile at a Z/D of 0.75 does show an increase in the turbulence level in the outer region of the boundary layer indicating that turbulent mixing is beginning to effect this portion of the profile. Finally, in the region downstream from the film cooling jet, the turbulence is strongly elevated at a Y of around 0.18 cm due to the mixing layer developing between the film cooling jet and the free stream. Figure 6.6 shows a comparison of u' profiles for the high turbulence case. Again, the base vane profile is compared with the three spanwise profiles with film cooling. Similar to the velocity profiles shown in figure 6.4, the turbulence profiles at Z/D locations of 0.0 and 0.75 are very uniform indicating spanwise mixing has redistributed the velocity deficit in the spanwise direction over this range. The turbulence profile at a Z/D of 1.5 shows a level between the base vane and the other two profiles indicating the spanwise mixing has significantly affected this profile also. The u' profile is elevated over the region between 0.05 cm and 0.3 cm due to the development of the mixing layer and is augmented by the free stream turbulence. For the high inlet turbulence case the mid profile peak in u' is closer to the wall because the large scale motions acting on the boundary layer have already mixed away a good portion of the velocity deficit in the spanwise and normal directions leaving the steepest portion of the gradient closer to the wall as compared to the low turbulence case.

A comparison between the base vane profile and three film cooling boundary layer profiles is shown in figure 6.7 for two staggered rows of holes. The hole to hole spacing in terms of diameters is three. The profiles directly downstream from the film cooling holes show a significant velocity deficit. The profile at a Z/D of 0.75 remains relatively unaffected by the film cooling jets in terms of its velocity deficit. The skin friction coefficient for this profile is noticeably elevated over the two downstream from holes. Figure 6.8 shows a comparison between the base vane profile and three profiles downstream from 2 rows of film cooling with the high inlet turbulence level. Unlike the low turbulence profiles all the film cooling profiles are similar due to the spanwise mixing enhanced by the external turbulence.

A comparison of u' turbulence profiles for the three spanwise film cooling profiles and the base vane profile with low inlet turbulence and two rows of holes is shown in figure 6.9. The base vane profile and the profile taken at a Z/D of 0.75 show similar trends but the elevated level of turbulence associated with the Z/D of 0.75 profile gives evidence of some production due to spanwise mixing. Finally, in the profiles downstream from the film cooling holes (Z/D of 0 and 1.5) the turbulence is strongly elevated but the peaks are dependent on the velocity gradients where production occurs. Figure 6.10 shows a comparison of u' profiles for the high turbulence case for two rows of holes. Again, the base vane profile is compared with the three spanwise profiles with

film cooling. Similar to the velocity profiles shown in figure 6.8, the turbulence profiles are all very uniform indicating spanwise mixing due to the free stream turbulence has efficiently redistributed the velocity deficit. The turbulence profiles all show broad peaks in u' away from the wall due to the production associated with the mixing layer which is additionally augmented by the free stream turbulence.

Pressure Surface Velocity Profiles with Film Cooling and Turbulence Effects

The velocity ratios chosen to study for the pressure surface film cooling were the same for the heat transfer and film cooling tests. Velocity ratios for film cooling are bound by the coolant and gas conditions and vane geometries. The static pressure on the pressure surface of a vane can vary significantly between the stagnation region and the trailing edge allowing for a wide range of velocity ratios. Velocity ratios of 0.5, 1.0, and 1.5 were chosen to provide a full range of mixing regimes (wake, equal velocity, and jet) with respect to the free stream.

One Row of Pressure Surface Holes. A comparison of the base vane velocity profiles with low and high inlet turbulence levels are shown in figure 6.11. The profiles indicate that the near wall velocity gradient is significantly higher for the high turbulence case compared to the low turbulence case. This higher near wall gradient is consistent with the higher level of heat transfer determined for the high turbulence level case. The location of the traverse points relative to the surface of the vane was determined by extrapolating the velocity gradient to the surface. Due to the acceleration and the turbulence this methodology results in an uncertainty as large as 0.004 cm. The measured velocity profile for the low turbulence condition is compared to a laminar finite difference calculation along the vane in figure 6.12. Once the absolute position of the measured velocity profile is set, it compares closely with the calculated profile. Setting the position of the profile with the largest near wall gradient has been found to significantly underestimate the shear stress. The streamwise velocity gradient is responsible for creating a significant change in the near wall velocity gradient. However, the location of the incremental velocity profile must be set by some methodology and extrapolating the near wall velocity gradient was chosen for convenience.

Velocity profiles for a single row of holes are shown in figures 6.12 and 6.13 for a velocity ratio of 1.5 with low and high inlet turbulence respectively. Similar to the suction surface data, figure 6.13 shows a comparison of three velocity profiles at different spanwise locations (in line with the hole, Z/D=0; between two holes, Z/D=1.5; and at the quarter spacing location , Z/D=0.75). The low turbulence base vane profile is also shown for comparison. The centerline profile (Z/D=1.5) shows a substantial mass addition, the bulk of which is well above the surface of the vane. The location of the bulge together with the relatively weak near wall velocity gradient indicates that the film cooling jet has separated from the surface. The profile at a Z/D of 0.75 also shows a peak in the velocity gradient but one which is much closer to the surface. This velocity overspeed is believed to be due to the acceleration of the free stream fluid around the blockage caused by the jet. The velocity profile near the wall is very steep indicating that the acceleration of

fluid has enhanced the skin friction in this region. The velocity profile at a Z/D of 1.5 in the middle of the two jets also shows a steeper near wall velocity gradient compared to the laminar profile and even shows a slight increase in velocity do to jet blockage. The spanwise variation in the velocity profile clearly indicates the film cooling jet has caused vorticity in the boundary layer. A comparison of the three velocity profiles for the high turbulence case is shown for the three spanwise locations in figure 6.14. The high turbulence base vane profile is also shown for comparison. The three profiles are surprisingly similar in contrast with the low turbulence case indicating the strength of the mixing. The close similarity of the profiles implies that the spanwise uniformity of the film cooling protection has improved with the mixing as well. The mass addition is clearly seen by the comparison with the base vane profile. The contrast between the low and high turbulence cases shown in figures 6.12 and 6.13 demonstrates the importance of the turbulence boundary condition in assessing the quality of the film cooling coverage and the augmentation of the heat transfer.

Velocity profiles for the low and high turbulence conditions are shown for a velocity ratio of 0.5 in figures 6.14 and 6.15. Figure 6.15 shows a comparison of the three film cooling velocity profiles with the base vane profile at low turbulence. Downstream from the jet, the velocity profile shows the influence of the film cooling. The jet, which is indicated by the velocity deficit, appears to be confined to a region of about one diameter above the surface. In the very near wall, the velocity profile looks consistent with the profiles at the other spanwise positions showing no indication of liftoff. The other spanwise positions show little influence from the jet. Additionally, the near wall velocity gradient appears to be a bit steeper for the three film cooling profiles when compared to the base vane profile. A comparison of the three film cooling velocity profiles with the base vane profile for the turbulence case is shown in figure 6.16. The spanwise uniformity of the three film cooling velocity profiles is quite good and the only contrast to the base vane profile is the small velocity deficit in the near wall region. Similar to the 1.5 velocity ratio, the difference between the high and low turbulence film cooling velocity profiles is dramatic.

The velocity profiles for the low and high turbulence conditions are shown for a velocity ratio of 1.0 in figures 6.16 and 6.17. The comparison of the three spanwise velocity profiles along with the base vane profile for the low turbulence condition is shown in figure 6.17. The profile downstream from the cooling hole shows a small bulge from the mass addition and a weaker near wall velocity gradient indicating jet liftoff has occurred. The very near wall comparison between the downstream profile and the other two spanwise profiles indicate that the jet blockage has introduced a significant level of vorticity into the boundary layer. Additionally, the near wall velocity gradients for of the off span profiles are steeper than the base vane profile gradient indicating the acceleration around the blockage has enhanced the skin friction. The excellent spanwise uniformity of the three high turbulence profiles is shown in figure 6.18. The film cooling profiles show evidence of mass addition when compared to the base vane profile. Again, the difference between the high and low turbulence film cooling velocity profiles shows the dramatic enhancement to mixing as a result of the external turbulence.

Two Staggered Rows of Holes. Velocity profiles for two rows of staggered holes and a velocity ratio of 1.5 are shown for the low and high turbulence conditions in figure 6.19 and 6.20. The three spanwise locations for the low turbulence condition are shown in figure 6.19. The velocity profiles taken downstream from the two rows of holes (Z/D = 0.0 and 1.5) show weaker near wall velocity gradients than the profile at a Z/D of 0.75 indicating some separation from the surface has occurred. The profile at Z/D of a 0.75 also shows a significantly higher velocity than the baseline case due to the acceleration around the blockage from the jets. The profile downstream from the upstream hole (Z/D=1.5) shows a peak velocity well away from the wall which suggests that its trajectory is affected by the second row of holes. The spanwise comparison of the three velocity profiles taken with high turbulence are shown for a velocity ratio of 1.5 in figure 6.20. The uniformity due to the spanwise mixing as well as the mass addition of the high velocity ratio jets is evident.

The spanwise comparison for the velocity ratio of 0.5 is shown for the low turbulence condition with two rows of holes in figure 6.21. The profiles downstream from the holes show velocity deficits and weaker near wall gradients. The downstream row has a lower velocity than the upstream row. Since the downstream row has a lower static pressure, more losses are generated across the holes while the upstream row has a short pressure gradient accelerating it. The profile at a Z/D of 0.75 has a steeper near wall gradient than the baseline profile but otherwise appears reasonably unaffected by the film cooling. The spanwise comparison of the three velocity profiles taken with high turbulence are shown for a velocity ratio of 0.5 in figure 6.22. The spanwise mixing produces excellent uniformity and the velocity deficit is apparent in contrast with the base vane profile.

The three velocity profiles for a velocity ratio of 1.0 are shown in figure 6.23 for the low turbulence condition with two rows of holes. The velocity profiles downstream from the holes show weaker near wall gradients than the profile at Z/D=0.75. Again, the downstream row has a lower velocity than the upstream row due to higher losses in the cooling holes. The profile at a Z/D of 0.75 is much fuller than the base vane profile and the near wall velocity differences indicates that significant vorticity exists in the boundary layer. The spanwise comparison of the three velocity profiles taken with the high turbulence condition are shown for a velocity ratio of 1.0 in figure 6.24. Again, the spanwise mixing produces excellent uniformity differing from the base vane profile with a steeper near wall velocity gradient.

All the comparisons of pressure surface velocity profiles for the high turbulence condition showed good spanwise uniformity due to the aggressive free stream turbulence enhanced mixing by the measurement point, an X/D of 9. Bons, MacArthur, and Rivir found that the jets from a single row of holes with a pitch to diameter ratio of three had merged by an X/D of 10. This evidence indicates that the high turbulence, in addition to dissipating cooling coverage in the normal direction also enhances the spanwise uniformity of effectiveness. Based on the analogy between momentum and thermal

energy transfer, these data indicate that the turbulence mixing of the high turbulence case has averaged out the film cooling protection on the pressure surface by an X/D of 9.

Velocity Profiles with Showerhead Cooling and Turbulence Effects

Showerhead cooling arrays are typically fed by a common plenum and the surface static pressure distribution across the five rows varies considerably. A typical coolant total to inlet total pressure ratio for a vane might be 1.02. For an exit Mach number of 0.7 this pressure ratio would equate to an equivalent pressure ratio {(Pc-Pt)/(Pt-Ps,ex)} of 0.07. Equivalent pressure ratios of 0.0175 and 0.35 were also chosen for investigation which correspond to coolant to inlet pressure ratios of 1.005 and 1.10 for a vane with an exit Mach number of 0.7.

Suction surface velocity profiles. Velocity profiles were taken at a location 59 diameters downstream from the last row of showerhead holes on the suction surface. The profiles for the low turbulence condition are shown in figure 6.25 in comparison with the base vane profile. The three profiles with showerhead cooling all show lower skin friction coefficients than the base vane profile but the base vane profile has a higher momentum thickness Reynolds number than all but the highest blowing ratio profile. This effect on the momentum thickness is interesting since the showerhead array would be expected to introduce low momentum fluid into the boundary layer. This effect may be due to a spanwise variation in boundary layer thickness due to the geometry of the showerhead array. The velocity profiles for the high turbulence condition and various pressure ratios, along with the base vane profile, are shown in figure 6.26. In comparison with the low turbulence case, the skin friction is higher in all cases. The momentum thickness Reynolds number is shown to grow substantially over the base vane value for all three pressure ratios. The base vane profile for the high turbulence case has a lower momentum thickness Reynolds number than the low turbulence base vane profile indicating that the turbulence changes the development of the boundary layer profile. The skin friction estimate for all cases was made using the Ludwieg-Tillman correlation.

Normal distributions of the streamwise fluctuating velocity, u', are shown for the low turbulence case over the various pressure ratios and for the base vane in figure 6.27. The highest pressure ratio shows an elevated level of turbulence while the extent of the u' distributions for the lower pressure ratios is consistent with comparatively thinner boundary layers than the base vane. The fluctuating velocity profile for the high turbulence condition is shown for the three showerhead pressure ratios and the base vane in figure 6.28. The profiles look consistent showing typical variations expected with this range of momentum thickness Reynolds numbers.

Pressure Surface Velocity Profiles. Velocity profiles were taken at a location 28 diameters downstream from the last row of showerhead holes on the pressure surface. The profiles for the low turbulence condition are shown in figure 6.29 in comparison with the base vane profile. The three profiles with showerhead cooling all appear to have steeper near wall velocity gradients indicating higher skin friction coefficients than the

base vane profile. Again, the Y position of these velocity profiles was determined by extrapolating the velocity gradient of points two and three to the vane surface. This procedure is known to overestimate the Y starting location of the points. The velocity profiles for the high turbulence condition and various pressure ratios along with the base vane profile are shown in figure 6.30. Due to the uncertainty of the Y location placement the data do not clearly show any significant difference.

Normal distributions of the streamwise fluctuating velocity, u', are shown for the low turbulence case over the various pressure ratios across the showerhead array and for the base vane in figure 6.31. The highest pressure ratio shows an elevated level of turbulence through most of the boundary layer while the near wall peak in u' is higher for the 0.07 pressure ratio distribution. The lower pressure ratio and the base vane profiles generally show insignificant levels of turbulence. The fluctuating velocity profile for the high turbulence condition is shown for the three showerhead pressure ratios and the base vane in figure 6.32. The profiles look consistent showing no significant differences.

Summary and Conclusions.

Velocity profiles downstream from film cooling arrays have been documented in this chapter to provide details of the interaction of turbulence and film cooling with vane surface boundary layer development. These data offer qualitative information which aids in visualizing how film cooling alters the development of the boundary layer and how turbulence mixes out the velocity and analogously temperature differences resulting from the film cooling jets in both the spanwise and normal directions. Additionally, the velocity and turbulence distributions represent useful quantitative information for grounding predictive comparisons.

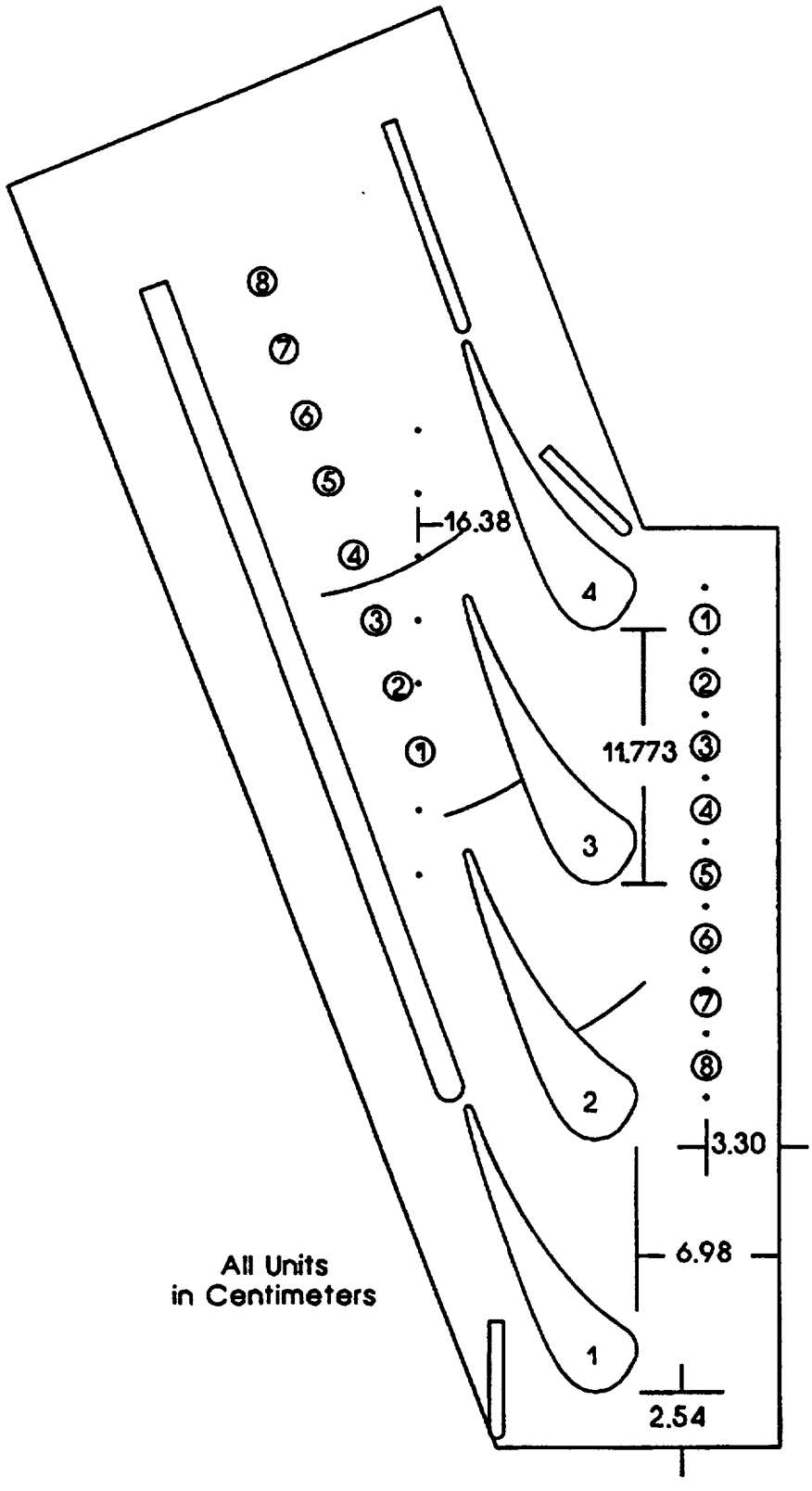

Figure 6.1 Schematic of cascade showing velocity measurement locations

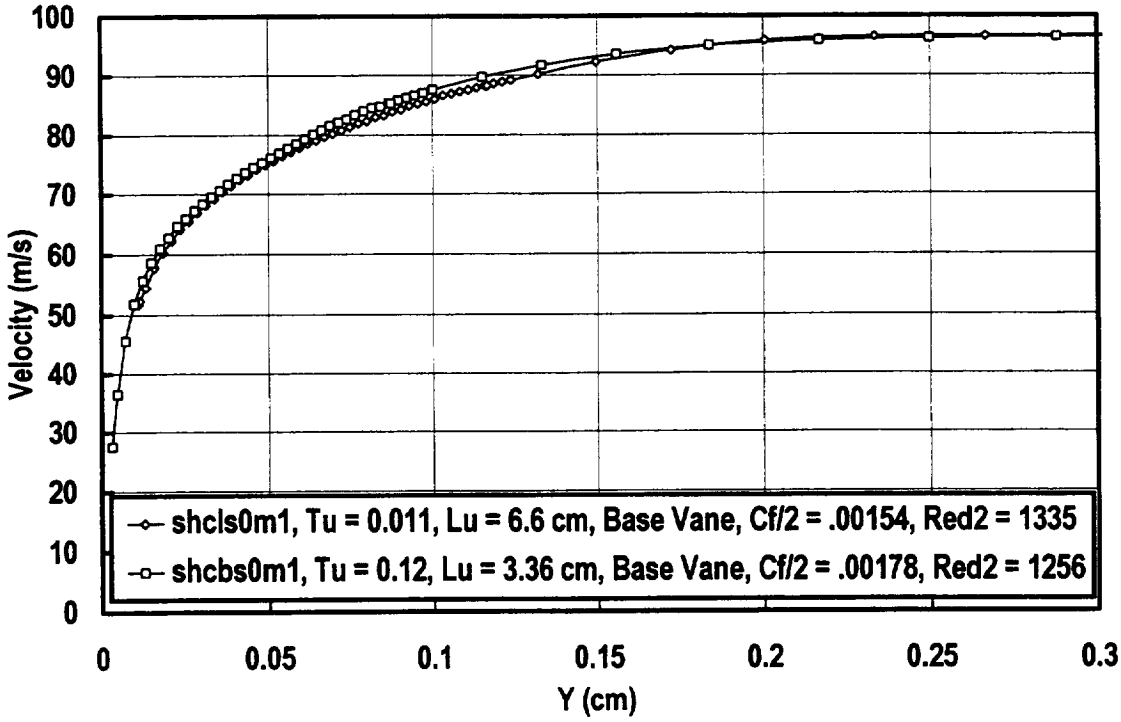

Figure 6.2 Baseline suction surface velocity profiles with high and low turbulence

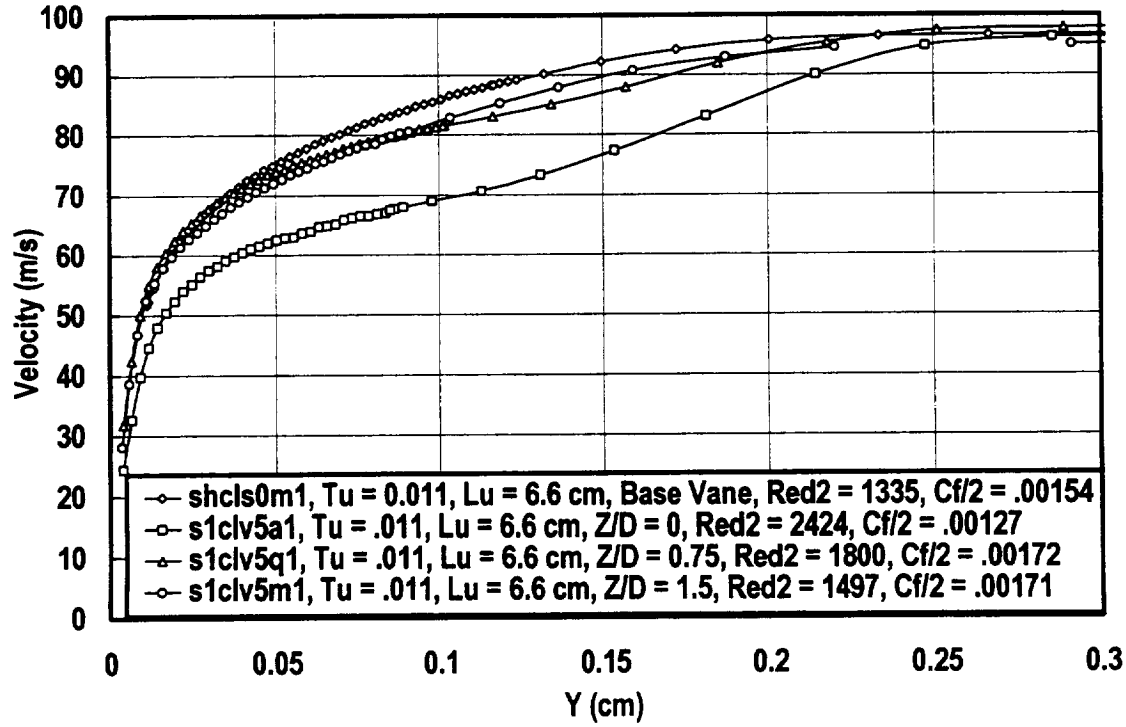

Figure 6.3 Spanwise comparison of suction surface velocity profiles with 1 row of 30° holes, low turbulence, X/D=12, VR=0.5, P/D=3

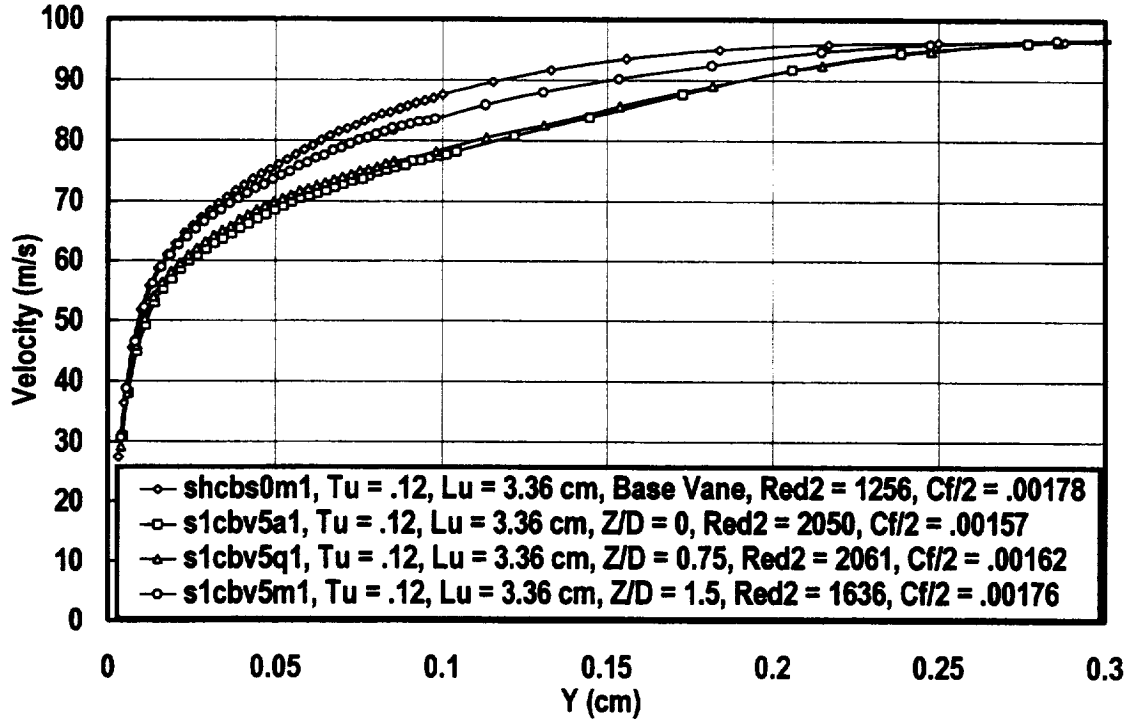

Figure 6.4 Spanwise comparison of suction surface velocity profiles with 1 row of 30° holes, comb(1), X/D=12, VR=0.5, P/D=3

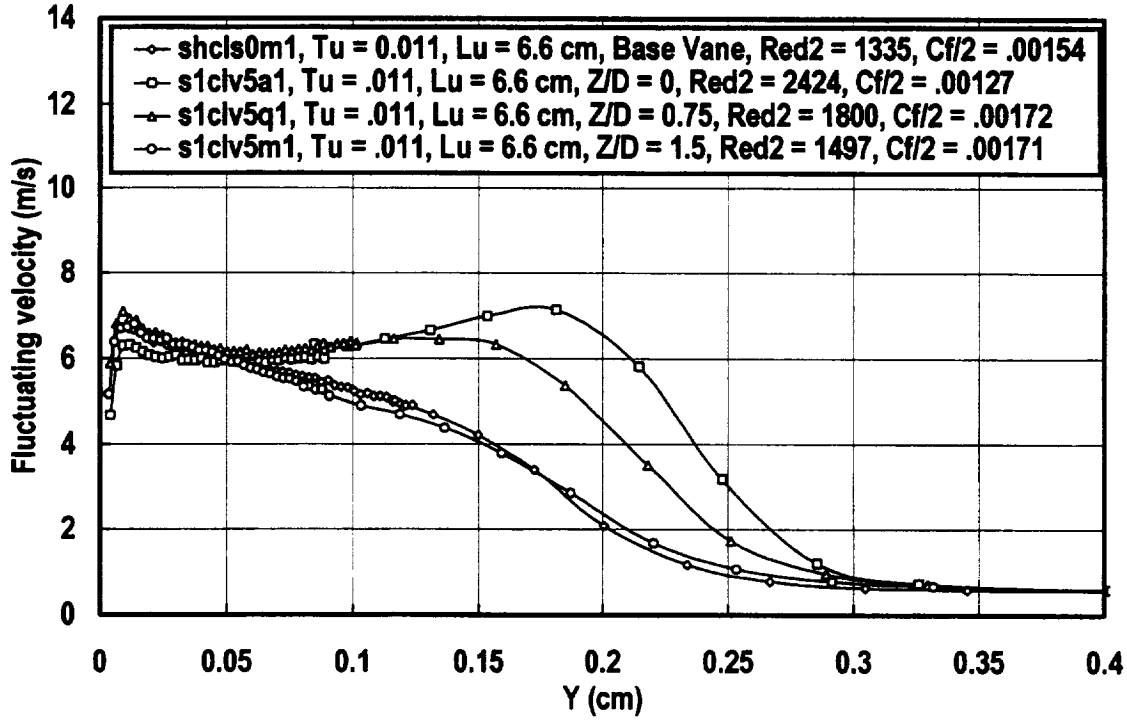

Figure 6.5 Spanwise comparison of suction surface fluctuating velocity profiles with 1 row of 30° holes, low turbulence, X/D=12, VR=0.5, P/D=3

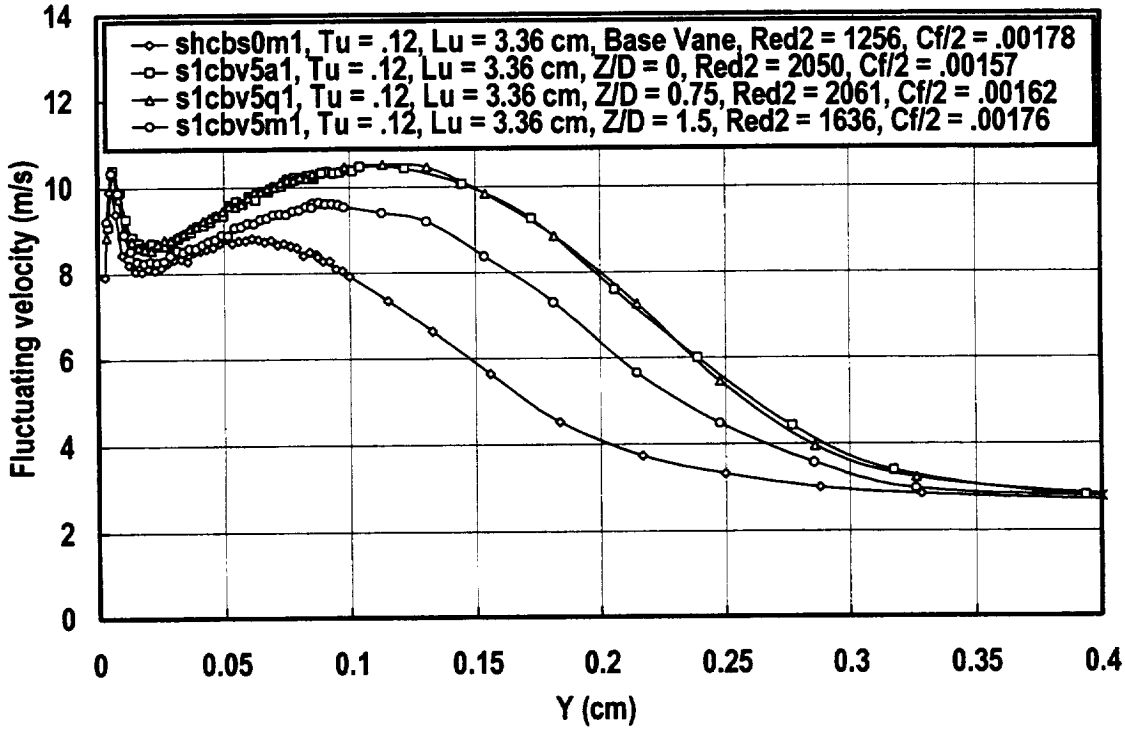

Figure 6.6 Spanwise comparison of suction surface fluctuating velocity profiles with 1 row of 30° holes, comb(1), X/D=12, VR=0.5, P/D=3

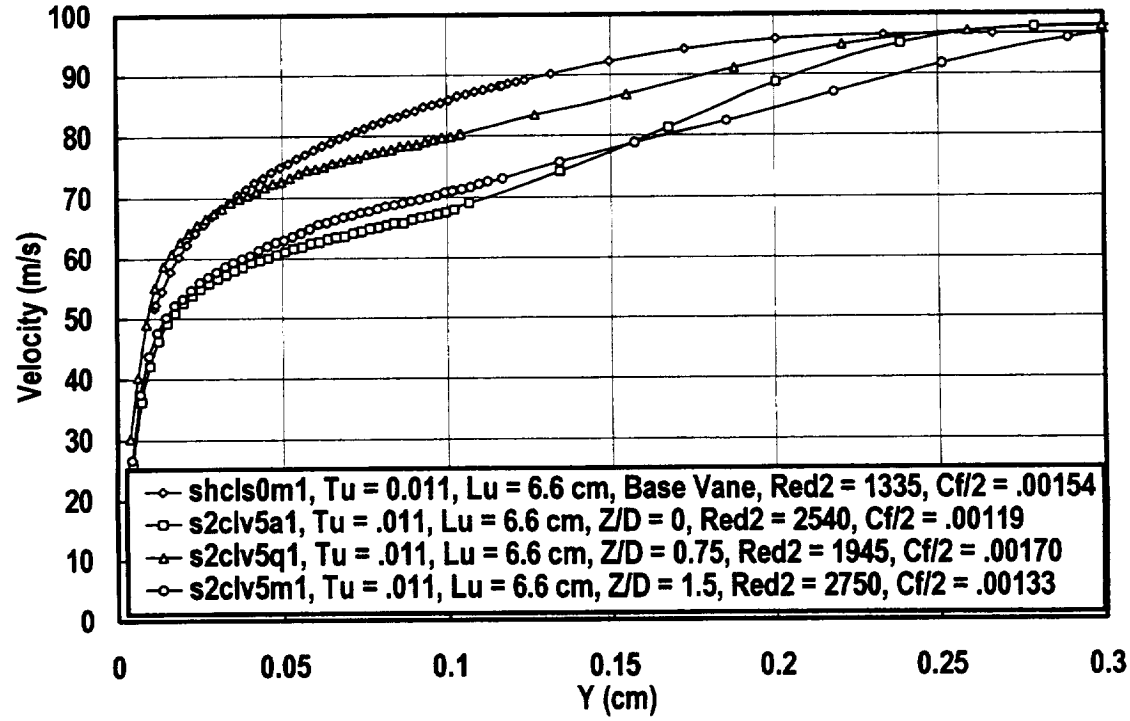

Figure 6.7 Spanwise comparison of suction surface velocity profiles with 2 rows of 30° holes, low turbulence, X/D=12, VR=0.5, P/D=3

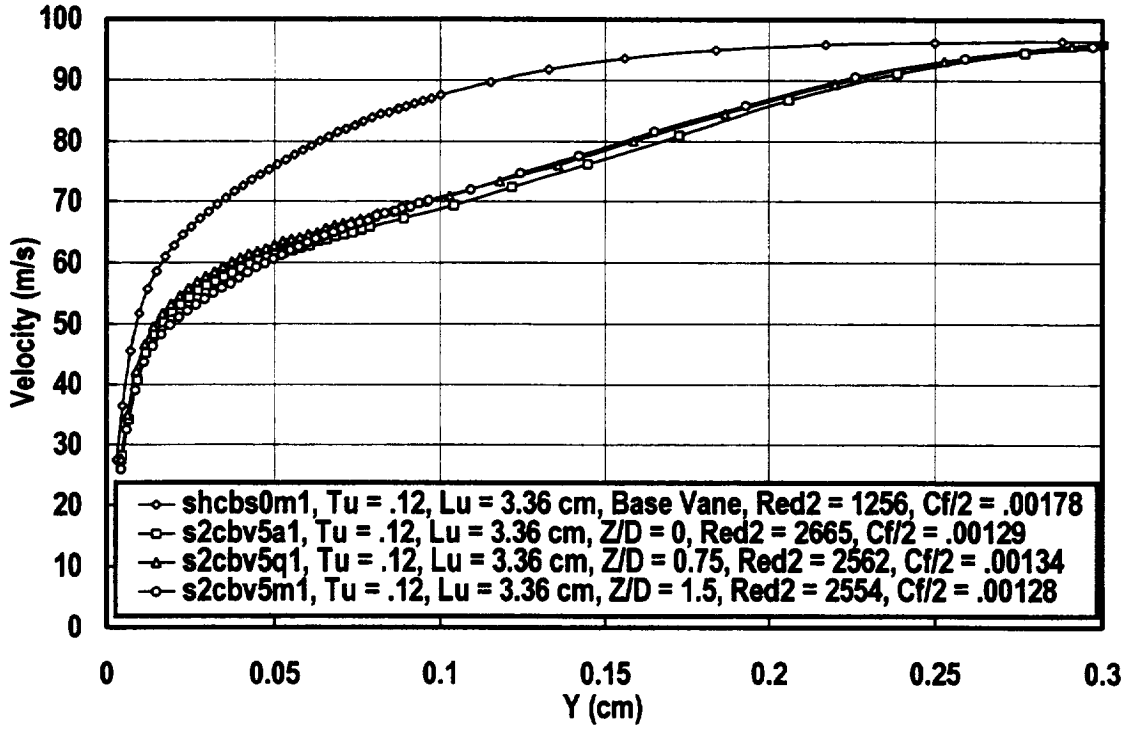

Figure 6.8 Spanwise comparison of suction surface velocity profiles with 2 rows of 30° holes, comb(1), X/D=12, VR=0.5, P/D=3

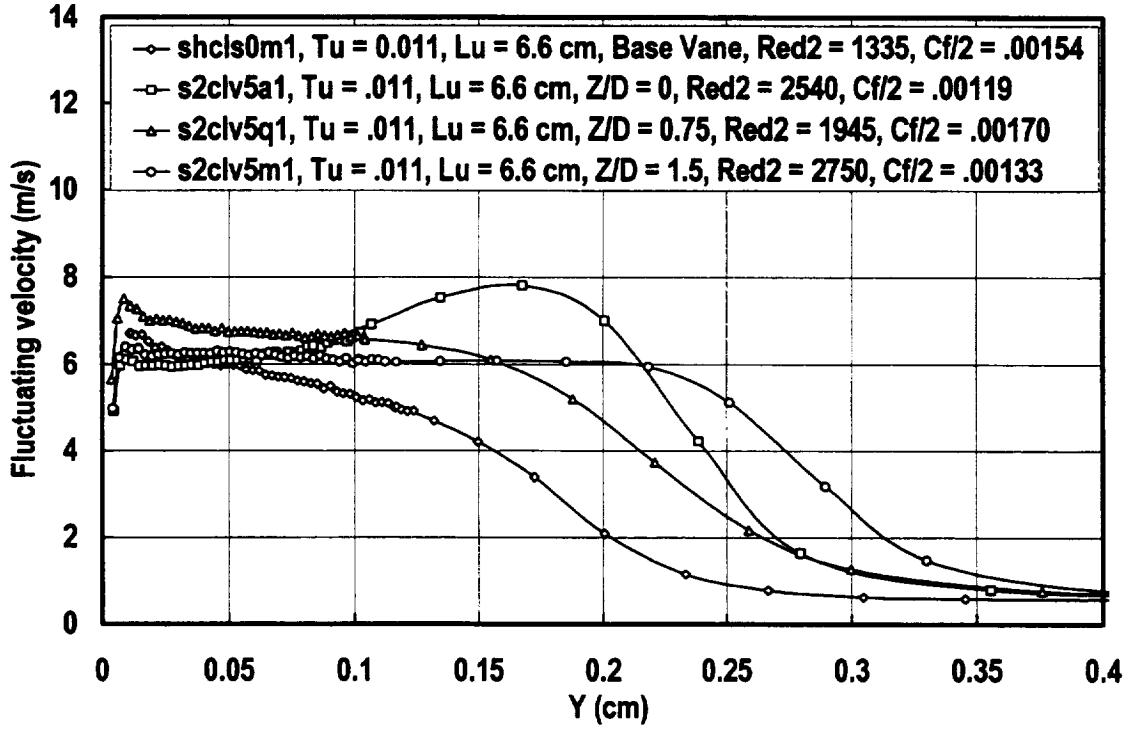

Figure 6.9 Spanwise comparison of suction surface fluctuating velocity profiles with 1 row of 30° holes, low turbulence, X/D=12, VR=0.5, P/D=3

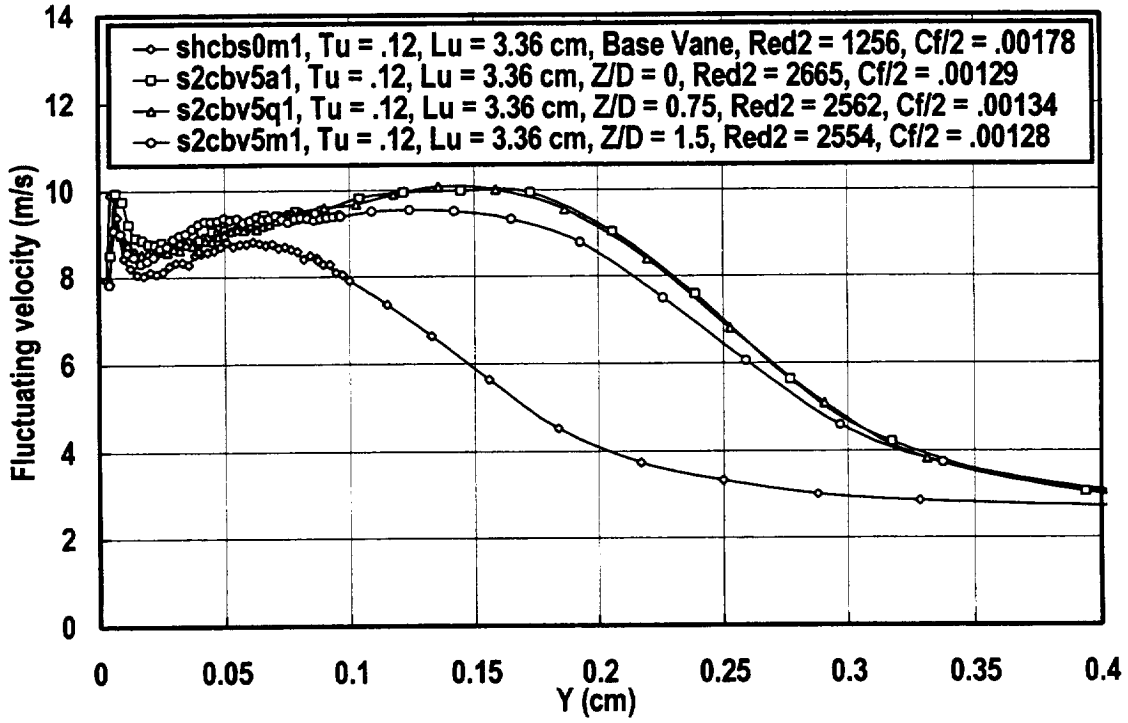

Figure 6.10 Spanwise comparison of suction surface fluctuating velocity profiles with 1 row of 30° holes, comb(1), X/D=12, VR=0.5, P/D=3

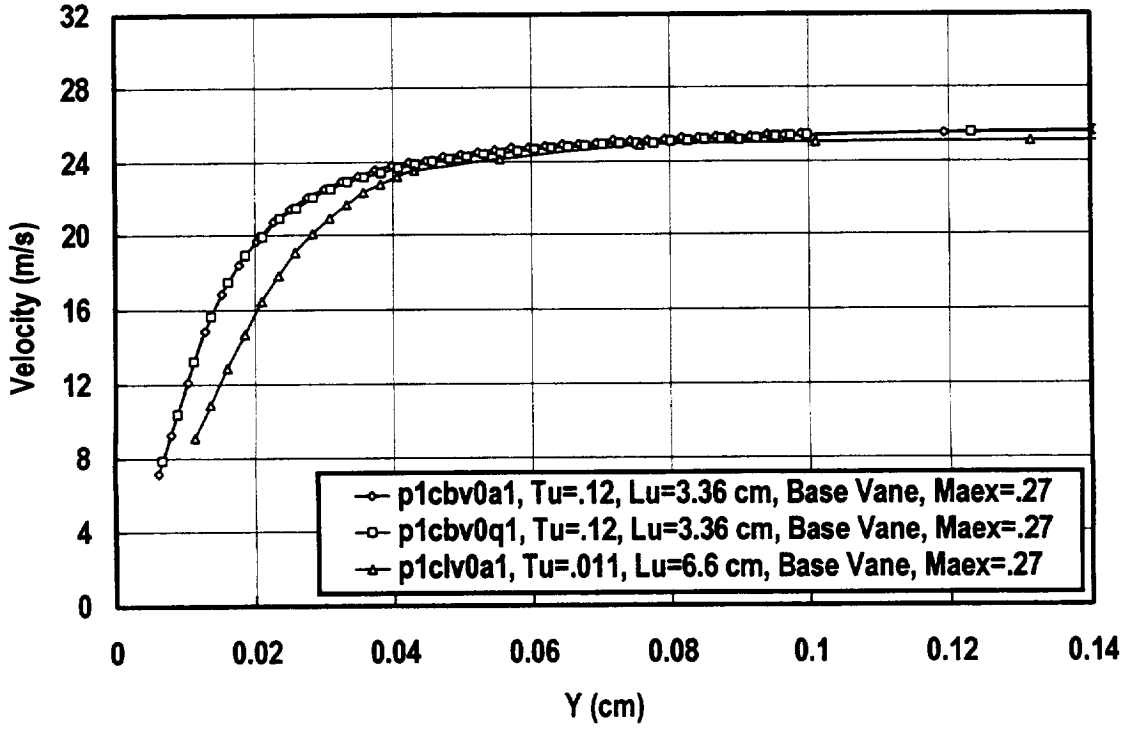

Figure 6.11 Baseline pressure surface velocity profiles with high and low turbulence

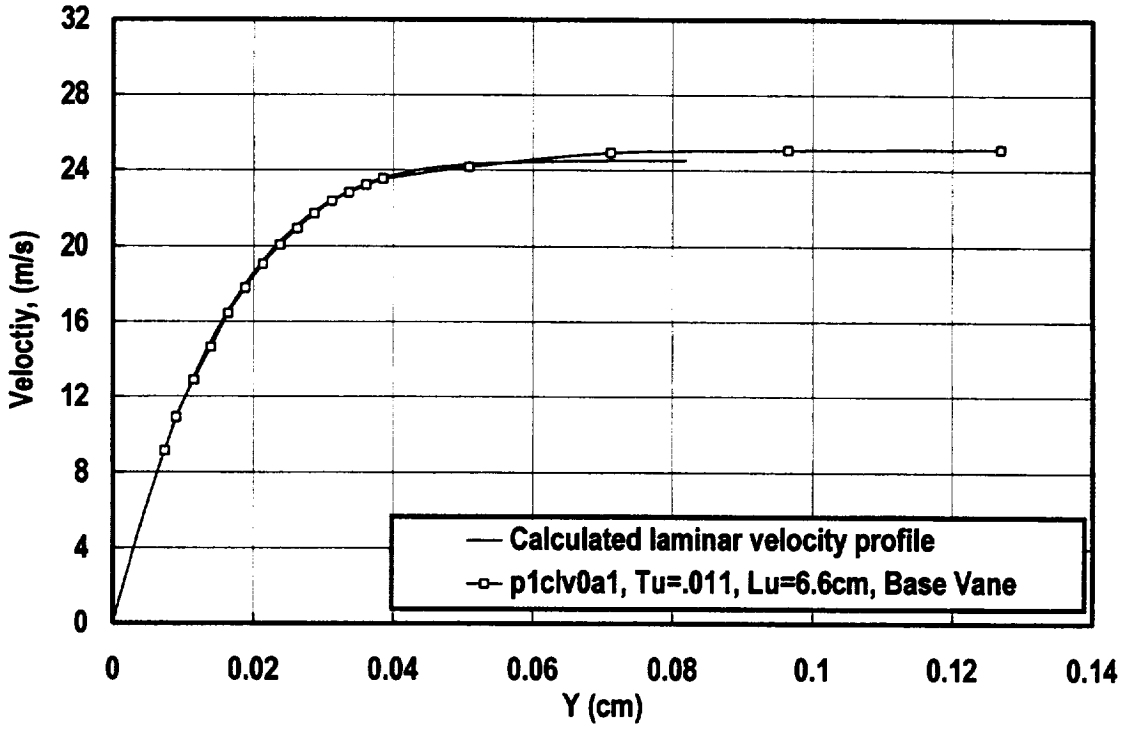

Figure 6.12 Calculated velocity profile compared to data with fitted offset

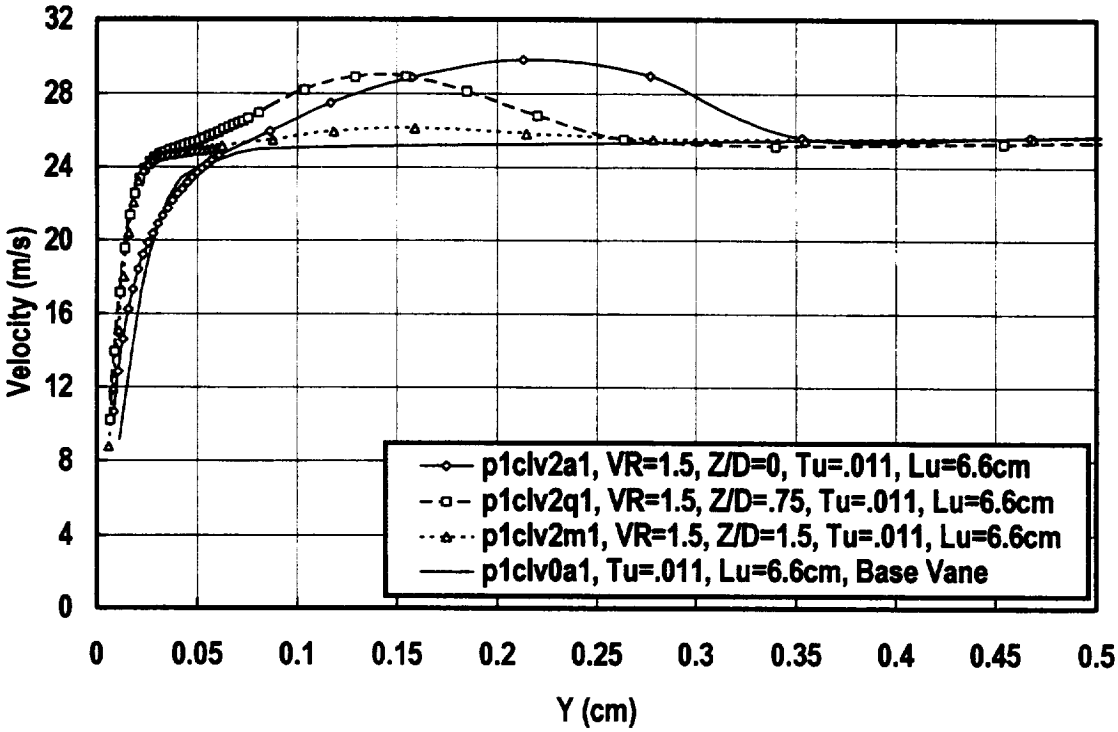

Figure 6.13 Spanwise comparison of pressure surface velocity profiles with 1 row of 30° holes, low turbulence, X/D=9, VR=1.5, P/D=3

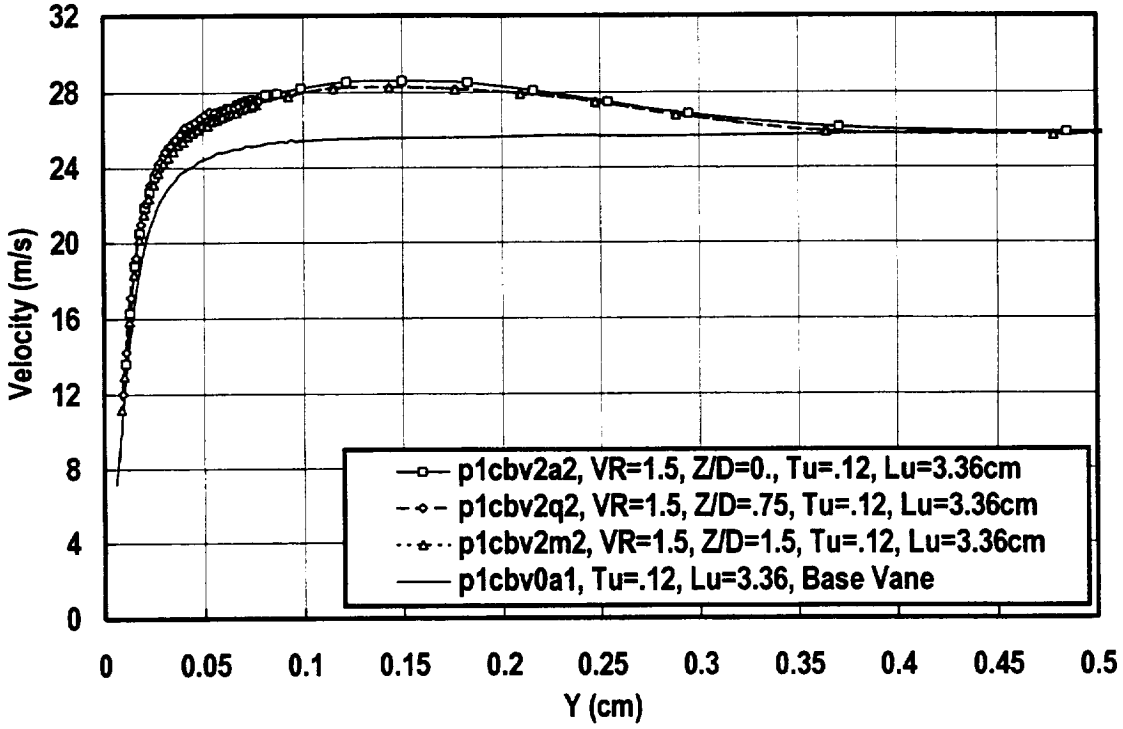

Figure 6.14 Spanwise comparison of pressure surface velocity profiles with 1 row of 30° holes, comb(1), X/D=9, VR=1.5, P/D=3

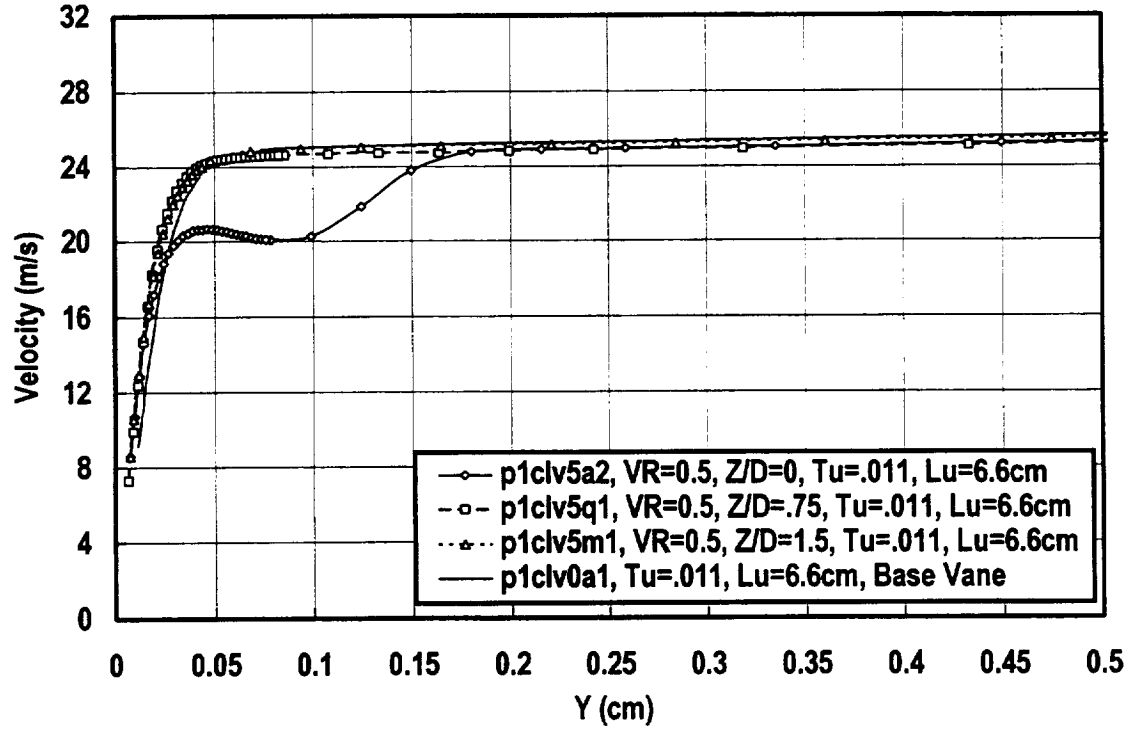

Figure 6.15 Spanwise comparison of pressure surface velocity profiles with 1 row of 30° holes, low turbulence, X/D=9, VR=0.5, P/D=3

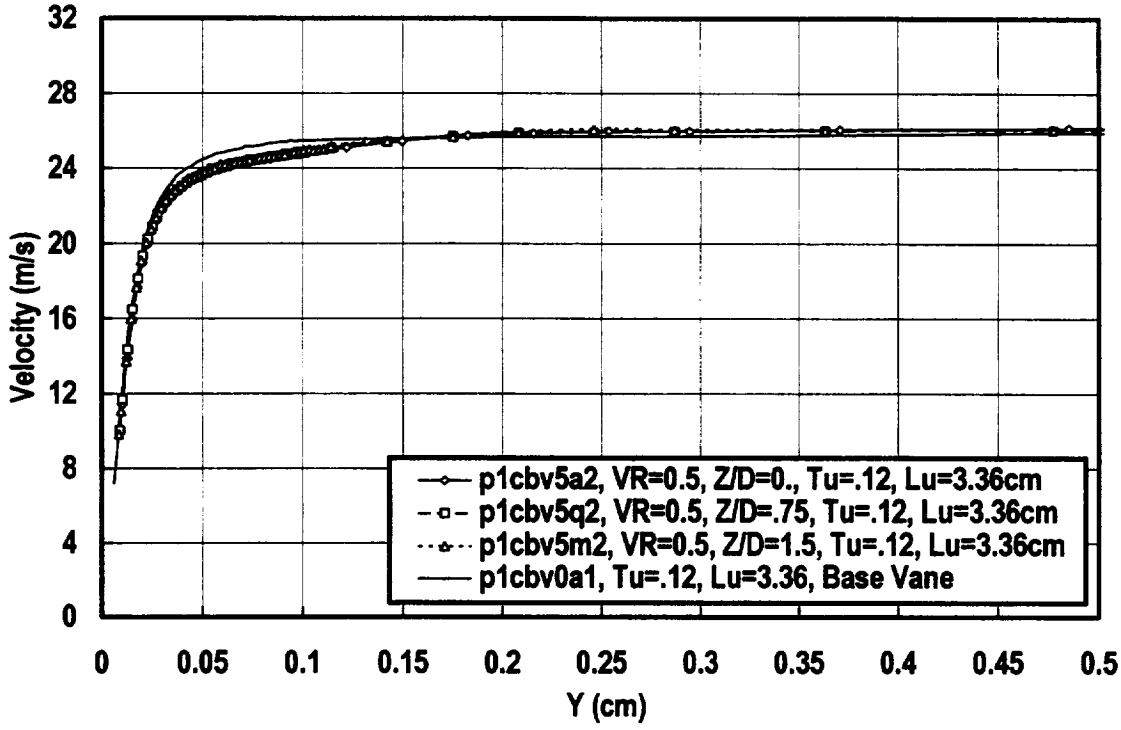

Figure 6.16 Spanwise comparison of pressure surface velocity profiles with 1 row of 30° holes, comb(1), X/D=9, VR=0.5, P/D=3

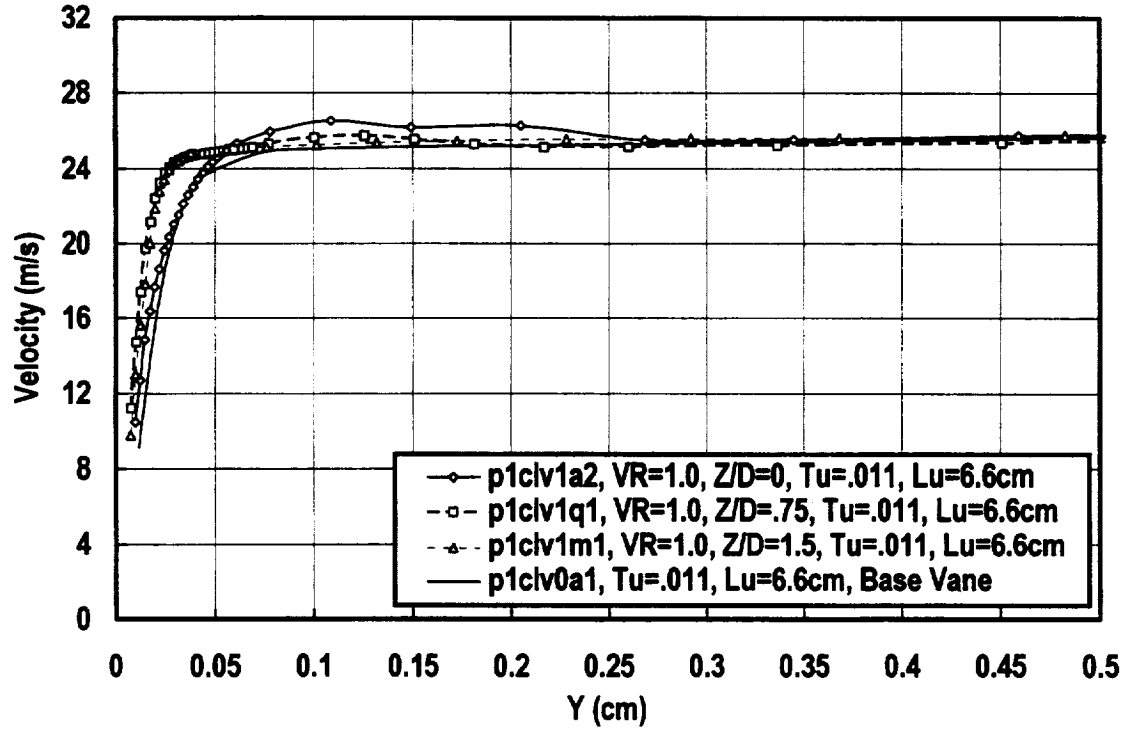

Figure 6.17 Spanwise comparison of pressure surface velocity profiles with 1 row of 30° holes, low turbulence, X/D=9, VR=1.0, P/D=3

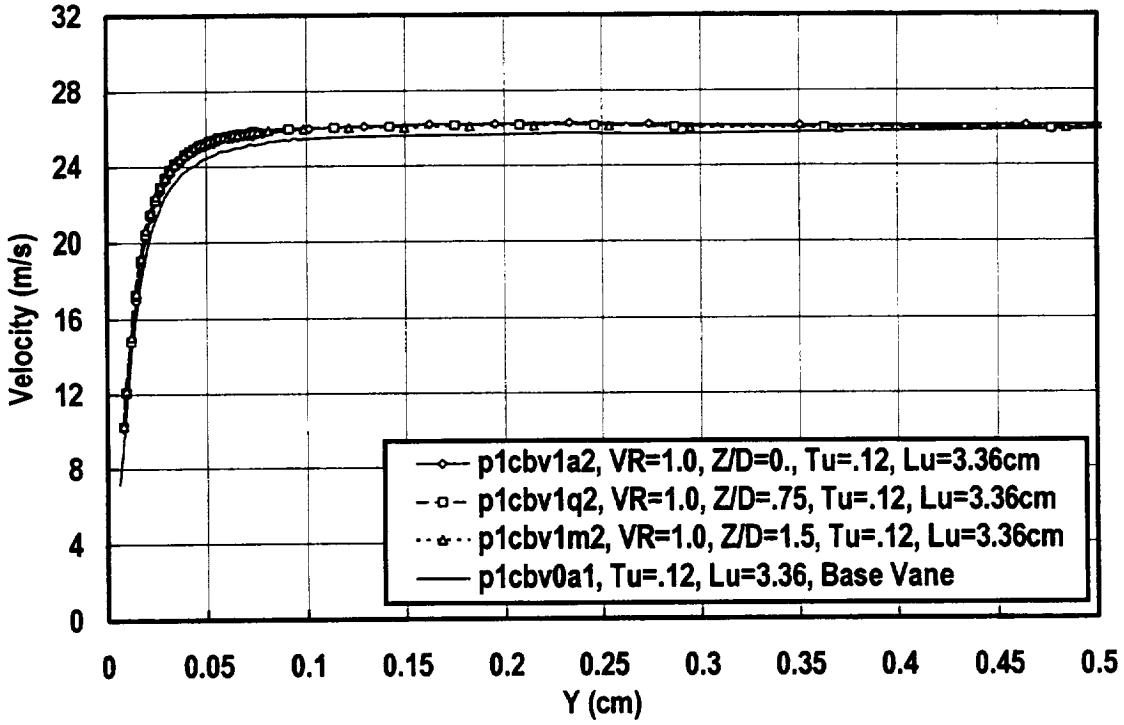

Figure 6.18 Spanwise comparison of pressure surface velocity profiles with 1 row of 30° holes, comb(1), X/D=9, VR=1.0, P/D=3

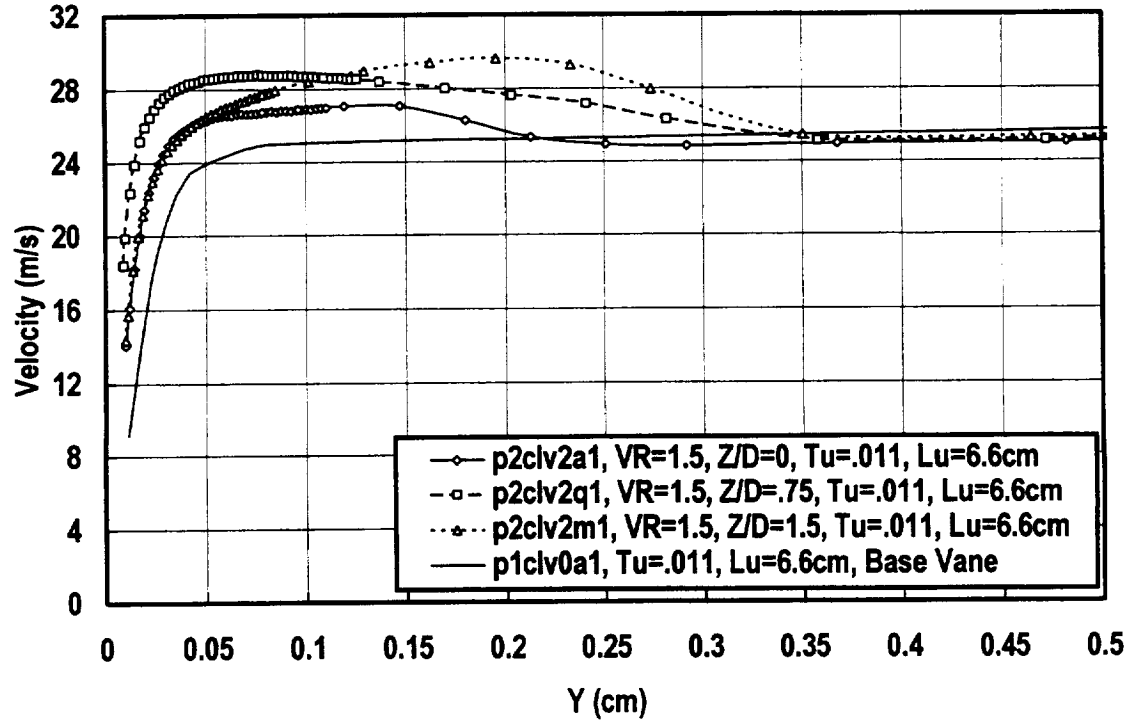

Figure 6.19 Spanwise comparison of pressure surface velocity profiles with 2 rows of 30° holes, low turbulence, X/D=9, VR=1.5, P/D=3

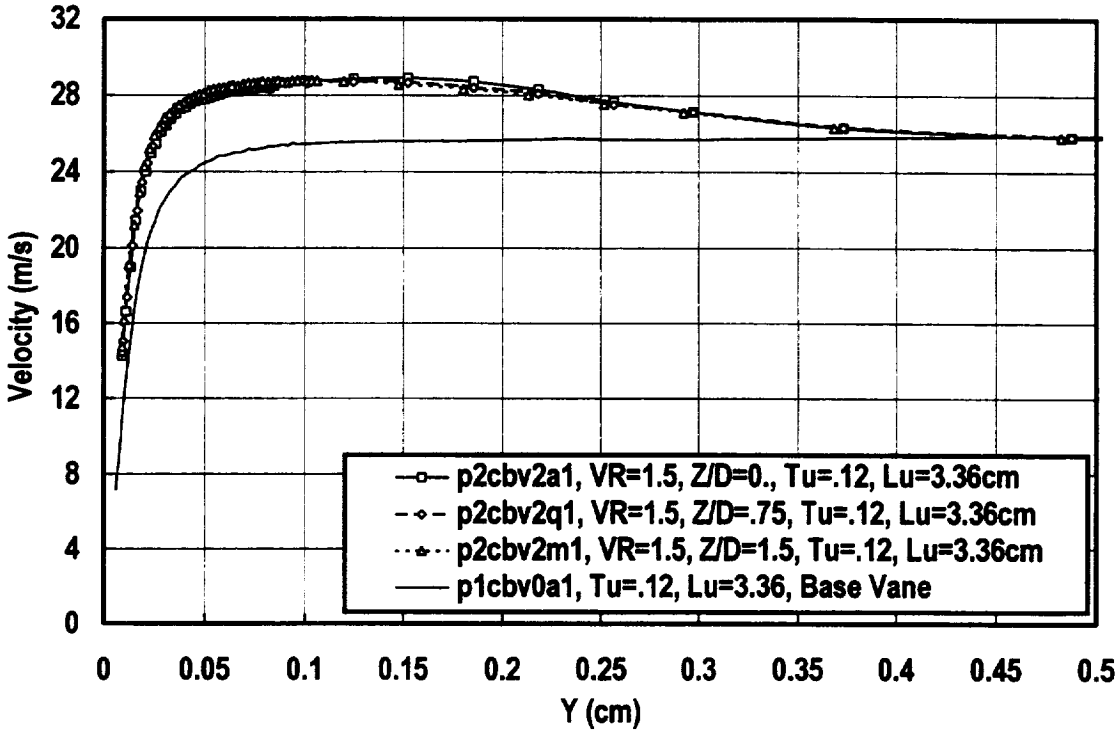

Figure 6.20 Spanwise comparison of pressure surface velocity profiles with 2 rows of 30° holes, comb(1) , X/D=9, VR=1.5, P/D=3

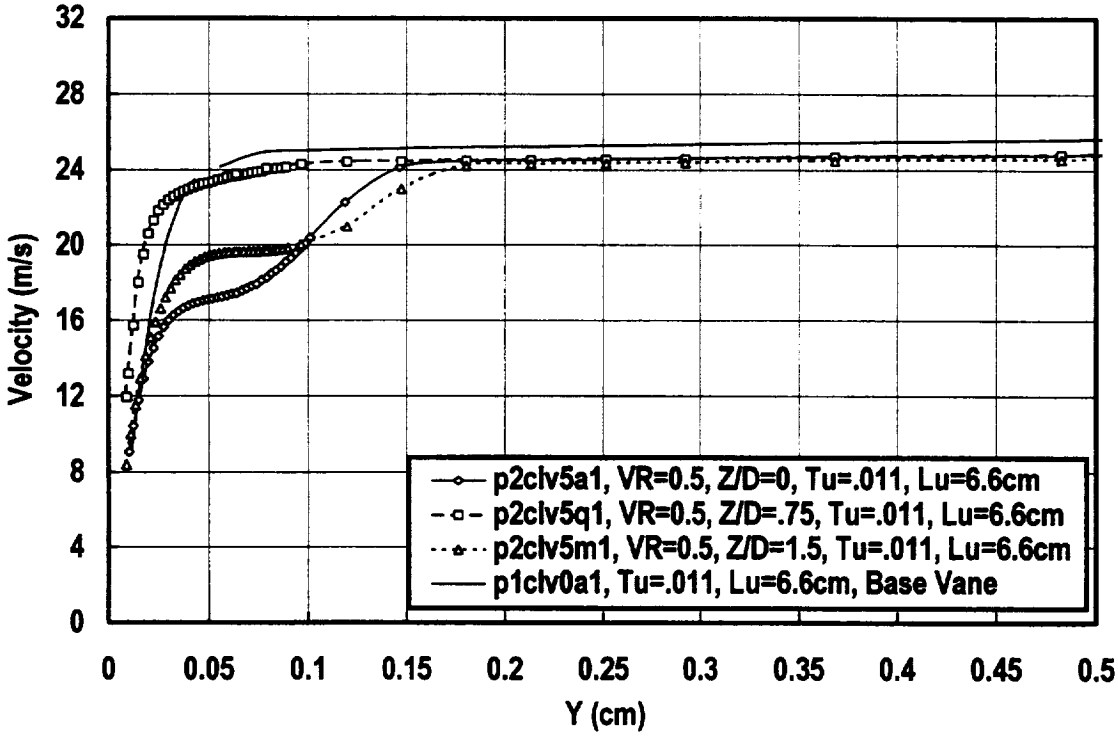

Figure 6.21 Spanwise comparison of pressure surface velocity profiles with 2 rows of 30° holes, low turbulence, X/D=9, VR=0.5, P/D=3

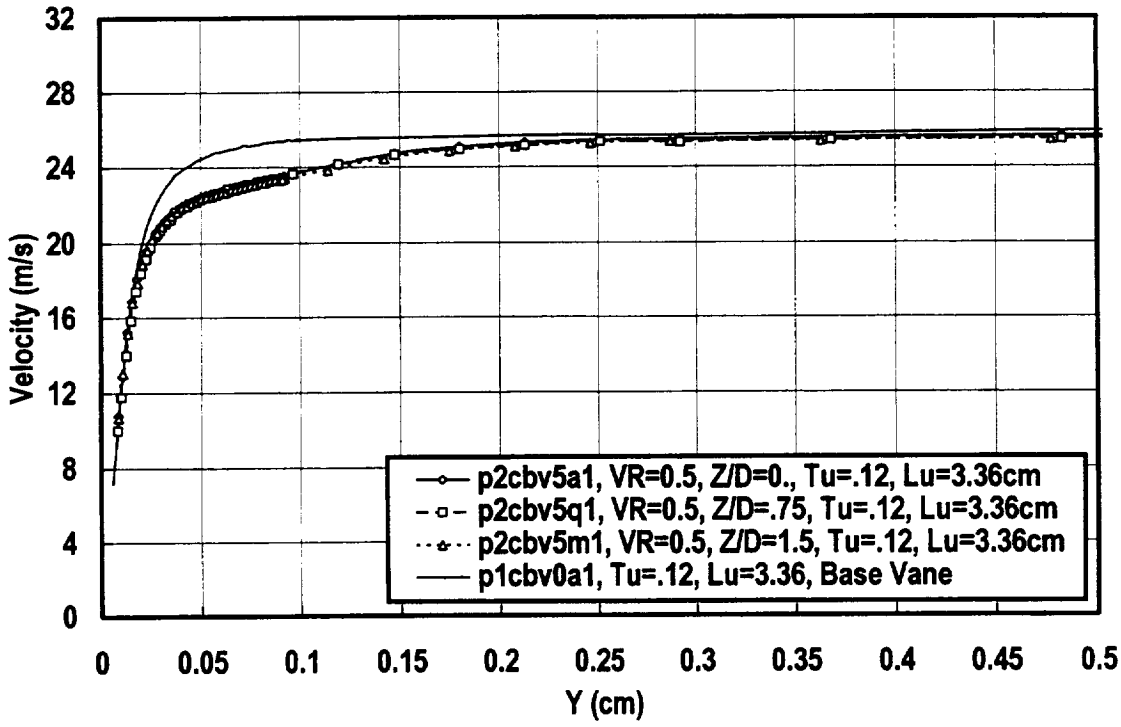

Figure 6.22 Spanwise comparison of pressure surface velocity profiles with 2 rows of 30° holes, comb(1), X/D=9, VR=0.5, P/D=3

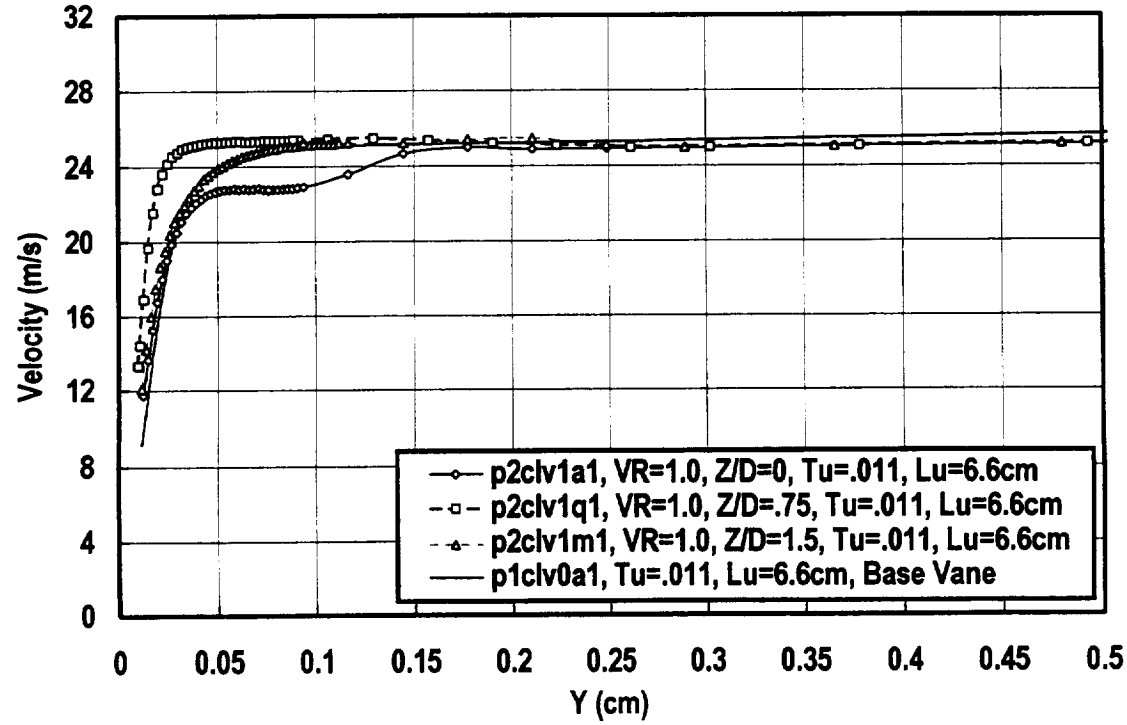

Figure 6.23 Spanwise comparison of pressure surface velocity profiles with 2 rows of 30° holes, low turbulence, X/D=9, VR=1.0, P/D=3

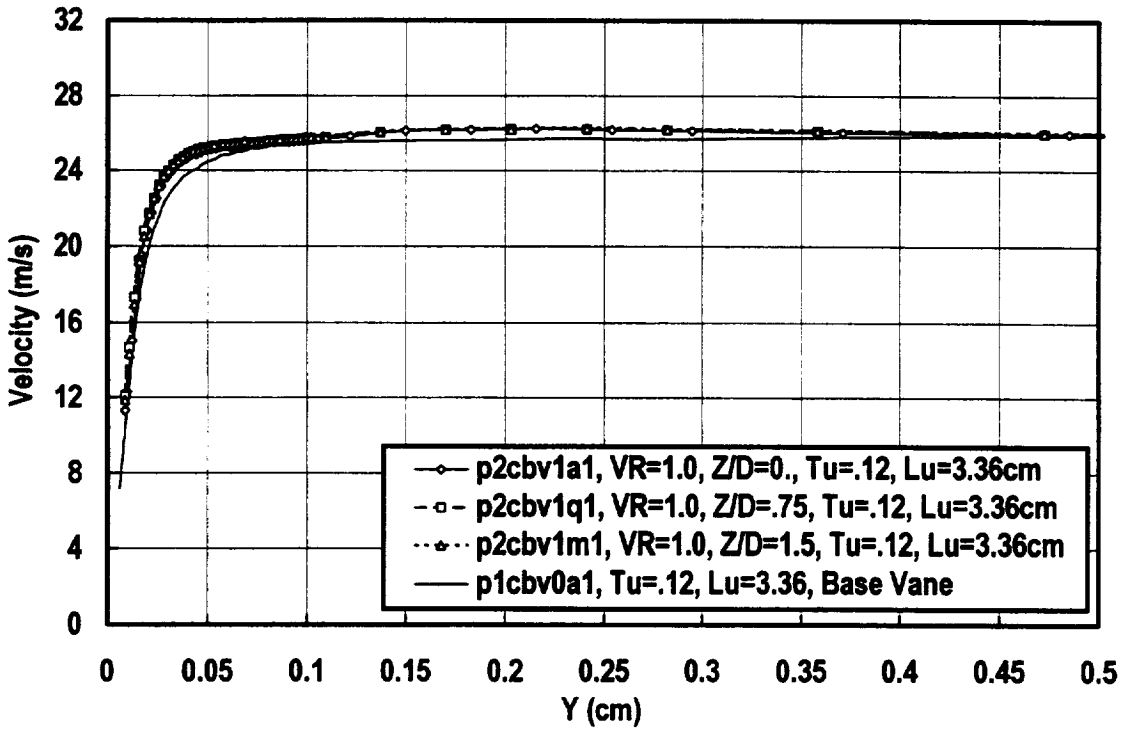

Figure 6.24 Spanwise comparison of pressure surface velocity profiles with 2 rows of 30° holes, comb(1), X/D=9, VR=1.0, P/D=3

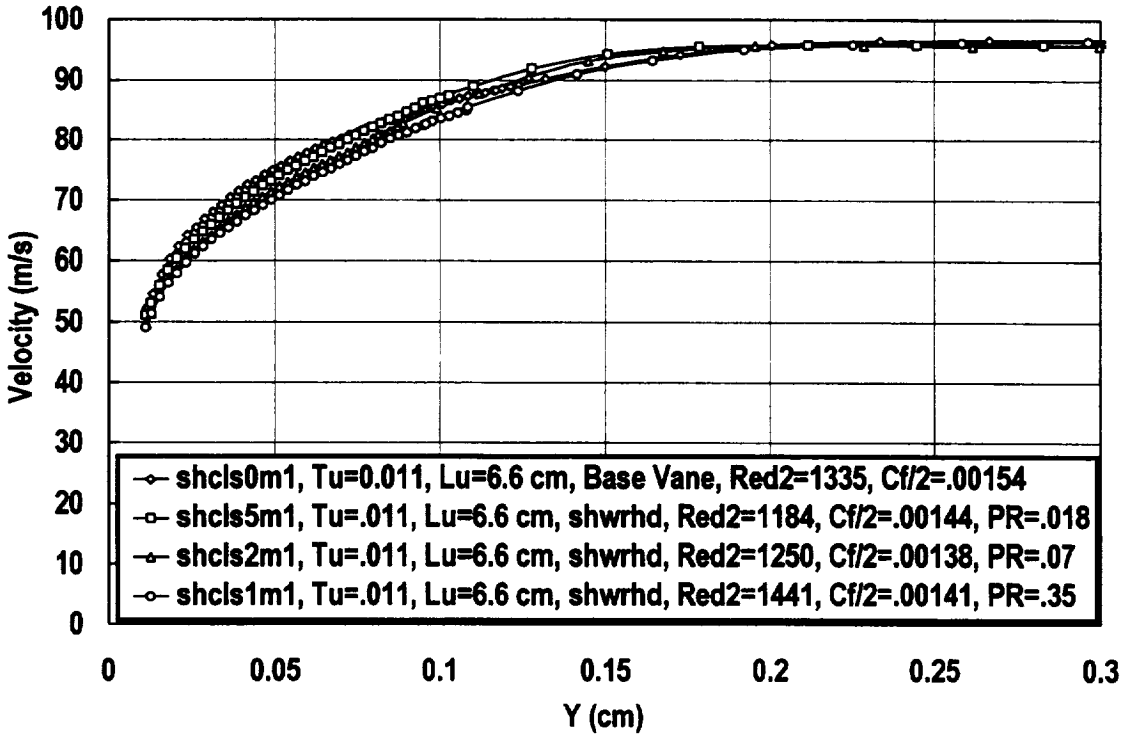

Figure 6.25 Comparison of suction surface velocity profiles with showerhead array for various pressure ratios, low turbulence.

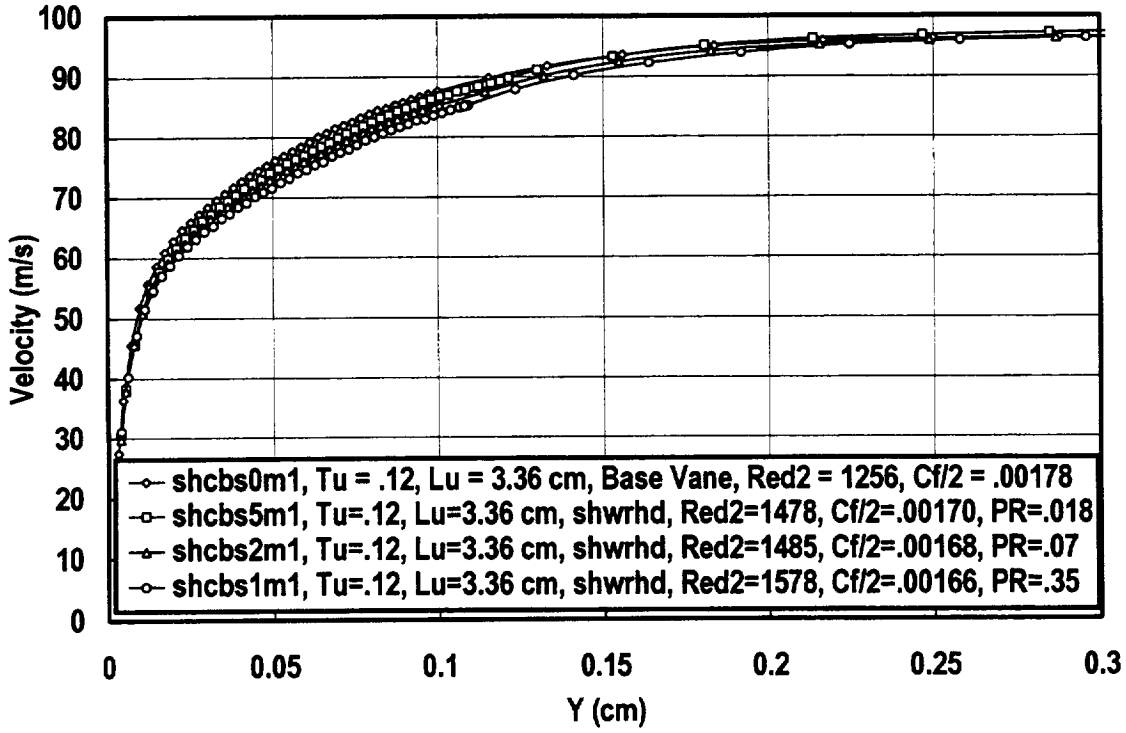

Figure 6.26 Comparison of suction surface velocity profiles with showerhead array for various pressure ratios, comb(1).

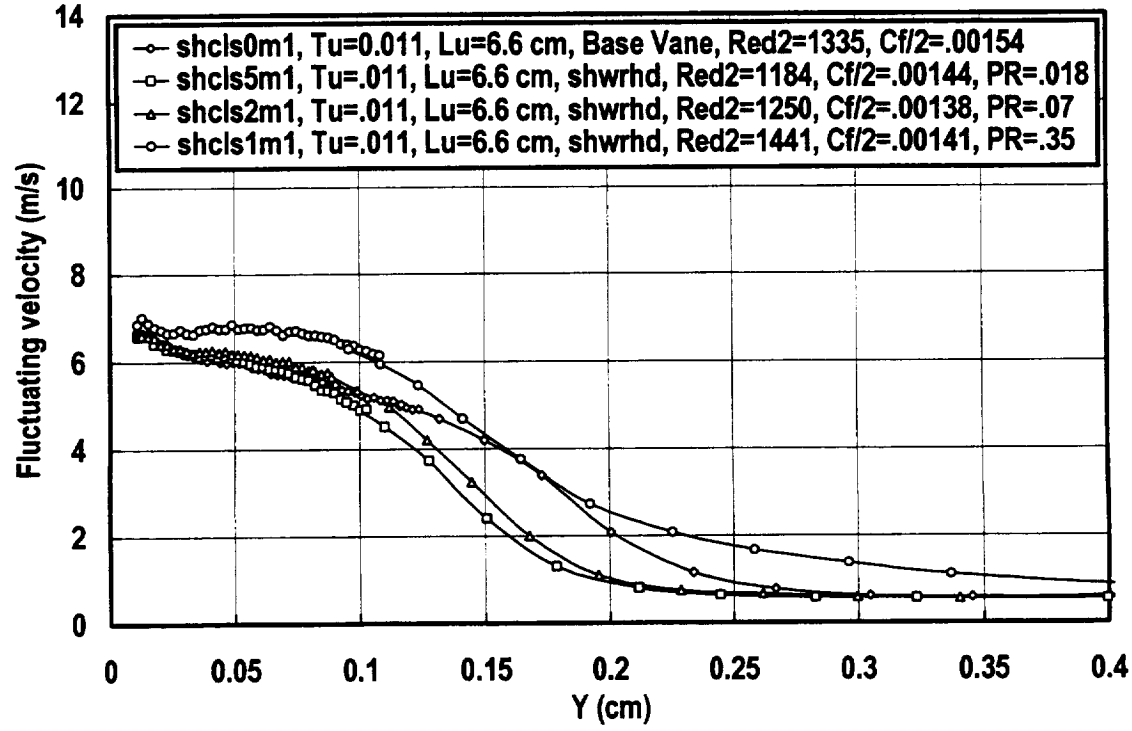

Figure 6.27 Comparison of suction surface fluctuating velocity profiles with showerhead array for various pressure ratios, low turbulence.

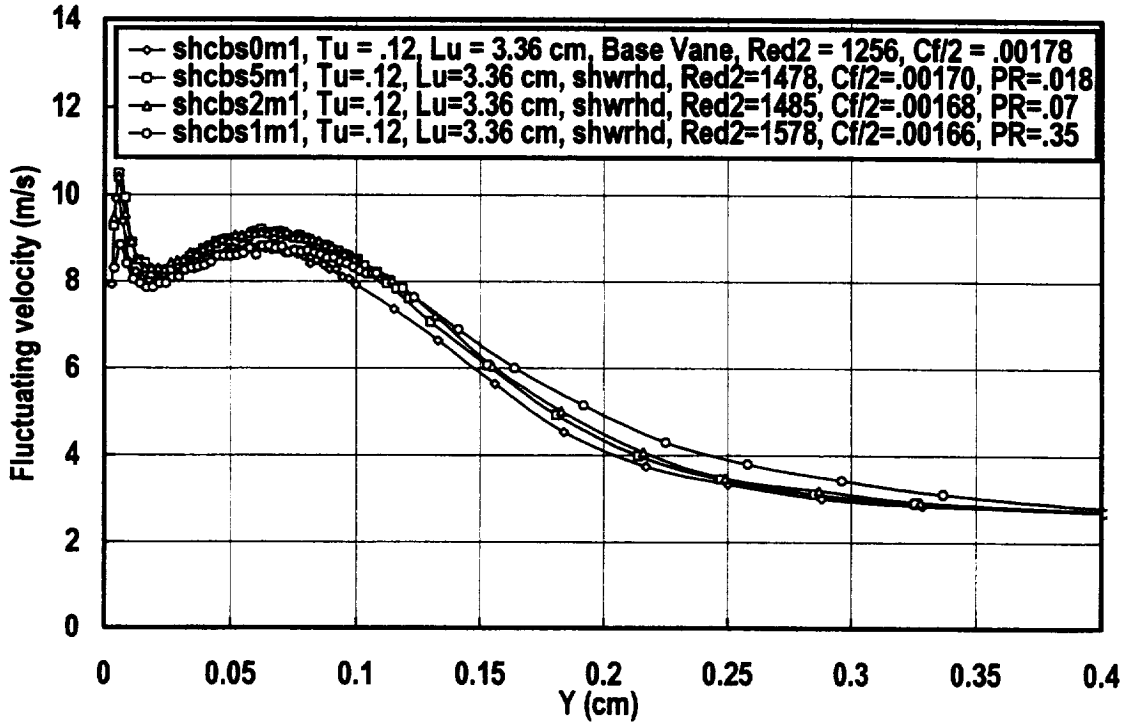

Figure 6.28 Comparison of suction surface fluctuating velocity profiles with showerhead array for various pressure ratios, comb(1).

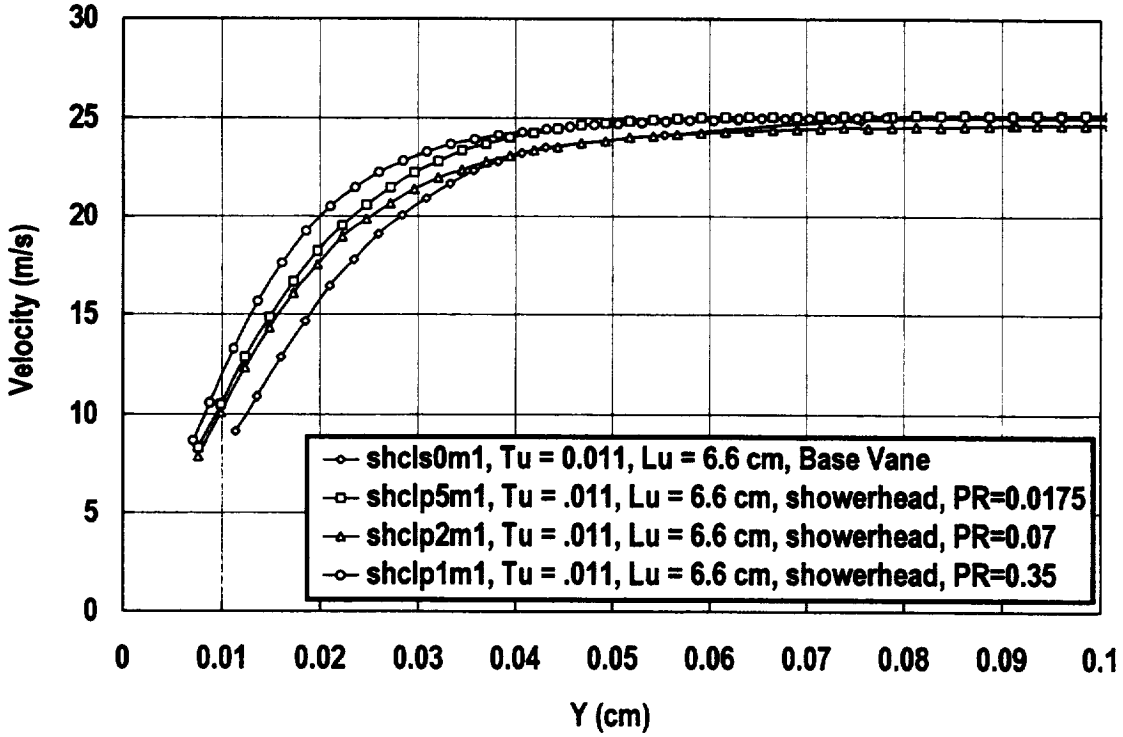

Figure 6.29 Comparison of pressure surface velocity profiles with showerhead array for various pressure ratios, low turbulence

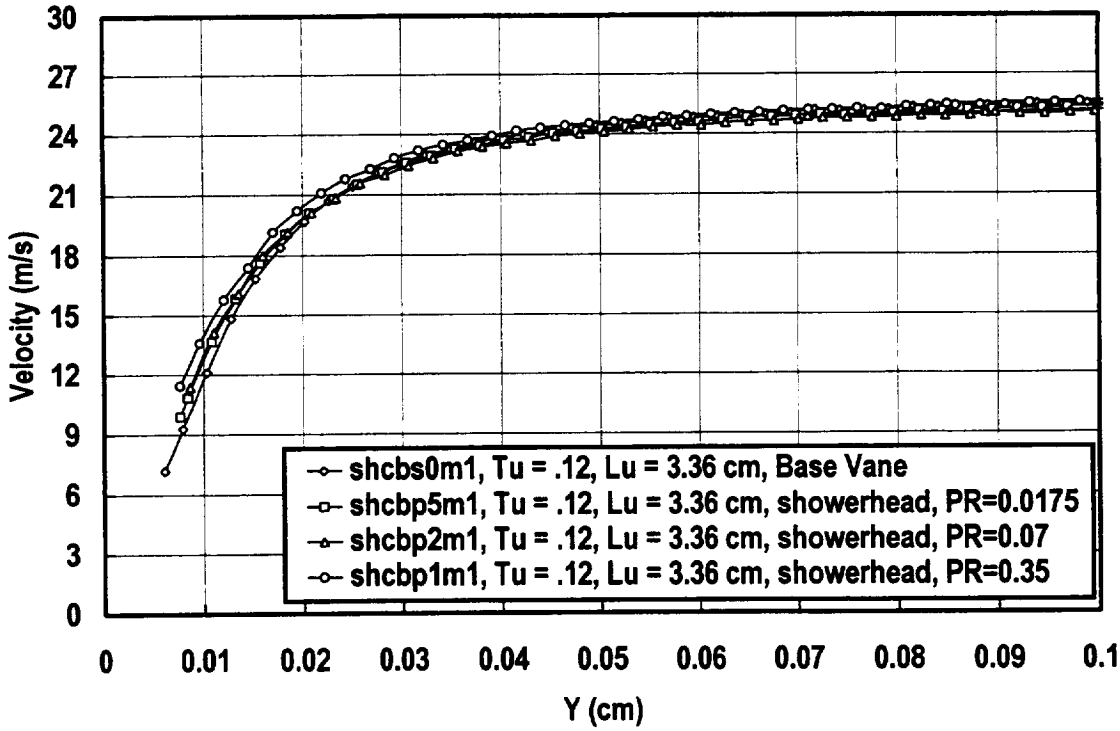

Figure 6.30 Comparison of pressure surface velocity profiles with showerhead array for various pressure ratios, comb(1)

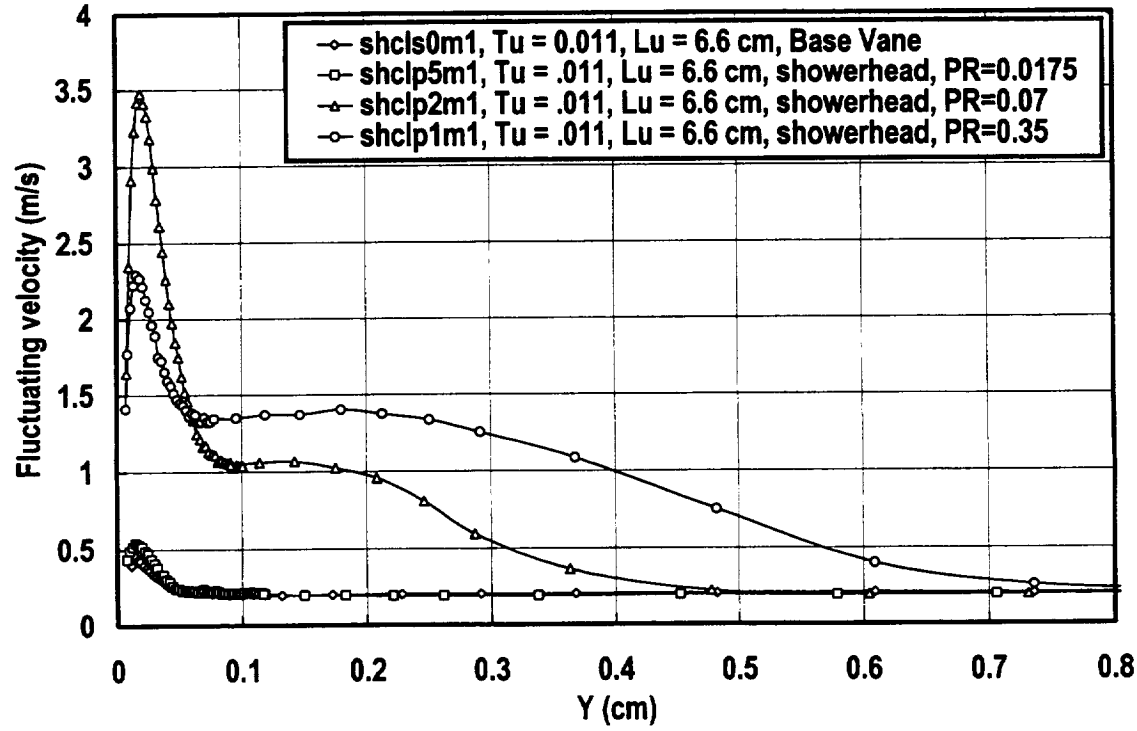

Figure 6.31 Comparison of pressure surface fluctuating velocity profiles with showerhead array for various pressure ratios, low turbulence

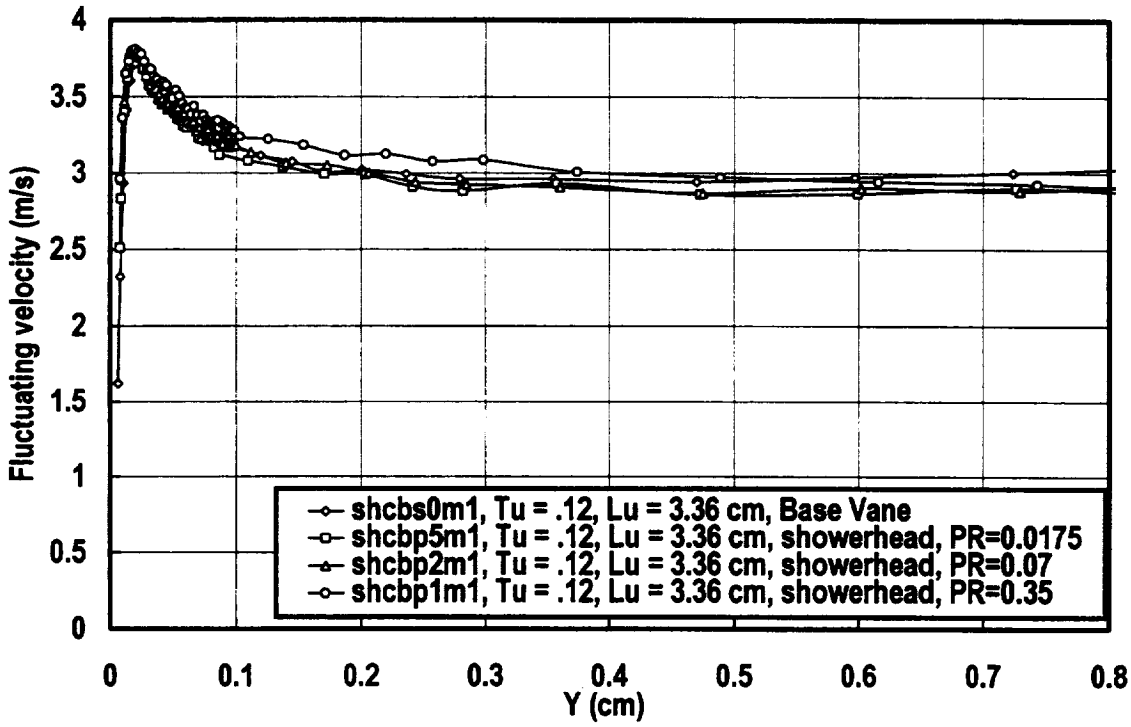

Figure 6.32 Comparison of pressure surface fluctuating velocity profiles with showerhead array for various pressure ratios, comb(1)

Chapter 7

Exit Losses with Film Cooling

Film cooling can be used to enhance engine performance by reducing the surface heat load on a turbine airfoil and allowing the component to run at a higher gas temperature. However, the losses associated with the film cooling need to be accounted for to estimate the overall performance of the system. In this chapter, the influence of the film cooling on aerodynamic performance for the three cooling configurations is examined. Exit total pressure loss distributions, normalized on the inlet total to exit static pressure difference are shown for the three configurations at three coolant to inlet total pressure ratios and for the two turbulence conditions.

The primary cause of profile losses on turbomachinery airfoils is boundary layer growth and trailing edge blockage (Glassman 1973). Denton (1993) in a comprehensive review of loss mechanisms in turbomachines suggests that mixing across gradients in the flow can result in increased losses even without the action of frictional forces. Ames and Plesniak (1995) reported a background total pressure loss of 1.5 percent in the core region of the flow at the exit of a vane cascade. These studies indicate that from the standpoint of a solid vane, midspan losses can occur due to boundary layer growth, trailing edge blockage, and the interaction of high turbulence with the flow. In this chapter we will examine the added influence of film cooling on losses.

From a fundamental standpoint, film cooling adds to losses by the addition of low momentum fluid into the boundary layer. The cooling air losses originate in the cooling passages and exit holes of the turbine airfoil. In addition to the momentum addition loss, film cooling can also generate losses by penetration into the flow causing a blockage to the boundary layer and free stream flow. This aspect of the loss is expected to be driven by the momentum of the fluid leaving the holes relative to the momentum of the passing free stream as well as the angle of injection relative to the flow along the surface of the airfoil. Lefebvre (1983) indicates that jet penetration has been correlated on the square root of the momentum flux ratio between the coolant and the gas and the sine of the angle. Another aspect of losses which we cannot examine in this study is the influence of density ratio on losses. Even if two streams of fluid have the same direction and total pressure, losses due to density differences will occur as the two streams of different velocities mix out.

Film cooling can also have a significant effect on boundary layer development. Mayle (1991) indicated that film cooling typically produced an immediate transition to turbulence. In addition to injecting low momentum fluid into the boundary layer, film cooling jets produce a blockage to the flow resulting in a local increase in the velocity field around the hole. Film cooling jets also create vorticity in the boundary layer. All these effects can have an influence to boundary layer development and the resulting

overall aerodynamic losses. The overall influence of film cooling on aerodynamic performance for a given configuration cannot always be predicted to first order by the simple mass injection model suggested in the previous paragraph.

Film Cooling Geometries

Three geometries were used for the aerodynamic losses tests. These geometries included a showerhead cooling array, a showerhead cooling array with 1 row of downstream cooling on both the pressure and suction surfaces, and a showerhead array with 2 rows of downstream cooling on the pressure and suction surfaces. The showerhead array consisted of five rows of 20° spanwise oriented 0.132 cm diameter holes spaced at 0.846 cm in the spanwise direction and by 0.508 cm in the stream wise direction. The single and double row of 30° streamwise oriented holes on the pressure surface had a diameter of 0.132 cm with a pitch to diameter ratio of 3. The double row geometry was constructed by drilling a staggered row 3 diameters upstream from the single row of holes. The average pressure coefficient was 0.058 for the single row and 0.055 for the double row. The single and double row of 30° streamwise oriented holes on the suction surface had a diameter of 0.159 cm with a pitch to diameter ratio of 3. The double row geometry was constructed by drilling a staggered row 3 diameters upstream from the single row of holes. The average pressure coefficient was 1.24 for the single row and 1.25 for the double row.

All the cooling arrays were fed with a common plenum for the aerodynamic tests. Three coolant to inlet pressure ratios were chosen for the tests, these were equivalent pressure ratios of 0.0175, 0.07 and 0.35. The equivalent pressure ratio was defined as the ratio of the coolant pressure less the inlet total pressure ratioed over the inlet total pressure less the averaged exit static pressure {PReqv = (Pc-Pt,in)/(Pt,in-Ps,ex)}. The typical coolant to total pressure ratio for a first stage vane is approximately 1.02. For an exit Mach number of 0.70 this equates to an equivalent pressure ratio of about 0.07. The other pressure ratios were taken to correspond to coolant to total pressure ratios of 1.005 and 1.10 for our typical first stage vane. These three pressure ratios produced velocity ratios of 0.76, 1.00, and 1.77 for the pressure surface arrays and velocity ratios of 0.67, 0.69, and 0.76 for the suction surface arrays for the three pressure ratios assuming the hole discharge coefficient was 0.67. The estimated level of uncertainty in the reported kinetic energy loss coefficient is +/- 0.25 percent.

Exit Losses

The exit total pressure surveys were taken at midspan at position 8 to determine profiles losses for the different geometries, pressure ratios and turbulence conditions. Figure 7.1 shows the total pressure loss profile from vane 2 for the base vane with both high and low turbulence conditions. The peak total pressure loss is highest for the low turbulence condition and the high turbulence case has the broadest width. The high turbulence case shows a loss which occurs in the core of the flow well away from the

edge of the wake. This loss was shown to be a strong function of turbulence level in Ames (1994) and Ames and Plesniak (1995). This loss is at least partly due to turbulent mixing across velocity gradients in the core of the flow. This "background loss" is negligible for the low turbulence condition but is very important for the close combustor condition.

Low Turbulence. The rows of the showerhead array are near the stagnation region of the vane so the pressure coefficients over the array are relatively low. The pressure coefficients over the five rows of holes of the showerhead array are 0.016, 0.016, 0.066, 0.158, and 0.327 starting from the pressure side to the suction side. The low pressure coefficients would tend to diminish the losses due to the showerhead film cooling while the slant wise injection would tend to increase the loss. A comparison of the total pressure loss surveys for the base vane and the showerhead array taken for the low turbulence condition over the three pressure ratios is shown in figure 7.2. The two lower pressure ratios show a slightly higher peak loss and a corresponding kinetic energy loss coefficient (Ebar) slightly higher than the base vane condition. The highest pressure ratio condition has a total pressure loss coefficient which is comparable to the base vane case even though the mass addition model would predict the loss would grow with increasing pressure ratio (or mass addition). At the highest pressure ratio, assuming a Cd of 0.67, the flow rate from the showerhead is expected to be about 0.6, 0.7, and 1.0 percent of the passage mass flow rate. A simple mass addition model would suggest that the loss associated with the showerhead would be equal to the local row mass flow rate times the local pressure coefficient. This estimate suggests the showerhead loss should be in the neighborhood of 0.10 to 0.13 percent. This difference would be difficult to determine experimentally. The differences in the data may be caused by small spanwise nonuniformities due to the showerhead array flow.

A comparison of the total pressure loss surveys for the base vane and the showerhead array with one row of downstream cooling taken for the low turbulence condition over the three pressure ratios is shown in figure 7.3. The addition of a single row of downstream cooling on the suction side should add significantly to the measured loss. The flow rate per unit length on the suction side is about 1 percent of the passage flow rate. With velocity ratios ranging from 0.67 to 0.76, the incremental mass addition model loss ought to be about 0.7 percent on the suction side. The mean increase in measured loss from the showerhead configuration averages only about 0.1 percent. This discrepancy between the simple model and the data is significant and the anomaly indicates that the film cooling must have a significant effect on the development of the suction surface boundary layer for this vane.

A comparison of the total pressure loss surveys for the base vane and the showerhead array with two rows of downstream cooling taken for the low turbulence condition over the three pressure ratios is shown in figure 7.4. The addition of a second row of downstream cooling on the suction side should add significantly to the measured loss. The flow rate per unit length on the suction side is about 2 percent of the passage flow rate. With velocity ratios ranging from 0.67 to 0.76, the incremental mass addition

model loss ought to be about 0.7 percent for the additional suction side row. The mean increase in measured loss from the showerhead with one downstream row configuration averages about 0.7 percent which is quite consistent with the simple mass addition model. The total measured losses are still about 0.5 percent less than the simple mass addition model would indicate. This difference supports the idea that for this vane configuration, the addition of suction surface cooling affects the development of the suction surface boundary layer which ultimately influences losses. However, the single wire measurements taken on the suction surface boundary layer show a significant increase in the momentum thickness with both one and two rows of film cooling.

A comparison of the exit loss surveys for the four vane configurations at the low turbulence condition is shown in figure 7.5 for an equivalent pressure ratio of 0.07. The data show no significant increase in exit losses with the addition of one downstream row of film cooling on the suction surface. The increment in losses with the addition of a second row of film cooling is clearly seen and is consistent with a simple mass addition model for losses.

A comparison of the surface static pressure distributions for the four vane configurations at the low turbulence condition is shown in figure 7.6 for an equivalent pressure ratio of 0.07. The pressure distributions show a reduction in the overspeed areas on the near suction surface due to the addition of the one and two rows of film cooling along with a reduced static pressure downstream of the holes indicating a local acceleration due to the blockage created by the film cooling mass addition. This change in the pressure profile could have an effect on the development of the boundary layer. However, the single wire profiles clearly show increases in momentum thickness with the addition of one and two rows of film cooling.

High Turbulence. A comparison of the total pressure loss surveys for the base vane and the showerhead array taken for the high turbulence condition over the three pressure ratios is shown in figure 7.7. The two lower pressure ratios show a slightly higher peak loss and a corresponding kinetic energy loss coefficient (Ebar) slightly higher than the base vane condition. The highest pressure ratio condition has a total pressure loss coefficient which is comparable to the base vane case even though a mass addition model would predict the loss would grow with increasing pressure ratio (or mass addition). At the highest pressure ratio, assuming a Cd of 0.67, the flow rate from the showerhead is expected to be about 0.6, 0.7, and 1.0 percent of the passage mass flow rate. A simple mass addition model would suggest that the loss associated with the showerhead would be equal to the local row mass flow rate times the local pressure coefficient, since the mass is injected normal to the flow. This estimate suggests the showerhead loss should be in the neighborhood of 0.10 to 0.13 percent. This difference would be difficult to determine experimentally. The differences in the data are within the experimental uncertainty of the loss coefficient and the only conclusion that can be drawn from the data is that showerhead cooling has only a minor effect on losses.

A comparison of the total pressure loss surveys for the base vane and the showerhead array with one row of downstream cooling taken for the high turbulence condition over the three pressure ratios is shown in figure 7.8. The addition of a single row of downstream cooling on the suction side should add significantly to the measured loss. The flow rate per unit length on the suction side is about 1 percent of the passage flow rate. With velocity ratios ranging from 0.67 to 0.76, the incremental mass addition model loss ought to be about 0.7 percent on the suction side. The mean increase in measured loss from the showerhead configuration averages only about 0.1 percent. This discrepancy between the simple model and the data is significant and the anomaly indicates that the film cooling may cause significant changes to the development of the suction surface boundary layer for this vane.

A comparison of the total pressure loss surveys for the base vane and the showerhead array with two rows of downstream cooling taken for the low turbulence condition over the three pressure ratios is shown in figure 7.9. The addition of a second row of downstream cooling on the suction side should add significantly to the measured loss. The flow rate per unit length on the suction side is about 2 percent of the passage flow rate. With velocity ratios ranging from 0.67 to 0.76, the incremental mass addition model loss ought to be about 0.7 percent for the additional suction side row. The mean increase in measured loss from the showerhead with one downstream row configuration averages about 0.4 percent which is reasonably consistent with the simple mass addition model. The total measured losses are still about 0.7 percent less than the simple mass addition model would indicate. This difference supports the idea that for this vane configuration, the addition of suction surface cooling affects the development of the suction surface boundary layer which ultimately influences losses. However, the single wire measurements taken on the suction surface boundary layer show a significant increase in the momentum thickness with both one and two rows of film cooling.

A comparison of the exit loss surveys for the four vane configurations at the low turbulence condition is shown in figure 7.10 for an equivalent pressure ratio of 0.07. The additional loss from showerhead cooling is about 0.3 percent which is about double the loss expected for the simple mass addition model. The data show no significant increase in exit losses with the addition of one downstream row of film cooling on the suction surface. The increment in losses with the addition of a second row of film cooling is clearly seen and is reasonably consistent with a simple mass addition model for losses.

A comparison of the surface static pressure distributions for the four vane configurations at the low turbulence condition is shown in figure 7.11 for an equivalent pressure ratio of 0.07. The pressure distributions show a reduction in the overspeed areas on the near suction surface due to the addition of the one and two rows of film cooling along with a reduced static pressure downstream of the holes indicating a local acceleration due to the blockage created by the film cooling mass addition. This change in the pressure profile could have an effect on the development of the boundary layer. However, the single wire profiles clearly show increases in momentum thickness with the addition of one and two rows of film cooling.

Summary and Conclusions

The losses generated by the addition of showerhead and downstream film cooling were examined for both low and high inlet turbulence by taking total pressure exit surveys. The data showed the significant difference in losses between the high and low turbulence condition but the incremental losses for the addition of film cooling were consistent between the two conditions. The losses due to the showerhead array were relatively small as expected, but the highest pressure ratio case showed no significant difference from the base vane case. The losses due to the addition of a single row of film cooling on the suction and pressure surface were surprisingly low, adding only about 0.1 percent to the overall loss. This incremental loss was much less than expected. The pressure distributions indicated that the addition of one and two rows of film cooling reduced the high velocity peak on the suction surface which may explain the low incremental loss. However, velocity profiles taken for a slightly lower velocity ratio on the suction surface showed a significant increase in the measured momentum thickness with the addition of a row of film cooling. Generally, the incremental loss for a second row of film cooling was more in line with the level of loss expected.

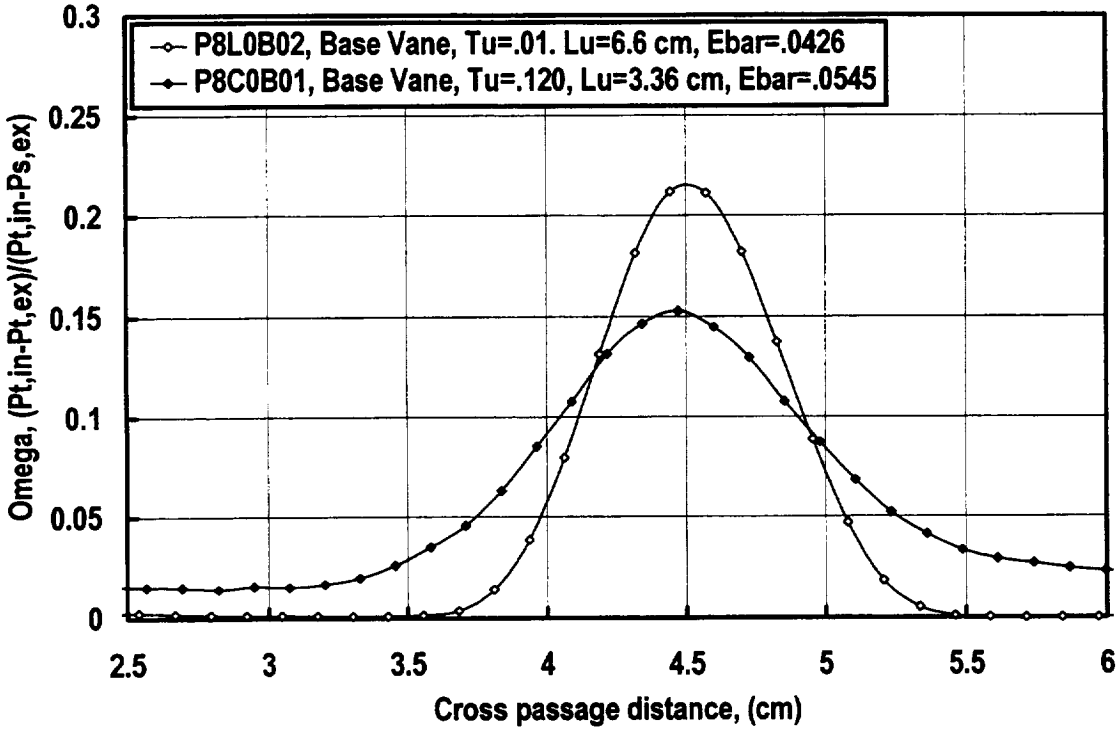

Figure 7.1 Comparison of exit total pressure loss surveys, position 8, vane 2 wake, base vane, low and high turbulence

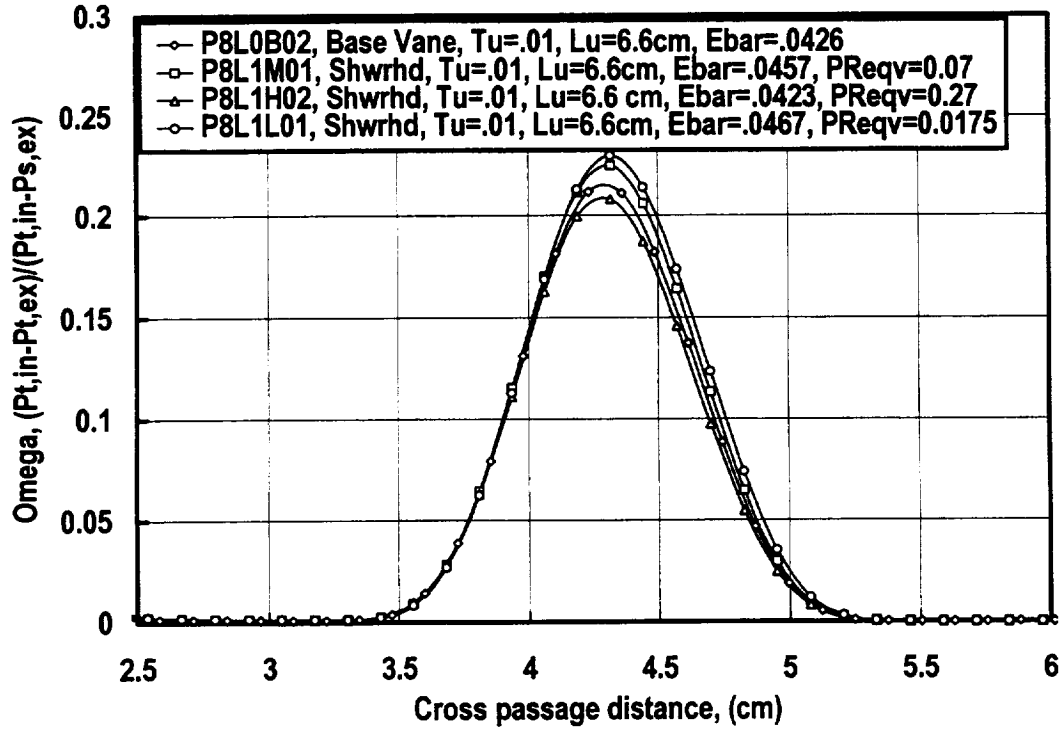

Figure 7.2 Comparison of exit total pressure loss surveys with pressure ratio, position 8, vane 2 wake, showerhead, low turbulence, $Ma_{ex} = 0.27$

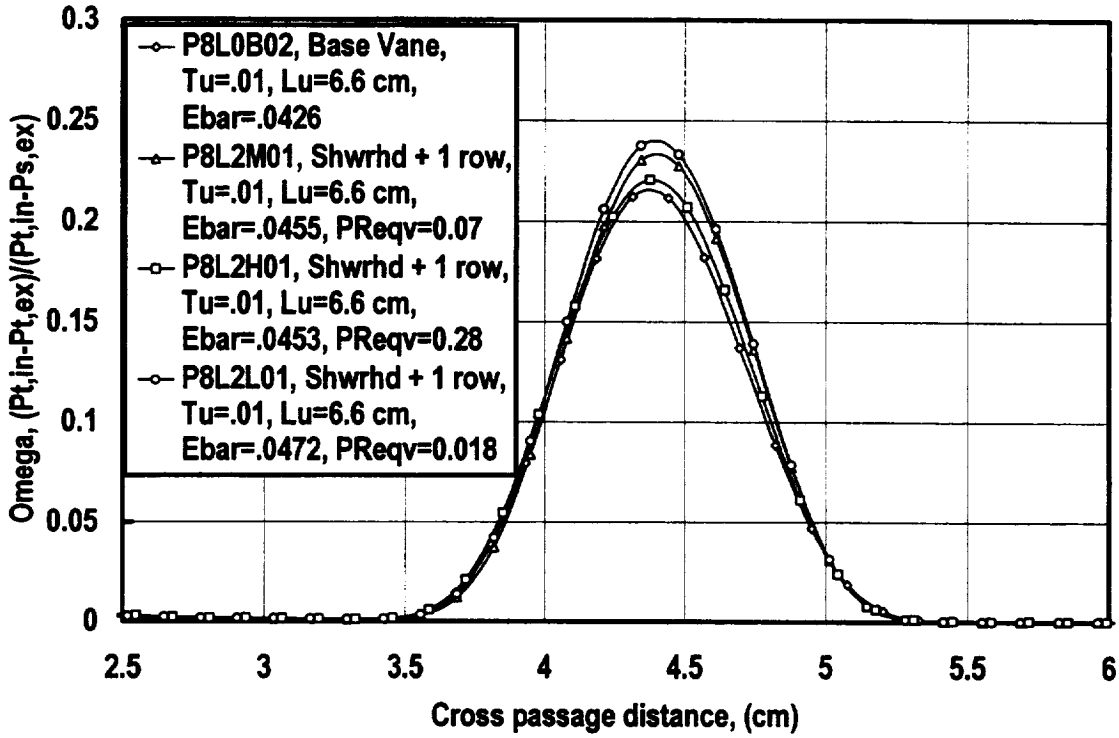

Figure 7.3 Comparison of exit total pressure loss surveys with pressure ratio, position 8, vane 2 wake, showerhead + 1 row, low turbulence, $Ma_{ex} = 0.27$

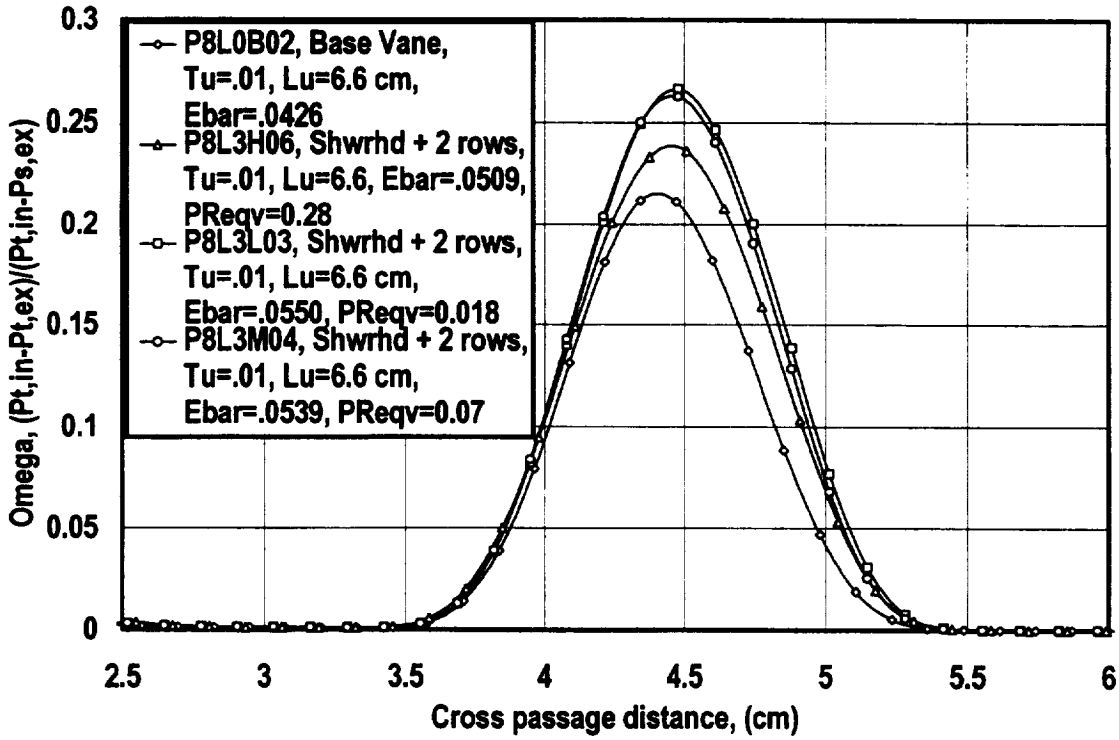

Figure 7.4 Comparison of exit total pressure loss surveys with pressure ratio, position 8, vane 2 wake, showerhead + 2 rows, low turbulence, $Ma_{ex} = 0.27$

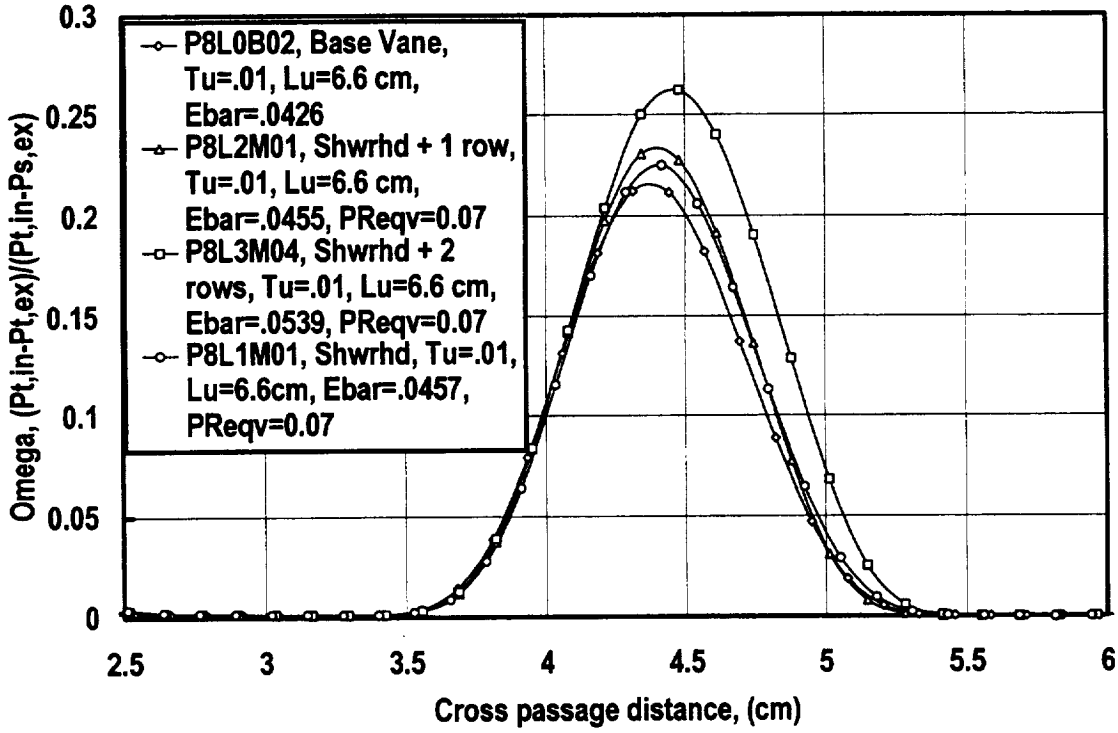

Figure 7.5 Comparison of exit total pressure loss surveys with geometry, position 8, PReqv = 0.07, low turbulence, Ma_{ex} = 0.27

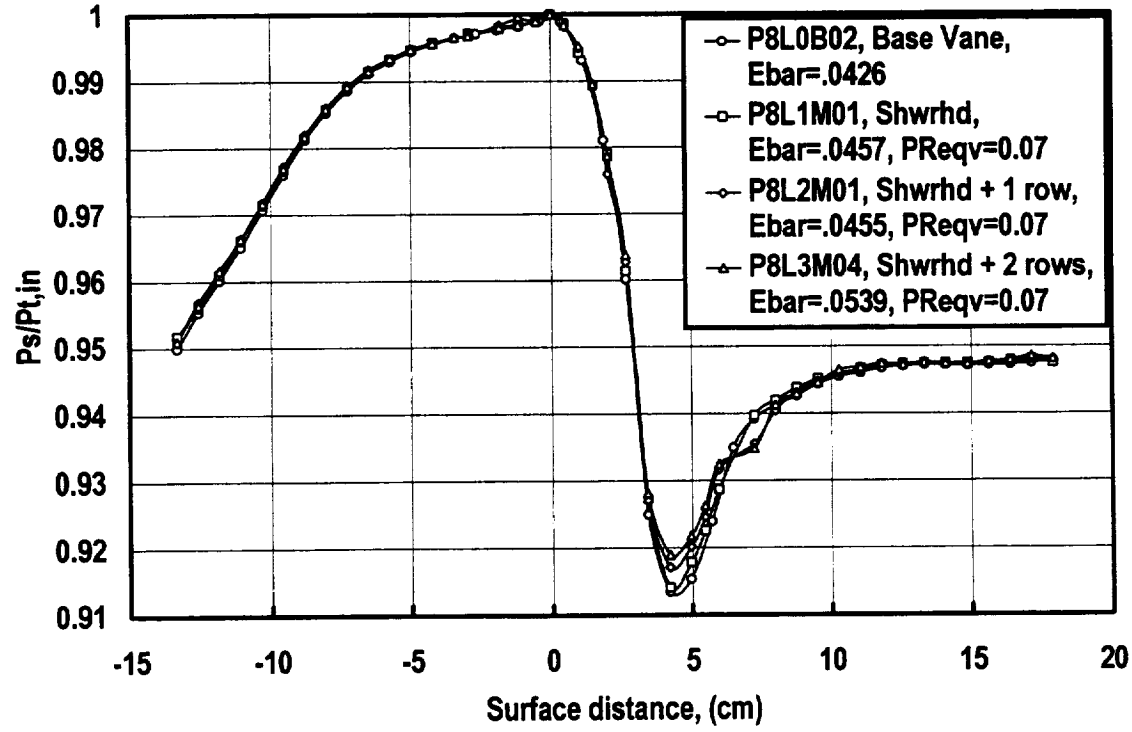

Figure 7.6 Comparison of C3X vane surface pressure distribution with geometry, position 8, Preqv = 0.07, Tu=0.01, Lu=6.6 cm, Ma_{ex} = 0.27

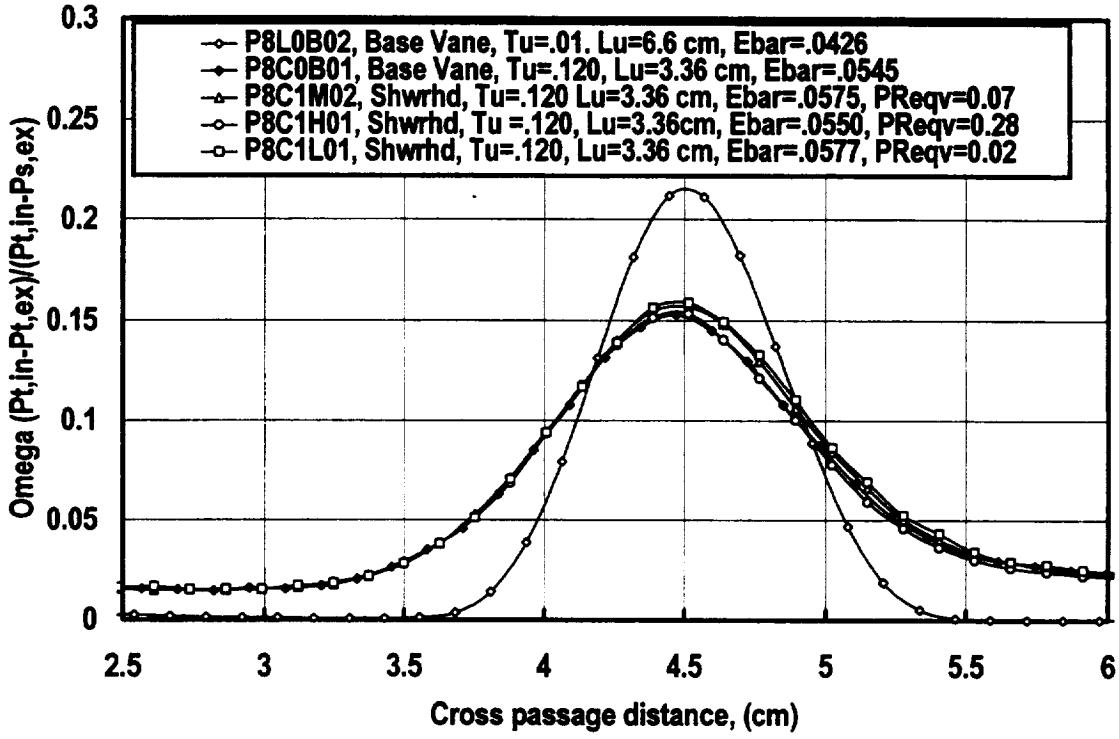

Figure 7.7 Comparison of exit total pressure loss surveys with pressure ratio, position 8, vane 2 wake, showerhead, comb(1), $Ma_{ex} = 0.27$

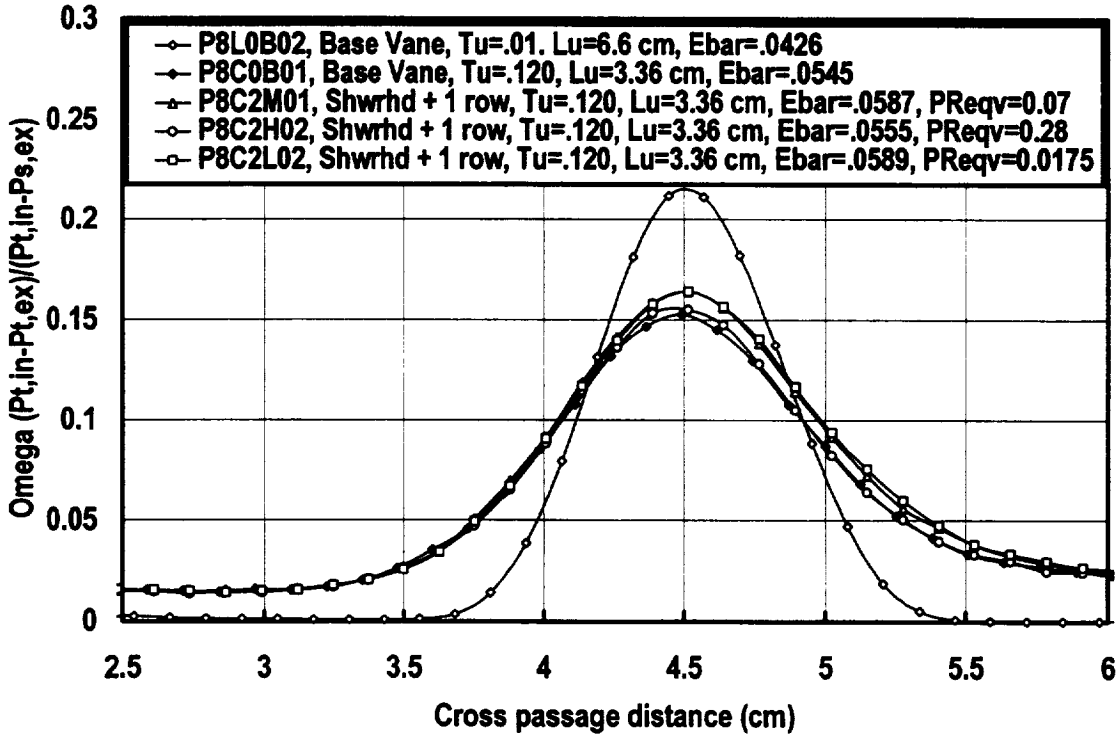

Figure 7.8 Comparison of exit total pressure loss surveys with pressure ratio, position 8, vane 2 wake, showerhead + 1 row, comb(1), $Ma_{ex} = 0.27$

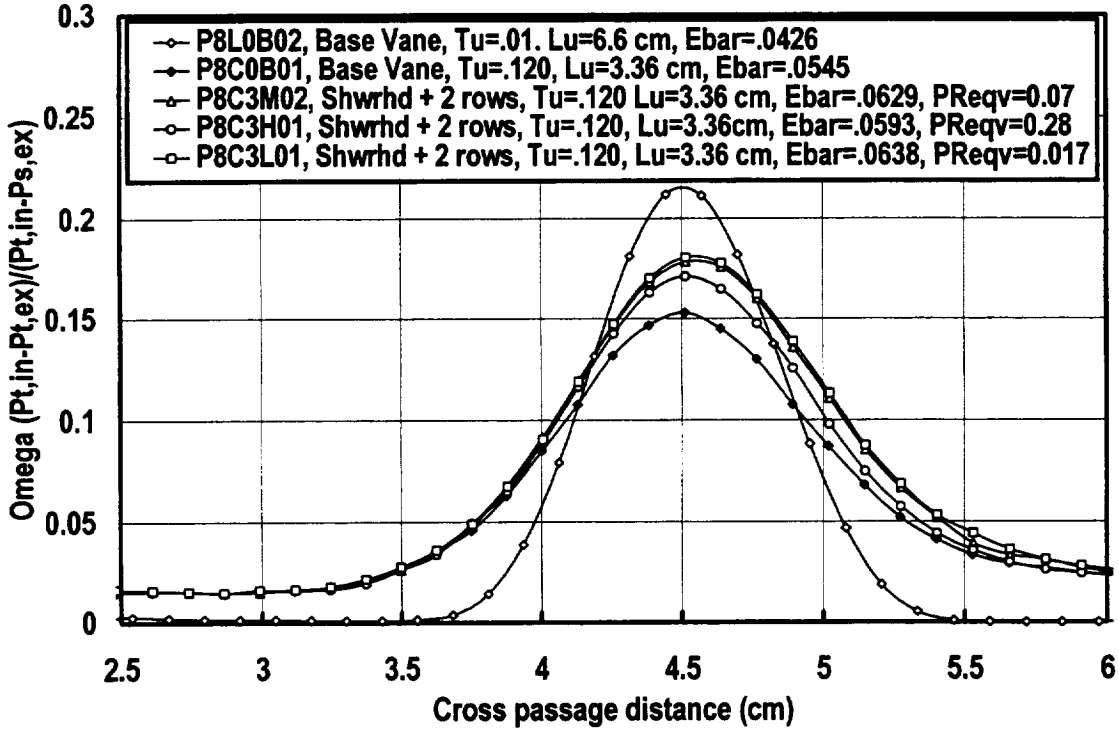

Figure 7.9 Comparison of exit total pressure loss surveys with pressure ratio, position 8, vane 2 wake, showerhead + 2 rows, comb(1), $Ma_{ex} = 0.27$

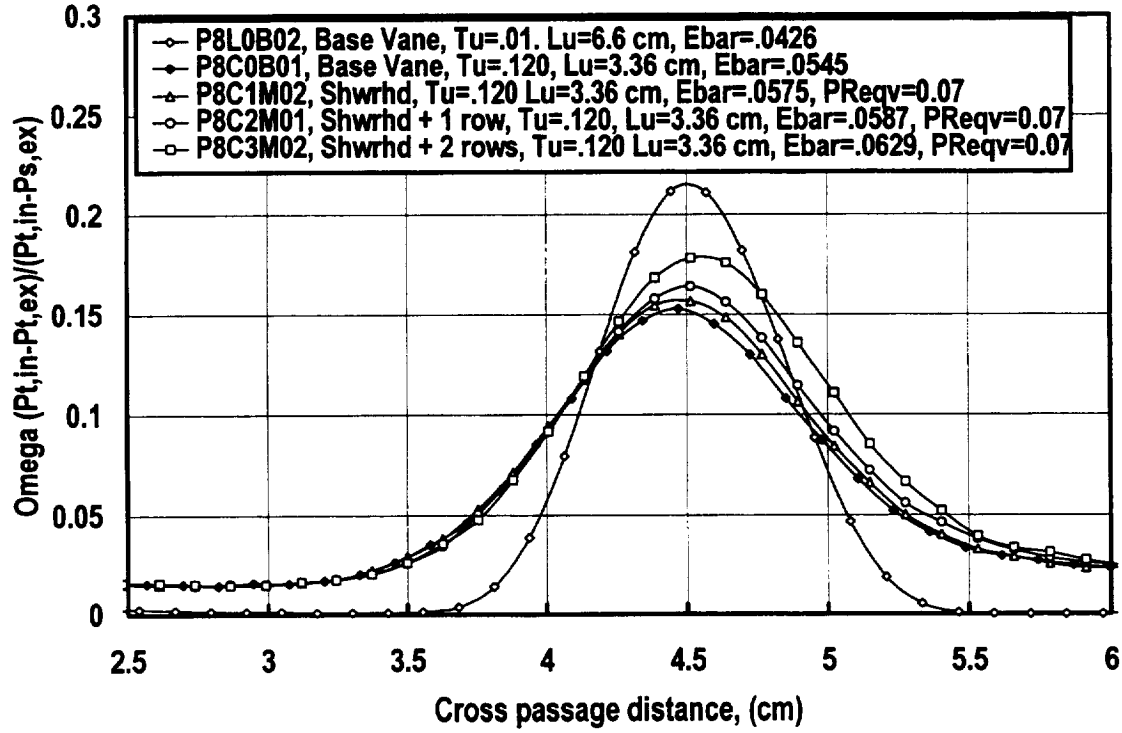

Figure 7.10 Comparison of exit total pressure loss surveys with geometry, position 8, PReqv = 0.07, comb(1), $Ma_{ex} = 0.27$

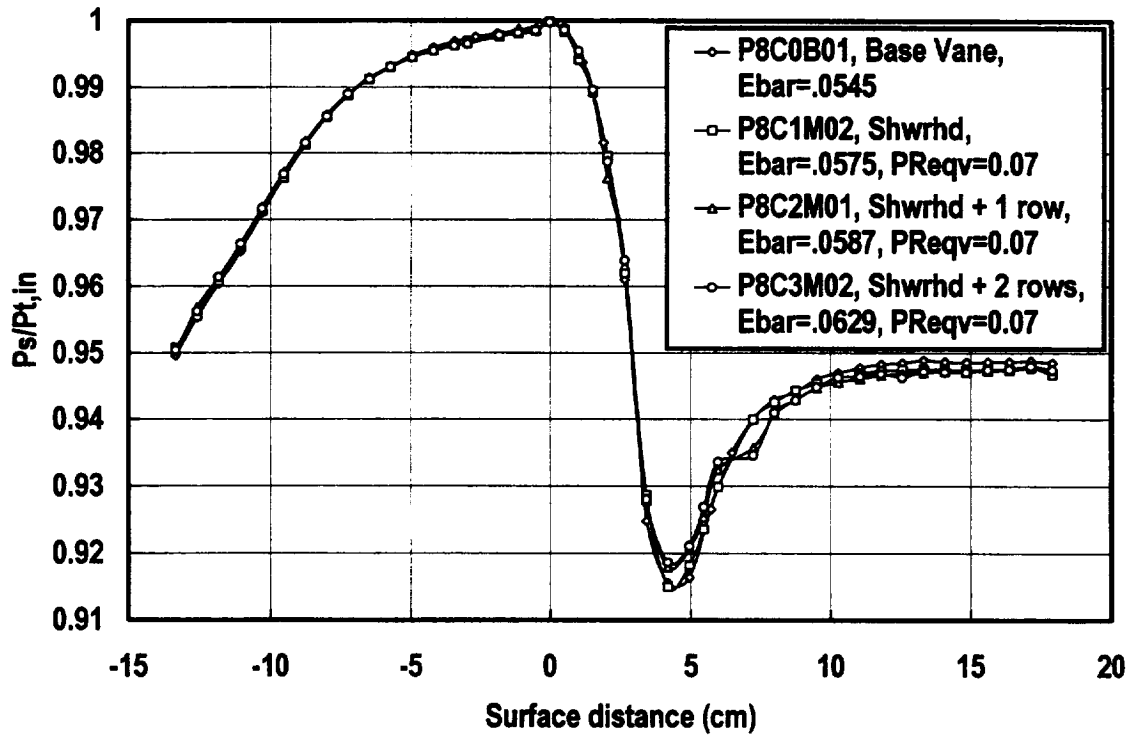

Figure 7.11 Comparison of C3X vane surface pressure distribution with geometry, position 8, Preqv = 0.07, comb(1), $Ma_{ex} = 0.27$

Chapter 8

Conclusions and Summary

The objective of this study was to investigate the influence of free stream turbulence on film cooling effectiveness and the interaction of discrete cooling jets on the surface heat transfer coefficient. The influence of high turbulence on flat plate film cooling has been previously reported but this study examines the influence of turbulence on film cooling for common vane configurations. Additionally, film cooling is known to influence the heat transfer coefficient distribution around and downstream of the hole arrays. Flat plate film cooling studies cannot develop boundary layers consistent with those found on turbomachinery airfoils. In this study the heat transfer distribution downstream from film cooling was examined as was the boundary layer developing downstream from the holes. In addition, the increase in profile losses due to the addition of film cooling has been examined. This chapter is intended to summarize the main results and conclusion from this study.

Heat Transfer with Film Cooling

Film cooling was found to have a substantial influence on heat transfer augmentation for both the high and low turbulence conditions for the laminar regions of the flow and exhibited a much smaller effect on the turbulent regions of the flow. Heat transfer augmentation due to film cooling was found to strongly depend on the velocity ratio or pressure ratio of the cooling array. The film cooling had the biggest influence near the holes for the high turbulence case. Also, the effect of film cooling was largest near the holes for the turbulence boundary layer on the suction surface for both cases. The influence of the film cooling on heat transfer was found to be more persistent in the laminar regions for the low turbulence cases. The low turbulence cases had significantly higher levels of augmentation than the high turbulence cases but the high turbulence cases all exhibited higher absolute levels of heat transfer for a given film cooling condition than the low turbulence cases. While the Stanton number augmentation ratios for the low turbulence cases were very high, they are not relevant from an engineering standpoint, since low turbulence levels do not exist at the entrance to first stage nozzles. However, the levels of Stanton number augmentation ratio found in the laminar regions for the high turbulence condition are substantial and heat transfer designers need to have both a general understanding of this problem and the design tools to deal with this situation. This heat transfer research should provide some of the needed understanding and these data can be used to help develop applicable tools. A more detailed understanding of the heat transfer problem is still needed in and around the holes and for arrays at different locations in terms of the pressure coefficient, on the pressure surface.

Film Cooling with High Turbulence

The influence of mock combustor turbulence was found to have a dramatic effect on pressure surface film cooling. The process of mixing film cooling protection away in the normal direction was found to be gradual but significant based on the results from the double row of

staggered holes on the pressure side, which are comparable to averaged effectiveness distributions. The high turbulence had reduced the effectiveness level to an average of 45 percent of the low turbulence level by the last measurement location. The single row of holes on the pressure side showed a more immediate reduction in effectiveness for the lowest velocity due to spanwise mixing as evidenced by the spanwise uniformity in velocity profiles. This strong spanwise mixing is also consistent with observations by Bons, MacArthur, and Rivir (1994). The influence of turbulence on cooling protection was less substantially reduced for the higher velocity ratios of the single row where the cooling protection was already poor.

The influence of turbulence on suction surface effectiveness was seen to be more complicated due to the interaction of the free stream turbulence with the suction surface boundary layer and the boundary layers corresponding interaction with the film cooling jets. The high turbulence produced a boundary layer with significantly higher skin friction and the fuller near wall profile apparently improved effectiveness in the near hole region. Further downstream, the effect of the turbulence was seen as the cooling performance of the high turbulence case deteriorated more rapidly.

The dissipation of cooling performance by the high inlet turbulence was found to be more substantial for the showerhead array on the suction surface. This difference was probably due to the longer streamwise distance the turbulence had to act. The highest pressure ratio showed a reduced influence of the turbulence due to the thermal dilution effect of the high mass flow rate. The level of cooling protection produced by the showerhead was poor on the pressure surface and showed regions of poor coverage. With the high turbulence, the protection was driven largely by the mass flow rate.

Generally, the turbulence was found to gradually mix away cooling protection in the normal direction producing effects that could be dramatic far downstream. The turbulence dissipated protection more rapidly in the spanwise direction. The pressure surface with its higher relative level of turbulence was affected more than the suction surface. Higher blowing and velocity ratios generally were less affected than lower blowing ratios due to the thermal dilution effect of the higher mass flows. More data is needed on the pressure surface in and around the holes and for arrays located in regions of higher relative velocities.

Velocity Profiles with Film Cooling

Velocity profiles downstream from film cooling arrays have been documented in this chapter to provide details of the interaction of turbulence and film cooling with vane surface boundary layer development. These data offer qualitative information which aids in visualizing how film cooling alters the development of the boundary layer and how turbulence mixes out the velocity and analogously temperature differences resulting from the film cooling jets in both the spanwise and normal directions. Additionally, the velocity and turbulence distributions represent useful quantitative information for grounding predictive comparisons.

Exit Losses with Film Cooling

The losses generated by the addition of showerhead and downstream film cooling were examined for both low and high inlet turbulence by taking total pressure exit surveys. The data showed the significant difference in losses between the high and low turbulence condition but the incremental losses for the addition of film cooling were consistent between the two conditions. The losses due to the showerhead array were relatively small as expected, but the highest pressure ratio case showed no significant difference from the base vane case. The losses due to the addition of a single row of film cooling on the suction and pressure surface were surprisingly low, adding only about 0.1 percent to the overall loss. This incremental loss was much less than expected. The pressure distributions indicated that the addition of one and two rows of film cooling reduced the high velocity peak on the suction surface which may explain the low incremental loss. However, velocity profiles taken for a slightly lower velocity ratio on the suction surface showed a significant increase in the measured momentum thickness with the addition of a row of film cooling. Generally, the incremental loss for a second row of film cooling was more in line with the level of loss expected.

References

1. Abhari, R.S., and Epstein, A.H., 1994, "An experimental study of film cooling in a rotating transonic turbine," ASME J. Turbomachinery, Vol. 116, p. 63.
2. Abuaf, N., Bunker, R., and Lee, C.P., 1995, "Heat transfer and film cooling effectiveness in a linear airfoil cascade," ASME paper no. 95-GT-3.
3. Ames, F.E., and Moffat, R.J., 1990, "Heat Transfer with High Intensity, Large Scale Turbulence: The Flat Plate Turbulent Boundary Layer and the Cylindrical Stagnation Point., Report No. HMT-44, Thermosciences Division of Mechanical Engineering, Stanford University.
4. Ames, F.E., 1994, "Experimental study of vane heat transfer and aerodynamics at elevated levels of turbulence," NASA CR 4633.
5. Ames, F.E., 1995, "The influence of large scale high intensity turbulence on vane heat transfer," ASME paper no. 95-GT-21.
6. Ames, F.E., and Plesniak, M.W., 1995, "The influence of large scale, high intensity turbulence on vane aerodynamic losses, wake growth, and the exit turbulence parameters," ASME paper no. 95-GT-290.
7. Bicen, A.F., and Jones, W.P., 1986, "Velocity characteristics of isothermal and combusting flows in a model combustor," Combust. Sci. and Technology, Vol. 49, p. 1.
8. Bons, J.P., MacArthur, C.D., and Rivir, R.B., 1994, "The effect of high freestream turbulence on film cooling effectiveness," ASME paper no. 94-GT-51.
9. Buck, F.A., and Prakash, C., 1995, "Design and evaluation of a single passage test model to obtain turbine airfoil film cooling effectiveness data," ASME paper no. 95-GT-19.
10. Crocker, M.L., and L'Ecuyer, M.R., 1988, "The effects of blowing ratio, density ratio, Reynolds number, and pitch-to-diameter ratio on film cooling effectiveness," Purdue University Thermal Sciences and Propulsion Center Report No. ME-TSPC-TR-88-17.
11. Denton, J.D., 1993, "Loss Mechanisms in Turbomachines," ASME Paper No. 93-GT-435, Presented at the International Gas Turbine and Aeroengine Congress and Exposition, Cincinnati, Ohio, May, 1993.
12. Dring, R.P., Blair, M.F., and Joslyn, H.D., 1980, "An experimental investigation of film cooling on a turbine rotor blade," J. of Engineering for Power, Vol.102, No.1, p.88.
13. Frota, M.F., 1982, "Analysis of the Uncertainties in Velocity Measurements and Technique for Turbulence Measurements in Complex Heated Flows with Multiple Hot-Wires," Ph.D. Dissertation, Dept. Mech. Engr., Stanford University.
14. Garg, V.K., Gaugler, R.E., 1993, "Heat transfer in film-cooled turbine blades," ASME paper no. 93-GT-81.
15. Gartshore, I.S., Salcudean, M., Barnea, Y., Zhang, K., and Aghadsi, F., 1993, "Some effects of coolant density on film cooling effectiveness," ASME paper no. 93-GT-76.
16. Glassman, A.J., editor, 1973, Turbine Design and Application, NASA SP-290, National Aeronautics and Space Administration, 1973.
17. Goebel, S.G., Abuaf, N., Lovett, J.A., and Lee, C.P., 1993, "Measurements of combustor velocity and turbulence profiles," ASME paper no. 93-GT-228.

18. Hancock, P.E., and Bradshaw, P. 1983, "The Effect of Free-Stream Turbulence on Turbulent Boundary Layer Flow and Heat Transfer," J. Fluids Engr., Vol. 105, p. 284.
19. Hinze, J., 1975, Turbulence, 2nd Ed., McGraw-Hill, New York.
20. Kays, W.M., 1987, "STAN7, a finite difference boundary layer code."
21. Kline, S.J., and McClintock, F.A., Jan., 1953, "Describing Uncertainties in Single Sample Experiments," Mech. Engr., p. 3.
22. Lefebvre, A.W., 1983, Gas Turbine Combustion, McGraw-Hill, New York.
23. L'Ecuyer, M.R., and Soechting, F.O., 1985, A model for correlating flat plate film cooling effectiveness for rows of round holes," *Heat Transfer and Cooling in Gas Turbines: AGARD Conference Proceedings No. 390*, 1985.
24. Mayle, R.E., 1991, "The role of laminar-turbulent transition in gas turbine engines," 1991 ASME International Gas Turbine Institute Scholar Award Paper, J. Turbomachinery, 113, pp. 509-537.
25. Mehendale, A.B., and Han, J.C., 1992, "Influence of high mainstream turbulence on leading edge film cooling heat transfer," ASME J. Turbomachinery, Vol. 114, p. 707.
26. Mehendale, A.B., Han, J.C., Ou, S., and Lee, C.P., 1994, "Unsteady wake over a linear turbine blade cascade with air and CO2 film injection: Part II -- Effect on film effectiveness and heat transfer distributions," ASME J. Turbomachinery, Vol. 116, p. 730.
27. Moss, R.W., and Oldfield, L.G., 1991, "Measurements of hot combustor turbulence spectra," ASME Paper no. 91-GT-351.
28. Moss, R.W., and Oldfield, L.G., 1992, "Measurements of the effect of free-stream turbulence length scale on heat transfer," ASME Paper 92-GT-244.
29. Moffat, R.J., 1980, "Experimental Methods in the Thermosciences," Dept. Mech. Engr., Stanford, University.
30. Nealy, D.A., Mihelc, M.S., Hylton, L.D., and Gladden, H.J., 1983, "Measurements of Heat Transfer Distribution Over the Surfaces of Highly Loaded Turbine Nozzle Guide Vanes," ASME paper No. 83-GT-53.
31. Nirmalan, N.V., and Hylton, L.D., 1990, "An experimental study of turbine vane heat transfer with leading edge and downstream film cooling," ASME J. Turbomachinery, Vol. 112, p. 477.
32. Ou, S. and Han, J.C., 1993, "Unsteady wake effect on film effectiveness and heat transfer coefficient from a turbine blade with one row of air and CO_2 film injection," ASME paper no. 93-WA/HT-57.
33. Ou, S., Han, J.C., Mehendale, A.B., and Lee, C.P., 1994, "Unsteady wake over a linear turbine blade cascade with air and CO_2 film injection: Part I -- Effect on heat transfer coefficients," ASME J. Turbomachinery, Vol. 116, p. 721.
34. Ou, S., Mehendale, A.B., and Han, J.C., 1992, "Influence of high mainstream turbulence on leading edge film cooling heat transfer: Effect of film hole row location," ASME Journal of Turbomachinery, Vol. 114, p. 716.
35. Rohsenow, Harnett, and Ganic, 1985 "Handbook of Heat Transfer Applications," 2nd Edition, McGraw-Hill Book Company.
36. Salcudean, M., Gartshore, I., Zhang, K., and McLean, I., 1994, "An experimental study of film cooling effectiveness near the leading edge of a turbine blade," J. of Turbomachinery, Vol. 116, p. 71.

37. Scrivener, C.T.J., 1990, "Heat transfer in aero engine gas turbines - part I," Journal of the Gas Turbine Society of Japan, June, 1990.
38. Simoneau, R.J., and Simon, F.F., 1993, "Progress towards understanding and predicting heat transfer in the turbine gas path," Int. J. Heat and Fluid Flow, Vol. 14, No. 2, June, 1993.
39. Takeishi, K., Aoki, S., Sato,T., and Tsukagoshi, K., 1991, "Film cooling on a gas turbine rotor blade," ASME paper no. 91-GT-279.
40. Thole, 1996, Private communication
41. White, F.M., 1974, Viscous Fluid Flow, McGraw-Hill, New York.
42. Wubben, F.J.W., 1991, "Single and Cross Hot Wire Anemometry in Incompressible Flow," Report LR-663, Faculty of Aerospace Engineering, Delft University of Technology
43. Zimmerman, D.R., 1979, Laser anemometer measurements at the exit of a T63-C20 combustor," NASA CR-159623.
44. Zimmerman, D.R., 1990, "Three-Dimensional Laser Anemometer Measurements in a Linear Turbine Vane Cascade," Forum on Turbulent Flows -- 1990, ASME FED Vol. 94, p. 143.

Appendix A.1 Inlet Turbulence Characteristics

	File	Tu	Vel (m/s)	Lx (cm)	Lu (cm)	Diss (m^2/s^3)	Y (cm)	Pos
Comb(1)	IR8CB1	0.1259	29.69	1.509	3.086	2542	3.810	6
	IR8CB2	0.1323	29.50	1.826	3.457	2580	2.540	6
	IR8CB3	0.1269	29.26	1.643	3.205	2396	5.080	6
	IR8CB4	0.1972	22.66	2.261	5.022	2661	0.127	6
	IR8CB5	0.1840	25.92	2.807	6.777	2414	0.318	6
	IR8CB6	0.1468	28.71	2.840	5.118	2197	1.016	6
	IR8CB7	0.1247	29.70	1.433	3.119	2439	3.810	2
	IR8CB8	0.1327	29.34	2.004	3.698	2390	2.540	2
	IR8CB9	0.1314	29.46	1.798	3.602	2415	5.080	2
	IR5CB1	0.1310	19.69	1.560	3.137	821	3.810	2
	IR5CB2	0.1360	19.37	1.567	3.193	858	3.810	6
Low Turb	IR8C21	0.0090	29.87	6.708	15.662	0.177	3.810	6
	IR8C22	0.0065	29.71	6.510	5.695	0.192	2.540	6
	IR8C23	0.0136	29.13	3.629	11.844	0.782	5.080	6
	IR8C24	0.0095	29.78	5.316	5.712	0.589	3.810	2
	IR8C25	0.0117	29.78	4.445	9.528	0.668	2.540	2
	IR8C26	0.0145	29.22	4.054	5.695	2.019	5.080	2
	IR5C21	0.0088	19.23	8.336	16.561	0.045	3.810	6
	IR5C22	0.0096	19.44	8.654	21.717	0.045	3.810	2

Appendix A.2 Vane Pressure Distributions

The three pages following this page contain pressure distributions for the two turbulence cases taken at three different exit Mach number conditions for the base vane. Additionally, pressure distributions are given for three film cooling geometries for three equivalent pressure ratios and for the two turbulence conditions. The pressure profiles are given in terms of the local vane static pressure ratioed by the inlet total pressure versus surface distance in centimeters. The position of 0.0 cm is taken as the nominal stagnation point with positive surface distance being the arc along the suction surface and negative distance is the arc along the pressure surface. The geometries of the base vane, the showerhead vane, the vane with a showerhead and one row of downstream film cooling on both the suction and pressure surface, and the vane with the showerhead and two rows of downstream film cooling are given in the heading of each profile. Additional information on the conditions is also given in the heading of the data sets. For these tests, all cooling arrays are fed with a common plenum.

Filename:	cvane51	cbvane52	pv02b02	pv8c0b01	pv0bh02	pv1c0b01
Geom:	Basevane	Basevane	Basevane	Basevane	Basevane	Basevane
Ma,ex	0.1697	0.1699	0.2703	0.2683	0.3472	0.3288
Ma,in	0.0537	0.0541	0.0786	0.0799	0.0985	0.0962
Tu,in	0.009	0.124	0.011	0.12	0.011	0.12
Lu,in (cm)	19.1	3.16	6.6	3.36	6.6	3.36
U0,in(m/s)	19.34	19.53	29.58	29.49	37.05	35.32
Surface	Ps(x)/Pt	Ps(x)/Pt	Ps(x)/Pt	Ps(x)/Pt	Ps(x)/Pt	Ps(x)/Pt
(cm)						
-13.335	0.979486	0.979571	0.949945	0.950048	0.919123	0.926124
-12.573	0.981577	0.981887	0.955264	0.956021	0.927754	0.934898
-11.811	0.983599	0.98384	0.960188	0.960943	0.935713	0.942162
-11.049	0.98556	0.98579	0.965174	0.965604	0.944441	0.949389
-10.287	0.987756	0.988014	0.970728	0.971136	0.952919	0.957463
-9.525	0.989903	0.990134	0.976052	0.976403	0.961718	0.965227
-8.763	0.991872	0.992027	0.981199	0.981252	0.96996	0.972631
-8.001	0.993551	0.993744	0.985311	0.985325	0.976573	0.978603
-7.239	0.995053	0.995103	0.98864	0.988568	0.98196	0.983439
-6.477	0.99615	0.996162	0.991184	0.991027	0.986024	0.987008
-5.715	0.996977	0.996926	0.992894	0.992752	0.988816	0.989471
-4.953	0.997687	0.997551	0.994462	0.994311	0.991322	0.991818
-4.191	0.998185	0.998019	0.99556	0.995442	0.993094	0.993421
-3.429	0.998583	0.998326	0.996475	0.996308	0.994514	0.994678
-2.667	0.998881	0.998606	0.997113	0.996885	0.995539	0.995569
-1.905	0.999162	0.998857	0.99771	0.997559	0.996449	0.996445
-1.143	0.999371	0.999039	0.998186	0.99797	0.997166	0.997069
-0.381	0.999756	0.999328	0.998958	0.998677	0.998374	0.998097
0.381	0.999669	0.999438	0.998868	0.998931	0.998286	0.998406
1.143	0.99689	0.997031	0.99311	0.993427	0.989309	0.990504
1.905	0.991512	0.992046	0.981034	0.981568	0.970352	0.97359
2.667	0.982967	0.983584	0.960215	0.961088	0.937763	0.944222
3.429	0.96822	0.969127	0.925035	0.927017	0.883415	0.895098
4.191	0.965301	0.965203	0.913412	0.915093	0.861556	0.876166
4.953	0.966208	0.965817	0.915417	0.916677	0.864218	0.877343
5.715	0.968632	0.96962	0.924037	0.927581	0.87935	0.893992
6.477	0.972871	0.973429	0.934928	0.935814	0.895641	0.905499
7.239	0.97563	0.975361	0.939216	0.939961	0.901819	0.911691
8.001	0.976501	0.976419	0.941219	0.942484	0.905716	0.9153
8.763	0.976872	0.976996	0.942668	0.943761	0.907492	0.917261
9.525	0.97764	0.977757	0.944358	0.945623	0.910457	0.919775
10.287	0.978016	0.978146	0.945455	0.946359	0.91204	0.921069
11.049	0.978315	0.978492	0.946037	0.947135	0.912958	0.92201
11.811	0.978442	0.978616	0.946744	0.947478	0.913725	0.922666
12.573	0.978538	0.97871	0.946991	0.947913	0.914279	0.922911
13.335	0.978699	0.978879	0.947212	0.948144	0.914512	0.923303
14.097	0.978651	0.978842	0.947165	0.947983	0.914481	0.923215
14.859	0.978679	0.978868	0.947116	0.947887	0.914211	0.92302
15.621	0.97868	0.978891	0.9472	0.94811	0.914566	0.923165
16.383	0.978661	0.978889	0.94728	0.948106	0.914803	0.923263
17.145	0.978704	0.97888	0.947509	0.948231	0.914848	0.923283
17.907	0.978748	0.978917	0.947731	0.94829	0.915423	0.923102

Filename:	p8l1l01	p8l1m01	p8l1h02	p8l2l01	p8l2m02	p8l2h01	p8l3l03	p8l3m04	p8l3h06
Geom:	Shwrhd	Shwrhd	Shwrhd	Shwhd+1	Shwhd+1	Shwhd+1	Shwhd+2	Shwhd+2	Shwhd+2
PReqv:	0.017559	0.074119	0.272727	0.017403	0.074717	0.275371	0.018525	0.070896	0.278274
Ma,ex:	0.270115	0.269702	0.270384	0.27084	0.269843	0.270331	0.269558	0.269835	0.270043
Ma,in:	0.078448	0.078001	0.078011	0.077503	0.076418	0.076145	0.076108	0.075887	0.07538
Tu,in:	0.011	0.011	0.011	0.011	0.011	0.011	0.011	0.011	0.011
Lu,in (cm)	6.6	6.6	6.6	6.6	6.6	6.6	6.6	6.6	6.6
U0,in (m/s	29.49	29.49	29.49	29.49	29.49	29.49	29.49	29.49	29.49
Surface	Ps(x)/Pt	Ps(x)/Pt	Ps(x)/Pt	Ps(x)/Pt	Ps(x)/Pt	Ps(x)/Pt	Ps(x)/Pt	Ps(x)/Pt	Ps(x)/Pt
(cm)									
-13.335	0.951414	0.95169	0.951154	0.950612	0.951142	0.950567	0.951145	0.951043	0.950692
-12.573	0.955825	0.956001	0.955796	0.956572	0.956889	0.956666	0.956724	0.956513	0.956482
-11.811	0.960806	0.960967	0.960736	0.96113	0.961571	0.961358	0.96152	0.961686	0.961418
-11.049	0.965986	0.966128	0.966118	0.966099	0.966435	0.966323	0.966523	0.966443	0.966564
-10.287	0.971361	0.971462	0.971403	0.971814	0.972005	0.97192	0.971861	0.971831	0.971748
-9.525	0.976492	0.976626	0.976435	0.977129	0.977474	0.977314	0.977017	0.977068	0.976964
-8.763	0.981529	0.981526	0.981474	0.981829	0.982039	0.981951	0.981862	0.981777	0.981738
-8.001	0.985605	0.985692	0.98569	0.985924	0.986182	0.98604	0.985976	0.985932	0.985883
-7.239	0.988908	0.988958	0.989004	0.989251	0.98943	0.989373	0.989325	0.989333	0.989246
-6.477	0.99142	0.991482	0.99148	0.991626	0.991836	0.991709	0.991638	0.99161	0.991579
-5.715	0.993221	0.993257	0.993253	0.993332	0.993419	0.993425	0.993391	0.993353	0.993426
-4.953	0.994668	0.994714	0.99469	0.994751	0.994838	0.994843	0.994792	0.994763	0.994806
-4.191	0.995796	0.995814	0.99584	0.995747	0.995812	0.995904	0.99569	0.99565	0.995688
-3.429				0.996517	0.996608	0.99665	0.996559	0.996605	0.996742
-2.946	0.997072	0.997099	0.997044	0.996849	0.996868	0.996739	0.996794	0.996818	0.996779
-1.829	0.997875	0.997913	0.997799	0.998001	0.99767	0.998401	0.998055	0.998053	0.99802
-1.143	0.998316	0.998348	0.998186	0.99868	0.99982	0.999183	0.998446	0.998423	0.998278
-0.508	0.998819	0.998838	0.998748	0.99892	0.998984	0.998598	0.998945	0.998929	0.998782
0	0.999962	0.99998	0.999968	0.999969	0.999965	1	1.00001	0.999993	0.999973
0.508	0.998553	0.9986	0.997807	0.998395	0.998078	0.998269	0.998636	0.998436	0.998801
1.016	0.994104	0.994151	0.993978	0.994973	0.994857	0.99551	0.99529	0.995294	0.995772
1.524	0.989204	0.989335	0.989503	0.989004	0.989135	0.988808	0.989607	0.989517	0.988688
2.032	0.978875	0.979043	0.978259	0.975679	0.975945	0.974662	0.978717	0.978664	0.977893
2.667	0.961249	0.961423	0.961478	0.962565	0.962769	0.962438	0.963939	0.963907	0.964034
3.429	0.927065	0.927344	0.927181	0.926443	0.927182	0.927289	0.927841	0.928234	0.928205
4.191	0.913714	0.914114	0.913923	0.916518	0.917235	0.917055	0.918822	0.918979	0.918936
4.953	0.917848	0.917901	0.917281	0.919852	0.920441	0.91992	0.92228	0.921863	0.92222
5.461	0.922219	0.922602	0.923217	0.924233	0.925036	0.925446	0.926644	0.926382	0.927294
5.969	0.927524	0.92877	0.929363	0.930717	0.931987	0.932365	0.931694	0.932445	0.934077
7.239	0.939494	0.93968	0.939417	0.935218	0.935985	0.935094	0.935148	0.934806	0.934608
8.001	0.941902	0.941953	0.941916	0.940082	0.940653	0.940374	0.941173	0.94125	0.941229
8.763	0.943819	0.94379	0.943768	0.942628	0.9432	0.942968	0.943029	0.943003	0.943
9.525	0.944919	0.945134	0.944915	0.944234	0.944868	0.944657	0.9447	0.94462	0.944514
10.287				0.945435	0.94594	0.945653	0.946644	0.94648	0.94666
11.049	0.946421	0.946651	0.946471	0.94606	0.946461	0.946321	0.946659	0.946896	0.94673
11.811	0.946948	0.94719	0.946949	0.946482	0.946824	0.946611	0.947264	0.947423	0.947232
12.573	0.947316	0.947403	0.947355	0.946768	0.947177	0.947059	0.947425	0.94724	0.947245
13.335	0.947329	0.947452	0.947413	0.946922	0.947237	0.947218	0.947629	0.947617	0.947549
14.097	0.947364	0.947413	0.947197	0.946826	0.947385	0.947153	0.947661	0.947424	0.947447
14.859	0.947298	0.947485	0.947162	0.947229	0.947756	0.947197	0.947552	0.94737	0.947279
15.621	0.947461	0.947564	0.947318	0.947184	0.947475	0.947288	0.947947	0.947759	0.947717
16.383	0.947567	0.947911	0.947566	0.947485	0.947407	0.949805	0.948039	0.94794	0.948035
17.145	0.947935	0.948095	0.947728	0.947926	0.948115	0.948008	0.948549	0.948507	0.948183
17.907	0.947308	0.947489	0.947203	0.947686	0.948203	0.947865	0.94842	0.948126	0.947752

Filename:	p8c1l01	p8c1m02	p8c1h01	p8c2l02	p8c2m01	p8c2h02	p8c3l01	p8c3m02	p8c3h01
Geom:	Shwrhd	Shwrhd	Shwrhd	Shwhd+1	Shwhd+1	Shwhd+1	Shwhd+2	Shwhd+2	Shwhd+2
PReqv:	0.021369	0.064856	0.276793	0.016423	0.070538	0.275255	0.015995	0.069533	0.281009
Ma,ex:	0.269378	0.270804	0.270749	0.269641	0.270648	0.270285	0.270264	0.2707	0.270286
Ma,in:	0.079189	0.079563	0.079142	0.078686	0.078772	0.078016	0.078733	0.078517	0.07807
Tu,in:	0.12	0.12	0.12	0.12	0.12	0.12	0.12	0.12	0.12
Lu,in (cm)	3.36	3.36	3.36	3.36	3.36	3.36	3.36	3.36	3.36
U0,in (m/s	29.49	29.49	29.49	29.49	29.49	29.49	29.49	29.49	29.49
Surface	Ps(x)/Pt	Ps(x)/Pt	Ps(x)/Pt	Ps(x)/Pt	Ps(x)/Pt	Ps(x)/Pt	Ps(x)/Pt	Ps(x)/Pt	Ps(x)/Pt
(cm)									
-13.335	0.951348	0.95076	0.950782	0.950591	0.95027	0.950524	0.950637	0.950458	0.950445
-12.573	0.956114	0.955586	0.955672	0.957133	0.956844	0.956959	0.956475	0.956305	0.956379
-11.811	0.961107	0.960783	0.960704	0.961644	0.961411	0.9615	0.961493	0.961416	0.961441
-11.049	0.966369	0.965814	0.965889	0.966518	0.966357	0.966485	0.966503	0.966332	0.966415
-10.287	0.971518	0.971224	0.97123	0.972004	0.971857	0.971955	0.971741	0.971662	0.971699
-9.525	0.976501	0.976234	0.976198	0.977273	0.977124	0.977251	0.976843	0.976805	0.97685
-8.763	0.981462	0.981258	0.981242	0.981892	0.981755	0.981866	0.981585	0.981537	0.981549
-8.001	0.985579	0.985455	0.98542	0.986047	0.985934	0.985851	0.985695	0.985619	0.985668
-7.239	0.988834	0.988721	0.988709	0.989169	0.989053	0.989108	0.989052	0.988996	0.989002
-6.477	0.991332	0.991231	0.991242	0.991504	0.991474	0.991518	0.99133	0.991256	0.991322
-5.715	0.993116	0.993015	0.993007	0.993197	0.993129	0.993212	0.993105	0.993088	0.99312
-4.953	0.994555	0.994499	0.994472	0.994604	0.99457	0.994629	0.994501	0.994491	0.994535
-4.191	0.995658	0.995594	0.9956	0.995614	0.995588	0.995629	0.995472	0.995446	0.99559
-3.429				0.996356	0.996337	0.996398	0.996288	0.996252	0.996426
-2.946	0.996936	0.996893	0.996851	0.99666	0.996615	0.996493	0.996507	0.996477	0.996513
-1.829	0.997731	0.997696	0.997645	0.997695	0.997675	0.997676	0.997733	0.997802	0.997762
-1.143	0.998102	0.998105	0.997994	0.998835	0.998769	0.998097	0.998103	0.998115	0.998061
-0.508	0.998516	0.99849	0.998468	0.998639	0.998624	0.99849	0.998489	0.998499	0.998398
0	0.999845	0.999901	0.999842	0.99989	0.999891	0.999874	0.999865	0.999804	0.999885
0.508	0.998693	0.998636	0.998065	0.998494	0.998351	0.99811	0.998759	0.998607	0.99862
1.016	0.994108	0.994165	0.994351	0.995171	0.995164	0.995324	0.995468	0.99543	0.995656
1.524	0.989568	0.98945	0.98954	0.989502	0.989322	0.988685	0.989708	0.989639	0.98876
2.032	0.979704	0.979598	0.97953	0.976457	0.976272	0.975721	0.978958	0.978742	0.97869
2.667	0.962344	0.962065	0.962071	0.963462	0.96321	0.963156	0.963958	0.963897	0.964124
3.429	0.929031	0.928554	0.928403	0.928112	0.927882	0.92798	0.928232	0.927993	0.928394
4.191	0.915997	0.914975	0.915248	0.918336	0.917944	0.918072	0.918636	0.918612	0.918851
4.953	0.919097	0.918198	0.918435	0.921005	0.920647	0.921168	0.921501	0.921061	0.921566
5.461	0.924129	0.923514	0.924251	0.926047	0.925427	0.926325	0.926968	0.926883	0.927753
5.969	0.930445	0.929826	0.930144	0.932937	0.932477	0.932815	0.933816	0.933621	0.934132
7.239	0.940619	0.939952	0.939935	0.936196	0.935697	0.93562	0.934696	0.934609	0.93446
8.001	0.942984	0.942492	0.942389	0.940863	0.94063	0.9407	0.941081	0.940976	0.941124
8.763	0.944828	0.944329	0.944133	0.943386	0.942937	0.943326	0.942944	0.942829	0.942941
9.525	0.945905	0.945403	0.945283	0.945064	0.944663	0.944956	0.944526	0.944809	0.944547
10.287				0.946002	0.945613	0.945838	0.946372	0.946292	0.946329
11.049	0.947292	0.946859	0.946783	0.946579	0.946129	0.946395	0.946595	0.946434	0.946546
11.811	0.94783	0.947337	0.947299	0.94698	0.946613	0.946896	0.946994	0.946822	0.946963
12.573	0.948028	0.947431	0.947604	0.947291	0.946865	0.947235	0.946421	0.946311	0.946165
13.335	0.948079	0.947517	0.947442	0.947485	0.947023	0.947382	0.947353	0.947204	0.947255
14.097	0.948179	0.94749	0.947623	0.94753	0.947162	0.947267	0.947379	0.947154	0.947353
14.859	0.947999	0.947405	0.947447	0.947508	0.947149	0.947268	0.947103	0.947053	0.947094
15.621	0.948017	0.947495	0.947414	0.94753	0.947297	0.947342	0.947565	0.947421	0.94748
16.383	0.948228	0.947597	0.947566	0.94807	0.947382	0.947564	0.947746	0.947519	0.94783
17.145	0.948426	0.947875	0.947736	0.948138	0.947738	0.947837	0.94819	0.947992	0.948125
17.907	0.947456	0.94672	0.946643	0.947971	0.947527	0.947575	0.947668	0.947421	0.947446

Appendix A.3 Vane Heat Transfer and Film Cooling Distributions

The three pages following this page contain heat transfer distributions for the two turbulence cases taken at three different exit Mach number conditions for the base vane. Additionally, heat transfer and film cooling distributions are given separately for one and two rows of suction surface film cooling, one and two rows of pressure surface film cooling, and for the showerhead array. The rows of film cooling were all investigated at three separate velocity ratios. At one velocity ratio, a lower exit Reynolds number was also run to indicate the influence of Reynolds number on heat transfer and film cooling. For the showerhead array three equivalent pressure ratios were run at one exit Reynolds number and a second Reynolds number was run at a single pressure ratio. All heat transfer and film cooling tests were run at the high and low turbulence condition. The heat transfer coefficient and Stanton number distributions are given in terms of surface distance with positive values for the suction surface arc and negative values for the pressure surface arc. Some Stanton number values were left blank to indicate that a particular point was not believed to be reliable. In drilling the suction surface film cooling array, one inner wall thermocouple was lost. For the pressure surface heat transfer and film cooling tests, the suction surface array was taped closed in order to provide an accurate measure of the film cooling flow and therefore accurate control of the velocity ratio. In this case two of the Stanton numbers were excluded. Finally, due to both lost thermocouples in the showerhead array and due to three dimensional conduction in and around the array, heat transfer and film cooling measurements are not given in the region in and around the holes. Adiabatic effectiveness levels are given only for the region downstream of the holes and the distance in terms of hole diameters is also given from the hole exit trailing edge.

File:	q2l5b04	Ts,ex (K)	297.90		File:	q25c5b04	Ts,ex (K)	299.77	
Ptot (Pa)	99364	Re,ex	813691		Ptot (Pa)	97171	Re,ex	514680	
Ttot (C)	29.09	q"	1397		Ttot (C)	28.35	q"	1542	
Ma,ex	0.2699	Tu,in	0.009		Ma,ex	0.1695	Tu,in	0.124	
Ma,in	0.0784	Lu,in (cm)	19.1		Ma,in	0.0517	Lu,in (cm)	3.16	
Ps,ex(Pa)	94460	U0,in(m/s)	19.34		Ps,ex(Pa)	95242	U0,in(m/s)	19.53	
Ps,in(Pa)'	98937				Ps,in(Pa)'	96989			
Surface	T surf	Taw	h	St	Surface	T surf	Taw	h	St
(cm)	(C)	(C)	W/m2/C		(cm)	(C)	(C)	W/m2/C	
-11.7094	45.28	28.86	67.20	0.001028	-11.7094	41.51	28.21	102.00	0.001558
-10.9474	45.53	28.91	71.17	0.001089	-10.9474	41.62	28.23	106.16	0.001622
-10.1854	45.68	28.93	72.08	0.001103	-10.1854	41.68	28.26	106.99	0.001635
-9.4234	46.13	28.94	70.27	0.001075	-9.4234	41.91	28.27	105.27	0.001608
-8.6614	46.57	28.96	68.92	0.001054	-8.6614	42.17	28.30	103.59	0.001583
-7.8994	46.88	28.98	68.42	0.001047	-7.8994	42.34	28.32	102.84	0.001571
-7.1374	47.20	29.00	67.70	0.001036	-7.1374	42.56	28.34	101.65	0.001553
-6.3754	47.52	29.00	66.84	0.001023	-6.3754	42.80	28.34	100.03	0.001528
-5.6134	47.72	28.99	66.43	0.001016	-5.6134	42.98	28.34	98.97	0.001512
-4.8514	47.77	28.99	66.62	0.001019	-4.8514	43.06	28.36	98.63	0.001507
-4.0894	47.61	29.00	67.54	0.001033	-4.0894	43.02	28.36	99.09	0.001514
-3.3274	47.22	29.01	67.87	0.001038	-3.3274	42.85	28.37	99.14	0.001515
-2.921	46.86	29.03	69.14	0.001058	-2.921	42.65	28.38	100.03	0.001528
-1.7272	44.70	29.29	85.33	0.001305	-1.7272	41.42	28.58	114.76	0.001753
-1.0414	42.67	29.31	100.48	0.001537	-1.0414	40.08	28.58	129.89	0.001984
-0.508	39.79	29.35	133.79	0.002047	-0.508	37.70	28.59	169.29	0.002586
0	38.49	29.37	153.69	0.002351	0	36.55	28.59	194.66	0.002974
0.508	37.95	29.30	163.41	0.0025	0.508	36.14	28.58	205.95	0.003147
1.016	38.57	29.29	148.50	0.002272	1.016	36.78	28.56	185.74	0.002838
1.524	38.68	29.23	145.99	0.002233	1.524	36.89	28.52	182.57	0.002789
2.032	38.52	29.19	148.51	0.002272	2.032	36.78	28.47	184.50	0.002819
2.7686	38.29	29.08	150.27	0.002299	2.7686	36.69	28.35	183.64	0.002806
3.5306	38.19	28.93	150.50	0.002302	3.5306	36.77	28.19	179.43	0.002741
4.2926	39.11	28.83	135.61	0.002075	4.2926	37.78	28.10	158.37	0.00242
5.0546	43.41	28.84	90.40	0.001383	5.0546	40.55	28.12	117.76	0.001799
5.8166	47.54	28.76	62.56	0.000957	5.8166	39.47	28.21	132.34	0.002022
7.1628	34.96	28.88	238.27	0.003645	7.1628	35.40	28.28	220.79	0.003373
7.6708	35.14	28.92	234.46	0.003587	7.6708	35.50	28.29	218.21	0.003334
8.1788	35.34	28.97	232.05	0.00355	8.1788	35.65	28.30	215.47	0.003292
8.9408	35.74	29.01	221.19	0.003384	8.9408	35.94	28.31	208.55	0.003186
9.7028	36.32	29.03	204.95	0.003135	9.7028	36.35	28.32	198.62	0.003035
10.4648	36.62	29.04	198.96	0.003044	10.4648	36.59	28.32	193.59	0.002958
11.2268	37.02	29.10	191.44	0.002929	11.2268	36.87	28.34	187.99	0.002872
11.9888	37.54	29.12	180.05	0.002754	11.9888	37.21	28.35	180.90	0.002764
12.7508	37.69	29.12	178.35	0.002728	12.7508	37.32	28.36	179.41	0.002741
13.5128	37.84	29.10	176.44	0.002699	13.5128	37.40	28.34	178.42	0.002726
14.2748	38.19	29.10	170.03	0.002601	14.2748	37.65	28.34	173.57	0.002652
15.0368	38.62	29.09	162.26	0.002482	15.0368	37.89	28.35	169.34	0.002587
15.7988	38.65	29.08	163.75	0.002505	15.7988	37.93	28.34	169.76	0.002594
16.5608	38.84	29.07	158.66	0.002427	16.5608	38.04	28.34	165.65	0.002531

File:	q3l8b01	Ts,ex (K)	294.53		File:	q3c8b06	Ts,ex (K)	295.20	
Ptot (Pa)	99364	Re,ex	831045		Ptot (Pa)	96224	Re,ex	804503	
Ttot (C)	25.67	q" (W/m2)	1805		Ttot (C)	26.37	q" (W/m2)	2210	
Ma,ex	0.2699	Tu,in	0.011		Ma,ex	0.2706	Tu,in	0.12	
Ma,in	0.0784	Lu,in (cm)	6.6		Ma,in	0.0799	Lu,in (cm)	3.36	
Ps,ex(Pa)	94460	U0,in(m/s)	29.58		Ps,ex(Pa)	91450	U0,in(m/s)	29.49	
Ps,in (Pa)	98937				Ps,in (Pa)	95795			
Surface	T surf	Taw	h	St	Surface	T surf	Taw	h	St
(cm)	(C)	(C)	W/m2/C		(cm)	(C)	(C)	W/m2/C	
-11.7094	42.45	25.20	84.12	0.000807	-11.7094	40.17	25.99	140.14	0.001386
-10.9474	42.68	25.26	88.82	0.000852	-10.9474	40.42	26.05	143.63	0.001421
-10.1854	42.86	25.32	90.00	0.000863	-10.1854	40.61	26.11	143.33	0.001418
-9.4234	43.40	25.38	87.71	0.000841	-9.4234	40.94	26.17	140.69	0.001392
-8.6614	43.91	25.43	86.01	0.000825	-8.6614	41.29	26.22	138.07	0.001366
-7.8994	44.25	25.47	85.44	0.00082	-7.8994	41.53	26.27	136.90	0.001354
-7.1374	44.61	25.52	84.64	0.000812	-7.1374	41.80	26.30	135.15	0.001337
-6.3754	44.96	25.54	83.61	0.000802	-6.3754	42.10	26.33	132.93	0.001315
-5.6134	45.19	25.56	83.18	0.000798	-5.6134	42.32	26.34	131.40	0.0013
-4.8514	45.25	25.57	83.43	0.0008	-4.8514	42.44	26.36	130.83	0.001294
-4.0894	45.10	25.60	84.50	0.000811	-4.0894	42.43	26.38	131.17	0.001297
-3.3274	44.67	25.61	85.21	0.000817	-3.3274	42.30	26.39	131.40	0.0013
-2.921	44.27	25.63	86.98	0.000834	-2.921	42.10	26.41	132.60	0.001312
-1.7272	41.92	25.85	106.99	0.001026	-1.7272	40.78	26.64	150.95	0.001493
-1.0414	39.79	25.87	125.07	0.0012	-1.0414	39.42	26.65	168.46	0.001666
-0.508	36.68	25.89	167.21	0.001604	-0.508	36.72	26.67	219.84	0.002174
0	35.31	25.90	192.14	0.001843	0	35.38	26.68	255.14	0.002524
0.508	34.81	25.86	202.72	0.001944	0.508	35.01	26.65	265.98	0.002631
1.016	35.47	25.82	184.53	0.00177	1.016	35.80	26.60	237.83	0.002352
1.524	35.54	25.71	181.34	0.001739	1.524	35.93	26.50	232.29	0.002298
2.032	35.33	25.61	183.82	0.001763	2.032	35.76	26.37	234.17	0.002316
2.7686	34.91	25.31	186.42	0.001788	2.7686	35.57	26.09	231.57	0.00229
3.5306	34.64	24.95	185.78	0.001782	3.5306	35.51	25.70	224.96	0.002225
4.2926	35.44	24.74	168.45	0.001616	4.2926	36.58	25.48	198.32	0.001962
5.0546	39.45	24.79	117.22	0.001124	5.0546	39.57	25.55	150.97	0.001493
5.8166	41.72	24.68	94.62	0.000908	5.8166	36.82	25.77	198.06	0.001959
7.1628	30.94	25.01	313.32	0.003005	7.1628	33.34	25.95	303.99	0.003007
7.6708	31.12	25.10	311.23	0.002985	7.6708	33.53	25.97	297.50	0.002943
8.1788	31.27	25.17	310.90	0.002982	8.1788	33.69	25.99	293.97	0.002908
8.9408	31.58	25.24	301.56	0.002892	8.9408	33.93	26.02	287.09	0.00284
9.7028	32.12	25.29	280.86	0.002694	9.7028	34.35	26.05	273.88	0.002709
10.4648	32.38	25.32	274.54	0.002633	10.4648	34.55	26.05	268.48	0.002656
11.2268	32.71	25.36	264.91	0.002541	11.2268	34.84	26.09	261.53	0.002587
11.9888	33.25	25.39	247.75	0.002376	11.9888	35.20	26.11	251.52	0.002488
12.7508	33.33	25.39	247.75	0.002376	12.7508	35.27	26.11	250.76	0.00248
13.5128	33.46	25.38	245.23	0.002352	13.5128	35.34	26.10	249.47	0.002467
14.2748	33.75	25.38	237.92	0.002282	14.2748	35.55	26.10	244.17	0.002415
15.0368	34.23	25.38	225.12	0.002159	15.0368	35.83	26.10	237.13	0.002345
15.7988	34.20	25.38	228.99	0.002196	15.7988	35.81	26.09	238.61	0.00236
16.5608	34.38	25.37	223.34	0.002142	16.5608	35.89	26.08	234.65	0.002321

File:	q3l1b07	Ts,ex (K)	292.36		File:	q3c1b03	Ts,ex (K)	292.10	
Ptot (Pa)	98340	Re,ex	950078		Ptot (Pa)	95421	Re,ex	954800	
Ttot (C)	24.99	q"	2126		Ttot (C)	25.20	q"	2799	
Ma,ex	0.3144	Tu,in	0.011		Ma,ex	0.3271	Tu,in	0.12	
Ma,in	0.0895	Lu,in (cm)	6.6		Ma,in	0.0952	Lu,in (cm)	3.36	
Ps,ex(Pa)	91828	U0,in(m/s)	33.74		Ps,ex(Pa)	88607	U0,in(m/s)	35.1348	
Ps,in (Pa)	97791				Ps,in (Pa)	94818			
Surface	T surf	Taw	h	St	Surface	T surf	Taw	h	St
(cm)	(C)	(C)	W/m2/C		(cm)	(C)	(C)	W/m2/C	
-11.7094	43.57	24.41	88.55	0.000747	-11.7094	40.36	24.67	160.91	0.001352
-10.9474	43.82	24.48	93.42	0.000788	-10.9474	40.77	24.74	162.90	0.001369
-10.1854	44.03	24.58	94.68	0.000799	-10.1854	41.09	24.82	161.33	0.001355
-9.4234	44.64	24.65	92.24	0.000778	-9.4234	41.53	24.91	157.88	0.001327
-8.6614	45.24	24.74	90.38	0.000763	-8.6614	41.98	25.00	154.57	0.001299
-7.8994	45.63	24.80	89.82	0.000758	-7.8994	42.27	25.06	153.00	0.001286
-7.1374	46.05	24.85	88.82	0.00075	-7.1374	42.60	25.11	150.96	0.001268
-6.3754	46.46	24.90	87.73	0.00074	-6.3754	42.97	25.16	148.38	0.001247
-5.6134	46.74	24.92	87.13	0.000735	-5.6134	43.24	25.20	146.68	0.001232
-4.8514	46.81	24.95	87.46	0.000738	-4.8514	43.41	25.23	145.77	0.001225
-4.0894	46.64	24.98	88.64	0.000748	-4.0894	43.44	25.26	145.87	0.001226
-3.3274	46.16	24.99	89.82	0.000758	-3.3274	43.33	25.27	145.88	0.001226
-2.921	45.70	25.01	91.86	0.000775	-2.921	43.13	25.29	147.14	0.001236
-1.7272	42.99	25.22	113.31	0.000956	-1.7272	41.62	25.51	167.50	0.001407
-1.0414	40.63	25.23	132.42	0.001117	-1.0414	40.13	25.53	185.60	0.001559
-0.508	37.14	25.26	177.71	0.0015	-0.508	37.01	25.55	242.75	0.00204
0	35.62	25.26	204.46	0.001725	0	35.46	25.57	283.01	0.002378
0.508	35.10	25.24	215.35	0.001817	0.508	35.09	25.53	292.71	0.002459
1.016	35.83	25.17	195.91	0.001653	1.016	36.04	25.46	260.62	0.00219
1.524	35.91	25.04	192.19	0.001622	1.524	36.17	25.31	254.16	0.002136
2.032	35.66	24.91	195.11	0.001646	2.032	35.99	25.15	255.46	0.002146
2.7686	35.14	24.52	197.63	0.001668	2.7686	35.67	24.73	253.23	0.002128
3.5306	34.77	24.03	196.68	0.00166	3.5306	35.56	24.17	244.10	0.002051
4.2926	35.63	23.75	177.87	0.001501	4.2926	36.75	23.83	214.51	0.001802
5.0546	40.09	23.84	123.49	0.001042	5.0546	40.23	23.94	163.46	0.001373
5.8166	41.58	23.68	106.96	0.000903	5.8166	36.38	24.26	229.03	0.001924
7.1628	30.57	24.15	340.54	0.002874	7.1628	32.75	24.52	344.76	0.002897
7.6708	30.82	24.26	335.44	0.00283	7.6708	32.97	24.57	337.73	0.002838
8.1788	30.96	24.33	335.53	0.002831	8.1788	33.13	24.60	334.16	0.002808
8.9408	31.29	24.42	326.20	0.002753	8.9408	33.40	24.64	326.50	0.002743
9.7028	31.88	24.49	304.12	0.002566	9.7028	33.86	24.68	311.88	0.00262
10.4648	32.14	24.53	297.78	0.002513	10.4648	34.10	24.69	305.58	0.002568
11.2268	32.49	24.56	287.72	0.002428	11.2268	34.37	24.72	298.63	0.002509
11.9888	33.08	24.59	268.58	0.002266	11.9888	34.78	24.74	286.87	0.00241
12.7508	33.14	24.61	269.83	0.002277	12.7508	34.84	24.75	286.40	0.002406
13.5128	33.27	24.59	267.15	0.002254	13.5128	34.92	24.73	284.61	0.002391
14.2748	33.58	24.60	259.33	0.002188	14.2748	35.16	24.73	278.23	0.002338
15.0368	34.11	24.59	244.79	0.002066	15.0368	35.47	24.73	269.98	0.002268
15.7988	34.04	24.58	249.76	0.002108	15.7988	35.42	24.72	272.33	0.002288
16.5608	34.23	24.58	244.05	0.002059	16.5608	35.49	24.72	268.58	0.002257

File:	s1v8q3l3	Ts,ex (K)	295.79	Tco (C)	47.80745			
Ptot (Pa)	99225	Re,ex	825324	VR	0.56			
Ttot (C)	26.95	q" (W/m2)	2644					
Ma,ex	0.2698	Tu,in	0.011					
Ma,in	0.0778	Lu,in (cm)	6.6					
Ps,ex(Pa)	94330	U0,in(m/s)	29.58					
Ps,in (Pa)	98807							
Surface	T surf	Taw	h	St	X/D	Taw,c(fc)	Naw	St/St0
(cm)	(C)	(C)	W/m2/C			(C)		
-11.7094	50.39	26.42	87.51	0.000842				
-10.9474	50.72	26.48	90.76	0.000874				
-10.1854	50.89	26.55	92.08	0.000886				
-9.4234	51.61	26.61	89.93	0.000866				
-8.6614	52.35	26.67	87.88	0.000846				
-7.8994	52.83	26.71	87.20	0.000839				
-7.1374	53.27	26.75	86.49	0.000833				
-6.3754	53.69	26.78	85.57	0.000824				
-5.6134	53.92	26.79	85.16	0.00082				
-4.8514	53.92	26.81	85.11	0.000819				
-4.0894	53.46	26.83	85.63	0.000824				
-3.3274	52.58	26.83	86.47	0.000832				
-2.921	51.79	26.81	95.42	0.000919				
-1.7272	45.50	26.91	114.60	0.001103				
-1.0414	43.92	26.95	125.57	0.001209				
-0.508	40.71	26.99	168.30	0.00162				
0	39.22	27.01	188.59	0.001815				
0.508	38.58	26.95	200.76	0.001933				
1.016	39.44	26.92	183.57	0.001767				
1.524	39.68	26.84	172.18	0.001657				
2.032	39.07	26.73	184.60	0.001777				
2.7686	39.12	26.54	181.12	0.001743				
3.5306	38.31	26.19	187.89	0.001809				
4.2926	40.47	26.06	137.23	0.001321				
5.0546	45.06	26.11	103.16	0.000993				
5.8166	37.94	25.41	183.09					
7.1628	33.95	26.08	326.71	0.003145	1.00	31.89	0.2672	1.0465
7.6708	34.03	26.17	344.89	0.00332	4.19	32.12	0.2749	1.1122
8.1788	34.59	26.22	327.01	0.003148	7.39	31.29	0.2350	1.0556
8.9408	35.23	26.31	311.41	0.002998	12.18	30.59	0.1992	1.0364
9.7028	36.03	26.35	288.15	0.002774	16.97	30.17	0.1782	1.0296
10.4648	36.43	26.38	280.01	0.002695	21.77	29.91	0.1645	1.0236
11.2268	36.92	26.44	269.49	0.002594	26.56	29.78	0.1562	1.0209
11.9888	37.70	26.47	251.07	0.002417	31.35	29.58	0.1458	1.0171
12.7508	37.82	26.49	250.95	0.002416	36.14	29.48	0.1401	1.0166
13.5128	38.03	26.47	247.32	0.002381	40.94	29.37	0.1359	1.0122
14.2748	38.42	26.49	240.09	0.002311	45.73	29.28	0.1311	1.0127
15.0368	39.08	26.48	227.26	0.002188	50.52	29.17	0.1259	1.0132
15.7988	39.09	26.48	230.25	0.002216	55.31	29.24	0.1293	1.0091
16.5608	39.40	26.48	221.92	0.002136	60.11	28.92	0.1145	0.9972

File:	s1v8q3h3	Ts,ex (K)	293.48	Tco (C)	46.84348			
Ptot (Pa)	96679	Re,ex	810465	VR	0.56			
Ttot (C)	24.58	q" (W/m2)	2695					
Ma,ex	0.2692	Tu,in	0.12					
Ma,in	0.0791	Lu,in (cm)	3.36					
Ps,ex(Pa)	91931	U0,in(m/s)	29.49					
Ps,in (Pa)	96257							
Surface	T surf	Taw	h	St	X/D	Taw,c(fc)	Naw	St/St0
(cm)	(C)	(C)	W/m2/C			(C)		
-11.7094	40.74	24.13	142.54	0.001406				
-10.9474	41.02	24.17	144.45	0.001425				
-10.1854	41.20	24.24	144.38	0.001424				
-9.4234	41.57	24.30	141.84	0.001399				
-8.6614	42.05	24.36	138.54	0.001366				
-7.8994	42.35	24.41	137.05	0.001352				
-7.1374	42.64	24.45	135.46	0.001336				
-6.3754	42.94	24.46	133.58	0.001317				
-5.6134	43.17	24.49	132.12	0.001303				
-4.8514	43.32	24.50	130.71	0.001289				
-4.0894	43.26	24.52	129.95	0.001282				
-3.3274	43.32	24.52	125.26	0.001235				
-2.921	43.44	24.51	131.99	0.001302				
-1.7272	38.85	24.57	158.49	0.001563				
-1.0414	37.99	24.60	169.25	0.001669				
-0.508	35.58	24.63	219.70	0.002167				
0	34.24	24.65	251.05	0.002476				
0.508	33.82	24.62	264.43	0.002608				
1.016	34.73	24.58	235.66	0.002324				
1.524	34.95	24.50	221.95	0.002189				
2.032	34.44	24.39	236.68	0.002334				
2.7686	34.83	24.19	219.69	0.002167				
3.5306	34.21	23.83	227.95	0.002248				
4.2926	35.77	23.69	191.38	0.001888				
5.0546	37.29	23.75	164.11	0.001619				
5.8166	32.08	23.87	288.56					
7.1628	32.07	23.90	314.90	0.003106	1.00	31.11	0.3142	1.0329
7.6708	32.03	23.92	334.25	0.003297	4.19	31.14	0.3151	1.1203
8.1788	32.45	23.95	320.60	0.003162	7.39	30.06	0.2669	1.0875
8.9408	32.89	23.97	308.56	0.003043	12.18	29.00	0.2198	1.0717
9.7028	33.40	24.00	293.16	0.002891	16.97	28.42	0.1936	1.0673
10.4648	33.69	24.02	286.02	0.002821	21.77	28.00	0.1747	1.0623
11.2268	34.07	24.04	275.86	0.002721	26.56	27.77	0.1639	1.0518
11.9888	34.56	24.07	262.88	0.002593	31.35	27.42	0.1471	1.0422
12.7508	34.69	24.07	260.29	0.002567	36.14	27.23	0.1388	1.0350
13.5128	34.84	24.07	257.35	0.002538	40.94	27.05	0.1307	1.0286
14.2748	35.10	24.08	251.17	0.002477	45.73	26.88	0.1228	1.0257
15.0368	35.49	24.09	242.16	0.002388	50.52	26.67	0.1134	1.0183
15.7988	35.55	24.09	242.24	0.002389	55.31	26.69	0.1143	1.0123
16.5608	35.72	24.08	234.86	0.002316	60.11	26.30	0.0973	0.9980

File:	s1v6q3l3	Ts,ex (K)	295.55	Tco (C)	45.31687			
Ptot (Pa)	99310	Re,ex	827816	VR	0.5			
Ttot (C)	26.72	q" (W/m2)	2645					
Ma,ex	0.2702	Tu,in	0.011					
Ma,in	0.0793	Lu,in (cm)	6.6					
Ps,ex(Pa)	94398	U0,in(m/s)	29.58					
Ps,in (Pa)	98874							
Surface	T surf	Taw	h	St	X/D	Taw,c(fc)	Naw	St/St0
(cm)	(C)	(C)	W/m2/C			(C)		
-11.7094	50.18	26.19	87.48	0.000841				
-10.9474	50.51	26.26	90.79	0.000872				
-10.1854	50.69	26.32	92.01	0.000884				
-9.4234	51.41	26.38	89.86	0.000864				
-8.6614	52.15	26.44	87.85	0.000844				
-7.8994	52.65	26.49	87.07	0.000837				
-7.1374	53.09	26.52	86.37	0.00083				
-6.3754	53.51	26.54	85.42	0.000821				
-5.6134	53.76	26.57	85.00	0.000817				
-4.8514	53.77	26.58	84.92	0.000816				
-4.0894	53.37	26.60	85.33	0.00082				
-3.3274	52.56	26.61	86.08	0.000827				
-2.921	51.86	26.60	94.74	0.00091				
-1.7272	45.52	26.70	114.55	0.001101				
-1.0414	43.87	26.74	125.86	0.001209				
-0.508	40.61	26.79	168.31	0.001617				
0	39.08	26.81	189.30	0.001819				
0.508	38.43	26.75	201.73	0.001939				
1.016	39.32	26.71	183.88	0.001767				
1.524	39.55	26.64	172.99	0.001662				
2.032	38.96	26.53	184.75	0.001775				
2.7686	39.00	26.33	181.38	0.001743				
3.5306	38.21	25.98	187.76	0.001804				
4.2926	40.34	25.85	138.68	0.001333				
5.0546	45.12	25.90	102.53	0.000985				
5.8166	37.78	25.20	173.90					
7.1628	33.91	25.90	325.71	0.00313	1.00	31.78	0.2998	1.0414
7.6708	33.88	25.96	346.94	0.003334	4.19	31.76	0.2968	1.1168
8.1788	34.33	26.00	331.54	0.003186	7.39	30.70	0.2405	1.0684
8.9408	34.98	26.09	313.98	0.003017	12.18	29.90	0.1962	1.0431
9.7028	35.80	26.13	289.10	0.002778	16.97	29.44	0.1706	1.0312
10.4648	36.21	26.17	280.41	0.002695	21.77	29.18	0.1558	1.0233
11.2268	36.73	26.23	268.99	0.002585	26.56	29.00	0.1440	1.0173
11.9888	37.51	26.26	250.33	0.002405	31.35	28.80	0.1319	1.0122
12.7508	37.64	26.27	249.84	0.002401	36.14	28.70	0.1261	1.0103
13.5128	37.84	26.26	246.69	0.002371	40.94	28.60	0.1211	1.0078
14.2748	38.21	26.27	239.79	0.002304	45.73	28.51	0.1164	1.0097
15.0368	38.87	26.26	226.85	0.00218	50.52	28.41	0.1116	1.0095
15.7988	38.87	26.26	229.99	0.00221	55.31	28.39	0.1108	1.0062
16.5608	39.17	26.25	222.27	0.002136	60.11	28.33	0.1078	0.9970

File:	s1v6q3h3	Ts,ex (K)	293.06	Tco (C)	44.23905			
Ptot (Pa)	97262	Re,ex	819558	VR	0.49			
Ttot (C)	24.19	q" (W/m2)	2702					
Ma,ex	0.2702	Tu,in	0.12					
Ma,in	0.0793	Lu,in (cm)	3.36					
Ps,ex(Pa)	92451	U0,in(m/s)	29.49					
Ps,in (Pa)	96835							
Surface	T surf	Taw	h	St	X/D	Taw,c(fc)	Naw	St/St0
(cm)	(C)	(C)	W/m2/C			(C)		
-11.7094	40.24	23.72	143.79	0.001404				
-10.9474	40.52	23.77	145.74	0.001423				
-10.1854	40.71	23.84	145.54	0.001421				
-9.4234	41.09	23.90	142.94	0.001396				
-8.6614	41.57	23.96	139.58	0.001363				
-7.8994	41.88	24.00	137.95	0.001347				
-7.1374	42.17	24.05	136.45	0.001332				
-6.3754	42.47	24.07	134.51	0.001313				
-5.6134	42.69	24.09	133.11	0.0013				
-4.8514	42.84	24.10	131.76	0.001286				
-4.0894	42.83	24.13	130.82	0.001277				
-3.3274	42.98	24.15	125.24	0.001223				
-2.921	43.25	24.15	129.75	0.001267				
-1.7272	38.54	24.22	160.16	0.001564				
-1.0414	37.64	24.23	171.20	0.001672				
-0.508	35.17	24.27	222.73	0.002175				
0	33.80	24.29	256.43	0.002504				
0.508	33.42	24.25	267.76	0.002614				
1.016	34.34	24.21	238.48	0.002329				
1.524	34.50	24.13	228.89	0.002235				
2.032	34.07	24.02	239.01	0.002334				
2.7686	34.35	23.82	228.08	0.002227				
3.5306	33.81	23.46	230.53	0.002251				
4.2926	35.45	23.31	192.22	0.001877				
5.0546	36.99	23.37	163.13	0.001593				
5.8166	32.00	23.50	261.41					
7.1628	31.77	23.65	301.85	0.002947	1.00	31.06	0.3561	0.9802
7.6708	31.78	23.62	310.81	0.003035	4.19	30.71	0.3402	1.0313
8.1788	32.00	23.59	312.10	0.003047	7.39	29.35	0.2762	1.0480
8.9408	32.41	23.61	303.46	0.002963	12.18	28.14	0.2173	1.0435
9.7028	32.96	23.62	287.29	0.002805	16.97	27.52	0.1872	1.0355
10.4648	33.26	23.64	280.79	0.002742	21.77	27.08	0.1655	1.0324
11.2268	33.60	23.66	272.76	0.002663	26.56	26.86	0.1541	1.0296
11.9888	34.10	23.68	259.89	0.002538	31.35	26.54	0.1377	1.0200
12.7508	34.23	23.69	257.98	0.002519	36.14	26.36	0.1287	1.0156
13.5128	34.38	23.68	255.01	0.00249	40.94	26.17	0.1200	1.0091
14.2748	34.64	23.69	249.48	0.002436	45.73	26.01	0.1120	1.0087
15.0368	35.02	23.69	240.88	0.002352	50.52	25.84	0.1035	1.0028
15.7988	35.07	23.69	241.15	0.002355	55.31	25.79	0.1013	0.9977
16.5608	35.23	23.69	234.65	0.002291	60.11	25.66	0.0953	0.9872

File:	s1v6q3k3	Ts,ex (K)	297.30	Tco (C)	42.2914			
Ptot (Pa)	99439	Re,ex	536186	VR	0.49			
Ttot (C)	25.89	q" (W/m2)	2035					
Ma,ex	0.1708	Tu,in	0.009					
Ma,in	0.0503	Lu,in (cm)	19.1					
Ps,ex(Pa)	97434	U0,in(m/s)	19.34					
Ps,in (Pa)	99263							
Surface	T surf	Taw	h	St	X/D	Taw,c(fc)	Naw	St/St0
(cm)	(C)	(C)	W/m2/C			(C)		
-11.7094	48.31	25.66	70.06	0.001034				
-10.9474	48.61	25.69	73.00	0.001077				
-10.1854	48.77	25.72	73.95	0.001091				
-9.4234	49.38	25.74	72.27	0.001067				
-8.6614	50.02	25.76	70.59	0.001042				
-7.8994	50.46	25.78	70.01	0.001033				
-7.1374	50.85	25.80	69.40	0.001024				
-6.3754	51.22	25.81	68.68	0.001014				
-5.6134	51.44	25.82	68.34	0.001009				
-4.8514	51.45	25.83	68.22	0.001007				
-4.0894	51.09	25.84	68.48	0.001011				
-3.3274	50.40	25.85	69.32	0.001023				
-2.921	49.95	25.86	75.84	0.001119				
-1.7272	44.07	25.94	91.35	0.001348				
-1.0414	42.36	25.96	101.60	0.001499				
-0.508	39.31	25.97	135.28	0.001997				
0	37.82	25.98	152.64	0.002253				
0.508	37.21	25.94	162.97	0.002405				
1.016	38.03	25.92	148.28	0.002189				
1.524	38.24	25.89	140.04	0.002067				
2.032	37.76	25.85	149.11	0.002201				
2.7686	37.84	25.77	147.07	0.002171				
3.5306	37.34	25.64	150.65	0.002224				
4.2926	39.34	25.59	111.48	0.001645				
5.0546	44.37	25.63	78.42	0.001157				
5.8166	41.81	25.42	92.03					
7.1628	33.87	25.60	243.56	0.003595	1.00	30.30	0.2785	0.9862
7.6708	33.74	25.61	261.45	0.003859	4.19	30.07	0.2643	1.0759
8.1788	34.18	25.61	249.84	0.003687	7.39	29.14	0.2092	1.0388
8.9408	34.83	25.65	235.60	0.003477	12.18	28.48	0.1681	1.0276
9.7028	35.70	25.66	215.81	0.003185	16.97	28.16	0.1485	1.0159
10.4648	36.17	25.68	208.25	0.003074	21.77	27.95	0.1349	1.0098
11.2268	36.70	25.72	199.67	0.002947	26.56	27.85	0.1271	1.0063
11.9888	37.50	25.74	185.65	0.00274	31.35	27.71	0.1176	0.9948
12.7508	37.73	25.74	183.57	0.002709	36.14	27.63	0.1131	0.9930
13.5128	37.99	25.73	180.59	0.002665	40.94	27.56	0.1096	0.9875
14.2748	38.44	25.73	174.31	0.002573	45.73	27.49	0.1052	0.9891
15.0368	39.09	25.73	165.53	0.002443	50.52	27.42	0.1014	0.9843
15.7988	39.18	25.73	166.74	0.002461	55.31	27.47	0.1036	0.9825
16.5608	39.50	25.72	159.46	0.002353	60.11	27.26	0.0916	0.9697

File:	s1v6q3g3	Ts,ex (K)	297.39	Tco (C)	45.16529			
Ptot (Pa)	98359	Re,ex	528845	VR	0.5			
Ttot (C)	25.97	q" (W/m2)	2036					
Ma,ex	0.1704	Tu,in	0.124					
Ma,in	0.0515	Lu,in (cm)	3.16					
Ps,ex(Pa)	96386	U0,in(m/s)	19.53					
Ps,in (Pa)	98176							
Surface	T surf	Taw	h	St	X/D	Taw,c(fc)	Naw	St/St0
(cm)	(C)	(C)	W/m2/C			(C)		
-11.7094	42.40	25.76	105.48	0.001578				
-10.9474	42.53	25.76	108.44	0.001622				
-10.1854	42.60	25.80	109.12	0.001632				
-9.4234	42.89	25.81	107.42	0.001607				
-8.6614	43.29	25.84	105.07	0.001572				
-7.8994	43.56	25.86	103.87	0.001554				
-7.1374	43.82	25.87	102.71	0.001537				
-6.3754	44.08	25.88	101.34	0.001516				
-5.6134	44.27	25.88	100.28	0.0015				
-4.8514	44.39	25.88	99.28	0.001485				
-4.0894	44.31	25.89	98.72	0.001477				
-3.3274	44.34	25.89	95.73	0.001432				
-2.921	44.56	25.89	100.66	0.001506				
-1.7272	40.05	25.95	122.49	0.001833				
-1.0414	39.01	25.97	132.43	0.001981				
-0.508	36.66	25.98	171.92	0.002572				
0	35.37	25.99	196.76	0.002944				
0.508	34.95	25.99	208.28	0.003116				
1.016	35.72	25.97	187.43	0.002804				
1.524	35.91	25.93	177.91	0.002662				
2.032	35.53	25.88	188.07	0.002814				
2.7686	35.76	25.80	182.06	0.002724				
3.5306	35.50	25.65	182.55	0.002731				
4.2926	37.42	25.59	133.30	0.001994				
5.0546	38.92	25.60	123.23	0.001844				
5.8166	34.70	25.64	192.21					
7.1628	34.37	25.65	226.76	0.003393	1.00	32.33	0.3424	1.0120
7.6708	34.17	25.65	247.30	0.0037	4.19	32.19	0.3351	1.1168
8.1788	34.50	25.65	238.48	0.003568	7.39	31.08	0.2782	1.0907
8.9408	34.98	25.68	227.81	0.003408	12.18	30.02	0.2228	1.0767
9.7028	35.57	25.69	213.82	0.003199	16.97	29.42	0.1917	1.0616
10.4648	35.94	25.72	207.05	0.003098	21.77	29.02	0.1700	1.0549
11.2268	36.34	25.71	199.03	0.002978	26.56	28.82	0.1599	1.0444
11.9888	36.84	25.73	189.24	0.002831	31.35	28.51	0.1432	1.0323
12.7508	37.04	25.73	186.39	0.002789	36.14	28.34	0.1339	1.0253
13.5128	37.20	25.74	184.22	0.002756	40.94	28.16	0.1247	1.0191
14.2748	37.51	25.75	179.07	0.002679	45.73	28.01	0.1163	1.0185
15.0368	37.85	25.75	173.71	0.002599	50.52	27.83	0.1071	1.0129
15.7988	37.96	25.76	173.13	0.00259	55.31	27.84	0.1072	1.0070
16.5608	38.15	25.76	166.63	0.002493	60.11	27.49	0.0894	0.9934

File:	s1v5q3l3	Ts,ex (K)	295.24	Tco (C)	43.89424			
Ptot (Pa)	99225	Re,ex	827288	VR	0.42			
Ttot (C)	26.39	q" (W/m2)	2646					
Ma,ex	0.2698	Tu,in	0.011					
Ma,in	0.0778	Lu,in (cm)	6.6					
Ps,ex(Pa)	94330	U0,in(m/s)	29.58					
Ps,in (Pa)	98807							
Surface	T surf	Taw	h	St	X/D	Taw,c(fc)	Naw	St/St0
(cm)	(C)	(C)	W/m2/C			(C)		
-11.7094	49.93	25.89	87.31	0.00084				
-10.9474	50.27	25.95	90.54	0.000871				
-10.1854	50.45	26.01	91.79	0.000883				
-9.4234	51.18	26.07	89.61	0.000862				
-8.6614	51.93	26.14	87.58	0.000842				
-7.8994	52.43	26.19	86.88	0.000836				
-7.1374	52.88	26.22	86.07	0.000828				
-6.3754	53.33	26.25	85.10	0.000818				
-5.6134	53.60	26.27	84.62	0.000814				
-4.8514	53.65	26.28	84.43	0.000812				
-4.0894	53.31	26.31	84.77	0.000815				
-3.3274	52.61	26.32	85.41	0.000821				
-2.921	52.06	26.32	93.54	0.0009				
-1.7272	45.64	26.43	114.13	0.001098				
-1.0414	43.88	26.46	125.88	0.001211				
-0.508	40.49	26.49	168.42	0.00162				
0	38.91	26.51	190.19	0.001829				
0.508	38.26	26.45	202.32	0.001946				
1.016	39.15	26.41	184.30	0.001772				
1.524	39.38	26.34	173.97	0.001673				
2.032	38.80	26.23	184.98	0.001779				
2.7686	38.82	26.03	181.86	0.001749				
3.5306	38.06	25.68	187.56	0.001804				
4.2926	40.17	25.55	140.64	0.001353				
5.0546	45.23	25.61	101.73	0.000978				
5.8166	37.66	24.90	184.55					
7.1628	33.94	25.67	324.06	0.003117	1.00	31.79	0.3362	1.0370
7.6708	33.70	25.69	351.55	0.003381	4.19	31.39	0.3127	1.1326
8.1788	34.04	25.71	336.99	0.003241	7.39	30.10	0.2418	1.0868
8.9408	34.71	25.79	315.93	0.003038	12.18	29.25	0.1912	1.0505
9.7028	35.57	25.84	289.05	0.00278	16.97	28.80	0.1638	1.0319
10.4648	35.99	25.87	279.59	0.002689	21.77	28.52	0.1473	1.0211
11.2268	36.50	25.93	268.17	0.002579	26.56	28.37	0.1358	1.0150
11.9888	37.29	25.96	249.36	0.002398	31.35	28.16	0.1228	1.0092
12.7508	37.40	25.97	249.15	0.002396	36.14	28.07	0.1169	1.0084
13.5128	37.60	25.96	245.96	0.002365	40.94	27.97	0.1122	1.0057
14.2748	37.96	25.96	239.21	0.002301	45.73	27.89	0.1078	1.0081
15.0368	38.61	25.96	226.64	0.00218	50.52	27.79	0.1021	1.0094
15.7988	38.60	25.96	229.91	0.002211	55.31	27.80	0.1026	1.0067
16.5608	38.90	25.95	221.93	0.002134	60.11	27.71	0.0981	0.9964

File:	s1v4q3h3.	Ts,ex (K)	293.99	Tco (C)	42.85379			
Ptot (Pa)	96837	Re,ex	811569	VR	0.42			
Ttot (C)	25.12	q" (W/m2)	2697					
Ma,ex	0.2698	Tu,in	0.12					
Ma,in	0.0789	Lu,in (cm)	3.36					
Ps,ex(Pa)	92062	U0,in(m/s)	29.49					
Ps,in (Pa)	96416							
Surface	T surf	Taw	h	St	X/D	Taw,c(fc)	Naw	St/St0
(cm)	(C)	(C)	W/m2/C			(C)		
-11.7094	41.21	24.66	143.30	0.001409				
-10.9474	41.49	24.71	145.25	0.001429				
-10.1854	41.68	24.77	145.06	0.001427				
-9.4234	42.06	24.83	142.49	0.001402				
-8.6614	42.53	24.89	139.15	0.001369				
-7.8994	42.85	24.94	137.47	0.001352				
-7.1374	43.14	24.98	135.97	0.001337				
-6.3754	43.45	25.00	133.98	0.001318				
-5.6134	43.69	25.03	132.48	0.001303				
-4.8514	43.86	25.04	131.02	0.001289				
-4.0894	43.87	25.06	129.95	0.001278				
-3.3274	44.07	25.08	124.92	0.001229				
-2.921	44.40	25.08	130.41	0.001283				
-1.7272	39.77	25.15	158.75	0.001561				
-1.0414	38.81	25.17	170.10	0.001673				
-0.508	36.31	25.20	220.30	0.002167				
0	34.91	25.22	253.66	0.002495				
0.508	34.51	25.18	265.58	0.002612				
1.016	35.42	25.15	236.89	0.00233				
1.524	35.66	25.07	223.58	0.002199				
2.032	35.16	24.96	237.23	0.002333				
2.7686	35.41	24.75	227.07	0.002233				
3.5306	34.92	24.39	228.49	0.002247				
4.2926	36.60	24.25	188.35	0.001853				
5.0546	38.24	24.30	160.63	0.00158				
5.8166	32.63	24.43	283.10					
7.1628	33.10	24.58	314.01	0.003089	1.00	31.70	0.3894	1.0272
7.6708	32.81	24.55	338.93	0.003334	4.19	31.06	0.3554	1.1329
8.1788	33.02	24.53	328.12	0.003227	7.39	29.60	0.2770	1.1099
8.9408	33.46	24.54	312.31	0.003072	12.18	28.43	0.2124	1.0818
9.7028	34.03	24.56	293.04	0.002882	16.97	27.88	0.1815	1.0640
10.4648	34.32	24.57	285.20	0.002805	21.77	27.46	0.1582	1.0564
11.2268	34.70	24.60	274.93	0.002704	26.56	27.28	0.1470	1.0454
11.9888	35.19	24.61	261.38	0.002571	31.35	26.99	0.1305	1.0334
12.7508	35.32	24.62	259.08	0.002548	36.14	26.84	0.1218	1.0274
13.5128	35.45	24.62	256.09	0.002519	40.94	26.68	0.1132	1.0208
14.2748	35.69	24.62	250.62	0.002465	45.73	26.54	0.1051	1.0207
15.0368	36.07	24.62	241.68	0.002377	50.52	26.40	0.0974	1.0135
15.7988	36.11	24.62	241.98	0.00238	55.31	26.38	0.0967	1.0085
16.5608	36.26	24.62	235.08	0.002312	60.11	26.11	0.0819	0.9962

File:	s2v6q3l3	Ts,ex (K)	293.21	Tco (C)	47.40627			
Ptot (Pa)	98520	Re,ex	829568	VR	0.58			
Ttot (C)	24.35	q" (W/m2)	2656					
Ma,ex	0.2702	Tu,in	0.011					
Ma,in	0.0793	Lu,in (cm)	6.6					
Ps,ex(Pa)	93647	U0,in(m/s)	29.58					
Ps,in (Pa)	98087							
Surface	T surf	Taw	h	St	X/D	Taw,c(fc)	Naw	St/St0
(cm)	(C)	(C)	W/m2/C			(C)		
-11.7094	47.61	23.75	88.45	0.000854				
-10.9474	47.94	23.80	91.62	0.000884				
-10.1854	48.09	23.87	93.03	0.000898				
-9.4234	48.77	23.93	90.98	0.000878				
-8.6614	49.46	23.99	89.11	0.00086				
-7.8994	49.90	24.03	88.54	0.000854				
-7.1374	50.29	24.07	87.92	0.000848				
-6.3754	50.62	24.09	87.20	0.000842				
-5.6134	50.74	24.10	87.04	0.00084				
-4.8514	50.62	24.10	87.07	0.00084				
-4.0894	49.90	24.11	88.14	0.000851				
-3.3274	48.58	24.09	89.71	0.000866				
-2.921	47.19	24.06	101.30	0.000978				
-1.7272	41.06	24.14	115.72	0.001117				
-1.0414	39.88	24.20	124.84	0.001205				
-0.508	37.13	24.27	168.50	0.001626				
0	35.75	24.28	186.79	0.001803				
0.508	35.11	24.23	200.15	0.001932				
1.016	36.04	24.22	182.28	0.001759				
1.524	36.27	24.13	168.53	0.001626				
2.032	35.57	24.04	186.91	0.001804				
2.7686	35.97	23.87	178.14	0.001719				
3.5306	34.88	23.52	190.70	0.00184				
4.2926	36.45	23.42	163.48	0.001578				
5.0546	40.68	23.38	109.17	0.001054				
5.8166	36.36	23.29	133.59					
7.1628	29.92	23.20	358.35	0.003458	1.00	34.70	0.4753	1.1508
7.6708	30.28	23.29	366.43	0.003536	4.19	35.59	0.5102	1.1846
8.1788	31.21	23.37	333.76	0.003221	7.39	34.59	0.4668	1.0801
8.9408	32.21	23.46	306.42	0.002957	12.18	33.21	0.4072	1.0224
9.7028	33.23	23.50	278.96	0.002692	16.97	32.32	0.3689	0.9993
10.4648	33.76	23.55	268.91	0.002595	21.77	31.74	0.3435	0.9855
11.2268	34.40	23.58	255.35	0.002464	26.56	31.40	0.3281	0.9698
11.9888	35.20	23.62	238.80	0.002305	31.35	30.89	0.3055	0.9698
12.7508	35.34	23.65	238.62	0.002303	36.14	30.62	0.2934	0.9691
13.5128	35.53	23.66	236.74	0.002285	40.94	30.37	0.2826	0.9713
14.2748	35.90	23.68	230.82	0.002228	45.73	30.11	0.2712	0.9761
15.0368	36.55	23.69	219.41	0.002117	50.52	29.80	0.2580	0.9806
15.7988	36.54	23.70	222.73	0.00215	55.31	29.63	0.2500	0.9787
16.5608	36.82	23.71	215.78	0.002082	60.11	29.40	0.2403	0.9721

File:	s2v6q3h3	Ts,ex (K)	293.38	Tco (C)	46.30915			
Ptot (Pa)	97493	Re,ex	823759	VR	0.57			
Ttot (C)	24.56	q" (W/m2)	2668					
Ma,ex	0.2714	Tu,in	0.12					
Ma,in	0.0786	Lu,in (cm)	3.36					
Ps,ex(Pa)	92628	U0,in(m/s)	29.49					
Ps,in (Pa)	97073							
Surface	T surf	Taw	h	St	X/D	Taw,c(fc)	Naw	St/St0
(cm)	(C)	(C)	W/m2/C			(C)		
-11.7094	40.44	24.06	142.97	0.001388				
-10.9474	40.70	24.12	145.20	0.001409				
-10.1854	40.88	24.19	145.07	0.001408				
-9.4234	41.25	24.25	142.61	0.001384				
-8.6614	41.72	24.30	139.20	0.001351				
-7.8994	42.03	24.35	137.58	0.001335				
-7.1374	42.30	24.39	136.19	0.001322				
-6.3754	42.58	24.42	134.39	0.001304				
-5.6134	42.75	24.44	133.13	0.001292				
-4.8514	42.84	24.44	131.96	0.001281				
-4.0894	42.66	24.45	131.58	0.001277				
-3.3274	42.49	24.41	127.43	0.001237				
-2.921	42.32	24.37	135.84	0.001318				
-1.7272	37.77	24.43	160.89	0.001562				
-1.0414	37.06	24.47	170.41	0.001654				
-0.508	34.89	24.53	221.50	0.00215				
0	33.59	24.54	253.47	0.00246				
0.508	33.24	24.52	264.72	0.002569				
1.016	34.15	24.48	235.40	0.002285				
1.524	34.37	24.40	219.75	0.002133				
2.032	33.82	24.30	238.82	0.002318				
2.7686	34.29	24.13	223.70	0.002171				
3.5306	33.56	23.76	232.09	0.002253				
4.2926	35.22	23.63	192.05	0.001864				
5.0546	36.30	23.65	169.56	0.001646				
5.8166	36.21	23.65	138.33					
7.1628	30.63	23.58	356.21	0.003457	1.00	35.44	0.5219	1.1499
7.6708	30.99	23.63	361.47	0.003508	4.19	36.53	0.5686	1.1923
8.1788	31.86	23.69	328.45	0.003188	7.39	35.82	0.5364	1.0964
8.9408	32.70	23.75	303.44	0.002945	12.18	34.36	0.4704	1.0372
9.7028	33.40	23.79	282.99	0.002747	16.97	33.21	0.4182	1.0139
10.4648	33.80	23.80	272.87	0.002648	21.77	32.37	0.3807	0.9973
11.2268	34.14	23.85	265.28	0.002575	26.56	31.76	0.3521	0.9953
11.9888	34.63	23.89	253.30	0.002458	31.35	31.00	0.3170	0.9882
12.7508	34.74	23.89	251.51	0.002441	36.14	30.55	0.2972	0.9842
13.5128	34.86	23.88	249.02	0.002417	40.94	30.17	0.2802	0.9795
14.2748	35.10	23.90	243.93	0.002368	45.73	29.78	0.2622	0.9803
15.0368	35.43	23.92	236.83	0.002299	50.52	29.34	0.2419	0.9801
15.7988	35.46	23.92	237.16	0.002302	55.31	29.05	0.2292	0.9754
16.5608	35.60	23.93	231.14	0.002243	60.11	28.77	0.2165	0.9666

File:	s2v4q3l3	Ts,ex (K)	292.61	Tco (C)	47.18046			
Ptot (Pa)	98520	Re,ex	831761	VR	0.43			
Ttot (C)	23.73	q" (W/m2)	2659					
Ma,ex	0.2702	Tu,in	0.011					
Ma,in	0.0793	Lu,in (cm)	6.6					
Ps,ex(Pa)	93647	U0,in(m/s)	29.58					
Ps,in (Pa)	98087							
Surface	T surf	Taw	h	St	X/D	Taw,c(fc)	Naw	St/St0
(cm)	(C)	(C)	W/m2/C			(C)		
-11.7094	47.06	23.14	88.22	0.000851				
-10.9474	47.41	23.19	91.36	0.000881				
-10.1854	47.55	23.26	92.81	0.000895				
-9.4234	48.27	23.32	90.61	0.000874				
-8.6614	48.96	23.38	88.80	0.000856				
-7.8994	49.41	23.42	88.17	0.00085				
-7.1374	49.81	23.45	87.53	0.000844				
-6.3754	50.17	23.48	86.77	0.000837				
-5.6134	50.32	23.48	86.49	0.000834				
-4.8514	50.23	23.49	86.55	0.000834				
-4.0894	49.62	23.50	87.40	0.000843				
-3.3274	48.46	23.49	88.76	0.000856				
-2.921	47.35	23.46	99.07	0.000955				
-1.7272	40.91	23.57	115.65	0.001115				
-1.0414	39.64	23.63	125.26	0.001208				
-0.508	36.77	23.70	168.62	0.001626				
0	35.33	23.71	188.14	0.001814				
0.508	34.68	23.67	201.74	0.001945				
1.016	35.64	23.64	182.60	0.00176				
1.524	35.90	23.56	170.22	0.001641				
2.032	35.25	23.46	187.49	0.001808				
2.7686	35.71	23.29	178.00	0.001716				
3.5306	34.73	22.93	190.49	0.001836				
4.2926	36.38	22.81	162.87	0.00157				
5.0546	41.07	22.78	107.01	0.001032				
5.8166	35.51	22.75	146.86					
7.1628	30.21	22.68	333.50	0.003215	1.00	35.34	0.5166	1.0698
7.6708	30.17	22.71	356.22	0.003434	4.19	34.69	0.4895	1.1504
8.1788	30.79	22.75	334.98	0.003229	7.39	32.72	0.4080	1.0830
8.9408	31.74	22.87	308.34	0.002973	12.18	31.07	0.3372	1.0277
9.7028	32.75	22.93	280.61	0.002705	16.97	30.17	0.2985	1.0042
10.4648	33.25	22.99	271.02	0.002613	21.77	29.59	0.2729	0.9922
11.2268	33.86	23.03	257.96	0.002487	26.56	29.26	0.2580	0.9788
11.9888	34.65	23.07	241.01	0.002324	31.35	28.80	0.2376	0.9778
12.7508	34.77	23.09	241.21	0.002325	36.14	28.53	0.2258	0.9786
13.5128	34.94	23.11	239.53	0.002309	40.94	28.29	0.2151	0.9817
14.2748	35.29	23.12	233.63	0.002252	45.73	28.07	0.2055	0.9870
15.0368	35.94	23.12	221.85	0.002139	50.52	27.81	0.1948	0.9905
15.7988	35.92	23.14	225.37	0.002173	55.31	27.65	0.1875	0.9892
16.5608	36.20	23.14	218.33	0.002105	60.11	27.46	0.1797	0.9826

File:	s2v4q3h3	Ts,ex (K)	293.80	Tco (C)	48.17318			
Ptot (Pa)	97493	Re,ex	822292	VR	0.41			
Ttot (C)	24.97	q" (W/m2)	2665					
Ma,ex	0.2714	Tu,in	0.12					
Ma,in	0.0786	Lu,in (cm)	3.36					
Ps,ex(Pa)	92628	U0,in(m/s)	29.49					
Ps,in (Pa)	97073							
Surface	T surf	Taw	h	St	X/D	Taw,c(fc)	Naw	St/St0
(cm)	(C)	(C)	W/m2/C			(C)		
-11.7094	40.86	24.50	142.82	0.001387				
-10.9474	41.13	24.55	144.89	0.001407				
-10.1854	41.31	24.61	144.81	0.001407				
-9.4234	41.67	24.67	142.37	0.001383				
-8.6614	42.16	24.73	138.93	0.001349				
-7.8994	42.45	24.78	137.43	0.001335				
-7.1374	42.74	24.82	135.88	0.00132				
-6.3754	43.02	24.84	134.03	0.001302				
-5.6134	43.22	24.87	132.70	0.001289				
-4.8514	43.32	24.88	131.52	0.001277				
-4.0894	43.20	24.89	130.93	0.001272				
-3.3274	43.15	24.87	126.41	0.001228				
-2.921	43.13	24.83	133.92	0.001301				
-1.7272	38.51	24.89	159.99	0.001554				
-1.0414	37.75	24.93	170.00	0.001651				
-0.508	35.50	24.97	220.97	0.002146				
0	34.19	24.99	253.18	0.002459				
0.508	33.82	24.97	264.98	0.002574				
1.016	34.76	24.94	235.45	0.002287				
1.524	34.97	24.85	221.32	0.00215				
2.032	34.45	24.74	238.24	0.002314				
2.7686	34.87	24.56	224.38	0.002179				
3.5306	34.22	24.19	230.74	0.002241				
4.2926	35.86	24.06	191.67	0.001862				
5.0546	37.11	24.08	166.81	0.00162				
5.8166	36.86	24.14	139.28					
7.1628	31.83	24.14	336.64	0.00327	1.00	38.77	0.6088	1.0875
7.6708	31.90	24.14	351.57	0.003415	4.19	38.08	0.5801	1.1604
8.1788	32.45	24.16	330.09	0.003206	7.39	35.93	0.4899	1.1026
8.9408	33.15	24.21	306.72	0.002979	12.18	33.61	0.3922	1.0491
9.7028	33.81	24.24	285.70	0.002775	16.97	32.26	0.3349	1.0244
10.4648	34.16	24.26	276.56	0.002686	21.77	31.34	0.2962	1.0115
11.2268	34.52	24.30	267.94	0.002602	26.56	30.73	0.2696	1.0060
11.9888	34.99	24.34	255.83	0.002485	31.35	30.02	0.2385	0.9988
12.7508	35.10	24.34	253.99	0.002467	36.14	29.60	0.2209	0.9946
13.5128	35.23	24.34	251.39	0.002442	40.94	29.26	0.2063	0.9895
14.2748	35.46	24.36	246.38	0.002393	45.73	28.92	0.1914	0.9909
15.0368	35.81	24.37	238.44	0.002316	50.52	28.57	0.1762	0.9874
15.7988	35.84	24.38	238.97	0.002321	55.31	28.33	0.1663	0.9835
16.5608	35.98	24.39	232.77	0.002261	60.11	28.10	0.1562	0.9741

File:	s2v4q3k3	Ts,ex (K)	296.27	Tco (C)	44.28832			
Ptot (Pa)	99551	Re,ex	538227	VR	0.4			
Ttot (C)	24.84	q" (W/m2)	1962					
Ma,ex	0.1705	Tu,in	0.009					
Ma,in	0.0502	Lu,in (cm)	19.1					
Ps,ex(Pa)	97551	U0,in(m/s)	19.34					
Ps,in (Pa)	99375							
Surface	T surf	Taw	h	St	X/D	Taw,c(fc)	Naw	St/St0
(cm)	(C)	(C)	W/m2/C			(C)		
-11.7094	46.17	24.61	70.89	0.001045				
-10.9474	46.49	24.63	73.66	0.001086				
-10.1854	46.62	24.66	74.80	0.001103				
-9.4234	47.18	24.68	73.12	0.001078				
-8.6614	47.76	24.71	71.58	0.001055				
-7.8994	48.14	24.73	71.09	0.001048				
-7.1374	48.48	24.75	70.57	0.00104				
-6.3754	48.77	24.75	69.97	0.001032				
-5.6134	48.88	24.75	69.84	0.00103				
-4.8514	48.79	24.76	69.87	0.00103				
-4.0894	48.21	24.76	70.51	0.00104				
-3.3274	47.20	24.75	71.95	0.001061				
-2.921	46.35	24.72	80.01	0.00118				
-1.7272	40.60	24.79	93.07	0.001372				
-1.0414	39.35	24.81	101.27	0.001493				
-0.508	36.89	24.84	135.30	0.001995				
0	35.62	24.86	151.22	0.002229				
0.508	35.05	24.83	162.79	0.0024				
1.016	35.87	24.82	148.33	0.002187				
1.524	36.13	24.78	138.80	0.002046				
2.032	35.68	24.73	150.96	0.002226				
2.7686	36.02	24.66	145.57	0.002146				
3.5306	35.42	24.50	151.89	0.002239				
4.2926	36.86	24.45	130.36	0.001922				
5.0546	41.41	24.45	81.35	0.001199				
5.8166	36.07	24.45	123.65					
7.1628	31.92	24.44	248.67	0.003666	1.00	33.02	0.4323	1.0058
7.6708	31.69	24.44	275.59	0.004063	4.19	32.10	0.3858	1.1328
8.1788	32.28	24.46	257.98	0.003803	7.39	30.51	0.3053	1.0715
8.9408	33.08	24.49	238.93	0.003523	12.18	29.38	0.2470	1.0410
9.7028	34.01	24.51	217.38	0.003205	16.97	28.92	0.2231	1.0222
10.4648	34.50	24.52	208.97	0.003081	21.77	28.56	0.2043	1.0122
11.2268	35.10	24.56	198.54	0.002927	26.56	28.42	0.1955	0.9995
11.9888	35.90	24.58	184.61	0.002722	31.35	28.18	0.1826	0.9881
12.7508	36.11	24.58	182.84	0.002696	36.14	28.03	0.1751	0.9880
13.5128	36.34	24.57	180.14	0.002656	40.94	27.90	0.1686	0.9839
14.2748	36.78	24.58	174.04	0.002566	45.73	27.78	0.1624	0.9864
15.0368	37.39	24.59	165.59	0.002441	50.52	27.65	0.1551	0.9835
15.7988	37.47	24.59	166.57	0.002456	55.31	27.56	0.1506	0.9804
16.5608	37.76	24.60	160.03	0.002359	60.11	27.43	0.1438	0.9721

File:	s2v4q3g3	Ts,ex (K)	297.00	Tco (C)	45.09728			
Ptot (Pa)	98124	Re,ex	529663	VR	0.4			
Ttot (C)	25.58	q" (W/m2)	1938					
Ma,ex	0.1708	Tu,in	0.124					
Ma,in	0.0507	Lu,in (cm)	3.16					
Ps,ex(Pa)	96146	U0,in(m/s)	19.53					
Ps,in (Pa)	97947							
Surface	T surf	Taw	h	St	X/D	Taw,c(fc)	Naw	St/St0
(cm)	(C)	(C)	W/m2/C			(C)		
-11.7094	41.25	25.36	104.90	0.001569				
-10.9474	41.37	25.38	107.96	0.001614				
-10.1854	41.44	25.41	108.63	0.001624				
-9.4234	41.70	25.43	107.15	0.001602				
-8.6614	42.08	25.45	104.74	0.001566				
-7.8994	42.32	25.47	103.71	0.001551				
-7.1374	42.56	25.49	102.55	0.001533				
-6.3754	42.80	25.49	101.19	0.001513				
-5.6134	42.94	25.50	100.32	0.0015				
-4.8514	43.00	25.50	99.55	0.001488				
-4.0894	42.82	25.50	99.24	0.001484				
-3.3274	42.67	25.49	96.71	0.001446				
-2.921	42.67	25.47	102.66	0.001535				
-1.7272	38.27	25.53	123.53	0.001847				
-1.0414	37.42	25.56	132.56	0.001982				
-0.508	35.40	25.59	172.46	0.002579				
0	34.23	25.61	197.21	0.002949				
0.508	33.87	25.57	207.60	0.003104				
1.016	34.62	25.56	186.72	0.002792				
1.524	34.83	25.52	176.49	0.002639				
2.032	34.46	25.48	188.72	0.002822				
2.7686	34.80	25.41	180.34	0.002697				
3.5306	34.44	25.25	183.54	0.002744				
4.2926	35.87	25.19	154.00	0.002303				
5.0546	37.50	25.20	125.83	0.001882				
5.8166	35.06	25.20	143.20					
7.1628	33.08	25.19	245.54	0.003672	1.00	37.28	0.6073	1.0952
7.6708	32.91	25.18	267.53	0.004	4.19	36.26	0.5563	1.2075
8.1788	33.39	25.20	250.92	0.003752	7.39	34.31	0.4578	1.1470
8.9408	34.11	25.24	230.22	0.003442	12.18	32.46	0.3638	1.0875
9.7028	34.81	25.25	212.36	0.003175	16.97	31.42	0.3107	1.0537
10.4648	35.21	25.27	204.09	0.003052	21.77	30.71	0.2743	1.0392
11.2268	35.58	25.30	196.94	0.002945	26.56	30.29	0.2519	1.0329
11.9888	36.06	25.33	187.38	0.002802	31.35	29.74	0.2231	1.0216
12.7508	36.22	25.33	184.88	0.002765	36.14	29.41	0.2065	1.0165
13.5128	36.37	25.32	182.38	0.002727	40.94	29.14	0.1931	1.0083
14.2748	36.63	25.33	177.78	0.002658	45.73	28.87	0.1791	1.0106
15.0368	36.95	25.33	172.53	0.00258	50.52	28.59	0.1649	1.0055
15.7988	37.04	25.33	171.86	0.00257	55.31	28.40	0.1554	0.9990
16.5608	37.20	25.34	166.11	0.002484	60.11	28.22	0.1459	0.9898

File:	s2v3q3l2.	Ts,ex (K)	292.13	Tco (C)	44.24634			
Ptot (Pa)	98520	Re,ex	832782	VR	0.32			
Ttot (C)	23.23	q" (W/m2)	2662					
Ma,ex	0.2699	Tu,in	0.011					
Ma,in	0.0770	Lu,in (cm)	6.6					
Ps,ex(Pa)	93656	U0,in(m/s)	29.58					
Ps,in (Pa)	98112							
Surface	T surf	Taw	h	St	X/D	Taw,c(fc)	Naw	St/St0
(cm)	(C)	(C)	W/m2/C			(C)		
-11.7094	46.65	22.67	88.04	0.000848				
-10.9474	47.00	22.73	91.17	0.000878				
-10.1854	47.16	22.80	92.54	0.000891				
-9.4234	47.87	22.86	90.46	0.000871				
-8.6614	48.59	22.91	88.48	0.000852				
-7.8994	49.05	22.96	87.85	0.000846				
-7.1374	49.46	22.99	87.19	0.00084				
-6.3754	49.84	23.02	86.39	0.000832				
-5.6134	50.03	23.03	86.07	0.000829				
-4.8514	49.99	23.03	85.99	0.000828				
-4.0894	49.45	23.04	86.72	0.000835				
-3.3274	48.45	23.03	87.81	0.000846				
-2.921	47.54	23.01	97.18	0.000936				
-1.7272	40.97	23.12	115.15	0.001109				
-1.0414	39.53	23.17	125.58	0.00121				
-0.508	36.54	23.24	168.75	0.001626				
0	35.07	23.25	188.96	0.00182				
0.508	34.40	23.21	202.81	0.001954				
1.016	35.38	23.17	183.11	0.001764				
1.524	35.62	23.10	171.51	0.001652				
2.032	35.00	22.99	187.26	0.001804				
2.7686	35.41	22.81	178.52	0.00172				
3.5306	34.49	22.45	190.17	0.001832				
4.2926	36.15	22.34	162.80	0.001568				
5.0546	41.09	22.31	106.17	0.001023				
5.8166	34.84	22.28	156.88					
7.1628	30.21	22.27	324.49	0.003126	1.00	33.68	0.5193	1.0401
7.6708	29.88	22.28	357.19	0.003441	4.19	31.94	0.4397	1.1526
8.1788	30.47	22.34	335.58	0.003233	7.39	29.88	0.3443	1.0840
8.9408	31.39	22.45	308.51	0.002972	12.18	28.50	0.2776	1.0274
9.7028	32.37	22.52	281.34	0.00271	16.97	27.78	0.2423	1.0060
10.4648	32.81	22.55	272.66	0.002626	21.77	27.30	0.2187	0.9974
11.2268	33.39	22.61	260.32	0.002508	26.56	27.05	0.2051	0.9868
11.9888	34.17	22.64	243.21	0.002343	31.35	26.70	0.1876	0.9859
12.7508	34.27	22.66	243.52	0.002346	36.14	26.49	0.1773	0.9871
13.5128	34.43	22.66	241.69	0.002328	40.94	26.29	0.1680	0.9898
14.2748	34.79	22.68	235.63	0.00227	45.73	26.13	0.1601	0.9946
15.0368	35.43	22.68	223.84	0.002156	50.52	25.94	0.1515	0.9986
15.7988	35.41	22.69	227.33	0.00219	55.31	25.83	0.1457	0.9970
16.5608	35.68	22.68	220.06	0.00212	60.11	25.69	0.1395	0.9895

File:	s2v3q3h3.	Ts,ex (K)	294.17	Tco (C)	46.70923			
Ptot (Pa)	97493	Re,ex	820951	VR	0.31			
Ttot (C)	25.36	q" (W/m2)	2663					
Ma,ex	0.2714	Tu,in	0.12					
Ma,in	0.0786	Lu,in (cm)	3.36					
Ps,ex(Pa)	92628	U0,in(m/s)	29.49					
Ps,in (Pa)	97073							
Surface	T surf	Taw	h	St	X/D	Taw,c(fc)	Naw	St/St0
(cm)	(C)	(C)	W/m2/C			(C)		
-11.7094	41.26	24.90	142.75	0.001387				
-10.9474	41.52	24.95	144.82	0.001407				
-10.1854	41.70	25.01	144.69	0.001406				
-9.4234	42.08	25.08	142.16	0.001382				
-8.6614	42.55	25.13	138.82	0.001349				
-7.8994	42.86	25.18	137.25	0.001334				
-7.1374	43.15	25.22	135.64	0.001318				
-6.3754	43.43	25.25	133.87	0.001301				
-5.6134	43.66	25.27	132.38	0.001287				
-4.8514	43.79	25.29	131.09	0.001274				
-4.0894	43.72	25.31	130.42	0.001268				
-3.3274	43.77	25.30	125.73	0.001222				
-2.921	43.89	25.28	132.43	0.001287				
-1.7272	39.24	25.34	159.43	0.001549				
-1.0414	38.40	25.35	169.86	0.001651				
-0.508	36.08	25.40	220.73	0.002145				
0	34.74	25.41	253.52	0.002464				
0.508	34.39	25.40	265.14	0.002577				
1.016	35.32	25.35	235.67	0.00229				
1.524	35.56	25.27	222.46	0.002162				
2.032	35.08	25.17	237.81	0.002311				
2.7686	35.45	24.97	224.67	0.002184				
3.5306	34.85	24.61	229.66	0.002232				
4.2926	36.50	24.46	191.08	0.001857				
5.0546	37.92	24.51	164.37	0.001598				
5.8166	36.98	24.65	151.50					
7.1628	32.90	24.69	327.86	0.003186	1.00	38.11	0.6097	1.0598
7.6708	32.55	24.65	355.57	0.003456	4.19	36.04	0.5164	1.1744
8.1788	32.95	24.65	334.83	0.003254	7.39	33.52	0.4020	1.1192
8.9408	33.59	24.67	309.89	0.003012	12.18	31.51	0.3103	1.0606
9.7028	34.21	24.70	289.17	0.00281	16.97	30.43	0.2604	1.0375
10.4648	34.54	24.71	279.85	0.00272	21.77	29.71	0.2274	1.0242
11.2268	34.89	24.73	270.64	0.00263	26.56	29.27	0.2064	1.0168
11.9888	35.36	24.77	257.92	0.002507	31.35	28.75	0.1814	1.0076
12.7508	35.48	24.77	255.69	0.002485	36.14	28.43	0.1668	1.0019
13.5128	35.60	24.77	253.05	0.002459	40.94	28.18	0.1551	0.9967
14.2748	35.84	24.79	247.71	0.002408	45.73	27.95	0.1442	0.9969
15.0368	36.19	24.80	239.75	0.00233	50.52	27.71	0.1327	0.9935
15.7988	36.23	24.81	240.06	0.002333	55.31	27.52	0.1237	0.9886
16.5608	36.38	24.81	233.52	0.00227	60.11	27.36	0.1167	0.9779

File:	p1v5q3l3	Ts,ex (K)	293.22	Tco (C)	36.17616			
Ptot (Pa)	98266	Re,ex	827413	VR	0.5			
Ttot (C)	24.35	q" (W/m2)	2554					
Ma,ex	0.2702	Tu,in	0.01					
Ma,in	0.0779	Lu,in (cm)	6.6					
Ps,ex(Pa)	93406	U0,in(m/s)	29.58					
Ps,in (Pa)	97849							
Surface	T surf	Taw	h	St	X/D	Taw,c(fc)	Naw	St/St0
(cm)	(C)	(C)	W/m2/C			(C)		
-11.7094	44.24	23.94	105.77	0.001023	68.33333	24.59	0.0533	1.2673
-10.9474	44.54	24.00	109.10	0.001055	62.45098	24.80	0.0658	1.2379
-10.1854	44.75	24.07	110.10	0.001064	56.56863	25.01	0.0776	1.2329
-9.4234	45.35	24.11	107.78	0.001042	50.68627	25.21	0.0906	1.2385
-8.6614	46.01	24.18	105.34	0.001018	44.80392	25.43	0.1039	1.2344
-7.8994	46.46	24.22	104.48	0.00101	38.92157	25.66	0.1208	1.2325
-7.1374	46.87	24.27	103.73	0.001003	33.03922	25.90	0.1372	1.2352
-6.3754	47.25	24.30	103.17	0.000997	27.15686	26.24	0.1636	1.2436
-5.6134	47.43	24.34	103.99	0.001005	21.27451	26.74	0.2031	1.2601
-4.8514	47.29	24.39	106.76	0.001032	15.39216	27.41	0.2561	1.2898
-4.0894	46.94	24.45	111.74	0.00108	9.509804	28.69	0.3617	1.3328
-3.3274	45.64	24.50	115.53	0.001117	3.627451	27.54	0.2605	1.3665
-2.921	44.54	24.54	109.71	0.001061	0.490196	24.19		1.2713
-1.7272	43.81	24.59	114.26	0.001105				
-1.0414	42.23	24.57	124.38	0.001202				
-0.508	38.69	24.56	166.33	0.001608				
0	36.98	24.56	190.81	0.001845				
0.508	36.43	24.53	201.12	0.001944				
1.016	37.38	24.49	182.58	0.001765				
1.524	37.63	24.40	175.94	0.001701				
2.032	37.14	24.29	184.10	0.00178				
2.7686	37.11	24.07	181.36	0.001753				
3.5306	36.44	23.70	186.06	0.001799				
4.2926	38.05	23.57	160.96	0.001556				
5.0546	44.47	23.59	100.06	0.000967				
5.8166	39.18	23.18	135.54					
7.1628	34.91	23.64	221.69					
7.6708	31.54	23.71	325.34	0.003145				
8.1788	31.91	23.72	311.67	0.003013				
8.9408	32.58	23.82	292.21	0.002825				
9.7028	33.27	23.86	273.67	0.002646				
10.4648	33.60	23.90	267.85	0.002589				
11.2268	34.03	23.94	258.88	0.002503				
11.9888	34.70	23.97	243.45	0.002354				
12.7508	34.83	23.98	242.67	0.002346				
13.5128	35.01	23.98	239.80	0.002318				
14.2748	35.32	23.99	234.03	0.002262				
15.0368	35.85	23.98	223.46	0.00216				
15.7988	35.89	23.99	225.05	0.002176				
16.5608	36.13	23.98	217.76	0.002105				

File:	p1v5q3h3	Ts,ex (K)	289.65	Tco (C)	36.82472			
Ptot (Pa)	97904	Re,ex	838129	VR	0.5			
Ttot (C)	20.74	q" (W/m2)	2578					
Ma,ex	0.2705	Tu,in	0.12					
Ma,in	0.0788	Lu,in (cm)	3.36					
Ps,ex(Pa)	93052	U0,in(m/s)	29.49					
Ps,in (Pa)	97479							
Surface	T surf	Taw	h	St	X/D	Taw,c(fc)	Naw	St/St0
(cm)	(C)	(C)	W/m2/C			(C)		
-11.7094	35.78	20.35	148.07	0.001427	68.33333	20.77	0.0253	1.0292
-10.9474	36.04	20.40	150.29	0.001448	62.45098	20.91	0.0308	1.0193
-10.1854	36.21	20.47	150.48	0.00145	56.56863	21.07	0.0366	1.0227
-9.4234	36.54	20.53	148.38	0.00143	50.68627	21.24	0.0437	1.0273
-8.6614	36.94	20.59	145.66	0.001403	44.80392	21.44	0.0521	1.0276
-7.8994	37.14	20.64	145.22	0.001399	38.92157	21.64	0.0616	1.0332
-7.1374	37.32	20.69	144.93	0.001396	33.03922	21.87	0.0735	1.0446
-6.3754	37.45	20.72	145.17	0.001399	27.15686	22.19	0.0908	1.0638
-5.6134	37.45	20.76	146.97	0.001416	21.27451	22.68	0.1194	1.0896
-4.8514	37.36	20.81	149.99	0.001445	15.39216	23.33	0.1574	1.1168
-4.0894	37.09	20.87	157.20	0.001515	9.509804	24.91	0.2535	1.1674
-3.3274	36.94	20.93	156.87	0.001511	3.627451	25.09	0.2616	1.1629
-2.921	36.47	20.98	152.21	0.001466	0.490196	22.29		1.1181
-1.7272	34.99	20.92	162.16	0.001562				
-1.0414	34.23	20.91	171.34	0.001651				
-0.508	31.69	20.91	222.45	0.002143				
0	30.22	20.91	260.51	0.00251				
0.508	29.98	20.88	267.40	0.002576				
1.016	30.92	20.83	237.53	0.002289				
1.524	31.15	20.74	228.49	0.002201				
2.032	30.76	20.63	238.46	0.002297				
2.7686	30.98	20.41	228.58	0.002202				
3.5306	30.61	20.03	227.49	0.002192				
4.2926	32.27	19.87	189.36	0.001824				
5.0546	34.00	19.93	160.62	0.001547				
5.8166	31.58	20.11	187.68					
7.1628	31.97	20.27	210.33					
7.6708	28.10	20.25	323.46	0.003116				
8.1788	28.35	20.22	311.63	0.003002				
8.9408	28.84	20.24	294.80	0.00284				
9.7028	29.27	20.27	282.97	0.002726				
10.4648	29.52	20.28	277.16	0.00267				
11.2268	29.77	20.31	271.69	0.002618				
11.9888	30.20	20.34	260.67	0.002511				
12.7508	30.29	20.32	258.84	0.002494				
13.5128	30.42	20.31	256.27	0.002469				
14.2748	30.64	20.31	251.17	0.00242				
15.0368	30.99	20.30	242.74	0.002339				
15.7988	31.02	20.30	243.01	0.002341				
16.5608	31.16	20.29	236.78	0.002281				

File:	p1v1q3l3	Ts,ex (K)	294.25	Tco (C)	46.77414			
Ptot (Pa)	99411	Re,ex	832843	VR	1			
Ttot (C)	25.39	q" (W/m2)	2552					
Ma,ex	0.2700	Tu,in	0.011					
Ma,in	0.0778	Lu,in (cm)	6.6					
Ps,ex(Pa)	94500	U0,in(m/s)	29.58					
Ps,in (Pa)	98991							
Surface	T surf	Taw	h	St	X/D	Taw,c(fc)	Naw	St/St0
(cm)	(C)	(C)	W/m2/C			(C)		
-11.7094	44.24	24.97	112.04	0.001073	68.33333	25.75	0.0361	1.3300
-10.9474	44.37	25.02	116.09	0.001112	62.45098	25.92	0.0411	1.3051
-10.1854	44.79	25.09	115.01	0.001102	56.56863	26.17	0.0496	1.2761
-9.4234	45.36	25.15	112.39	0.001076	50.68627	26.39	0.0576	1.2795
-8.6614	46.02	25.21	109.47	0.001049	44.80392	26.64	0.0666	1.2709
-7.8994	46.48	25.25	108.01	0.001035	38.92157	26.95	0.0790	1.2624
-7.1374	46.79	25.29	107.37	0.001028	33.03922	27.22	0.0898	1.2668
-6.3754	47.05	25.32	106.81	0.001023	27.15686	27.62	0.1073	1.2757
-5.6134	47.04	25.36	107.86	0.001033	21.27451	28.16	0.1309	1.2949
-4.8514	46.69	25.40	110.43	0.001058	15.39216	28.71	0.1548	1.3218
-4.0894	45.53	25.44	118.52	0.001135	9.509804	29.63	0.1965	1.4006
-3.3274	44.14	25.49	124.85	0.001196	3.627451	28.20	0.1274	1.4632
-2.921	43.38	25.53	118.74	0.001137	0.490196	25.34		1.3632
-1.7272	44.06	25.60	115.87	0.00111				
-1.0414	42.78	25.59	124.36	0.001191				
-0.508	39.43	25.58	166.72	0.001597				
0	37.79	25.58	190.32	0.001823				
0.508	37.22	25.56	201.63	0.001931				
1.016	38.17	25.51	182.75	0.00175				
1.524	38.42	25.43	175.17	0.001678				
2.032	37.90	25.32	184.51	0.001767				
2.7686	37.90	25.10	181.52	0.001739				
3.5306	37.15	24.74	186.87	0.00179				
4.2926	38.69	24.62	161.84	0.00155				
5.0546	44.76	24.67	101.28	0.00097				
5.8166	36.52	24.47	199.53					
7.1628	35.54	24.69	225.54					
7.6708	32.36	24.74	330.23	0.003163				
8.1788	32.82	24.76	312.73	0.002995				
8.9408	33.51	24.84	292.62	0.002803				
9.7028	34.18	24.88	275.09	0.002635				
10.4648	34.53	24.93	268.91	0.002576				
11.2268	34.97	24.97	259.44	0.002485				
11.9888	35.63	24.99	244.17	0.002339				
12.7508	35.76	25.00	242.99	0.002327				
13.5128	35.94	25.00	240.03	0.002299				
14.2748	36.23	25.01	234.56	0.002247				
15.0368	36.73	25.01	224.34	0.002149				
15.7988	36.78	25.00	224.84	0.002154				
16.5608	37.02	25.00	217.71	0.002085				

File:	p1v1q3h3	Ts,ex (K)	289.84	Tco (C)	37.44804			
Ptot (Pa)	97904	Re,ex	837460	VR	1			
Ttot (C)	20.93	q" (W/m2)	2578					
Ma,ex	0.2705	Tu,in	0.12					
Ma,in	0.0788	Lu,in (cm)	3.36					
Ps,ex(Pa)	93052	U0,in(m/s)	29.49					
Ps,in (Pa)	97479							
Surface	T surf	Taw	h	St	X/D	Taw,c(fc)	Naw	St/St0
(cm)	(C)	(C)	W/m2/C			(C)		
-11.7094	36.16	20.53	145.64	0.001404	68.33333	21.15	0.0365	1.0127
-10.9474	36.41	20.58	147.98	0.001426	62.45098	21.35	0.0457	1.0039
-10.1854	36.59	20.65	148.17	0.001428	56.56863	21.54	0.0526	1.0073
-9.4234	36.93	20.70	145.87	0.001406	50.68627	21.73	0.0612	1.0103
-8.6614	37.36	20.77	142.97	0.001378	44.80392	21.95	0.0706	1.0089
-7.8994	37.58	20.82	142.37	0.001372	38.92157	22.16	0.0808	1.0133
-7.1374	37.75	20.87	142.00	0.001368	33.03922	22.40	0.0924	1.0238
-6.3754	37.86	20.90	142.06	0.001369	27.15686	22.71	0.1092	1.0414
-5.6134	37.76	20.94	144.13	0.001389	21.27451	23.13	0.1330	1.0688
-4.8514	37.39	20.98	148.54	0.001432	15.39216	23.61	0.1597	1.1063
-4.0894	36.27	21.02	162.45	0.001566	9.509804	24.56	0.2152	1.2067
-3.3274	34.74	21.07	180.36	0.001738	3.627451	23.97	0.1771	1.3374
-2.921	34.33	21.11	173.30	0.00167	0.490196	21.56		1.2735
-1.7272	34.68	21.12	165.56	0.001596				
-1.0414	34.09	21.11	172.96	0.001667				
-0.508	31.64	21.11	225.18	0.00217				
0	30.20	21.12	263.33	0.002538				
0.508	29.95	21.09	270.69	0.002609				
1.016	30.89	21.04	240.33	0.002316				
1.524	31.13	20.96	229.97	0.002216				
2.032	30.70	20.85	241.70	0.002329				
2.7686	30.92	20.62	230.95	0.002226				
3.5306	30.48	20.23	230.59	0.002222				
4.2926	32.10	20.05	191.33	0.001844				
5.0546	33.69	20.10	163.51	0.001576				
5.8166	31.96	20.26	176.16					
7.1628	32.01	20.47	210.18					
7.6708	28.04	20.44	331.64	0.003196				
8.1788	28.35	20.42	317.43	0.003059				
8.9408	28.88	20.44	299.04	0.002882				
9.7028	29.33	20.46	286.73	0.002763				
10.4648	29.60	20.48	280.83	0.002706				
11.2268	29.88	20.50	274.56	0.002646				
11.9888	30.32	20.52	262.66	0.002531				
12.7508	30.42	20.51	261.21	0.002517				
13.5128	30.55	20.50	258.39	0.00249				
14.2748	30.77	20.50	253.13	0.00244				
15.0368	31.12	20.50	244.67	0.002358				
15.7988	31.15	20.50	245.33	0.002364				
16.5608	31.30	20.50	238.79	0.002301				

File:	p1v1q3k5	Ts,ex (K)	295.91	Tco (C)	39.3687			
Ptot (Pa)	98314	Re,ex	533351	VR	1			
Ttot (C)	24.49	q" (W/m2)	1909					
Ma,ex	0.1708	Tu,in	0.009					
Ma,in	0.0504	Lu,in (cm)	19.1					
Ps,ex(Pa)	96332	U0,in(m/s)	19.34					
Ps,in (Pa)	98139							
Surface	T surf	Taw	h	St	X/D	Taw,c(fc)	Naw	St/St0
(cm)	(C)	(C)	W/m2/C			(C)		
-11.7094	42.42	24.29	88.16	0.001313	68.33333	24.79	0.0327	1.2771
-10.9474	42.60	24.32	91.41	0.001361	62.45098	24.94	0.0410	1.2503
-10.1854	42.93	24.35	90.67	0.00135	56.56863	25.06	0.0477	1.2246
-9.4234	43.42	24.37	88.61	0.00132	50.68627	25.20	0.0555	1.2276
-8.6614	43.99	24.39	86.22	0.001284	44.80392	25.38	0.0659	1.2178
-7.8994	44.36	24.41	85.28	0.00127	38.92157	25.58	0.0784	1.2133
-7.1374	44.61	24.44	84.93	0.001265	33.03922	25.80	0.0907	1.2212
-6.3754	44.77	24.45	84.80	0.001263	27.15686	26.04	0.1067	1.2350
-5.6134	44.65	24.47	86.10	0.001282	21.27451	26.36	0.1274	1.2617
-4.8514	44.18	24.49	88.69	0.001321	15.39216	26.60	0.1421	1.2959
-4.0894	42.95	24.52	96.18	0.001432	9.509804	27.00	0.1667	1.3861
-3.3274	41.95	24.57	98.90	0.001473	3.627451	26.06	0.1008	1.4186
-2.921	41.20	24.64	95.91	0.001428	0.490196	24.65		1.3504
-1.7272	41.46	24.69	93.82	0.001397				
-1.0414	40.27	24.68	100.91	0.001503				
-0.508	37.38	24.65	134.66	0.002005				
0	35.89	24.65	154.33	0.002298				
0.508	35.43	24.61	162.36	0.002418				
1.016	36.26	24.59	147.82	0.002201				
1.524	36.50	24.57	142.05	0.002115				
2.032	36.11	24.51	149.65	0.002229				
2.7686	36.18	24.43	147.57	0.002198				
3.5306	35.73	24.29	151.50	0.002256				
4.2926	37.18	24.25	131.74	0.001962				
5.0546	43.34	24.32	78.73	0.001172				
5.8166	43.53	24.20	73.76					
7.1628	35.04	24.26	171.73					
7.6708	32.38	24.30	231.67	0.00345				
8.1788	32.63	24.30	226.97	0.00338				
8.9408	33.29	24.32	211.61	0.003151				
9.7028	33.91	24.33	200.22	0.002982				
10.4648	34.31	24.34	194.41	0.002895				
11.2268	34.71	24.37	188.65	0.002809				
11.9888	35.33	24.38	178.15	0.002653				
12.7508	35.56	24.38	175.78	0.002618				
13.5128	35.77	24.37	173.14	0.002578				
14.2748	36.13	24.38	167.85	0.0025				
15.0368	36.59	24.37	161.23	0.002401				
15.7988	36.70	24.38	160.70	0.002393				
16.5608	36.94	24.37	154.48	0.0023				

File:	p1v1q3g2	Ts,ex (K)	292.43	Tco (C)	39.20832			
Ptot (Pa)	98827	Re,ex	544332	VR	1			
Ttot (C)	20.99	q" (W/m2)	1964					
Ma,ex	0.1709	Tu,in	0.124					
Ma,in	0.0513	Lu,in (cm)	3.16					
Ps,ex(Pa)	96834	U0,in(m/s)	19.53					
Ps,in (Pa)	98645							
Surface	T surf	Taw	h	St	X/D	Taw,c(fc)	Naw	St/St0
(cm)	(C)	(C)	W/m2/C			(C)		
-11.7094	36.71	20.82	107.01	0.001576	68.33333	21.55	0.0397	1.0112
-10.9474	36.82	20.84	110.46	0.001627	62.45098	21.71	0.0478	1.0029
-10.1854	36.86	20.87	111.58	0.001643	56.56863	21.86	0.0538	1.0052
-9.4234	37.10	20.89	110.41	0.001626	50.68627	22.01	0.0610	1.0108
-8.6614	37.44	20.93	108.60	0.001599	44.80392	22.23	0.0709	1.0104
-7.8994	37.61	20.95	108.33	0.001595	38.92157	22.43	0.0808	1.0152
-7.1374	37.73	20.98	108.35	0.001595	33.03922	22.67	0.0924	1.0273
-6.3754	37.80	21.00	108.62	0.0016	27.15686	22.99	0.1095	1.0465
-5.6134	37.64	21.03	110.73	0.001631	21.27451	23.48	0.1347	1.0783
-4.8514	37.25	21.04	114.19	0.001681	15.39216	24.01	0.1636	1.1158
-4.0894	36.10	21.08	126.04	0.001856	9.509804	25.09	0.2213	1.2259
-3.3274	34.80	21.11	136.57	0.002011	3.627451	24.09	0.1647	1.3276
-2.921	34.39	21.17	131.90	0.001942	0.490196	21.80		1.2709
-1.7272	34.33	21.11	126.73	0.001866				
-1.0414	33.63	21.09	133.65	0.001968				
-0.508	31.34	21.07	174.27	0.002566				
0	30.02	21.07	202.96	0.002989				
0.508	29.78	21.05	208.65	0.003072				
1.016	30.59	21.03	187.98	0.002768				
1.524	30.79	21.01	181.46	0.002672				
2.032	30.48	20.96	190.06	0.002799				
2.7686	30.74	20.86	183.18	0.002697				
3.5306	30.55	20.71	183.05	0.002696				
4.2926	32.04	20.65	154.05	0.002268				
5.0546	34.08	20.69	124.16	0.001828				
5.8166	32.78	20.76	126.12					
7.1628	31.96	20.83	165.34					
7.6708	28.91	20.83	236.88	0.003488				
8.1788	29.10	20.81	231.56	0.00341				
8.9408	29.71	20.82	216.60	0.003189				
9.7028	30.17	20.82	207.73	0.003059				
10.4648	30.49	20.82	202.34	0.002979				
11.2268	30.78	20.82	197.53	0.002909				
11.9888	31.23	20.84	189.29	0.002787				
12.7508	31.39	20.83	187.43	0.00276				
13.5128	31.54	20.83	185.52	0.002732				
14.2748	31.82	20.83	180.85	0.002663				
15.0368	32.16	20.83	175.49	0.002584				
15.7988	32.24	20.82	175.23	0.00258				
16.5608	32.42	20.82	169.33	0.002493				

File:	p1v2q3l8.	Ts,ex (K)	294.64	Tco (C)	48.05292			
Ptot (Pa)	99411	Re,ex	831430	VR	1.5			
Ttot (C)	25.79	q" (W/m2)	2552					
Ma,ex	0.2700	Tu,in	0.011					
Ma,in	0.0778	Lu,in (cm)	6.6					
Ps,ex(Pa)	94500	U0,in(m/s)	29.58					
Ps,in (Pa)	98991							
Surface	T surf	Taw	h	St	X/D	Taw,c(fc)	Naw	St/St0
(cm)	(C)	(C)	W/m2/C			(C)		
-11.7094	43.18	25.36	124.07	0.001189	68.33333	26.74	0.0609	1.4738
-10.9474	43.01	25.42	130.63	0.001252	62.45098	26.95	0.0679	1.4696
-10.1854	43.27	25.48	129.90	0.001245	56.56863	27.09	0.0714	1.4422
-9.4234	43.55	25.54	128.70	0.001234	50.68627	27.25	0.0761	1.4662
-8.6614	43.88	25.59	127.14	0.001219	44.80392	27.40	0.0806	1.4771
-7.8994	44.03	25.63	126.99	0.001217	38.92157	27.53	0.0847	1.4852
-7.1374	43.99	25.68	128.29	0.00123	33.03922	27.66	0.0885	1.5145
-6.3754	43.92	25.70	129.50	0.001241	27.15686	27.82	0.0945	1.5477
-5.6134	43.63	25.74	132.60	0.001271	21.27451	28.07	0.1042	1.5930
-4.8514	43.24	25.78	136.21	0.001306	15.39216	28.36	0.1158	1.6314
-4.0894	42.34	25.81	145.27	0.001392	9.509804	29.19	0.1518	1.7179
-3.3274	42.17	25.84	141.43	0.001356	3.627451	28.21	0.1070	1.6586
-2.921	42.17	25.85	125.39	0.001202	0.490196	25.34		1.4405
-1.7272	43.75	26.00	116.99	0.001121				
-1.0414	42.64	25.99	124.75	0.001196				
-0.508	39.48	25.99	167.38	0.001604				
0	37.91	25.98	190.13	0.001822				
0.508	37.35	25.97	202.00	0.001936				
1.016	38.28	25.92	183.52	0.001759				
1.524	38.52	25.83	174.62	0.001674				
2.032	37.98	25.73	185.28	0.001776				
2.7686	38.01	25.52	181.75	0.001742				
3.5306	37.18	25.17	188.54	0.001807				
4.2926	38.68	25.04	163.24	0.001565				
5.0546	44.40	25.10	102.84	0.000986				
5.8166	36.77	24.74	192.15					
7.1628	35.56	25.10	229.61					
7.6708	32.57	25.15	335.05	0.003211				
8.1788	33.08	25.16	314.70	0.003016				
8.9408	33.77	25.24	294.04	0.002818				
9.7028	34.36	25.29	278.22	0.002667				
10.4648	34.73	25.33	270.47	0.002592				
11.2268	35.11	25.37	262.49	0.002516				
11.9888	35.68	25.39	248.76	0.002384				
12.7508	35.86	25.40	246.13	0.002359				
13.5128	36.04	25.40	243.04	0.002329				
14.2748	36.36	25.41	236.77	0.002269				
15.0368	36.80	25.40	227.57	0.002181				
15.7988	36.91	25.41	227.05	0.002176				
16.5608	37.15	25.41	219.74	0.002106				

File:	p1v2q3h5.	Ts,ex (K)	290.92	Tco (C)	43.13975			
Ptot (Pa)	97904	Re,ex	833495	VR	1.5			
Ttot (C)	22.02	q" (W/m2)	2574					
Ma,ex	0.2705	Tu,in	0.12					
Ma,in	0.0788	Lu,in (cm)	3.36					
Ps,ex(Pa)	93052	U0,in(m/s)	29.49					
Ps,in (Pa)	97479							
Surface	T surf	Taw	h	St	X/D	Taw,c(fc)	Naw	St/St0
(cm)	(C)	(C)	W/m2/C			(C)		
-11.7094	37.13	21.61	146.98	0.001419	68.33	22.78	0.0541	1.0238
-10.9474	37.36	21.68	149.62	0.001445	62.45	23.06	0.0645	1.0169
-10.1854	37.48	21.73	150.21	0.00145	56.57	23.27	0.0718	1.0230
-9.4234	37.78	21.79	148.25	0.001431	50.69	23.52	0.0810	1.0286
-8.6614	38.10	21.85	146.12	0.001411	44.80	23.77	0.0902	1.0331
-7.8994	38.20	21.90	146.45	0.001414	38.92	24.03	0.1002	1.0443
-7.1374	38.23	21.94	147.28	0.001422	33.04	24.27	0.1098	1.0638
-6.3754	38.11	21.97	149.23	0.001441	27.16	24.54	0.1214	1.0959
-5.6134	37.68	21.99	154.44	0.001491	21.27	24.84	0.1347	1.1474
-4.8514	36.96	22.03	162.81	0.001572	15.39	25.04	0.1424	1.2149
-4.0894	35.53	22.06	182.10	0.001758	9.51	25.40	0.1584	1.3552
-3.3274	34.39	22.07	196.75	0.0019	3.63	24.60	0.1198	1.4617
-2.921	34.26	22.07	183.95	0.001776	0.49	21.55		1.3542
-1.7272	35.41	22.17	164.93	0.001592				
-1.0414	34.93	22.17	171.08	0.001652				
-0.508	32.63	22.18	222.31	0.002147				
0	31.26	22.18	258.29	0.002494				
0.508	30.97	22.16	268.11	0.002589				
1.016	31.93	22.11	237.16	0.00229				
1.524	32.18	22.02	225.45	0.002177				
2.032	31.72	21.91	238.74	0.002305				
2.7686	31.97	21.70	228.06	0.002202				
3.5306	31.45	21.34	229.74	0.002218				
4.2926	33.03	21.19	191.39	0.001848				
5.0546	34.57	21.26	163.96	0.001583				
5.8166	32.94	21.46	176.78					
7.1628	34.25	21.56	189.75					
7.6708	28.69	21.53	353.26	0.003411				
8.1788	29.07	21.50	332.33	0.003209				
8.9408	29.76	21.52	304.75	0.002943				
9.7028	30.27	21.54	289.75	0.002798				
10.4648	30.58	21.56	282.46	0.002727				
11.2268	30.89	21.59	275.26	0.002658				
11.9888	31.35	21.60	262.93	0.002539				
12.7508	31.50	21.60	260.21	0.002512				
13.5128	31.65	21.58	256.78	0.002479				
14.2748	31.90	21.59	251.23	0.002426				
15.0368	32.26	21.59	242.81	0.002344				
15.7988	32.31	21.58	242.62	0.002343				
16.5608	32.47	21.57	235.77	0.002276				

File:	p2v5q3l3	Ts,ex (K)	294.34	Tco (C)	42.56142			
Ptot (Pa)	98738	Re,ex	827087	VR	0.5			
Ttot (C)	25.49	q" (W/m2)	2586					
Ma,ex	0.2701	Tu,in	0.011					
Ma,in	0.0777	Lu,in (cm)	6.6					
Ps,ex(Pa)	93858	U0,in(m/s)	29.58					
Ps,in (Pa)	98321							
Surface	T surf	Taw	h	St	X/D	Taw,c(fc)	Naw	St/St0
(cm)	(C)	(C)	W/m2/C			(C)		
-11.7094	42.52	25.05	130.58	0.001259	68.33333	26.53	0.0842	1.5605
-10.9474	42.57	25.12	135.51	0.001307	62.45098	26.77	0.0945	1.5336
-10.1854	42.74	25.19	136.08	0.001312	56.56863	27.02	0.1054	1.5199
-9.4234	43.09	25.25	134.26	0.001295	50.68627	27.26	0.1161	1.5388
-8.6614	43.54	25.31	131.81	0.001271	44.80392	27.50	0.1272	1.5406
-7.8994	43.85	25.34	130.83	0.001262	38.92157	27.83	0.1442	1.5393
-7.1374	44.09	25.39	130.43	0.001258	33.03922	28.17	0.1621	1.5490
-6.3754	44.33	25.41	130.26	0.001256	27.15686	28.80	0.1978	1.5662
-5.6134	44.53	25.43	131.12	0.001264	21.27451	29.88	0.2601	1.5847
-4.8514	44.71	25.45	132.60	0.001279	15.39216	31.43	0.3496	1.5978
-4.0894	44.77	25.47	136.76	0.001319	9.509804	34.38	0.5213	1.6270
-3.3274	43.70	25.47	142.21	0.001371	3.627451	33.18	0.4512	1.6778
-2.921	42.25	25.47	142.63	0.001375	0.490196	29.22		1.6485
-1.7272	43.76	25.64	118.82	0.001146				
-1.0414	43.02	25.66	124.16	0.001197				
-0.508	39.66	25.67	166.75	0.001608				
0	38.00	25.69	190.95	0.001841				
0.508	37.40	25.64	202.44	0.001952				
1.016	38.38	25.60	183.17	0.001766				
1.524	38.64	25.52	175.27	0.00169				
2.032	38.11	25.40	185.12	0.001785				
2.7686	38.19	25.19	181.09	0.001746				
3.5306	37.46	24.81	186.84	0.001802				
4.2926	39.11	24.68	161.29	0.001555				
5.0546	44.87	24.65	103.87	0.001002				
5.8166	36.26	24.33	205.88					
7.1628	35.74	24.81	227.40					
7.6708	32.28	24.86	343.91	0.003316				
8.1788	32.77	24.89	323.35	0.003118				
8.9408	33.51	24.97	299.60	0.002889				
9.7028	34.15	25.02	281.43	0.002714				
10.4648	34.50	25.06	273.93	0.002641				
11.2268	34.93	25.12	264.42	0.00255				
11.9888	35.50	25.14	250.40	0.002414				
12.7508	35.66	25.15	248.23	0.002394				
13.5128	35.83	25.14	244.72	0.00236				
14.2748	36.12	25.15	238.90	0.002304				
15.0368	36.55	25.15	229.61	0.002214				
15.7988	36.64	25.15	229.47	0.002213				
16.5608	36.86	25.13	221.98	0.00214				

File:	p2v5q3h4	Ts,ex (K)	293.78	Tco (C)	39.97			
Ptot (Pa)	97164	Re,ex	814284	VR	0.5			
Ttot (C)	24.90	q" (W/m2)	2559					
Ma,ex	0.2695	Tu,in	0.12					
Ma,in	0.0789	Lu,in (cm)	3.36					
Ps,ex(Pa)	92382	U0,in(m/s)	29.49					
Ps,in (Pa)	96742							
Surface	T surf	Taw	h	St	X/D	Taw,c(fc)	Naw	St/St0
(cm)	(C)	(C)	W/m2/C			(C)		
-11.7094	39.90	24.51	148.03	0.001452	68.33333	25.12	0.0391	1.0475
-10.9474	40.15	24.57	150.37	0.001475	62.45098	25.28	0.0462	1.0382
-10.1854	40.29	24.63	150.85	0.00148	56.56863	25.47	0.0547	1.0436
-9.4234	40.58	24.69	149.34	0.001465	50.68627	25.71	0.0663	1.0526
-8.6614	40.95	24.75	146.89	0.001441	44.80392	25.95	0.0784	1.0550
-7.8994	41.11	24.79	146.96	0.001441	38.92157	26.23	0.0947	1.0645
-7.1374	41.23	24.85	147.45	0.001446	33.03922	26.54	0.1118	1.0820
-6.3754	41.27	24.88	148.70	0.001459	27.15686	26.99	0.1395	1.1093
-5.6134	41.14	24.92	152.44	0.001495	21.27451	27.69	0.1839	1.1505
-4.8514	40.87	24.98	158.22	0.001552	15.39216	28.62	0.2429	1.1993
-4.0894	40.28	25.04	172.60	0.001693	9.509804	30.90	0.3928	1.3049
-3.3274	39.80	25.12	178.95	0.001755	3.627451	31.48	0.4282	1.3505
-2.921	39.19	25.17	176.43	0.001731	0.490196	28.88		1.3195
-1.7272	38.52	25.19	167.36	0.001642				
-1.0414	38.25	25.17	170.38	0.001671				
-0.508	35.82	25.16	221.10	0.002169				
0	34.41	25.17	257.73	0.002528				
0.508	34.07	25.14	268.75	0.002636				
1.016	35.02	25.09	237.62	0.002331				
1.524	35.29	25.00	226.57	0.002222				
2.032	34.86	24.90	238.14	0.002336				
2.7686	35.09	24.67	227.89	0.002235				
3.5306	34.63	24.30	229.34	0.002249				
4.2926	36.26	24.13	191.13	0.001875				
5.0546	38.24	24.21	158.52	0.001555				
5.8166	35.71	24.36	188.79					
7.1628	36.31	24.54	208.65					
7.6708	32.21	24.50	326.07	0.003198				
8.1788	32.50	24.47	312.47	0.003065				
8.9408	33.06	24.49	292.38	0.002868				
9.7028	33.51	24.51	280.03	0.002747				
10.4648	33.76	24.53	274.76	0.002695				
11.2268	34.07	24.56	267.62	0.002625				
11.9888	34.50	24.58	256.51	0.002516				
12.7508	34.62	24.58	254.86	0.0025				
13.5128	34.74	24.56	252.24	0.002474				
14.2748	34.96	24.57	247.19	0.002425				
15.0368	35.30	24.56	239.28	0.002347				
15.7988	35.34	24.56	239.43	0.002348				
16.5608	35.50	24.55	232.71	0.002283				

File:	p2v1q3l3	Ts,ex (K)	294.12	Tco (C)	47.76778			
Ptot (Pa)	98738	Re,ex	827876	VR	1			
Ttot (C)	25.26	q" (W/m2)	2587					
Ma,ex	0.2701	Tu,in	0.011					
Ma,in	0.0777	Lu,in (cm)	6.6					
Ps,ex(Pa)	93858	U0,in(m/s)	29.58					
Ps,in (Pa)	98321							
Surface	T surf	Taw	h	St	X/D	Taw,c(fc)	Naw	St/St0
(cm)	(C)	(C)	W/m2/C			(C)		
-11.7094	41.83	24.75	134.63	0.001298	68.33333	28.68	0.1707	1.6083
-10.9474	41.90	24.82	139.11	0.001341	62.45098	28.97	0.1809	1.5738
-10.1854	41.99	24.88	140.20	0.001351	56.56863	29.35	0.1952	1.5654
-9.4234	42.31	24.92	138.30	0.001333	50.68627	29.69	0.2086	1.5845
-8.6614	42.73	24.97	135.63	0.001307	44.80392	29.97	0.2192	1.5847
-7.8994	43.03	25.01	134.24	0.001294	38.92157	30.30	0.2323	1.5789
-7.1374	43.26	25.05	133.27	0.001285	33.03922	30.60	0.2443	1.5822
-6.3754	43.45	25.06	132.36	0.001276	27.15686	31.15	0.2681	1.5907
-5.6134	43.40	25.07	133.43	0.001286	21.27451	31.92	0.3018	1.6120
-4.8514	42.90	25.09	137.68	0.001327	15.39216	32.66	0.3337	1.6584
-4.0894	41.09	25.09	155.63	0.0015	9.509804	33.50	0.3706	1.8508
-3.3274	38.72	25.11	182.09	0.001755	3.627451	30.36	0.2318	2.1476
-2.921	38.60	25.05	165.68	0.001597	0.490196	25.98		1.9142
-1.7272	42.49	25.30	119.41	0.001151				
-1.0414	41.99	25.35	123.64	0.001192				
-0.508	38.91	25.39	167.06	0.00161				
0	37.35	25.40	190.03	0.001832				
0.508	36.80	25.36	201.06	0.001938				
1.016	37.74	25.32	182.83	0.001762				
1.524	38.00	25.24	173.29	0.00167				
2.032	37.41	25.12	185.24	0.001785				
2.7686	37.52	24.93	180.83	0.001743				
3.5306	36.64	24.55	188.35	0.001815				
4.2926	38.20	24.44	162.33	0.001565				
5.0546	43.33	24.42	106.28	0.001024				
5.8166	36.30	24.15	184.00					
7.1628	35.04	24.55	230.26					
7.6708	31.81	24.60	348.94	0.003363				
8.1788	32.40	24.64	324.62	0.003129				
8.9408	33.14	24.72	300.96	0.002901				
9.7028	33.80	24.76	282.82	0.002726				
10.4648	34.18	24.81	275.06	0.002651				
11.2268	34.61	24.86	265.67	0.002561				
11.9888	35.18	24.89	251.46	0.002424				
12.7508	35.34	24.90	249.02	0.0024				
13.5128	35.51	24.89	245.53	0.002367				
14.2748	35.80	24.90	239.62	0.00231				
15.0368	36.22	24.90	230.55	0.002222				
15.7988	36.31	24.89	230.26	0.002219				
16.5608	36.53	24.89	222.73	0.002147				

File:	p2v1q3h3	Ts,ex (K)	293.86	Tco (C)	47.58			
Ptot (Pa)	97164	Re,ex	813994	VR	1			
Ttot (C)	24.98	q" (W/m2)	2561					
Ma,ex	0.2695	Tu,in	0.12					
Ma,in	0.0789	Lu,in (cm)	3.36					
Ps,ex(Pa)	92382	U0,in(m/s)	29.49					
Ps,in (Pa)	96742							
Surface	T surf	Taw	h	St	X/D	Taw,c(fc)	Naw	St/St0
(cm)	(C)	(C)	W/m2/C			(C)		
-11.7094	40.20	24.60	146.12	0.001433	68.33333	26.29	0.0736	1.0341
-10.9474	40.45	24.66	148.51	0.001457	62.45098	26.56	0.0830	1.0256
-10.1854	40.61	24.72	148.93	0.001461	56.56863	26.88	0.0945	1.0305
-9.4234	40.94	24.79	146.96	0.001442	50.68627	27.29	0.1100	1.0360
-8.6614	41.33	24.85	144.42	0.001417	44.80392	27.74	0.1274	1.0374
-7.8994	41.53	24.89	144.21	0.001415	38.92157	28.26	0.1486	1.0447
-7.1374	41.66	24.95	144.44	0.001417	33.03922	28.81	0.1706	1.0600
-6.3754	41.70	24.99	145.53	0.001428	27.15686	29.59	0.2037	1.0859
-5.6134	41.48	25.02	149.35	0.001465	21.27451	30.68	0.2508	1.1273
-4.8514	40.95	25.07	156.38	0.001534	15.39216	31.96	0.3059	1.1855
-4.0894	39.39	25.10	179.27	0.001759	9.509804	34.26	0.4075	1.3555
-3.3274	37.02	25.13	219.09	0.002149	3.627451	32.94	0.3481	1.6537
-2.921	36.13	25.15	217.78	0.002136	0.490196	28.03		1.6289
-1.7272	37.99	25.26	169.20	0.00166				
-1.0414	37.87	25.24	170.64	0.001674				
-0.508	35.60	25.24	222.03	0.002178				
0	34.24	25.25	258.52	0.002536				
0.508	33.93	25.22	268.87	0.002638				
1.016	34.87	25.17	238.04	0.002335				
1.524	35.11	25.09	226.39	0.002221				
2.032	34.65	24.98	239.83	0.002353				
2.7686	34.92	24.77	228.44	0.002241				
3.5306	34.33	24.42	233.07	0.002286				
4.2926	35.91	24.27	193.79	0.001901				
5.0546	37.65	24.35	162.84	0.001597				
5.8166	36.17	24.51	171.42					
7.1628	35.85	24.65	213.30					
7.6708	32.08	24.60	332.53	0.003262				
8.1788	32.48	24.58	314.86	0.003089				
8.9408	33.06	24.60	295.13	0.002895				
9.7028	33.53	24.62	282.69	0.002773				
10.4648	33.81	24.64	276.72	0.002715				
11.2268	34.13	24.67	269.64	0.002645				
11.9888	34.57	24.68	257.98	0.002531				
12.7508	34.68	24.68	256.29	0.002514				
13.5128	34.81	24.66	253.62	0.002488				
14.2748	35.04	24.66	248.33	0.002436				
15.0368	35.39	24.66	240.13	0.002356				
15.7988	35.43	24.65	240.19	0.002356				
16.5608	35.59	24.64	233.41	0.00229				

File:	p2v1q3k3	Ts,ex (K)	296.95	Tco (C)	45.24			
Ptot (Pa)	98755	Re,ex	533056	VR	1			
Ttot (C)	25.54	q" (W/m2)	1931					
Ma,ex	0.1707	Tu,in	0.009					
Ma,in	0.0503	Lu,in (cm)	19.1					
Ps,ex(Pa)	96766	U0,in(m/s)	19.37					
Ps,in (Pa)	98580							
Surface	T surf	Taw	h	St	X/D	Taw,c(fc)	Naw	St/St0
(cm)	(C)	(C)	W/m2/C			(C)		
-11.7094	41.18	25.33	109.25	0.001623	68.33333	28.35	0.1516	1.5791
-10.9474	41.24	25.37	112.93	0.001678	62.45098	28.41	0.1530	1.5412
-10.1854	41.36	25.39	113.10	0.001681	56.56863	28.65	0.1640	1.5243
-9.4234	41.62	25.41	111.62	0.001659	50.68627	28.85	0.1736	1.5430
-8.6614	41.99	25.44	109.19	0.001622	44.80392	28.98	0.1791	1.5389
-7.8994	42.27	25.44	107.79	0.001602	38.92157	29.23	0.1915	1.5302
-7.1374	42.49	25.47	106.99	0.00159	33.03922	29.52	0.2047	1.5349
-6.3754	42.65	25.47	106.47	0.001582	27.15686	30.10	0.2344	1.5472
-5.6134	42.55	25.47	108.10	0.001606	21.27451	31.01	0.2802	1.5807
-4.8514	41.98	25.48	112.92	0.001678	15.39216	31.87	0.3236	1.6463
-4.0894	40.20	25.48	130.56	0.00194	9.509804	32.80	0.3704	1.8775
-3.3274	38.41	25.50	145.01	0.002155	3.627451	29.57	0.2060	2.0754
-2.921	38.46	25.48	130.70	0.001942	0.490196	26.45		1.8362
-1.7272	41.43	25.66	97.65	0.001451				
-1.0414	41.05	25.67	100.12	0.001488				
-0.508	38.34	25.69	134.33	0.001996				
0	36.91	25.69	153.07	0.002274				
0.508	36.38	25.66	162.90	0.002421				
1.016	37.22	25.64	148.07	0.0022				
1.524	37.47	25.61	141.08	0.002096				
2.032	37.04	25.55	149.77	0.002226				
2.7686	37.16	25.48	147.34	0.002189				
3.5306	36.63	25.33	151.63	0.002253				
4.2926	38.08	25.28	131.41	0.001953				
5.0546	43.76	25.29	79.94	0.001188				
5.8166	42.83	25.18	80.51					
7.1628	35.81	25.29	173.66					
7.6708	33.16	25.32	238.40	0.003543				
8.1788	33.50	25.33	230.46	0.003424				
8.9408	34.23	25.38	213.31	0.00317				
9.7028	34.84	25.39	201.81	0.002999				
10.4648	35.24	25.41	195.69	0.002908				
11.2268	35.66	25.44	189.04	0.002809				
11.9888	36.20	25.46	179.76	0.002671				
12.7508	36.42	25.47	176.91	0.002629				
13.5128	36.60	25.45	174.31	0.00259				
14.2748	36.91	25.46	169.51	0.002519				
15.0368	37.27	25.45	164.19	0.00244				
15.7988	37.40	25.46	163.00	0.002422				
16.5608	37.61	25.45	156.71	0.002329				

File:	p2v1q3g4	Ts,ex (K)	296.45	Tco (C)	46.55			
Ptot (Pa)	98453	Re,ex	530991	VR	1			
Ttot (C)	25.02	q" (W/m2)	1933					
Ma,ex	0.1702	Tu,in	0.124					
Ma,in	0.0512	Lu,in (cm)	3.16					
Ps,ex(Pa)	96482	U0,in(m/s)	19.53					
Ps,in (Pa)	98272							
Surface	T surf	Taw	h	St	X/D	Taw,c(fc)	Naw	St/St0
(cm)	(C)	(C)	W/m2/C			(C)		
-11.7094	40.56	24.88	107.63	0.001608	68.33333	26.43	0.0715	1.0316
-10.9474	40.67	24.91	111.31	0.001663	62.45098	26.81	0.0878	1.0251
-10.1854	40.69	24.94	112.63	0.001682	56.56863	27.09	0.0993	1.0292
-9.4234	40.91	24.97	111.74	0.001669	50.68627	27.44	0.1146	1.0377
-8.6614	41.21	25.00	110.26	0.001647	44.80392	27.86	0.1324	1.0406
-7.8994	41.35	25.03	110.42	0.001649	38.92157	28.31	0.1526	1.0497
-7.1374	41.43	25.07	110.93	0.001657	33.03922	28.84	0.1755	1.0669
-6.3754	41.41	25.09	112.21	0.001676	27.15686	29.59	0.2097	1.0966
-5.6134	41.14	25.12	115.71	0.001728	21.27451	30.67	0.2591	1.1430
-4.8514	40.59	25.18	121.97	0.001822	15.39216	31.96	0.3174	1.2090
-4.0894	39.07	25.23	141.58	0.002115	9.509804	34.42	0.4310	1.3968
-3.3274	37.06	25.29	167.58	0.002503	3.627451	32.54	0.3410	1.6525
-2.921	36.33	25.33	164.85	0.002462	0.490196	27.97		1.6112
-1.7272	37.57	25.31	132.10	0.001973				
-1.0414	37.42	25.27	133.22	0.00199				
-0.508	35.29	25.24	173.41	0.00259				
0	34.01	25.24	201.17	0.003005				
0.508	33.69	25.21	209.99	0.003137				
1.016	34.49	25.18	188.20	0.002811				
1.524	34.71	25.15	180.25	0.002692				
2.032	34.37	25.10	190.12	0.00284				
2.7686	34.62	25.00	183.25	0.002737				
3.5306	34.33	24.89	185.07	0.002764				
4.2926	35.79	24.83	155.46	0.002322				
5.0546	37.83	24.89	124.77	0.001864				
5.8166	36.29	24.94	133.51					
7.1628	36.09	24.98	163.07					
7.6708	32.77	24.96	240.47	0.003592				
8.1788	33.02	24.93	232.59	0.003474				
8.9408	33.69	24.92	215.00	0.003211				
9.7028	34.18	24.93	205.82	0.003074				
10.4648	34.51	24.94	200.57	0.002996				
11.2268	34.85	24.97	195.47	0.00292				
11.9888	35.31	24.96	186.82	0.002791				
12.7508	35.49	24.96	184.53	0.002756				
13.5128	35.63	24.94	182.44	0.002725				
14.2748	35.91	24.94	177.91	0.002657				
15.0368	36.25	24.94	172.63	0.002578				
15.7988	36.35	24.93	171.97	0.002569				
16.5608	36.54	24.92	165.86	0.002477				

File:	p2v2q3l3	Ts,ex (K)	293.95	Tco (C)	44.66			
Ptot (Pa)	98738	Re,ex	828513	VR	1.5			
Ttot (C)	25.08	q" (W/m2)	2590					
Ma,ex	0.2701	Tu,in	0.011					
Ma,in	0.0777	Lu,in (cm)	6.6					
Ps,ex(Pa)	93858	U0,in(m/s)	29.58					
Ps,in (Pa)	98321							
Surface	T surf	Taw	h	St	X/D	Taw,c(fc)	Naw	St/St0
(cm)	(C)	(C)	W/m2/C			(C)		
-11.7094	42.48	24.49	125.90	0.001213	68.33333	30.22	0.2844	1.5035
-10.9474	42.53	24.53	130.33	0.001256	62.45098	30.66	0.3044	1.4740
-10.1854	42.49	24.59	132.67	0.001278	56.56863	31.08	0.3234	1.4809
-9.4234	42.69	24.63	131.95	0.001271	50.68627	31.49	0.3426	1.5113
-8.6614	42.88	24.67	131.35	0.001266	44.80392	31.86	0.3598	1.5342
-7.8994	42.84	24.70	132.73	0.001279	38.92157	32.17	0.3743	1.5607
-7.1374	42.66	24.73	135.09	0.001302	33.03922	32.43	0.3866	1.6034
-6.3754	42.26	24.74	138.96	0.001339	27.15686	32.81	0.4051	1.6696
-5.6134	41.40	24.74	147.28	0.001419	21.27451	33.23	0.4262	1.7788
-4.8514	40.09	24.75	160.80	0.001549	15.39216	33.59	0.4443	1.9363
-4.0894	37.50	24.74	197.79	0.001906	9.509804	34.17	0.4735	2.3515
-3.3274	35.12	24.75	242.82	0.00234	3.627451	30.63	0.2956	2.8629
-2.921	35.91	24.70	197.67	0.001905	0.490196	24.46		2.2831
-1.7272	41.58	25.02	120.28	0.001159				
-1.0414	41.21	25.09	123.59	0.001191				
-0.508	38.30	25.15	167.67	0.001616				
0	36.80	25.17	189.79	0.001829				
0.508	36.28	25.13	200.53	0.001932				
1.016	37.23	25.09	182.60	0.001759				
1.524	37.46	25.00	171.80	0.001655				
2.032	36.82	24.89	185.86	0.001791				
2.7686	37.00	24.71	180.40	0.001738				
3.5306	36.03	24.33	189.70	0.001828				
4.2926	37.56	24.22	163.33	0.001574				
5.0546	42.31	24.20	108.06	0.001041				
5.8166	37.26	23.95	150.42					
7.1628	34.52	24.31	231.88					
7.6708	31.44	24.38	352.91	0.003401				
8.1788	32.08	24.43	326.23	0.003144				
8.9408	32.85	24.54	302.42	0.002914				
9.7028	33.46	24.57	285.79	0.002754				
10.4648	33.87	24.62	277.25	0.002672				
11.2268	34.29	24.67	268.36	0.002586				
11.9888	34.89	24.69	253.84	0.002446				
12.7508	35.10	24.70	250.61	0.002415				
13.5128	35.29	24.70	247.22	0.002382				
14.2748	35.60	24.70	240.96	0.002322				
15.0368	36.08	24.69	230.95	0.002225				
15.7988	36.17	24.69	230.98	0.002226				
16.5608	36.42	24.68	223.05	0.002149				

File:	p2v2q3h3	Ts,ex (K)	292.27	Tco (C)	46.83			
Ptot (Pa)	97164	Re,ex	819647	VR	1.5			
Ttot (C)	23.37	q" (W/m2)	2561					
Ma,ex	0.2695	Tu,in	0.12					
Ma,in	0.0789	Lu,in (cm)	3.36					
Ps,ex(Pa)	92382	U0,in(m/s)	29.49					
Ps,in (Pa)	96742							
Surface	T surf	Taw	h	St	X/D	Taw,c(fc)	Naw	St/St0
(cm)	(C)	(C)	W/m2/C			(C)		
-11.7094	38.74	22.98	144.49	0.001414	68.33333	25.52	0.1066	1.0199
-10.9474	39.00	23.04	146.89	0.001437	62.45098	25.99	0.1239	1.0116
-10.1854	39.13	23.10	147.55	0.001443	56.56863	26.47	0.1421	1.0182
-9.4234	39.44	23.16	145.93	0.001428	50.68627	27.00	0.1622	1.0259
-8.6614	39.79	23.21	143.74	0.001406	44.80392	27.56	0.1842	1.0297
-7.8994	39.89	23.27	144.36	0.001412	38.92157	28.17	0.2081	1.0430
-7.1374	39.92	23.31	145.43	0.001423	33.03922	28.79	0.2326	1.0644
-6.3754	39.75	23.34	148.27	0.001451	27.15686	29.60	0.2664	1.1033
-5.6134	39.17	23.37	155.52	0.001521	21.27451	30.58	0.3073	1.1707
-4.8514	38.17	23.40	167.86	0.001642	15.39216	31.50	0.3457	1.2691
-4.0894	35.89	23.42	204.50	0.002001	9.509804	32.77	0.3992	1.5421
-3.3274	33.36	23.42	259.89	0.002543	3.627451	30.42	0.2988	1.9563
-2.921	33.02	23.42	241.53	0.002363	0.490196	24.38		1.8017
-1.7272	36.05	23.59	169.47	0.001658				
-1.0414	35.96	23.59	170.71	0.00167				
-0.508	33.77	23.59	222.78	0.002179				
0	32.43	23.61	258.75	0.002531				
0.508	32.17	23.59	267.66	0.002619				
1.016	33.09	23.54	237.80	0.002326				
1.524	33.32	23.45	225.14	0.002203				
2.032	32.82	23.35	240.62	0.002354				
2.7686	33.13	23.14	228.29	0.002233				
3.5306	32.47	22.81	234.56	0.002295				
4.2926	34.04	22.65	194.50	0.001903				
5.0546	35.56	22.73	166.14	0.001625				
5.8166	34.95	22.90	157.34					
7.1628	33.89	23.01	215.47					
7.6708	30.33	22.97	335.22	0.00328				
8.1788	30.76	22.94	315.84	0.00309				
8.9408	31.37	22.96	295.44	0.00289				
9.7028	31.83	22.98	283.72	0.002776				
10.4648	32.13	23.00	277.34	0.002713				
11.2268	32.44	23.03	270.72	0.002648				
11.9888	32.91	23.04	258.55	0.002529				
12.7508	33.02	23.04	256.87	0.002513				
13.5128	33.16	23.02	254.21	0.002487				
14.2748	33.40	23.03	248.70	0.002433				
15.0368	33.76	23.02	240.30	0.002351				
15.7988	33.80	23.02	240.55	0.002353				
16.5608	33.96	23.01	233.69	0.002286				

File:	shp5q3l3	Ts,ex (K)	294.51	Tco (C)	43.73			
Ptot (Pa)	99456	Re,ex	834248	PReqv	0.0175			
Ttot (C)	25.68	q" (W/m2)	2508					
Ma,ex	0.2707	Tu,in	0.011					
Ma,in	0.0775	Lu,in (cm)	6.6					
Ps,ex(Pa)	94518	U0,in(m/s)	29.58					
Ps,in (Pa)	99039							
Surface	T surf	Taw	h	St	X/D	Taw,c(fc)	Naw	St/St0
(cm)	(C)	(C)	W/m2/C			(C)		
-11.7094	44.51	25.15	105.86	0.001012	87.94118	26.18	0.0555	1.2536
-10.9474	44.84	25.23	108.25	0.001034	82.05882	26.10	0.0469	1.2140
-10.1854	45.21	25.29	107.53	0.001027	76.17647	26.31	0.0555	1.1902
-9.4234	45.68	25.35	105.65	0.00101	70.29412	26.44	0.0590	1.2000
-8.6614	46.10	25.40	104.22	0.000996	64.41176	26.59	0.0650	1.2072
-7.8994	46.45	25.44	103.33	0.000987	58.52941	26.78	0.0730	1.2049
-7.1374	46.64	25.48	103.31	0.000987	52.64706	26.94	0.0798	1.2159
-6.3754	46.88	25.51	102.69	0.000981	46.76471	27.13	0.0890	1.2235
-5.6134	46.92	25.52	102.97	0.000984	40.88235	27.36	0.1009	1.2332
-4.8514	46.86	25.55	103.37	0.000988	35	27.60	0.1127	1.2344
-4.0894	46.21	25.57	106.62	0.001019	29.11765	27.90	0.1282	1.2570
-3.3274	45.18	25.58	110.07	0.001052	23.23529	28.21	0.1450	1.2869
-2.921	43.45	25.59	120.48	0.001151	20.09804	27.30	0.0940	1.3799
-1.7272	40.30	25.76	146.97	0.001404	10.88235	27.87	0.1170	1.3685
-1.0414	39.03	25.79	164.00	0.001567	5.588235	28.90	0.1736	1.3063
-0.508	35.90	25.81	248.64					
0	40.33	25.84	148.22					
0.508	36.72	25.77	217.30					
1.016	33.15	25.70	379.88					
1.524	32.93	25.62	372.67					
2.032	32.57	25.50	382.47					
2.7686	33.88	25.30	280.08	0.002676	11.66667	32.16	0.3722	1.4967
3.5306	34.67	24.86	239.11	0.002285	17.54902	30.51	0.2993	1.2822
4.2926	35.33	24.66	225.40	0.002154	23.43137	31.12	0.3388	1.3330
5.0546	39.13	24.70	150.42	0.001437	29.31373	30.01	0.2790	1.2783
5.8166	36.58	24.48	183.77	0.001756	35.19608	29.90	0.2458	1.9348
7.1628	32.89	24.90	309.05	0.002953	45.59	28.90	0.2126	0.9826
7.6708	33.30	24.97	299.02	0.002857	49.51	28.76	0.2022	0.9571
8.1788	33.73	25.05	288.72	0.002759	53.43	28.38	0.1784	0.9251
8.9408	34.29	25.12	276.96	0.002646	59.31	28.28	0.1698	0.9150
9.7028	34.82	25.19	264.40	0.002526	65.20	28.10	0.1572	0.9378
10.4648	35.17	25.22	257.19	0.002458	71.08	27.98	0.1489	0.9332
11.2268	35.59	25.28	248.62	0.002376	76.96	27.93	0.1432	0.9350
11.9888	36.13	25.30	235.96	0.002255	82.84	27.76	0.1336	0.9488
12.7508	36.23	25.32	235.72	0.002252	88.73	27.69	0.1286	0.9479
13.5128	36.39	25.30	232.93	0.002226	94.61	27.59	0.1241	0.9462
14.2748	36.74	25.31	226.00	0.002159	100.49	27.51	0.1196	0.9463
15.0368	37.18	25.30	216.93	0.002073	106.37	27.38	0.1131	0.9600
15.7988	37.24	25.30	217.60	0.002079	112.25	27.42	0.1151	0.9467
16.5608	37.51	25.29	208.80	0.001995	118.14	27.18	0.1023	0.9314

File:	shp5q3h3	Ts,ex (K)	294.84	Tco (C)	44.36			
Ptot (Pa)	97693	Re,ex	815782	PReqv	0.0175			
Ttot (C)	25.98	q" (W/m2)	2510					
Ma,ex	0.2698	Tu,in	0.12					
Ma,in	0.0791	Lu,in (cm)	3.36					
Ps,ex(Pa)	92875	U0,in(m/s)	29.49					
Ps,in (Pa)	97266							
Surface	T surf	Taw	h	St	X/D	Taw,c(fc)	Naw	St/St0
(cm)	(C)	(C)	W/m2/C			(C)		
-11.7094	40.48	25.56	144.40	0.00141	87.94118	25.80	0.0127	1.0172
-10.9474	40.79	25.61	145.41	0.00142	82.05882	25.81	0.0111	0.9993
-10.1854	41.05	25.67	144.41	0.00141	76.17647	25.93	0.0137	0.9945
-9.4234	41.40	25.74	141.86	0.001385	70.29412	26.01	0.0146	0.9953
-8.6614	41.76	25.79	139.41	0.001361	64.41176	26.11	0.0173	0.9967
-7.8994	41.99	25.84	138.39	0.001351	58.52941	26.22	0.0202	0.9978
-7.1374	42.21	25.89	137.31	0.001341	52.64706	26.31	0.0231	1.0029
-6.3754	42.48	25.92	135.55	0.001323	46.76471	26.43	0.0279	1.0066
-5.6134	42.62	25.94	134.89	0.001317	40.88235	26.58	0.0347	1.0134
-4.8514	42.60	25.97	135.15	0.00132	35	26.75	0.0424	1.0198
-4.0894	42.26	25.99	137.94	0.001347	29.11765	26.98	0.0542	1.0380
-3.3274	41.48	26.00	143.99	0.001406	23.23529	27.29	0.0698	1.0817
-2.921	40.88	26.02	144.56	0.001411	20.09804	26.53	0.0279	1.0761
-1.7272	38.89	26.14	167.74	0.001638	10.88235	27.59	0.0797	1.0969
-1.0414	37.89	26.13	185.11	0.001807	5.588235	28.72	0.1422	1.0847
-0.508	34.69	26.12	299.16					
0	38.12	26.16	184.90					
0.508	35.77	26.06	251.65					
1.016	33.42	25.97	384.95					
1.524	33.53	25.98	359.33					
2.032	32.97	25.82	382.75					
2.7686	34.08	25.63	283.04	0.002763	11.66667	30.91	0.2818	1.2065
3.5306	34.46	25.26	256.19	0.002501	17.54902	29.18	0.2050	1.1242
4.2926	35.22	25.11	237.38	0.002318	23.43137	29.86	0.2468	1.1815
5.0546	37.87	25.17	173.68	0.001696	29.31373	28.41	0.1688	1.1356
5.8166	35.56	25.41	219.14	0.00214	35.19608	28.43	0.1455	1.0921
7.1628	32.97	25.48	324.18	0.003165	45.59	27.79	0.1221	1.0527
7.6708	33.24	25.50	314.74	0.003073	49.51	27.54	0.1085	1.0443
8.1788	33.58	25.51	303.36	0.002962	53.43	27.20	0.0899	1.0186
8.9408	33.97	25.53	292.01	0.002851	59.31	27.02	0.0789	1.0040
9.7028	34.38	25.56	280.24	0.002736	65.20	26.92	0.0722	1.0101
10.4648	34.66	25.57	272.64	0.002662	71.08	26.80	0.0656	1.0024
11.2268	34.95	25.59	265.32	0.00259	76.96	26.77	0.0624	1.0014
11.9888	35.34	25.61	254.40	0.002484	82.84	26.67	0.0568	0.9984
12.7508	35.41	25.61	253.51	0.002475	88.73	26.61	0.0533	0.9979
13.5128	35.52	25.60	250.88	0.002449	94.61	26.53	0.0495	0.9927
14.2748	35.78	25.60	244.58	0.002388	100.49	26.49	0.0474	0.9888
15.0368	36.07	25.60	237.44	0.002318	106.37	26.42	0.0436	0.9884
15.7988	36.09	25.59	237.83	0.002322	112.25	26.43	0.0447	0.9839
16.5608	36.27	25.59	229.94	0.002245	118.14	26.32	0.0390	0.9673

File:	shp2q3l3	Ts,ex (K)	294.41	Tco (C)	45.67			
Ptot (Pa)	99456	Re,ex	834637	PReqv	0.07			
Ttot (C)	25.57	q" (W/m2)	2506					
Ma,ex	0.2707	Tu,in	0.011					
Ma,in	0.0775	Lu,in (cm)	6.6					
Ps,ex(Pa)	94518	U0,in(m/s)	29.58					
Ps,in (Pa)	99039							
Surface	T surf	Taw	h	St	X/D	Taw,c(fc)	Naw	St/St0
(cm)	(C)	(C)	W/m2/C			(C)		
-11.7094	43.85	25.04	108.82	0.00104	87.94118	26.08	0.0505	1.2885
-10.9474	44.44	25.12	109.29	0.001044	82.05882	25.95	0.0402	1.2255
-10.1854	44.52	25.18	110.86	0.001059	76.17647	26.16	0.0478	1.2269
-9.4234	45.02	25.24	108.56	0.001037	70.29412	26.26	0.0499	1.2328
-8.6614	45.49	25.29	106.66	0.001019	64.41176	26.42	0.0553	1.2351
-7.8994	45.76	25.33	106.22	0.001015	58.52941	26.61	0.0628	1.2383
-7.1374	46.00	25.37	105.78	0.001011	52.64706	26.76	0.0685	1.2447
-6.3754	46.23	25.40	105.11	0.001004	46.76471	26.96	0.0769	1.2521
-5.6134	46.23	25.41	105.59	0.001009	40.88235	27.21	0.0885	1.2644
-4.8514	46.09	25.45	106.36	0.001016	35	27.48	0.1004	1.2698
-4.0894	45.43	25.46	109.40	0.001045	29.11765	27.81	0.1163	1.2895
-3.3274	44.11	25.47	114.70	0.001096	23.23529	28.26	0.1381	1.3408
-2.921	42.30	25.48	124.67	0.001191	20.09804	26.66	0.0584	1.4276
-1.7272	39.57	25.65	146.25	0.001397	10.88235	26.97	0.0658	1.3615
-1.0414	38.04	25.68	166.51	0.001591	5.588235	27.74	0.1029	1.3261
-0.508	34.09	25.70	289.74					
0	39.36	25.73	153.85					
0.508	35.84	25.66	223.74					
1.016	32.35	25.60	385.91					
1.524	31.82	25.51	415.16					
2.032	32.10	25.39	372.18					
2.7686	33.15	25.19	287.59	0.002748	11.66667	31.97	0.3313	1.5366
3.5306	33.92	24.75	249.25	0.002381	17.54902	30.94	0.2959	1.3363
4.2926	34.46	24.55	236.64	0.002261	23.43137	31.57	0.3325	1.3992
5.0546	38.06	24.60	157.36	0.001503	29.31373	30.37	0.2740	1.3371
5.8166	35.40	24.37	195.63	0.001869	35.19608	30.15	0.2487	2.0593
7.1628	32.51	24.79	312.00	0.002981	45.59	29.45	0.2233	0.9918
7.6708	32.94	24.86	303.33	0.002898	49.51	29.43	0.2195	0.9707
8.1788	33.44	24.94	291.22	0.002782	53.43	29.06	0.1990	0.9330
8.9408	33.97	25.02	280.80	0.002683	59.31	29.00	0.1930	0.9275
9.7028	34.51	25.08	268.28	0.002563	65.20	28.76	0.1788	0.9514
10.4648	34.87	25.11	260.85	0.002492	71.08	28.65	0.1719	0.9464
11.2268	35.25	25.17	253.19	0.002419	76.96	28.54	0.1644	0.9519
11.9888	35.76	25.19	240.67	0.002299	82.84	28.31	0.1522	0.9675
12.7508	35.81	25.21	241.52	0.002307	88.73	28.17	0.1449	0.9710
13.5128	35.95	25.19	238.90	0.002282	94.61	28.04	0.1391	0.9703
14.2748	36.27	25.20	232.27	0.002219	100.49	27.92	0.1329	0.9724
15.0368	36.72	25.19	222.69	0.002128	106.37	27.78	0.1264	0.9853
15.7988	36.69	25.19	225.44	0.002154	112.25	27.76	0.1255	0.9806
16.5608	36.96	25.18	216.16	0.002065	118.14	27.44	0.1103	0.9640

File:	shp2q3h3	Ts,ex (K)	294.63	Tco (C)	44.55			
Ptot (Pa)	97693	Re,ex	816499	PReqv	0.07			
Ttot (C)	25.77	q" (W/m2)	2511					
Ma,ex	0.2698	Tu,in	0.12					
Ma,in	0.0791	Lu,in (cm)	3.36					
Ps,ex(Pa)	92875	U0,in(m/s)	29.49					
Ps,in (Pa)	97266							
Surface	T surf	Taw	h	St	X/D	Taw,c(fc)	Naw	St/St0
(cm)	(C)	(C)	W/m2/C			(C)		
-11.7094	40.23	25.36	144.99	0.001415	87.94118	25.72	0.0188	1.0209
-10.9474	40.56	25.41	145.92	0.001424	82.05882	25.73	0.0170	1.0026
-10.1854	40.82	25.48	144.91	0.001414	76.17647	25.86	0.0203	0.9977
-9.4234	41.16	25.53	142.31	0.001389	70.29412	25.96	0.0227	0.9981
-8.6614	41.51	25.59	140.03	0.001367	64.41176	26.09	0.0259	1.0007
-7.8994	41.72	25.63	139.11	0.001358	58.52941	26.20	0.0300	1.0027
-7.1374	41.94	25.68	138.14	0.001348	52.64706	26.34	0.0352	1.0087
-6.3754	42.19	25.70	136.45	0.001332	46.76471	26.48	0.0411	1.0130
-5.6134	42.29	25.73	136.11	0.001328	40.88235	26.67	0.0499	1.0222
-4.8514	42.23	25.76	136.73	0.001334	35	26.86	0.0586	1.0313
-4.0894	41.78	25.78	140.42	0.001371	29.11765	27.15	0.0731	1.0563
-3.3274	40.84	25.79	147.97	0.001444	23.23529	27.48	0.0904	1.1112
-2.921	40.09	25.80	149.59	0.00146	20.09804	26.60	0.0424	1.1132
-1.7272	37.89	25.90	177.56	0.001733	10.88235	27.68	0.0954	1.1607
-1.0414	36.76	25.89	198.72	0.00194	5.588235	28.65	0.1480	1.1641
-0.508	33.35	25.84	346.39					
0	36.88	25.88	205.30					
0.508	34.77	25.77	272.15					
1.016	32.66	25.67	400.72					
1.524	32.69	25.68	389.02					
2.032	32.51	25.54	379.10					
2.7686	33.61	25.39	286.57	0.002797	11.66667	30.96	0.2909	1.2211
3.5306	33.97	25.02	260.77	0.002545	17.54902	29.43	0.2258	1.1439
4.2926	34.64	24.88	244.37	0.002385	23.43137	30.26	0.2738	1.2159
5.0546	37.20	24.94	178.29	0.00174	29.31373	28.67	0.1901	1.1653
5.8166	34.86	25.20	229.00	0.002235	35.19608	28.83	0.1661	1.1409
7.1628	32.59	25.25	329.31	0.003214	45.59	27.99	0.1421	1.0690
7.6708	32.90	25.27	319.31	0.003116	49.51	27.79	0.1305	1.0591
8.1788	33.27	25.28	306.06	0.002987	53.43	27.37	0.1085	1.0273
8.9408	33.70	25.31	294.06	0.00287	59.31	27.16	0.0966	1.0107
9.7028	34.12	25.33	281.83	0.002751	65.20	27.06	0.0903	1.0154
10.4648	34.42	25.35	273.82	0.002673	71.08	26.91	0.0814	1.0064
11.2268	34.71	25.37	266.56	0.002602	76.96	26.88	0.0790	1.0057
11.9888	35.10	25.39	255.50	0.002494	82.84	26.76	0.0717	1.0024
12.7508	35.17	25.39	254.70	0.002486	88.73	26.67	0.0671	1.0023
13.5128	35.28	25.38	252.04	0.00246	94.61	26.59	0.0632	0.9969
14.2748	35.54	25.38	245.51	0.002396	100.49	26.53	0.0600	0.9922
15.0368	35.83	25.39	238.40	0.002327	106.37	26.45	0.0558	0.9921
15.7988	35.86	25.38	238.72	0.00233	112.25	26.46	0.0567	0.9872
16.5608	36.04	25.39	230.73	0.002252	118.14	26.33	0.0493	0.9703

File:	shp2q3k3.	Ts,ex (K)	298.47	Tco (C)	44.85			
Ptot (Pa)	99670	Re,ex	531793	PReqv	0.07			
Ttot (C)	27.04	q" (W/m2)	1895					
Ma,ex	0.1698	Tu,in	0.009					
Ma,in	0.0499	Lu,in (cm)	19.1					
Ps,ex(Pa)	97683	U0,in(m/s)	19.37					
Ps,in (Pa)	99496							
Surface	T surf	Taw	h	St	X/D	Taw,c(fc)	Naw	St/St0
(cm)	(C)	(C)	W/m2/C			(C)		
-11.7094	44.72	26.76	85.61	0.00127	87.94	27.62	0.0474	1.2354
-10.9474	45.06	26.80	87.50	0.001298	82.06	27.57	0.0426	1.1923
-10.1854	45.20	26.83	88.00	0.001306	76.18	27.67	0.0469	1.1841
-9.4234	45.59	26.85	86.34	0.001281	70.29	27.72	0.0483	1.1918
-8.6614	45.96	26.86	84.93	0.00126	64.41	27.82	0.0535	1.1952
-7.8994	46.21	26.88	84.46	0.001253	58.53	27.98	0.0613	1.1971
-7.1374	46.37	26.89	84.30	0.001251	52.65	28.10	0.0675	1.2076
-6.3754	46.56	26.89	83.76	0.001243	46.76	28.27	0.0767	1.2154
-5.6134	46.57	26.89	84.11	0.001248	40.88	28.49	0.0890	1.2281
-4.8514	46.45	26.90	84.59	0.001255	35.00	28.74	0.1024	1.2314
-4.0894	45.86	26.91	87.05	0.001292	29.12	29.07	0.1205	1.2499
-3.3274	44.78	26.91	90.36	0.001341	23.24	29.49	0.1437	1.2913
-2.921	43.17	26.94	98.92	0.001468	20.10	28.26	0.0741	1.3876
-1.7272	40.48	27.08	116.69	0.001731	10.88	28.44	0.0766	1.3262
-1.0414	39.08	27.10	133.41	0.001979	5.59	29.38	0.1285	1.2877
-0.508	36.49	27.12	205.24					
0	40.29	27.14	123.41					
0.508	37.26	27.11	179.40					
1.016	34.26	27.07	307.09					
1.524	34.39	27.01	277.78					
2.032	34.09	26.98	293.61					
2.7686	35.06	26.90	223.73	0.003319	11.67	33.47	0.3661	1.4439
3.5306	35.92	26.72	194.85	0.002891	17.55	32.44	0.3159	1.2557
4.2926	36.67	26.64	183.17	0.002718	23.43	32.88	0.3426	1.3100
5.0546	40.12	26.62	121.16	0.001798	29.31	32.00	0.2949	1.2999
5.8166	38.98	26.44	130.92	0.001942	35.20	31.31	0.2635	2.0297
7.1628	34.76	26.59	232.03	0.003443	45.59	30.83	0.2322	0.9445
7.6708	35.18	26.66	223.36	0.003314	49.51	30.68	0.2212	0.9240
8.1788	35.66	26.71	214.39	0.003181	53.43	30.33	0.1995	0.8960
8.9408	36.26	26.77	204.29	0.003031	59.31	30.18	0.1887	0.8957
9.7028	36.80	26.79	194.35	0.002884	65.20	29.93	0.1742	0.9197
10.4648	37.19	26.82	188.12	0.002791	71.08	29.78	0.1644	0.9170
11.2268	37.59	26.87	182.34	0.002705	76.96	29.72	0.1588	0.9237
11.9888	38.11	26.88	173.36	0.002572	82.84	29.51	0.1464	0.9338
12.7508	38.25	26.89	172.19	0.002555	88.73	29.42	0.1410	0.9363
13.5128	38.43	26.87	169.86	0.00252	94.61	29.30	0.1352	0.9337
14.2748	38.80	26.88	164.25	0.002437	100.49	29.21	0.1296	0.9369
15.0368	39.19	26.87	158.69	0.002354	106.37	29.08	0.1228	0.9485
15.7988	39.27	26.87	158.56	0.002353	112.25	29.00	0.1184	0.9392
16.5608	39.55	26.86	151.14	0.002242	118.14	28.91	0.1139	0.9239

File:	shp2q3g3	Ts,ex (K)	297.24	Tco (C)	42.77			
Ptot (Pa)	99082	Re,ex	531439	PReqv	0.07			
Ttot (C)	25.80	q" (W/m2)	1926					
Ma,ex	0.1698	Tu,in	0.124					
Ma,in	0.0514	Lu,in (cm)	3.16					
Ps,ex(Pa)	97107	U0,in(m/s)	19.53					
Ps,in (Pa)	98899							
Surface	T surf	Taw	h	St	X/D	Taw,c(fc)	Naw	St/St0
(cm)	(C)	(C)	W/m2/C			(C)		
-11.7094	40.88	25.60	106.30	0.001583	87.94118	25.94	0.0193	1.0160
-10.9474	41.04	25.63	108.92	0.001622	82.05882	25.92	0.0173	1.0002
-10.1854	41.17	25.65	108.98	0.001623	76.17647	26.01	0.0210	0.9930
-9.4234	41.42	25.68	107.53	0.001601	70.29412	26.07	0.0229	0.9957
-8.6614	41.71	25.71	105.95	0.001578	64.41176	26.15	0.0262	0.9970
-7.8994	41.88	25.72	105.43	0.00157	58.52941	26.24	0.0306	0.9994
-7.1374	42.06	25.74	104.75	0.00156	52.64706	26.35	0.0357	1.0046
-6.3754	42.26	25.75	103.74	0.001545	46.76471	26.48	0.0430	1.0110
-5.6134	42.32	25.76	103.68	0.001544	40.88235	26.66	0.0529	1.0212
-4.8514	42.21	25.77	104.45	0.001556	35	26.84	0.0630	1.0324
-4.0894	41.75	25.78	107.54	0.001602	29.11765	27.15	0.0806	1.0579
-3.3274	40.85	25.79	113.11	0.001685	23.23529	27.46	0.0984	1.1122
-2.921	40.17	25.79	114.08	0.001699	20.09804	26.85	0.0626	1.1118
-1.7272	37.87	25.91	136.98	0.00204	10.88235	27.66	0.1036	1.1636
-1.0414	36.74	25.91	154.86	0.002307	5.588235	28.67	0.1639	1.1623
-0.508	34.01	25.90	258.66					
0	36.85	25.91	162.07					
0.508	34.91	25.88	221.21					
1.016	32.97	25.85	344.04					
1.524	33.33	25.84	294.00					
2.032	32.82	25.79	320.14					
2.7686	33.87	25.70	229.66	0.003421	11.66667	30.88	0.3032	1.2191
3.5306	34.31	25.55	209.76	0.003124	17.54902	29.49	0.2284	1.1397
4.2926	35.14	25.50	194.45	0.002896	23.43137	30.14	0.2688	1.1969
5.0546	37.76	25.51	137.69	0.002051	29.31373	28.96	0.1994	1.1398
5.8166	36.15	25.62	160.31	0.002388	35.19608	28.59	0.1716	1.1809
7.1628	33.36	25.64	245.44	0.003656	45.59	28.10	0.1439	1.0837
7.6708	33.64	25.65	237.16	0.003532	49.51	27.82	0.1271	1.0595
8.1788	34.01	25.64	227.27	0.003385	53.43	27.47	0.1063	1.0282
8.9408	34.50	25.66	216.56	0.003225	59.31	27.25	0.0930	1.0123
9.7028	34.95	25.67	206.84	0.003081	65.20	27.13	0.0854	1.0152
10.4648	35.28	25.68	200.57	0.002987	71.08	27.00	0.0769	1.0100
11.2268	35.61	25.69	194.34	0.002895	76.96	26.95	0.0739	1.0078
11.9888	36.01	25.70	186.14	0.002772	82.84	26.85	0.0672	1.0031
12.7508	36.14	25.70	184.44	0.002747	88.73	26.76	0.0620	1.0022
13.5128	36.28	25.69	182.23	0.002714	94.61	26.68	0.0578	0.9957
14.2748	36.58	25.70	176.79	0.002633	100.49	26.62	0.0536	0.9929
15.0368	36.87	25.69	171.96	0.002561	106.37	26.55	0.0503	0.9899
15.7988	36.95	25.69	171.61	0.002556	112.25	26.56	0.0508	0.9855
16.5608	37.16	25.69	164.35	0.002448	118.14	26.43	0.0435	0.9672

File:	shp1q3l3	Ts,ex (K)	294.27	Tco (C)	41.06			
Ptot (Pa)	99916	Re,ex	838895	PReqv	0.35			
Ttot (C)	25.43	q" (W/m2)	2509					
Ma,ex	0.2707	Tu,in	0.011					
Ma,in	0.0775	Lu,in (cm)	6.6					
Ps,ex(Pa)	94956	U0,in(m/s)	29.58					
Ps,in (Pa)	99497							
Surface	T surf	Taw	h	St	X/D	Taw,c(fc)	Naw	St/St0
(cm)	(C)	(C)	W/m2/C			(C)		
-11.7094	42.22	24.90	120.15	0.001142	87.94118	25.65	0.0460	1.4159
-10.9474	41.92	24.98	127.72	0.001214	82.05882	25.61	0.0391	1.4254
-10.1854	42.13	25.04	127.37	0.001211	76.17647	25.73	0.0429	1.4029
-9.4234	42.36	25.10	126.47	0.001202	70.29412	25.80	0.0434	1.4293
-8.6614	42.49	25.16	126.46	0.001202	64.41176	25.93	0.0484	1.4575
-7.8994	42.59	25.20	126.74	0.001205	58.52941	26.01	0.0514	1.4705
-7.1374	42.52	25.23	128.29	0.00122	52.64706	26.14	0.0571	1.5025
-6.3754	42.53	25.26	128.64	0.001223	46.76471	26.24	0.0619	1.5252
-5.6134	42.36	25.27	130.33	0.001239	40.88235	26.37	0.0695	1.5532
-4.8514	42.06	25.31	132.41	0.001259	35	26.47	0.0736	1.5733
-4.0894	41.16	25.33	139.40	0.001325	29.11765	26.62	0.0823	1.6354
-3.3274	39.79	25.33	150.36	0.00143	23.23529	26.82	0.0945	1.7493
-2.921	39.06	25.35	152.68	0.001452	20.09804	26.14	0.0502	1.7401
-1.7272	37.15	25.52	169.43	0.001611	10.88235	26.78	0.0810	1.5699
-1.0414	35.82	25.54	192.48	0.00183	5.588235	27.32	0.1144	1.5256
-0.508	31.59	25.56	357.08					
0	34.47	25.59	229.39					
0.508	32.61	25.52	293.09					
1.016	30.69	25.46	410.86					
1.524	29.83	25.37	486.00					
2.032	31.06	25.26	363.07					
2.7686	32.23	25.05	290.61	0.002763	11.66667	29.18	0.2581	1.5453
3.5306	32.10	24.61	287.55	0.002734	17.54902	28.79	0.2537	1.5343
4.2926	32.58	24.41	267.46	0.002543	23.43137	29.57	0.3101	1.5740
5.0546	34.89	24.46	197.21	0.001875	29.31373	28.38	0.2364	1.6678
5.8166	32.81	24.23	237.80	0.002261	35.19608	28.65	0.2247	2.4913
7.1628	31.53	24.65	326.95	0.003109	45.59	28.15	0.2129	1.0344
7.6708	31.95	24.72	319.91	0.003042	49.51	28.17	0.2112	1.0190
8.1788	32.50	24.80	305.17	0.002902	53.43	27.82	0.1854	0.9731
8.9408	33.02	24.88	294.30	0.002798	59.31	27.60	0.1685	0.9675
9.7028	33.53	24.94	281.85	0.00268	65.20	27.53	0.1603	0.9948
10.4648	33.87	24.98	274.41	0.002609	71.08	27.39	0.1502	0.9908
11.2268	34.22	25.04	267.04	0.002539	76.96	27.32	0.1423	0.9993
11.9888	34.72	25.05	254.01	0.002415	82.84	27.23	0.1361	1.0164
12.7508	34.79	25.07	254.40	0.002419	88.73	27.15	0.1296	1.0180
13.5128	34.93	25.06	251.76	0.002394	94.61	27.08	0.1264	1.0177
14.2748	35.23	25.06	244.96	0.002329	100.49	27.02	0.1224	1.0207
15.0368	35.66	25.05	235.14	0.002236	106.37	26.97	0.1197	1.0354
15.7988	35.76	25.05	234.51	0.00223	112.25	26.99	0.1212	1.0152
16.5608	36.08	25.05	225.17	0.002141	118.14	26.79	0.1088	0.9995

File:	shp1q3h3	Ts,ex (K)	294.59	Tco (C)	43.24			
Ptot (Pa)	97693	Re,ex	816662	PReqv	0.35			
Ttot (C)	25.72	q" (W/m2)	2512					
Ma,ex	0.2698	Tu,in	0.12					
Ma,in	0.0791	Lu,in (cm)	3.36					
Ps,ex(Pa)	92875	U0,in(m/s)	29.49					
Ps,in (Pa)	97266							
Surface	T surf	Taw	h	St	X/D	Taw,c(fc)	Naw	St/St0
(cm)	(C)	(C)	W/m2/C			(C)		
-11.7094	39.85	25.29	148.44	0.001449	87.94118	25.90	0.0340	1.0451
-10.9474	40.16	25.34	149.53	0.001459	82.05882	25.90	0.0312	1.0272
-10.1854	40.39	25.41	148.61	0.00145	76.17647	26.03	0.0352	1.0230
-9.4234	40.68	25.46	146.39	0.001429	70.29412	26.14	0.0385	1.0266
-8.6614	40.96	25.53	144.63	0.001411	64.41176	26.27	0.0419	1.0335
-7.8994	41.11	25.57	144.19	0.001407	58.52941	26.41	0.0475	1.0392
-7.1374	41.24	25.62	143.94	0.001405	52.64706	26.55	0.0529	1.0509
-6.3754	41.36	25.65	143.19	0.001397	46.76471	26.70	0.0599	1.0629
-5.6134	41.31	25.68	144.08	0.001406	40.88235	26.89	0.0692	1.0819
-4.8514	41.08	25.70	146.05	0.001425	35	27.06	0.0775	1.1015
-4.0894	40.37	25.71	152.42	0.001488	29.11765	27.30	0.0905	1.1466
-3.3274	39.11	25.72	164.04	0.001601	23.23529	27.63	0.1090	1.2318
-2.921	38.08	25.71	170.45	0.001663	20.09804	26.61	0.0510	1.2683
-1.7272	35.72	25.79	208.72	0.002037	10.88235	27.57	0.1020	1.3644
-1.0414	34.67	25.77	234.31	0.002287	5.588235	28.30	0.1447	1.3724
-0.508	31.30	25.66	409.32					
0	33.87	25.70	264.59					
0.508	32.58	25.58	316.69					
1.016	31.23	25.47	402.45					
1.524	30.68	25.47	450.91					
2.032	31.37	25.37	376.38					
2.7686	32.66	25.25	293.22	0.002862	11.66667	29.76	0.2507	1.2493
3.5306	32.73	24.88	280.97	0.002742	17.54902	29.21	0.2359	1.2324
4.2926	33.27	24.76	263.45	0.002571	23.43137	30.08	0.2879	1.3107
5.0546	35.17	24.82	204.01	0.001991	29.31373	28.47	0.1985	1.3334
5.8166	33.18	25.09	261.74	0.002554	35.19608	28.84	0.1773	1.3039
7.1628	31.98	25.13	335.01	0.003269	45.59	27.96	0.1560	1.0874
7.6708	32.35	25.14	325.38	0.003175	49.51	27.95	0.1554	1.0791
8.1788	32.83	25.15	308.94	0.003015	53.43	27.48	0.1291	1.0369
8.9408	33.33	25.17	295.77	0.002886	59.31	27.31	0.1184	1.0165
9.7028	33.77	25.21	284.34	0.002775	65.20	27.23	0.1121	1.0244
10.4648	34.11	25.22	275.12	0.002685	71.08	27.11	0.1045	1.0111
11.2268	34.42	25.25	267.61	0.002612	76.96	27.07	0.1007	1.0096
11.9888	34.82	25.27	256.79	0.002506	82.84	26.96	0.0937	1.0074
12.7508	34.91	25.28	255.51	0.002494	88.73	26.88	0.0892	1.0054
13.5128	35.05	25.27	252.45	0.002464	94.61	26.80	0.0850	0.9985
14.2748	35.32	25.27	245.73	0.002398	100.49	26.74	0.0815	0.9930
15.0368	35.61	25.27	238.91	0.002332	106.37	26.66	0.0773	0.9941
15.7988	35.65	25.28	239.05	0.002333	112.25	26.67	0.0775	0.9885
16.5608	35.84	25.27	230.93	0.002254	118.14	26.51	0.0689	0.9710

Appendix A.4 Vane Velocity Profiles

This appendix contains 65 velocity and turbulence profiles taken for the various vane, film cooling, and turbulence conditions investigated in this study. The profiles were taken in a two step process. First, the probe was set very close to the surface and traversed outward. Next the probe was set about 0.1 cm off the surface and stepped in small increments until the probe rested on the surface. This two step process was developed due to backlash found in the traversing mechanism off the surface which caused too large an uncertainty in the position of the first several Y increments. The process of stepping into the surface eliminated the backlash problem. These data sets were taken back to back and the relative position of the outward profile was determined by fitting the velocity and turbulence data to the inward profile. The absolute position of the profile was set differently on the suction and pressure surfaces. On the suction surface, the profile was integrated to determine the displacement and momentum thicknesses and the skin friction was estimated using the Ludwieg-Tillman correlation. Next, the absolute position of the data was determined by fitting to the inner region profile of a canonical boundary layer. The methodology used on the suction surface is believed to provide a reasonably good estimate of the absolute Y position of first two data points. On the pressure surface due to the high acceleration, the turbulence, and the film cooling jet interaction, the data could not be estimated with a Blasius profile. The position of the first unrestrained point off the surface was typically set by extrapolating the first unrestrained velocity gradient near the surface. Based on boundary layer calculations, this method typically overestimated the relative position of the profile by between 0.0025 cm and 0.004 cm but was found to be adequate for comparison purposes in chapter 6. For this reason, a certain amount of judgment will be needed for using these pressure surface data for comparison purposes.

Basically, the pressure surface velocity profiles were taken at a location equivalent to 9 diameters or 1.14 cm downstream from the trailing edge of the last row of film cooling holes. On the suction surface the profiles were taken at a location equivalent to 12 diameters or 1.90 cm downstream from the trailing edge of the last row of film cooling holes. More specific information on the vane and film cooling geometries is given in chapters 2 and 6.

Geom:	base vane			Geom:	base vane	
VR	N/A	Low		VR	N/A	Comb(1)
Red2	1334.869	Tu=.011		Red2	1256.234	Tu=.12
Uinf	96.683	Lu=6.6		Uinf	96.53	Lu=3.36
Cf/2	0.001542			Cf/2	0.001777	
filename	shcls0m1			filename	shcbs0m1	
Y(cm)	U(y)(m/s)	u' (m/s)		Y(cm)	U(y)(m/s)	u' (m/s)
0.011176	51.78599	6.712914		0.0012	27.46052	7.923022
0.011557	52.30751	6.704149		0.00185	36.3876	9.911083
0.013335	54.58946	6.665853		0.002862	45.53821	9.395157
0.015906	57.82011	6.682675		0.003874	51.75736	8.445668
0.018477	60.29589	6.52776		0.004887	55.72598	8.217164
0.021048	62.2977	6.382293		0.005899	58.61858	8.059175
0.023619	64.20162	6.413258		0.006911	60.96312	8.034049
0.02619	65.51977	6.31648		0.007923	62.8185	8.120158
0.028761	66.96658	6.223212		0.008935	64.64575	8.074261
0.031332	68.15625	6.168334		0.009948	65.90699	8.133054
0.033903	69.22547	6.115618		0.01096	67.22305	8.256624
0.036474	70.49108	6.073151		0.011972	68.34888	8.33665
0.039045	71.45778	6.025453		0.012984	69.56253	8.344554
0.041616	72.50191	6.072326		0.013996	70.60743	8.287964
0.044186	73.21836	5.996885		0.015008	71.68536	8.506665
0.046757	74.19838	5.968957		0.016021	72.64709	8.533963
0.049328	74.95803	6.006849		0.017033	73.60699	8.573911
0.051899	75.60715	5.98626		0.018045	74.45324	8.615059
0.05447	76.47464	5.968521		0.019057	75.2586	8.695732
0.057041	77.13533	5.878699		0.020069	76.11785	8.806683
0.059612	77.84725	5.854969		0.021082	76.8932	8.701381
0.062183	78.53133	5.846104		0.022094	77.71781	8.75352
0.064754	79.06874	5.7492		0.023106	78.48262	8.760991
0.067325	79.66207	5.727383		0.024118	79.24067	8.811396
0.069896	80.15038	5.704588		0.02513	80.07419	8.775507
0.072467	80.78219	5.690143		0.026143	80.75141	8.734662
0.075038	81.30275	5.672038		0.027155	81.49451	8.767799
0.077609	81.90477	5.609586		0.028167	81.96947	8.662968
0.08018	82.27593	5.590412		0.029179	82.58056	8.693635
0.082751	82.91645	5.553727		0.030191	83.24139	8.633148
0.085322	83.20596	5.547004		0.031203	83.9015	8.591446
0.087893	83.84846	5.433208		0.032216	84.44837	8.409224
0.090464	84.19056	5.492581		0.033228	84.72808	8.494549
0.093035	84.84999	5.363058		0.03424	85.27872	8.429332
0.095606	85.18237	5.331174		0.035252	85.73338	8.284986
0.098177	85.54597	5.317515		0.036264	86.2078	8.287504
0.100748	85.95319	5.241401		0.037277	86.62819	8.099054
0.103318	86.60058	5.160257		0.038289	87.04822	8.054264
0.105889	86.88213	5.188686				
0.10846	87.29991	5.114539		0.0344	85.29004	8.385085
0.111031	87.53853	5.122197		0.0394	87.57542	7.916979
0.113602	87.88754	5.101202		0.0454	89.7261	7.360009
0.116173	88.28162	4.995927		0.0524	91.7296	6.634806
0.118744	88.63668	4.956635		0.0614	93.56276	5.640775
0.121315	88.89008	4.908844		0.0724	94.97914	4.52504
0.123886	89.18269	4.918952		0.0854	95.8634	3.746595
				0.0984	96.19091	3.336327
0.11684	88.28558	5.017423		0.1134	96.4094	3.011626
0.13208	90.19621	4.693402		0.1294	96.41975	2.855067
0.14986	92.24601	4.202666		0.1594	96.52836	2.713092

Geom:	base vane			Geom:	base vane	
VR	N/A	Low		VR	N/A	Comb(1)
Red2	1334.869	Tu=.011		Red2	1334.869	Tu=.12
Uinf	96.683	Lu=6.6		Uinf	96.683	Lu=3.36
Cf/2	0.001542			Cf/2	0.001542	
filename	shcls0m1			filename	shcls0m1	
Y(cm)	U(y)(m/s)	u' (m/s)		Y(cm)	U(y)(m/s)	u' (m/s)
0.17272	94.20459	3.390915		0.519176	96.2682	2.559402
0.20066	95.86593	2.085635		0.646176	96.09127	2.448097
0.23368	96.49223	1.156826		0.773176	95.72332	2.386625
0.2667	96.59792	0.783927		0.900176	95.47133	2.30397
0.3048	96.68327	0.626365		1.027176	95.17091	2.264051
0.34544	96.59449	0.593287		1.154176	94.90389	2.2618
0.42164	96.51868	0.574532		1.281176	94.56467	2.229805
0.53594	96.36883	0.57436		1.408176	94.2261	2.272136
0.66294	96.15106	0.554676		1.535176	93.88136	2.241632
0.78994	95.93546	0.572747		1.662176	93.71208	2.228511
0.91694	95.69402	0.567925		1.789176	93.34748	2.236999
1.04394	95.48313	0.581613		1.916176	93.06066	2.238082
1.17094	95.23858	0.557198		2.043176	92.75008	2.230065
1.29794	94.91699	0.611397		2.170176	92.35567	2.269716
1.42494	94.78516	0.549943		2.297176	92.03795	2.255777
1.55194	94.5509	0.54636		2.424176	91.6538	2.3011
1.67894	94.24196	0.574527		2.551176	91.32895	2.331919
1.80594	94.03622	0.523301		2.678176	91.02336	2.33831
1.93294	93.63248	0.598944		2.805176	90.62595	2.38895
2.05994	93.44544	0.555983		2.932176	90.32618	2.499248
2.18694	93.11662	0.53087		3.059176	89.91846	2.99508
2.31394	92.77682	0.551336		3.186176	88.46511	5.062054
2.44094	92.60863	0.531714		3.313176	81.95772	8.811504
2.56794	92.27171	0.532253		3.440176	70.08456	9.769164
2.69494	91.81929	0.585768		3.567176	67.85828	10.67316
2.82194	91.52457	0.55267		3.694176	77.08378	10.09856
2.94894	91.12787	0.62724		3.821176	84.39468	6.721316
3.07594	90.80441	1.00558		3.948176	87.10302	4.705296
3.20294	90.36657	2.622535				
3.32994	84.49741	7.480835				
3.45694	65.9567	9.331752				
3.58394	62.13349	7.916819				
3.71094	76.5213	5.984825				
3.83794	87.24913	2.804719				
3.96494	90.39857	0.835239				

Geom:	1 row SS	Low		Geom:	1 row SS	Low		Geom:	1 row SS	Low
VR	0.5	Tu=.011		VR	0.5	Tu=.011		VR	0.5	Tu=.011
Red2	2424.642	Lu=6.6		Red2	1800.217	Lu=6.6		Red2	1497.256	Lu=6.6
Uinf	95.69			Uinf	95.69			Uinf	95.69	
Cf/2	0.001268			Cf/2	0.001717			Cf/2	0.001713	
Z/D =	0			Z/D =	0.75			Z/D =	1.5	
filename	s1clv5a1			filename	s1clv5q1			filename	s1clv5m1	
Y(cm)	U(y)(m/s)	u' (m/s)		Y(cm)	U(y)(m/s)	u' (m/s)		Y(cm)	U(y)(m/s)	u' (m/s)
0.004064	24.70879	4.742		0.004064	32.17451	5.949411		0.003556	28.52399	5.229768
0.006635	33.018	5.906313		0.006635	42.82211	6.900479		0.005842	39.03747	6.461369
0.009206	40.17305	6.373932		0.009206	50.65892	7.181069		0.008413	47.31764	6.787768
0.011777	45.07832	6.39326		0.011777	55.64914	7.009827		0.010984	53.04938	6.816294
0.014348	48.46721	6.315626		0.014348	58.73386	6.969002		0.013555	56.01263	6.882171
0.016919	51.00249	6.22616		0.016919	61.14346	6.76981		0.016126	58.57618	6.675289
0.01949	52.91348	6.149938		0.01949	63.13474	6.662609		0.018697	60.39928	6.550894
0.022061	54.61724	6.10931		0.022061	64.77432	6.684723		0.021268	62.02112	6.545684
0.024632	55.77361	6.078269		0.024632	66.07749	6.61065		0.023839	63.383	6.503197
0.027203	57.07489	6.104023		0.027203	67.34307	6.519613		0.02641	64.50124	6.543864
0.029774	58.13961	6.14474		0.029774	68.45488	6.438701		0.028981	65.63918	6.403428
0.032345	58.87014	6.028709		0.032345	69.63493	6.455434		0.031552	66.79053	6.394563
0.034915	59.76683	6.038458		0.034915	70.55554	6.399248		0.034123	67.72343	6.402059
0.037486	60.39156	6.021741		0.037486	71.2307	6.391362		0.036693	68.7523	6.341308
0.040057	61.12303	6.070889		0.040057	72.04127	6.359982		0.039264	69.68845	6.266912
0.042628	61.75346	5.977935		0.042628	72.82635	6.363901		0.041835	70.56525	6.261746
0.045199	62.1908	5.978441		0.045199	73.48498	6.272929		0.044406	71.40604	6.221674
0.04777	62.7107	6.025036		0.04777	74.32034	6.303397		0.046977	72.11434	6.134275
0.050341	63.17381	6.080889		0.050341	74.71452	6.228966		0.049548	72.83176	6.045193
0.052912	63.5192	5.998424		0.052912	75.21864	6.235315		0.052119	73.55128	5.9865
0.055483	63.68529	5.989179		0.055483	75.8988	6.226083		0.05469	74.245	6.001309
0.058054	64.3245	5.9675		0.058054	76.35033	6.276719		0.057261	74.85059	5.914564
0.060625	64.65649	5.937807		0.060625	76.75417	6.162801		0.059832	75.33501	5.853343
0.063196	65.41309	6.038406		0.063196	77.23723	6.20838		0.062403	76.14316	5.817059
0.065767	65.55733	5.97107		0.065767	77.72148	6.178398		0.064974	76.54132	5.746779
0.068338	65.81841	6.045135		0.068338	78.06946	6.199114		0.067545	77.10155	5.707704
0.070909	66.52251	6.0246		0.070909	78.60271	6.207589		0.070116	77.70553	5.638114
0.07348	66.80397	6.088687		0.07348	79.00798	6.2703		0.072687	78.26559	5.598442
0.076051	67.16483	6.048393		0.076051	79.50989	6.247762		0.075258	78.72845	5.585213
0.078622	67.20252	6.077305		0.078622	79.84075	6.289683		0.077829	79.21873	5.529414
0.081193	67.55854	6.092597		0.081193	80.2608	6.304338		0.0804	79.57153	5.484524
0.083764	67.69935	6.040444		0.083764	80.50275	6.259682		0.082971	80.20599	5.408307
0.086335	68.44297	6.115785		0.086335	80.66604	6.369645		0.085542	80.66525	5.326351
0.088906	68.65929	6.061916		0.088906	80.92316	6.42412		0.088113	81.22234	5.323441
				0.091477	81.33138	6.337871				
0.08509	68.22388	6.400661		0.094047	81.80753	6.417525		0.080772	79.39007	5.401938
0.09779	69.7366	6.359175		0.096618	81.99022	6.418975		0.090932	81.48452	5.188977
0.11303	71.47641	6.531547		0.099189	82.18683	6.470624		0.103632	83.80192	4.962239
0.13081	74.1425	6.734203		0.10176	82.47105	6.44405		0.118872	86.23289	4.756344
0.15367	78.15878	7.065138						0.136652	88.89146	4.428087
0.18161	84.04636	7.217289		0.088646	81.0421	6.424232		0.159512	91.74284	3.831741
0.21463	91.02499	5.88575		0.101346	82.43333	6.377929		0.187452	93.99341	2.883841
0.24765	95.82695	3.207159		0.116586	83.97588	6.534965		0.220472	95.59174	1.694136
0.28575	97.30525	1.199996		0.134366	86.02763	6.523989		0.253492	96.08138	1.071509
0.32639	97.31166	0.737035		0.157226	88.9079	6.403308		0.291592	96.12878	0.790781
0.40259	97.33438	0.598648		0.185166	92.95915	5.426662		0.332232	96.29356	0.675407
0.51689	97.14843	0.570072		0.218186	96.51148	3.540719		0.408432	96.04816	0.585842
0.64389	96.94128	0.57594		0.251206	98.47099	1.739662		0.522732	95.90043	0.563611
0.77089	96.61088	0.583592		0.289306	98.93123	0.965351		0.649732	95.65867	0.575834
0.89789	96.20975	0.564113		0.329946	99.0265	0.720045		0.776732	95.40742	0.530054

Geom:	1 row SS	Low		Geom:	1 row SS	Low		Geom:	1 row SS	Low
VR	0.5	Tu=.011		VR	0.5	Tu=.011		VR	0.5	Tu=.011
Red2	2424.642	Lu=6.6		Red2	1800.217	Lu=6.6		Red2	1497.256	Lu=6.6
Uinf	95.69			Uinf	95.69			Uinf	95.69	
Cf/2	0.001268			Cf/2	0.001717			Cf/2	0.001713	
Z/D =	0			Z/D =	0.75			Z/D =	1.5	
filename	s1clv5a1			filename	s1clv5q1			filename	s1clv5m1	
Y(cm)	U(y)(m/s)	u' (m/s)		Y(cm)	U(y)(m/s)	u' (m/s)		Y(cm)	U(y)(m/s)	u' (m/s)
1.02489	96.09315	0.602404		0.406146	98.71956	0.602338		0.903732	95.01151	0.6229
1.15189	95.82159	0.570117		0.520446	98.5792	0.589116		1.030732	94.81324	0.549083
1.27889	95.66726	0.557049		0.647446	98.26199	0.599771		1.157732	94.45725	0.553929
1.40589	95.40675	0.549251		0.774446	98.0427	0.608342		1.284732	94.12397	0.588172
1.53289	95.16396	0.553487		0.901446	97.75465	0.563572		1.411732	93.86685	0.566002
1.65989	94.83986	0.572708		1.028446	97.46487	0.550271		1.538732	93.47054	0.559765
1.78689	94.41947	0.548048		1.155446	97.18097	0.559331		1.665732	93.14528	0.549736
1.91389	94.17484	0.549618		1.282446	96.80792	0.58383		1.792732	92.84206	0.532207
2.04089	93.66299	0.648939		1.409446	96.38998	0.565922		1.919732	92.4297	0.540856
2.16789	93.47451	0.554815		1.536446	96.13272	0.562939		2.046732	92.20786	0.550665
2.29489	93.25403	0.586622		1.663446	95.72266	0.542863		2.173732	91.8598	0.531067
2.42189	92.82961	0.589038		1.790446	95.35877	0.543118		2.300732	91.52764	0.525294
2.54889	92.44185	0.604044		1.917446	95.04788	0.543876		2.427732	91.07052	0.549928
2.67589	92.2083	0.539808		2.044446	94.66174	0.535097		2.554732	90.86341	0.527962
2.80289	91.89713	0.565997		2.171446	94.34162	0.546705		2.681732	90.40335	0.558092
2.92989	91.60321	0.650799		2.298446	93.88832	0.54457		2.808732	90.01138	0.582096
3.05689	91.18509	1.06608		2.425446	93.61109	0.58266		2.935732	89.67607	0.662756
3.18389	90.67636	2.860282		2.552446	93.22242	0.568633		3.062732	89.36526	1.088031
3.31089	84.4579	7.615436		2.679446	93.115	0.599524		3.189732	88.76638	2.815142
3.43789	66.39395	9.507979		2.806446	92.62984	0.595549		3.316732	82.97824	7.156377
3.56489	62.16102	8.090754		2.933446	92.2716	0.673246		3.443732	65.872	8.943935
3.69189	76.68693	6.210872		3.060446	91.96404	1.078825		3.570732	61.61853	8.100101
3.81889	87.3226	2.947207		3.187446	91.6325	2.813867		3.697732	75.65012	6.353478
3.94589	90.79671	0.880719		3.314446	85.4654	7.342182		3.824732	85.9359	2.830907
				3.441446	68.04588	9.356989		3.951732	89.02715	0.883305
				3.568446	62.96941	8.493327				
				3.695446	77.20457	6.702637				
				3.822446	88.11232	3.089239				
				3.949446	91.81939	0.982262				

Geom:	1 row SS	Comb(1)		Geom:	1 row SS	Comb(1)		Geom:	1 row SS	Comb(1)
VR	0.5	Tu = .12		VR	0.5	Tu = .12		VR	0.5	Tu = .12
Red2	2050.275	Lu=3.36		Red2	2061.382	Lu=3.36		Red2	1635.795	Lu=3.36
Uinf	95.69			Uinf	95.69			Uinf	95.69	
Cf/2	0.001567			Cf/2	0.001625			Cf/2	0.001765	
Z/D =	0			Z/D =	0.75			Z/D =	1.5	
filename	s1cbv5a1.pm			filename	s1cbv5q1			filename	s1cbv5m1	
Y(cm)	U(y)(m/s)	u' (m/s)		Y(cm)	U(y)(m/s)	u' (m/s)		Y(cm)	U(y)(m/s)	u' (m/s)
0.004318	30.9037	9.085595		0.00381	29.23835	8.852057		0.00381	30.74427	9.210737
0.006096	38.10333	10.40093		0.005842	38.00054	10.33231		0.005588	38.82829	10.34133
0.008667	44.91878	9.885712		0.008413	45.86933	9.747141		0.008159	46.53196	9.886864
0.011238	49.23725	9.260709		0.010984	50.34291	9.039175		0.01073	52.16358	8.912351
0.013809	52.95793	8.837937		0.013555	53.96557	8.745083		0.013301	56.13631	8.527543
0.01638	55.23953	8.713859		0.016126	56.39155	8.62123		0.015872	58.9547	8.283377
0.018951	56.91176	8.622285		0.018697	58.16086	8.582298		0.018443	60.94728	8.24454
0.021522	58.54915	8.692049		0.021268	59.60028	8.547383		0.021014	62.69661	8.283796
0.024093	59.91586	8.639064		0.023839	60.94685	8.686188		0.023585	64.07259	8.265524
0.026664	60.81485	8.641729		0.02641	62.06848	8.774981		0.026156	65.4058	8.293861
0.029235	61.89468	8.698517		0.028981	63.17636	8.767527		0.028727	66.61985	8.424786
0.031806	62.90812	8.808533		0.031552	64.22186	8.861011		0.031298	67.68251	8.541702
0.034377	63.71622	8.883519		0.034123	65.12711	8.92567		0.033869	68.60557	8.50307
0.036947	64.55076	8.95727		0.036693	65.73122	9.04196		0.036439	69.63029	8.585171
0.039518	65.44558	9.091333		0.039264	66.91463	9.093063		0.03901	70.45659	8.582691
0.042089	66.14109	9.116002		0.041835	67.63745	9.226025		0.041581	71.26991	8.662943
0.04466	67.00072	9.190107		0.044406	68.48341	9.280933		0.044152	72.11665	8.740891
0.047231	67.70652	9.321434		0.046977	69.19279	9.363916		0.046723	72.76859	8.783322
0.049802	68.48869	9.336721		0.049548	69.85752	9.454552		0.049294	73.5863	8.887385
0.052373	69.16174	9.581149		0.052119	70.41766	9.572175		0.051865	74.30383	8.881269
0.054944	69.87562	9.667425		0.05469	70.9705	9.553637		0.054436	74.91056	9.054836
0.057515	70.51096	9.618196		0.057261	71.67911	9.624261		0.057007	75.7997	9.083662
0.060086	70.86922	9.784141		0.059832	72.091	9.771567		0.059578	76.40553	9.161099
0.062657	71.28906	9.707838		0.062403	72.55745	9.895436		0.062149	77.12916	9.159273
0.065228	71.7617	9.904349		0.064974	72.97273	9.91147		0.06472	77.58451	9.250192
0.067799	72.27097	9.893917		0.067545	73.53076	9.978631		0.067291	78.41788	9.279603
0.07037	72.8185	10.016		0.070116	73.9755	10.00841		0.069862	78.88622	9.362185
0.072941	73.33558	10.01673		0.072687	74.42794	10.11133		0.072433	79.49924	9.381236
0.075512	73.76546	10.18854		0.075258	75.06213	10.17665		0.075004	80.13914	9.361854
0.078083	74.19066	10.22115		0.077829	75.21797	10.16034		0.077575	80.50191	9.451069
0.080654	74.79189	10.18999		0.0804	75.70375	10.23449		0.080146	81.04077	9.475822
0.083225	75.1451	10.27234		0.082971	76.24084	10.21191		0.082717	81.52078	9.554097
0.085796	75.50172	10.19349		0.085542	76.72702	10.2768		0.085288	81.77385	9.630245
0.088367	75.90478	10.31056						0.087859	82.43434	9.65011
0.090938	76.64582	10.36463		0.085344	76.47401	10.31474		0.09043	82.76674	9.605295
0.093509	76.72665	10.31956		0.098044	78.24791	10.46553		0.093001	83.21162	9.617541
0.096079	77.16937	10.34523		0.113284	80.47155	10.52438		0.095571	83.3297	9.590932
0.09865	77.51698	10.40436		0.131064	82.52342	10.45828				
0.101221	77.6972	10.36861		0.153924	85.75606	9.834874		0.08509	82.11664	9.535787
				0.181864	89.1093	8.839299		0.09779	83.6713	9.536713
0.0762	73.61149	10.1007		0.214884	92.48408	7.270461		0.11303	85.96426	9.399848
0.0889	75.8881	10.32757		0.247904	94.81637	5.458602		0.13081	87.98388	9.190594
0.10414	78.24097	10.47028		0.286004	96.39891	3.966113		0.15367	90.31788	8.388435
0.12192	80.74625	10.43161		0.326644	96.84497	3.239043		0.18161	92.50236	7.311219
0.14478	83.87607	10.06297		0.402844	96.9267	2.833624		0.21463	94.68076	5.670187
0.17272	87.62916	9.253727		0.517144	96.93156	2.59356		0.24765	95.90001	4.485882
0.20574	91.75111	7.597719		0.644144	96.69976	2.480229		0.28575	96.64051	3.587903
0.23876	94.46095	5.999078		0.771144	96.38794	2.409624		0.32639	96.8961	2.990634
0.27686	96.07034	4.426989		0.898144	96.08165	2.401533		0.40259	96.99827	2.791375
0.3175	96.93508	3.414504		1.025144	95.82652	2.29195		0.51689	96.84477	2.586685

Geom:	1 row SS	Comb(1)		Geom:	1 row SS	Comb(1)		Geom:	1 row SS	Comb(1)
VR	0.5	Tu = .12		VR	0.5	Tu = .12		VR	0.5	Tu = .12
Red2	2050.275	Lu=3.36		Red2	2061.382	Lu=3.36		Red2	1635.795	Lu=3.36
Uinf	95.69			Uinf	95.69			Uinf	95.69	
Cf/2	0.001567			Cf/2	0.001625			Cf/2	0.001765	
Z/D =	0			Z/D =	0.75			Z/D =	1.5	
filename	s1cbv5a1.prn			filename	s1cbv5q1			filename	s1cbv5m1	
Y(cm)	U(y)(m/s)	u' (m/s)		Y(cm)	U(y)(m/s)	u' (m/s)		Y(cm)	U(y)(m/s)	u' (m/s)
0.3937	97.04929	2.820058		1.152144	95.47297	2.290423		0.64389	96.69792	2.495327
0.508	96.98661	2.587732		1.279144	95.21441	2.266376		0.77089	96.38588	2.405526
0.635	96.83664	2.512323		1.406144	94.85535	2.238292		0.89789	96.09622	2.356027
0.762	96.49258	2.443916		1.533144	94.51804	2.23124		1.02489	95.8849	2.312594
0.889	96.19979	2.360105		1.660144	94.27333	2.245102		1.15189	95.91238	2.351777
1.016	95.97285	2.313584		1.787144	93.9203	2.254325		1.27889	96.56229	2.271257
1.143	95.42404	2.291395		1.914144	93.62783	2.218154		1.40589	96.18805	2.313163
1.27	95.08712	2.245712		2.041144	93.20773	2.267185		1.53289	95.81851	2.280762
1.397	94.93291	2.237696		2.168144	92.8895	2.297543		1.65989	95.51279	2.284931
1.524	94.86253	2.259643		2.295144	92.57883	2.268116		1.78689	95.06205	2.270242
1.651	94.46397	2.257217		2.422144	92.16273	2.313163		1.91389	94.65909	2.305899
1.778	93.9975	2.251017		2.549144	91.85052	2.336048		2.04089	94.39699	2.289818
1.905	93.75611	2.268621		2.676144	91.51917	2.354243		2.16789	94.0521	2.280543
2.032	93.48392	2.250483		2.803144	91.09204	2.394471		2.29489	93.61482	2.348847
2.159	93.21523	2.269826		2.930144	90.75071	2.489263		2.42189	93.297	2.334153
2.286	92.77551	2.300523		3.057144	90.34449	2.933467		2.54889	92.89783	2.370483
2.413	92.51023	2.303095		3.184144	89.07405	4.971366		2.67589	92.38319	2.421049
2.54	91.98765	2.317209		3.311144	82.86707	8.571074		2.80289	92.10735	2.421051
2.667	91.54446	2.348709		3.438144	71.04594	9.7414		2.92989	91.69193	2.521906
2.794	91.32684	2.433763		3.565144	68.02428	10.33491		3.05689	91.37875	2.941864
2.921	90.86468	2.491889		3.692144	76.93856	10.01929		3.18389	90.20108	4.880807
3.048	90.48182	2.870972		3.819144	84.24867	6.965636		3.31089	84.33461	8.49328
3.175	89.36926	4.712679		3.946144	87.12519	4.806068		3.43789	72.4168	9.892316
3.302	83.49924	8.41335						3.56489	68.68516	10.47855
3.429	71.70689	9.672148						3.69189	77.34826	10.30039
3.556	67.86068	10.38532						3.81889	84.89297	7.135881
3.683	76.6019	10.23375						3.94589	87.92975	5.019738
3.81	84.27468	7.048472								
3.937	87.34454	4.879697								
3.32994	84.49741	7.480835								
3.45694	65.9567	9.331752								
3.58394	62.13349	7.916819								
3.71094	76.5213	5.984825								
3.83794	87.24913	2.804719								
3.96494	90.39857	0.835239								

Geom:	2 rows SS			Geom:	2 rows SS			Geom:	2 rows SS	
VR	0.5	Low		VR	0.5	Low		VR	0.5	Low
Red2	2540.111	Tu=.011		Red2	1944.579	Tu=.011		Red2	2750.859	Tu=.011
Uinf	95.69	Lu=6.6		Uinf	95.69	Lu=6.6		Uinf	95.69	Lu=6.6
Cf/2	0.001185			Cf/2	0.001705			Cf/2	0.001329	
Z/D =	0			Z/D =	0.75			Z/D =	1.5	
filename	s2clv5a1			filename	s2clv5q1			filename	s2clv5m1	
Y(cm)	U(y)(m/s)	u' (m/s)		Y(cm)	U(y)(m/s)	u' (m/s)		Y(cm)	U(y)(m/s)	u' (m/s)
0.004572	26.35442	4.966235		0.00381	30.6473	5.700989		0.004318	27.02883	5.033887
0.007143	36.64045	6.033792		0.006096	40.73294	7.135633		0.006889	37.88717	6.226165
0.009714	42.63555	6.177768		0.008667	49.61647	7.582066		0.00946	44.3494	6.471651
0.012285	46.85353	6.129824		0.011238	55.78617	7.422785		0.012031	48.23711	6.407388
0.014856	49.7088	6.020198		0.013809	59.47602	7.355209		0.014602	50.74623	6.435749
0.017427	51.43824	6.03583		0.01638	61.50182	7.186426		0.017173	52.73066	6.291822
0.019998	53.16785	6.031393		0.018951	63.51993	7.092		0.019744	53.87011	6.26052
0.022569	54.43111	6.053474		0.021522	64.92915	7.127974		0.022315	55.34365	6.300808
0.02514	55.56398	6.028975		0.024093	66.29005	7.094633		0.024886	56.66898	6.312958
0.027711	56.47962	6.00288		0.026664	67.2387	7.104226		0.027457	57.49881	6.319855
0.030282	57.2593	6.026627		0.029235	68.16312	7.053043		0.030028	58.38404	6.286688
0.032853	57.86516	6.029833		0.031806	68.97469	7.031018		0.032599	59.32421	6.345252
0.035423	58.57894	6.057144		0.034377	69.93388	6.959027		0.035169	59.98475	6.330785
0.037994	59.16069	6.037597		0.036947	70.71451	6.897146		0.03774	60.64713	6.336145
0.040565	59.9319	6.094685		0.039518	71.20674	6.918815		0.040311	61.12248	6.333566
0.043136	60.31694	6.125752		0.042089	71.85091	6.904444		0.042882	62.07959	6.322024
0.045707	60.70887	6.126739		0.04466	72.53742	6.842094		0.045453	62.79636	6.369359
0.048278	61.32085	6.172575		0.047231	73.18447	6.911301		0.048024	63.36932	6.349815
0.050849	61.776	6.166105		0.049802	73.4342	6.815753		0.050595	63.68955	6.364005
0.05342	62.27358	6.157237		0.052373	74.12413	6.827266		0.053166	64.28139	6.350231
0.055991	62.60696	6.187968		0.054944	74.82323	6.842814		0.055737	64.85355	6.314437
0.058562	63.13024	6.188301		0.057515	75.35057	6.841273		0.058308	65.5732	6.285084
0.061133	63.38823	6.151578		0.060086	75.51767	6.817132		0.060879	66.29579	6.320696
0.063704	63.87597	6.299096		0.062657	75.8548	6.801826		0.06345	66.58118	6.28609
0.066275	64.12548	6.294297		0.065228	76.53341	6.808069		0.066021	66.97776	6.344186
0.068846	64.28767	6.337915		0.067799	76.70258	6.763742		0.068592	67.49389	6.29488
0.071417	64.8088	6.256782		0.07037	77.25533	6.777159		0.071163	67.73994	6.240137
0.073988	65.08171	6.349629		0.072941	77.35676	6.743986		0.073734	68.18847	6.215466
0.076559	65.51951	6.327269		0.075512	77.9817	6.794529		0.076305	68.43044	6.259993
0.07913	65.69736	6.377598		0.078083	78.30969	6.73037		0.078876	68.80357	6.221432
0.081701	66.05265	6.481202		0.080654	78.49129	6.674855		0.081447	69.23158	6.261137
0.084272	66.3133	6.470034		0.083225	78.74585	6.72068		0.084018	69.49124	6.203538
0.086843	66.4135	6.46022		0.085796	79.26638	6.764796		0.086589	69.73183	6.271055
0.089414	66.97385	6.567582		0.088367	79.44482	6.726676		0.08916	70.12093	6.192852
0.091985	67.35892	6.633192		0.090938	79.56541	6.709009		0.091731	70.4036	6.169398
0.094555	67.57064	6.651544		0.093509	80.00784	6.746742		0.094301	70.74436	6.135348
0.097126	67.88323	6.601954		0.096079	80.31992	6.789962		0.096872	71.02183	6.2099
0.099697	68.19224	6.714533		0.09865	80.61131	6.684953		0.099443	71.63335	6.095947
0.102268	68.60667	6.799284		0.101221	80.75536	6.727875		0.102014	71.85988	6.181278
				0.103792	81.10075	6.704974		0.104585	72.07127	6.12844
0.08382	66.39846	6.502641						0.107156	72.47567	6.182562
0.10668	69.73607	6.996878		0.10414	81.17011	6.647449		0.109727	72.9408	6.167147
0.13462	75.03622	7.611299		0.127	84.42952	6.5172		0.112298	73.41351	6.127995
0.16764	82.21592	7.899888		0.15494	87.7583	6.186425				
0.20066	89.74984	7.08836		0.18796	92.17031	5.252046		0.1016	71.83696	6.162534
0.23876	96.10817	4.27504		0.22098	95.9071	3.769514		0.11684	73.87488	6.123504
0.2794	98.80434	1.662906		0.25908	98.2049	2.194196		0.13462	76.63998	6.142572
0.3556	98.909	0.804112		0.29972	98.93197	1.298882		0.15748	79.74648	6.154447
0.4699	98.61871	0.654667		0.37592	99.06094	0.776235		0.18542	83.31052	6.135393
0.5969	98.54471	0.607439		0.49022	98.82603	0.633708		0.21844	88.02839	6.010734

Geom:	2 rows SS			Geom:	2 rows SS			Geom:	2 rows SS	
VR	0.5	Low		VR	0.5	Low		VR	0.5	Low
Red2	2540.111	Tu=.011		Red2	1944.579	Tu=.011		Red2	2750.859	Tu=.011
Uinf	95.69	Lu=6.6		Uinf	95.69	Lu=6.6		Uinf	95.69	Lu=6.6
Cf/2	0.001185			Cf/2	0.001705			Cf/2	0.001329	
Z/D =	0			Z/D =	0.75			Z/D =	1.5	
filename	s2clv5a1			filename	s2clv5q1			filename	s2clv5m1	
Y(cm)	U(y)(m/s)	u' (m/s)		Y(cm)	U(y)(m/s)	u' (m/s)		Y(cm)	U(y)(m/s)	u' (m/s)
0.7239	97.99162	0.669347		0.61722	98.46252	0.588314		0.25146	92.7954	5.173824
0.8509	97.92433	0.554943		0.74422	98.18734	0.615958		0.28956	96.99065	3.21587
0.9779	97.47461	0.583257		0.87122	97.902	0.650709		0.3302	98.67903	1.50062
1.1049	97.34901	0.567296		0.99822	97.62355	0.58841		0.4064	98.82014	0.745473
1.2319	96.93429	0.586723		1.12522	97.41178	0.568222		0.5207	98.7134	0.640412
1.3589	96.63489	0.561235		1.25222	96.84383	0.59194		0.6477	98.45641	0.618725
1.4859	96.27205	0.573545		1.37922	96.75968	0.576476		0.7747	97.77527	0.643395
1.6129	96.13284	0.574176		1.50622	96.35367	0.597339		0.9017	97.68818	0.597374
1.7399	95.6963	0.585999		1.63322	95.93275	0.590021		1.0287	97.33799	0.565592
1.8669	95.24442	0.565404		1.76022	95.56376	0.559694		1.1557	97.06516	0.576893
1.9939	94.77269	0.582079		1.88722	95.35545	0.581485		1.2827	96.81521	0.58517
2.1209	94.65153	0.542308		2.01422	94.91468	0.578003		1.4097	96.23286	0.62815
2.2479	94.23591	0.547644		2.14122	94.63979	0.5722		1.5367	96.09963	0.582313
2.3749	93.84762	0.589376		2.26822	94.33409	0.578046		1.6637	95.73975	0.571411
2.5019	93.62596	0.602109		2.39522	94.04405	0.573706		1.7907	95.17242	0.614614
2.6289	93.27162	0.593657		2.52222	93.65784	0.593768		1.9177	95.0513	0.557728
2.7559	92.85545	0.596769		2.64922	93.25141	0.55455		2.0447	94.78125	0.598885
2.8829	92.47221	0.654752		2.77622	92.79136	0.580555		2.1717	94.2635	0.57874
3.0099	92.08627	0.93693		2.90322	92.23677	0.645898		2.2987	93.85495	0.55993
3.1369	91.78487	2.228397		3.03022	92.22691	0.982612		2.4257	93.43808	0.580701
3.2639	88.4024	6.206252		3.15722	91.54326	2.289199		2.5527	93.32693	0.599301
3.3909	72.25623	9.477423		3.28422	87.80044	6.321476		2.6797	93.08337	0.553737
3.5179	61.60372	8.279602		3.41122	72.26889	9.462072		2.8067	92.52245	0.598191
3.6449	73.89941	7.424563		3.53822	62.11903	8.31621		2.9337	92.16317	0.674257
3.7719	86.52705	3.804791		3.66522	74.40319	7.466167		3.0607	91.91345	1.090117
3.8989	91.44041	1.233956		3.79222	86.35371	3.611181		3.1877	91.38504	2.782626
				3.91922	91.79327	1.168768		3.3147	85.78883	7.185553
								3.4417	68.5058	9.258586
								3.5687	63.34339	8.379216
								3.6957	77.3699	6.616049
								3.8227	88.11646	3.033943
								3.9497	91.7326	0.946282

Geom:	2 rows SS	Comb(1)		Geom:	2 rows SS	Comb(1)		Geom:	2 rows SS	Comb(1)
VR	0.5	Tu = .12		VR	0.5	Tu = .12		VR	0.5	Tu = .12
Red2	2664.845	Lu=3.36		Red2	2562.256	Lu=3.36		Red2	2554.234	Lu=3.36
Uinf	95.69			Uinf	95.69			Uinf	95.69	
Cf/2	0.00129			Cf/2	0.001344			Cf/2	0.001281	
Z/D =	0			Z/D =	0.75			Z/D =	1.5	
filename	s2cbv5a1			filename	s2cbv5q1			filename	s2cbv5m1	
Y(cm)	U(y)(m/s)	u' (m/s)		Y(cm)	U(y)(m/s)	u' (m/s)		Y(cm)	U(y)(m/s)	u' (m/s)
0.004572	28.15473	8.507309		0.004318	27.66413	7.945191		0.004318	25.9961	7.821551
0.006604	34.20665	9.943918		0.00635	34.96064	9.222383		0.006096	32.49869	9.085509
0.009175	40.71885	9.746228		0.008921	42.25544	8.979564		0.008667	38.99011	9.011624
0.011746	45.14738	9.222797		0.011492	46.64205	8.76489		0.011238	43.66619	8.572092
0.014317	48.21562	8.908839		0.014063	49.56751	8.600801		0.013809	46.38417	8.467235
0.016888	50.31506	8.8506		0.016634	51.78345	8.530588		0.01638	48.34492	8.315723
0.019459	52.02076	8.763277		0.019205	53.28637	8.577992		0.018951	49.84258	8.37781
0.02203	53.18082	8.743453		0.021776	54.60048	8.544871		0.021522	51.09876	8.470677
0.024601	54.36327	8.790905		0.024347	55.86103	8.605068		0.024093	52.23112	8.6598
0.027172	55.44688	8.664068		0.026918	56.91071	8.579204		0.026664	53.24911	8.707151
0.029743	56.28893	8.753323		0.029489	57.79556	8.661711		0.029235	54.16198	8.872409
0.032314	56.96208	8.747894		0.03206	58.54972	8.629637		0.031806	55.1246	8.962995
0.034885	57.68092	8.827257		0.034631	59.38306	8.764209		0.034377	55.95459	9.000189
0.037455	58.35669	8.974664		0.037201	60.11222	8.730573		0.036947	56.68045	9.110736
0.040026	59.04443	8.85259		0.039772	60.76036	8.631143		0.039518	57.54338	9.227323
0.042597	59.75144	8.905038		0.042343	61.42512	8.85593		0.042089	58.47369	9.293832
0.045168	60.35187	9.055726		0.044914	61.83997	8.834161		0.04466	59.31748	9.293732
0.047739	60.77478	9.001152		0.047485	62.33271	8.945517		0.047231	59.96072	9.298798
0.05031	61.26462	9.088649		0.050056	62.8558	8.989599		0.049802	60.61816	9.356862
0.052881	61.61204	9.174667		0.052627	63.55061	9.067128		0.052373	61.26203	9.323297
0.055452	62.03325	9.099068		0.055198	63.95142	9.11616		0.054944	62.07629	9.35432
0.058023	62.45197	9.11667		0.057769	64.24807	9.083842		0.057515	62.57846	9.258952
0.060594	62.76899	9.170851		0.06034	64.71421	9.212417		0.060086	63.28543	9.312508
0.063165	63.50656	9.285948		0.062911	64.98079	9.108591		0.062657	63.94719	9.387563
0.065736	63.82613	9.425077		0.065482	65.69804	9.18276		0.065228	64.50781	9.33079
0.068307	64.36674	9.341036		0.068053	66.15925	9.233436		0.067799	65.08492	9.347041
0.070878	64.66494	9.407973		0.070624	66.47447	9.310055		0.07037	65.59988	9.415118
0.073449	64.96999	9.388261		0.073195	66.74914	9.360259		0.072941	66.22398	9.335833
0.07602	65.42574	9.310207		0.075766	67.18825	9.411999		0.075512	66.56784	9.268826
0.078591	65.89855	9.511764		0.078337	67.32465	9.348445		0.078083	66.96486	9.349995
				0.080908	68.06605	9.494302		0.080654	67.71277	9.36647
0.0762	65.49974	9.437052						0.083225	68.07315	9.357219
0.0889	67.2632	9.539045		0.08001	67.59829	9.501257		0.085796	68.31818	9.319864
0.10414	69.37162	9.833177		0.09017	69.31923	9.601344		0.088367	68.8917	9.344801
0.12192	72.43959	9.957387		0.10287	70.96273	9.685433		0.090938	69.20466	9.365162
0.14478	76.17062	9.996114		0.11811	73.40533	9.90569		0.093509	69.7378	9.386589
0.17272	80.90759	9.949295		0.13589	76.07189	10.08589		0.096079	70.05773	9.438857
0.20574	86.75403	9.041574		0.15875	80.06496	10.01459				
0.23876	91.13058	7.583194		0.18669	84.54867	9.55422		0.08636	68.42744	9.477809
0.27686	94.45884	5.625377		0.21971	89.44954	8.391565		0.09652	70.20692	9.407475
0.3175	95.7571	4.211362		0.25273	93.14172	6.798932		0.10922	72.01373	9.510889
0.3937	96.67887	3.053278		0.29083	95.62591	5.091869		0.12446	74.7007	9.545928
0.508	96.81891	2.640827		0.33147	96.8543	3.828437		0.14224	77.61954	9.517669
0.635	96.57947	2.516267		0.40767	97.29386	2.990699		0.1651	81.61519	9.325964
0.762	96.31535	2.429473		0.52197	97.3371	2.669385		0.19304	85.88284	8.779691
0.889	96.03885	2.359524		0.64897	97.18775	2.508587		0.22606	90.55518	7.492825
1.016	95.79323	2.292843		0.77597	96.66495	2.436052		0.25908	93.55505	6.054881
1.143	95.43296	2.254883		0.90297	96.42616	2.376344		0.29718	95.5709	4.590439
1.27	95.20281	2.221699		1.02997	96.18565	2.292052		0.33782	96.45592	3.740227
1.397	94.68405	2.232674		1.15697	95.79573	2.279634		0.41402	96.95068	3.016776

Geom:	2 rows SS	Comb(1)		Geom:	2 rows SS	Comb(1)		Geom:	2 rows SS	Comb(1)
VR	0.5	Tu = .12		VR	0.5	Tu = .12		VR	0.5	Tu = .12
Red2	2664.845	Lu=3.36		Red2	2562.256	Lu=3.36		Red2	2554.234	Lu=3.36
Uinf	95.69			Uinf	95.69			Uinf	95.69	
Cf/2	0.00129			Cf/2	0.001344			Cf/2	0.001281	
Z/D =	0			Z/D =	0.75			Z/D =	1.5	
filename	s2cbv5a1			filename	s2cbv5q1			filename	s2cbv5m1	
Y(cm)	U(y)(m/s)	u' (m/s)		Y(cm)	U(y)(m/s)	u' (m/s)		Y(cm)	U(y)(m/s)	u' (m/s)
1.524	94.30058	2.217386		1.28397	95.56673	2.27152		0.52832	96.89543	2.675766
1.651	94.0401	2.207805		1.41097	95.29124	2.251616		0.65532	96.64552	2.589899
1.778	93.99897	2.216703		1.53797	94.96806	2.231527		0.78232	96.32595	2.465887
1.905	93.44596	2.222589		1.66497	94.63337	2.239363		0.90932	96.00827	2.372942
2.032	93.09256	2.248539		1.79197	94.31114	2.235158		1.03632	95.70179	2.33728
2.159	92.65281	2.246172		1.91897	93.99032	2.226985		1.16332	95.36167	2.310888
2.286	92.39154	2.232135		2.04597	93.66808	2.272939		1.29032	95.02307	2.306237
2.413	92.06722	2.245022		2.17297	93.22224	2.257668		1.41732	94.72273	2.289296
2.54	91.68589	2.31174		2.29997	92.85911	2.26429		1.54432	94.30844	2.265822
2.667	91.41985	2.340549		2.42697	92.6824	2.310855		1.67132	94.11848	2.269025
2.794	91.01102	2.360445		2.55397	92.20379	2.315826		1.79832	93.6925	2.290645
2.921	90.52821	2.473924		2.68097	91.84489	2.358745		1.92532	93.39507	2.255982
3.048	90.2947	2.874902		2.80797	91.56648	2.412928		2.05232	93.06643	2.278182
3.175	89.00185	4.803159		2.93497	91.28754	2.52858		2.17932	92.71397	2.312265
3.302	82.65501	8.700994		3.06197	90.7372	2.99001		2.30632	92.34678	2.32292
3.429	70.83649	9.685112		3.18897	89.23537	5.224709		2.43332	92.05158	2.381662
3.556	68.24213	10.42404		3.31597	82.56342	8.845275		2.56032	91.66522	2.359179
3.683	77.27505	9.965522		3.44297	70.61938	9.746576		2.68732	91.25678	2.384864
3.81	84.49803	6.75075		3.56997	69.31686	10.63499		2.81432	90.83321	2.433176
3.937	87.20111	4.815722		3.69697	78.43531	9.838133		2.94132	90.51791	2.533871
				3.82397	85.29771	6.635118		3.06832	90.09996	2.987458
				3.95097	87.83091	4.667714		3.19532	88.78786	5.093758
								3.32232	82.11311	8.812264
								3.44932	70.23338	9.650993
								3.57632	68.41277	10.45135
								3.70332	77.25266	9.833592
								3.83032	84.46754	6.634108
								3.95732	87.04393	4.749412
								3.5687	63.34339	8.379216
								3.6957	77.3699	6.616049
								3.8227	88.11646	3.033943
								3.9497	91.7326	0.946282

Geom:	Showerhd	Low		Geom:	Showerhd	Low		Geom:	Showerhd	Low
PReqv	0.0175	Tu=.011		PReqv	0.07	Tu=.011		PReqv	0.35	Tu=.011
Red2	1184.33	Lu=6.6		Red2	1249.654	Lu=6.6		Red2	1441.993	Lu=6.6
Uinf	95.89			Uinf	95.69			Uinf	95.69	
Cf/2	0.001439			Cf/2	0.00138			Cf/2	0.001414	
Z/D =	N/A			Z/D =	N/A			Z/D =	N/A	
filename	shcls5m1			filename	shcls2a1			filename	shcls1a1	
Y(cm)	U(y)(m/s)	u' (m/s)		Y(cm)	U(y)(m/s)	u' (m/s)		Y(cm)	U(y)(m/s)	u' (m/s)
0.011176	51.14561	6.582716		0.01143	49.66076	6.593658		0.011176	49.05934	6.868401
0.0127	53.09492	6.60539		0.012776	51.40384	6.623189		0.012954	51.41631	7.022609
0.015271	56.02822	6.612893		0.015347	54.38044	6.600062		0.015525	54.16112	6.887659
0.017842	58.53997	6.415126		0.017918	56.74583	6.575298		0.018096	56.49978	6.790098
0.020413	60.41885	6.418615		0.020489	58.58617	6.420236		0.020667	58.07438	6.732818
0.022984	61.90623	6.295325		0.02306	60.27726	6.413838		0.023238	59.77763	6.663221
0.025555	63.50711	6.284596		0.025631	61.70631	6.322873		0.025809	61.13068	6.673716
0.028126	64.85764	6.251338		0.028202	63.05989	6.319805		0.02838	62.31216	6.74154
0.030697	65.98912	6.195872		0.030773	64.11153	6.266624		0.030951	63.45827	6.663436
0.033268	67.14661	6.198111		0.033344	65.42819	6.216372		0.033522	64.56092	6.63989
0.035839	68.35639	6.122067		0.035915	66.57012	6.252543		0.036093	65.55668	6.741633
0.03841	69.41117	6.165806		0.038486	67.57369	6.251906		0.038664	66.53713	6.760678
0.040981	70.44781	6.167296		0.041057	68.71921	6.271874		0.041235	67.60181	6.810044
0.043551	71.38512	6.094884		0.043628	69.62864	6.22806		0.043805	68.33734	6.756445
0.046122	72.4601	6.131769		0.046199	70.50249	6.266404		0.046376	69.20736	6.760042
0.048693	73.17642	6.093258		0.04877	71.33439	6.184038		0.048947	70.05519	6.854091
0.051264	74.08546	6.039591		0.051341	72.25203	6.181196		0.051518	70.78777	6.762076
0.053835	75.01543	6.004467		0.053912	72.87553	6.16991		0.054089	71.68444	6.779679
0.056406	75.61601	5.961998		0.056482	73.82068	6.150668		0.05666	72.52312	6.794097
0.058977	76.50949	5.890089		0.059053	74.50117	6.113583		0.059231	73.07483	6.744403
0.061548	77.11021	5.900964		0.061624	75.30132	6.05595		0.061802	73.98936	6.746421
0.064119	77.99213	5.842595		0.064195	75.91955	6.075442		0.064373	74.58887	6.816899
0.06669	78.7541	5.845692		0.066766	76.60757	6.000552		0.066944	75.21122	6.735675
0.069261	79.28432	5.788647		0.069337	77.26025	6.022877		0.069515	75.98096	6.628217
0.071832	80.08959	5.748393		0.071908	77.81212	6.022369		0.072086	76.65586	6.699431
0.074403	80.71268	5.660244		0.074479	78.7022	5.904859		0.074657	77.30287	6.709694
0.076974	81.52343	5.616681		0.07705	79.41369	5.887294		0.077228	78.07359	6.661324
0.079545	82.15713	5.583756		0.079621	80.05437	5.806677		0.079799	78.63596	6.611735
0.082116	82.77655	5.473647		0.082192	80.87668	5.787768		0.08237	79.48521	6.612216
0.084687	83.42388	5.357459		0.084763	81.37668	5.736994		0.084941	80.19479	6.583477
0.087258	83.91183	5.3477		0.087334	82.22266	5.762789		0.087512	80.71949	6.565206
0.089829	84.71044	5.293693						0.090083	81.22616	6.520791
0.0924	85.3396	5.149152		0.08128	80.90352	5.819791		0.092654	81.91434	6.42334
0.094971	85.92231	5.082004		0.0889	82.79736	5.66649		0.095225	82.42205	6.411667
0.097542	86.48193	4.997538		0.09906	85.27393	5.350223		0.097796	83.09673	6.383098
0.100113	86.94334	4.88629		0.11176	87.77822	4.960261		0.100367	83.62141	6.287861
0.102683	87.36321	4.917584		0.127	90.54373	4.207507		0.102937	83.99902	6.250434
				0.14478	93.16349	3.241138		0.105508	84.53372	6.186432
0.094742	86.1564	5.081168		0.16764	94.76358	1.998321		0.108079	84.85976	6.152465
0.109982	89.0103	4.512203		0.19558	95.69212	1.093034				
0.127762	91.86005	3.735785		0.2286	95.77267	0.75509		0.095758	82.64729	6.305681
0.150622	94.28844	2.405863		0.26162	95.58776	0.678084		0.108458	85.44773	5.950708
0.178562	95.58021	1.295976		0.29972	95.69164	0.592846		0.123698	88.21777	5.471546
0.211582	95.83134	0.806274		0.34036	95.64153	0.567883		0.141478	90.9842	4.690793
0.244602	95.85579	0.649559		0.41656	95.43051	0.612811		0.164338	93.23827	3.758217
0.282702	95.8259	0.588373		0.53086	95.36982	0.587656		0.192278	95.04602	2.739422
0.323342	95.89103	0.572925		0.65786	95.23283	0.577214		0.225298	95.84792	2.080735
0.399542	95.72497	0.555971		0.78486	95.01424	0.563255		0.258318	96.16412	1.670248
0.513842	95.48327	0.595192		0.91186	94.82138	0.570682		0.296418	96.38944	1.377493
0.640842	95.34535	0.556615		1.03886	94.55338	0.53393		0.337058	96.22344	1.115752

Geom:	Showerhd	Low		Geom:	Showerhd	Low		Geom:	Showerhd	Low
PReqv	0.0175	Tu=.011		PReqv	0.07	Tu=.011		PReqv	0.35	Tu=.011
Red2	1184.33	Lu=6.6		Red2	1249.654	Lu=6.6		Red2	1441.993	Lu=6.6
Uinf	95.89			Uinf	95.69			Uinf	95.69	
Cf/2	0.001439			Cf/2	0.00138			Cf/2	0.001414	
Z/D =	N/A			Z/D =	N/A			Z/D =	N/A	
filename	shcls5m1			filename	shcls2a1			filename	shcls1a1	
Y(cm)	U(y)(m/s)	u' (m/s)		Y(cm)	U(y)(m/s)	u' (m/s)		Y(cm)	U(y)(m/s)	u' (m/s)
0.767842	95.08241	0.554244		1.16586	94.28198	0.530394		0.413258	96.03599	0.847834
0.894842	94.8641	0.544705		1.29286	94.0802	0.547247		0.527558	95.79688	0.665415
1.021842	94.73579	0.548019		1.41986	93.77673	0.589546		0.654558	95.64226	0.590465
1.148842	94.42542	0.577377		1.54686	93.58139	0.534082		0.781558	95.27606	0.552781
1.275842	94.27195	0.573452		1.67386	93.33804	0.547034		0.908558	95.10273	0.533821
1.402842	93.98472	0.541606		1.80086	93.07443	0.527476		1.035558	94.87606	0.523675
1.529842	93.73632	0.536834		1.92786	92.86267	0.552709		1.162558	94.58348	0.526925
1.656842	93.58096	0.536671		2.05486	92.61678	0.518635		1.289558	94.446	0.546268
1.783842	93.23443	0.558723		2.18186	92.24995	0.535166		1.416558	94.11706	0.547033
1.910842	92.93293	0.56032		2.30886	91.93446	0.536105		1.543558	93.81739	0.529167
2.037842	92.63898	0.542313		2.43586	91.641	0.542256		1.670558	93.57301	0.575806
2.164842	92.33749	0.560449		2.56286	91.27171	0.602046		1.797558	93.34921	0.541784
2.291842	92.10356	0.517506		2.68986	90.87041	0.525584		1.924558	92.99966	0.503595
2.418842	91.79332	0.528088		2.81686	90.57183	0.561405		2.051558	92.71068	0.579442
2.545842	91.40482	0.539077		2.94386	90.21473	0.638618		2.178558	92.42598	0.556118
2.672842	91.16118	0.534812		3.07086	89.84845	1.040388		2.305558	92.13007	0.53364
2.799842	90.66631	0.592776		3.19786	89.4471	2.809034		2.432558	91.80824	0.525736
2.926842	90.38539	0.651152		3.32486	83.19165	7.541925		2.559558	91.49696	0.534159
3.053842	90.12327	0.93058		3.45186	65.32411	9.404777		2.686558	91.16618	0.524295
3.180842	89.68159	2.338838		3.57886	61.1402	7.904376		2.813558	90.81556	0.55454
3.307842	85.3328	6.705765		3.70586	75.44002	6.057652		2.940558	90.30739	0.631285
3.434842	68.35647	9.484248		3.83286	86.13448	2.866102		3.067558	90.08833	1.041372
3.561842	60.1088	7.981367		3.95986	89.58116	0.841588		3.194558	89.70918	2.702546
3.688842	73.2333	6.696161						3.321558	84.0252	7.380477
3.815842	85.07066	3.239774						3.448558	65.94253	9.387269
3.942842	89.51823	1.007654						3.575558	61.05391	8.066925
								3.702558	75.44702	6.214016
								3.829558	86.04928	2.944587
								3.956558	89.65902	0.867003

Geom:	Showerhd	Comb(1)		Geom:	Showerhd	Comb(1)		Geom:	Showerhd	Comb(1)
PReqv	0.0175	Tu = .12		PReqv	0.07	Tu = .12		PReqv	0.35	Tu = .12
Red2	1477.982	Lu=3.36		Red2	1484.68	Lu=3.36		Red2	1578.808	Lu=3.36
Uinf	95.69			Uinf	95.69			Uinf	95.69	
Cf/2	0.001703			Cf/2	0.001682			Cf/2	0.001658	
Z/D =	N/A			Z/D =	N/A			Z/D =	N/A	
filename	shcbs5m1			filename	shcbs2m1			filename	shcbs1m1	
Y(cm)	U(y)(m/s)	u' (m/s)		Y(cm)	U(y)(m/s)	u' (m/s)		Y(cm)	U(y)(m/s)	u' (m/s)
0.00381	30.53606	9.28597		0.00381	30.28353	9.474075		0.004064	30.69817	8.301992
0.005588	38.23386	10.49118		0.005588	38.50659	10.40723		0.00635	39.66415	8.846759
0.008159	45.51683	9.926656		0.008159	46.38374	9.562769		0.008921	46.41092	8.409705
0.01073	51.09848	8.900343		0.01073	51.61176	8.918233		0.011492	50.8014	8.049985
0.013301	54.92216	8.494893		0.013301	55.3801	8.503254		0.014063	53.86815	7.94817
0.015872	57.66822	8.418845		0.015872	58.03339	8.304015		0.016634	56.21324	7.855289
0.018443	59.86271	8.169907		0.018443	60.09324	8.301665		0.019205	57.92338	7.864779
0.021014	61.65781	8.242157		0.021014	61.83747	8.301853		0.021776	59.55797	7.952942
0.023585	63.33975	8.177675		0.023585	63.30019	8.278336		0.024347	61.0349	7.948435
0.026156	64.71064	8.232164		0.026156	64.93742	8.426942		0.026918	62.17471	8.086909
0.028727	66.12003	8.371378		0.028727	66.06151	8.477178		0.029489	63.45369	8.099787
0.031298	67.1711	8.434165		0.031298	67.48163	8.504177		0.03206	64.38558	8.267076
0.033869	68.43408	8.565319		0.033869	68.49744	8.65246		0.034631	65.54305	8.314844
0.036439	69.3886	8.640768		0.036439	69.59189	8.615253		0.037201	66.3357	8.330822
0.03901	70.37461	8.738619		0.03901	70.38959	8.747441		0.039772	67.40905	8.369251
0.041581	71.47555	8.807718		0.041581	71.20782	8.792435		0.042343	68.0894	8.450739
0.044152	72.31425	8.908241		0.044152	72.31973	8.883314		0.044914	69.13461	8.586187
0.046723	72.92271	8.937203		0.046723	73.08273	8.981911		0.047485	69.86921	8.588044
0.049294	74.07742	8.973642		0.049294	74.06497	8.926829		0.050056	70.49392	8.589691
0.051865	74.76067	8.909229		0.051865	74.72669	9.072724		0.052627	71.37671	8.605019
0.054436	75.64198	9.004308		0.054436	75.65208	9.058504		0.055198	72.09781	8.654095
0.057007	76.37647	9.020328		0.057007	76.26974	9.124706		0.057769	72.97308	8.761221
0.059578	76.99966	9.142424		0.059578	77.11827	9.10449		0.06034	73.55601	8.61613
0.062149	77.84267	9.204366		0.062149	77.64978	9.134914		0.062911	74.31305	8.81708
0.06472	78.42632	9.131976		0.06472	78.46507	9.103698		0.065482	74.82466	8.827305
0.067291	79.09228	9.023622		0.067291	79.2561	9.14487		0.068053	75.72939	8.774242
0.069862	79.84219	9.142585		0.069862	79.95136	9.112368		0.070624	76.32288	8.808424
0.072433	80.64243	9.058137		0.072433	80.65593	9.139204		0.073195	76.85249	8.664304
0.075004	81.31445	9.011804		0.075004	81.35548	9.023063		0.075766	77.60232	8.718419
0.077575	81.92935	9.058592		0.077575	81.93548	9.009412		0.078337	78.3555	8.682205
0.080146	82.56753	8.989144		0.080146	82.77343	8.994459		0.080908	78.86768	8.718751
0.082717	83.17271	8.888892		0.082717	83.13708	8.976834		0.083479	79.46809	8.663246
0.085288	83.67928	8.836423		0.085288	83.82196	8.93563		0.08605	80.04874	8.616294
0.087859	84.3487	8.820259		0.087859	84.27993	8.838386		0.088621	80.51609	8.547016
0.09043	84.74075	8.728213		0.09043	84.89786	8.807482		0.091192	81.00335	8.551192
0.093001	85.27087	8.69519		0.093001	85.40863	8.616663		0.093763	81.5354	8.460635
0.095571	85.83447	8.613781		0.095571	85.89037	8.638733		0.096333	81.78798	8.421921
0.098142	86.21815	8.496		0.098142	86.40228	8.59589		0.098904	82.35619	8.336316
0.100713	86.7077	8.499169		0.100713	86.65626	8.514427		0.101475	82.83004	8.252914
0.103284	86.99369	8.359258						0.104046	83.25282	8.189181
0.105855	87.59599	8.211081		0.09906	86.32864	8.521049		0.106617	83.7106	8.187943
0.108426	87.74797	8.209724		0.1143	88.84058	8.039255		0.109188	84.07513	8.10346
0.110997	88.22522	8.058716		0.13208	91.48599	7.202649				
0.113568	88.56771	8.014138		0.15494	93.88625	6.049598		0.108204	83.93678	8.184623
0.116139	88.91346	7.832366		0.18288	95.64952	5.005491		0.123444	86.62881	7.623262
0.11871	89.24773	7.840941		0.2159	96.73768	4.063896		0.141224	88.86435	6.896955
0.121281	89.72926	7.612272		0.24892	97.42188	3.471538		0.164084	90.85492	5.999764
				0.28702	97.72144	3.186307		0.192024	92.51481	5.146352
0.112268	88.42236	7.962951		0.32766	97.86523	2.931794		0.225044	93.86932	4.298116
0.130048	91.00274	7.071861		0.40386	97.9459	2.729982		0.258064	94.47822	3.799821

Geom:	Showerhd	Comb(1)		Geom:	Showerhd	Comb(1)		Geom:	Showerhd	Comb(1)
PReqv	0.0175	Tu = .12		PReqv	0.07	Tu = .12		VR	0.35	Tu = .12
Red2	1477.982	Lu=3.36		Red2	1484.68	Lu=3.36		Red2	1578.808	Lu=3.36
Uinf	95.69			Uinf	95.69			Uinf	95.69	
Cf/2	0.001703			Cf/2	0.001682			Cf/2	0.001658	
Z/D =	N/A			Z/D =	N/A			Z/D =	N/A	
filename	shcbs5m1			filename	shcbs2m1			filename	shcbs1m1	
Y(cm)	U(y)(m/s)	u' (m/s)		Y(cm)	U(y)(m/s)	u' (m/s)		Y(cm)	U(y)(m/s)	u' (m/s)
0.152908	93.25747	6.064413		0.51816	97.74497	2.531317		0.296164	94.91576	3.420999
0.180848	95.04508	4.918068		0.64516	97.49564	2.435928		0.336804	95.21149	3.105155
0.213868	96.18288	3.991047		0.77216	97.33137	2.38871		0.413004	95.21628	2.766532
0.246888	96.78106	3.450159		0.89916	97.03978	2.336887		0.527304	95.17866	2.497525
0.284988	97.16649	3.107761		1.02616	96.68065	2.282885		0.654304	94.88368	2.341543
0.325628	97.22655	2.911069		1.15316	96.43048	2.264812		0.781304	94.52761	2.281705
0.401828	97.29985	2.710705		1.28016	96.14257	2.272747		0.908304	94.22903	2.23003
0.516128	97.26318	2.529784		1.40716	95.86391	2.241503		1.035304	93.94576	2.212243
0.643128	97.00949	2.448164		1.53416	95.59497	2.280357		1.162304	93.65887	2.178419
0.770128	96.75673	2.378399		1.66116	95.22956	2.268616		1.289304	93.30463	2.187832
0.897128	96.4567	2.335453		1.78816	94.98626	2.245893		1.416304	93.05941	2.192945
1.024128	96.13311	2.300952		1.91516	94.64497	2.273073		1.543304	92.65143	2.165931
1.151128	95.9662	2.293489		2.04216	94.28338	2.270374		1.670304	92.42913	2.180379
1.278128	95.6664	2.261566		2.16916	93.96022	2.29435		1.797304	92.07384	2.189516
1.405128	95.38915	2.294997		2.29616	93.65498	2.303616		1.924304	91.67166	2.191866
1.532128	95.18936	2.302903		2.42316	93.33491	2.341267		2.051304	91.37074	2.182748
1.659128	94.78382	2.26618		2.55016	93.10468	2.369465		2.178304	91.09762	2.190754
1.786128	94.45251	2.255827		2.67716	92.64249	2.390116		2.305304	90.76009	2.217158
1.913128	94.18034	2.26767		2.80416	92.37054	2.429555		2.432304	90.34693	2.236208
2.040128	93.9951	2.314863		2.93116	91.96503	2.527556		2.559304	90.1376	2.241539
2.167128	93.61545	2.268863		3.05816	91.56479	2.945438		2.686304	89.82975	2.273149
2.294128	93.23103	2.296492		3.18516	90.5649	4.683276		2.813304	89.40945	2.35886
2.421128	92.89394	2.332362		3.31216	84.74714	8.641446		2.940304	88.91274	2.430498
2.548128	92.57422	2.347345		3.43916	73.11026	9.778446		3.067304	88.61792	2.945074
2.675128	92.24503	2.377261		3.56616	68.70544	10.49507		3.194304	87.19576	5.110282
2.802128	91.88986	2.409398		3.69316	77.0796	10.58973		3.321304	80.53207	8.802429
2.929128	91.60594	2.49245		3.82016	85.0428	7.270712		3.448304	69.09077	9.656534
3.056128	91.08402	2.871758		3.94716	88.36395	5.099961		3.575304	67.43074	10.50014
3.183128	90.17314	4.611034						3.702304	76.57567	9.693415
3.310128	84.86093	8.314949						3.829304	83.2844	6.486391
3.437128	73.22781	9.810813						3.956304	85.93688	4.506208
3.564128	68.37268	10.36325								
3.691128	76.31007	10.52725								
3.818128	84.5449	7.286524								
3.945128	87.97981	5.022678								

Geom:	Basevane			Geom:	Basevane			Geom:	Basevane	
VR	N/A			VR	N/A			VR	N/A	
Tu	0.12			Tu	0.12			Tu	0.011	
Lu (cm)	3.36			Lu (cm)	3.36			Lu (cm)	6.6	
Comb(1)				Comb(1)				Low Tu		
Z/D =	N/A			Z/D =	N/A			Z/D =	N/A	
filename	p1cbv0a1			filename	p1cbv0q1			filename	p1clv0a1	
Y(cm)	U(y)(m/s)	u' (m/s)		Y(cm)	U(y)(m/s)	u' (m/s)		Y(cm)	U(y)(m/s)	u' (m/s)
0.006096	7.156882	1.621544		0.006604	7.866478	1.890348		0.011379	9.116917	0.396813
0.007899	9.265553	2.321499		0.008752	10.39201	2.615354		0.013581	10.88153	0.462816
0.010361	12.10729	2.931601		0.011213	13.25196	3.173993		0.016042	12.87127	0.422316
0.012822	14.82478	3.413612		0.013675	15.63151	3.463191		0.018504	14.64615	0.422424
0.015283	16.84018	3.604752		0.016136	17.46817	3.653756		0.020965	16.45015	0.39391
0.017745	18.40279	3.707875		0.018597	18.93001	3.690218		0.023426	17.80726	0.377574
0.020206	19.68439	3.740971		0.021059	19.9103	3.704779		0.025888	19.07637	0.363003
0.022667	20.71172	3.717592		0.02352	20.89136	3.672164		0.028349	20.0629	0.341426
0.025129	21.42959	3.71528		0.025981	21.49084	3.68572		0.03081	20.91934	0.325408
0.02759	22.07364	3.68066		0.028443	22.07573	3.623259		0.033272	21.68742	0.311917
0.030051	22.54072	3.674947		0.030904	22.54378	3.601331		0.035733	22.35308	0.294283
0.032513	22.95968	3.624436		0.033365	22.93602	3.624345		0.038194	22.80054	0.27532
0.034974	23.24372	3.605166		0.035827	23.18312	3.57432		0.040656	23.21427	0.256931
0.037435	23.60637	3.54131		0.038288	23.41208	3.533115		0.043117	23.52331	0.252724
0.039897	23.79917	3.537649		0.040749	23.6867	3.492917				
0.042358	23.98435	3.526608		0.043211	23.8723	3.487927		0.055372	24.16321	0.230398
0.044819	24.08486	3.474923		0.045672	24.03027	3.480302		0.075692	24.91555	0.208019
0.047281	24.31388	3.467167		0.048134	24.18287	3.414648		0.101092	25.06985	0.20108
0.049742	24.42841	3.472193		0.050595	24.28479	3.438549		0.131572	25.13519	0.192878
0.052204	24.54021	3.404247		0.053056	24.4381	3.3441		0.172212	25.21554	0.197802
0.054665	24.65508	3.424943		0.055518	24.51157	3.33137		0.228092	25.28082	0.199757
0.057126	24.80567	3.390129		0.057979	24.60398	3.368858		0.291592	25.37844	0.199684
0.059588	24.80961	3.363957		0.06044	24.70132	3.369734		0.367792	25.48328	0.200083
0.062049	24.88245	3.379196		0.062902	24.78678	3.352417		0.482092	25.65322	0.202647
0.06451	24.96761	3.351512		0.065363	24.82716	3.31018		0.609092	25.8212	0.206495
0.066972	24.97713	3.308683		0.067824	24.86406	3.279602		0.736092	25.99408	0.199919
0.069433	25.04309	3.336005		0.070286	24.95988	3.30034		0.863092	26.19177	0.204555
0.071894	25.18379	3.350801		0.072747	25.01149	3.304951		0.990092	26.36601	0.21593
0.074356	25.13953	3.303226		0.075208	25.01813	3.288713		1.117092	26.56835	0.204379
0.076817	25.17663	3.342867		0.07767	25.01775	3.272995		1.244092	26.74279	0.212881
0.079278	25.21887	3.312789		0.080131	25.11561	3.3168		1.371092	26.94878	0.21693
0.08174	25.31026	3.290574		0.082592	25.14992	3.259716		1.498092	27.20704	0.208192
0.084201	25.32043	3.294173		0.085054	25.21783	3.300242		1.625092	27.42258	0.219767
0.086662	25.34976	3.270228		0.087515	25.2352	3.273919		1.752092	27.66327	0.213458
0.089124	25.39606	3.278685		0.089976	25.19734	3.227207		1.879092	27.89731	0.217865
0.091585	25.3564	3.242726		0.092438	25.25475	3.225671		2.006092	28.12675	0.212857
0.094046	25.48137	3.234919		0.094899	25.31936	3.2579		2.133092	28.3426	0.216879
0.096508	25.39286	3.262302		0.09736	25.39703	3.207226		2.260092	28.61648	0.221217
0.098969	25.50024	3.233826		0.099822	25.41665	3.204836		2.387092	28.842	0.225035
								2.514092	29.10617	0.216971
0.09652	25.43075	3.185318		0.08255	25.22839	3.297076		2.641092	29.3571	0.218193
0.11938	25.52971	3.114201		0.09525	25.34596	3.219865		2.768092	29.54299	0.229307
0.14478	25.57674	3.074263		0.12319	25.57514	3.165284		2.895092	29.82504	0.22011
0.17018	25.60292	3.007795		0.14097	25.63247	3.164956		3.022092	30.06456	0.21948
0.20066	25.65591	3.02027		0.16383	25.69349	3.104606		3.149092	30.27819	0.223971
0.23622	25.70899	2.994097		0.18923	25.75899	3.060505		3.276092	30.51087	0.21742
0.2794	25.67796	2.959652		0.21463	25.7879	3.043411		3.403092	30.70281	0.22526
0.3556	25.7637	2.960368		0.24511	25.85708	3.006374		3.530092	30.89853	0.223648
0.4699	25.88481	2.941521		0.28067	25.85485	2.987122		3.657092	31.08595	0.231112
0.5969	25.91601	2.972245		0.32385	25.89874	2.975504		3.784092	31.28138	0.233914

Geom:	Basevane			Geom:	Basevane			Geom:	Basevane	
VR	N/A			VR	N/A			VR	N/A	
Tu	0.12			Tu	0.12			Tu	0.011	
Lu (cm)	3.36			Lu (cm)	3.36			Lu (cm)	6.6	
Comb(1)				Comb(1)				Low Tu		
Z/D =	N/A			Z/D =	N/A			Z/D =	N/A	
filename	p1cbv0a1			filename	p1cbv0q1			filename	p1clv0a1	
Y(cm)	U(y)(m/s)	u' (m/s)		Y(cm)	U(y)(m/s)	u' (m/s)		Y(cm)	U(y)(m/s)	u' (m/s)
0.7239	26.03152	3.001411		0.40005	25.90969	3.001661		3.911092	31.47922	0.222742
0.8509	26.25509	3.038525		0.51435	25.98852	2.955427				
0.9779	26.41495	3.03922		0.64135	26.08348	2.972708				
1.1049	26.62736	3.137475		0.76835	26.26279	3.01428				
1.2319	26.78637	3.190267		0.89535	26.36255	3.05629				
1.3589	27.03376	3.193506		1.02235	26.54623	3.120905				
1.4859	27.20964	3.205679		1.14935	26.7435	3.126674				
1.6129	27.52814	3.251679		1.27635	26.93917	3.15736				
1.7399	27.78675	3.269842		1.40335	27.1856	3.231457				
1.8669	28.15704	3.3161		1.53035	27.4251	3.22752				
1.9939	28.51486	3.412869		1.65735	27.65704	3.303697				
2.1209	28.76943	3.457812		1.78435	27.84685	3.269877				
2.2479	29.0118	3.438383		1.91135	28.03747	3.377991				
2.3749	29.26577	3.493145		2.03835	28.34689	3.380959				
2.5019	29.46098	3.47332		2.16535	28.53327	3.385883				
2.6289	29.71351	3.5566		2.29235	28.81213	3.414891				
2.7559	29.92712	3.587531		2.41935	29.05426	3.437703				
2.8829	30.18612	3.578462		2.54635	29.35994	3.508754				
3.0099	30.42994	3.565583		2.67335	29.53252	3.485989				
3.1369	30.57464	3.645644		2.80035	29.78337	3.531578				
3.2639	30.81793	3.593765		2.92735	29.94627	3.531411				
3.3909	31.01446	3.622055		3.05435	30.29496	3.554056				
3.5179	31.1895	3.671378		3.18135	30.41011	3.572476				
3.6449	31.39644	3.666115		3.30835	30.65929	3.60311				
3.7719	31.59813	3.696785		3.43535	30.83858	3.620415				
3.8989	31.70064	3.676057		3.56235	31.01346	3.636437				
				3.68935	31.23672	3.652563				
				3.81635	31.42259	3.659098				
				3.94335	31.54664	3.642791				

Geom:	1 row PS			Geom:	1 row PS			Geom:	1 row PS	
VR	1.5			VR	1.5			VR	1.5	
Tu	0.12			Tu	0.12			Tu	0.12	
Lu (cm)	3.36			Lu (cm)	3.36			Lu (cm)	3.36	
Comb(1)				Comb(1)				Comb(1)		
Z/D =	0			Z/D =	0.75			Z/D =	1.5	
filename	p1cbv2a2			filename	p1cbv2q2			filename	p1cbv2m2	
Y(cm)	U(y)(m/s)	u' (m/s)		Y(cm)	U(y)(m/s)	u' (m/s)		Y(cm)	U(y)(m/s)	u' (m/s)
0.010668	13.6264	3.494592		0.009398	12.03177	3.162633		0.008738	11.20551	2.944606
0.013005	16.29816	3.920946		0.011176	14.22758	3.656388		0.01016	12.96357	3.333786
0.015466	18.79954	4.186494		0.013637	17.12866	4.049404		0.012621	15.87226	3.892973
0.017927	20.49122	4.311976		0.016099	19.21554	4.252309		0.015083	18.3562	4.188231
0.020389	21.85002	4.360471		0.01856	20.97119	4.360709		0.017544	20.18911	4.27056
0.02285	22.69885	4.295174		0.021021	22.10643	4.33968		0.020005	21.51415	4.251241
0.025311	23.47467	4.237002		0.023483	23.09642	4.344065		0.022467	22.38147	4.295866
0.027773	24.0419	4.230338		0.025944	23.77266	4.279317		0.024928	23.1211	4.24272
0.030234	24.49502	4.150079		0.028405	24.31754	4.263178		0.027389	23.72785	4.150765
0.032696	25.00062	4.12416		0.030867	24.8555	4.199998		0.029851	24.24533	4.173657
0.035157	25.2537	4.046865		0.033328	25.17088	4.158642		0.032312	24.5759	4.062551
0.037618	25.5334	4.037357		0.035789	25.52365	4.102398		0.034773	24.90558	4.06487
0.04008	25.82179	4.019327		0.038251	25.78871	4.054684		0.037235	25.23816	3.97074
0.042541	25.98674	3.965823		0.040712	26.13779	4.102797		0.039696	25.3931	3.954805
0.045002	26.13577	3.989194		0.043173	26.28045	4.043705		0.042157	25.69654	3.922279
0.047464	26.38493	3.954407		0.045635	26.42499	3.999372		0.044619	25.8778	3.921594
0.049925	26.55228	3.926148		0.048096	26.62485	3.973458		0.04708	26.05296	3.92553
0.052386	26.65231	3.875467		0.050557	26.81276	3.94213		0.049541	26.27263	3.926148
0.054848	26.76457	3.87396		0.053019	26.98698	3.974462		0.052003	26.2633	3.834368
0.057309	26.93741	3.84892		0.05548	26.95107	3.925949		0.054464	26.48961	3.84716
0.05977	27.02554	3.856742		0.057941	26.82746	3.873059		0.056925	26.55966	3.834705
0.062232	27.15392	3.820782		0.060403	26.97734	3.842099		0.059387	26.68032	3.830518
0.064693	27.12812	3.843756		0.062864	27.18554	3.907984		0.061848	26.79113	3.827075
0.067154	27.346	3.8526		0.065325	27.19659	3.84612		0.064309	26.90029	3.822332
0.069616	27.4468	3.78779		0.067787	27.29722	3.810018		0.066771	26.93048	3.793958
0.072077	27.54694	3.827868		0.070248	27.44575	3.863588		0.069232	27.10382	3.785271
0.074538	27.5858	3.80145		0.072709	27.43144	3.845112		0.071693	27.20843	3.842432
0.077	27.5901	3.804429		0.075171	27.49786	3.824006		0.074155	27.2241	3.842875
0.079461	27.75809	3.779536		0.077632	27.54376	3.802835		0.076616	27.37177	3.81771
0.081922	27.7697	3.797084								
0.084384	27.86234	3.777805		0.052578	26.75066	3.836556		0.05969	26.73866	3.805238
0.086845	27.9225	3.79254		0.067818	27.30342	3.781297		0.07493	27.35682	3.766895
				0.085598	27.79589	3.741613		0.09271	27.77379	3.793455
0.06604	27.40743	3.818998		0.108458	28.10113	3.687886		0.11557	28.20436	3.690617
0.08128	27.85721	3.789054		0.136398	28.30274	3.579762		0.14351	28.2594	3.611283
0.09906	28.22204	3.707879		0.169418	28.18981	3.460595		0.17653	28.15495	3.513163
0.12192	28.56288	3.643984		0.202438	27.99118	3.404399		0.20955	27.90513	3.438163
0.14986	28.62105	3.505412		0.240538	27.38317	3.271046		0.24765	27.4797	3.305027
0.18288	28.52278	3.491804		0.281178	26.75768	3.200489		0.28829	26.78819	3.219413
0.2159	28.09959	3.375857		0.357378	25.95748	3.045573		0.36449	25.90484	3.05761
0.254	27.50989	3.302383		0.471678	25.69733	3.069623		0.47879	25.71894	3.072559
0.29464	26.86579	3.214433		0.598678	25.71286	3.007739		0.60579	25.85835	3.019741
0.37084	26.15618	3.079867		0.725678	25.87745	3.076762		0.73279	25.94859	3.08098
0.48514	25.87402	3.075396		0.852678	26.08173	3.078659		0.85979	26.08393	3.09479
0.61214	26.01407	3.073099		0.979678	26.20302	3.095934		0.98679	26.25785	3.143057
0.73914	26.11639	3.085479		1.106678	26.43489	3.117356		1.11379	26.46942	3.173644
0.86614	26.338	3.118214		1.233678	26.64477	3.141131		1.24079	26.67473	3.157747
0.99314	26.4538	3.139341		1.360678	26.84663	3.212197		1.36779	26.80724	3.217426
1.12014	26.61582	3.167078		1.487678	27.0104	3.258837		1.49479	27.16132	3.266089
1.24714	26.81368	3.215529		1.614678	27.28248	3.291948		1.62179	27.26409	3.265764

Geom:	1 row PS			Geom:	1 row PS			Geom:	1 row PS	
VR	1.5			VR	1.5			VR	1.5	
Tu	0.12			Tu	0.12			Tu	0.12	
Lu (cm)	3.36			Lu (cm)	3.36			Lu (cm)	3.36	
Comb(1)				Comb(1)				Comb(1)		
Z/D =	0			Z/D =	0.75			Z/D =	1.5	
filename	p1cbv2a2			filename	p1cbv2q2			filename	p1cbv2m2	
Y(cm)	U(y)(m/s)	u' (m/s)		Y(cm)	U(y)(m/s)	u' (m/s)		Y(cm)	U(y)(m/s)	u' (m/s)
1.37414	27.06051	3.218331		1.741678	27.49108	3.317692		1.74879	27.52166	3.317249
1.50114	27.25962	3.25476		1.868678	27.74636	3.372168		1.87579	27.7987	3.352687
1.62814	27.46654	3.290489		1.995678	28.07105	3.372172		2.00279	27.99991	3.39451
1.75514	27.73744	3.350372		2.122678	28.27489	3.40523		2.12979	28.29013	3.377194
1.88214	28.01558	3.424431		2.249678	28.49499	3.389764		2.25679	28.55876	3.42377
2.00914	28.2047	3.461853		2.376678	28.71177	3.471899		2.38379	28.7375	3.487031
2.13614	28.53448	3.430144		2.503678	28.95125	3.469802		2.51079	28.97764	3.503139
2.26314	28.71168	3.459154		2.630678	29.27232	3.481003		2.63779	29.22099	3.495663
2.39014	28.92915	3.504824		2.757678	29.45764	3.523879		2.76479	29.47718	3.503254
2.51714	29.26616	3.524134		2.884678	29.69983	3.528554		2.89179	29.72891	3.516392
2.64414	29.53544	3.578174		3.011678	29.90865	3.573967		3.01879	29.96248	3.552079
2.77114	29.69925	3.563328		3.138678	30.19116	3.596247		3.14579	30.23356	3.538926
2.89814	29.98182	3.569492		3.265678	30.39894	3.580393		3.27279	30.32751	3.597307
3.02514	30.16551	3.608154		3.392678	30.77021	3.625605		3.39979	30.65054	3.599759
3.15214	30.43354	3.650905		3.519678	31.00632	3.641171		3.52679	30.83853	3.625908
3.27914	30.63764	3.654467		3.646678	31.28102	3.684125		3.65379	31.00659	3.639076
3.40614	30.80552	3.662761		3.773678	31.38099	3.711897		3.78079	31.10456	3.664923
3.53314	31.03481	3.690495		3.900678	31.62804	3.684053		3.90779	31.42707	3.661361
3.66014	31.23551	3.638781								
3.78714	31.43532	3.678407								
3.91414	31.57591	3.673358								

Geom:	1 row PS			Geom:	1 row PS			Geom:	1 row PS	
VR	1			VR	1			VR	1	
Tu	0.12			Tu	0.12			Tu	0.12	
Lu (cm)	3.36			Lu (cm)	3.36			Lu (cm)	3.36	
Comb(1)				Comb(1)				Comb(1)		
Z/D =	0			Z/D =	0.75			Z/D =	1.5	
filename	p1cbv1a2			filename	p1cbv1q2			filename	p1cbv1m2	
Y(cm)	U(y)(m/s)	u' (m/s)		Y(cm)	U(y)(m/s)	u' (m/s)		Y(cm)	U(y)(m/s)	u' (m/s)
0.007874	10.15881	2.529483		0.007874	10.22943	2.557197		0.008001	10.30245	2.551284
0.0095	12.07772	2.967293		0.009398	12.09355	2.988155		0.00955	12.21053	3.039739
0.011961	14.74901	3.404597		0.011859	14.81509	3.455055		0.012012	15.05275	3.482246
0.014422	16.9765	3.671698		0.014321	17.26475	3.770357		0.014473	17.38196	3.810875
0.016884	18.84309	3.868172		0.016782	19.06238	3.882711		0.016934	19.23562	3.897619
0.019345	20.19947	3.903047		0.019243	20.41432	3.931998		0.019396	20.66326	3.964732
0.021806	21.30494	3.868206		0.021705	21.46549	3.848507		0.021857	21.58782	3.910198
0.024268	22.1609	3.815582		0.024166	22.21477	3.801636		0.024318	22.42804	3.863849
0.026729	22.69374	3.757822		0.026627	22.89908	3.69326		0.02678	22.96211	3.807086
0.02919	23.21319	3.653331		0.029089	23.40006	3.698508		0.029241	23.41891	3.681165
0.031652	23.62163	3.597102		0.03155	23.81617	3.692528		0.031702	23.80135	3.679256
0.034113	24.00616	3.551543		0.034011	24.14115	3.566942		0.034164	24.1058	3.590974
0.036574	24.2892	3.491276		0.036473	24.30728	3.509193		0.036625	24.41707	3.50049
0.039036	24.50352	3.445455		0.038934	24.63601	3.463623		0.039086	24.63771	3.47239
0.041497	24.67379	3.390287		0.041395	24.79774	3.428099		0.041548	24.80178	3.433923
0.043958	24.82366	3.366816		0.043857	24.93088	3.384394		0.044009	25.02921	3.356828
0.04642	24.96156	3.308143		0.046318	25.09795	3.338856		0.04647	25.16884	3.350735
0.048881	25.08901	3.268654		0.048779	25.17587	3.307686		0.048932	25.23949	3.314904
0.051342	25.18515	3.258248		0.051241	25.31027	3.295468		0.051393	25.36517	3.277842
0.053804	25.24235	3.216416		0.053702	25.3802	3.259843		0.053855	25.41702	3.28224
0.056265	25.34877	3.243489		0.056163	25.50871	3.229135		0.056316	25.5342	3.223455
0.058726	25.4824	3.190024		0.058625	25.53751	3.180015		0.058777	25.5747	3.166565
0.061188	25.48201	3.151686		0.061086	25.59927	3.14912		0.061239	25.56676	3.180965
0.063649	25.51257	3.139801		0.063547	25.65141	3.16748		0.0637	25.68532	3.172191
0.06611	25.55581	3.114451		0.066009	25.69979	3.098924		0.066161	25.72136	3.147021
0.068572	25.60433	3.103992		0.06847	25.72973	3.135626		0.068623	25.71919	3.145256
0.071033	25.6394	3.103542		0.070931	25.67616	3.13347		0.071084	25.796	3.118553
0.073494	25.61927	3.090837		0.073393	25.83036	3.099212		0.073545	25.82704	3.096099
0.075956	25.73146	3.100137		0.075854	25.81622	3.08557		0.076007	25.85078	3.122542
0.078417	25.74382	3.040855								
				0.07366	25.85612	3.092309		0.06604	25.67672	3.15476
0.07874	25.7659	3.13874		0.09144	25.97165	3.039467		0.08128	25.88933	3.118491
0.1016	25.99533	3.017979		0.1143	26.02759	2.986741		0.09906	25.98098	3.009676
0.12954	26.10048	2.995448		0.14224	26.07272	2.993289		0.12192	26.03894	3.014518
0.16256	26.22365	2.989971		0.17526	26.15156	2.984876		0.14986	26.0161	2.990925
0.19558	26.2237	3.020063		0.20828	26.1725	2.978203		0.18288	26.0793	3.002166
0.23368	26.28322	3.023764		0.24638	26.1296	3.03123		0.2159	26.12763	2.982351
0.27432	26.21862	3.003849		0.28702	26.0621	2.981429		0.254	26.10276	2.977897
0.35052	26.13471	2.995709		0.36322	26.01163	3.048584		0.29464	25.98314	2.972801
0.46482	26.12765	3.036039		0.47752	25.92047	2.999962		0.37084	25.93816	3.00954
0.59182	26.15768	3.069342		0.60452	26.09222	3.052242		0.48514	25.97098	3.047824
0.71882	26.29922	3.086584		0.73152	26.11111	3.029215		0.61214	26.04373	3.032548
0.84582	26.39713	3.116211		0.85852	26.34835	3.09639		0.73914	26.06639	3.043032
0.97282	26.58723	3.087033		0.98552	26.47153	3.125538		0.86614	26.22605	3.067758
1.09982	26.68431	3.138451		1.11252	26.60712	3.137914		0.99314	26.38898	3.111651
1.22682	26.92742	3.209835		1.23952	26.73145	3.155188		1.12014	26.55486	3.143381
1.35382	27.08951	3.242769		1.36652	27.0227	3.223451		1.24714	26.82177	3.182325
1.48082	27.32141	3.289932		1.49352	27.20399	3.286884		1.37414	27.04334	3.251218
1.60782	27.56485	3.316977		1.62052	27.44088	3.304705		1.50114	27.15952	3.263575
1.73482	27.82056	3.309173		1.74752	27.66674	3.341825		1.62814	27.42323	3.298222

Geom:	1 row PS			Geom:	1 row PS			Geom:	1 row PS	
VR	1			VR	1			VR	1	
Tu	0.12			Tu	0.12			Tu	0.12	
Lu (cm)	3.36			Lu (cm)	3.36			Lu (cm)	3.36	
Comb(1)				Comb(1)				Comb(1)		
Z/D =	0			Z/D =	0.75			Z/D =	1.5	
filename	p1cbv1a2			filename	p1cbv1q2			filename	p1cbv1m2	
Y(cm)	U(y)(m/s)	u' (m/s)		Y(cm)	U(y)(m/s)	u' (m/s)		Y(cm)	U(y)(m/s)	u' (m/s)
1.86182	28.08397	3.349463		1.87452	27.86493	3.386269		1.75514	27.66625	3.279413
1.98882	28.34297	3.41369		2.00152	28.13415	3.373513		1.88214	27.92492	3.385176
2.11582	28.54685	3.466387		2.12852	28.33243	3.435276		2.00914	28.15486	3.388119
2.24282	28.79472	3.449328		2.25552	28.6571	3.428132		2.13614	28.34333	3.41398
2.36982	29.05691	3.493989		2.38252	28.92507	3.458858		2.26314	28.59514	3.424259
2.49682	29.30978	3.487872		2.50952	29.10251	3.498805		2.39014	28.89759	3.460825
2.62382	29.52307	3.550282		2.63652	29.43312	3.538517		2.51714	29.08428	3.510173
2.75082	29.88679	3.561209		2.76352	29.64804	3.512344		2.64414	29.31368	3.546507
2.87782	30.0774	3.604193		2.89052	29.83598	3.574172		2.77114	29.56257	3.549332
3.00482	30.28287	3.598725		3.01752	30.04755	3.600012		2.89814	29.85623	3.560099
3.13182	30.5058	3.615032		3.14452	30.37543	3.635744		3.02514	30.0996	3.544568
3.25882	30.76736	3.650434		3.27152	30.59097	3.603558		3.15214	30.26578	3.559903
3.38582	30.94733	3.659612		3.39852	30.77096	3.622038		3.27914	30.44372	3.58069
3.51282	31.1738	3.673063		3.52552	30.95779	3.647268		3.40614	30.75608	3.628123
3.63982	31.30852	3.702352		3.65252	31.1813	3.642322		3.53314	30.84408	3.651291
3.76682	31.58064	3.655001		3.77952	31.3876	3.629433		3.66014	31.07925	3.612739
3.89382	31.7568	3.67221		3.90652	31.50104	3.656499		3.78714	31.25619	3.634464
								3.91414	31.43381	3.677055

Geom:	1 row PS			Geom:	1 row PS			Geom:	1 row PS	
VR	0.5			VR	0.5			VR	0.5	
Tu	0.12			Tu	0.12			Tu	0.12	
Lu (cm)	3.36			Lu (cm)	3.36			Lu (cm)	3.36	
Comb(1)				Comb(1)				Comb(1)		
Z/D =	0			Z/D =	0.75			Z/D =	1.5	
filename	p1cbv5a2			filename	p1cbv5q2			filename	p1cbv2m2	
Y(cm)	U(y)(m/s)	u' (m/s)		Y(cm)	U(y)(m/s)	u' (m/s)		Y(cm)	U(y)(m/s)	u' (m/s)
0.00889	9.930879	2.558936		0.00889	10.03564	2.595729		0.008636	9.832409	2.543872
0.010262	11.39357	2.893141		0.010338	11.64543	2.947319		0.009728	11.05546	2.869266
0.012723	13.86122	3.311217		0.012799	14.34065	3.397756		0.01219	13.70598	3.306498
0.015184	15.94142	3.550379		0.01526	16.4846	3.606768		0.014651	15.98368	3.536998
0.017646	17.66629	3.692758		0.017722	18.10851	3.714742		0.017112	17.6688	3.664578
0.020107	18.96577	3.713742		0.020183	19.32573	3.703042		0.019574	19.0722	3.725806
0.022568	19.93913	3.701985		0.022644	20.24087	3.692194		0.022035	20.04844	3.704254
0.02503	20.74018	3.679407		0.025106	20.89969	3.623534		0.024496	20.76911	3.65592
0.027491	21.27531	3.621719		0.027567	21.52837	3.614921		0.026958	21.38487	3.626493
0.029952	21.8043	3.607306		0.030029	21.96475	3.568435		0.029419	21.89708	3.563467
0.032414	22.17235	3.590165		0.03249	22.30871	3.585509		0.03188	22.28965	3.559662
0.034875	22.46395	3.491581		0.034951	22.61267	3.493515		0.034342	22.58241	3.517599
0.037336	22.76995	3.460254		0.037413	22.84838	3.462304		0.036803	22.83514	3.490324
0.039798	22.96381	3.464125		0.039874	23.03124	3.440361		0.039264	23.04912	3.430592
0.042259	23.18748	3.418523		0.042335	23.21726	3.426118		0.041726	23.27891	3.422337
0.04472	23.35271	3.394767		0.044797	23.39549	3.395675		0.044187	23.42809	3.396815
0.047182	23.49305	3.404836		0.047258	23.50416	3.402016		0.046648	23.53918	3.358787
0.049643	23.62977	3.353147		0.049719	23.60408	3.38614		0.04911	23.67187	3.397252
0.052104	23.76934	3.368541		0.052181	23.74795	3.37346		0.051571	23.78671	3.367706
0.054566	23.87938	3.335677		0.054642	23.92071	3.380391		0.054032	23.88134	3.38807
0.057027	24.0216	3.366341		0.057103	23.93147	3.341101		0.056494	24.01422	3.330775
0.059488	24.00752	3.341347		0.059565	24.01844	3.356932		0.058955	24.17863	3.351526
0.06195	24.09006	3.371633		0.062026	24.10132	3.341544		0.061416	24.17871	3.364441
0.064411	24.14075	3.368026		0.064487	24.22951	3.373036		0.063878	24.18584	3.336637
0.066872	24.24284	3.348741		0.066949	24.21844	3.363389		0.066339	24.30502	3.345676
0.069334	24.26146	3.332413		0.06941	24.30983	3.33572		0.0688	24.30894	3.343534
0.071795	24.40003	3.341589		0.071871	24.34408	3.347513		0.071262	24.35737	3.359529
0.074256	24.36731	3.308947		0.074333	24.38357	3.30996		0.073723	24.436	3.360573
0.076718	24.44265	3.346561		0.076794	24.42965	3.351416		0.076184	24.45811	3.346092
0.079179	24.45547	3.359438		0.079255	24.46771	3.337048		0.078646	24.52769	3.316541
0.08164	24.53348	3.344438		0.081717	24.53042	3.328665		0.081107	24.57778	3.355344
0.084102	24.49175	3.366878		0.084178	24.59071	3.357407		0.083568	24.64831	3.357189
0.086563	24.59799	3.383594		0.086639	24.59627	3.366155		0.08603	24.64509	3.330722
0.089024	24.64649	3.358634		0.089101	24.64073	3.301855		0.088491	24.66872	3.360432
0.091486	24.71067	3.372606		0.091562	24.72898	3.37668		0.090952	24.72079	3.372185
0.093947	24.71672	3.387402		0.094023	24.7281	3.34359		0.093414	24.77773	3.356126
0.096408	24.73487	3.375555		0.096485	24.76191	3.352993		0.095875	24.83333	3.373228
0.09887	24.75566	3.359895		0.098946	24.81893	3.339419		0.098336	24.87174	3.399265
0.101331	24.80688	3.381421		0.101407	24.82236	3.399827		0.100798	24.942	3.396607
								0.103259	24.97809	3.385473
0.08128	24.47337	3.360282		0.07366	24.40334	3.34222		0.10572	24.93898	3.348043
0.09906	24.78867	3.344477		0.09144	24.6875	3.393929		0.108182	24.97498	3.359709
0.12192	25.10275	3.363437		0.1143	25.04825	3.375562		0.110643	25.00944	3.409154
0.14986	25.43924	3.30832		0.14224	25.4	3.34138		0.113104	25.0814	3.372881
0.18288	25.72459	3.17256		0.17526	25.68972	3.244362		0.115566	25.10925	3.35958
0.2159	25.84266	3.161307		0.20828	25.86341	3.131381				
0.254	25.99351	3.062124		0.24638	25.88078	3.060866		0.07366	24.4325	3.369576
0.29464	25.96807	3.052583		0.28702	25.92741	3.067918		0.09144	24.71525	3.326356
0.37084	26.04598	2.999825		0.36322	25.99256	3.02935		0.1143	25.1399	3.375004
0.48514	26.15138	3.015037		0.47752	26.02061	2.993005		0.14224	25.44633	3.300099

Geom:	1 row PS			Geom:	1 row PS			Geom:	1 row PS	
VR	0.5			VR	0.5			VR	0.5	
Tu	0.12			Tu	0.12			Tu	0.12	
Lu (cm)	3.36			Lu (cm)	3.36			Lu (cm)	3.36	
Comb(1)				Comb(1)				Comb(1)		
Z/D =	0			Z/D =	0.75			Z/D =	1.5	
filename	p1cbv5a2			filename	p1cbv5q2			filename	p1cbv2m2	
Y(cm)	U(y)(m/s)	u' (m/s)		Y(cm)	U(y)(m/s)	u' (m/s)		Y(cm)	U(y)(m/s)	u' (m/s)
0.61214	26.09927	3.012326		0.60452	26.14734	3.02156		0.17526	25.65697	3.21586
0.73914	26.24633	3.055595		0.73152	26.25809	3.039726		0.20828	25.91171	3.163921
0.86614	26.34987	3.077335		0.85852	26.36477	3.111657		0.24638	26.05789	3.083339
0.99314	26.5059	3.135614		0.98552	26.5656	3.119357		0.28702	26.03065	3.029293
1.12014	26.65791	3.197632		1.11252	26.66877	3.190673		0.36322	26.01797	2.999838
1.24714	26.95168	3.184637		1.23952	26.82989	3.214784		0.47752	26.08414	2.99701
1.37414	27.0612	3.26505		1.36652	27.07555	3.235739		0.60452	26.14495	2.957616
1.50114	27.33843	3.264764		1.49352	27.28928	3.267531		0.73152	26.24228	3.070969
1.62814	27.54222	3.318185		1.62052	27.51403	3.312403		0.85852	26.36831	3.062183
1.75514	27.80305	3.318219		1.74752	27.79855	3.321521		0.98552	26.53839	3.112637
1.88214	28.0138	3.385742		1.87452	28.02308	3.341237		1.11252	26.72422	3.140505
2.00914	28.27132	3.396491		2.00152	28.18934	3.391313		1.23952	26.96857	3.189427
2.13614	28.46578	3.432814		2.12852	28.45259	3.422138		1.36652	27.10714	3.225205
2.26314	28.81033	3.480798		2.25552	28.67618	3.452796		1.49352	27.39739	3.274963
2.39014	29.02936	3.489056		2.38252	28.97759	3.49326		1.62052	27.58576	3.328986
2.51714	29.24837	3.496672		2.50952	29.27295	3.497011		1.74752	27.8877	3.317568
2.64414	29.51396	3.516615		2.63652	29.48036	3.499973		1.87452	27.99992	3.36638
2.77114	29.69974	3.593728		2.76352	29.71835	3.57748		2.00152	28.27362	3.39489
2.89814	30.00854	3.552402		2.89052	29.96034	3.578652		2.12852	28.54636	3.441503
3.02514	30.27866	3.60003		3.01752	30.21657	3.615144		2.25552	28.80437	3.40953
3.15214	30.48757	3.617338		3.14452	30.40614	3.626638		2.38252	29.10277	3.476111
3.27914	30.62717	3.643234		3.27152	30.61469	3.622088		2.50952	29.32567	3.513318
3.40614	30.87844	3.61778		3.39852	30.87469	3.662609		2.63652	29.52515	3.548964
3.53314	31.03761	3.665405		3.52552	31.0627	3.632127		2.76352	29.80297	3.549039
3.66014	31.26567	3.658943		3.65252	31.22511	3.612505		2.89052	30.03972	3.564928
3.78714	31.42149	3.706859		3.77952	31.48853	3.69351		3.01752	30.16767	3.575285
3.91414	31.68176	3.666308		3.90652	31.56676	3.659623		3.14452	30.53932	3.605518
								3.27152	30.68629	3.639373
								3.39852	30.96778	3.623175
								3.52552	31.12621	3.626387
								3.65252	31.32249	3.653136
								3.77952	31.47723	3.651636
								3.90652	31.67295	3.683323

Geom:	1 row PS			Geom:	1 row PS			Geom:	1 row PS	
VR	1.5			VR	1.5			VR	1.5	
Tu	0.011			Tu	0.011			Tu	0.011	
Lu (cm)	6.6			Lu (cm)	6.6			Lu (cm)	6.6	
Low Tu				Low Tu				Low Tu		
Z/D =	0			Z/D =	0.75			Z/D =	1.5	
filename	p1clv2a1			filename	p1clv1q1			filename	p1clv2m1	
Y(cm)	U(y)(m/s)	u' (m/s)		Y(cm)	U(y)(m/s)	u' (m/s)		Y(cm)	U(y)(m/s)	u' (m/s)
0.008636	10.65112	2.22752		0.006604	10.21369	1.258838		0.006096	8.761798	0.67095
0.010668	12.84097	2.47699		0.009065	13.92511	1.51462		0.008382	11.93649	0.861323
0.013129	14.6027	2.562793		0.011527	17.16155	1.551543		0.010843	15.09423	0.93287
0.015591	16.23022	2.502906		0.013988	19.54702	1.466567		0.013305	18.00649	0.914215
0.018052	17.31188	2.486524		0.016449	21.38609	1.360123		0.015766	20.38391	0.870006
0.020513	18.41951	2.456945		0.018911	22.57038	1.271198		0.018227	22.1082	0.788667
0.022975	19.22974	2.385695		0.021372	23.38501	1.217096		0.020689	23.23024	0.711821
0.025436	19.84714	2.371185		0.023833	23.91637	1.172174		0.02315	23.84179	0.673364
0.027897	20.34299	2.340866		0.026295	24.28198	1.137729		0.025611	24.16493	0.658051
0.030359	20.88521	2.351716		0.028756	24.51403	1.141099		0.028073	24.40118	0.635927
0.03282	21.35667	2.31054		0.031217	24.68936	1.116948		0.030534	24.5302	0.621537
0.035281	21.77032	2.256685		0.033679	24.82132	1.169222		0.032995	24.61008	0.625245
0.037743	22.19276	2.230692		0.03614	24.92648	1.169931		0.035457	24.67042	0.615852
0.040204	22.55113	2.240084		0.038601	24.99819	1.194306		0.037918	24.6927	0.611939
0.042665	22.81736	2.196274		0.041063	25.09746	1.226128		0.040379	24.73831	0.621949
0.045127	23.17193	2.190845		0.043524	25.18869	1.282128		0.042841	24.77745	0.635273
0.047588	23.44506	2.17648		0.045985	25.26982	1.309155		0.045302	24.81727	0.628685
0.050049	23.69414	2.136439		0.048447	25.36703	1.338717		0.047763	24.87424	0.655284
0.052511	23.93211	2.12156		0.050908	25.44709	1.38234		0.050225	24.89345	0.677356
0.054972	24.13755	2.125683		0.053369	25.55041	1.456908		0.052686	24.90859	0.645549
0.057433	24.37004	2.126535		0.055831	25.67115	1.51264		0.055147	24.95638	0.669405
				0.058292	25.77553	1.547203		0.057609	24.99991	0.69625
0.054972	24.13755	2.125683		0.060753	25.91006	1.608286		0.06007	25.01469	0.702131
0.057433	24.37004	2.126535		0.063215	26.06664	1.64733		0.062531	25.06715	0.715438
0.06096	24.61787	2.098525		0.065676	26.18408	1.699056				
0.08636	25.94494	2.032279		0.068137	26.28537	1.731424		0.062484	25.12927	0.723849
0.11684	27.50442	2.103109		0.070599	26.41453	1.758167		0.087884	25.45543	0.888772
0.15748	28.83964	2.343225		0.07306	26.51508	1.81481		0.118364	25.92499	1.078959
0.21336	29.80951	2.64191		0.075522	26.66202	1.820079		0.159004	26.10353	1.075524
0.27686	28.93021	2.583991						0.214884	25.79781	0.845957
0.35306	25.59972	0.872227		0.080772	26.96883	1.914767		0.278384	25.50782	0.518908
0.46736	25.64383	0.223349		0.103632	28.17442	2.142815		0.354584	25.49094	0.277067
0.59436	25.84029	0.201818		0.129032	28.87741	2.165899		0.468884	25.58421	0.21091
0.72136	26.04138	0.202203		0.154432	28.89227	2.156863		0.595884	25.72577	0.209112
0.84836	26.21143	0.201256		0.184912	28.11341	2.055488		0.722884	25.88517	0.20496
0.97536	26.40898	0.202931		0.220472	26.80691	1.709409		0.849884	26.09056	0.201734
1.10236	26.54877	0.206067		0.263652	25.51622	1.007027		0.976884	26.2422	0.214159
1.22936	26.7589	0.207389		0.339852	25.12952	0.330629		1.103884	26.44504	0.207555
1.35636	26.97756	0.213932		0.454152	25.26938	0.206025		1.230884	26.66654	0.204234
1.48336	27.24732	0.205049		0.581152	25.44092	0.20074		1.357884	26.85718	0.205373
1.61036	27.46224	0.21831		0.708152	25.61874	0.195101		1.484884	27.10587	0.203008
1.73736	27.70692	0.210696		0.835152	25.77662	0.210697		1.611884	27.33937	0.207795
1.86436	27.96009	0.209052		0.962152	25.97859	0.197988		1.738884	27.55037	0.217848
1.99136	28.20598	0.220214		1.089152	26.17692	0.208772		1.865884	27.82027	0.218875
2.11836	28.43116	0.212249		1.216152	26.39014	0.205212		1.992884	28.09832	0.206306
2.24536	28.71992	0.220195		1.343152	26.62269	0.202296		2.119884	28.343	0.215744
2.37236	28.94189	0.225856		1.470152	26.84779	0.203294		2.246884	28.58755	0.218711
2.49936	29.22229	0.21264		1.597152	27.0886	0.208213		2.373884	28.85128	0.210352
2.62636	29.49978	0.224877		1.724152	27.32975	0.209458		2.500884	29.0905	0.218698
2.75336	29.77378	0.217675		1.851152	27.59589	0.208302		2.627884	29.37196	0.213248

Geom:	1 row PS			Geom:	1 row PS			Geom:	1 row PS	
VR	1.5			VR	1.5			VR	1.5	
Tu	0.011			Tu	0.011			Tu	0.011	
Lu (cm)	6.6			Lu (cm)	6.6			Lu (cm)	6.6	
Low Tu				Low Tu				Low Tu		
Z/D =	0			Z/D =	0.75			Z/D =	1.5	
filename	p1clv2a1			filename	p1clv1q1			filename	p1clv2m1	
Y(cm)	U(y)(m/s)	u' (m/s)		Y(cm)	U(y)(m/s)	u' (m/s)		Y(cm)	U(y)(m/s)	u' (m/s)
2.88036	29.99666	0.221208		1.978152	27.83816	0.212542		2.754884	29.60824	0.22448
3.00736	30.23758	0.231411		2.105152	28.12932	0.209889		2.881884	29.85218	0.22225
3.13436	30.49613	0.223677		2.232152	28.36952	0.206097		3.008884	30.08728	0.224693
3.26136	30.7235	0.220275		2.359152	28.64793	0.214312		3.135884	30.34232	0.226293
3.38836	30.93206	0.223322		2.486152	28.9139	0.218843		3.262884	30.5858	0.225248
3.51536	31.14503	0.223886		2.613152	29.17969	0.205775		3.389884	30.82899	0.221391
3.64236	31.33082	0.240581		2.740152	29.42327	0.21626		3.516884	31.0318	0.217146
3.76936	31.59643	0.226101		2.867152	29.67916	0.221252		3.643884	31.27634	0.220288
3.89636	31.78894	0.225705		2.994152	29.91484	0.219333		3.770884	31.47261	0.213999
				3.121152	30.15587	0.223279		3.897884	31.64482	0.221295
				3.248152	30.38471	0.222057				
				3.375152	30.62474	0.224061				
				3.502152	30.83027	0.222266				
				3.629152	31.05551	0.218654				
				3.756152	31.24849	0.219409				
				3.883152	31.44043	0.230104				

Geom:	1 row PS			Geom:	1 row PS			Geom:	1 row PS	
VR	1			VR	1			VR	1	
Tu	0.011			Tu	0.011			Tu	0.011	
Lu (cm)	6.6			Lu (cm)	6.6			Lu (cm)	6.6	
Low Tu				Low Tu				Low Tu		
Z/D =	0			Z/D =	0.75			Z/D =	1.5	
filename	p1clv1a1			filename	p1clv1q1			filename	p1clv1m1	
Y(cm)	U(y)(m/s)	u' (m/s)		Y(cm)	U(y)(m/s)	u' (m/s)		Y(cm)	U(y)(m/s)	u' (m/s)
0.009652	10.47378	1.932211		0.00762	11.20392	0.759528		0.007366	9.794534	0.570865
0.012113	12.70681	2.148295		0.010081	14.69775	0.862328		0.009827	13.00249	0.631783
0.014575	14.84879	2.186894		0.012543	17.39962	0.893256		0.012289	15.64404	0.640547
0.017036	16.36009	2.124274		0.015004	19.7139	0.819882		0.01475	17.82854	0.637221
0.019497	17.6784	2.05703		0.017465	21.12994	0.743691		0.017211	20.01121	0.595461
0.021959	18.6244	1.994502		0.019927	22.41655	0.650834		0.019673	21.88118	0.518978
0.02442	19.62025	1.958322		0.022388	23.21949	0.568724		0.022134	22.81042	0.430418
0.026881	20.33126	1.910559		0.024849	23.75986	0.50704		0.024595	23.3924	0.397207
0.029343	21.02073	1.891442		0.027311	24.06244	0.483144		0.027057	23.92183	0.356016
0.031804	21.52002	1.839484		0.029772	24.32388	0.475453		0.029518	24.28327	0.310174
0.034265	22.13177	1.84314		0.032233	24.44941	0.466804		0.031979	24.42504	0.293633
0.036727	22.60862	1.781652		0.034695	24.56813	0.456582		0.034441	24.61152	0.284922
0.039188	23.0142	1.731621		0.037156	24.6497	0.485374		0.036902	24.74977	0.26974
0.041649	23.4154	1.698296		0.039617	24.70791	0.479867		0.039363	24.83681	0.268125
0.044111	23.75588	1.645114		0.042079	24.7601	0.499959				
0.046572	24.104	1.571317		0.04454	24.79319	0.510579		0.0381	24.81964	0.270196
0.049033	24.34313	1.548476		0.047001	24.81919	0.52236		0.05588	25.05117	0.252786
0.051495	24.5947	1.49064		0.049463	24.86465	0.530132		0.0762	25.17164	0.260853
0.053956	24.82909	1.455249		0.051924	24.8927	0.549642		0.1016	25.28442	0.271827
0.056417	25.00864	1.430051		0.054385	24.9293	0.565015		0.13208	25.40457	0.270346
0.058879	25.16227	1.379787		0.056847	24.97395	0.584985		0.17272	25.47724	0.257757
0.06134	25.35598	1.372562		0.059308	25.00479	0.608476		0.2286	25.57553	0.226555
				0.061769	25.03077	0.61381		0.2921	25.58872	0.209102
0.06134	25.35598	1.372562		0.064231	25.05994	0.643598		0.3683	25.65623	0.200374
0.078232	25.96393	1.294342		0.066692	25.10545	0.666755		0.4826	25.79238	0.203333
0.108712	26.53695	1.4422		0.069153	25.15354	0.672401		0.6096	25.92303	0.202409
0.149352	26.18919	1.650287						0.7366	26.10555	0.203088
0.205232	26.29037	1.574977		0.05969	25.00588	0.607561		0.8636	26.2661	0.206127
0.268732	25.52944	0.688733		0.07747	25.33665	0.753669		0.9906	26.44083	0.214453
0.344932	25.55377	0.225034		0.10033	25.6356	0.86166		1.1176	26.60487	0.206484
0.459232	25.75318	0.204397		0.12573	25.72772	0.855402		1.2446	26.83133	0.206014
0.586232	25.89433	0.196975		0.15113	25.56147	0.730008		1.3716	27.0344	0.204826
0.713232	26.06708	0.212229		0.18161	25.31116	0.531321		1.4986	27.23706	0.219208
0.840232	26.23278	0.210234		0.21717	25.15262	0.34722		1.6256	27.46504	0.217957
0.967232	26.39107	0.201469		0.26035	25.15942	0.231331		1.7526	27.74165	0.206843
1.094232	26.58653	0.202831		0.33655	25.22565	0.198228		1.8796	27.94552	0.213416
1.221232	26.77151	0.211955		0.45085	25.36665	0.196073		2.0066	28.22885	0.216254
1.348232	26.97768	0.205716		0.57785	25.53381	0.200726		2.1336	28.48814	0.212874
1.475232	27.17161	0.208815		0.70485	25.68479	0.19733		2.2606	28.72789	0.211556
1.602232	27.45131	0.206926		0.83185	25.87661	0.199215		2.3876	28.9962	0.215455
1.729232	27.6972	0.214857		0.95885	26.03977	0.196539		2.5146	29.27075	0.215758
1.856232	27.93277	0.213952		1.08585	26.23948	0.201974		2.6416	29.49151	0.230034
1.983232	28.19807	0.209987		1.21285	26.44752	0.207986		2.7686	29.78941	0.2152
2.110232	28.43327	0.210157		1.33985	26.65657	0.204855		2.8956	30.0425	0.221006
2.237232	28.68268	0.21005		1.46685	26.89489	0.211194		3.0226	30.25732	0.222468
2.364232	28.95016	0.21725		1.59385	27.12459	0.210046		3.1496	30.49295	0.219728
2.491232	29.163	0.229407		1.72085	27.38262	0.204711		3.2766	30.73842	0.229395
2.618232	29.46273	0.215733		1.84785	27.63834	0.207717		3.4036	30.94762	0.223668
2.745232	29.68618	0.223671		1.97485	27.87233	0.217768		3.5306	31.16654	0.221968
2.872232	29.98237	0.21671		2.10185	28.12876	0.211983		3.6576	31.35185	0.23697

Geom:	1 row PS			Geom:	1 row PS			Geom:	1 row PS	
VR	1			VR	1			VR	1	
Tu	0.011			Tu	0.011			Tu	0.011	
Lu (cm)	6.6			Lu (cm)	6.6			Lu (cm)	6.6	
Low Tu				Low Tu				Low Tu		
Z/D =	0			Z/D =	0.75			Z/D =	1.5	
filename	p1clv1a1			filename	p1clv1q1			filename	p1clv1m1	
Y(cm)	U(y)(m/s)	u' (m/s)		Y(cm)	U(y)(m/s)	u' (m/s)		Y(cm)	U(y)(m/s)	u' (m/s)
2.999232	30.2169	0.220082		2.22885	28.41196	0.20923		3.7846	31.59401	0.223867
3.126232	30.45796	0.217664		2.35585	28.66046	0.213695		3.9116	31.72433	0.236436
3.253232	30.68221	0.227992		2.48285	28.93814	0.212318				
3.380232	30.88041	0.221611		2.60985	29.17207	0.222396				
3.507232	31.09259	0.224819		2.73685	29.42999	0.213636				
3.634232	31.30085	0.220334		2.86385	29.682	0.217558				
3.761232	31.49612	0.226917		2.99085	29.91879	0.226052				
3.888232	31.68613	0.222234		3.11785	30.18907	0.217723				
				3.24485	30.41812	0.223645				
				3.37185	30.62833	0.225159				
				3.49885	30.88274	0.221329				
				3.62585	31.06337	0.227232				
				3.75285	31.26639	0.223383				
				3.87985	31.45406	0.212847				
				3.756152	31.24849	0.219409				
				3.883152	31.44043	0.230104				

Geom:	1 row PS			Geom:	1 row PS			Geom:	1 row PS	
VR	0.5			VR	0.5			VR	0.5	
Tu	0.011			Tu	0.011			Tu	0.011	
Lu (cm)	6.6			Lu (cm)	6.6			Lu (cm)	6.6	
Low Tu				Low Tu				Low Tu		
Z/D =	0			Z/D =	0.75			Z/D =	1.5	
filename	p1clv5a2			filename	p1clv5q1			filename	p1clv5m1	
Y(cm)	U(y)(m/s)	u' (m/s)		Y(cm)	U(y)(m/s)	u' (m/s)		Y(cm)	U(y)(m/s)	u' (m/s)
0.00762	8.582598	1.081549		0.006604	7.30282	0.556921		0.00762	8.782814	0.409846
0.009652	10.70136	1.330626		0.009065	9.888276	0.786862		0.009398	10.82422	0.460977
0.012113	12.87149	1.516541		0.011527	12.35452	0.928099		0.011859	13.22003	0.495973
0.014575	14.64007	1.551806		0.013988	14.71926	1.055249		0.014321	15.28607	0.490923
0.017036	16.09538	1.572453		0.016449	16.56794	1.084843		0.016782	17.07581	0.517785
0.019497	17.20255	1.556156		0.018911	18.24155	1.068163		0.019243	18.59088	0.499956
0.021959	18.15759	1.520996		0.021372	19.52888	1.034772		0.021705	19.76204	0.495686
0.02442	18.81725	1.522408		0.023833	20.63008	0.943257		0.024166	20.82239	0.481349
0.026881	19.37164	1.478812		0.026295	21.49743	0.858023		0.026627	21.64977	0.466523
0.029343	19.77023	1.476262		0.028756	22.15859	0.755508		0.029089	22.43968	0.431813
0.031804	20.05584	1.460247		0.031217	22.70403	0.658588		0.03155	22.91348	0.406462
0.034265	20.29851	1.474305		0.033679	23.12803	0.571339		0.034011	23.39296	0.368553
0.036727	20.417	1.482838		0.03614	23.47819	0.491867		0.036473	23.76232	0.352856
0.039188	20.56797	1.471555		0.038601	23.74662	0.431774		0.038934	24.10047	0.317302
0.041649	20.60814	1.483863		0.041063	23.93009	0.375302		0.041395	24.32043	0.297273
0.044111	20.61615	1.497813		0.043524	24.08134	0.335808		0.043857	24.50132	0.27572
0.046572	20.64832	1.489193		0.045985	24.18867	0.31152				
0.049033	20.63143	1.484217		0.048447	24.26904	0.287667		0.043857	24.50132	0.27572
0.051495	20.60114	1.500831		0.050908	24.34629	0.274301		0.04826	24.87002	0.253396
0.053956	20.54151	1.486825		0.053369	24.37723	0.267145		0.06858	25.33849	0.219225
0.056417	20.48976	1.505176		0.055831	24.42797	0.263819		0.09398	25.47957	0.205966
0.058879	20.43274	1.505465		0.058292	24.44378	0.262122		0.12446	25.55027	0.213136
0.06134	20.35915	1.500428		0.060753	24.48708	0.256205		0.1651	25.62403	0.204178
0.063801	20.31067	1.483226		0.063215	24.50329	0.254002		0.22098	25.69141	0.206113
0.066263	20.27024	1.505358		0.065676	24.51795	0.250727		0.28448	25.76741	0.203115
0.068724	20.18537	1.475894		0.068137	24.5342	0.255565		0.36068	25.87493	0.207321
0.071185	20.13657	1.478981		0.070599	24.55506	0.257212		0.47498	25.99964	0.203143
0.073647	20.11313	1.481114		0.07306	24.56373	0.250375		0.60198	26.13926	0.209512
0.076108	20.08385	1.481303		0.075522	24.58594	0.249465		0.72898	26.31876	0.210772
0.07857	20.06259	1.494434		0.077983	24.5888	0.250146		0.85598	26.4634	0.216447
				0.080444	24.61424	0.252328		0.98298	26.66153	0.206647
0.0762	20.08108	1.481715		0.082906	24.58312	0.261957		1.10998	26.84626	0.210139
0.09906	20.2505	1.643692		0.085367	24.62289	0.257199		1.23698	27.04975	0.208444
0.12446	21.86328	1.794163						1.36398	27.25884	0.209645
0.14986	23.78879	1.25166		0.08255	24.63121	0.254032		1.49098	27.47981	0.212752
0.18034	24.78804	0.503345		0.10795	24.67541	0.250228		1.61798	27.70002	0.209862
0.2159	24.91379	0.253974		0.13335	24.72656	0.233991		1.74498	27.93169	0.213407
0.25908	24.97475	0.201972		0.16383	24.71683	0.220169		1.87198	28.17551	0.210574
0.33528	25.065	0.205401		0.19939	24.80576	0.200703		1.99898	28.44278	0.210478
0.44958	25.2495	0.196829		0.24257	24.89032	0.200537		2.12598	28.69098	0.215129
0.57658	25.40531	0.200063		0.31877	24.95494	0.202243		2.25298	28.95595	0.219709
0.70358	25.54632	0.207729		0.43307	25.10983	0.19656		2.37998	29.19577	0.221969
0.83058	25.77506	0.203063		0.56007	25.28741	0.203157		2.50698	29.43216	0.218959
0.95758	25.944	0.202924		0.68707	25.46863	0.197633		2.63398	29.69509	0.217085
1.08458	26.12789	0.201165		0.81407	25.62887	0.204778		2.76098	29.98548	0.223725
1.21158	26.32306	0.206815		0.94107	25.80892	0.200014		2.88798	30.21581	0.223779
1.33858	26.53628	0.206254		1.06807	25.99254	0.202831		3.01498	30.4677	0.220975
1.46558	26.71294	0.207992		1.19507	26.22169	0.199358		3.14198	30.68638	0.222639
1.59258	26.98535	0.205426		1.32207	26.43632	0.20061		3.26898	30.93404	0.224072
1.71958	27.2098	0.211424		1.44907	26.64702	0.200082		3.39598	31.13961	0.224923

Geom:	1 row PS			Geom:	1 row PS			Geom:	1 row PS	
VR	0.5			VR	0.5			VR	0.5	
Tu	0.011			Tu	0.011			Tu	0.011	
Lu (cm)	6.6			Lu (cm)	6.6			Lu (cm)	6.6	
Low Tu				Low Tu				Low Tu		
Z/D =	0			Z/D =	0.75			Z/D =	1.5	
filename	p1clv5a2			filename	p1clv5q1			filename	p1clv5m1	
Y(cm)	U(y)(m/s)	u' (m/s)		Y(cm)	U(y)(m/s)	u' (m/s)		Y(cm)	U(y)(m/s)	u' (m/s)
1.84658	27.44223	0.212787		1.57607	26.86835	0.214918		3.52298	31.36255	0.233728
1.97358	27.7424	0.213584		1.70307	27.1065	0.207776		3.64998	31.56092	0.235246
2.10058	27.96592	0.217951		1.83007	27.37492	0.198335		3.77698	31.76428	0.240805
2.22758	28.23953	0.209283		1.95707	27.63006	0.209675		3.90398	31.93592	0.231855
2.35458	28.47824	0.216073		2.08407	27.86916	0.206162				
2.48158	28.7653	0.218584		2.21107	28.1233	0.215995				
2.60858	29.01068	0.213694		2.33807	28.37979	0.215626				
2.73558	29.27135	0.214582		2.46507	28.66382	0.211712				
2.86258	29.5433	0.210602		2.59207	28.90269	0.212688				
2.98958	29.76439	0.216205		2.71907	29.1621	0.217083				
3.11658	30.00346	0.221739		2.84607	29.3945	0.213037				
3.24358	30.24983	0.216148		2.97307	29.67274	0.214473				
3.37058	30.4511	0.213811		3.10007	29.88724	0.215294				
3.49758	30.66943	0.218305		3.22707	30.11271	0.215287				
3.62458	30.84983	0.225664		3.35407	30.29524	0.232348				
3.75158	31.07176	0.223167		3.48107	30.55381	0.219889				
3.87858	31.27489	0.219458		3.60807	30.77313	0.218944				
				3.73507	30.94518	0.220838				
				3.86207	31.1594	0.233367				

Geom:	2 rows PS			Geom:	2 rows PS			Geom:	2 rows PS	
VR	1.5			VR	1.5			VR	1.5	
Tu	0.12			Tu	0.12			Tu	0.12	
Lu (cm)	3.36			Lu (cm)	3.36			Lu (cm)	3.36	
Comb(1)				Comb(1)				Comb(1)		
Z/D =	0			Z/D =	0.75			Z/D =	1.5	
filename	p2cbv2a1			filename	p2cbv2q1			filename	p2cbv2m1	
Y(cm)	U(y)(m/s)	u' (m/s)		Y(cm)	U(y)(m/s)	u' (m/s)		Y(cm)	U(y)(m/s)	u' (m/s)
0.009144	14.2352	3.240164		0.009144	14.4206	3.252343		0.009144	14.76625	3.346348
0.010871	16.61401	3.765818		0.009601	15.0332	3.383291		0.010185	16.18373	3.710842
0.013333	18.97005	3.987508		0.011633	17.38084	3.934447		0.012647	19.08701	4.043266
0.015794	21.43535	4.043607		0.014095	20.10901	4.17829		0.015108	21.22725	4.209338
0.018255	22.9718	3.991982		0.016556	21.95664	4.228247		0.017569	22.91413	4.232056
0.020717	24.00696	3.851259		0.019017	23.43752	4.162044		0.020031	24.25213	4.123641
0.023178	24.94933	3.780397		0.021479	24.43876	4.010401		0.022492	25.18122	3.998511
0.025639	25.44979	3.724231		0.02394	25.30021	3.921194		0.024953	25.87055	3.905721
0.028101	26.06785	3.660635		0.026401	25.87321	3.869721		0.027415	26.31319	3.826982
0.030562	26.38862	3.552805		0.028863	26.34307	3.770768		0.029876	26.79194	3.764959
0.033023	26.73979	3.503105		0.031324	26.69251	3.674448		0.032337	27.01213	3.705516
0.035485	27.01057	3.391099		0.033785	27.02854	3.620838		0.034799	27.33381	3.595962
0.037946	27.25718	3.372994		0.036247	27.28389	3.529531		0.03726	27.4808	3.529538
0.040407	27.34939	3.303845		0.038708	27.47158	3.488866		0.039721	27.62893	3.466759
0.042869	27.51945	3.260083		0.041169	27.64223	3.436938		0.042183	27.81064	3.461145
0.04533	27.66516	3.259692		0.043631	27.82337	3.376797		0.044644	27.96583	3.39221
0.047791	27.75654	3.21199		0.046092	27.80567	3.330969		0.047105	28.04884	3.332528
0.050253	27.76787	3.177527		0.048553	27.94587	3.316174		0.049567	28.06985	3.350603
0.052714	27.86915	3.15568		0.051015	28.03931	3.280835		0.052028	28.2397	3.279945
0.055175	27.96502	3.160243		0.053476	28.10777	3.22436		0.05449	28.32287	3.252828
0.057637	28.02014	3.112724		0.055937	28.12792	3.224925		0.056951	28.35124	3.245157
0.060098	28.12797	3.088392		0.058399	28.23052	3.198749		0.059412	28.38022	3.202801
0.062559	28.17911	3.086269		0.06086	28.25416	3.209407		0.061874	28.44934	3.211088
0.065021	28.24755	3.086384		0.063321	28.34775	3.166041		0.064335	28.48228	3.22377
0.067482	28.20219	3.059594		0.065783	28.38645	3.119617		0.066796	28.44531	3.17591
0.069943	28.27859	3.072647		0.068244	28.39557	3.105439		0.069258	28.56617	3.195266
0.072405	28.30226	3.038715		0.070705	28.42827	3.107844		0.071719	28.60941	3.178548
0.074866	28.33848	3.037117		0.073167	28.46651	3.14693		0.07418	28.60588	3.154685
0.077327	28.40013	3.042074		0.075628	28.53943	3.119		0.076642	28.62246	3.148783
0.079789	28.41265	3.011891		0.078089	28.52949	3.09103		0.079103	28.60196	3.154084
0.08225	28.36425	3.034685		0.080551	28.50539	3.105443		0.081564	28.64495	3.111185
0.084711	28.50132	3.028319		0.083012	28.55556	3.086062		0.084026	28.7037	3.157872
								0.086487	28.75634	3.14088
0.06858	28.27704	3.107528		0.06858	28.34843	3.129369		0.088948	28.66638	3.101186
0.08382	28.50925	3.028512		0.08382	28.54278	3.087024		0.09141	28.66037	3.130346
0.1016	28.69064	3.036919		0.1016	28.61898	3.044705		0.093871	28.75658	3.111315
0.12446	28.82996	3.050112		0.12446	28.67037	3.062073		0.096332	28.73507	3.080882
0.1524	28.87929	3.106424		0.1524	28.62281	3.091584		0.098794	28.76037	3.097825
0.18542	28.6962	3.135246		0.18542	28.37669	3.128575		0.101255	28.721	3.102816
0.21844	28.29906	3.163091		0.21844	28.08817	3.130508		0.103716	28.77875	3.116549
0.25654	27.65097	3.149075		0.25654	27.50793	3.125696		0.106178	28.74043	3.057036
0.29718	27.12944	3.106313		0.29718	27.09243	3.119669				
0.37338	26.27959	2.977162		0.37338	26.29622	2.989872		0.0635	28.48037	3.181531
0.48768	25.80461	2.958194		0.48768	25.82016	3.011462		0.07874	28.69161	3.128981
0.61468	25.79116	2.959719		0.61468	25.77736	2.91619		0.09652	28.74668	3.044788
0.74168	25.87015	2.95591		0.74168	25.80604	2.93737		0.11938	28.69458	3.100205
0.86868	25.97977	2.976601		0.86868	25.96424	2.917002		0.14732	28.54638	3.067443
0.99568	26.07265	2.995802		0.99568	26.08688	2.950846		0.18034	28.30798	3.134664
1.12268	26.35022	3.010921		1.12268	26.18467	2.969205		0.21336	28.03221	3.129998
1.24968	26.45666	3.015382		1.24968	26.36778	3.033624		0.25146	27.52599	3.167702

Geom:	2 rows PS			Geom:	2 rows PS			Geom:	2 rows PS	
VR	1.5			VR	1.5			VR	1.5	
Tu	0.12			Tu	0.12			Tu	0.12	
Lu (cm)	3.36			Lu (cm)	3.36			Lu (cm)	3.36	
Comb(1)				Comb(1)				Comb(1)		
Z/D =	0			Z/D =	0.75			Z/D =	1.5	
filename	p2cbv2a1			filename	p2cbv2q1			filename	p2cbv2m1	
Y(cm)	U(y)(m/s)	u' (m/s)		Y(cm)	U(y)(m/s)	u' (m/s)		Y(cm)	U(y)(m/s)	u' (m/s)
1.37668	26.58382	3.077529		1.37668	26.58374	3.091014		0.2921	27.07513	3.113881
1.50368	26.84244	3.112971		1.50368	26.74503	3.079343		0.3683	26.28185	3.031183
1.63068	26.97286	3.13467		1.63068	26.93171	3.103896		0.4826	25.80883	2.937636
1.75768	27.21123	3.178157		1.75768	27.19937	3.123399		0.6096	25.77048	2.978485
1.88468	27.45933	3.194679		1.88468	27.39959	3.178846		0.7366	25.79746	2.949437
2.01168	27.66252	3.229063		2.01168	27.59639	3.203088		0.8636	26.03647	2.92565
2.13868	27.84292	3.264635		2.13868	27.81292	3.239424		0.9906	26.10664	2.984086
2.26568	28.11983	3.326866		2.26568	28.03528	3.277563		1.1176	26.27984	2.994262
2.39268	28.37614	3.320661		2.39268	28.24675	3.266872		1.2446	26.45763	3.007738
2.51968	28.54529	3.356609		2.51968	28.47009	3.337885		1.3716	26.60924	3.049041
2.64668	28.83218	3.336183		2.64668	28.77951	3.333108		1.4986	26.74049	3.092115
2.77368	29.04491	3.399611		2.77368	28.99025	3.390859		1.6256	27.05449	3.135066
2.90068	29.24126	3.413139		2.90068	29.24482	3.404521		1.7526	27.20297	3.170748
3.02768	29.40477	3.397304		3.02768	29.33707	3.396226		1.8796	27.42134	3.170987
3.15468	29.60483	3.428766		3.15468	29.58667	3.391671		2.0066	27.61467	3.20334
3.28168	29.87533	3.47592		3.28168	29.79361	3.43764		2.1336	27.80192	3.275842
3.40868	30.09268	3.467321		3.40868	30.00237	3.445463		2.2606	28.0289	3.232699
3.53568	30.27588	3.49925		3.53568	30.14042	3.410708		2.3876	28.32889	3.308341
3.66268	30.47074	3.497672		3.66268	30.36684	3.461185		2.5146	28.53382	3.340454
3.78968	30.62321	3.50908		3.78968	30.56407	3.513263		2.6416	28.78238	3.322554
3.91668	30.73125	3.530203		3.91668	30.68647	3.470888		2.7686	29.04267	3.367062
								2.8956	29.21987	3.388906
								3.0226	29.43743	3.418236
								3.1496	29.64335	3.426273
								3.2766	29.80521	3.449229
								3.4036	30.07777	3.449186
								3.5306	30.14405	3.47604
								3.6576	30.43604	3.465314
								3.7846	30.50611	3.513532
								3.9116	30.7087	3.509132

Geom:	2 rows PS			Geom:	2 rows PS			Geom:	2 rows PS	
VR	1			VR	1			VR	1	
Tu	0.12			Tu	0.12			Tu	0.12	
Lu (cm)	3.36			Lu (cm)	3.36			Lu (cm)	3.36	
Comb(1)				Comb(1)				Comb(1)		
Z/D =	0			Z/D =	0.75			Z/D =	1.5	
filename	p2cbv1a1			filename	p2cbv1q1			filename	p2cbv1m1	
Y(cm)	U(y)(m/s)	u' (m/s)		Y(cm)	U(y)(m/s)	u' (m/s)		Y(cm)	U(y)(m/s)	u' (m/s)
0.00889	11.30841	2.720385		0.00889	12.08291	2.927926		0.00889	11.85722	2.789107
0.009754	12.32339	3.032247		0.010998	14.67244	3.506718		0.010973	14.34461	3.386076
0.012215	15.03027	3.609506		0.01346	17.3021	3.80819		0.013434	16.93871	3.674824
0.014676	17.23426	3.770229		0.015921	19.22436	3.886001		0.015895	19.16713	3.772714
0.017138	19.50237	3.855794		0.018382	20.78923	3.812053		0.018357	20.52411	3.773492
0.019599	20.8429	3.800167		0.020844	21.72219	3.762915		0.020818	21.69869	3.715353
0.02206	21.75352	3.692214		0.023305	22.50723	3.618638		0.023279	22.54228	3.553521
0.024522	22.50967	3.544107		0.025766	23.21337	3.505507		0.025741	23.16565	3.461271
0.026983	23.15604	3.471762		0.028228	23.679	3.446519		0.028202	23.68181	3.384793
0.029444	23.6087	3.3826		0.030689	23.98758	3.311075		0.030664	23.97865	3.259035
0.031906	23.94215	3.276445		0.03315	24.27229	3.208336		0.033125	24.32675	3.184181
0.034367	24.22223	3.150217		0.035612	24.54531	3.151301		0.035586	24.51213	3.087564
0.036828	24.45463	3.099414		0.038073	24.69909	3.074113		0.038048	24.73101	3.04313
0.03929	24.59726	3.03712		0.040534	24.8807	3.051212		0.040509	24.89683	2.995686
0.041751	24.80327	3.004403		0.042996	24.99238	2.999178		0.04297	25.01541	2.934767
0.044212	24.84117	2.963852		0.045457	25.12949	2.962621		0.045432	25.06247	2.867599
0.046674	24.93986	2.941477		0.047918	25.17169	2.924029		0.047893	25.14764	2.859662
0.049135	25.08508	2.907649		0.05038	25.19876	2.890026		0.050354	25.24051	2.86715
0.051596	25.10458	2.860946		0.052841	25.2083	2.845112		0.052816	25.28722	2.783987
0.054058	25.14234	2.834842		0.055302	25.26988	2.851794		0.055277	25.31832	2.785378
0.056519	25.21935	2.845842		0.057764	25.38104	2.841296		0.057738	25.40841	2.748186
0.05898	25.27947	2.80567		0.060225	25.36257	2.802782		0.0602	25.39475	2.774438
0.061442	25.2284	2.780054		0.062686	25.40373	2.820696		0.062661	25.41951	2.742708
0.063903	25.29474	2.827676		0.065148	25.42148	2.837703		0.065122	25.43406	2.737648
0.066364	25.31693	2.818022		0.067609	25.42115	2.781872		0.067584	25.4398	2.752167
0.068826	25.36812	2.774651		0.07007	25.44818	2.823073		0.070045	25.47751	2.748894
0.071287	25.41384	2.790041		0.072532	25.47376	2.840706		0.072506	25.46343	2.735808
0.073748	25.43509	2.809784		0.074993	25.47879	2.79005		0.074968	25.52258	2.721858
0.07621	25.38525	2.801768		0.077454	25.48417	2.820229		0.077429	25.51203	2.73331
0.078671	25.44132	2.75212		0.079916	25.53338	2.785436		0.07989	25.60298	2.74156
0.081132	25.5015	2.772248		0.082377	25.58302	2.79713		0.082352	25.59465	2.747647
0.083594	25.47059	2.784223		0.084838	25.56498	2.77164		0.084813	25.62988	2.723068
0.086055	25.54981	2.775563		0.0873	25.54609	2.773971		0.087274	25.58098	2.706105
0.088516	25.53465	2.773959		0.089761	25.64799	2.827847		0.089736	25.60973	2.736783
0.090978	25.51043	2.758129		0.092222	25.59297	2.817666		0.092197	25.67993	2.730117
0.093439	25.53877	2.784239		0.094684	25.63045	2.78239		0.094658	25.66945	2.712903
0.0959	25.56215	2.763404		0.097145	25.66957	2.787513		0.09712	25.69457	2.732623
0.098362	25.58819	2.794069		0.099606	25.70997	2.775304		0.099581	25.76728	2.736146
0.100823	25.60391	2.773016		0.102068	25.70059	2.81304		0.102042	25.75546	2.738233
0.103284	25.64033	2.797832								
0.105746	25.68168	2.799796		0.05334	25.27711	2.824249		0.05334	25.33216	2.765683
				0.06858	25.43988	2.783293		0.06858	25.54959	2.72401
0.06604	25.34374	2.795392		0.08636	25.59412	2.811358		0.08636	25.65886	2.734293
0.08128	25.50436	2.775869		0.10922	25.77144	2.776636		0.10922	25.79601	2.781165
0.09906	25.63641	2.785145		0.13716	26.04011	2.838804		0.13716	26.05409	2.78615
0.12192	25.82862	2.796976		0.17018	26.17124	2.872615		0.17018	26.17724	2.835156
0.14986	26.11326	2.855592		0.2032	26.20989	2.845964		0.2032	26.19232	2.820289
0.18288	26.17591	2.8469		0.2413	26.19551	2.876123		0.2413	26.2498	2.8154
0.2159	26.24115	2.872503		0.28194	26.13839	2.913259		0.28194	26.18865	2.779952
0.254	26.17955	2.873085		0.35814	26.09178	2.91429		0.35814	26.12363	2.83445

Geom:	2 rows PS			Geom:	2 rows PS			Geom:	2 rows PS	
VR	1			VR	1			VR	1	
Tu	0.12			Tu	0.12			Tu	0.12	
Lu (cm)	3.36			Lu (cm)	3.36			Lu (cm)	3.36	
Comb(1)				Comb(1)				Comb(1)		
Z/D =	0			Z/D =	0.75			Z/D =	1.5	
filename	p2cbv1a1			filename	p2cbv1q1			filename	p2cbv1m1	
Y(cm)	U(y)(m/s)	u' (m/s)		Y(cm)	U(y)(m/s)	u' (m/s)		Y(cm)	U(y)(m/s)	u' (m/s)
0.29464	26.13379	2.896936		0.47244	25.97132	2.925786		0.47244	26.01195	2.81782
0.37084	26.03877	2.89767		0.59944	26.06585	2.933193		0.59944	26.04535	2.837592
0.48514	25.96284	2.912724		0.72644	26.09592	2.959818		0.72644	26.10742	2.855507
0.61214	26.0528	2.930625		0.85344	26.23776	2.957177		0.85344	26.21945	2.883208
0.73914	26.08967	2.937619		0.98044	26.31815	3.013499		0.98044	26.32721	2.844615
0.86614	26.16479	2.914349		1.10744	26.38741	2.960026		1.10744	26.43219	2.904892
0.99314	26.31041	2.994375		1.23444	26.57528	3.024469		1.23444	26.65126	2.935726
1.12014	26.45768	3.012884		1.36144	26.82254	3.060613		1.36144	26.82277	2.976956
1.24714	26.62747	3.045727		1.48844	26.95417	3.077455		1.48844	27.02266	2.996296
1.37414	26.81386	3.064095		1.61544	27.17077	3.112928		1.61544	27.10279	3.03229
1.50114	27.00004	3.137896		1.74244	27.35661	3.142757		1.74244	27.34918	3.092328
1.62814	27.18488	3.104899		1.86944	27.61968	3.166638		1.86944	27.5455	3.093449
1.75514	27.36603	3.14228		1.99644	27.83274	3.210899		1.99644	27.82147	3.096818
1.88214	27.58133	3.173596		2.12344	27.9893	3.22666		2.12344	28.04647	3.144425
2.00914	27.81019	3.245477		2.25044	28.26945	3.272788		2.25044	28.2024	3.176023
2.13614	27.97999	3.263317		2.37744	28.48783	3.301053		2.37744	28.40552	3.207399
2.26314	28.26798	3.284007		2.50444	28.74287	3.355885		2.50444	28.62063	3.254261
2.39014	28.46797	3.33902		2.63144	28.95992	3.377141		2.63144	28.91345	3.269118
2.51714	28.75913	3.343243		2.75844	29.15331	3.362417		2.75844	29.14926	3.301951
2.64414	28.89593	3.382679		2.88544	29.35297	3.402667		2.88544	29.29991	3.321418
2.77114	29.11568	3.382223		3.01244	29.58709	3.437694		3.01244	29.59887	3.337168
2.89814	29.43111	3.392674		3.13944	29.78323	3.426826		3.13944	29.72967	3.342103
3.02514	29.50323	3.428346		3.26644	29.95585	3.469187		3.26644	29.95798	3.399459
3.15214	29.76295	3.439386		3.39344	30.15141	3.473871		3.39344	30.23059	3.417136
3.27914	29.98238	3.473441		3.52044	30.37543	3.462811		3.52044	30.36249	3.33663
3.40614	30.17683	3.470194		3.64744	30.53921	3.477814		3.64744	30.57864	3.391198
3.53314	30.43236	3.498924		3.77444	30.69735	3.542809		3.77444	30.68979	3.40068
3.66014	30.5899	3.509839		3.90144	30.86267	3.524659		3.90144	30.83333	3.416781
3.78714	30.69716	3.494985								
3.91414	30.80283	3.54178								

Geom:	2 rows PS			Geom:	2 rows PS			Geom:	2 rows PS	
VR	0.5			VR	0.5			VR	0.5	
Tu	0.12			Tu	0.12			Tu	0.12	
Lu (cm)	3.36			Lu (cm)	3.36			Lu (cm)	3.36	
Comb(1)				Comb(1)				Comb(1)		
Z/D =	0			Z/D =	0.75			Z/D =	1.5	
filename	p2cbv5a1			filename	p2cbv5q1			filename	p2cbv5m1	
Y(cm)	U(y)(m/s)	u' (m/s)		Y(cm)	U(y)(m/s)	u' (m/s)		Y(cm)	U(y)(m/s)	u' (m/s)
0.00889	10.78041	2.919373		0.008636	10.00017	2.665793		0.00889	10.66532	2.853011
0.01082	12.87247	3.383524		0.010338	11.75088	3.080002		0.011217	13.04573	3.273
0.013282	15.21397	3.58354		0.012799	13.96282	3.462323		0.013678	15.15924	3.522492
0.015743	16.88827	3.646367		0.01526	15.83005	3.610705		0.01614	16.82503	3.592627
0.018204	18.08736	3.617293		0.017722	17.40513	3.660755		0.018601	17.86423	3.568853
0.020666	18.88241	3.607698		0.020183	18.39952	3.577124		0.021062	18.88442	3.564276
0.023127	19.58595	3.511872		0.022644	19.13678	3.54076		0.023524	19.63109	3.521582
0.025588	20.07335	3.467125		0.025106	19.76424	3.478988		0.025985	20.22275	3.446335
0.02805	20.61993	3.408155		0.027567	20.3774	3.420135		0.028446	20.56407	3.411608
0.030511	20.95798	3.398267		0.030029	20.68779	3.380838		0.030908	20.89544	3.338943
0.032972	21.2403	3.359381		0.03249	21.03086	3.341879		0.033369	21.23066	3.313314
0.035434	21.49495	3.252738		0.034951	21.23953	3.299852		0.03583	21.47533	3.306967
0.037895	21.70471	3.255817		0.037413	21.62997	3.283843		0.038292	21.66189	3.278226
0.040356	21.93952	3.226316		0.039874	21.78461	3.25517		0.040753	21.88497	3.26912
0.042818	22.06805	3.219175		0.042335	21.94548	3.228953		0.043214	21.97523	3.21644
0.045279	22.19182	3.208573		0.044797	22.08942	3.202511		0.045676	22.12597	3.196344
0.04774	22.31735	3.217883		0.047258	22.17804	3.190293		0.048137	22.24602	3.175828
0.050202	22.44378	3.151015		0.049719	22.31444	3.195109		0.050599	22.39003	3.160727
0.052663	22.53007	3.194421		0.052181	22.41194	3.188031		0.05306	22.4174	3.140362
0.055125	22.5996	3.197005		0.054642	22.50122	3.177757		0.055521	22.48196	3.162859
0.057586	22.63291	3.167243		0.057103	22.61823	3.156075		0.057983	22.58912	3.171031
0.060047	22.73412	3.16752		0.059565	22.62501	3.188692		0.060444	22.67083	3.167865
0.062509	22.85496	3.155301		0.062026	22.66089	3.182699		0.062905	22.70731	3.123429
0.06497	22.91796	3.178859		0.064487	22.75012	3.158008		0.065367	22.8327	3.15705
0.067431	22.96897	3.218598		0.066949	22.8448	3.153855		0.067828	22.83592	3.152017
0.069893	23.03006	3.226207		0.06941	22.90137	3.192529		0.070289	22.93105	3.164778
0.072354	23.1028	3.172409		0.071871	22.98463	3.190876		0.072751	22.99179	3.193748
0.074815	23.09873	3.192898		0.074333	23.04232	3.176015		0.075212	23.0568	3.193913
0.077277	23.1555	3.202183		0.076794	23.09445	3.201166		0.077673	23.09297	3.195769
0.079738	23.25131	3.197171		0.079255	23.20704	3.204906		0.080135	23.17983	3.179501
0.082199	23.30684	3.222714		0.081717	23.23299	3.171512		0.082596	23.20165	3.193988
0.084661	23.36391	3.198498		0.084178	23.28662	3.211914		0.085057	23.29823	3.203337
0.087122	23.39029	3.232482		0.086639	23.37298	3.222253		0.087519	23.34594	3.186707
0.089583	23.4295	3.200662		0.089101	23.35669	3.214278		0.08998	23.31379	3.193222
0.092045	23.51443	3.231875		0.091562	23.42367	3.183026		0.092441	23.42424	3.22378
0.0635	22.79401	3.164675		0.0635	22.82887	3.165864		0.09144	23.36933	3.208492
0.07874	23.24358	3.208641		0.07874	23.17308	3.18561		0.1143	23.81599	3.225492
0.09652	23.67542	3.208981		0.09652	23.62706	3.196621		0.14224	24.43661	3.193511
0.11938	24.14163	3.246323		0.11938	24.13756	3.228321		0.17526	24.83704	3.083089
0.14732	24.72388	3.219212		0.14732	24.64569	3.167331		0.20828	25.06002	3.047153
0.18034	25.06636	3.097325		0.18034	24.94515	3.087469		0.24638	25.25885	2.964318
0.21336	25.29307	3.068489		0.21336	25.13733	3.017488		0.28702	25.35447	2.889968
0.25146	25.43703	3.030148		0.25146	25.33931	2.950509		0.36322	25.37251	2.860682
0.2921	25.47758	2.933134		0.2921	25.30703	2.889435		0.47752	25.44213	2.864222
0.3683	25.5725	2.865051		0.3683	25.42416	2.873398		0.60452	25.46656	2.858127
0.4826	25.63654	2.859994		0.4826	25.46107	2.829792		0.73152	25.5333	2.846125
0.6096	25.66611	2.85297		0.6096	25.50629	2.835425		0.85852	25.62387	2.885181
0.7366	25.71088	2.877536		0.7366	25.58528	2.843233		0.98552	25.71942	2.878394
0.8636	25.8269	2.878932		0.8636	25.66973	2.891349		1.11252	25.9367	2.932974

Geom:	2 rows PS			Geom:	2 rows PS			Geom:	2 rows PS	
VR	0.5			VR	0.5			VR	0.5	
Tu	0.12			Tu	0.12			Tu	0.12	
Lu (cm)	3.36			Lu (cm)	3.36			Lu (cm)	3.36	
Comb(1)				Comb(1)				Comb(1)		
Z/D =	0			Z/D =	0.75			Z/D =	1.5	
filename	p2cbv5a1			filename	p2cbv5q1			filename	p2cbv5m1	
Y(cm)	U(y)(m/s)	u' (m/s)		Y(cm)	U(y)(m/s)	u' (m/s)		Y(cm)	U(y)(m/s)	u' (m/s)
0.9906	25.90651	2.919537		0.9906	25.82812	2.929097		1.23952	26.10412	2.923103
1.1176	26.07617	2.96575		1.1176	25.95342	2.915895		1.36652	26.24244	2.980989
1.2446	26.26143	2.984065		1.2446	26.13107	2.968312		1.49352	26.42302	3.016185
1.3716	26.33002	2.986143		1.3716	26.26627	2.988881		1.62052	26.61378	3.020403
1.4986	26.62592	3.017971		1.4986	26.44642	3.001195		1.74752	26.73756	3.044248
1.6256	26.79151	3.084967		1.6256	26.73274	3.051676		1.87452	27.03814	3.088429
1.7526	26.99003	3.121165		1.7526	26.91743	3.112449		2.00152	27.22787	3.131379
1.8796	27.23632	3.146253		1.8796	26.99461	3.119389		2.12852	27.38681	3.153063
2.0066	27.41499	3.172548		2.0066	27.30283	3.191239		2.25552	27.60068	3.141319
2.1336	27.5876	3.190045		2.1336	27.43064	3.220047		2.38252	27.84467	3.245625
2.2606	27.87863	3.233807		2.2606	27.69032	3.2032		2.50952	28.09336	3.234183
2.3876	27.97779	3.273001		2.3876	27.95228	3.239085		2.63652	28.27237	3.266762
2.5146	28.28268	3.27488		2.5146	28.09522	3.256966		2.76352	28.52206	3.2815
2.6416	28.53062	3.299683		2.6416	28.36442	3.287589		2.89052	28.66564	3.266169
2.7686	28.7502	3.311089		2.7686	28.58296	3.341697		3.01752	28.93775	3.310047
2.8956	28.91594	3.338163		2.8956	28.77327	3.316275		3.14452	29.10858	3.370331
3.0226	29.17986	3.33337		3.0226	29.07573	3.368182		3.27152	29.27035	3.327348
3.1496	29.32908	3.389527		3.1496	29.17365	3.382025		3.39852	29.48289	3.375596
3.2766	29.46958	3.387446		3.2766	29.40329	3.360999		3.52552	29.65183	3.352602
3.4036	29.70568	3.428867		3.4036	29.61089	3.364543		3.65252	29.81943	3.381664
3.5306	29.90695	3.411354		3.5306	29.77992	3.393371		3.77952	29.98895	3.415334
3.6576	30.06986	3.430258		3.6576	29.92605	3.425668		3.90652	30.19973	3.434165
3.7846	30.29259	3.452047		3.7846	30.08346	3.461568				
3.9116	30.37453	3.419789		3.9116	30.20147	3.443402				

Geom:	2 rows PS			Geom:	2 rows PS			Geom:	2 rows PS	
VR	1.5			VR	1.5			VR	1.5	
Tu	0.011			Tu	0.011			Tu	0.011	
Lu (cm)	6.6			Lu (cm)	6.6			Lu (cm)	6.6	
Low Tu				Low Tu				Low Tu		
Z/D =	0			Z/D =	0.75			Z/D =	1.5	
filename	p2clv2a3			filename	p2cbv2q1			filename	p2clv2m1	
Y(cm)	U(y)(m/s)	u' (m/s)		Y(cm)	U(y)(m/s)	u' (m/s)		Y(cm)	U(y)(m/s)	u' (m/s)
0.01016	14.06373	2.344474		0.00889	18.38993	2.747325		0.01016	14.35899	2.608629
0.011938	16.09757	2.54808		0.009906	19.87258	2.896854		0.011278	15.70081	2.785743
0.014399	18.21381	2.596064		0.012367	22.34971	2.850969		0.013739	18.12898	2.854325
0.016861	19.98571	2.541551		0.014829	23.89386	2.797699		0.0162	19.93812	2.80136
0.019322	21.41229	2.480078		0.01729	25.1755	2.689111		0.018662	21.12487	2.707277
0.021783	22.40767	2.399451		0.019751	25.93453	2.539874		0.021123	22.24723	2.623958
0.024245	23.21675	2.329511		0.022213	26.45948	2.41867		0.023584	22.9753	2.536946
0.026706	23.94339	2.273349		0.024674	26.88818	2.330628		0.026046	23.66612	2.470203
0.029167	24.4536	2.173585		0.027135	27.27718	2.246414		0.028507	24.15728	2.372609
0.031629	24.93048	2.132086		0.029597	27.56832	2.149703		0.030968	24.64161	2.28693
0.03409	25.28034	2.101617		0.032058	27.76698	2.072479		0.03343	25.00644	2.245602
0.036551	25.50809	2.054918		0.034519	27.93208	2.000074		0.035891	25.26255	2.181317
0.039013	25.71426	2.020377		0.036981	28.05201	1.943608		0.038352	25.55431	2.166844
0.041474	25.88127	1.988847		0.039442	28.18342	1.903235		0.040814	25.76936	2.113912
0.043935	26.0506	1.957914		0.041903	28.32046	1.856657		0.043275	25.97089	2.08363
0.046397	26.17055	1.94179		0.044365	28.35274	1.811631		0.045736	26.18399	2.030643
0.048858	26.25769	1.928042		0.046826	28.41679	1.780531		0.048198	26.34612	1.997917
0.051319	26.3056	1.915734		0.049287	28.52522	1.761771		0.050659	26.50899	1.962659
0.053781	26.42093	1.928682		0.051749	28.53922	1.762145		0.05312	26.63243	1.953486
0.056242	26.47012	1.919615		0.05421	28.57069	1.728502		0.055582	26.74164	1.924769
0.058703	26.52397	1.906142		0.056671	28.61232	1.739799		0.058043	26.89857	1.914616
0.061165	26.5458	1.924403		0.059133	28.64416	1.720104		0.060504	27.00312	1.880368
0.063626	26.54469	1.923813		0.061594	28.67814	1.719211		0.062966	27.09229	1.906241
0.066087	26.62727	1.943535		0.064055	28.67744	1.69864		0.065427	27.20919	1.877391
0.068549	26.65202	1.958454		0.066517	28.72749	1.708349		0.067888	27.31443	1.850365
0.07101	26.62532	1.946041		0.068978	28.70739	1.705724		0.07035	27.38981	1.848754
0.073471	26.63598	1.94914		0.071439	28.7377	1.675575		0.072811	27.51728	1.840803
0.075933	26.67594	1.960932		0.073901	28.73455	1.703367		0.075272	27.56744	1.838916
0.078394	26.69546	1.994671		0.076362	28.7716	1.704294		0.077734	27.69315	1.815968
0.080856	26.7326	1.982094		0.078824	28.75846	1.706285		0.080195	27.76509	1.805479
0.083317	26.77311	1.990209		0.081285	28.74034	1.722601		0.082656	27.82985	1.821764
0.085778	26.72716	2.004426		0.083746	28.71633	1.698477		0.085118	27.94444	1.796689
0.08824	26.81533	1.999164		0.086208	28.71872	1.71921				
0.090701	26.80498	2.040972		0.088669	28.73016	1.716307		0.07874	27.72989	1.807009
0.093162	26.79226	2.003443		0.09113	28.73905	1.71353		0.1016	28.37982	1.767263
0.095624	26.84196	2.030835		0.093592	28.72448	1.713845		0.12954	28.95164	1.753758
0.098085	26.85542	2.044994		0.096053	28.69087	1.757885		0.16256	29.39755	1.809536
0.100546	26.90497	2.059689		0.098514	28.69171	1.719226		0.19558	29.60353	1.940164
0.103008	26.86503	2.042891		0.100976	28.67237	1.740827		0.23368	29.29437	2.174337
0.105469	26.91359	2.047885		0.103437	28.66859	1.745575		0.27432	27.96124	2.241872
0.10793	26.93417	2.056477		0.105898	28.64521	1.741208		0.35052	25.43457	0.936346
0.110392	26.9661	2.059605		0.10836	28.62036	1.749024		0.46482	25.265	0.221542
				0.110821	28.59804	1.761079		0.59182	25.41511	0.195712
0.07874	26.72987	1.97017		0.113282	28.57936	1.727056		0.71882	25.5123	0.204301
0.09652	26.86641	2.046751		0.115744	28.56588	1.763619		0.84582	25.68648	0.197992
0.11938	27.06378	2.03193		0.118205	28.55823	1.77842		0.97282	25.85578	0.194779
0.14732	27.05482	1.988122		0.120666	28.53	1.764948		1.09982	26.03199	0.195137
0.18034	26.23827	1.736694		0.123128	28.50235	1.776327		1.22682	26.2175	0.193124
0.21336	25.34131	1.150471		0.125589	28.53	1.764948		1.35382	26.41446	0.197098
0.25146	24.94682	0.614434						1.48082	26.61252	0.206125

Geom:	2 rows PS			Geom:	2 rows PS			Geom:	2 rows PS	
VR	1.5			VR	1.5			VR	1.5	
Tu	0.011			Tu	0.011			Tu	0.011	
Lu (cm)	6.6			Lu (cm)	6.6			Lu (cm)	6.6	
Low Tu				Low Tu				Low Tu		
Z/D =	0			Z/D =	0.75			Z/D =	1.5	
filename	p2clv2a3			filename	p2cbv2q1			filename	p2clv2m1	
Y(cm)	U(y)(m/s)	u' (m/s)		Y(cm)	U(y)(m/s)	u' (m/s)		Y(cm)	U(y)(m/s)	u' (m/s)
0.2921	24.86632	0.370249		0.10922	28.62457	1.723725		1.60782	26.84187	0.203303
0.3683	24.96344	0.22989		0.13716	28.38805	1.75938		1.73482	27.07162	0.193775
0.4826	25.05036	0.198556		0.17018	28.0054	1.803635		1.86182	27.28203	0.209953
0.6096	25.19259	0.196456		0.2032	27.63066	1.83541		1.98882	27.54819	0.197675
0.7366	25.32163	0.19253		0.2413	27.1751	1.829891		2.11582	27.79799	0.20473
0.8636	25.44386	0.19488		0.28194	26.29741	1.584738		2.24282	28.05274	0.199874
0.9906	25.61302	0.191728		0.35814	25.12553	0.588208		2.36982	28.32079	0.205497
1.1176	25.72148	0.201953		0.47244	25.14426	0.212269		2.49682	28.56031	0.217149
1.2446	25.93495	0.194612		0.59944	25.28827	0.199702		2.62382	28.81651	0.200713
1.3716	26.11713	0.19465		0.72644	25.40595	0.197873		2.75082	29.05844	0.205899
1.4986	26.30339	0.202401		0.85344	25.5416	0.204634		2.87782	29.33178	0.203776
1.6256	26.5217	0.191437		0.98044	25.73341	0.193454		3.00482	29.56518	0.206948
1.7526	26.74647	0.197449		1.10744	25.91433	0.195471		3.13182	29.79845	0.205242
1.8796	26.95737	0.198507		1.23444	26.09609	0.194596		3.25882	30.04041	0.206383
2.0066	27.21023	0.195544		1.36144	26.2743	0.199278		3.38582	30.23864	0.220884
2.1336	27.42896	0.194909		1.48844	26.47993	0.200002		3.51282	30.45944	0.213249
2.2606	27.68287	0.199541		1.61544	26.71788	0.196432		3.63982	30.65597	0.209954
2.3876	27.95708	0.210803		1.74244	26.93131	0.207205		3.76682	30.87174	0.207633
2.5146	28.17281	0.201481		1.86944	27.19083	0.200983		3.89382	31.03909	0.205318
2.6416	28.42257	0.199731		1.99644	27.41975	0.20648				
2.7686	28.67185	0.205171		2.12344	27.67939	0.199375				
2.8956	28.89956	0.201278		2.25044	27.9361	0.212789				
3.0226	29.1346	0.201108		2.37744	28.17027	0.205957				
3.1496	29.34417	0.203746		2.50444	28.42539	0.202552				
3.2766	29.581	0.210265		2.63144	28.68771	0.20588				
3.4036	29.78908	0.203106		2.75844	28.92721	0.206868				
3.5306	30.02399	0.206386		2.88544	29.1721	0.212045				
3.6576	30.17442	0.21872		3.01244	29.41914	0.205131				
3.7846	30.36185	0.211939		3.13944	29.64947	0.207277				
3.9116	30.57331	0.207453		3.26644	29.88636	0.199711				
				3.39344	30.11634	0.206219				
				3.52044	30.31982	0.213059				
				3.64744	30.50647	0.212807				
				3.77444	30.70272	0.207159				
				3.90144	30.90139	0.21528				

Geom:	2 rows PS			Geom:	2 rows PS			Geom:	2 rows PS	
VR	1			VR	1			VR	1	
Tu	0.011			Tu	0.011			Tu	0.011	
Lu (cm)	6.6			Lu (cm)	6.6			Lu (cm)	6.6	
Low Tu				Low Tu				Low Tu		
Z/D =	0			Z/D =	0.75			Z/D =	1.5	
filename	p2clv1a1			filename	p2clv1q1			filename	p2clv1m1	
Y(cm)	U(y)(m/s)	u' (m/s)		Y(cm)	U(y)(m/s)	u' (m/s)		Y(cm)	U(y)(m/s)	u' (m/s)
0.012192	11.74524	1.854901		0.009652	13.29395	1.716034		0.01143	12.1065	2.280081
0.014653	13.6306	1.930924		0.010541	14.42192	1.81828		0.013716	14.21176	2.386722
0.017115	15.24518	1.967703		0.012573	16.89795	2.000376		0.016177	16.00474	2.355606
0.019576	16.78271	1.964128		0.015034	19.6551	1.917758		0.018639	17.5307	2.269994
0.022037	18.02473	1.868595		0.017496	21.54821	1.742342		0.0211	18.64874	2.192732
0.024499	19.00513	1.838435		0.019957	22.82198	1.571564		0.023561	19.48621	2.094454
0.02696	19.8667	1.778964		0.022418	23.60997	1.4184		0.026023	20.37188	1.987896
0.029421	20.5043	1.689125		0.02488	24.15749	1.321356		0.028484	21.03647	1.91301
0.031883	21.05254	1.637794		0.027341	24.54064	1.239877		0.030945	21.54289	1.825646
0.034344	21.48423	1.572512		0.029802	24.7121	1.204997		0.033407	21.95223	1.738176
0.036805	21.81038	1.528423		0.032264	24.9117	1.146989		0.035868	22.38186	1.692556
0.039267	22.05935	1.480368		0.034725	25.00964	1.147565		0.038329	22.75246	1.601623
0.041728	22.26017	1.468917		0.037186	25.06805	1.110084		0.040791	23.01503	1.534975
0.044189	22.45783	1.460907		0.039648	25.13175	1.103009		0.043252	23.34207	1.478001
0.046651	22.57947	1.431229		0.042109	25.18419	1.100642		0.045713	23.54115	1.416059
0.049112	22.66144	1.429133		0.04457	25.23454	1.096135		0.048175	23.73965	1.400457
0.051573	22.7385	1.439906		0.047032	25.25248	1.106883		0.050636	23.90923	1.328786
0.054035	22.78095	1.439865		0.049493	25.27813	1.09304		0.053097	24.0351	1.305915
0.056496	22.78694	1.433955		0.051954	25.2804	1.09206		0.055559	24.20035	1.271547
0.058957	22.83203	1.456882		0.054416	25.29893	1.110079		0.05802	24.30279	1.262493
0.061419	22.78498	1.452937		0.056877	25.29398	1.104846		0.060481	24.40322	1.239874
0.06388	22.83395	1.446524		0.059338	25.31745	1.114777		0.062943	24.53307	1.233314
0.066341	22.78316	1.464815		0.0618	25.31921	1.132171		0.065404	24.59506	1.214929
0.068803	22.80731	1.454535		0.064261	25.29603	1.127018		0.067865	24.67445	1.206356
0.071264	22.85876	1.474621		0.066722	25.3143	1.141246		0.070327	24.72845	1.19184
0.073725	22.79107	1.465544		0.069184	25.33696	1.135988		0.072788	24.81246	1.191473
0.076187	22.75798	1.476583		0.071645	25.30841	1.141148		0.075249	24.87576	1.186664
0.078648	22.78044	1.489094		0.074106	25.36393	1.129299		0.077711	24.93506	1.199274
0.08111	22.79143	1.498817		0.076568	25.36475	1.146221		0.080172	24.95119	1.205518
0.083571	22.81902	1.520696		0.079029	25.37911	1.132295		0.082634	25.0221	1.199772
0.086032	22.8344	1.527406		0.081491	25.3722	1.130791		0.085095	25.04784	1.194171
0.088494	22.83964	1.555314		0.083952	25.37772	1.125598		0.087556	25.07611	1.219118
0.090955	22.86958	1.538017		0.086413	25.36382	1.141311		0.090018	25.08388	1.2201
				0.088875	25.37992	1.121985		0.092479	25.12642	1.224551
0.0762	22.78584	1.47735		0.091336	25.39695	1.124707		0.09494	25.1681	1.252478
0.09398	22.91842	1.571012						0.097402	25.15459	1.244541
0.11684	23.58793	1.667313		0.0889	25.3934	1.121884		0.099863	25.20052	1.253327
0.14478	24.66758	1.33219		0.10668	25.45156	1.046009		0.102324	25.18532	1.26569
0.1778	25.01481	0.776948		0.12954	25.47721	0.942011		0.104786	25.19595	1.282715
0.21082	24.89021	0.416698		0.15748	25.37494	0.820737		0.107247	25.19802	1.281939
0.24892	24.93425	0.246914		0.1905	25.24551	0.663737		0.109708	25.19799	1.267497
0.28956	24.96816	0.212371		0.22352	25.09585	0.488467		0.11217	25.25953	1.293579
0.36576	25.06549	0.198371		0.26162	24.99712	0.317159				
0.48006	25.14913	0.194947		0.30226	25.01367	0.230895		0.09398	25.24954	1.267391
0.60706	25.27987	0.197184		0.37846	25.0885	0.196597		0.11684	25.25758	1.32965
0.73406	25.37538	0.201643		0.49276	25.19678	0.195017		0.14478	25.23729	1.310154
0.86106	25.52319	0.194824		0.61976	25.30742	0.192563		0.1778	25.43403	1.195839
0.98806	25.67469	0.195715		0.74676	25.44342	0.20098		0.21082	25.48041	0.992041
1.11506	25.80995	0.19885		0.87376	25.55954	0.194488		0.24892	25.1424	0.644996
1.24206	25.98627	0.195438		1.00076	25.71716	0.192235		0.28956	24.9829	0.322979

Geom:	2 rows PS			Geom:	2 rows PS			Geom:	2 rows PS	
VR	1			VR	1			VR	1	
Tu	0.011			Tu	0.011			Tu	0.011	
Lu (cm)	6.6			Lu (cm)	6.6			Lu (cm)	6.6	
Low Tu				Low Tu				Low Tu		
Z/D =	0			Z/D =	0.75			Z/D =	1.5	
filename	p2clv1a1			filename	p2clv1q1			filename	p2clv1m1	
Y(cm)	U(y)(m/s)	u' (m/s)		Y(cm)	U(y)(m/s)	u' (m/s)		Y(cm)	U(y)(m/s)	u' (m/s)
1.36906	26.17968	0.200092		1.12776	25.86658	0.199607		0.36576	25.05833	0.197824
1.49606	26.36854	0.196016		1.25476	26.02286	0.205493		0.48006	25.18147	0.196044
1.62306	26.58609	0.204106		1.38176	26.22204	0.198345		0.60706	25.31823	0.198743
1.75006	26.78904	0.210525		1.50876	26.40291	0.201887		0.73406	25.41628	0.193458
1.87706	27.02493	0.200444		1.63576	26.60574	0.196798		0.86106	25.54085	0.19723
2.00406	27.23309	0.209469		1.76276	26.81828	0.204323		0.98806	25.69821	0.194605
2.13106	27.48082	0.20437		1.88976	27.04885	0.197945		1.11506	25.81333	0.198513
2.25806	27.73887	0.200818		2.01676	27.27529	0.207931		1.24206	26.01074	0.19562
2.38506	27.98737	0.20325		2.14376	27.53225	0.199533		1.36906	26.16947	0.202811
2.51206	28.20311	0.214447		2.27076	27.78097	0.204765		1.49606	26.37507	0.192754
2.63906	28.44983	0.20642		2.39776	28.0049	0.20579		1.62306	26.5781	0.195301
2.76606	28.67654	0.20833		2.52476	28.25784	0.200142		1.75006	26.77464	0.203069
2.89306	28.92948	0.20327		2.65176	28.50304	0.206501		1.87706	27.01477	0.203451
3.02006	29.1741	0.209615		2.77876	28.71566	0.203861		2.00406	27.23175	0.207001
3.14706	29.33919	0.224445		2.90576	28.98034	0.202445		2.13106	27.46372	0.212736
3.27406	29.59793	0.219438		3.03276	29.20651	0.208101		2.25806	27.71528	0.199127
3.40106	29.81591	0.219647		3.15976	29.42681	0.205998		2.38506	27.93631	0.211275
3.52806	30.0236	0.209461		3.28676	29.66818	0.213322		2.51206	28.20043	0.206094
3.65506	30.21283	0.207698		3.41376	29.86962	0.209302		2.63906	28.43617	0.203851
3.78206	30.38882	0.219097		3.54076	30.07848	0.211991		2.76606	28.66888	0.205688
3.90906	30.56195	0.212659		3.66776	30.28477	0.21295		2.89306	28.91841	0.204534
				3.79476	30.43856	0.221278		3.02006	29.14852	0.208483
				3.92176	30.64852	0.213522		3.14706	29.34382	0.214171
								3.27406	29.58601	0.214239
								3.40106	29.79471	0.215511
								3.52806	29.97804	0.225271
								3.65506	30.20903	0.21429
								3.78206	30.34496	0.21846
								3.90906	30.53298	0.218238

Geom:	2 rows PS			Geom:	2 rows PS			Geom:	2 rows PS	
VR	0.5			VR	0.5			VR	0.5	
Tu	0.011			Tu	0.011			Tu	0.011	
Lu (cm)	6.6			Lu (cm)	6.6			Lu (cm)	6.6	
Low Tu				Low Tu				Low Tu		
Z/D =	0			Z/D =	0.75			Z/D =	1.5	
filename	p2clv5a1			filename	p2clv5q1			filename	p2clv5m1	
Y(cm)	U(y)(m/s)	u' (m/s)		Y(cm)	U(y)(m/s)	u' (m/s)		Y(cm)	U(y)(m/s)	u' (m/s)
0.01016	9.039479	1.567436		0.00889	11.9329	1.518183		0.00889	8.549638	1.408072
0.012395	10.43055	1.64861		0.009888	13.16695	1.648147		0.010922	10.18738	1.555574
0.014857	11.76551	1.662103		0.01235	15.71432	1.81136		0.013383	11.76144	1.668982
0.017318	12.90873	1.649436		0.014811	18.00078	1.75751		0.015845	13.18179	1.66563
0.019779	13.83948	1.613758		0.017272	19.51275	1.635232		0.018306	14.41385	1.678986
0.022241	14.52942	1.581459		0.019734	20.59013	1.48358		0.020767	15.40033	1.636958
0.024702	15.14525	1.546692		0.022195	21.31747	1.362621		0.023229	16.24426	1.572929
0.027163	15.64852	1.577488		0.024656	21.82279	1.249174		0.02569	16.98136	1.520589
0.029625	16.00081	1.55978		0.027118	22.13674	1.163298		0.028151	17.57057	1.471249
0.032086	16.27198	1.532057		0.029579	22.39394	1.080973		0.030613	18.06443	1.43809
0.034547	16.48203	1.54106		0.03204	22.58198	1.024225		0.033074	18.50767	1.382739
0.037009	16.66485	1.52662		0.034502	22.73567	0.978034		0.035535	18.80528	1.334731
0.03947	16.79024	1.54666		0.036963	22.85117	0.94381		0.037997	19.12172	1.330178
0.041931	16.89406	1.520188		0.039424	22.95145	0.92031		0.040458	19.31899	1.28848
0.044393	16.96571	1.517242		0.041886	23.06569	0.893724		0.042919	19.51881	1.276655
0.046854	17.0646	1.532028		0.044347	23.16758	0.885028		0.045381	19.64829	1.292883
0.049315	17.11802	1.530844		0.046808	23.24474	0.863405		0.047842	19.77255	1.254231
0.051777	17.1603	1.536452		0.04927	23.2996	0.858502		0.050303	19.84664	1.260122
0.054238	17.22846	1.573087		0.051731	23.37409	0.831744		0.052765	19.89954	1.252465
0.056699	17.26356	1.564408		0.054192	23.44895	0.812659		0.055226	19.95181	1.25815
0.059161	17.32751	1.588684		0.056654	23.50177	0.824857		0.057687	19.99275	1.243916
0.061622	17.43228	1.618899		0.059115	23.58456	0.802033		0.060149	20.01185	1.240315
0.064083	17.45121	1.640676		0.061576	23.63847	0.777856		0.06261	20.03824	1.261294
0.066545	17.57891	1.70138		0.064038	23.68678	0.761087		0.065071	20.04441	1.238466
0.069006	17.6938	1.769078		0.066499	23.73882	0.753547		0.067533	20.04819	1.243914
0.071467	17.82068	1.802195		0.06896	23.78175	0.73333		0.069994	20.05874	1.231786
0.073929	17.92118	1.851048		0.071422	23.84175	0.698843		0.072455	20.0644	1.246722
0.07639	18.12836	1.928586		0.073883	23.89574	0.688335		0.074917	20.08226	1.245544
0.078851	18.25881	1.964546		0.076344	23.91909	0.680467		0.077378	20.08706	1.244931
0.081313	18.48651	2.045876		0.078806	24.01408	0.653769		0.07984	20.10936	1.241801
0.083774	18.6395	2.056263		0.081267	24.05161	0.616311		0.082301	20.10854	1.264766
0.086235	18.85769	2.145304		0.083728	24.06598	0.600041		0.084762	20.16861	1.2686
0.088697	19.12825	2.194884		0.08619	24.10081	0.573471		0.087224	20.18637	1.303311
0.091158	19.32984	2.242126		0.088651	24.1397	0.57354		0.089685	20.24628	1.325929
0.093619	19.56627	2.258006								
0.096081	19.81691	2.268949		0.0635	23.77059	0.712398		0.0635	20.04463	1.250897
0.098542	20.06142	2.306092		0.07874	24.06684	0.575169		0.07874	20.10524	1.255364
0.101003	20.37404	2.308124		0.09652	24.2836	0.479843		0.09652	20.43694	1.436956
				0.11938	24.42789	0.387587		0.11938	21.39864	1.69388
0.095504	19.82616	2.286553		0.14732	24.46142	0.306988		0.14732	23.46084	1.383965
0.118364	22.28216	2.003298		0.18034	24.49409	0.236891		0.18034	24.71187	0.492787
0.146304	24.13529	0.866168		0.21336	24.52898	0.211158		0.21336	24.80793	0.26143
0.179324	24.48147	0.340977		0.25146	24.55875	0.199465		0.25146	24.84123	0.214142
0.212344	24.51095	0.220219		0.2921	24.58722	0.199618		0.2921	24.88807	0.195142
0.250444	24.57608	0.193152		0.3683	24.7022	0.19471		0.3683	24.98605	0.192498
0.291084	24.62519	0.187384		0.4826	24.80482	0.196198		0.4826	25.07583	0.20655
0.367284	24.70136	0.189846		0.6096	24.9275	0.201622		0.6096	25.23902	0.199431
0.481584	24.81331	0.186347		0.7366	25.077	0.192895		0.7366	25.35643	0.195285
0.608584	24.93099	0.191327		0.8636	25.20324	0.193816		0.8636	25.47483	0.201809
0.735584	25.07043	0.197723		0.9906	25.33172	0.20749		0.9906	25.58838	0.209587

Geom:	2 rows PS			Geom:	2 rows PS			Geom:	2 rows PS	
VR	0.5			VR	0.5			VR	0.5	
Tu	0.011			Tu	0.011			Tu	0.011	
Lu (cm)	6.6			Lu (cm)	6.6			Lu (cm)	6.6	
Low Tu				Low Tu				Low Tu		
Z/D =	0			Z/D =	0.75			Z/D =	1.5	
filename	p2clv5a1			filename	p2clv5q1			filename	p2clv5m1	
Y(cm)	U(y)(m/s)	u' (m/s)		Y(cm)	U(y)(m/s)	u' (m/s)		Y(cm)	U(y)(m/s)	u' (m/s)
0.862584	25.21749	0.192325		1.1176	25.51198	0.19823		1.1176	25.78812	0.192832
0.989584	25.36636	0.187071		1.2446	25.66293	0.195865		1.2446	25.97454	0.194021
1.116584	25.51507	0.187123		1.3716	25.83556	0.194217		1.3716	26.16429	0.196444
1.243584	25.67862	0.189454		1.4986	26.05864	0.198435		1.4986	26.38334	0.190073
1.370584	25.88264	0.187312		1.6256	26.23044	0.202875		1.6256	26.54917	0.198957
1.497584	26.07911	0.189391		1.7526	26.45823	0.194434		1.7526	26.77328	0.204681
1.624584	26.29142	0.190878		1.8796	26.69208	0.198116		1.8796	27.02387	0.194377
1.751584	26.4812	0.201321		2.0066	26.93904	0.195676		2.0066	27.24906	0.19667
1.878584	26.71955	0.195468		2.1336	27.17795	0.195676		2.1336	27.47107	0.202654
2.005584	26.93892	0.19891		2.2606	27.41296	0.196311		2.2606	27.705	0.213281
2.132584	27.17984	0.192199		2.3876	27.59374	0.212508		2.3876	27.95765	0.204494
2.259584	27.40721	0.203556		2.5146	27.87244	0.206606		2.5146	28.17536	0.21046
2.386584	27.66344	0.202857		2.6416	28.10385	0.203036		2.6416	28.43185	0.203884
2.513584	27.90094	0.197552		2.7686	28.30195	0.213001		2.7686	28.66889	0.202479
2.640584	28.11701	0.192954		2.8956	28.56052	0.204597		2.8956	28.91472	0.205169
2.767584	28.37471	0.198617		3.0226	28.79698	0.20784		3.0226	29.14767	0.211024
2.894584	28.59889	0.19739		3.1496	29.01262	0.209367		3.1496	29.37132	0.204732
3.021584	28.8243	0.208884		3.2766	29.24705	0.205459		3.2766	29.57788	0.21227
3.148584	29.0599	0.193851		3.4036	29.41603	0.211187		3.4036	29.80078	0.21242
3.275584	29.2465	0.204515		3.5306	29.63019	0.205931		3.5306	29.99477	0.210897
3.402584	29.48653	0.204562		3.6576	29.85001	0.206692		3.6576	30.18615	0.206778
3.529584	29.69951	0.202213		3.7846	29.99595	0.207139		3.7846	30.36119	0.205325
3.656584	29.88629	0.196481		3.9116	30.15756	0.209194		3.9116	30.51022	0.220531
3.783584	30.04061	0.217088								
3.910584	30.20545	0.208858								

Geom:	Showerhd			Geom:	Showerhd			Geom:	Showerhd	
PReqv	0.0175			PReqv	0.07			PReqv	0.35	
Tu	0.12			Tu	0.12			Tu	0.12	
Lu (cm)	3.36			Lu (cm)	3.36			Lu (cm)	3.36	
Comb(1)				Comb(1)				Comb(1)		
Z/D =	N/A			Z/D =	N/A			Z/D =	N/A	
filename	shcbp5m1			filename	shcbp2m1			filename	shcbp1m1	
Y(cm)	U(y)(m/s)	u' (m/s)		Y(cm)	U(y)(m/s)	u' (m/s)		Y(cm)	U(y)(m/s)	u' (m/s)
0.00762	9.894217	2.510873		0.008636	11.54329	2.956003		0.00762	11.26621	2.959796
0.008382	10.83826	2.831236		0.011097	14.36268	3.469269		0.009652	13.38322	3.365274
0.010843	13.65251	3.401926		0.013559	16.34344	3.70269		0.012113	15.567	3.653397
0.013305	15.84334	3.621136		0.01602	18.26679	3.800296		0.014575	17.15493	3.729818
0.015766	17.64958	3.750778		0.018481	19.42664	3.796175		0.017036	18.86864	3.801767
0.018227	19.02989	3.761187		0.020943	20.43727	3.778821		0.019497	19.91072	3.808865
0.020689	20.07665	3.72205		0.023404	21.18085	3.759952		0.021959	20.79016	3.791813
0.02315	20.79655	3.752908		0.025865	21.90415	3.75475		0.02442	21.46742	3.777583
0.025611	21.5221	3.683464		0.028327	22.32747	3.676615		0.026881	21.94986	3.728254
0.028073	22.11793	3.633087		0.030788	22.79734	3.576501		0.029343	22.47289	3.679122
0.030534	22.57957	3.575387		0.033249	23.17882	3.610472		0.031804	22.85952	3.680042
0.032995	22.91691	3.544295		0.035711	23.50981	3.592487		0.034265	23.14174	3.632001
0.035457	23.26476	3.548239		0.038172	23.72328	3.517681		0.036727	23.35023	3.613306
0.037918	23.41961	3.481524		0.040633	23.89949	3.488338		0.039188	23.55975	3.5848
0.040379	23.69724	3.45124		0.043095	24.03057	3.453849		0.041649	23.81002	3.596639
0.042841	23.81435	3.46976		0.045556	24.24606	3.453058		0.044111	23.94933	3.577845
0.045302	24.04365	3.418942		0.048017	24.38493	3.426492		0.046572	24.05587	3.499848
0.047763	24.11375	3.431707		0.050479	24.50144	3.41691		0.049033	24.15911	3.490547
0.050225	24.26176	3.394584		0.05294	24.58935	3.430286		0.051495	24.25239	3.543046
0.052686	24.3395	3.359219		0.055401	24.71913	3.379666		0.053956	24.35681	3.50419
0.055147	24.45591	3.350844		0.057863	24.82689	3.393754		0.056417	24.48236	3.456204
0.057609	24.54433	3.313632		0.060324	24.8046	3.342536		0.058879	24.53337	3.428654
0.06007	24.58368	3.300187		0.062785	24.93306	3.327975		0.06134	24.61286	3.420806
0.062531	24.69314	3.329314		0.065247	24.98624	3.337604		0.063801	24.67015	3.386247
0.064993	24.81332	3.33064		0.067708	25.01479	3.275874		0.066263	24.71582	3.438435
0.067454	24.83889	3.29051		0.070169	25.07583	3.303904		0.068724	24.78303	3.383273
0.069915	24.88801	3.230914		0.072631	25.15569	3.261088		0.071185	24.81344	3.342564
0.072377	24.9564	3.273988		0.075092	25.17104	3.274377		0.073647	24.85121	3.380756
0.074838	24.91541	3.212137		0.077554	25.17594	3.288343		0.076108	24.88765	3.346505
0.0773	24.98263	3.247617		0.080015	25.21334	3.24266		0.07857	24.8711	3.332882
0.079761	25.04015	3.218611		0.082476	25.26698	3.230515		0.081031	24.98013	3.336356
0.082222	25.13523	3.168145		0.084938	25.25823	3.243371		0.083492	25.02118	3.333179
0.084684	25.09641	3.210491		0.087399	25.28938	3.201474		0.085954	25.0094	3.296482
0.087145	25.18866	3.204295		0.08986	25.41374	3.226239		0.088415	25.04424	3.332319
0.089606	25.19497	3.193704		0.092322	25.35761	3.202742		0.090876	25.05865	3.315823
0.092068	25.25749	3.183138		0.094783	25.36815	3.193594		0.093338	25.15871	3.307412
0.094529	25.25808	3.170917		0.097244	25.42487	3.188802		0.095799	25.18077	3.29121
0.09699	25.29593	3.188899		0.099706	25.47587	3.182657		0.09826	25.19473	3.279903
0.08636	25.26103	3.121354		0.07112	25.23792	3.226984		0.08509	25.10113	3.34819
0.10922	25.40294	3.082339		0.0889	25.41451	3.189102		0.10287	25.28655	3.240378
0.13716	25.52864	3.042291		0.11176	25.6356	3.137936		0.12573	25.4041	3.22326
0.17018	25.61848	2.993709		0.1397	25.75193	3.068283		0.15367	25.50833	3.184641
0.2032	25.72943	2.988224		0.17272	25.84438	3.053857		0.18669	25.5804	3.118941
0.2413	25.72395	2.90941		0.20574	25.85407	3.002578		0.21971	25.62569	3.126142
0.28194	25.73226	2.882788		0.24384	25.89276	2.942233		0.25781	25.64647	3.078866
0.35814	25.79964	2.930842		0.28448	25.92366	2.925436		0.29845	25.76088	3.087423
0.47244	25.8379	2.860669		0.36068	26.00725	2.906851		0.37465	25.74496	3.009089
0.59944	25.87699	2.866816		0.47498	26.09262	2.867532		0.48895	25.93818	2.971563
0.72644	26.05115	2.90263		0.60198	26.1788	2.900734		0.61595	26.03901	2.944312

Geom:	Showerhd			Geom:	Showerhd			Geom:	Showerhd	
PReqv	0.0175			PReqv	0.07			PReqv	0.35	
Tu	0.12			Tu	0.12			Tu	0.12	
Lu (cm)	3.36			Lu (cm)	3.36			Lu (cm)	3.36	
Comb(1)				Comb(1)				Comb(1)		
Z/D =	N/A			Z/D =	N/A			Z/D =	N/A	
filename	shcbp5m1			filename	shcbp2m1			filename	shcbp1m1	
Y(cm)	U(y)(m/s)	u' (m/s)		Y(cm)	U(y)(m/s)	u' (m/s)		Y(cm)	U(y)(m/s)	u' (m/s)
0.85344	26.22293	2.871906		0.72898	26.25976	2.882652		0.74295	26.19536	2.928086
0.98044	26.31798	2.924428		0.85598	26.39509	2.934408		0.86995	26.37077	2.888939
1.10744	26.52691	2.971226		0.98298	26.57257	2.933742		0.99695	26.49344	2.93897
1.23444	26.66086	2.994068		1.10998	26.73567	2.967863		1.12395	26.66811	2.982217
1.36144	26.86469	3.024983		1.23698	26.90692	3.009867		1.25095	26.82932	2.983064
1.48844	27.08662	3.067576		1.36398	27.07946	3.027381		1.37795	27.05532	3.035531
1.61544	27.28367	3.104104		1.49098	27.24603	3.059454		1.50495	27.27522	3.018783
1.74244	27.46337	3.118397		1.61798	27.4979	3.075932		1.63195	27.36375	3.090963
1.86944	27.70004	3.176319		1.74498	27.62667	3.14781		1.75895	27.61845	3.091455
1.99644	27.98236	3.168009		1.87198	27.93323	3.171645		1.88595	27.82233	3.12866
2.12344	28.15541	3.220787		1.99898	28.18702	3.175922		2.01295	27.95029	3.153273
2.25044	28.35227	3.247367		2.12598	28.32234	3.230268		2.13995	28.29852	3.18409
2.37744	28.54857	3.258111		2.25298	28.57467	3.251543		2.26695	28.44625	3.223788
2.50444	28.78166	3.267516		2.37998	28.76286	3.272388		2.39395	28.64555	3.223409
2.63144	29.01435	3.286836		2.50698	28.99799	3.269706		2.52095	28.81846	3.290005
2.75844	29.18657	3.299235		2.63398	29.22591	3.303676		2.64795	29.06412	3.309589
2.88544	29.38193	3.340346		2.76098	29.43181	3.341761		2.77495	29.19761	3.268372
3.01244	29.61492	3.376613		2.88798	29.61107	3.360045		2.90195	29.42678	3.308765
3.13944	29.83479	3.360263		3.01498	29.8147	3.408572		3.02895	29.66082	3.370762
3.26644	29.99336	3.385671		3.14198	30.07726	3.377706		3.15595	29.87043	3.354028
3.39344	30.18235	3.360711		3.26898	30.14784	3.431521		3.28295	30.06383	3.377259
3.52044	30.38787	3.431976		3.39598	30.36036	3.3895		3.40995	30.21655	3.375896
3.64744	30.47795	3.422939		3.52298	30.63473	3.45217		3.53695	30.44239	3.43458
3.77444	30.63457	3.441598		3.64998	30.75408	3.449522		3.66395	30.57622	3.453847
3.90144	30.78273	3.443858		3.77698	30.9017	3.499815		3.79095	30.73721	3.445389
				3.90398	31.02844	3.453189		3.91795	30.86682	3.442299

Geom:	Showerhd			Geom:	Showerhd			Geom:	Showerhd	
PReqv	0.0175			PReqv	0.07			PReqv	0.35	
Tu	0.011			Tu	0.011			Tu	0.011	
Lu (cm)	6.6			Lu (cm)	6.6			Lu (cm)	6.6	
Low Tu				Low Tu				Low Tu		
Z/D =	N/A			Z/D =	N/A			Z/D =	N/A	
filename	shclp5m1			filename	shclp2m1			filename	shclp1m1	
Y(cm)	U(y)(m/s)	u' (m/s)		Y(cm)	U(y)(m/s)	u' (m/s)		Y(cm)	U(y)(m/s)	u' (m/s)
0.00762	8.296853	0.433612		0.00762	7.858206	1.644312		0.007112	8.665696	1.410246
0.009906	10.5058	0.488208		0.009906	10.10836	2.345793		0.008763	10.5887	1.771815
0.012367	12.8673	0.514551		0.012367	12.33378	2.913598		0.011224	13.30795	2.071444
0.014829	14.84659	0.541052		0.014829	14.33221	3.230793		0.013686	15.66625	2.223086
0.01729	16.65426	0.526945		0.01729	16.08734	3.419794		0.016147	17.61908	2.290385
0.019751	18.22451	0.516326		0.019751	17.54431	3.476003		0.018608	19.2324	2.267748
0.022213	19.51082	0.486386		0.022213	18.93678	3.411122		0.02107	20.52065	2.216349
0.024674	20.59187	0.468726		0.024674	19.84771	3.327161		0.023531	21.48106	2.125415
0.027135	21.47606	0.430662		0.027135	20.67155	3.183049		0.025992	22.2617	2.047155
0.029597	22.24555	0.404685		0.029597	21.39705	2.991994		0.028454	22.8329	1.961656
0.032058	22.81125	0.378638		0.032058	21.97914	2.783612		0.030915	23.26897	1.89047
0.034519	23.33358	0.333589		0.034519	22.37399	2.610429		0.033376	23.69437	1.746863
0.036981	23.67469	0.332564		0.036981	22.77823	2.441576		0.035838	23.92962	1.725457
0.039442	24.0244	0.302597		0.039442	23.08226	2.26081		0.038299	24.16999	1.652623
0.041903	24.25371	0.284885		0.041903	23.35145	2.09969		0.04076	24.29361	1.592164
0.044365	24.46021	0.258199		0.044365	23.52651	1.973984		0.043222	24.43829	1.559704
0.046826	24.66591	0.240279		0.046826	23.73191	1.843009		0.045683	24.57403	1.510838
0.049287	24.73517	0.23889		0.049287	23.83368	1.747606		0.048144	24.67075	1.470967
0.051749	24.85134	0.22475		0.051749	24.02058	1.621535		0.050606	24.72343	1.445587
0.05421	24.91448	0.226957		0.05421	24.09528	1.519323		0.053067	24.7828	1.432122
0.056671	24.96787	0.221278		0.056671	24.18217	1.458683		0.055528	24.82916	1.399636
0.059133	25.02487	0.22482		0.059133	24.25169	1.360024		0.05799	24.88999	1.360853
0.061594	25.05047	0.224705		0.061594	24.30029	1.333934		0.060451	24.88843	1.381286
0.064055	25.05942	0.219751		0.064055	24.36938	1.245047		0.062912	24.92564	1.346968
0.066517	25.07298	0.217114		0.066517	24.42878	1.211693		0.065374	24.99235	1.324422
0.068978	25.0507	0.236438		0.068978	24.4666	1.161439		0.067835	24.97927	1.324766
0.071439	25.099	0.222927		0.071439	24.50201	1.169114		0.070296	25.00499	1.350504
0.073901	25.08976	0.217628		0.073901	24.53724	1.126409		0.072758	24.97029	1.322403
0.076362	25.12862	0.214043		0.076362	24.52716	1.112413		0.075219	25.0167	1.324353
0.078824	25.09467	0.224844		0.078824	24.55649	1.107223				
0.081285	25.14986	0.220439		0.081285	24.58661	1.067338		0.062992	24.98412	1.367365
0.083746	25.13611	0.207552		0.083746	24.57719	1.073675		0.078232	25.07365	1.344235
0.086208	25.15234	0.210309		0.086208	24.6086	1.061263		0.096012	25.1348	1.34634
0.088669	25.12257	0.207937		0.088669	24.63163	1.056554		0.118872	25.11087	1.368755
0.09113	25.13494	0.205111		0.09113	24.67011	1.060384		0.146812	25.20719	1.368381
0.093592	25.15396	0.208053		0.093592	24.68368	1.026543		0.179832	25.2306	1.402342
0.096053	25.15349	0.206167		0.096053	24.68327	1.042288		0.212852	25.32332	1.373784
0.098514	25.16797	0.206937		0.098514	24.68196	1.037672		0.250952	25.44007	1.333061
0.100976	25.1677	0.211591		0.100976	24.70144	1.035949		0.291592	25.50963	1.250315
0.103437	25.17821	0.211951						0.367792	25.66455	1.083829
0.105898	25.19126	0.2106		0.09144	24.67148	1.045145		0.482092	25.79005	0.753427
0.10836	25.17605	0.215484		0.1143	24.7763	1.058385		0.609092	25.97869	0.398618
0.110821	25.16122	0.207864		0.14224	24.80104	1.065295		0.736092	26.1761	0.256723
0.113282	25.17933	0.208948		0.17526	24.86185	1.023235		0.863092	26.35471	0.217077
0.115744	25.15947	0.209607		0.20828	24.88565	0.958475		0.990092	26.51446	0.202764
0.118205	25.22682	0.201799		0.24638	25.12644	0.808668		1.117092	26.7202	0.201774
				0.28702	25.37322	0.595776		1.244092	26.92536	0.200933
0.11684	25.2247	0.204948		0.36322	25.54519	0.362749		1.371092	27.15047	0.198144
0.14986	25.30153	0.193656		0.47752	25.68642	0.218654		1.498092	27.34596	0.198916
0.18288	25.32163	0.195368		0.60452	25.84055	0.191603		1.625092	27.56797	0.194576

Geom:	Showerhd			Geom:	Showerhd			Geom:	Showerhd	
PReqv	0.0175			PReqv	0.07			PReqv	0.35	
Tu	0.011			Tu	0.011			Tu	0.011	
Lu (cm)	6.6			Lu (cm)	6.6			Lu (cm)	6.6	
Low Tu				Low Tu				Low Tu		
Z/D =	N/A			Z/D =	N/A			Z/D =	N/A	
filename	shclp5m1			filename	shclp2m1			filename	shclp1m1	
Y(cm)	U(y)(m/s)	u' (m/s)		Y(cm)	U(y)(m/s)	u' (m/s)		Y(cm)	U(y)(m/s)	u' (m/s)
0.22098	25.39202	0.189771		0.73152	25.99651	0.191582		1.752092	27.80097	0.198006
0.26162	25.44363	0.19088		0.85852	26.16706	0.200747		1.879092	28.01803	0.198763
0.33782	25.52948	0.187839		0.98552	26.36944	0.197291		2.006092	28.23131	0.205134
0.45212	25.67669	0.193788		1.11252	26.52755	0.199377		2.133092	28.44713	0.206651
0.57912	25.83622	0.191186		1.23952	26.72989	0.2027		2.260092	28.69712	0.202866
0.70612	26.01968	0.191308		1.36652	26.95412	0.193725		2.387092	28.9504	0.206689
0.83312	26.16983	0.196194		1.49352	27.13046	0.196799		2.514092	29.17472	0.201197
0.96012	26.34591	0.196917		1.62052	27.36922	0.200713		2.641092	29.41375	0.196417
1.08712	26.51941	0.196617		1.74752	27.58304	0.204746		2.768092	29.64465	0.204707
1.21412	26.73291	0.196841		1.87452	27.83438	0.198294		2.895092	29.87411	0.201608
1.34112	26.92695	0.206855		2.00152	28.05374	0.209383		3.022092	30.07998	0.20562
1.46812	27.11911	0.204187		2.12852	28.28036	0.20781		3.149092	30.29692	0.202163
1.59512	27.37799	0.197276		2.25552	28.53734	0.199838		3.276092	30.50239	0.20505
1.72212	27.62348	0.199547		2.38252	28.75929	0.198007		3.403092	30.688	0.205714
1.84912	27.81989	0.21211		2.50952	29.00671	0.200287		3.530092	30.87903	0.210978
1.97612	28.09739	0.202319		2.63652	29.21546	0.207049		3.657092	31.05528	0.205702
2.10312	28.35391	0.194357		2.76352	29.47777	0.202314		3.784092	31.20588	0.217572
2.23012	28.55582	0.203177		2.89052	29.69167	0.203103		3.911092	31.38739	0.212367
2.35712	28.80415	0.205289		3.01752	29.91967	0.208129				
2.48412	29.0464	0.200442		3.14452	30.11182	0.204811				
2.61112	29.27335	0.222134		3.27152	30.3281	0.218719				
2.73812	29.50768	0.201382		3.39852	30.54099	0.210008				
2.86512	29.72326	0.206609		3.52552	30.75216	0.208566				
2.99212	29.97866	0.208096		3.65252	30.91202	0.219823				
3.11912	30.15023	0.2058		3.77952	31.12489	0.211518				
3.24612	30.37783	0.214993		3.90652	31.27375	0.206331				
3.37312	30.57997	0.209236								
3.50012	30.723	0.231544								
3.62712	30.95987	0.208815								
3.75412	31.11813	0.217555								
3.88112	31.33346	0.211709								

Appendix A.5 Turbulent Scales of Velocity Profiles

This appendix contains integral and energy scales taken inside the boundary layers with and without film cooling. An estimate for the dissipation based on the spectrum is also given. Typically, velocity time records were taken for two locations in each boundary layer. The data sets consisted of 40 records of 8192 points. Each data set was analyzed using an FFT algorithm then the 40 spectrums were averaged. The dissipation was estimated from the spectrum as detailed in chapter 3 and an inverse FFT was used to calculated the autocorrelation in time. The integral time scale was estimated by integrating the spectrum to the first zero crossing and Taylor's hypothesis was used to estimate the integral scale. The energy scale was defined as $Lu = 1.5\ u'^3/\varepsilon$ after Hancock and Bradshaw. The different vane geometries are given in the column "Geo" and the symbols relate to the following geometries, turbulence conditions, and film cooling conditions:

Geo	vane geometry
BV	base vane
P1	one row of pressure surface film cooling
P2	two rows of pressure surface film cooling
S1	one row of suction surface film cooling
S2	two rows of suction surface film cooling
SHP	showerhead array taken on the pressure surface
SHS	showerhead array taken on the suction surface
T	turbulence geometry
L	low turbulence configuration
C	combustor or high turbulence configuration
Z/D	spanwise location of measurement relative to hole centerline of downstream row of holes
VR	velocity ratio of film cooling array
PR	equivalent pressure ratio of showerhead array

Filename	Vinlet	ew,in	Re,hw	Vhw	Tu	Tau	Lx	e	Lu	Y loc	Geo	T	Z/D	VR	PR
	m/s			m/s		s	cm	m2/s3	cm	cm					
p1cbpm	29.38	9.101	5.953	19.22	0.1938	0.000371	0.713	6797	1.14	0.0193	BV	C	N/A		
p1cba4	29.46	9.123	7.883	25.46	0.1226	0.000452	1.15	2057	2.216	0.1033	BV	C	N/A		
p1cbqp	29.56	9.177	8.465	27.26	0.1154	0.000537	1.463	1883	2.479	1.506	BV	C	N/A		
shs0m4	28.74	8.93	26.9	86.57	0.0927	0.000199	1.719	74283	1.043	0.0943	BV	C	N/A		
shl0m4	28.9	8.803	26.77	87.87	0.0553	1.52E-05	0.133	85942	0.2	0.1135	BV	L	N/A		
p1c1a4	29.54	8.853	7.512	25.07	0.053	0.00013	0.326	2800	0.125	0.0574	P1	L	0	1	
p1c1a6	29.53	8.853	7.966	26.57	0.0521	0.000104	0.277	6064	0.066	0.1089	P1	L	0	1	
p1c2a4	29.52	8.832	7.382	24.67	0.0835	8.08E-05	0.199	8482	0.154	0.0637	P1	L	0	1.5	
p1c2a9	29.51	8.825	8.762	29.3	0.0845	3.98E-05	0.116	23132	0.098	0.2502	P1	L	0	1.5	
p1c2m7	29.54	8.872	7.878	26.23	0.0397	0.000126	0.329	1834	0.092	0.1582	P1	L	1.5	1.5	
p1c2q4	29.16	8.893	8.893	29.16	0.0727	8.63E-05	0.252	8790	0.163	0.1335	P1	L	0.75	1.5	
p1c5a2	29.51	8.887	6.521	21.65	0.058	0.00067	1.45	1311	0.227	0.0465	P1	L	0	0.5	
p1c5a4	29.53	8.892	6.27	20.82	0.0695	2.26E-05	0.047	10503	0.043	0.108	P1	L	0	0.5	
p2l1a1	29.54	9.551	5.735	17.74	0.1062	0.000131	0.233	4921	0.204	0.0215	P2	L	0	1	
p2l1a4	29.55	9.549	7.455	23.07	0.0683	6.67E-05	0.154	8139	0.072	0.0992	P2	L	0	1	
p2l1m1	29.44	9.449	6.068	18.9	0.1124	0.000133	0.252	4362	0.33	0.0218	P2	L	1.5	1	
p2l1m4	29.56	9.488	8.118	25.29	0.0492	0.000176	0.446	3412	0.085	0.102	P2	L	1.5	1	
p2l1q1	29.5	9.497	6.588	20.46	0.0894	0.000157	0.321	1875	0.49	0.0161	P2	L	0.75	1	
p2l1q4	29.51	9.502	8.197	25.46	0.0394	0.000121	0.309	2072	0.073	0.1142	P2	L	0.75	1	
p2l2a1	29.55	9.578	6.527	20.14	0.1242	9.38E-05	0.189	9921	0.236	0.0171	P2	L	0	1.5	
p2l2a4	29.53	9.57	8.711	26.87	0.0736	5.62E-05	0.151	13126	0.088	0.0988	P2	L	0	1.5	
p2l2m1	29.51	9.377	6.548	20.61	0.133	0.00011	0.226	10186	0.303	0.0176	P2	L	1.5	1.5	
p2l2m4	29.54	9.382	8.982	28.27	0.0603	7.44E-05	0.21	6932	0.107	0.0977	P2	L	1.5	1.5	
p2l2q1	29.62	9.387	6.398	20.19	0.1421	0.000115	0.232	9536	0.371	0.0102	P2	L	0.75	1.5	
p2l2q4	29.53	9.361	9.104	28.72	0.0569	7.06E-05	0.203	6128	0.107	0.0939	P2	L	0.75	1.5	
p2l5a1	29.52	9.545	4.315	13.34	0.1212	0.000354	0.472	2359	0.269	0.0185	P2	L	0	0.5	
p2l5a4	29.54	9.549	6.429	19.88	0.1131	3.07E-05	0.061	34152	0.05	0.0967	P2	L	0	0.5	
p2l5m1	29.64	9.484	4.622	14.44	0.1097	0.000599	0.865	930	0.642	0.0184	P2	L	1.5	0.5	
p2l5m4	29.59	9.47	6.484	20.26	0.062	0.0002	0.406	5257	0.057	0.087	P2	L	1.5	0.5	
p2l5q1	29.55	9.586	6.237	19.22	0.0845	0.000238	0.457	1744	0.369	0.0168	P2	L	0.75	0.5	
p2l5q4	29.61	9.604	7.899	24.35	0.0095	2.25E-05	0.055	203	0.009	0.107	P2	L	0.75	0.5	
shp1l1	29.5	9.026	5.285	17.28	0.1354	0.00022	0.38	3241	0.592	0.0157	SHP	L	N/A		0.35
shp1l4	29.51	9.02	7.666	25.08	0.0503	0.000105	0.263	1230	0.245	0.1099	SHP	L	N/A		0.35
shp2l1	29.56	8.999	5.337	17.53	0.1962	0.000778	1.364	2220	2.749	0.0192	SHP	L	N/A		0.07
shp2l4	29.51	8.98	7.548	24.81	0.0385	0.000114	0.282	659	0.198	0.102	SHP	L	N/A		0.07
shp5l1	29.65	8.975	5.235	17.29	0.0228	0.000569	0.984	5.447	1.688	0.0183	SHP	L	N/A		0.02
shp5l4	29.67	8.978	7.621	25.18	0.0132	0.001208	3.042	0.581	9.483	0.1037	SHP	L	N/A		0.02
shl1a1	28.62	8.661	16.13	53.29	0.1287	3.64E-05	0.194	182393	0.265	0.0147	SHS	L	N/A		0.35
shl1a4	28.6	8.654	25.39	83.91	0.0736	7.37E-05	0.619	124544	0.284	0.1023	SHS	L	N/A		0.35
shl2a1	28.77	8.74	15.79	51.99	0.1264	2.86E-05	0.149	173651	0.245	0.0133	SHS	L	N/A		0.07
shl2a4	28.69	8.715	26.03	85.7	0.0598	1.5E-05	0.129	112154	0.18	0.1012	SHS	L	N/A		0.07
shl5a1	28.67	8.714	15.83	52.07	0.1254	3.22E-05	0.168	170380	0.245	0.0119	SHS	L	N/A		0.02
shl5a4	28.72	8.734	26.52	87.22	0.0536	1.3E-05	0.113	89301	0.171	0.1018	SHS	L	N/A		0.02

Filename	Vinlet	ew,in	Re,hw	Vhw	Tu	Tau	Lx	e	Lu	Y loc	Geo	T	Z/D	VR	PR
	m/s			m/s		s	cm	m2/s3	cm	cm					
s1l5a1	28.62	8.572	13.36	44.62	0.1472	4.75E-05	0.212	142726	0.298	0.0115	S1	L	0	0.5	
s1l5a4	28.6	8.563	21.14	70.59	0.0876	1.27E-05	0.09	217124	0.163	0.1053	S1	L	0	0.5	
s1l5m1	28.71	8.7	15.05	49.66	0.1369	3.12E-05	0.155	164461	0.287	0.0095	S1	L	1.5	0.5	
s1l5m4	28.67	8.681	25.16	83.11	0.0602	1.3E-05	0.108	118207	0.159	0.0998	S1	L	1.5	0.5	
s1l5q1	28.68	8.559	12.37	41.44	0.1643	7.85E-05	0.325	179320	0.264	0.0063	S1	L	0.75	0.5	
s1l5q4	28.64	8.558	24.33	81.42	0.0767	1.18E-05	0.096	206195	0.177	0.0919	S1	L	0.75	0.5	
s2l5a1	28.75	8.667	10.5	34.84	0.1683	8.66E-05	0.302	99012	0.305	0.0067	S2	L	0	0.5	
s2l5a4	28.7	8.65	20.37	67.57	0.0968	1.78E-05	0.12	230862	0.182	0.0945	S2	L	0	0.5	
s2l5m1	28.73	8.591	10.61	35.48	0.1703	5.84E-05	0.207	102924	0.321	0.0063	S2	L	1.5	0.5	
s2l5m4	28.77	8.601	21.16	70.77	0.0861	1.89E-05	0.134	164140	0.207	0.0945	S2	L	1.5	0.5	
s2l5q1	28.72	8.632	10.1	33.6	0.1843	0.000125	0.421	124521	0.286	0.0045	S2	L	0.75	0.5	
s2l5q4	28.66	8.611	24.22	80.6	0.0813	1.32E-05	0.107	215267	0.196	0.0984	S2	L	0.75	0.5	
p1s1a1	29.46	9.353	6.262	19.72	0.195	0.00033	0.651	7068	1.207	0.0185	P1	C	0	1	
p1s1a4	29.42	9.341	8.2	25.83	0.115	0.000387	1	3794	1.036	0.0851	P1	C	0	1	
p1s1m1	29.4	9.269	6.22	19.73	0.1962	0.000338	0.667	7419	1.173	0.0178	P1	C	1.5	1	
p1s1m4	29.4	9.27	8.168	25.91	0.1154	0.000351	0.908	4146	0.967	0.0853	P1	C	1.5	1	
p1s1q1	29.42	9.313	6.25	19.75	0.1964	0.000316	0.624	7113	1.23	0.018	P1	C	0.75	1	
p1s1q4	29.43	9.306	8.181	25.88	0.1168	0.000402	1.041	4029	1.028	0.0773	P1	C	0.75	1	
p1s2a1	29.35	9.15	6.48	20.78	0.2064	0.000361	0.749	8816	1.343	0.0176	P1	C	0	1.5	
p1s2a4	29.39	9.155	8.755	28.11	0.1312	0.000336	0.944	12432	0.605	0.0936	P1	C	0	1.5	
p1s2m1	29.3	9.196	6.409	20.42	0.2063	0.00033	0.673	8481	1.323	0.018	P1	C	1.5	1.5	
p1s2m4	29.41	9.229	8.759	27.91	0.1323	0.000315	0.878	11775	0.641	0.0999	P1	C	1.5	1.5	
p1s2q1	29.39	9.189	6.643	21.25	0.2029	0.000322	0.685	8895	1.351	0.0192	P1	C	0.75	1.5	
p1s2q4	29.29	9.154	8.802	28.16	0.1307	0.000322	0.906	11569	0.647	0.1166	P1	C	0.75	1.5	
p1s5a1	29.42	9.177	5.901	18.92	0.1922	0.000283	0.535	8137	0.886	0.02	P1	C	0	0.5	
p1s5a4	29.36	9.157	7.728	24.78	0.1306	0.00043	1.064	3357	1.514	0.1	P1	C	0	0.5	
p1s5m1	29.36	9.121	5.984	19.26	0.1953	0.000334	0.642	8126	0.982	0.02	P1	C	1.5	0.5	
p1s5m4	29.38	9.124	7.766	25.01	0.1356	0.000433	1.084	3444	1.698	0.1107	P1	C	1.5	0.5	
p1s5q1	29.3	9.123	5.759	18.49	0.1965	0.000291	0.539	8255	0.872	0.0185	P1	C	0.75	0.5	
p1s5q4	29.4	9.156	7.698	24.72	0.1346	0.000391	0.967	3492	1.583	0.0913	P1	C	0.75	0.5	
p2s1a1	29.3	8.899	5.892	19.4	0.1974	0.000268	0.519	9116	0.923	0.017	P2	C	0	1	
p2s1a4	29.35	8.916	7.778	25.6	0.1056	0.000316	0.809	5432	0.546	0.1002	P2	C	0	1	
p2s1m1	29.36	9.117	6.019	19.39	0.1926	0.000276	0.535	8335	0.937	0.0163	P2	C	1.5	1	
p2s1m4	29.19	9.063	7.789	25.09	0.1079	0.000341	0.855	4742	0.628	0.102	P2	C	1.5	1	
p2s1q1	29.35	8.912	6.032	19.86	0.1931	0.000263	0.521	8550	0.99	0.0169	P2	C	0.75	1	
p2s1q4	29.35	8.921	7.789	25.63	0.1067	0.000285	0.731	5092	0.602	0.0947	P2	C	0.75	1	
p2s2a1	29.32	8.884	6.371	21.03	0.1909	0.000235	0.494	13165	0.737	0.0154	P2	C	0	1.5	
p2s2a4	29.27	8.862	8.721	28.8	0.1032	0.000253	0.729	12303	0.32	0.1195	P2	C	0	1.5	
p2s2m1	29.27	8.856	6.683	22.09	0.1875	0.000321	0.71	12541	0.85	0.0164	P2	C	1.5	1.5	
p2s2m4	29.35	8.878	8.697	28.76	0.104	0.000282	0.81	10581	0.379	0.0988	P2	C	1.5	1.5	
p2s2q1	29.39	8.895	6.569	21.71	0.1895	0.00028	0.607	13015	0.802	0.0162	P2	C	0.75	1.5	
p2s2q4	29.36	8.885	8.662	28.62	0.1043	0.000264	0.756	11260	0.354	0.1021	P2	C	0.75	1.5	
p2s5a1	29.22	9.11	5.411	17.35	0.2066	0.000253	0.439	9377	0.737	0.0167	P2	C	0	0.5	
p2s5a4	29.33	9.145	7.334	23.52	0.1364	0.000349	0.82	4306	1.151	0.0901	P2	C	0	0.5	
p2s5m1	29.3	9.098	5.399	17.39	0.2061	0.000251	0.436	9277	0.744	0.0175	P2	C	1.5	0.5	
p2s5m4	29.2	9.068	7.312	23.55	0.1335	0.000377	0.888	4135	1.127	0.1007	P2	C	1.5	0.5	
p2s5q1	29.27	9.107	5.33	17.13	0.2108	0.000246	0.421	9660	0.731	0.0172	P2	C	0.75	0.5	
p2s5q4	29.24	9.096	7.305	23.48	0.1326	0.00037	0.87	4208	1.076	0.0908	P2	C	0.75	0.5	

Filename	Vinlet	ew,in	Re,hw	Vhw	Tu	Tau	Lx	e	Lu	Y loc	Geo	T	Z/D	VR	PR
	m/s			m/s		s	cm	m2/s3	cm	cm					
shp1h1	29.28	8.994	6.006	19.56	0.1923	0.000328	0.642	7440	1.072	0.018	SHP	C	N/A		0.35
shp1h4	29.45	9.049	7.759	25.25	0.1258	0.000413	1.042	2620	1.835	0.0994	SHP	C	N/A		0.35
shp2h1	29.5	9.082	5.795	18.82	0.1983	0.000348	0.655	7327	1.064	0.0167	SHP	C	N/A		0.07
shp2h4	29.28	9.022	7.807	25.34	0.1202	0.000419	1.062	2015	2.102	0.0905	SHP	C	N/A		0.07
shp5h1	29.35	8.979	5.762	18.83	0.1985	0.000354	0.667	7401	1.059	0.0174	SHP	C	N/A		0.02
shp5h4	29.34	8.974	7.821	25.58	0.1211	0.000424	1.084	1837	2.426	0.1108	SHP	C	N/A		0.02
shs1m1	28.11	8.77	12.97	41.58	0.2073	0.000325	1.351	147652	0.65	0.0071	SHS	C	N/A		0.35
shs1m4															
shs2m1	28.35	8.721	11.29	36.7	0.2723	0.0005	1.834	130107	1.151	0.0052	SHS	C	N/A		0.07
shs2m4	28.37	8.733	26.33	85.54	0.101	0.000217	1.853	94911	1.019	0.0937	SHS	C	N/A		0.07
shs5m1	28.34	8.704	11.78	38.36	0.2727	0.000525	2.014	135097	1.271	0.0056	SHS	C	N/A		0.02
shs5m4	28.25	8.711	26.55	86.13	0.0983	0.000222	1.91	82937	1.098	0.0976	SHS	C	N/A		0.02
s1s5a1	28.41	8.492	10.4	34.78	0.2805	0.000402	1.398	138019	1.009	0.0053	S1	C	0	0.5	
s1s5a4	28.26	8.515	22.9	76.01	0.1339	0.000211	1.606	175394	0.902	0.0887	S1	C	0	0.5	
s1s5m1	28.21	8.658	12.09	39.39	0.2605	0.000514	2.026	137881	1.175	0.0058	S1	C	1.5	0.5	
s1s5m4	28.44	8.722	25.54	83.29	0.1124	0.000242	2.017	121354	1.015	0.0947	S1	C	1.5	0.5	
s1s5q1	28.46	8.703	12.84	41.98	0.2406	0.000387	1.625	147031	1.051	0.0071	S1	C	0.75	0.5	
s1s5q4	28.59	8.724	23.99	78.61	0.1324	0.000214	1.683	162121	1.044	0.1005	S1	C	0.75	0.5	
s2s5a1	28.2	8.479	10.9	36.25	0.2714	0.000357	1.294	160097	0.892	0.0074	S2	C	0	0.5	
s2s5a4	28.07	8.437	20.67	68.76	0.139	0.000126	0.865	260730	0.502	0.0997	S2	C	0	0.5	
s2s5m1	28.18	8.462	11.72	39.03	0.2367	0.000317	1.238	197867	0.597	0.0087	S2	C	1.5	0.5	
s2s5m4	28.16	8.455	21.21	70.63	0.1343	0.000121	0.855	251935	0.508	0.0995	S2	C	1.5	0.5	
s2s5q1	28.13	8.454	12.6	41.92	0.2144	0.000223	0.935	195426	0.557	0.0088	S2	C	0.75	0.5	
s2s5q4	28.09	8.444	20.9	69.54	0.1435	0.00013	0.902	246086	0.606	0.0919	S2	C	0.75	0.5	

REPORT DOCUMENTATION PAGE

Form Approved
OMB No. 0704-0188

1. AGENCY USE ONLY (*Leave blank*)	2. REPORT DATE	3. REPORT TYPE AND DATES COVERED
	September 1996	Final Contractor Report

4. TITLE AND SUBTITLE

Experimental Study of Vane Heat Transfer and Film Cooling at Elevated Levels of Turbulence

5. FUNDING NUMBERS

WU-505-62-10
C-NAS3-25950

6. AUTHOR(S)

Forrest E. Ames

7. PERFORMING ORGANIZATION NAME(S) AND ADDRESS(ES)

Allison Engine Company
P.O. Box 420
Indianapolis, Indiana 46206-0420

8. PERFORMING ORGANIZATION REPORT NUMBER

E-10419

9. SPONSORING/MONITORING AGENCY NAME(S) AND ADDRESS(ES)

National Aeronautics and Space Administration
Lewis Research Center
Cleveland, Ohio 44135-3191

10. SPONSORING/MONITORING AGENCY REPORT NUMBER

NASA CR-198525

11. SUPPLEMENTARY NOTES

Project Manager, Steven A. Hippensteele, Internal Fluid Mechanics Division, NASA Lewis Research Center, organization code 2630, (216) 433-5897.

12a. DISTRIBUTION/AVAILABILITY STATEMENT

Unclassified - Unlimited
Subject Category 34

This publication is available from the NASA Center for AeroSpace Information, (301) 621-0390.

12b. DISTRIBUTION CODE

13. ABSTRACT (*Maximum 200 words*)

This report documents the results of an experimental study on the influence of high level turbulence on vane film cooling and the influence of film cooling on vane heat transfer. Three different cooling configurations were investigated which included one row of film cooling on both pressure and suction surfaces, two staggered rows of film cooling on both suction and pressure surfaces, and a showerhead cooling array. The turbulence had a strong influence on film cooling effectiveness, particularly on the pressure surface where local turbulence levels were the highest. For the single row of holes, the spanwise mixing quickly reduced centerline effectiveness levels while mixing in the normal direction was more gradual. The film cooling had a strong influence on the heat transfer in the laminar regions of the vane. The effect of film cooling on heat transfer was noticeable in the turbulent regions but augmentation ratios were significantly lower. In addition to heat transfer and film cooling, velocity profiles were taken downstream of the film cooling rows at three spanwise locations. These profile comparisons documented the strong spanwise mixing due to the high turbulence. Total pressure exit measurements were also documented for the three configurations.

14. SUBJECT TERMS

Gas turbine heat transfer; Film cooling; Turbulence; Vane aerodynamics

15. NUMBER OF PAGES

229

16. PRICE CODE

A11

17. SECURITY CLASSIFICATION OF REPORT	18. SECURITY CLASSIFICATION OF THIS PAGE	19. SECURITY CLASSIFICATION OF ABSTRACT	20. LIMITATION OF ABSTRACT
Unclassified	Unclassified	Unclassified	